



UNIVERSITEIT VAN PRETORIA
UNIVERSITY OF PRETORIA
YUNIBESITHI YA PRETORIA



UNIVERSITEIT VAN PRETORIA
UNIVERSITY OF PRETORIA
YUNIBESITHI YA PRETORIA

Faculty of Engineering, Built Environment and
Information Technology

INVESTIGATION OF RHEOLOGICAL RESPONSE, COHESION AND ADHESION FATIGUE DAMAGE OF BITUMINOUS ROAD SEAL MATERIALS

ESTIMÉ MAMBULA WA KANYINDA MUKANDILA

University of Pretoria

**INVESTIGATION OF RHEOLOGICAL RESPONSE,
COHESION AND ADHESION FATIGUE DAMAGE OF
BITUMINOUS ROAD SEAL MATERIALS**

ESTIMÉ MAMBULA WA KANYINDA MUKANDILA

Thesis submitted in partial fulfilment of the requirements for the degree
Doctor of Philosophy
in the
Department of Civil Engineering
Faculty of Engineering, Built Environment and Information Technology
University of Pretoria

Pretoria

June 2016

Thesis summary

INVESTIGATION OF RHEOLOGICAL RESPONSE, COHESION AND ADHESION FATIGUE DAMAGE OF BITUMINOUS ROAD SEAL MATERIALS

ESTIMÉ MAMBULA WA KANYINDA MUKANDILA

Promoter: Professor Doctor Wynand J vdM Steyn

Co-Promoter: Doctor Terence Ian Milne

Department: Civil Engineering

University: University of Pretoria

Degree: Philosophiae Doctor (Engineering)

Most of the current seal designs are based on the volumetric properties of materials and voids. In order to improve seal design, the possibility of introducing mechanistic principles into the seal design was investigated. Introducing mechanistic concepts into the seal design meant that principles such as elasticity and viscoelasticity could be used in terms of stress-strain to explain phenomena such as damage in the seal structure. Viscoelastic parameters of bituminous materials such as complex modulus (G^*) and phase angle (δ) are key elements in the understanding of performance, damage and failure of seal bituminous materials. Two main failure parameters of seal are cohesion failure (fatigue cracking due to ageing of binder and loss of elasticity) and adhesion failure or stripping (occurring between stone to bitumen or bitumen to base).

The aim of this study was to model the response of a seal's binder and the cohesion and adhesion damage of seals materials This Research also investigates the testing procedure of Cohesion Fatigue Damage (CFD) and Adhesion Fatigue Damage (AFD) of bituminous seal material using the Dynamic Shear Rheometer (DSR). The research was based on the Lifetime Optimisation Tool (LOT) research programme from Delft University of Technology.

The response model was performed by means of the DSR parallel plate and modelled using the linear viscoelastic rheological master curves. In addition to the binder models an ageing model was developed base on the G^* master curve using the recovered field-aged bitumens and the fresh binder from the plant.

The modelling of CFD and AFD of the seal was based on investigated DRS test protocols results and was established on the "stiffness reduction" principle of materials under the action of cyclic stress.

From the ageing model it appeared that PAV ageing does not necessary simulate the long term ageing of bitumen. An investigation into ageing of non-modified and modified binder is suggested (e.g. by comparing PAV ageing with Q-sun ageing). The recovery of bitumen method needs to be revisited using technique such centrifugal force.

The CFD and AFD models offer a practical advantage consisting of the possibility to be adapted and incorporated in the recursive simulation models as developed in the South African Road Design System (SARDS). It was observed that the generalised model for CFD depends more on stress, while the generalised model for AFD appears to depend more on temperature. This observation seems to agree with the fact that adhesion damage is more sensitive to temperature change, whereas cohesion damage is more prone to be influenced by applied fatigue stress. The CFD and AFD models provide an indication of non-linear development of the fatigue damage during-life period within bitumen and between bitumen and stone in the case of seal. This is represented by the modelling of the change of G^* , as suggested in this investigation.

Statement by the author

The author hereby states that all the research work reported in this dissertation was initiated by him and that he was solely responsible for the experimental planning and control of the various tests discussed, as well as the interpretation and reporting of all the results.

The preparation of the materials for testing and the execution of the tests (Dynamic Shear Rheometer (DSR)) were performed by him or delegated to the available technicians, under his direct supervision.



To God be the Glory

Acknowledgments

I would like to express my gratitude to the following organisation and peoples for their contribution to the success of this of this thesis:

- The South African National Roads Agency Ltd (SANRAL), which made possible this work, through the South African Road Design System (SARDS).
- TOSAS in general and Johan Muller in particular: for providing major of bitumen used in the research
- Prof Wynand Steyn, the Promoter of this Thesis, for his leadership, his “always positive attitude” and his support.
- Dr Terence Milne, the Co-promoter of this Thesis, he always challenge me believe in me.
- The team of the “Thin surfacing” research group of the SARDS: Prof Kim Jenkins, Gerrie Van Zyl, Johan Gerber and Stephen Bredenhann. All discussion, comment and review made possible this research.
- The team of Civil Engineering and Geosciences, Section of Pavement Engineering Delft University of Technology. Prof Andre Moolenaar, Prof Scarpas, Prof Sandra Erkens, Dr Rien Hurman, Dr Milliyon Woldekidan, Dr Diederik Van Lent, Dr Jian Qiu, Dr Mo Liatong Mo. I appreciate the background knowledge transfer and continuous support.
- Aurecon and WorleyParsons for the support and opportunity offer to pursue and complete Thesis.
- Dr Emile Horak, for his endless support and kind advices, he inspires me.
- Dr Hechter Theyse, his scientific guidance was a contribution to the progress of this research.
- Dr Arno Hefer, for all discussions and support.
- Dr Phil Paige Green, for your advices.
- Prof Alex Visser, for the knowledge transfer.
- Sasol especially Jacques van Heerden, for allowing DSR testing in the Laboratory
- SRT: Hennie Loots and Phumzile Dlamini, for the DSR testing and support

- CSIR: Benoit Verhaeghe, Georges Mturi, Keneilwe Mogonedi, Johan O'Connell, Dr Morris de Beer, Dr Joseph Anochie Boateng, Dr Martin Mgangira, Julius Komba. The support in testing, advices and all discussions are appreciated.
- Dr Raelized Du plooy for your support and knowledge share.
- Frances Jordan for editing inputs.
- My family: Marie-colette, Esther Daniela Israel and Gracia, for all supports and love,
- My parents: Remy Kanyinda and Charlotte Lubuya. I am grateful for the life you gave me. You are wonderful!
- Bienvenu Lukwichi Omari, for all discussion and your inputs.
- Dr Jeff Banutelo and is family, for your opening your house to me during my research time in Sasolburg.
- To All my big family and all my Friends, receive my gratitude.

Table of Contents

List of Figures.....	x
List of Tables.....	xvi
List of Abbreviations.....	xviii
List of Symbols.....	xix
List of Units	xix
1 INTRODUCTION	1
1.1 Background.....	1
1.2 Problem Statement	1
1.3 Objectives	3
1.4 Scope and Extent of the Research.....	4
References.....	7
2 LITERATURE REVIEW	8
2.1 Introduction	8
2.2 Surfacing Seals.....	10
2.3 Seal Components.....	12
2.3.1 Bituminous binder	12
2.3.2 Aggregate	15
2.4 Seal Design.....	17
2.5 Seal Modelling.....	19
2.6 Ageing of Bituminous Binder.....	23
2.6.1 Background on bitumen ageing	23
2.6.2 Some bitumen ageing methods	24
2.6.3 Comments on ageing methods	29
2.7 Rheology and Visco-elasticity	29
2.7.1 Introduction	29
2.7.2 Definitions related to visco-elasticity	32

2.7.3	Linear visco-elasticity concepts for frequency domain	36
2.8	Visco-elasticity of Bituminous Material	39
2.9	Rheological Modelling of Linear Visco-elastic Properties of Bituminous Materials	41
2.9.1	Construction of master curves	42
2.9.2	Black space diagrams and Cole-Cole diagrams	48
2.9.3	Mathematical models	51
2.9.4	Mechanical models	56
2.10	Cohesion and Adhesion	64
2.10.1	Introduction	64
2.10.2	Adhesion and cohesion mechanisms.....	66
2.10.3	Moisture damage effects on adhesion	68
2.10.4	Conclusion on cohesion and adhesion	69
2.11	Fatigue of Bituminous Materials.....	69
2.11.1	Introduction	69
2.11.2	Fatigue mechanism.....	72
2.12	Summary of Literature Review and Research Recommendations	75
2.13	References.....	79
3	EXPERIMENTAL PROGRAMME	88
3.1	Introduction	88
3.2	Bituminous Materials Used for the Experiment	90
3.3	Basic description of the Dynamic Shear Rheometer (DSR)	90
3.3.1	Bitumen frequency sweep response test using the DSR	95
3.3.2	DSR testing for cohesion fatigue damage and adhesion fatigue damage tests	96
3.3.3	Special DSR setups for cohesion fatigue damage test	96
3.3.4	Special DSR setups for adhesion fatigue tests	97

3.4	Sample Preparation and Conditioning.....	97
3.4.1	Water conditioning by vacuum vessel.....	98
3.4.2	Ageing by Q-SUN	99
3.5	Development of Testing Procedures for Cohesion and Adhesion Fatigue Damage	100
3.5.1	Stabilisation of testing temperature in the chamber	101
3.5.2	Choice of testing parameters	101
3.5.3	Choice of testing mode: strain controlled vs. stress controlled.....	103
3.5.4	Impact of changes in DSR geometry configuration on the test output ..	105
3.5.5	Pure shear test mode vs. combined shear and normal stress test mode....	108
3.5.6	Choice of binder film thickness between stone columns in the adhesion test.....	112
3.5.7	Repeatability of tests.....	113
3.5.8	Binder fatigue related to change in sample radius	115
3.5.9	Use of parallel plates for cohesion fatigue damage test.....	116
3.6	Testing Approach Adopted.....	116
3.7	Testing Protocols	117
3.7.1	Bitumen frequency sweep response protocol	117
3.7.2	Cohesion fatigue damage test protocol.....	119
3.7.3	Adhesion fatigue damage test protocol.....	122
3.8	Summary.....	125
	References.....	126
4	RESULTS, INTERPRETATION AND MODELLING CONCEPT OF COHESION AND ADHESION FATIGUE DAMAGE.....	130
4.1	Introduction	130
4.2	Bitumen Response Outcome	130
4.2.1	Results of the mathematical models	130

4.2.2	Mechanical model results	133
4.2.3	Comparison between different models.....	136
4.3	Cohesion and Adhesion Fatigue Damage Outcome	138
4.4	End–life Damage Principle	141
4.5	Principle of Damage During-life Period	142
4.6	Summary.....	144
	References.....	144
5	RHEOLOGICAL RESPONSE, COHESION AND ADHESION FATIGUE DAMAGE MODELS OF BITUMINOUS ROAD SEAL MATERIALS	145
5.1	Introduction	145
5.2	Models Based on Response Data.....	145
5.2.1	Principle of development of ageing model	145
5.2.2	Ageing model of a seal’s bitumen	146
5.2.3	5.2.3 Discussion of the ageing model	154
5.3	Fatigue Damage Modelling	156
5.3.1	Background to fatigue life	156
5.3.2	Fatigue damage model of cohesion and adhesion using the end-life principle.....	161
5.3.3	Fatigue damage model of cohesion and adhesion in the during-life period	170
5.4	Summary.....	185
	References.....	187
6	INPUT PARAMETERS FOR SEAL MODELLING AND SEAL DESIGN	189
6.1	Introduction	189
6.2	Use of Rheological Response, Cohesion and Adhesion Fatigue Damage Parameters	189
6.3	Summary.....	192
	References.....	192

7	CONCLUSION AND RECOMMENDATIONS	193
7.1	Conclusion	193
7.2	Recommendations	196
	REFERENCES.....	199
	APPENDICES	212
A	OVERVIEW OF SEAL DESIGN.....	213
A.1	Introduction	213
A.2	Seal Design Approach in South Africa	215
A.2.1	Calculation of application rate of binder	216
A.2.2	Calculation of different void fractions necessary for the design	216
A.2.3	Determination of binder application rate	218
A.2.4	Calculation of spread rate of aggregate	219
A.2.5	Other aspects considered in the seal design process.....	220
A.3	McLeod Seal Design Approach.....	222
A.4	Austroroads Seal Design Approach	225
A.5	References.....	229
B	FORMULAE OF SOME MATHEMATICAL VISCO-ELASTIC MODELS	230
B.1	Modified Van der Poel's nomograph	230
B.2	Jongepier and Kuilman's Model	230
B.3	Dobson's Model	231
B.4	Dickinson and Witt's Model	232
B.5	Christensen and Anderson (CA) Model.....	233
B.6	Fractional Model.....	233
B.7	Christensen, Anderson and Marasteanu (CAM) Model.....	234
B.8	Bahia and Co-workers' Model	235
B.9	Al-Qadi and Co-workers' Model	235
B.10	Polynomial Model.....	236

B.11	Sigmoidal Model.....	236
B.12	The LCPC Master Curve Construction Method.....	237
B.13	Generalised Logistic Sigmoidal Model	237
B.14	New Complex Modulus and Phase Angle Predictive Model.....	238
B.15	References.....	238
C	DEVELOPMENT OF MECHANICAL MODEL.....	239
C.1	Maxwell Model and Generalised Maxwell Model.....	240
C.2	Kelvin-Voigt model and generalised Kelvin-Voigt model	247
C.3	References.....	250
D	BITUMEN CLASSICATION TEST RESULTS.....	251
E	BITUMEN RESPONSE DATA	258
E.1	Arrhenius and WLF graphs	259
	70/100.....	259
	SE1	261
	KRS 60	263
	SR1	265
E.2	Shift factor parameters (Arrhenius and WLF) and CA model parameters .	267
E.3	Prony series model parameters	270
	Prony parameters for 70/100 bitumen	271
	Prony parameters for SE1 bitumen.....	271
	Prony parameters for KRS 60 bitumen	272
	Prony parameters for SR1 bitumen	272
E.4	Huet-Sayegh model parameters	273
E.5	2S2P1D model parameters.....	274
E.6	Complex moduli and phase angle data for different models	275
E.7	Complex moduli and phase angle graphs for different models	293
	70/100.....	294

SE1	296
KRS 60	298
SR1	300
F	COHESION AND ADHESION FATIGUE DAMAGE TESTING DATA..... 302
F.1	Complex modulus and deflection output data of cohesion fatigue tests: ... 302
F.2	Complex modulus and deflection output graph of cohesion fatigue tests.. 303
F.3	Complex modulus and deflection output data of adhesion fatigue damage tests 306
F.4	Complex modulus and deflection output graph of adhesion fatigue damage tests 307
G	DATA ON AGEING MODEL OF SEAL'S BITUMEN 309
G.1	Initial information on the 70/100 bitumen recovered..... 310
G.2	Initial information on the SE1 bitumen recovered..... 311
G.3	Prony series parameters for recovered bitumen from field-aged seals 312
	Prony parameters for recovered bitumen from 70/100 field-aged seals 312
	Prony parameters for recovered bitumen from SE1 field-aged seals..... 314
G.4	Complex modulus Prony data for all 70/100 bitumens 316
G.5	Complex modulus Prony data for all SE1 bitumens 321
G.6	Combined graph for all 70/100 G * Prony series bitumens..... 325
G.7	Combined graph for all SE1 G * Prony series bitumens..... 326
G.8	Complex modulus Prony data of all 70/100 bitumen case studies at 10, 62.83 and 100 rad/s 327
G.9	Complex modulus Prony data of all SE1 bitumen case studies at 10, 62.83 and 100 rad/s 328
G.10	70/100 seal's ageing model data at 10, 62.83 and 100 rad/s 329
G.11	SE1 seal's ageing model data at 10, 62.83 and 100 rad/s 332
H	END-LIFE DAMAGE MODEL DATA OF BITUMINOUS SEAL MATERIALS . 335
H.1	Graphs of coefficients "a" and "b" for cohesion fatigue damage model 335

H.2	Graphs of coefficients “a” and “b” for adhesion fatigue damage model.....	336
I	DATA OF DAMAGE MODEL DURING-LIFE OF BITUMINOUS SEAL MATERIALS	337
I.1	Graphs of damage as function of normalised number of repetitions for cohesion fatigue damage.....	338
I.2	Graphs of damage as function of normalised number of repetitions for adhesion fatigue damage.....	348
I.3	Initial Nelder coefficients for cohesion fatigue damage	353
I.4	Initial Nelder coefficients for adhesion fatigue damage	355
I.5	Graphic development of relationship between the initial Nelder coefficients and stress level for cohesion fatigue damage	356
I.6	Graphic development of relationship between the initial Nelder coefficients and stress level for adhesion fatigue damage.....	363
I.7	Graphic development of relationship for adjusted model coefficients and global model coefficients in the case of CFD	367
	Coefficient “ a_C ”	368
	Coefficient “ b_C ”	370
	Coefficient “ c_C ”	373
	Coefficient “ w_C ”	375
I.8	Graphic development of relationship for adjusted model coefficients and global model coefficients in the case of AFD	377
	Coefficient “ a_A ”	378
	Coefficient “ b_A ”	381
	Coefficient “ c_A ”	384
	Coefficient “ w_A ”	387
I.9	Graphs of normalised cohesion fatigue damage model per temperature..	389
I.10	Graph of normalised adhesion fatigue damage model per temperature ...	391

I.11	Values of adjusted model coefficients in the case of cohesion fatigue damage.....	392
I.12	Values of adjusted model coefficients in the case of adhesion fatigue damage.....	394

List of Figures

Figure 1-1: Schematic representation of scope of work	5
Figure 1-2: Research flow chart	6
Figure 2-1: Types of seals commonly used in South Africa (TRH 3, 2007)	11
Figure 2-2: Broad chemical composition of bitumen	14
Figure 2-3: Design process for single seal (after Marais, 1981)	18
Figure 2-4: Seal geometry model: model overview and partial cross-section (after Huurman, 2010)	21
Figure 2-5: Example of running seal model under CAPA-3D FEM (after Milne, 2004)	22
Figure 2-6: Changes in bitumen composition during ageing (after Chipperfield <i>et al.</i> , 1970 and SABITA, 2007)	28
Figure 2-7: Dynamic (complex) modulus.....	37
Figure 2-8: Graphical representation of the complex modulus	39
Figure 2-9: Typical material response to step loads (as adapted from Soleimani, 2009 and Molenaar, 2010).....	40
Figure 2-10: Example of complex modulus and phase angle master curves for bitumen	44
Figure 2-11: Example of a black space diagram (70/100_Unaged_Uncondition_WLF)	49
Figure 2-12: Example of a modified Cole-Cole diagram (70/100_Unaged_Uncondition_WLF)	50
Figure 2-13: Meaning of the four parameters related in the CA model.....	54
Figure 2-14: Maxwell model (spring and dashpot in series)	58
Figure 2-15: Kelvin-Voigt model	59
Figure 2-16: Prony series	60
Figure 2-17: Huet-Sayegh model	62

Figure 2-18: 2S2P1D model.....	63
Figure 2-19: Cohesion and adhesion (adapted from von Fraunhofer, 2011).....	65
Figure 2-20: Contact angle of liquid on a solid surface.....	68
Figure 2-21: Tensile stress–strain curves for brittle and ductile materials taken to fracture (after Domone and Illstone, 2010)	70
Figure 2-22: Representation of brittle and ductile fractures (after Domone and Illstone, 2010)	71
Figure 2-23 : Graph determination of fatigue life using dissipated energy ratio (extracted from Sybilski et al., 2013).....	74
Figure 3-1: DSR and its accessories	91
Figure 3-2: Schematic representation of DSR operation.	92
Figure 3-3: DSR Parallel plate configuration	93
Figure 3-4 : Representation of Shear stress and strain in bitumen during DSR test. 93	
Figure 3-5: Bitumen column configuration for the DSR cohesion fatigue damage test	96
Figure 3-6: Stone column configuration for the DSR adhesion fatigue damage test	97
Figure 3-7: 10.9 mm and 6 mm stone columns	98
Figure 3-8: Water conditioning by vacuum vessel	99
Figure 3-9: External view of the Q-SUN	99
Figure 3-10: Loading of bitumen samples	99
Figure 3-11: Q-SUN testing parameters.....	100
Figure 3-12: Samples after Q-SUN test.....	100
Figure 3-13: Complex modulus vs. time in strain-controlled mode at different temperatures for adhesion (DoI_70-100_Unaged-Cond_25C_0.75%_31.4_10.9)	104
Figure 3-14: Complex modulus and deflection angle vs. time in stress-controlled mode at different temperatures for adhesion (DoI_70-100_Unaged_Uncond_25C_62.8_10.9_ stress controlled)	105

Figure 3-15: Comparison of parallel plate–stone column configurations based on the complex modulus.....	106
Figure 3-16: Complex modulus–DSR gap relationship.....	108
Figure 3-17: Presentation of shear and normal stress on a Mohr-Coulomb graph .	109
Figure 3-18: Comparison between pure shear and combined shear and normal force for DSR cohesion fatigue damage test at 25 °C	110
Figure 3-19: Comparison between pure shear and combined shear and normal force for DSR cohesion fatigue damage test at 10 °C	111
Figure 3-20: Comparison between pure shear and combined shear and normal force for DSR adhesion test at 25 °C.....	111
Figure 3-21: Comparison between pure shear and combined shear and normal force for DSR adhesion test at 20 °C.....	112
Figure 3-22: Example of visual inspection of adhesion failure.....	113
Figure 3-23: Frequency sweep comparison of CA complex modulus results between DSR-MCR302 (from the CSIR) DSR-AR 2000 (from TU Delft).....	114
Figure 3-24: Frequency sweep comparison of CA phase angle results between DSR-MCR302 (from the CSIR) DSR-AR 2000 (from TU Delft)	114
Figure 3-25: Example of repeatability of fatigue test performed on the same DSR	115
Figure 3-26: Three views of the split mould.....	120
Figure 3-27: Two views of the clamping system.....	120
Figure 3-28: Illustration of rings.....	120
Figure 3-29: Bitumen poured into the mould	121
Figure 3-30: Bitumen column samples in the split mould	121
Figure 3-31: Fitting stones in the clamping system	123
Figure 3-32: Zero gap between two stone columns	123
Figure 3-33: Placing a droplet of bitumen on the lower stone column	124
Figure 3-34: Joining the two stone columns together using the bitumen film	124

Figure 3-35: Trimming the bitumen film to fit the stone column	124
Figure 4-1: Complex modulus and phase angle master curves using the Arrhenius method and the CA formula	131
Figure 4-2: Complex modulus and phase angle master curves using the WLF method and the CA formula	132
Figure 4-3: Mechanical model – Prony series	133
Figure 4-4: Mechanical model – HS model	135
Figure 4-5: Mechanical model – 2S2P1D model	136
Figure 4-6: Complex moduli comparison for different models for 70/100-Unaged-Unconditioned bitumen	137
Figure 4-7: Phase angle comparison for different models for 70/100-Unaged-Unconditioned bitumen	137
Figure 4-8: Phase angle comparison for different models for SR1-Unaged-Unconditioned bitumen	138
Figure 4-9: Complex modulus and deflection output of the cohesion fatigue damage test	140
Figure 4-10: Complex modulus and deflection output of the adhesion fatigue damage test	141
Figure 5-1: Combined graph for all 70/100 G^* Prony series	147
Figure 5-2: Relationship between G^* and time for 70/100 bitumen at 62.83 rad/s .	149
Figure 5-3: Combined graph of seal's bitumen ageing model for 70/100	150
Figure 5-4: Relationship between modelled and Prony series G^* in the ageing model for 70/100	150
Figure 5-5: Combined graph of seal's bitumen ageing model for SE1	151
Figure 5-6: Relationship between modelled and Prony series G^* in the ageing model for SE1	151
Figure 5-7: Graph of ageing model of 70/100 seal's bitumen based on average G^* from the three reference frequencies	153

Figure 5-8: Graph of ageing model of SE1 seal’s bitumen based on average G^* from the three reference frequencies 154

Figure 5-9: End-life cohesion fatigue model for 70/100 bitumen modelled at 25 °C 163

Figure 5-10: Cohesion fatigue damage transfer function for 70/100 bitumen 164

Figure 5-11: Adhesion fatigue damage transfer function between dolorite and 70/100 bitumen 165

Figure 5-12: Relationship between coefficient “a” and the temperature for cohesion fatigue damage model with 70/100 bitumen binder 165

Figure 5-13: Correlation between modelled and laboratory-based shear stress in the case of cohesion fatigue damage 167

Figure 5-14: Correlation between modelled and laboratory-based shear stress in the case of adhesion fatigue damage 168

Figure 5-15: Reversed fatigue results under stress-controlled and strain–controlled conditions (after Domone and Illstone, 2010) 168

Figure 5-16: comparison cohesion-adhesion failure times 169

Figure 5-17: Damage calculated from DSR results (D_C -calc) and initial modelled damage (D'_C) vs. normalised number of repetitions at 5mNm – 25 °C 173

Figure 5-18: Combination of all Nelder Coefficients b'_C on a unique graph 176

Figure 5-19: Relationship between β'_C1 and temperature 177

Figure 5-20: Plot of global damage model for CFD in the case of the 70/100 bitumen modelled at the temperature of 25 °C 180

Figure 5-21: Normalised cohesion fatigue damage model during seal life 182

Figure 5-22: Normalised adhesion fatigue damage model during seal life 182

Figure 5-23: Correlation between damage calculated from laboratory data and modelled damage in the case of cohesion fatigue damage 183

Figure 5-24: Correlation between damage calculated from laboratory data and modelled damage in the case of adhesion fatigue damage 184

Figure 6-1: Cycling process representing the integration of seal modelling 190

Figure A-1:Principles applied for design of the binder application rate (after TRH 3, 2007).....	213
Figure A-2: Schematic illustration of the modified tray test.....	214
Figure A-3: Flowchart for design of aggregate and binder application rates for seals (adapted from ASSDPG, 2001)	228
FigureC-1: Hookean spring model	239
Figure C-2: Newtonian dashpot model.....	239
Figure C-3: Maxwell model.....	240
Figure C-4: Standard linear solid model	242
FigureC-5: Prony series	244
Figure C-6: Kelvin-Voigt model	247
FigureC-7: Generalised Kelvin-Voigt model	249

List of Tables

Table 3-1: Binders specification tests.....	89
Table 3-2: Guide to choice of plate size and gap as a function of testing temperature	95
Table 3-3: Testing parameters for cohesion fatigue damage and adhesion fatigue damage.....	102
Table 3-4: Description of test setups for geometry configuration changes	106
Table 3-5: Data for complex modulus – DSR–gap relationship.....	107
Table 3-6: Preparation temperature of bitumen for DSR test	117
Table 3-7: Test parameters for binder response	118
Table 3-8 : Values of frequencies (in Hz) used in frequency test	118
Table 3-9: Matrix for binder film shear response tests using the DSR.....	119
Table 3-10: Test parameters for cohesion fatigue damage test	122
Table 3-11: Test parameters for cohesion fatigue damage test	125
Table 4-1: Shift factors and CA parameters for 70/100-Unaged-Unconditioned bitumen	132
Table 4-2: Prony parameters for 70/100-Unaged-Unconditioned bitumen	134
Table 4-3: HS model parameters	135
Table 4-4: 2S2P1D model parameters	136
Table 4-5: Testing parameters for cohesion damage	139
Table 4-6: Testing parameters for adhesion fatigue damage	139
Table 5-1: Values of constants of seal’s bitumen ageing model for 70/100 and SE1	149
Table 5-2: G^* values for 70/100 and SE1 at the three reference frequencies	152
Table 5-3: Modelled aged time of PAV and Q-SUN for 70/100 and SE1 at the three reference frequencies	152

Table 5-4: Data for average G^* and estimated aged time for PAV and Q-SUN aged bitumen	153
Table 5-5: Number of repetitions to failure at different stress levels and temperatures for cohesion fatigue damage test.....	162
Table 5-6: Number of repetitions to failure at different stress levels and temperatures for adhesion fatigue damage test.....	162
Table 5-7: Values of model constants in the cohesion and adhesion fatigue damage models	166
Table 5-8: Initial values of Nelder coefficients in the case of cohesion within 70/100 bitumen at 25 °C and at different stress levels.....	173
Table 5-9: Values of global coefficients for cohesion fatigue damage (CFD)	174
Table 5-10: Values of global coefficients for adhesion fatigue damage (AFD)	175
Table 5-11: Information on the relationship between global model coefficients and stress level and/or temperature, based on observed trends	178
Table 5-12: Values of adjusted model coefficients in the case of cohesion fatigue damage tested at 25 °C and at different stress levels.....	181
Table 5-13: coefficient of determination and Standard Error of Estimate for CFD and AFD.....	183
Table 6-1: Rheological response, cohesion and adhesion fatigue damage parameters used as inputs in seal modelling	191
Table A-1: Recommended values applied in single seal and double seal design ..	221

List of Abbreviations

AADT	Average Annual Daily Traffic
AFD	Adhesion Fatigue Damage
ALD	Average Least Dimension
ARRB	Australian Road Research Board
ASSDPG	Austrroads Sprayed Seal Design Project Group
BVF	Basic Voids Factor
CA	Christensen and Anderson (model)
CBR	California Bearing ratio
CFD	Cohesion Fatigue Damage
DSR	Dynamic Shear Rheometer
ELT	Effective Layer Thickness
ELVs	Equivalent Light Vehicles
FE	Finite element (analysis/method)
FI	Flakiness Index
ME	Mechanistic–empirical (design method)
PAV	Pressure ageing vessel
PF	Polymer Factor
PTTSP	Partial Time Temperature Superposition Principle
RTFOT	Rolling Thin Film Oven Test
SANRAL	South African National Roads Agency Limited
SARDS	South African Road Design System
SBS	Styrene butadiene styrene
SFE	Surface Free Energy
TTSP	Time Temperature Superposition Principle
UV	Ultraviolet
WLF	Williams Landel Ferry

List of Key Symbols

α_T	Shift factor
δ	Phase angle
G^*	Complex modulus
τ	Shear stress
ω	Angular frequency
D_A	Cohesion damage
D_C	Adhesion damage
N_f	Number of repetitions to failure
N_n	Normalised Number of repetitions

List of Special Units

nm	nanometres
mNm	millinewtonmeter



INTRODUCTION

1 INTRODUCTION

1.1 Background

The South African National Roads Agency Limited (SANRAL) and the South African roads industry require the modelling to be developed to the stage where performance evaluation of different seal types in different environments can be carried out, using mechanistic performance modelling and assessment.

The damage models for evaluating the performance prediction for road seals (referred to as “seals”) and thin-layer bituminous road surfacings currently included in the South African Pavement Design Method (SAPDM) are insufficiently detailed and need to be developed further. The available mechanistic seal design, developed by Milne (2004), is at prototype stage and needs improvement.

The performance of seals is dependent on the material components of the seal and the climate in which the seal is constructed. The seal structure consists mainly of a combination of bituminous binder and aggregates. Traffic and weather conditions induce stresses in the seal. These stresses dictate the behaviour of the bitumen, and interaction between the aggregate and the bitumen, consequently affecting the lifespan and performance of the seal.

1.2 Problem Statement

One of the main functions of a surfacing seal is to protect the underlying layers from the abrasive and destructive forces of traffic and the environment (TRH 3, 2007). Milne (2004) reported that, in practice, seal binders did not always provide the expected additional benefits and at times exhibited characteristics that could in fact promote rapid deterioration of the layer’s serviceability, affecting the long-term life of the pavement structure.

To ensure that seals fulfil all their functions, the following issues should be clarified:

- Binder behaviour
- Binder and aggregate interaction
- Changes in binder–aggregate bond over time
- The time at which, and the position at which, the binder–aggregate bond fails



INTRODUCTION

- The time at which, and the position at which, the bond within the binder fails.

These issues can be addressed by investigating the performance of the different material components of the seal. Such a performance investigation can be carried out at two levels: (i) the response mechanism and (ii) the damage mechanism of bituminous seal materials. The response mechanism characterises the materials in working conditions, while the damage mechanism is characteristic of the failure conditions of the materials. Knowledge of the response and damage mechanisms should be considered as key factors in predicting successfully the life of bituminous seal materials.

In this study the response model will be expressed in terms of a visco-elastic and rheological analysis of the bituminous binder. The damage model will be investigated through the cohesion within the binder and adhesion at the binder–aggregate interface.

The aim of investigating the performance of bituminous seal materials is thus to gain a comprehensive understanding of the response and damage mechanisms in order to control failures of the seal. Milne *et al.* (2004) reported the following seal failure parameters:

- Fatigue cracking (ageing of binder and loss of elasticity)
- Low-temperature cracking (brittleness)
- Adhesion failure or stripping (stone to bitumen, and bitumen to base)
- Moisture damage
- Early rutting of the supporting base
- Permanent deformation or loss of texture: punching, rotation of seal stone reducing voids (associated with bleeding)
- Aggregate crushing or polishing.

Valuable information on the seal failure can be gained by investigating the following:

- Changes in the visco-elastic and rheological properties of the bituminous binder due to the action of traffic and the environment
- Interactions between seal material components (binder cohesion and aggregate–binder adhesion)
- Effect of the base layer on seal material components.



INTRODUCTION

Visco-elasticity and rheology are often characterised by the complex modulus (G^*), the phase angle (δ) and the viscosity (ν). Yusoff *et al.* (2011) reported that the principal parameters representing the visco-elastic rheological properties of bitumen are the magnitude of the complex modulus (G^*) and the phase angle (δ). These parameters can be used to characterise cohesion and adhesion in the damage model.

From the above statements and ideas, the following questions can be raised on the performance and life of a seal:

- Can a model that uses visco-elastic parameters express factors affecting the response of bitumen, such as ageing?
- Can the fatigue damage of cohesion within the binder be represented by a model using visco-elastic parameters?
- Can the fatigue damage of adhesion between the aggregate and the binder be represented by a model using visco-elastic parameters?

1.3 Objectives

This study aims to model the response and the damage of bituminous road seal materials.

The response focuses on:

- 1) The presentation of a seal's binder response model that can be used to characterise the different types of bitumen used in South African seals during early seal life and when the seal is aged
- 2) Modelling the ageing of bitumen and exploring ageing methods that could better simulate the field ageing of seal binders

The damage investigates:

- 3) The development of a cohesion fatigue damage (CFD) model within the binder and an adhesion fatigue damage (AFD) model between stone and binder.

The binder response parameters and damage parameters obtained from these models are intended to be used as inputs in the modelling of the seal system.



INTRODUCTION

1.4 Scope and Extent of the Research

This study forms part of the research that has been undertaken under SANRAL South African Road Design System (SARDS) Project in the field of road surfacing seal. Milne (2015) reported on the evolution of this SARDS project and presented the link between different components forming part of the seal system modelling. The bituminous materials component of the SARDS seal project was investigated through this study. This study focused on the response and damage of seal materials (namely bituminous binder and stone aggregates) as presented in Figure 1-1.

The response model investigated only fresh binder (for the newly constructed seal scenario) and aged binder (for the old seal scenario). The intermediary stage where self-healing occurs within the seal was considered to be outside the scope of this study. The damage model was explored only for fresh bitumen.

This study was based on the Lifetime Optimisation Tool (LOT) research programme from Delft University of Technology in Netherlands (Huurman, 2007). From LOT research, the Dynamic Shear Rheometer (DSR) was selected as the main laboratory equipment in this study. The DSR addresses both the loading time and temperature behaviour dependency of bituminous binders (Asphalt Institute, 1997), which are essential parameters in this study. Moreover, the Dynamic Shear Rheometer (DSR) in South Africa motivated the use of the device as the main laboratory equipment in this study. The benefits and limitations identified in using the DSR could help in the testing procedures and results analysis during its implementation stage in the country. In Figure 1-1 the various types of DSR set-ups are illustrated with photo insets and indicated where in the bituminous binder and stone aggregate matrix simulations are performed.

In the modelling part of the research, no stone-to-stone contact within the seal was considered. This is because it appears that there is almost always a film of binder between stones, especially in the case of pre-coated stone.

During this research, stone cracking and/or breaking under applied loads was not considered as it was assumed that for well-designed seals, the stones were strong enough to prevent breaking under traffic load.

INTRODUCTION

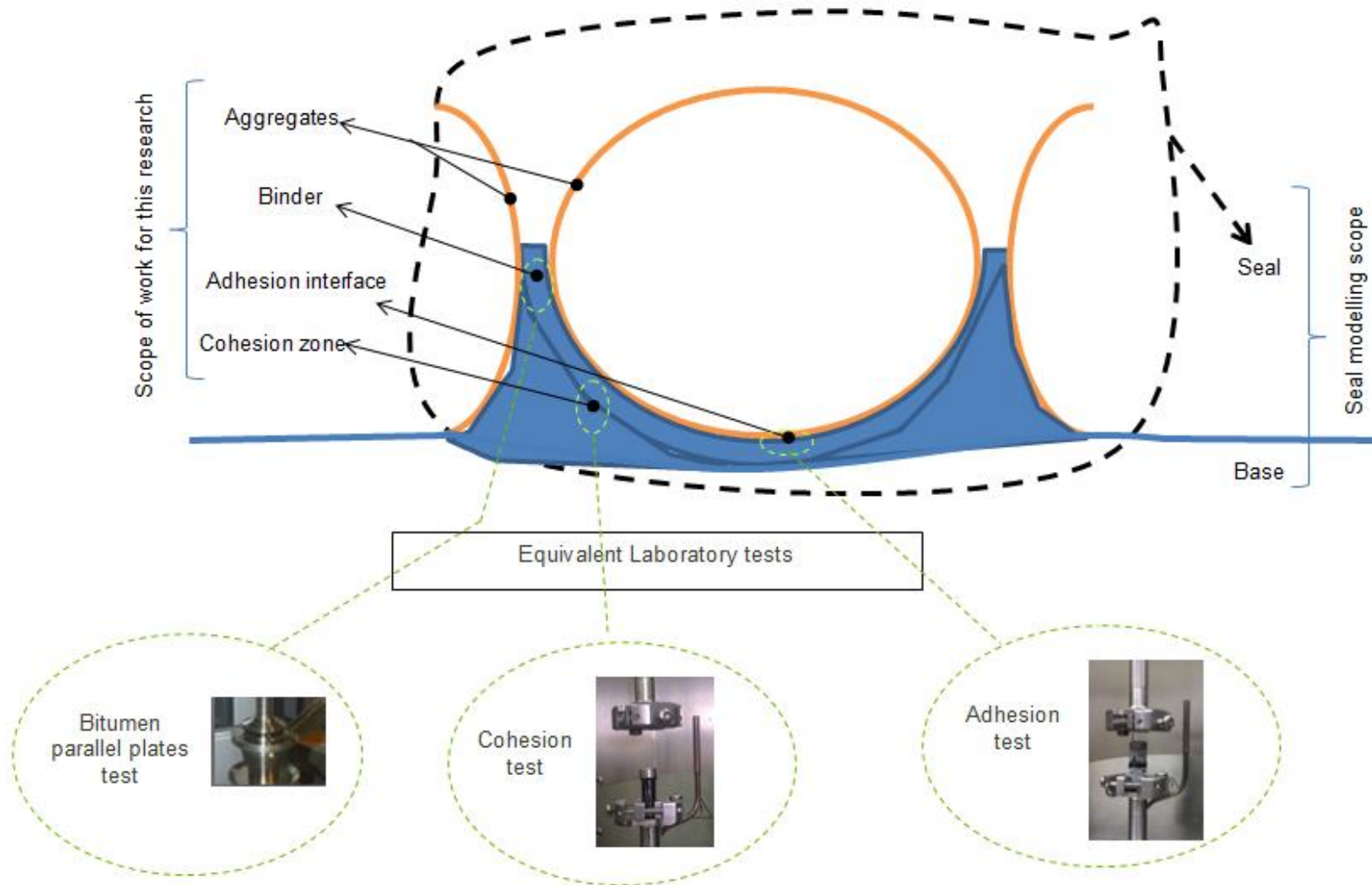


Figure 1-1: Schematic representation of scope of work

INTRODUCTION

The research considered specific types of binder and stone available in South Africa.

For the response model, the following bitumens were used:

- 70/100 penetration grade
- 60% cationic spray grade
- Styrene butadiene styrene (SBS) polymer-modified bitumen (SE1)
- Bitumen rubber (SR1).

The 70/100 penetration grade bitumen binder and dolerite aggregate (DoI) were selected for the damage model.

The research flow chart is shown in Figure 1-2.

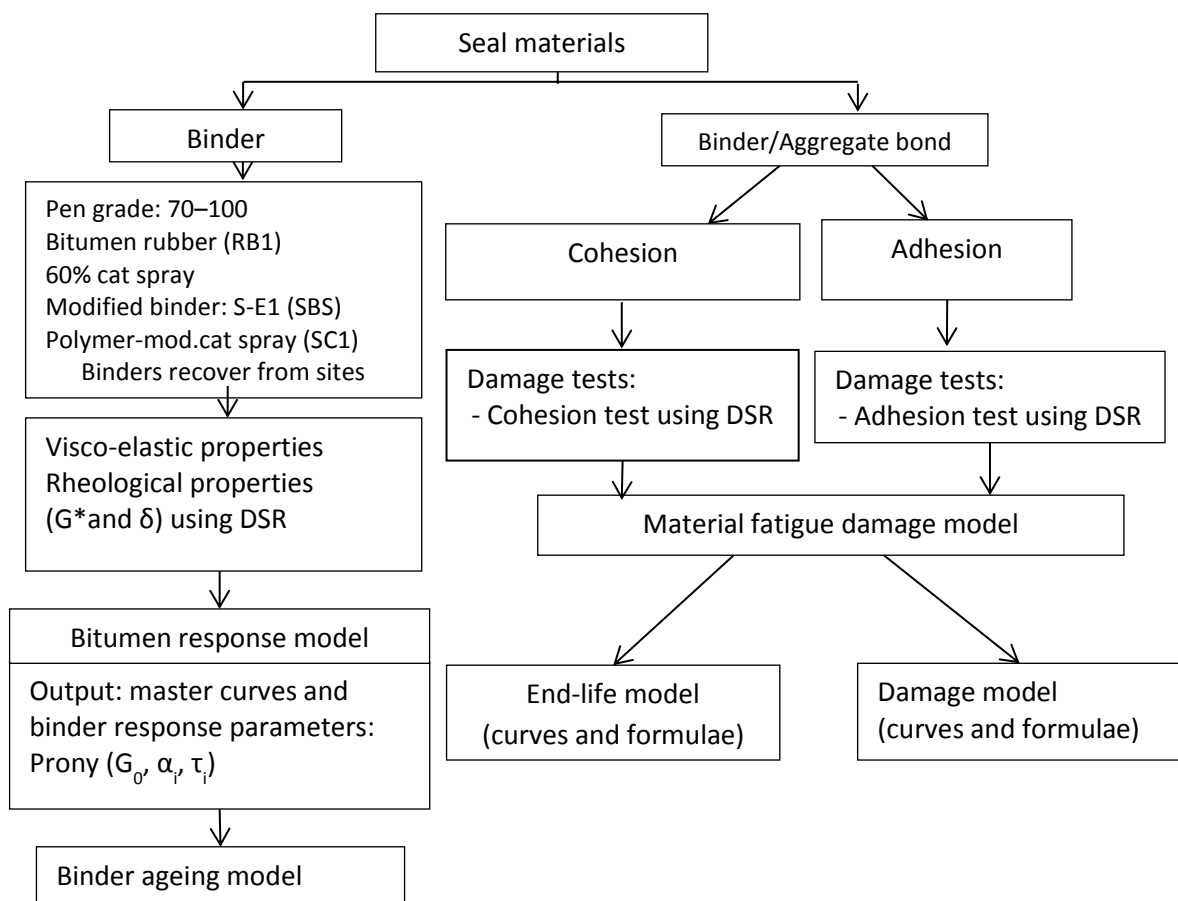


Figure 1-2: Research flow chart



INTRODUCTION

It can be concluded that evaluating the performance of a seal requires material characterisation. The characterisation can be done at two levels: (i) the response and (ii) the damage assessment. The damage assessment consists of cohesion fatigue damage (CFD) investigation and adhesion fatigue damage (AFD) investigation. The DSR was the main laboratory device identified for assessing both response and damage with the aim of modelling these phenomena

References

- Asphalt Institute, 1997, *Performance-graded Asphalt Binder Specification and Testing*, Superpave Series No. 1 (SP-1), Lexington, KY, US.
- Huurman M., 2007, *Lifetime Optimisation Tool (LOT)*, Main report, Technical University of Delft, Netherlands.
- Milne T. I., 2004, *Towards a performance-related seal design method for bitumen and modified road seal binders*. PhD thesis, University of Stellenbosch, South Africa.
- Milne T. I., Huurman M., Van de Ven M. F. C., Jenkins K. J., Scarpas A. and Kasbergen C., 2004, *Towards mechanistic behaviour of flexible road surfacing seals using a prototype FEM model*. Proceedings of the 8th Conference on Asphalt Pavements for Southern Africa, Sun City, South Africa.
- Milne T.I., 2015, Overview of enhancements to road surfacing seal design methodologies through seal system and materials modelling, *Proceedings of the 11th Conference on Asphalt Pavements for Southern Africa*, Sun City, South Africa, 16–19 August 2015, pp. 510–521.
- TRH 3, 2007, see SANRAL (South African National Roads Agency Limited) 2007.
- SANRAL (South African National Roads Agency Limited), 2007, *Design and Construction of Surfacing Seals*. Technical Recommendations for Highways (TRH 3), Version 1.5, May 2007, Pretoria, South Africa.
- Yusoff N. I. M., Shaw M. T. and Airey G. D., 2011, Modelling the linear visco-elastic rheological properties of bituminous binders. *Construction and Building Materials*, 25(5): 2171–2189.



2 LITERATURE REVIEW

2.1 Introduction

The scope of this research highlights the response and fatigue damage characterisation of seal materials. These two concepts will be developed in order to produce the parameters required as input into the seal design which forms part of the pavement design.

The “pavement design” concept is well known and is generally described as being constituted of two approaches, namely the empirical method and the mechanistic method, also called the analytical method. Desai (2002) describes mechanistic design methods as being methods based on principles of mechanics, such as elasticity, plasticity and visco-elasticity, while empirical methods are based on experience or index properties (e.g. value of California Bearing Ratio (CBR), limiting deflections). Paterson (1987), Li and Kumar (2003), and Schram and Abdelrahman (2009) stated that the empirical method uses observed performance from full-scale experiments to determine empirical relationships by regression analysis, while the mechanistic design method identifies the effects of the physical causes of stresses (i.e. loading, environment and material properties) on the performance of the pavement structure. In some cases both approaches are combined, this is called the Mechanistic–Empirical (ME) method.

In South Africa, an ME design method has been used since the early 1970s (Maree and Freeme, 1981).

Jooste (2004) defined ME design as a two-step process, involving firstly the calculation of expected material responses under simulated loading, and secondly the estimation of how many load applications the material can withstand, at the calculated response level, before it cracks or deforms to an unacceptable level.

Theyse *et al.* (1996) reported that the ME analysis process, as applied in South Africa, comprised the following steps: the material and load characterisation, structural analysis, pavement response, transfer functions and predicted pavement life. The material characterisation included layer thickness and elastic material



LITERATURE REVIEW

properties for each layer in the pavement structure. The standard design load was defined as a 40 kN dual wheel load at 350 mm spacing between centres and a uniform contact pressure of 520 kPa. The structural analysis involved a linear elastic, static analysis of the multi-layer system. The pavement response to the loading condition was expressed in terms of stress (σ) and strain (ϵ) at the critical position in the pavement structure, determined by the material type used in each layer of the pavement structure. A transfer function related the stress-strain condition to the number of loads that could be sustained at a stress-strain level before the pavement reached a certain terminal condition.

Theyse *et al.* (1996, 2011) listed the following critical parameters determining the fatigue life of different pavement materials:

- The maximum horizontal tensile strain at the bottom of the asphalt layers
- The maximum tensile strain at the bottom of cemented layers
- The safety factor against shear failure or major and minor principal stresses in the granular materials
- The vertical strain on top of the subgrade material.

Theyse *et al.* (2007) reported that the ME design procedure available in South Africa has remained unchanged since the late 1970s in terms of the load input, material characteristics, primary pavement response model and damage models or transfer functions. The method was implemented in a number of software packages, starting in the late 1990s, which exposed it to a wide user group, and it has therefore come under increasing scrutiny and criticism. This has progressed to the point where it was stated that although, the method is a valuable design tool, it is overly sensitive to changes in input variables, leading to inadmissible and counter-intuitive results in some cases, and providing unrealistic structural capacity estimates for certain pavement types. It does not assess all materials equally, based on their true performance potential. The method focuses largely on the effect of load magnitude (stress condition) on the structural capacity of a pavement, ignoring the effects of construction and environmental conditions.



LITERATURE REVIEW

Theyse *et al.* (2007, 2011) reported that SANRAL had undertaken to address this issue and to revise the South African pavement design method for flexible and rigid pavements by introducing the South African Road Design System (SARDS). The improvement of the seal modelling forms part of this revision; consequently, any new development resulting from this research should contribute to the SARDS.

The purpose of this literature review is to investigate essential concepts related to seal bituminous materials, such as ageing of bitumen, rheology, adhesion, cohesion and fatigue damage.

2.2 Surfacing Seals

A surfacing seal is a thin surfacing or overlay forming part of a road pavement structure. TRH 3 (2007) states that a seal consists of a coat of bituminous binder sprayed onto the road surfacing which is immediately covered with a layer of aggregate (stone or sand). Janisch and Gaillard (1998) state that the reason for seal work is to protect the pavement from the deteriorating effects of sun and water. The seal combats this situation by providing a waterproof membrane which mitigates the effect of the sun on the pavement and helps the pavement to shed water, thus preventing it from entering the base material. The seal also increases surface friction through the additional texture of the aggregate it contains.

TRH 3 (2007) lists the following principal functions of a seal:

- It provides a waterproof cover to the underlying pavement.
- It provides a safe all-weather skid resistant surface.
- It protects the underlying layer from the destructive forces of traffic and the environment.

Good adhesion between the aggregate and the binder film is achieved by rolling compaction. The rolling compaction initiates the process of orientating aggregate particles in a mosaic pattern, and moving the binder into voids between the aggregates. This process is completed by the action of traffic, to obtain a relatively impermeable pavement surfacing.

LITERATURE REVIEW

The Southern African Bitumen Association (SABITA, 1993) and the California Department of Transportation (Caltrans, 2003) state that multiple layers can be placed and various binder and aggregate types can be used to address specific distress modes or traffic situations.

TRH 3 (2007) lists the following types of seal: single seal, double seal, Cape seal, slurry seal, sand seal, inverted double seal, geotextile seal, split seal choked, seal and graded aggregate (Otta) seals. The first five are commonly used in South Africa and are illustrated in Figure 2-1. To develop seal materials characteristics, this thesis used the single seal as a prototype because of its simplicity, allowing different components to be assessed.

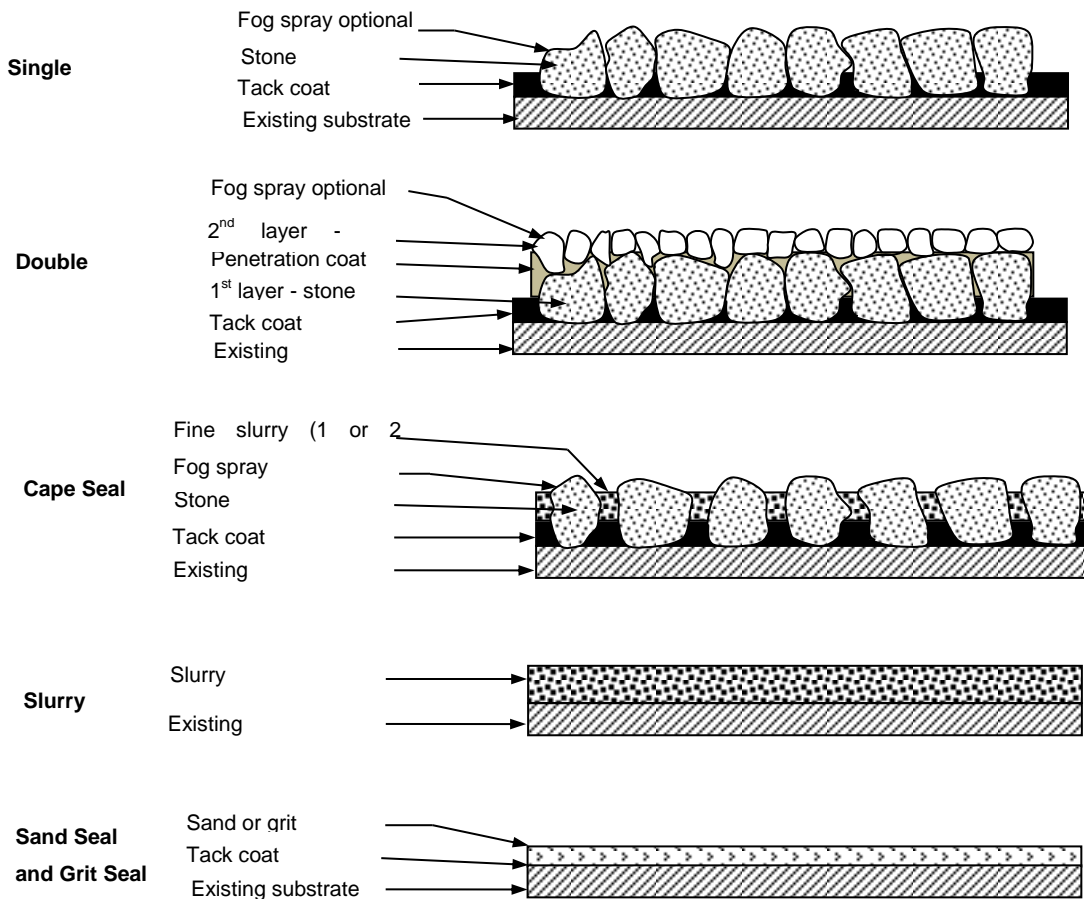


Figure 2-1: Types of seals commonly used in South Africa (TRH 3, 2007)



LITERATURE REVIEW

Seals form a major part of surfaced roads in South Africa. Approximately 150 000 km (20 per cent) of the total road network in South Africa is surfaced. Most of these roads are surfaced or resurfaced with seals (TRH 3, 2007).

After a certain period of service, surfacing seals reach failure status.

2.3 Seal Components

The seal structure consists of a combination of bituminous binder, aggregate and a certain percentage of voids. Bituminous binder and aggregate are discussed in this section.

2.3.1 Bituminous binder

2.3.1.1 Definition

Bitumen is the most used binder for road surfacing. In the past, coal was also used for this purpose. Tar is deemed to be hazardous for health and is no longer allowed for use in many countries, including South Africa. This thesis deals only with bituminous binders.

The term “bituminous” identifies the bitumen itself, any derivative of bitumen or any combination of bitumen with other road materials such as aggregate or filler.

SABITA (2007) defines bitumen as a dark brown to black viscous liquid or solid, consisting essentially of hydrocarbons and their derivatives. It softens gradually when heated. Bitumen is obtained by refining petroleum crude oil, but it is also found as a naturally occurring deposit. As a binder, bitumen is a strong adhesive, highly waterproof and a durable material. The bitumen also provides some flexibility to mixtures of mineral aggregates, with which it is usually combined. It is highly resistant to the action of most acids, alkalis and salts, but soluble in trichloroethylene. Although solid or semi-solid at ambient temperatures, bitumen can be readily liquefied by applying heat, by dissolving it in petroleum solvent, or by emulsifying it in water. The properties of bitumen are dependent on the crude oil source.



LITERATURE REVIEW

According to the Asphalt Academy (2007), the main purposes of bituminous products are:

- to act as an organic glue and waterproofing agent when combined with naturally occurring inorganic stone and sand
- to provide appropriate behavioural characteristics to the materials in service. This will improve their ability to withstand the environmental conditions to which they may be exposed.

2.3.1.2 Bitumen composition

The UK's Road Research Laboratory (1962), SABITA (2007), Read and Whiteoak (2003), and Xiang *et al.* (2010) state that bitumen is a complex combination of hydrocarbons with small quantities of sulphur, oxygen and nitrogen, and trace quantities of metals such as vanadium, nickel, iron, magnesium and calcium. The chemical natures of the crude oils from which bitumens are derived reflect different geological conditions during their formation. Elementary analysis of bitumen manufactured from a variety of crude oils shows that most bitumens contain 82 to 88 per cent carbon, 8 to 11 per cent hydrogen, 0 to 6 per cent sulphur, 0 to 1.5 per cent oxygen, and 0 to 1 per cent nitrogen. The precise composition varies according to the source of crude oil from which the bitumen originates, modifications induced during manufacture and ageing in service. The bitumen presents a kind of colloid dispersion system composed of asphaltenes, saturates, aromatics and resins. In this system, solid-state asphaltenes, with an average size of 100 nm, form the disperse phase, while saturates and aromatics constitute the continuous liquid phase. Resins contribute to good dispersion of the disperse phase in the continuous phase. Therefore the stability and macroscopic properties of the bitumen (colloidal system) depend on the composition of the group components. Figure 2-2 represents this chemical subdivision of bitumen components.

LITERATURE REVIEW

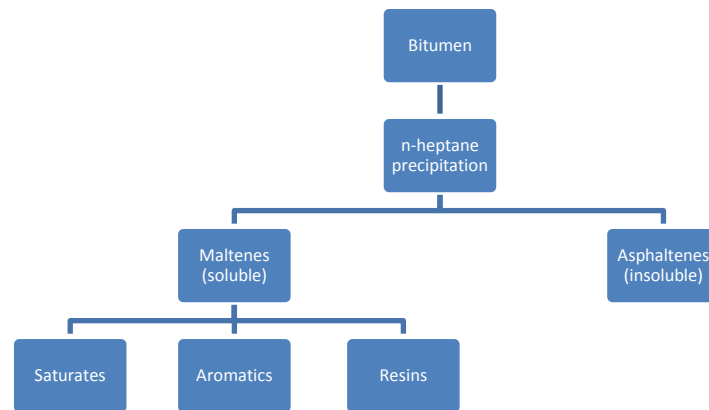


Figure 2-2: Broad chemical composition of bitumen

SABITA (2007) states that the weak interaction between molecules of bitumen results in Newtonian behaviour at high temperatures, where the viscosity change is directly proportional to the temperature change.

2.3.1.3 Characteristics of bitumen

The Road Research Laboratory (1962) states that bituminous binders are supplied in various grades having, at normal temperatures, a wide range of consistencies from fluid to hard and brittle. The consistency of bitumen is dependent on the temperature, the applied load and the mixing oil (in the case of cutback) or water (in the case of an emulsion).

The behaviour of a bituminous binder is determined by its consistency range. The bituminous binder is commonly classified as a visco-elastic material, but can be solid (brittle or elastic) or viscous (non-Newtonian or Newtonian).

The visco-elastic character of bitumen results in its varied response behaviour under various loading times and temperature changes (SABITA, 2007).

In the seal, bitumen is a major component that provides waterproofing characteristics. It acts as the binder that holds the aggregate together and makes it adhere to the base.

The loss of bitumen properties with time is known as bitumen ageing. The ageing of bitumen is detailed in Section 2.6.



LITERATURE REVIEW

The flow characteristics of bitumen are referred to as its rheological properties. This is dealt with in Section 2.7.

2.3.2 Aggregate

As defined by the US Department of the Army (1952) and Weinert (1980), rock is a firm and coherent or consolidated naturally formed solid substance constituted of one or more minerals. Rock makes up the crust of the earth.

A small piece of rock is often called a stone. Stone can be considered as a rock that has been cut into pieces, trimmed or engineered for the purposes of construction, jewellery, etc. In this research the term “stone” will represent the pieces of rock that have been cored for the purpose of the adhesion fatigue damage test using the DSR.

Basic sources of road building materials are either natural rocks or slags derived from a metallurgical process. Natural rocks occur as massive outcrops or as gravels, the latter being derived from the former. Natural rocks are classified by petrologists according to their mode of origin into three main classes: igneous, sedimentary and metamorphic (Road Research Laboratory, 1962; Weinert, 1980; Das, 1990).

Weinert (1980) states that in chemical rock analysis, the percentage of oxides such as silica (SiO_2) is used to classify rocks. If SiO_2 makes up more than 60 per cent of the material, this should be regarded as *acid* for road construction purposes. If the SiO_2 component is less than 60 per cent, the construction material is known to be *basic*.

Weinert (1980) and Akzo Nobel (2009) state that aggregates of the acidic type possess surfaces that tend to be negatively charged, and that those of basic type are characterised by surfaces that tend to be positively charged. Acidic aggregates include those with high silica contents, while basic aggregates include carbonates.

In this research, the aggregate used as cored stone was dolerite, which is a basic stone.



2.3.2.1 Characteristics of seal aggregates

As one of the two major components of the seal, aggregate plays an important role and should comply with certain characteristics. TRH 3 (2007) states that the seal's aggregate has four functions:

- to provide resistance to abrasive wheel loads and transfer the wheel load to the underlying pavement structure
- to provide a skid-resistant surface
- to provide a structure to accommodate the elastic and impermeable bituminous binder and have sufficient voids to prevent the binder flushing to the surface under loading
- to protect the binder from harmful ultra-violet (UV) rays of the sun.

Aggregate properties (such as size, shape, grading, cleanliness, moisture content, toughness, soundness, durability, fracture, polish resistance and porosity) influence seal performance (Shuler *et al.*, 2011).

As stated in Section 1.4, in this research dolerite (base type aggregate) was used as stone in the adhesion fatigue damage test. The dolerite is one of the common aggregates used for seal in South Africa. This dolerite was sourced from Trichardt crushers in Trichardt, Mpumalanga province, South Africa.

2.3.2.2 General description of Dolerite

According to Hergt *et al.* (1989), dolerite is an igneous rock, thus rock initially molten and injected as a fluid into older sedimentary rocks. Emplacement probably occurred over a period of 20 million years, and the average age of the rock is middle Jurassic.

Leaman (1973) and Lurie (1984) define dolerite as a basic intrusive hypabyssal rock with SiO₂ content varying between 45 and 52 per cent. The essential minerals contained in the dolerite are plagioclase, feldspar and pyroxene (augite), which constitute between about 60 per cent and 80 per cent of the rock's total composition. The accessory minerals are quartz, orthoclase, chlorite (20 to 40 per cent) and magnetite (2 to 3 per cent).



2.4 Seal Design

Most of the seal designs currently used are based on work developed by Hanson (1935), who made the first attempt to rationalise the single seal design. Holtrop (2008) states that the rate of application of the binder and the aggregate spread rate are both of major importance in achieving satisfactory performance for the service conditions of seals. These two concepts are related to the volumetric and void assessment of the seal layer.

A certain amount of empty space is present in a single or double seal layer (Semmeling, 1987). Some of these voids are lost during the life of the seal because of the effects of traffic on aggregate embedment at the bottom of the layer and the wear of the aggregate at the top of the seal layer. A portion of the voids must be left unfilled with binder to ensure good skid resistance. An overview of seal design methods is presented in Appendix A.

In general, the principles applied to the design of the binder application rate are based on the same concept (some of the variations in seal design are also presented in Appendix A). A schematic flowchart illustrating the design process of a single seal, based on South African experience, is presented in Figure 2-3. This flowchart, from Marais (1981), was based on the Average Least Dimension (ALD) of stone. However, Semmelink (1987) and TRH 3 (2007) later emphasised the use of the Effective Layer Thickness (ELT) of the seal in the seal design.

LITERATURE REVIEW

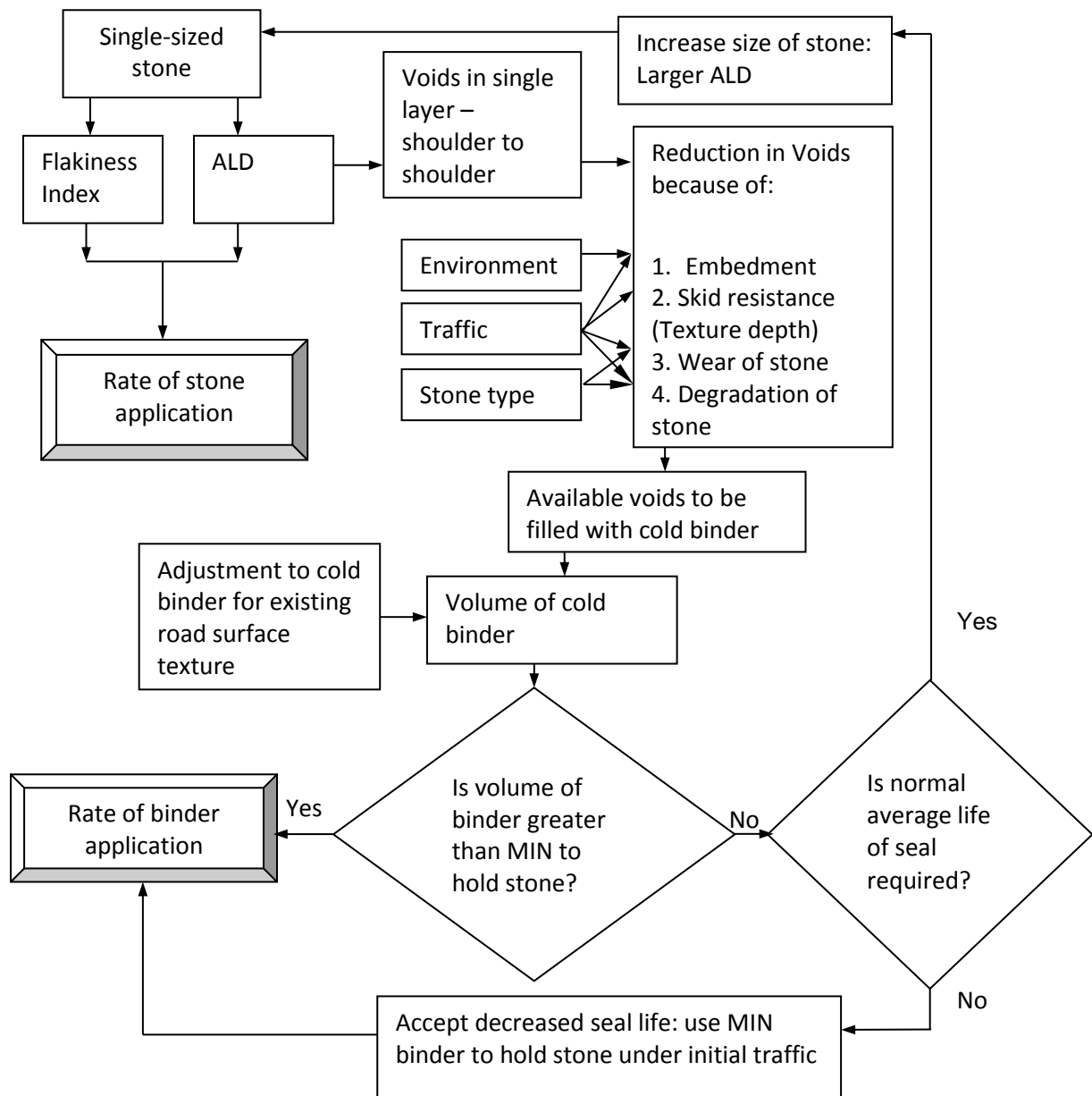


Figure 2-3: Design process for single seal (after Marais, 1981)

In summary, the seal design philosophy reported in the literature (such as Hanson, 1935; Marais, 1981; Semmelink, 1987; Holtrop, 2008) aims to calculate the portion of voids within the seal layer that needs to be filled in order to minimise loss of stone and to provide the surface texture required for minimum skid resistance. The ultimate objective is to maximise the seal life of different classes of roads. The principle of



LITERATURE REVIEW

seal design is based on the volumetric properties of the seal materials and the amount of voids trapped in the seal. Some design values are chosen experimentally or empirically.

It can be noted that the forces of traffic and of the environment that act on the seal seem to be under-considered in the design. Although the volumetric properties and the concept of voids in the seal do play a role in seal performance, volumetric design lacks the part of mechanistic analysis that takes into account parameters such as stress and/or strain interactions in the seal structure and the durability of the seal.

It has been suggested that mechanistic analysis expressed in terms of stress-strain interactions can be used to develop response and damage models of seals. These models will reflect the action of traffic (vehicle loading, tyre pressure, traffic abrasive action on aggregate, etc.), the environment (water sensitivity, temperature action, ageing of binder, etc.) and material characteristics, and should be further analysed for the improvement of seal performance. For this reason seal modelling work was initiated, especially as developed in Section 2.5.

The Road Research Laboratory (1962) defined the durability of bitumen as its degree of resistance to changes caused by the weather and traffic. Extensive work on seal durability has been done in Australia. Oliver (2004), Oliver and Boer (2008) and Oliver (2011) reported on a study on predicting the life of a seal by means of correlating bitumen hardening with factors such as bitumen viscosity, bitumen film thickness and seal aggregate size. These studies involved the use of an Australian Road Research Board (ARRB) test method and modelled the prediction of seal life. In South Africa, research has been done on the durability of bitumen by modifying the Rolling Thin Film Oven Test (RTFOT) to simulate long-term ageing of bitumen (Muller and Jenkins, 2011). The ageing of bitumen is discussed in detail in Section 2.6.

2.5 Seal Modelling

The current seal design is based on the volumetric properties of materials and voids, as presented in Section 2.4. In order to improve seal design, the possibility of introducing mechanistic principles into the seal design was investigated, in South



LITERATURE REVIEW

Africa (Milne *et al.*, 2004) and elsewhere in the world (Huurman, 2010; Kathirgamanathan *et al.*, 2012).

Introducing mechanistic concepts into the seal design meant that principles such as elasticity and visco-elasticity could be used in terms of stress-strain in the seal structure.

Milne (2004) developed an initial prototype numerical model of seal performance, which determined failure and fatigue criteria to assess the seal's expected lifetime. This numerical model used Finite Element (FE) analysis because of the complexity of seal geometry and the ability of FE analysis to model complex stress analysis problems. CAPA-3D was the specific FE used in the development of this prototype. Huurman (2010) stated that a seal might mechanistically be designed on the basis of a meso-mechanical analysis due to its limited thickness. The meso-mechanical analysis can consider a small volume of material and, in the analysis, the seal must be represented as it is, i.e. individual stones sitting in the bitumen. Thus the design of seals might benefit from FE modelling of the seal's meso-structure. At meso-scale, the constituent materials such as binders and stones are assigned different material properties (Woldekidan, 2011). The interactions of these constituent materials dictate the bulk-scale response behaviour.

Huurman (2010) developed a subsequent model that addressed some of the limitations from Milne's first prototype. The object of developing the numerical model was to determine the relative performance of the seal in terms of the number of wheel load repetitions to stripping of stone (loss of adhesion), cracking of binder (loss of cohesion), crushing of stone, embedment of stone and flushing (penetration of stone into the base). This performance is studied through the stresses and strains that develop in various relevant structural components of the seal (Huurman, 2010).

The elements included in the model were as follows:

- *Geometry of seal model:* represent the seal structure in terms of meshes using meso-scale analysis
- *Numerical model of applied loads:* three components of stress (vertical, lateral and longitudinal) induced by rolling wheels and driven wheels

LITERATURE REVIEW

- FE method (FEM) material parameters and behaviour :

The following materials were included:

- *Bitumen binder*: modelled using visco-elastic model such as generalised Burgers model
- *Aggregates*: modelled using linear elastic principle
- *Mastic underlayer*: bituminous material between the stone and base, the stiffness of which was used in the model
- *Interface*: between stone and bitumen which was modelled on the elastic properties of stone and bitumen
- *Base layer*: unbound material with stress-dependent behaviour and minimum visco-elastic deformation
- *Environment* (temperature regime).

Figure 2-4 illustrates a seal geometry model, and Figure 2-5 presents an example of running the seal model under CAPA-3D FEM.

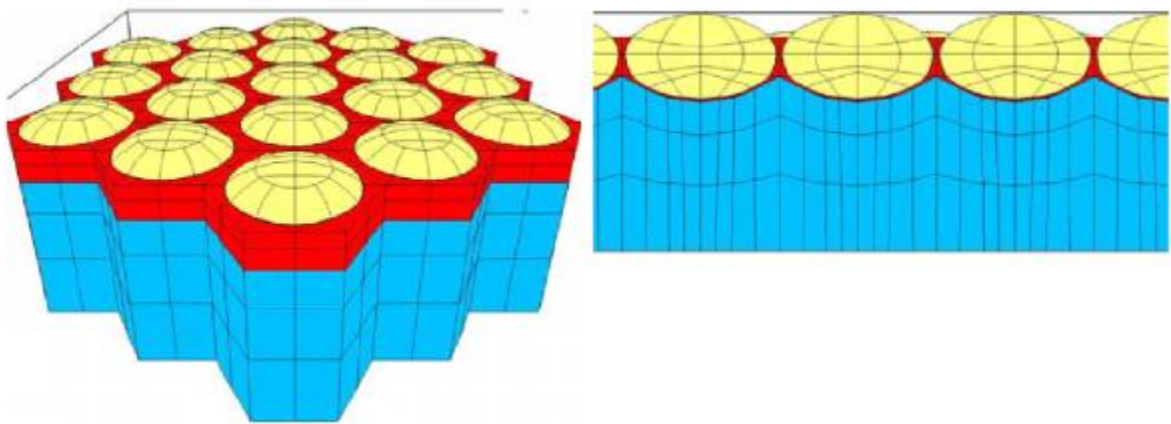


**Figure 2-4: Seal geometry model: model overview and partial cross-section
(after Huurman, 2010)**

LITERATURE REVIEW

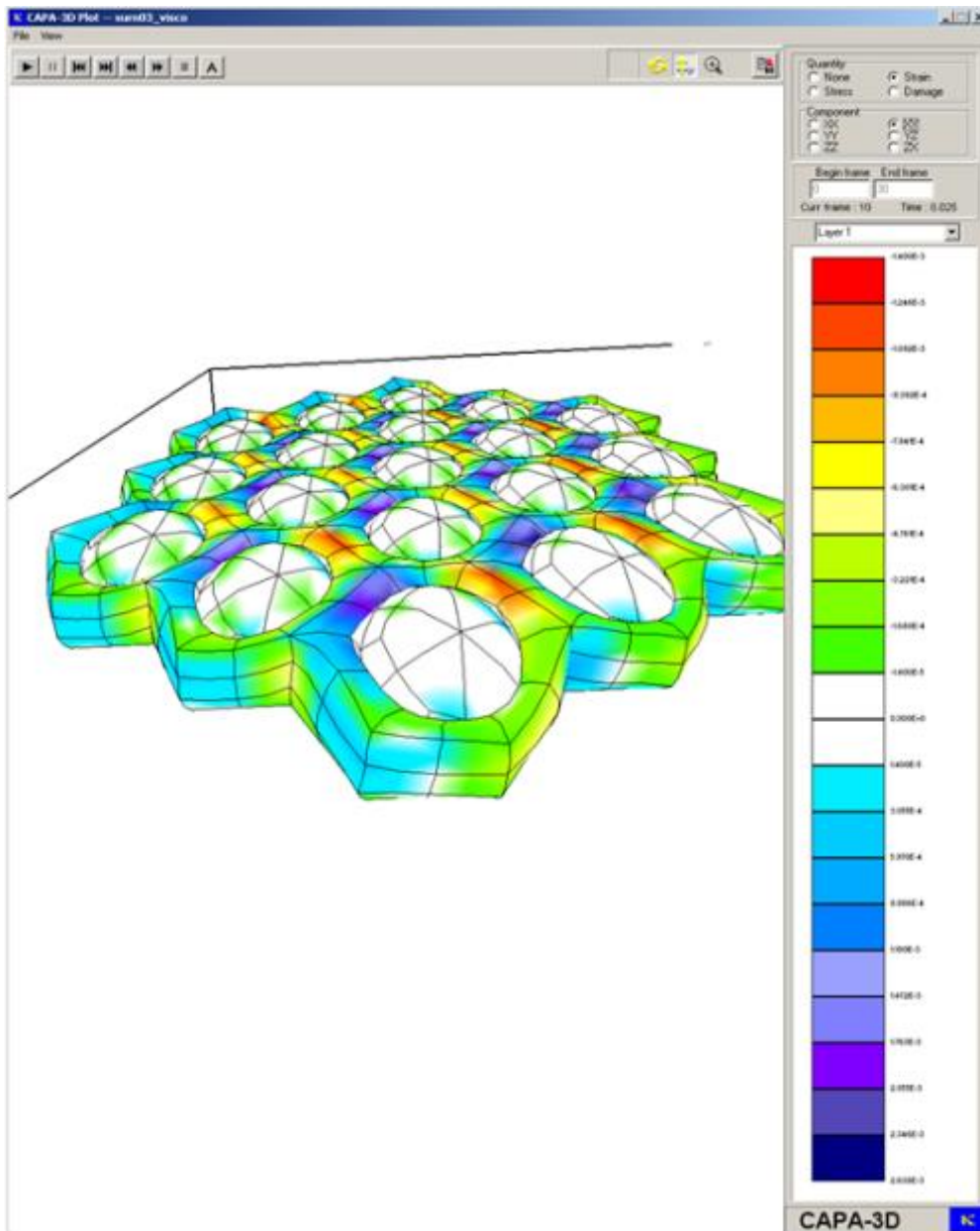


Figure 2-5: Example of running seal model under CAPA-3D FEM (after Milne, 2004)

Although the prototype numerical seal model demonstrated the ability to use mechanistic-type analysis to model a seal, Milne (2004) suggested that the model needed more refinement. In this regard, Milne (2004) and Huurman (2010) reported that:



LITERATURE REVIEW

- no information about damage development in the types of bitumen considered was available
- bitumen data for bitumen material parameters were borrowed from previous work.

Among the recommendations made by Milne (2004), the following were of interest for this research:

- research into specific bitumen parameters to improve the visco-elastic parameters of the Burgers model used in Milne's work
- further assessment of the materials testing system of fatigue relationships for cracking, and determination of adhesion yield stress for stone loss.

2.6 Ageing of Bituminous Binder

2.6.1 Background on bitumen ageing

Any material is subject to the influence of environmental factors during its lifetime. These factors include (but are not limited to) temperature, ultraviolet (UV) exposure, rainfall and humidity. The absorption of UV radiation results in the degradation of materials, which changes their chemical composition. Changes in the chemical characteristics of a material are also reflected in changes in its physical properties, such as its strength and deformability (Hagos, 2008).

According to the UK Road Research Laboratory (1962), Vallerga (1981) and Janisch and Gaillard (1998), all bituminous surfacing materials change with time under the action of weather and traffic. The bitumen becomes softer in warm weather and harder in cold weather, but the exposed binder hardens continually as a result of atmospheric influences (sun, wind and water). The bitumen hardens after heating, mainly due to volatilisation, and in the long term it hardens mainly due to oxidation. The terms "age hardening" and "ageing" are regularly used to describe the phenomenon of "hardening". Hardening is associated primarily with loss of the volatile components of bitumen during the construction phase, and progressive oxidation of the in-place material in the field. Both factors cause an increase in viscosity and stiffness of the bitumen. This may lead to brittle condition,



LITERATURE REVIEW

disintegration of stone-bitumen bonds and cracking failures because the material is unable to bend and flex when exposed to traffic and temperature changes.

Bell (1989) stated that ageing of asphalt mixtures occurs in essentially two phases, short term and long term. Short-term ageing is due primarily to volatilisation of the bitumen during construction, whereas long-term ageing is due to oxidation and steric hardening in the field.

2.6.2 Some bitumen ageing methods

Bell (1989) reported that the most promising methods for simulating short-term ageing of mixtures are extended heating and extended mixing. Microwave heating should also be considered. The most promising methods for long-term ageing of mixtures are pressure oxidation, extended oven ageing, UV treatment, and alternate ageing and moisture treatment.

Muller and Jenkins (2011) split ageing test methods into two categories: short-term ageing (including methods such as the Rolling Thin Film Oven (RTFO), thin film oven and rotating flask tests) and long-term ageing (which consists of methods such as pressure ageing vessel, rotating cylinder ageing test and long-term rotating flask test).

According to Hagos (2008), the effect of UV radiation from sunlight is an important factor to consider during the ageing process of bituminous materials. The light from the sun basically consists of three components: ultraviolet (UV), visible (VIS) and infrared (IR) light. The shorter wavelengths have a greater influence on the degradation of a material, since the higher energies absorbed by the material may exceed the bond energies. Xenon arc lights are able to produce radiation that simulates the natural (sunlight) spectrum in the UV region (i.e. 295 to 400 nm).

Attempts have been made to accelerate the ageing of bitumen in the laboratory through the effect of temperature, pressure or the simulation of weather conditions. The most common ageing methods used are:

- the Rolling Thin Film Oven Test (RTFOT): ASTM D2872 as described by SABITA (2007)

LITERATURE REVIEW

- the Pressure Ageing Vessel (PAV) method: different variants of the PAV method are used, such as PAV-ageing, AASHTO R28 or ASTM D6521-13 as described by ASTM, 2013).

Another ageing method that is often used for bituminous roofing and waterproofing materials is the accelerated weathering test using the Xenon-Arc method as described in ASTM D 4798-01 (ASTM, 2002).

Hagos (2008) reported the use of a specific weatherometer to simulate the ageing of bitumen. This weatherometer used an artificial light source (Xenon-Arc lights) that closely simulates the UV and visible part of solar radiation. In setting up an accelerated weathering procedure, not only temperature, but all factors of weathering in real life need to be taken into account to simulate “natural ageing”. In order to accelerate the ageing process, the weathering test should be conducted at an elevated temperature. Nevertheless, care should be taken to conduct the tests at realistic temperatures to avoid deviation from the chemical reactions that take place in practice. To determine the realistic conditions of weathering, it is imperative to analyse prevailing weather conditions. In this case 1 000 hours of UV exposure in a weathering chamber was selected to simulate the effect of UV radiation. Hagos concluded that laboratory ageing methods are not as severe as long-term field ageing as laboratory ageing could not simulate the complex nature of field ageing.

This weatherometer had the following features:

- rain and humidity functions for weathering testing
- measurement and control of Chamber Air Temperature (CHT) (max. 70 °C during light phase)
- air-cooled Xenon lamps with adjustable power range between 1.7 and 2.1 kW
- static, flat sample array, maximum exposure area 3 081 cm²
- specimen tray with 5° slope (as recommended in many standards) for optimum spray water drain
- measurement and control of irradiance, broad band in the UV range (300 to 400 nm) in W/m², or narrow band at 340 nm or at 420 nm in W/(m²nm); switch between control points without having to change hardware



LITERATURE REVIEW

- measurement and control of Black Standard Temperature (BST, max. 100°C during light phase) or Black Panel Temperature (BPT) at sample level
- selectable temperature control: CHT or dual control of CHT and BST/BPT
- measurement and control of relative humidity
- ultrasonic humidification and specimen spray system.

It was suggested to improve the ageing protocol in order to make a reasonable prediction of long term field ageing (e.g. reducing humidity from 70 per cent to 50 per cent and increasing the temperature of exposure of the thin layer of binder up to 90 °C).

Muller and Jenkins (2011) investigated two modifications of the RTFOT test for simulating long-term ageing in order to compare the results with PAV ageing:

- extended RTFOT test conditions at 163 °C (ERTFOT163). The test duration extended to 325 minutes
- extended RTFOT test conditions at 100 °C (ERTFOT100sra). The test duration extended for 48 hours and a temperature of 100 °C was maintained around the inner surface of each container during the test. At this temperature, the bitumen does not flow continuously in thin films and an electroplated steel rod 129 mm long, with a diameter of 8 mm, is inserted into each glass bottle to ensure that a thin film is continuously spread on the inside of the glass bottles; this system is referred to as “Steel Rod Assistance” (SRA).

They concluded that the extended method was promising for simulating long-term ageing.

Ma *et al.* (2008) aged binder by RTFOT before UV exposure. The UV ageing was done in a UV irradiation chamber using mercury-arc lamps and the oven set to a temperature of 40 °C. The exposure time was two months (with film binder analysed at an interval of 1 month). After ageing, the following was observed:

- Asphaltenes and resins increase with UV ageing time.
- Aromatics decrease with UV ageing time.
- Due to their nature, saturates change only slightly due to age.



LITERATURE REVIEW

- The generic fractions of bitumen are transformed from light mass molecules to large molecules after UV ageing. This transformation is represented by the following sequence: aromatics → resins → asphaltenes.
- Typical functional groups of carbonyls and sulphoxides appear in the bitumen after UV irradiation.
- Quantities of carbonyl and sulphoxide groups increase with increasing UV ageing time.
- After UV irradiation, the bitumen increases in viscosity and Penetration Index; it becomes solid-like and the temperature susceptibility decreases.

They concluded that the influence of UV irradiation changes the chemical properties of bitumen components. Consequently, temperature susceptibility becomes lower due to increased viscosity; this influences mainly the low-temperature properties of bitumen.

Xiang *et al.* (2010) investigated photo-oxidative ageing (ageing in an atmospheric environment, which is referred to as “outdoor ageing”). They found that the performance of bitumen decreases very fast in the 3 months of outdoor ageing, and that the extent of decrease slows down after 9 months of outdoor ageing. The group components analysis revealed that, after outdoor ageing, asphaltenes increase, the content of saturates and aromatics decreases, and the content of resins exhibits a slight variation. Comparing outdoor ageing with laboratory-simulated UV ageing, they concluded that outdoor ageing is greater than in laboratory-simulated UV radiation ageing.

Chipperfield *et al.* (1970) and SABITA (2007) reported that air-blowing of bitumen from a given vacuum residue results in a significant increase in the asphaltene content, as well as a significant decrease in aromatics, while the saturate and resin content are substantially unchanged. Major changes in viscosity and the relative proportions of chemical components take place during the construction of hot-mix asphalt layers. Figure 2-6 illustrates these changes in terms of the Ageing Index (viscosity ratio of recovered bitumen to original bitumen) and the broad chemical components. Although the Ageing Index continues to increase in the long term, the overall changes in the chemical composition after construction are minor.



LITERATURE REVIEW

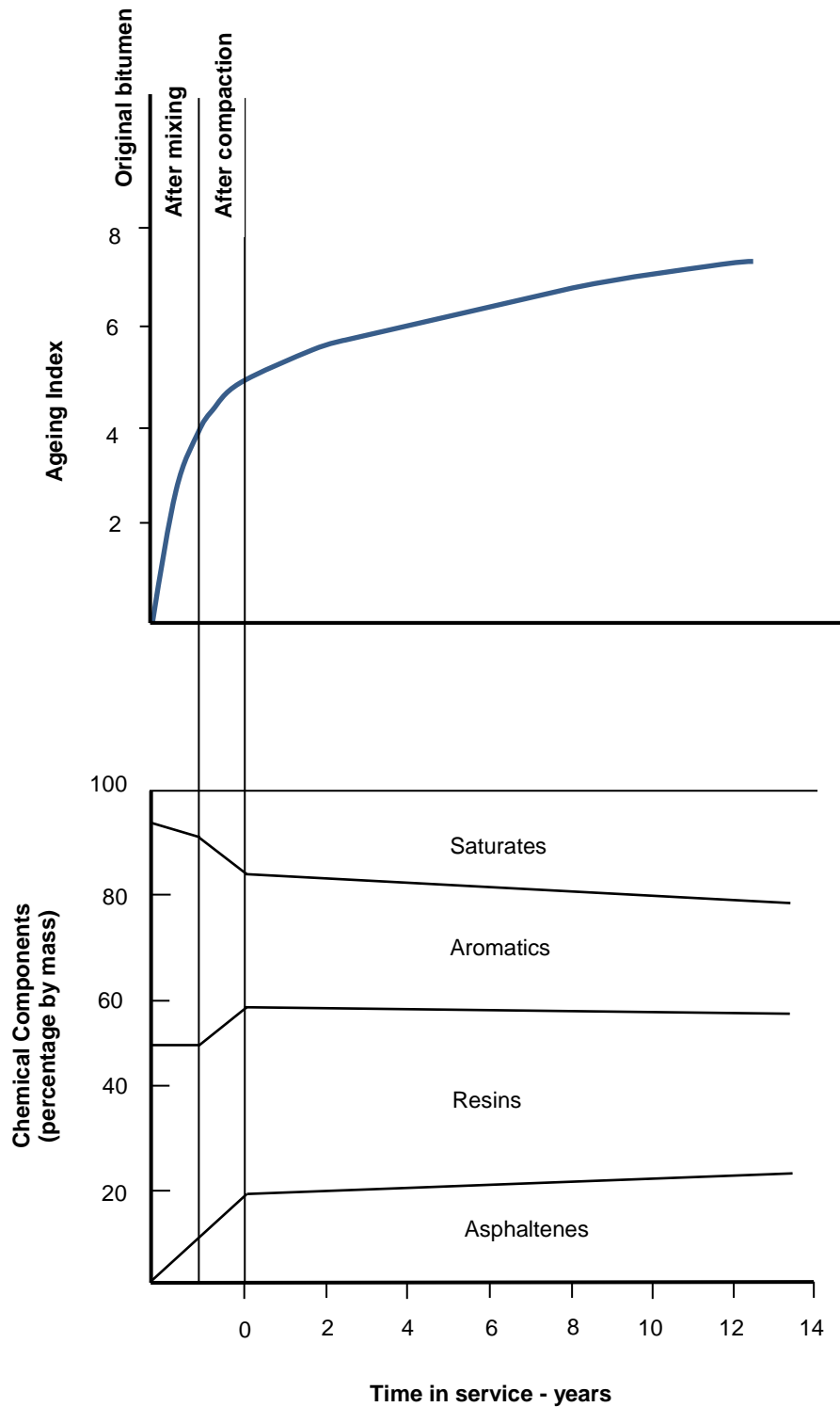


Figure 2-6: Changes in bitumen composition during ageing (after Chipperfield *et al.*, 1970 and SABITA, 2007)



2.6.3 Comments on ageing methods

The ageing process of bituminous material is determined by two major factors: the temperature and the weather conditions. The pressure is an additional factor that is used to accelerate the oxidation of bitumen in the laboratory, but it does not play a significant role in the field ageing of pavement. Simulation of ageing can be subdivided into short-term ageing and long-term ageing. Short-term ageing reflects the loss of volatiles that generally occurs during the hot phase of bituminous material preparation in the plant or during construction. Long-term ageing represents the oxidation process of bituminous material during its lifetime. It appears to be difficult to simulate field ageing with laboratory ageing. Woo *et al.* (2007) reported that the issue of developing an accelerated binder ageing test, which would rank this mode of ageing the same as pavement ageing, is challenging at best and fundamentally impossible at worst, because of the different effects of time, temperature and pressure on different materials. Although the simulation of the ageing is possible, the accurate representation of specific field condition appears difficult due to the high number of variables. The availability of oxygen due to air voids in the pavement is a key variable.

However, a better field-ageing simulation should represent long-term ageing in a relative short testing time and should take into account the field micro-climate.

2.7 Rheology and Visco-elasticity

2.7.1 Introduction

According to Barnes *et al.* (1993), and Read and Whiteoak (2003), the term “rheology” was invented by Professor Bingham, a physical chemist working at Lafayette College, Easton, in Pennsylvania. He created the term "rheology", from the Greek $\rho\epsilon\omega$ (rheo), meaning flow. But the discipline of rheology is much older. The first formal scientific description of a rheological phenomenon, by Isaac Newton, suggested that “the resistance which arises from the lack of slipperiness of the parts of a liquid, other things being equal, is proportional to the velocity with which the parts of the liquid are separated from one another. This could be stated as: “the



LITERATURE REVIEW

shear stress is proportional to the shear rate”, and the constant of proportionality could be called “the viscosity of the liquid”. As it is now known, Newton's postulate applies only to a limited class of low molecular weight liquids, over finite ranges of shear rate or stress. Rheology is usually more concerned with materials whose behaviour is non-Newtonian, in that their viscosity is a function of shear rate or stress. Such materials include polymers, paints, inks, creams, gels, shampoos, drilling fluids, adhesives and many foodstuffs. The definition of rheology already given would allow a study of the behaviour of all matter.

The deformation and flow of matter (or material) are part of the behaviour of the material. Among the fundamental behaviours of materials are the Hookean elastic solids and Newtonian viscous liquids, i.e. there are both elastic solid and viscous liquid materials.

It is reported in the literature (Barnes *et al.*, 1993; Macosko, 1994) that in 1678, Robert Hooke used an apparatus based on springs to prove that when a weight attached to the springs or to a long wire was doubled, the extension doubled. In this way he established his law (Hooke's Law): “the force is proportional to the change in length”. Later Thomas Young did some work in the elastic domain and suggested that the strain is proportional to the stress; he referred to the “constant of proportionality” as the “modulus of the material”.

The modulus of the material represents its “stiffness”. In this particular case it is called Young's Modulus or elastic modulus. Hooke's law is represented by Equation 2-1 and Equation 2-2.

$$\sigma = E\varepsilon \quad \text{Equation 2-1}$$

where

σ is the stress [Pa]

E is the stiffness or elastic modulus (Young's Modulus) [Pa]

ε is the strain [m/m]

$$\varepsilon = \frac{x}{L} \quad \text{Equation 2-2}$$



LITERATURE REVIEW

where

X is the displacement [m]

L is the initial length of the spring or elastic material [m]

Barnes *et al.* (1993) state that Newton gave attention to liquids and in the *Principia* published in 1687, there appears the following hypothesis associated with steady simple shearing flow: “The resistance which arises from the lack of slipperiness of the parts of the liquid, other things being equal, is proportional to the velocity with which the parts of the liquid are separated from one another”. This lack of slipperiness is what we now call “viscosity”. It is synonymous with “internal friction” and is a measure of “resistance to flow”. The force per unit area required to produce the motion is given by Equation 2-3 and is proportional to the “velocity gradient” (or “shear rate”) U/d , as per Equation 2-4. In other words, “if the force doubled, the velocity gradient will doubled”. The constant of proportionality “ η ” is called the “coefficient of viscosity”. In the 19th century, Navier and Stokes independently developed a consistent three-dimensional theory for what is now called a Newtonian viscous liquid. The governing equations for such a fluid are called the Navier-Stokes equations.

$$\tau = \frac{F}{A} \quad \text{Equation 2-3}$$

$$\tau = \frac{U}{d} \eta \quad \text{Equation 2-4}$$

where

U is the velocity of a given moving “plane” of liquid in relation to a fixed liquid “plane” in a liquid flow [m/s]

d is the distance between the fixed “plane” and the moving “plane” in the liquid flow [m/s].



LITERATURE REVIEW

Stress-strain behaviour defines the response of materials to a load. When stress or strain is applied to a material, rearrangements take place inside the material as the response to that stimulus. Materials that are able to return to their original shape after the removal of stress are known as elastic materials. The stress-strain behaviour of these materials is time-independent and can be characterised by an elastic modulus (Soleimani, 2009).

Barnes *et al.* (1993) and Macosko (1994) reported that during the 19th century, scientists began to notice that a number of materials exhibited time dependence in their elastic response. When materials such as silk, gum rubber, pitch and even glass were loaded in shear or extension, an instantaneous deformation, as expected for a Hookean solid, was followed by a continuous deformation or “creep.” When the load was removed, part of the deformation recovered instantly, more recovered with time and in some materials there was a permanent set. This time-dependent response is known as visco-elasticity. These materials dissipate the input energy, which leads to permanent deformation and they are characterised by their elastic and viscous moduli (Soleimani, 2009).

The work of Maxwell, Voigt, Kelvin, Boltzmann, Weber, Markovitz and others showed that the distinction between viscous liquids and elastic solids was not as clear as had previously been thought. It was observed a “fluid-like” behaviour in some solids; similarly a “solid-like” behaviour was noticed in certain liquid. Most of the materials, such as non-Newtonian, are also viscos-elastic, in that they exhibit aspects of both types of behaviour (Barnes *et al.* (1993).

2.7.2 Definitions related to visco-elasticity

Barnes *et al.* (1993) and Macosko (1994) described “visco-elasticity” as the time-dependent response of material which is typical of all polymeric materials. The word visco-elastic means the simultaneous existence of viscous and elastic properties in a material. It is assumed that all real materials are visco-elastic, i.e. in all materials both viscous and elastic properties coexist. The particular response of a sample in a given experiment depends on the time-scale of the experiment, in relation to a natural time of the material. Thus, if the experiment is relatively slow, the sample will



LITERATURE REVIEW

appear to be viscous rather than elastic, whereas if the experiment is relatively fast, it will appear to be elastic rather than viscous. At intermediate time-scales, mixed, i.e. visco-elastic, response is observed.

Woldekidan (2011), Jansen (2006), Flügge (1975) and Ferry (1980) state that visco-elastic material behaviour, expressed as creep and relaxation functions, is usually determined from laboratory experiments. These functions are the “fingerprints” of the material. Relaxation and creep tests are the two used experimental methods most commonly to investigate the time-dependent behaviour of visco-elastic materials.

A creep test is characterised by an increasing deformation with time, under a constant stress. In a relaxation test, a constant strain is applied, resulting in decreasing stress with time. Relaxation and creep tests are particularly suitable for investigating the visco-elastic properties of materials for loading times longer than 1 second. These are referred to as “time domain tests”. For short loading times, which correspond to high-frequency loadings, these tests cannot provide complete material information. This is mainly because, in practice, it takes a finite time, typically about 0.1 to 1 seconds, to apply a constant stress or constant strain to the material. Accurate material information for short time-scales, about a fraction of a second, can therefore not be obtained from time domain tests. For this reason material information for short loading times is indirectly obtained from dynamic tests.

In a dynamic test, material information is obtained as a function of loading frequency. This type of test is known as a “frequency domain test”. This information can then be converted into time domain data using Laplace or Fourier transforms. For conducting dynamic tests, a device such as a Dynamic Shear Rheometer (DSR) is commonly used. Dynamic tests performed in the frequency domain apply a periodically varying strain or stress signal, with a fixed frequency, to obtain intrinsic material information.

Macosko (1994) reported that during the conversion of stress relaxation data to a relaxation modulus, for small strain (strains < 0.5) the stress relaxation – relaxation modulus relationship is linear and independent of strain. For larger strains (strains > 0.5), the relaxation modulus is no longer independent of strain; this is known as non-linear visco-elastic behaviour. According to Barnes *et al.* (1993), in the



LITERATURE REVIEW

linear theory of visco-elasticity, material parameters (such as the viscosity coefficient and rigidity modulus) are not allowed to change with changes in variables such as strain or strain rate. This independence between linear visco-elasticity parameters allows the time derivatives to be expressed as ordinary partial derivatives; thus the linear theory is applicable only to small changes in the variables. The general differential equation for linear visco-elasticity (also known as constitutive) can thus be written as per Equation 2-5 in the time domain.

$$\left(1 + \alpha_1 \frac{\partial}{\partial t} + \alpha_2 \frac{\partial^2}{\partial t^2} + \dots + \alpha_n \frac{\partial^n}{\partial t^n}\right) \sigma = \left(\beta_0 + \beta_1 \frac{\partial}{\partial t} + \beta_2 \frac{\partial^2}{\partial t^2} + \dots + \beta_m \frac{\partial^m}{\partial t^m}\right) \gamma \quad \text{Equation 2-5}$$

Where t is time [s]

If in Equation 2-5, β_0 is the only non-zero parameter, this equation can be written as Equation 2-6, which is the equation of Hookean elasticity (i.e. linear solid behaviour).

$$\sigma = \beta_0 \gamma \quad \text{Equation 2-6}$$

where β_0 is the rigidity modulus [Pa]

If β_1 is the only non-zero parameter in Equation 2-5, this represents Newtonian viscous flow, the constant β_1 , being the coefficient of viscosity as presented in Equation 2-7.

$$\sigma = \beta_1 \frac{\partial \gamma}{\partial t} \quad \text{Equation 2-7}$$

If $\beta_0 = G$ and $\beta_1 = \eta$ are both non-zero, while the other constants are zero, Equation 2-5 is expressed as Equation 2-8. This equation, which is one of the simplest models of visco-elasticity, is called the “Kelvin model”, although the name “Voigt” is also used.

$$\sigma = G\gamma + \eta \frac{\partial \gamma}{\partial t} \quad \text{Equation 2-8}$$



LITERATURE REVIEW

As reported in Section 2.7.2, dynamic testing (such as DSR testing) is recommended in the frequency domain. One of the dynamic testing output parameters is the shear modulus, which represents the stiffness of a material.

Barnes *et al.* (1993); McNaught and Wilkinson (1997) and Meyers and Chawla (1999) state that while Young's modulus (E) describes the material's response to linear stress (like pulling on the ends of a wire or putting a weight on top of a column), the shear modulus (G) describes the material's response to shear stress (like cutting it with dull scissors). The shear modulus is related to the deformation of a solid when it experiences a force parallel to one of its surfaces, while its opposite face experiences an opposing force (such as friction). One possible definition of a fluid would be a material with zero shear modulus.

Shear modulus can be expressed as a function of Young' modulus, as presented in Equation 2-9.

$$G = \frac{E}{2(1+\nu)} \quad \text{Equation 2-9}$$

where

G is the shear modulus [Pa]

E is the elastic modulus

ν is the Poisson ratio

It is usual to characterise the stiffness of pavement materials by the resilient modulus or dynamic modulus. Loulizi *et al.* (2006) reported that the hot-mix asphalt resilient modulus test can be performed by loading a cylindrical sample along and parallel to its vertical diametric plane to allow the development of a relatively uniform state of tensile stresses perpendicular to the load direction. The loading consists of a Haversine pulse with a duration of 0.03 seconds, followed by a rest period of 0.97 seconds. The vertical and horizontal deformations at the centre of the sample that result from the applied pulse load are recorded as the output of the test. The dynamic modulus test, known also as the complex modulus test, is performed by applying sinusoidal vertical loads to cylindrical specimens and measuring the



LITERATURE REVIEW

corresponding vertical deformation. The test is usually performed at different temperatures and at different frequencies. Loulizi *et al.* concluded that the dynamic modulus test provides a better characterisation of hot-mix asphalt than the resilient modulus test because it provides full characterisation of the mix over various temperatures and loading frequencies.

The Mechanistic-Empirical (M-E) Design Guide, developed in the National Cooperative Highway Research Program (NCHRP), used the dynamic modulus as a fundamental input in the design process (NCHRP, 2004). Research on the testing protocol of the dynamic modulus has been reported, such as the work done by Tran and Hall (2005) and Dougan *et al.* (2003).

2.7.3 Linear visco-elasticity concepts for frequency domain

Dougan *et al.* (2003) reported that for linear visco-elastic materials, the stress-strain relationship under a continuous sinusoidal loading is defined by its complex dynamic modulus (E^*). This is a complex number that relates stress to strain for linear visco-elastic materials subjected to continuously applied sinusoidal loading in the frequency domain. The complex modulus is defined as the ratio of the amplitude of the sinusoidal stress and the amplitude of the sinusoidal strain at any given time (t), and the angular load frequency (ω). According to Clyne *et al.* (2003) and Ferry (1980), the evaluation of complex modulus tests requires an understanding of linear visco-elasticity concepts. The fundamental concepts of linear visco-elasticity for the one-dimensional case of a sinusoidal loading can be expressed as per Equation 2-10 to Equation 2-13. The resulting steady-state response is presented in Equation 2-7.

$$\sigma = \sigma_0 \sin(\omega t) \quad \text{Equation 2-10}$$

$$\omega = 2\pi f \quad \text{Equation 2-11}$$

$$\varepsilon = \varepsilon_0 \sin(\omega t - \delta) \quad \text{Equation 2-12}$$

LITERATURE REVIEW

$$E^* = \frac{\sigma}{\varepsilon} = \frac{\sigma_0 \sin(\omega t)}{\varepsilon_0 \sin(\omega t - \delta)} = \frac{\sigma_0 e^{i\omega t}}{\varepsilon_0 e^{i(\omega t - \delta)}}$$

Equation 2-13

where

 σ_0 is the peak (maximum) stress [Pa] ε_0 is the peak (maximum) strain [Pa] δ is the phase angle [$^\circ$] ω is the angular velocity [rad/s] f is frequency t is time [s] i is an imaginary component of the complex modulus

Mathematically, the dynamic modulus is defined as the absolute value of the complex modulus, and is given by Equation 2-14.

$$|E^*| = \frac{\sigma_0}{\varepsilon_0}$$

Equation 2-14

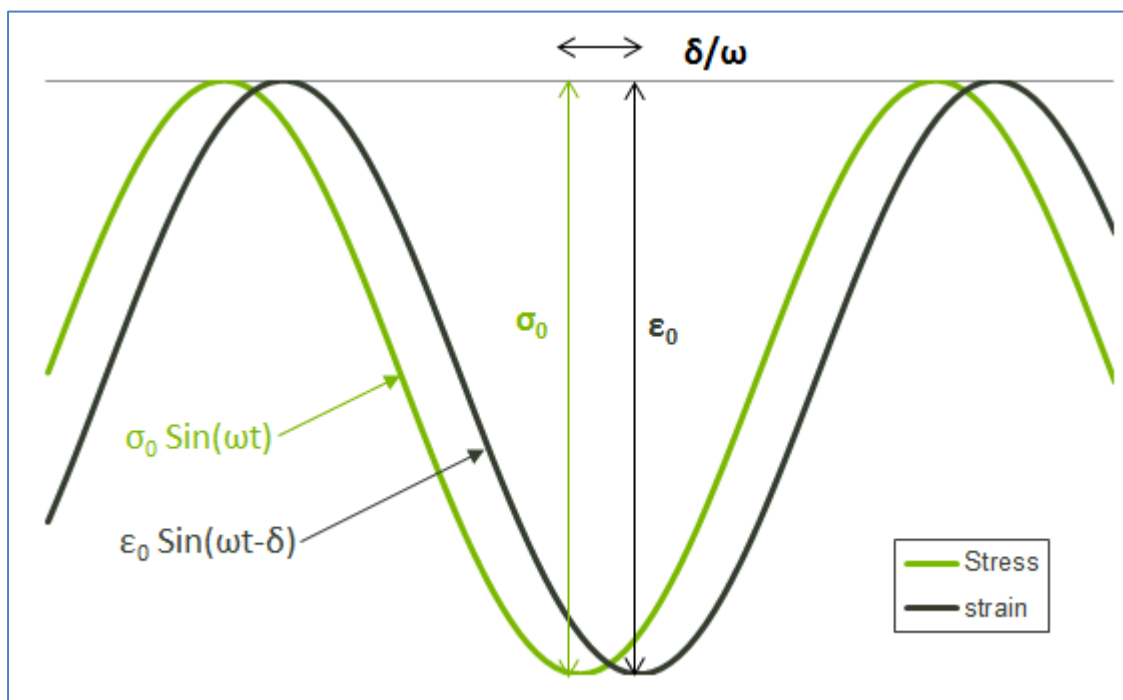


Figure 2-7: Dynamic (complex) modulus

LITERATURE REVIEW

In the case of shear stress, the stiffness is the dynamic shear modulus or complex modulus (G^*).

The complex modulus (G^*) is a time-dependent parameter, so that its magnitude depends on the angular frequency (ω). The shear stress (τ), and shear strain (γ), vary sinusoidally with time, thus the complex modulus (G^*) is calculated from the absolute or peak-to-peak stress and strain values (Anderson *et al.*, 1991). Yusoff *et al.* (2011) define the absolute value of the complex modulus ($|G^*|$) as the ratio of maximum (shear) stress to maximum strain when the material is subjected to shear loading. In addition, the phase angle (δ) is the phase difference between stress and strain in harmonic oscillation. If δ equals 90° , bitumen can be considered to be purely viscous in nature, whereas a δ of 0° corresponds to a purely elastic behaviour. Between these two extremes, the material behaviour can be considered to have a combination of viscous and elastic responses according to its nature.

A complex number G^* has two components, i.e. the real part (G') and the imaginary part (G''), as presented in Equation 2-15 and Equation 2-16.

Liao (2007) states that the real part or the storage modulus (elastic modulus) is the “in-phase” component related to the energy stored in the material for every loading cycle; $G'(\omega)$ is given by Equation 2-17. The imaginary part or the loss modulus (viscous modulus) is the “out-of-phase” component related to the energy lost per cycle in permanent flow; $G''(\omega)$ is given by Equation 2-18. In addition to these two components, the complex modulus and the phase angle are also characterised by the loss tangent ($\tan\delta$) as defined in Equation 2-19. The absolute value of the complex modulus is given by Equation 2-20.

$$G^*(\omega) = G'(\omega) + iG''(\omega) \quad \text{Equation 2-15}$$

with

$$i = \sqrt{-1} \quad \text{Equation 2-16}$$

$$G'(\omega) = G^*(\omega)\cos\delta \quad \text{Equation 2-17}$$

LITERATURE REVIEW

$$G''(\omega) = G^*(\omega)\sin\delta \quad \text{Equation 2-18}$$

$$\tan(\delta) = \frac{G''}{G'} \quad \text{Equation 2-19}$$

$$|G^*| = \sqrt{G'^2 + G''^2} \quad \text{Equation 2-20}$$

The relationship between the absolute value and the storage and loss modulus is represented graphically in Figure 2-8.

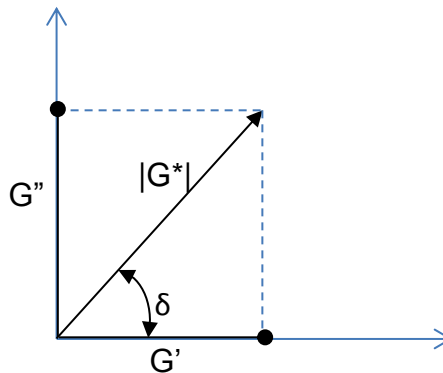


Figure 2-8: Graphical representation of the complex modulus

2.8 Visco-elasticity of Bituminous Material

Molenaar (2010) reported that pavement performance is governed by the magnitude of the applied stresses, their number of repetitions and the ability of the materials to withstand these stresses. To be able to calculate the stresses, the stiffness moduli of the different materials should be known. In addition, the stress/strength characteristics and the resistance of the material to fatigue and permanent deformation need to be known. Bituminous materials, which are part of the pavement structure, exhibit a visco-elastic, visco-plastic behaviour. These behaviours are illustrated when the bituminous material is subjected to a step load, as presented in Figure 2-9.

LITERATURE REVIEW

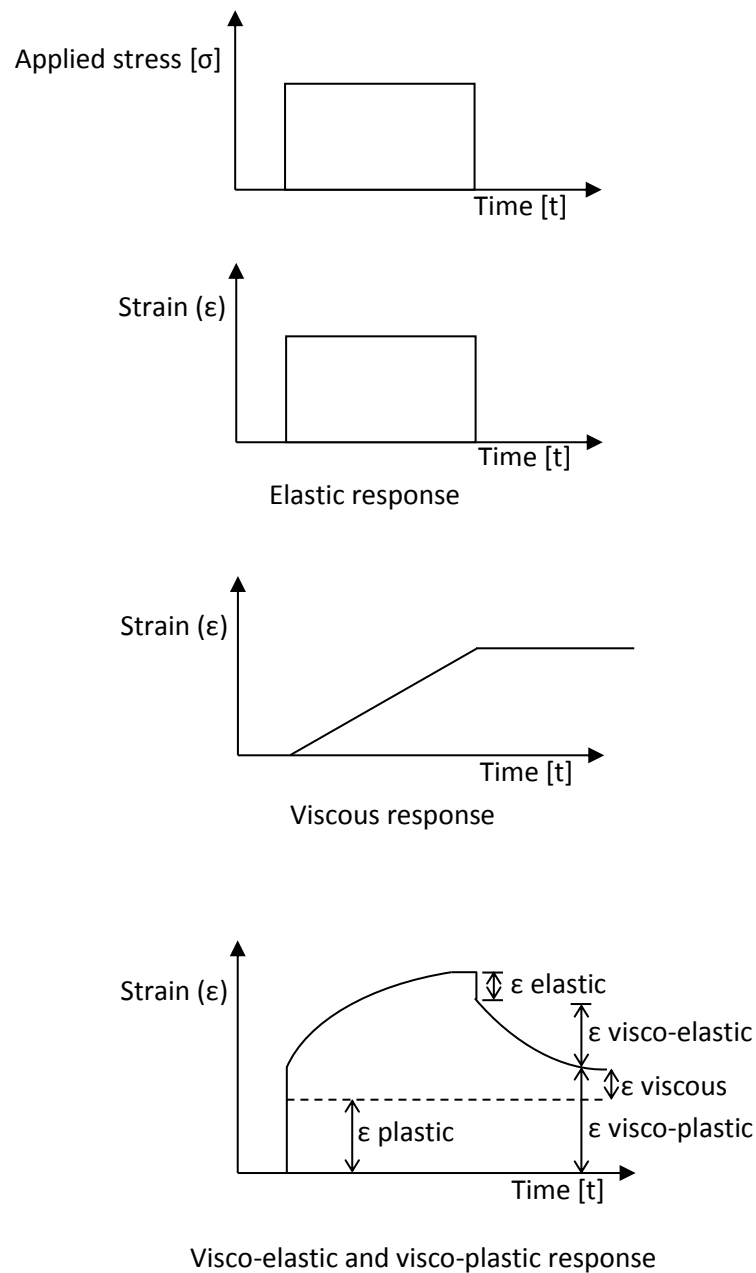


Figure 2-9: Typical material response to step loads (as adapted from Soleimani, 2009 and Molenaar, 2010)

The Asphalt Academy (2007) also states that bituminous binders behave as visco-elastic materials, with their behaviour influenced by loading time as well as

LITERATURE REVIEW

temperature. At high temperatures or long loading times, binders behave as viscous liquids, and consequently produce large permanent deformation. At low temperatures or short loading times, they behave as elastic (brittle) solids, with most of the deformation being recovered at the end of the loading period.

The rheological characteristics of bitumen at a particular temperature are determined by both the constitution (chemical composition) and structure (physical arrangement) of the molecules in the material. Changes to the constitution, structure or both will result in a change to the rheology (Read and Whiteoak, 2003).

Yusoff *et al.* (2011) define rheology as the study and evaluation of the flow and permanent deformation of time- and temperature-dependent materials, such as bitumen, that are stressed (usually shear stress or extensional stress) through the application of force. The colloidal structure (asphaltenes and resins) defines the rheological properties of bitumen, ranging from Newtonian-dominated behaviour to non-Newtonian-dominated behaviour. Understanding the flow and deformation of bitumen in asphalt is important in terms of pavement performance.

The visco-elastic characteristics and modelling of bituminous materials are the main focus of the rest of this research. The core principles of modelling the visco-elastic behaviour of bituminous material are presented in Section 2.9.

2.9 Rheological Modelling of Linear Visco-elastic Properties of Bituminous Materials

It has been reported in the literature (Di Benedetto *et al.*, 2007, 2013; Di Benedetto and Corté, 2005; Airey *et al.*, 2003; Olard and Di Benedetto, 2003) that bituminous materials have linear visco-elastic behaviour for low strain levels. If these materials are considered as isotropic, the linear properties are characterised by the complex modulus E^* and the complex Poisson's ratio ν^* for the three-dimensional description. It has been shown that the Poisson's ratio is a complex number, which is also dependent on frequency and temperature. This dependency should be taken into account to obtain better simulations. Nevertheless, in order to simplify the FE calculation, it was decided to consider the Poisson's ratio as a constant real number. In what follows it has been classically taken to be equal to 0.35.



LITERATURE REVIEW

Normally, the linear visco-elastic rheological properties of bitumen are presented in the form of complex modulus (G^*) and phase angle (δ) master curves.

Yusoff (2012), Mohammad *et al.* (2005), Anderson *et al.* (1994) and Van der Poel (1954) stressed the importance of models as a valuable tool for fitting or describing the rheological properties of bituminous binders and asphalt mixtures. Such models originated from the development of Van der Poel's first nomograph in the 1950s.

The approach used for modelling the linear visco-elastic properties of bitumen is based on the construction of master curves, determination of the mathematical model and determination of the mechanical model.

2.9.1 Construction of master curves

Molenaar (2010) reported that the stiffness characteristics of both bitumen and asphaltic mixes depend on both temperature and loading time. On the other hand, it is not practical to perform tests over the entire temperature and loading time domain in order to determine this dependency. Stiffness values covering the entire time and temperature domain can be obtained by using the equivalency principle between frequency and temperature (resulting from the so-called "thermorheologically simple behaviour" of bitumen and bituminous materials). The equivalency principle allows the construction of master curves, relating stiffness to load frequency, given a certain temperature.

Regarding the description of a thermorheologically simple material, Lakes (2009) reported that in some materials visco-elasticity arises from a molecular rearrangement process which occurs under stress, or from a diffusion process under stress. The speed of such processes depends on the speed of molecular motion, of which temperature is a measure. If all the processes contributing to the visco-elasticity of a material are accelerated to the same extent by a temperature rise, then Equation 2-21 and Equation 2-22 can be applied. For such a material, a change in temperature stretches or shrinks the effective timescale. This temperature change corresponds to a horizontal shift of the material property curves on the log time or log frequency axis. This material obeys the Time-Temperature Superposition Principle (TTSP) and is called thermorheologically simple.



LITERATURE REVIEW

$$E(t, T) = E(\xi, T_s)$$

Equation 2-21

where

$$\xi = \frac{t}{\alpha(T)}$$

Equation 2-22

and where

ξ is the reduced time

T is the temperature measured during the process

T_s is the reference temperature

t is time

$\alpha(T)$ is the shift factor

It is reported in the literature, such as Yusoff (2012), Bonaquist (2008), Chailleux *et al.* (2006), Clyne *et al.* (2003), Dougan *et al.* (2003), Pellinen and Witczak (2002) and Anderson *et al.* (1994), that the analysis of complex modulus test data often involves generating so-called “master curves”. For thermorheologically simple materials, the shift to the reference temperature allows the alignment of various isotherm curves to form a single and continuous line – the master curve. This curve allows comparisons to be made over extended ranges of frequencies or temperatures. Master curves are generated using the TTSP. In addition to the complex modulus, master curves can be constructed for a phase angle. Figure 2-10 shows an example of complex modulus and phase angle master curves. The shift factor ($\alpha(T)$) is the amount of shifting required at each temperature to form the master curve and it defines the required shift at a given temperature. The actual frequency is multiplied by this shift factor to obtain a reduced frequency (ω_r) for the master curve. The relationship between the frequency and the reduced frequency is given by Equation 2-23 and Equation 2-24. At the reference temperature, the shift factor $\alpha(T) = 1$. The amount of shift required at each temperature to form the master curve describes the temperature dependency of the material.

LITERATURE REVIEW

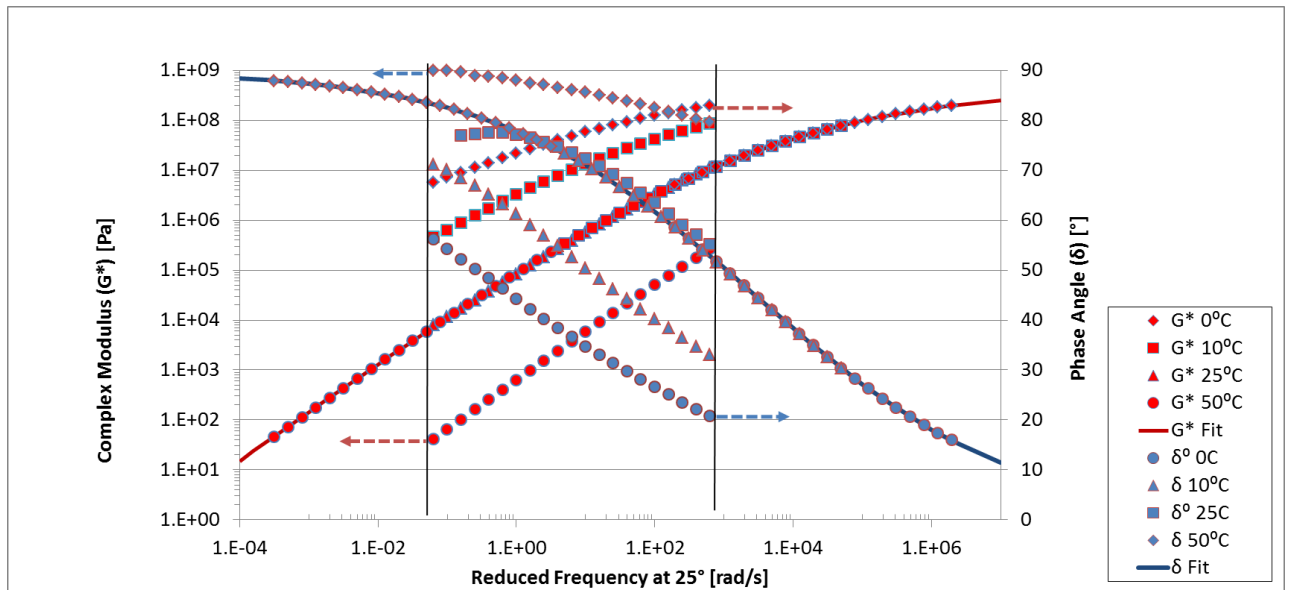


Figure 2-10: Example of complex modulus and phase angle master curves for bitumen

$$\omega_r = \alpha(T)\omega$$

Equation 2-23

$$\log(\omega_r) = \log(f\omega) + \log[\alpha(T)]$$

Equation 2-24

where

ω is the angular frequency [rad/s]

ω_r is the reduced frequency [rad/s]

Yusoff (2012), Yusoff *et al.* (2011) and Anderson *et al.* (1994) reported the use of different shift factor methods such as a random shift, Williams, Landel and Ferry (WLF), Arrhenius, Log-Linear, Viscosity Temperature Susceptibility (VTS) and Laboratoire Central des Ponts et Chaussées (LCPC) methods. The methods and



equations of determining the shift factor are presented as indicated in Section 2.9.1.1 to Section 2.9.1.6.

2.9.1.1 Numerical, non-linear least squares shift

Yusoff (2012) and Pellinen and Witczak (2002) reported that the numerical, non-functional form shift approach uses a solver function such as the MS Excel Spreadsheet to assess all the shift factors simultaneously with the coefficients of a model using a non-linear least squares fitting. In this process, no functional form for the relationship of α_T versus temperature is assumed.

2.9.1.2 The Arrhenius equation

According to Lakes (2009), the Arrhenius shift factor was developed based on the fact that the shift factor depends on temperature and on the material. Many materials exhibit temperature-dependent creep behaviour represented by the Arrhenius relation (see Equation 2-25).

$$\tau^{-1} = \nu_0 e^{\left(-\frac{H}{RT}\right)}$$

Equation 2-25

where

τ is the time constant

ν_0 is the characteristic frequency

T is absolute temperature

H is the activation energy

R is the constant for a perfect gas, 8.314 J/(mol.K)

Yusoff (2012), Molenaar (2010) and Medani and Huurman (2003) reported that the Arrhenius equation is a commonly used formula for the shift factor. Anderson *et al.* (1994) stated that Arrhenius function is necessary to describe the time-temperature dependency in the low temperature region, below the glass transition temperature, and in the high-temperature Newtonian region. It can be described by Equation 2-26:



LITERATURE REVIEW

$$\log a_T = C \left(\frac{1}{T} - \frac{1}{T_s} \right) = \left(\frac{\Delta H}{R} \right) \left(\frac{1}{T} - \frac{1}{T_s} \right) \quad \text{Equation 2-26}$$

where

T is the temperature considered

T_s is the reference temperature

R is the constant for a perfect gas, 8.314 J/(mol.K)

ΔH is the apparent activation energy

C is a constant

From Equation 2-26, Equation 2-27 is derived.

$$\alpha_T = e^{\left(\frac{\Delta H}{R} \left(\frac{1}{T} - \frac{1}{T_s} \right) \right)} \quad \text{Equation 2-27}$$

2.9.1.3 The Williams, Landel and Ferry (WLF) equation

According to Mangiafico (2014), Yusoff (2012), Lakes (2009) Williams, Landel and Ferry (1955) discovered the WLF equation, which has been widely used to describe the relationship between the shift factor a_T and temperature dependency by means of Equation 2-28. Anderson *et al.* (1994) reported that The Williams-Landers-Ferry (WLF) equation is valid in the intermediate or visco-elastic region.

$$\log a_T = \frac{-C_1(T-T_s)}{C_2+T-T_s} \quad \text{Equation 2-28}$$

where

T is the temperature

T_s is the reference temperature



C_1 and C_2 are constants

2.9.1.4 The Log-Linear Equation

Yusoff (2012) and Pellinen and Witczak (2002) discussed the Log-Linear Relation. In this relation, a_T is determined using Equation 2-29.

$$\log \alpha \left(\frac{T}{T_s} \right) = \beta (T - T_s) \quad \text{Equation 2-29}$$

where

β : is the slope of the straight-line relationship between $\log a_T$ and temperature

2.9.1.5 The Viscosity Temperature Susceptibility (VTS) equation

Yusoff (2012), Garcia and Thompson (2007) and Pellinen and Witczak (2002) state that a_T can be expressed as a function of binder viscosity using the viscosity temperature susceptibility (VTS) concept. The VTS relation is presented in Equation 2-30.

$$\log(\alpha_T) = C(10^{A+VTS[\log(T_R)]} - 10^{A+VTS[\log(T_R)_0]}) \quad \text{Equation 2-30}$$

where

C is a constant

T_R is the temperature of interest [Rankine]

$(T_R)_0$ is the reference temperature [Rankine]

A is the regression intercept

VTS is the regression slope of viscosity temperature susceptibility

2.9.1.6 The Laboratoire Central des Ponts et Chaussées (LCPC) approach

Chailleux *et al.* (2006) developed a mathematically based procedure in order to construct master curves from dynamic measurements. In this method a shift factor is calculated gradually for close isotherms, at only one frequency. For measurements taken at temperatures $T_1, T_2, \dots, T_i, T_{i+1}, \dots, T_n$, master curve construction related to a



LITERATURE REVIEW

reference temperature T_{ref} (with ref between 1 and n) is made using cumulatives of $\log(\alpha_{(T_i, T_{i+1})})$. Hence, a shift factor needs to be applied for an isotherm T_i according to the reference temperature T_{ref} . This is given by Equation 2-31.

$$\log(\alpha_{(T_i, T_{ref})}) = \sum_{j=i}^{j=ref} \frac{\log(|G^*(T_j, \omega)|) - \log(|G^*(T_{j+1}, \omega)|)}{\delta_{avr}^{(T_j, T_{j+1})}(\omega)} \times \frac{\pi}{2} \quad \text{Equation 2-31}$$

where

ω is the angular frequency

$\delta_{avr}^{(T_j, T_{j+1})}(\omega)$ is the average of two phase angles measured at T_j and T_{j+1} (for ω)

$|G^*(T_j, \omega)|$ is the absolute value of the complex modulus measured at T_j (for ω)

$|G^*(T_{j+1}, \omega)|$ is the absolute value of the complex modulus measured at T_{j+1} (for ω)

2.9.1.7 Choice of shift factor methods

The WLF and the Arrhenius shift factor methods are those most often used in the literature. Although Anderson *et al.* (1994) found that the Arrhenius equation is better than the WLF equation at low temperatures, they both appear to be simple and provide acceptable and comparable results. These two equations were adopted in this thesis.

2.9.2 Black space diagrams and Cole-Cole diagrams

King *et al.* (2012) reported that black space diagrams are simple rheological plots of G^* versus δ , that can conveniently analyse rheological data over all test temperatures and frequencies with no mathematical shifts required to account for the TTSP. A black space diagram captures phase changes in the binder, such as wax crystallisation which is known to cause low-temperature physical hardening. Such effects can be missed if the TTSP incorrectly over-shifts data to align individual frequency sweeps. Soleimani (2009) reported that a black space diagram is very sensitive to morphology. In addition, temperature-independent curves can be

LITERATURE REVIEW

constructed when the material obeys the TTSP. Typically, the expected visco-elastic behaviour describes a decreasing phase angle and increasing complex modulus as the temperature decreases. The black space diagram will appear discontinuous for the following reasons:

- The sample is tested in the non-linear region.
- The sample is not rheologically simple (i.e. phase transitions occur over the studied temperature and frequency range).
- The sample is tested outside of the testing machine resolution.

An example of a black space diagram is given in Figure 2-11.

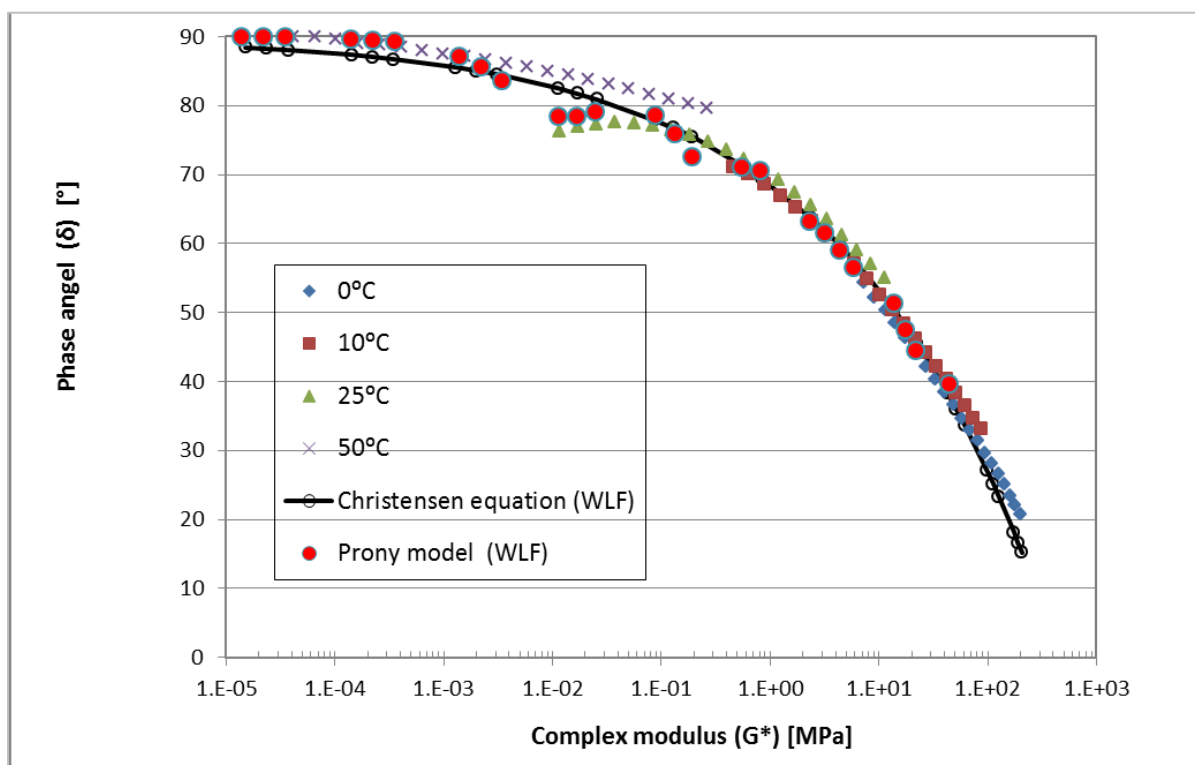


**Figure 2-11: Example of a black space diagram
(70/100_Unaged_Uncondition_WLF)**

Placet *et al.* (2009) reported that the Cole-Cole diagram was initially developed by Kenneth Stewart Cole and Robert Hugh Cole (Cole and Cole 1941, 1942). This diagram represents a convenient way to summarise the visco-elastic properties of materials. It allows the visualisation of the relaxation mechanisms of visco-elastic materials. Soleimani (2009) states that modified Cole-Cole diagrams, also known as

LITERATURE REVIEW

Han plots, represent changes between the elastic and viscous components of the complex modulus. Such graphs are useful for interpreting the relative elasticity or viscosity of a particular asphalt over a range of temperatures. If a straight line is plotted such that $G' = G''$, its intercept with the Han curve shows the crossover frequency between G' and G'' . Data on the left or above the straight line represent a behaviour dominated by the viscous or loss modulus, while data on the right and under the line indicate that the elastic modulus dominates the behaviour of the sample under the given testing condition. An example of a modified Cole-Cole diagram is given in Figure 2-12.

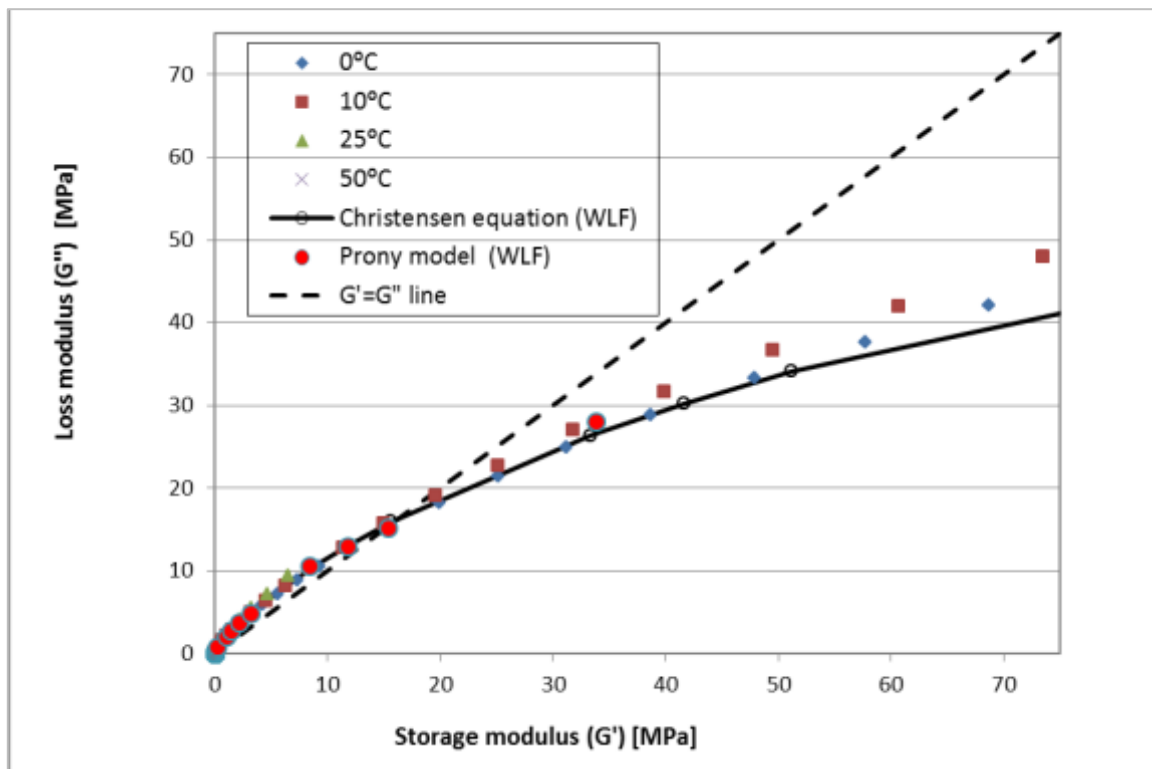


**Figure 2-12: Example of a modified Cole-Cole diagram
(70/100_Unaged_Uncondition_WLF)**

Di Benedetto *et al.* (2011) state that when plotted in a black or Cole-Cole diagram, the normalised moduli of materials derived from the same binder produce curves that superimpose on each other. This confirms that time and temperature are dependent for these materials. According to Olard and Di Benedetto (2003), some polymer-modified materials do not have a unique black space diagram. However, they



LITERATURE REVIEW

produce unique G^* master curves at a reference temperature. Hence, the value of G^* at any temperature can be obtained, provided the shift factor is known. This property is called “Partial Time-Temperature Superposition Principle” (PTTSP) as the shifting procedure gives a unique and continuous master curve for G^* . Woldekidan (2011), Lakes (2009) and Ferry (1980) reported that for thermorheologically complex materials, the change in temperature could be modelled with a vertical shift factor in addition to the horizontal shift factor. The vertical shift factor (β_T) is applied to a corrected or reduced modulus (E_p). The general formulation of this principle is given in Equation 2-32.

$$E(t, T) = \beta_T E_p(t, \alpha_T\{T\}, T_R) \quad \text{Equation 2-32}$$

where

β_T is the vertical shift factor for a given temperature $\{T\}$

T_R is the reference temperature [K]

$\alpha_T\{T\}$ is the horizontal shift factor for a given temperature $\{T\}$

E_p is the reduced modulus (obtained after horizontal shifting)

t is the time

2.9.3 Mathematical models

2.9.3.1 Introduction

Yusoff *et al.* (2011) state that various researchers have used explicit empirical algebraic equations to characterise the master curves of the complex modulus for bitumen. Among these mathematical models, the following can be listed:

- Jongepier and Kuilman’s model
- Dobson’s model
- Dickinson and Witt’s model
- Christensen and Anderson (CA) model
- Fractional model
- Christensen, Anderson and Marasteanu (CAM) model
- Modified Christensen model



LITERATURE REVIEW

- Anderson and Marasteanu model
- Al-Qadi and co-workers' model
- Polynomial model, sigmoidal model
- LCPC master curve construction method
- New complex modulus and phase angle predictive model
- Generalised logistic sigmoidal model

A brief description and the formulae of these models are provided in Appendix B.

This thesis makes use of the Christensen and Anderson (CA) model due to its simplicity, as stated by Yusoff *et al.* (2011) and Anderson *et al.* (1994).

2.9.3.2 Christensen and Anderson (CA) model

Anderson *et al.* (2008) reported that during the development of the Strategic Highway Research Program (SHRP), there was a need to describe the relaxation modulus, with all other rheological functions being generated from the relaxation modulus. Christensen recognised that the relaxation modulus is skewed, not symmetrical. This induced them to investigate a skewed function. Their development process is presented as follows:

- Characterisation of the complex modulus as a function of four primary parameters: glassy modulus (G_{glassy}), steady state viscosity (η_0), crossover frequency (ω_{cross}), and Rheological Index (R). These four parameters are presented in Figure 2-13.
- Yusoff *et al.* (2011) and Yusoff (2012) reported:
 - o The glassy modulus (G_{glassy}) is the value that the complex modulus or stiffness modulus approaches at low temperatures and high frequencies (short loading times).
 - o The steady-state viscosity (η_0) is the steady-state, or Newtonian viscosity. In dynamic testing, it is approximated as the limit of the complex viscosity $|\eta^*|$, as the phase angle approaches 90° . The 45° line that the dynamic master curve approaches at low frequencies is



LITERATURE REVIEW

often referred to as the “viscous asymptote”. It is indicative of the steady-state viscosity, and the value of η_0 is binder specific.

- The crossover frequency (ω_{cross}) is the frequency at a given temperature where $\tan \delta$ is 1. At this point, the storage and loss moduli are equal. For most bitumens, the crossover frequency is nearly equal to the point at which the viscous asymptote intersects the glassy modulus. The crossover frequency can be thought of as a hardness parameter that indicates the general consistency of a given bitumen at the selected temperature and is binder specific.
- The Rheological Index (R) indicates the difference between G_{glassy} and the dynamic shear complex modulus at the crossover frequency, $G^*(\omega_{cross})$. It is directly proportional to the width of the relaxation spectrum and indicates rheological type. R is not a measure of temperature, but reflects the change in modulus with frequency or leading time, and therefore is a measure of the shear rate dependency of bitumen. R is binder specific.

- Use of the Weibull function to model the relaxation spectrum: This function is given by Equation 2-33.

$$F(x) = \frac{m}{b} e^{\left\{\frac{x-a}{b}\right\} \left[1 + \left\{\frac{x-a}{b}\right\}\right]^{-(m+1)}} \quad \text{Equation 2-33}$$

where

$F(x)$ is the probability density function

m is the skewness parameter

x is an independent parameter

b is a scale parameter

a is a location parameter

- Integrate the function to obtain a cumulative Weibull function: the cumulative Weibull function is presented in Equation 2-34.

LITERATURE REVIEW

$$1 - P(x) = \left[1 + \left\{ \frac{x-a}{b} \right\}^b \right]^{-m} \quad \text{Equation 2-34}$$

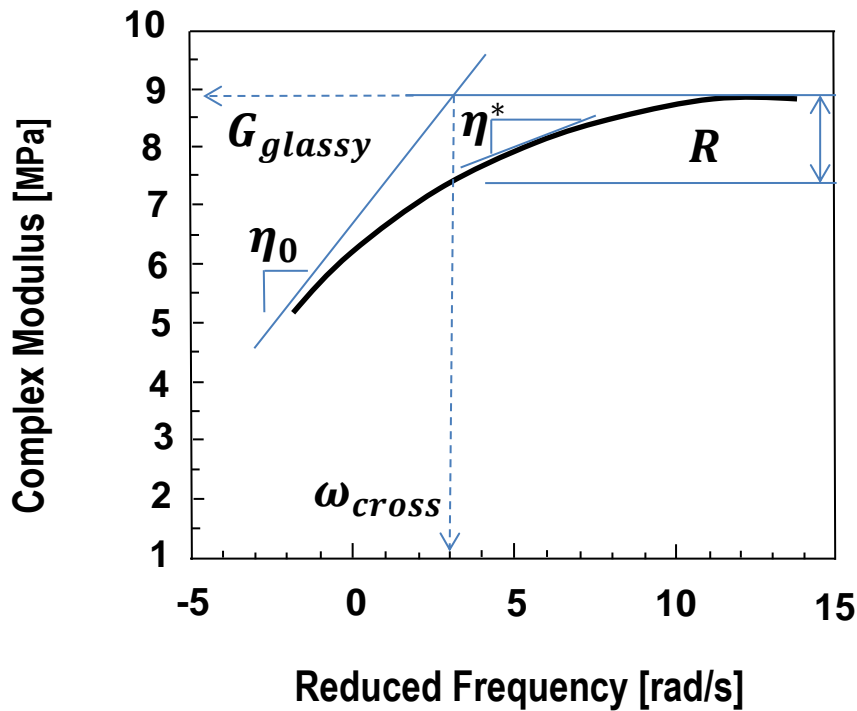


Figure 2-13: Meaning of the four parameters related in the CA model

- Substituting rheological parameters in the cumulative Weibull function: the result of this substitution is presented in Equation 2-35 and Equation 2-36.

$$G^* = G_{glassy} \left[1 + \left\{ \frac{\omega}{\omega_{cross}} \right\}^{\left(\frac{\log 2}{R} \right)} \right]^{-\frac{R}{\log 2}} \quad \text{Equation 2-35}$$

where

G^* is the measured complex modulus

G_{glassy} is the Glassy modulus

R is the Rheological Index (shape factor)

ω is the test frequency



LITERATURE REVIEW

ω_{cross} is the crossover frequency (location parameter)

$$\delta = \frac{90}{\left[1 + \left\{\frac{\omega}{\omega_{cross}}\right\}^{\frac{\log 2}{R}}\right]} \quad \text{Equation 2-36}$$

where

δ is the measured phase angle

- Estimate for Rheological Index: from the combination of Equation 2-35 and Equation 2-36, the Rheological Index can be expressed as per Equation 2-37.

$$R = \frac{\log 2 \left\{ \log \left(\frac{G^*}{G_{glassy}} \right) \right\}}{\log \left(1 - \frac{\delta}{90} \right)} \quad \text{Equation 2-37}$$

Yusoff (2012), Yusoff *et al.* (2011) and Anderson *et al.* (1994) reported that Equation 2-37 is reasonably accurate within the region where δ is between 10° and 70° , and that the best results are obtained near the crossover point, where $\delta = 45^\circ$. For this reason a second set of parameters was defined to characterise the visco-elastic behaviour at high temperatures and/or low frequencies (secondary region). The secondary region, which represents the viscous state of a material, was characterised by a transition phase angle (δ_v), a limiting modulus in the viscous flow region ($G_{glassy v}$), a location parameter for the viscous flow region ($\omega_{cross v}$), and a transition angular frequency between the two regions (ω_v). The formulae for δ_v , $G_{glassy v}$, ($\omega_{cross v}$) and ω_v are given respectively in Equation 2-38, Equation 2-39, Equation 2-40 and Equation 2-41.

$$\delta_v = 90 \left(\frac{\eta_0 \omega_{cross}}{G_{glassy}} \right)^{\frac{\log 2}{R-0.81}} \quad \text{Equation 2-38}$$



LITERATURE REVIEW

$$G_{glassyv} = G_{glassy} \left[\frac{90}{(90-\delta_v)} \right]^{0.81 - \frac{R}{\log 2}} \quad \text{Equation 2-39}$$

$$\omega_{crossv} = \omega_{cross} \left[\frac{(90-\delta_v)}{\delta_v} \right]^{\frac{R}{\log 2} - 0.81} \quad \text{Equation 2-40}$$

$$\omega_v = \omega_{cross} \left[\frac{(90-\delta_v)}{\delta_v} \right]^{\frac{R}{\log 2}} \quad \text{Equation 2-41}$$

In Equation 2-38, η_0 represents the steady-state viscosity. The other parameters in these equations are as previously defined.

Yusoff (2012) and Yusoff *et al.* (2011) state that, in practice, the primary parameters are of more interest and can be applied with confidence to temperatures up to about 45 °C under typical traffic loading times. They also mention that in the equations developed for the secondary region, the WLF equation was used. However, for characterisation of visco-elastic properties in the Newtonian region (lower temperature in the secondary region), the Arrhenius function was used to describe the shift factor.

Despite all the complexity presented by the use of the secondary region, in general it is not necessary to use the parameters for the viscous flow region. Thus, the CA model appears to be simple, accurate and intensively used.

2.9.4 Mechanical models

2.9.4.1 Background

Flügge (1975), Ferry (1980), Barnes *et al.* (1993), Woldekidan (2011), and Yusoff (2012) reported that since visco-elastic materials show a combination of viscous and elastic behaviour, it is useful to consider the simple behaviour of analogue mechanical models, constructed from linear springs and dashpots, to describe the visco-elastic behaviour of bituminous materials. In the mechanical models, Hookean



LITERATURE REVIEW

deformation is represented by a spring and Newtonian flow by a dashpot. The spring is an element characterising a simple material in which the force is proportional to the extension, while the dashpot is an element describing a simple material in which the force is proportional to the rate of extension. The extension (ε_s) of the spring follows Equation 2-1 and the strain in the dashpot (ε_d) obeys the law given in Equation 2-42. Many particular combinations of such springs and dashpots (also called “discrete assembly”) have been used to represent the behaviour of more complex materials such as bitumen and polymers. Complex materials are described by connecting the basic elements in series or in parallel. The simplest are the Maxwell and Kelvin-Voigt models.

$$\sigma = \eta \dot{\varepsilon}_d$$

Equation 2-42

where

$\dot{\varepsilon}_d$ is the strain rate of the dashpot

η is the viscosity

It should be noted that the dot is used to indicate time differentiation: e.g. $\dot{\varepsilon}_d = \frac{\partial \varepsilon_d}{\partial t}$.

This type of dot will have the same meaning throughout this document.

Roylance (2001) reported that when an improved fit to experimental data is necessary, additional spring and dashpot elements may be used in the Maxwell and Kelvin-Voigt models. This results in the generalisation of these models. The generalised Maxwell model is also known as a Prony series.

Di Benedetto *et al.* (2013) discuss other analogically based models, also called “continuous spectrum” model, such as the Huet-Sayegh model and the 2S2P1D model (two springs, two parabolic elements and one dashpot), which is a generalisation of the Huet-Sayegh model. Details on some of these models are presented in Section 2.9.4.2 to Section 2.9.4.6. An overview of the mechanical model is presented in Appendix C.

2.9.4.2 Maxwell model

The Maxwell model is a spring and dashpot in series as presented in Figure 2-14.

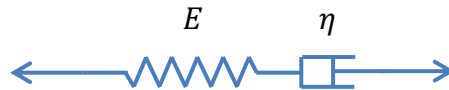


Figure 2-14: Maxwell model (spring and dashpot in series)

Flügge (1975) reported that since in the Maxwell model both elements are connected in series, the total elongation is given in Equation 2-43.

$$\varepsilon = \varepsilon_s + \varepsilon_d \tag{Equation 2-43}$$

where the subscripts “s” and “d” in strain terms refer to the spring and dashpot elements respectively. Used in the same context for stress, these subscripts will also have the same meaning.

It can also be stated that the stress in the spring in the model is equal to the stress in the dashpot and it is equivalent to the stress in the Maxwell system. This relation is presented in Equation 2-44.

$$\sigma = \sigma_s = \sigma_d \tag{Equation 2-44}$$

Woldekidan (2011) and Roylance (2001) reported that the Maxwell time-dependent stress relation is developed by combining Equation 2-1, Equation 2-42 and Equation 2-43 to obtain Equation 2-45.

$$\sigma + \frac{\eta}{E} \dot{\sigma} = \eta \dot{\varepsilon} \tag{Equation 2-45}$$

where

$\frac{\eta}{E}$ is a relaxation time constant, usually denoted as τ

LITERATURE REVIEW

By transforming and integrating Equation 2-45,

$$\sigma = \sigma_0 e^{\left(-\frac{t}{\tau}\right)}$$

2.9.4.3 Kelvin-Voigt Model

Roylance (2001) reported that the Maxwell model is suitable for relaxation loading, but it simulates creep loading poorly. The Kelvin-Voigt model is appropriated for creep. It is presented in Figure 2-15.

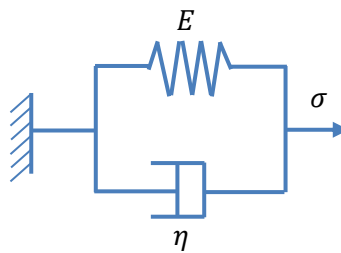


Figure 2-15: Kelvin-Voigt model

The stress applied in the Kelvin-Voigt model and the strain generated (as represented in Figure 2-15) are presented in Equation 2-46 and Equation 2-47.

$$\sigma = \sigma_s + \sigma_d \tag{Equation 2-46}$$

$$\varepsilon = \varepsilon_s = \varepsilon_d \tag{Equation 2-47}$$

By substituting Equation 2-1 and Equation 2-42 in Equation 2-46, Equation 2-48 is obtained.

$$\sigma = E\varepsilon_s + \eta\dot{\varepsilon}_d \tag{Equation 2-48}$$

Roylance (2001) developed Equation 2-48 to obtain the constitutive law expressed by Equation 2-49.

$$\frac{\varepsilon(t)}{R} = \frac{R \left(1 - e^{-\frac{t}{\tau}}\right)}{E}$$

Equation 2-49

with

$$R = \sigma(t)$$

Equation 2-50

where $\sigma(t)$ is a constant representing the case of creep.

2.9.4.4 Prony series

Roylance (2001) reported that the Wiechert model, also known as Prony series, is an array of Maxwell units in parallel as presented in Figure 2-16. Prony series is suitable for describing a scenario of the stress resulting from an imposed strain.

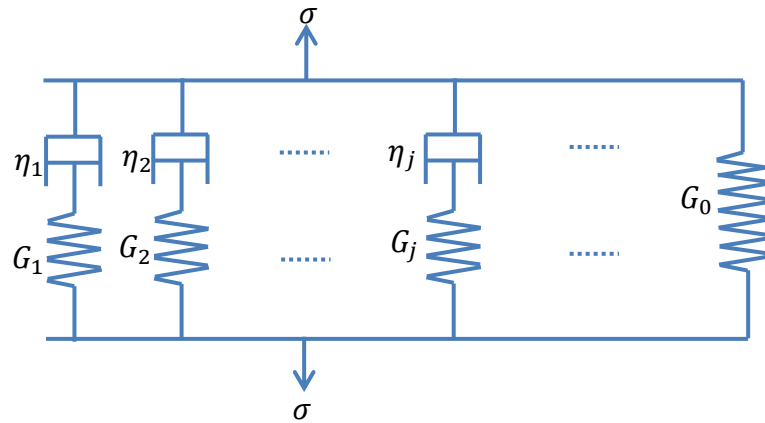


Figure 2-16: Prony series

Huurman and Woldekidan (2007) and Dassault Systèmes (2012) reported that in FE packages such as ABAQUS, the Prony series is incorporated as the primary linear visco-elasticity model. A Prony series model is implemented on the basis of the bulk and shear moduli, K and G .

The initial response is defined by the initial elastic modulus (E_0) and the initial Poisson's ratio (ν_0). These inputs are translated to K_0 and G_0 via Equation 2-51 to Equation 2-54.

$$G_0 = \frac{E_0}{2(1+\nu_0)}$$

Equation 2-51



LITERATURE REVIEW

$$K_0 = \frac{E_0}{3(1+\nu_0)} \quad \text{Equation 2-52}$$

$$\nu_0 = \frac{3K_0 - 2G_0}{6K_0 + 2G_0} \quad \text{Equation 2-53}$$

$$E_0 = \frac{9K_0G_0}{3K_0 + G_0} \quad \text{Equation 2-54}$$

For dynamic data obtained in the frequency domain (e.g. data from the DSR), a transformation from the time domain to the frequency domain in Prony series formulation is required. Using Fourier transforms, the expression for the time-dependent shear modulus can be written in the frequency domain as per Equation 2-55 and Equation 2-56.

$$G'(\omega) = G_0 \left[1 - \sum_{j=1}^N \frac{\alpha_j \tau_j^2 \omega^2}{1 + \tau_j^2 \omega^2} \right] \quad \text{Equation 2-55}$$

$$G''(\omega) = G_0 \left[\sum_{j=1}^N \frac{\alpha_j \tau_j \omega}{1 + \tau_j^2 \omega^2} \right] \quad \text{Equation 2-56}$$

where

G' is the storage modulus

G'' is the loss modulus

ω is the angular frequency

N is the number of terms in the Prony series

α_j is the stiffness reduction ratio for the j^{th} Prony element [without unit]

τ_j is the relaxation time for the j^{th} Prony element [with units of time]

2.9.4.5 Huet-Sayegh model

Olard and Di Benedetto (2003) state that the Huet-Sayegh model is a visco-elastic model using a parabolic creep function called the “parabolic element”. The Huet-Sayegh model was developed to improve the Huet model in fitting the response of bituminous mixes at low frequencies and/or high temperature. The adaptation of the Huet model was done by introducing a spring of small rigidity (G) compared with G in parallel. The Huet-Sayegh model is presented in Figure 2-17 and formulated in Equation 2-57 and Equation 2-58.

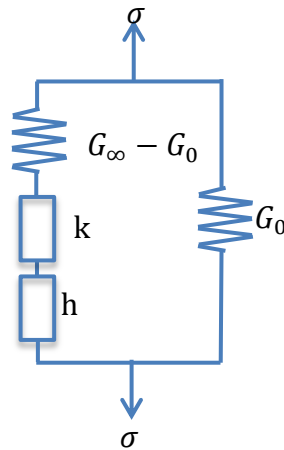


Figure 2-17: Huet-Sayegh model

$$G^*(\omega, T) = G_0 + \frac{(G_\infty - G_0)}{1 + \zeta(i\omega\tau(T))^{-k} + (i\omega\tau(T))^{-h}}$$

Equation 2-57

where

i is the complex number as defined in Equation 2-16

G^* is the complex modulus

G_0 is the static modulus

G_∞ is the limit of the complex modulus when $\omega\tau$ tends to infinite

ω is the angular frequency

LITERATURE REVIEW

h is the parabolic element characteristic (exponents such as $1 > h > k > 0$)

ζ is a dimensionless constant

$\tau(T)$ is the characteristic time, which value varies only with temperature (T); it is expressed by Equation 2-58.

$$\tau(T) = \exp(a + bT + cT^2) \quad \text{Equation 2-58}$$

2.9.4.6 2S2P1D model

Olard and Di Benedetto (2003) stated that the Huet-Sayegh model, at very low frequencies (for $G_0 = 0$), becomes equivalent to a parabolic element instead of linear dashpot. For this reason, the model is not suitable for binder at very low frequencies. To address this problem, a linear dashpot was added to the Huet-Sayegh model; thus, the new model is constituted with two springs, two parabolic elements and one dashpot. This model is named 2S2P1D and is exhibited in Figure 2-18 and expressed as per Equation 2-59 and Equation 2-60.

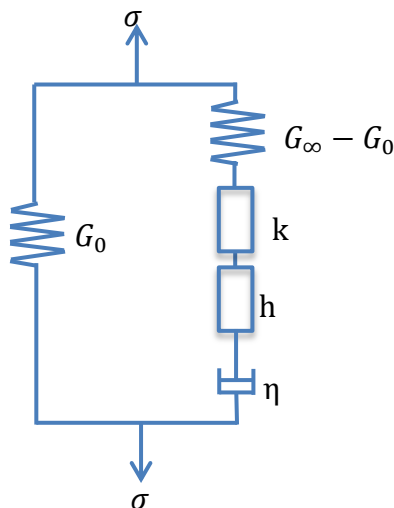


Figure 2-18: 2S2P1D model



LITERATURE REVIEW

$$G^*(\omega, T) = G_0 + \frac{(G_\infty - G_0)}{1 + \zeta(i\omega\tau(T))^{-k} + (i\omega\tau(T))^{-h} + (i\omega\beta\tau(T))^{-1}} \quad \text{Equation 2-59}$$

where

β is a dimensionless constant and can be expressed by Equation 2-60.

$$\beta = \frac{\eta}{\tau(T)(G_\infty - G_0)} \quad \text{Equation 2-60}$$

The other parameters in Equation 2-59 are as defined for the Huet-Sayegh equation.

2.10 Cohesion and Adhesion

2.10.1 Introduction

Read and Whiteoak (2003) state that the primary function of bitumen is to act as an adhesive. It is required either to bind aggregate particles together or to provide a bond between particles and an existing surface.

In the literature, the term “cohesion” is closely related to adhesion, especially when these two concepts are associated with the failure of a material. Von Fraunhofer (2011) states that “cohesion” is the molecular attraction by which the particles of a body are united throughout the mass, while “adhesion” is the molecular attraction exerted between the surfaces of bodies in contact. Therefore, cohesion is an attraction process that occurs between similar molecules, primarily as the result of chemical bonds that have formed between the individual components of the adhesive. In contrast, adhesion is any attraction process between dissimilar molecular species, which have been brought into direct contact such that the adhesive clings to the applied surface or substrate. Thus, cohesion may be defined as the internal strength of an adhesive due to various interactions within that adhesive that bind the mass together, whereas adhesion is the bonding of one material to another, namely an adhesive to a substrate, due to a number of different possible interactions at the adhesive-substrate surface interface. These differences are shown schematically in Figure 2-19.

LITERATURE REVIEW

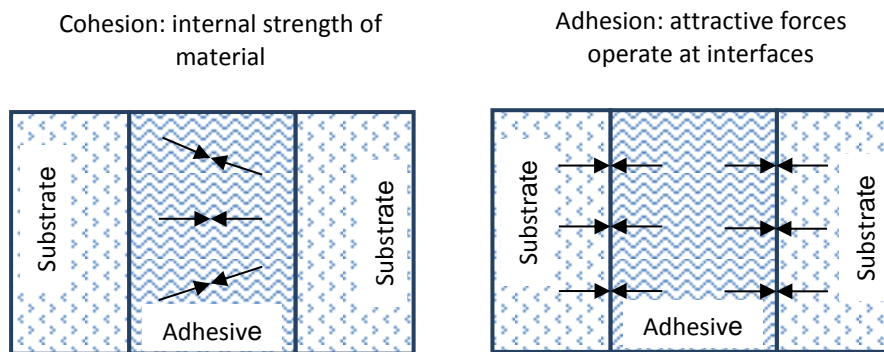


Figure 2-19: Cohesion and adhesion (adapted from von Fraunhofer, 2011)

Dorn (1994) and Petrucci *et al.* (2007) reported that cohesive force is the strength of the adhesive itself resulting in mechanical entangling and interlocking of the adhesive molecules and their physical and/or chemical affinity for each other. This creates intermolecular forces such as those from hydrogen bonding and Van der Waals forces. On the other hand, adhesive force is the result of the mechanical interlocking between adhesive and the material surface roughness (mechanical adhesion) and the physical and/or chemical interactions between the adhesive and the material. The forces involved in adhesion are mechanical (i.e. sticking together) and electrostatic forces (attraction due to opposing charges).

Petrucci *et al.* (2007) and Burnett *et al.* (2008) state that when a liquid comes into contact with a surface, both cohesive and adhesive forces will act on it. These forces govern the shape that the liquid takes on. If the cohesion force of a liquid is significantly greater than its adhesion force with the solid, then the molecules of the liquid will have more affinity with themselves than with the solid surface. In this case, the liquid divides into a number of small, roughly spherical beads which stand on the surface, maintaining minimal contact with the surface. Similarly, if the cohesion force of the liquid is significantly less than its adhesion force with the solid, then the liquid will spread out to form a thin film over the solid surface; this process is known as “wetting”.



2.10.2 Adhesion and cohesion mechanisms

According to Bhasin (2006), the physico-chemical character of the aggregate plays a role in adhesion. Several mechanisms are responsible for the adhesion and debonding of aggregate and bituminous binder. These mechanisms are grouped into mechanical, physical or chemical interactions between the bitumen and the aggregate. The mechanical contribution to adhesion is due to mechanical interlocking, expressed as the “surface roughness”. The chemical contribution to adhesion at the interface of aggregate and bitumen is due to the formation of chemical bonds (weak bonds). The physical contribution to the adhesion is based on surface energy principle from thermodynamic theory.

The principal factors affecting bitumen-aggregate adhesion are related to:

- *Aggregate properties*: mineralogy, surface texture, porosity, dust, durability surface area, absorption shape
- *Bitumen properties*: rheology, electrical polarity, constitution
- *Bituminous material properties*: void content, permeability, bitumen content, bitumen film thickness, filler type, aggregate grading, type of bituminous mixture
- *External factors*: rainfall, humidity, water pH, presence of salts, temperature, temperature cycling, traffic, moisture content, design, workmanship, weathering, drainage

According to various literature reviews, such as Schultz and Nadrin (1994), Newby *et al.* (1995), Hefer (2004), Van Lent (2008) and Vert *et al.* (2012), traditional theories of adhesion are based on thermodynamic theory. This theory is based on the concept that an adhesive will adhere to a substrate due to established physical intermolecular forces at the interface, provided that intimate contact is achieved. Adhesion requires energy from chemical and/or physical linkages. The physical energy is generally expressed in terms of the Surface Free Energy (SFE) of the materials involved in the adhesive bond. The adhesion strength is proportional to the SFE.



LITERATURE REVIEW

Burnett *et al.* (2008) state that the surface energy is analogous to the surface tension of a liquid. Surface energy describes the interaction between cohesive and adhesive forces which, in turn, dictate whether wetting will occur. In practical terms, the higher the surface energy, the more reactive the surface.

Generally, the SFE of solids is determined by indirect methods. Indirect methods use the work of adhesion (the work required to separate two materials brought together forming a new interface) of a solid as it interacts with various liquids and gases to assess the SFE of the solid. Examples of interactions between solids and liquids or gases are the formation of contact angles, vapour adsorption, evolution of heat when solids are immersed in a liquid, etc.

The following are some devices that can be used to determine the SFE of a solid:

- *Wilhelmy plate*: measuring of the dynamic contact angle between different probe liquids with the solid
- *Sessile drop method device*: measuring of the static contact angle between different probe liquids with the solid
- *Universal sorption device (USD)*: measuring the adsorption isotherms for different probes with the solid
- *Micro calorimeter*: measuring the heat of immersion for different probes with the solid
- *Inverse gas chromatography (IGC)*: measuring the retention times for different probes with the solid

Various methods have been used to measure the SFE of solids, such as the contact angle approach, the gas adsorption method and inverse gas chromatography (IGC).

Contact angles are commonly used to measure the SFE of solids. When a drop of liquid is placed on a clean, smooth horizontal surface, it either spreads over the solid surface or takes the form of a drop with a finite contact angle between the solid and liquid phases. Figure 2-20 schematises the surface forces acting on a liquid drop; the interfacial energy between the solid and the liquid is represented by γ_{SL} ; γ_{SV} and γ_{LV} are the surface free energies of the solid and liquid in the presence of the vapour "V".

LITERATURE REVIEW

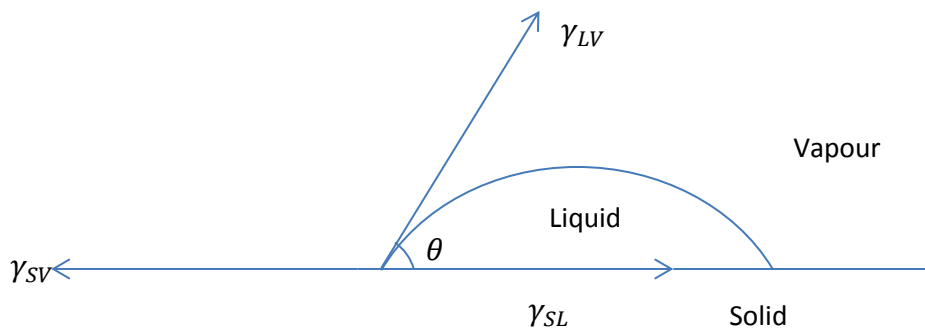


Figure 2-20: Contact angle of liquid on a solid surface

2.10.3 Moisture damage effects on adhesion

Moisture damage affects bitumen-aggregate adhesion. Howson *et al.* (2009) state that moisture damage is assessed using the mechanical properties of a material or based on fundamental material properties that affect physical adhesion between the bitumen and aggregate, and the propensity to lose this bond in the presence of water. The surface energy and fatigue resistance are some of these properties. The SFE is the energy required to form a unit area of new surface.

According to Tarrer and Wagh (1993), there are five different mechanisms by which stripping of bitumen from an aggregate surface may occur, namely detachment, displacement, spontaneous emulsification, pore pressure and hydraulic scouring. These mechanisms may act individually or together to cause adhesion failure in bituminous materials. A brief description of each of the suggested mechanisms of stripping follows:

- *Detachment*: The peeling of bitumen from aggregate is due to the presence of a layer of water. This phenomenon is explained by a much lower SFE of water compared with that of bitumen; thus the water wets the aggregate easily, then the bitumen and consequently the water replaces the bitumen in the bond.
- *Displacement*: Water penetrates the aggregate through a break and displaces the bitumen by thermodynamic principles or by chemical reaction.



LITERATURE REVIEW

- *Spontaneous emulsification*: The stripping in this case is due to the combination of water and bitumen in an inverted emulsion presenting two phases: the continuous phase (bitumen) and the discontinuous phase (water). The evaporation of water could restore the initial adhesion.
- *Pore pressure*: In this mechanism, water is trapped in asphalt mix voids and its circulation is restricted; this causes stripping of the bitumen film from the aggregate.
- *Hydraulic scouring*: This mechanism is caused by the action of vehicle tyres on a saturated pavement surface. The stripping is due to the tyre's pumping action on the water through the surface voids.

Although moisture damage caused by adhesion is generally described by the thermodynamic approach, Newby *et al.* (1995) state that the adhesion of a visco-elastic binder is better controlled by the interfacial slippage, irrespective of the SFE level developed by the adhesion interface.

2.10.4 Conclusion on cohesion and adhesion

Cohesion and adhesion are two related concepts, especially in the case of bond failure between two different materials. They are described by mechanical, physical mechanisms or chemical interactions. The physical mechanism, which is generally described by the thermodynamic approach, is the most developed in the literature.

In this research, cohesion within the bitumen and adhesion between the aggregate and the bitumen will be investigated and assessed using the DSR in the fatigue testing mode. This protocol of the investigation appears to be more suitable for a mechanical approach to the assessment. Thus, the thermodynamic and chemical interaction approaches to cohesion and adhesion will not be considered.

2.11 Fatigue of Bituminous Materials

2.11.1 Introduction

The fatigue concept is generally associated with the failure and fracture concepts. Elucidation of the two last concepts will enhance understanding of the fatigue

LITERATURE REVIEW

concept. Domone and Illstone (2010) define “fracture” as the separation of a material or its components into two or more pieces under the action of a static or slowly changing imposed load, at temperatures that are low compared with the material melting temperature. On the other hand, “failure” refers to a material or its components that is/are rendered unfit for further service. Failure can occur without fracture (e.g. by excessive deformation or by reduction of a load-supporting area due to wear or corrosion). In general, fracture modes range from brittle to ductile, depending on the type of material and the applied load. Brittle fracture occurs when a material absorbs little or no energy prior to fracture. Ductile fracture applies to a material that can sustain noticeable plastic deformation and energy absorption prior to fracture. Brittle and ductile fracture behaviour in terms of tensile stress–strain is presented in Figure 2-21. The area under the stress–strain curve up to fracture is a measure of the energy absorbed per unit volume of material, and is called the “toughness” of the material. Ductile materials exhibit much higher values of toughness than do brittle materials. Figure 2-22 illustrates typical deformation related to brittle and ductile fracture. In the case of ductile fracture, the sample can experience a considerable change in shape prior to fracture.

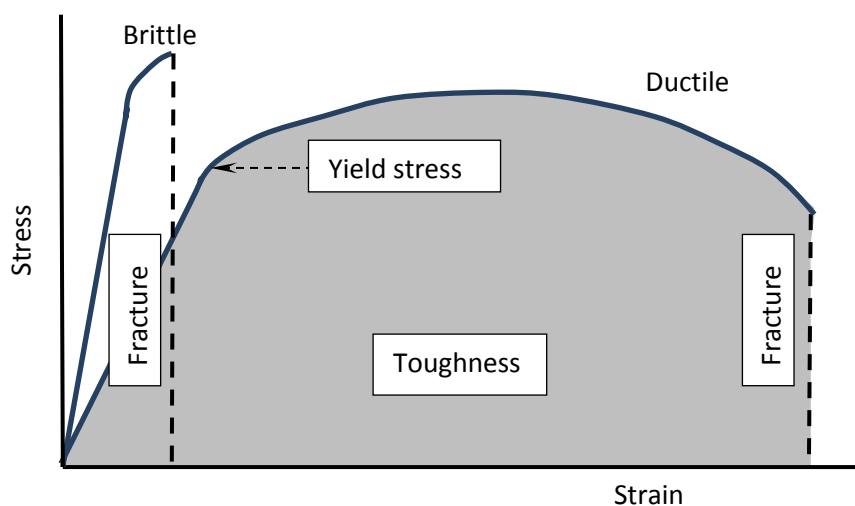


Figure 2-21: Tensile stress–strain curves for brittle and ductile materials taken to fracture (after Domone and Illstone, 2010)

LITERATURE REVIEW

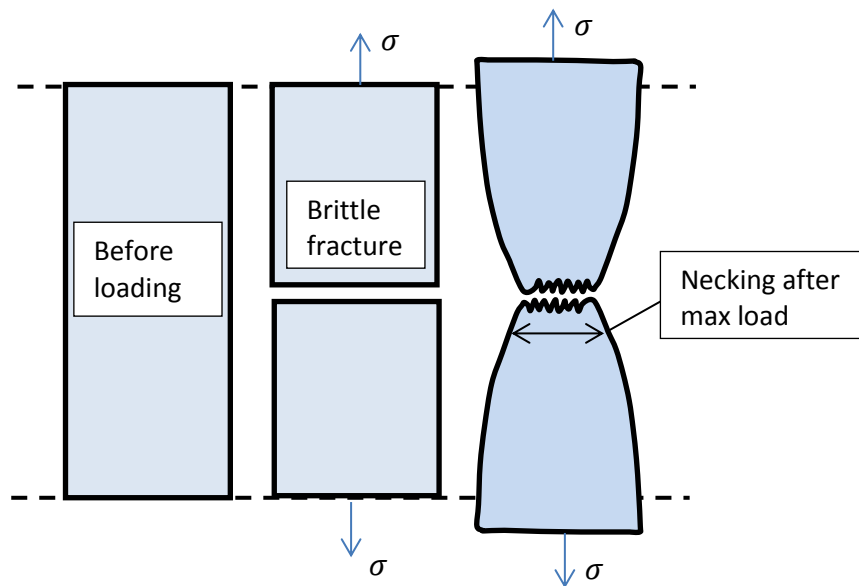


Figure 2-22: Representation of brittle and ductile fractures (after Domone and Illstone, 2010)

According to Airey *et al.* (2006), Domone and Illstone (2010) and Sybilski *et al.* (2013), in engineering materials exposed to complex mechanical and environmental loading (e.g. temperature and humidity variation, etc.) constant microstructural (or structural, depending on material types) changes occur, causing a drop in strength. In general, such effects are complex, but at macroscopic scale can be seen as so-called “material damage”. Thus, fatigue can be described as the phenomenon of material fracture under repeated or fluctuating stress having a maximum value of generally less than the tensile strength of the material. In the case of road pavements, which generally carry loads that are considerably lower than the load capacity, but in a cyclically repeatable way, it can be assumed that high cycle fatigue can occur. The most basic damages that occur in the asphalt pavement are permanent deformation and cracking. The “fatigue resistance” of a bituminous mixture is, therefore, the ability of the mixture to resist cracking and fracture under this repeated bending.



2.11.2 Fatigue mechanism

Domone and Illstone (2010) state that fatigue failure usually originates from a region of concentrated stress, such as an impure particle in the material, or at an engineering feature, such as a hole or notch. Once a fatigue crack has initiated, it grows under the action of the cyclic stress until its length is such that its associated stress intensity factor equals the fracture toughness of the material, at which point fast fracture occurs. The crack growth region of the fatigue fracture face is relatively smooth, whereas, in the case of a ductile metal, the fast fracture region is rougher and characteristic of local plastic deformation. Fatigue failure does not normally involve gross plastic deformation and hence shows similarities with brittle fracture. Ductile metals are particularly prone to fatigue failure, but ceramics and polymers can also suffer from the same phenomenon. Fatigue performance, in its simplest form, is characterised in the laboratory by plotting the experimental stress range versus the number of cycles to failure. This is also called “fatigue life”.

In their work on fatigue of bitumen and bituminous mixes, Pell *et al.* (1961) found that the factor controlling the fatigue life of bitumen and bituminous mixes is the magnitude of the applied tensile strain, rather than stress. The effects of temperature and loading speed can be accounted for by their effect on the stiffness of the specimen. However, it was clear that under certain conditions in a constant-strain test, particularly at low stresses, the measured fatigue life includes a considerable length of time necessary to propagate the crack or cracks sufficiently to terminate the test. They suggested that the definition of failure as implied in “constant-strain” tests and in “constant-stress” tests should be clearly understood. In “constant-strain” tests, crack propagation may have to be taken into account, whereas in “constant-stress” tests, the initiation of a crack appears to be followed by immediate and catastrophic failure of the specimen, which causes the test machine to stop. This implies that the constant-stress test continuously applies the same load whereas the constant-strain test reduces the load as the sample weakens to keep the strain constant. Consequently, catastrophic failure does not occur in the case of constant-strain test.

Airey *et al.* (2006) and Sybilski *et al.* (2013) associated and defined fatigue failure as an arbitrary 50 per cent reduction in initial stiffness (for the controlled strain tests) or



LITERATURE REVIEW

complete fracture of the specimen (for the controlled stress tests). On the other hand, Van Dijk (1975), Hopman *et al.* (1989) Pronk *et al.* (1996) and Sybilski *et al.* (2013) reported a new definition of fatigue life base on dissipated energy. Part of energy generated during fatigue test is related to mechanical fatigue of the sample and interpreted as dissipated energy. A sudden change of dissipated energy during a fatigue test is considered as the starting point of sample degradation. The Dissipated energy is expressed by Equation 2-61. The fatigue life can be determined based on the dissipated fatigue criterion. This is a graphical criterion using a Dissipated Energy Ratio (DER) expressed as function of the number of load cycles to determine the fatigue life. In this criterion, the fatigue life is characterised by the position on the graph where the function is no longer linear. The DER is expressed by Equation 2-62 and graphical representations of DER for controlled strain mode and controlled stress mode are schematised in Figure 2-23. From Figure 2-23, reveals that the use of intersection between two tangents (resulting in point A) overestimates the fatigue life; while the determination of the point of deviation from linear part results in point B. Therefore, the determination of the transition point between the linear part and curve part of the function appears to be subjective.

$$W_n = \pi \sigma_n \varepsilon_n \sin \delta_n \quad \text{Equation 2-61}$$

where

W_n is the dissipated energy [J/m³]

σ_n is the stress amplitude [MPa]

ε_n is the strain amplitude [$\mu\text{mm}/\text{mm}$]

δ_n is the phase angle [°]

$$W_n = \frac{n w_0}{w_n} \quad \text{Equation 2-62}$$

where

n is the number of loading cycle

w_0 is the energy dissipated in the first cycle

w_n is the energy dissipated in the nth cycle

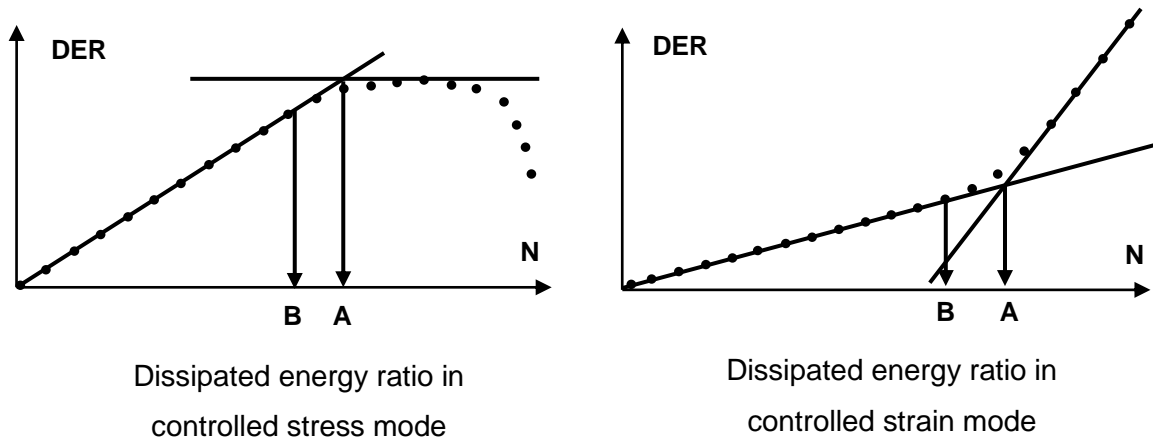


Figure 2-23 : Graph determination of fatigue life using dissipated energy ratio (extracted from Sybilski et al., 2013)

Due to the subjectivity of this graphical method, Rowe and Bouldin (2000) developed a precise mathematical method using the so-called “reduced dissipated energy ratio. Two equations were introduced for reduced dissipated energy ratio: the reduced dissipated energy ratio in stress controlled mode (as presented in Equation 2-63) and reduced dissipated energy ratio in strain controlled mode presented in Equation 2-64.

$$R_n^\sigma = n E_n \quad \text{Equation 2-63}$$

$$R_n^\sigma = \frac{n}{E_n} \quad \text{Equation 2-64}$$

where

n is the number of loading cycle

E_n is the stiffness modulus in nth cycle [MPa]

Sybilski *et al.* (2013) reported that the determination of fatigue life using of strain controlled reduced dissipated energy ratio equation was not as easy as in the situation of stress controlled.



LITERATURE REVIEW

In this research, fatigue will be investigated in terms of cohesion failure and adhesion failure. It should be mentioned that in some literature sources, such as Domone and Illstone (2010), it seems to be suggested that fatigue is more likely to occur in the form of ductile fracture than brittle fracture, and fatigue is frequently correlated with a high number of applied stress cycles (more than 1 000). Furthermore, according to Newby *et al.* (1995), the adhesion of a visco-elastic adhesive might be controlled by the interfacial slippage, which can be considered as a brittle fracture. This implies that adhesion might be considered as a “non-fatigue” mechanism. Despite these observations, in this research adhesion will be considered as a fatigue mechanism, due to the fact that the DSR cycling load applied to the sample and the interface stiffness reduction (which is a characteristic of fatigue) are monitored.

2.12 Summary of Literature Review and Research Recommendations

A seal is constituted of stone and bituminous binder. The binder provides the visco-elastic properties in the seal structure. The traffic loading and environmental forces applied to the seal generate changes within the seal structure. Most of these changes can be defined as “damage” and are characterised mainly by ageing of the bituminous binder and the effect of water on the seal structure. The damage affects the performance and life of the road pavement. The damage and failure of the seal manifest as permanent deformation (rutting), adhesion failure between stone and binder (loss of stone) and cohesion failure within the bituminous binder (cracking).

Based on the visco-elastic and rheological properties of bituminous materials, the damage can be expressed in terms of stiffness reduction of the seal materials.

Evaluation of the performance of a seal requires material characterisation, which can be done at two levels: (i) response and (ii) damage assessment. The response focuses on the bitumen’s “working” characteristics, based on the modelling of visco-elastic materials, while the damage consists of investigations into the cohesion fatigue damage (CFD) and adhesion fatigue damage (AFD) of the seal materials, based on the stiffness reduction principle of materials under the action of cyclic stress. The DSR was the main laboratory device used to identify both response and damage with the aim of modelling these phenomena.



LITERATURE REVIEW

In this context, the literature review has covered fundamental concepts related to the characterisation of bituminous seal materials. The following are fundamental concepts:

- 1) *Seal composition and importance*: The seal consists of bitumen and aggregate. The bitumen acts as the binder that holds the aggregate together and to the base. The aggregate provides abrasion protection and the bitumen provides waterproofing. It is the bitumen that gives these materials their rheological and visco-elastic characteristics, allowing the seal to respond to traffic loading and environmental actions. The visco-elastic characteristics of the seal response are represented by parameters such as the complex modulus (G^*) and the phase angle (δ). Thus, the seal responds by mitigating stripping (adhesion failure), cracking (cohesion failure) and deformation.
- 2) *Seal design*: The principle of seal design is based on the volumetric properties of seal materials and the amount of voids trapped in the seal. Some design values are chosen experimentally or empirically. Nevertheless, the forces of traffic and of the environment that act on the seal seem to be under-considered in the design. Although volumetric properties and the void concept of seals play a role in seal performance, the volumetric design lacks mechanistic analysis which takes into account parameters such as stress and/or strain interactions in the seal structure and the durability of the seal.
- 3) *Seal modelling*: This modelling initiated the development of the mechanistic analysis of seals expressed in terms of stress-strain interactions. In this thesis seal modelling will be further developed by using response and damage models of the seal. These models will reflect the action of traffic (vehicle loading, tyre pressure, traffic abrasive action on aggregate, etc.), the environment (water sensitivity, temperature action, ageing of binder, etc.) and material characteristics, and should be further analysed for the improvement of seal performance.
- 4) *Ageing and durability of bituminous binder*: One of the reasons for cohesion failure in seals is the loss of bitumen properties with time, which is known as bitumen ageing. The ageing process of bituminous material is determined by the temperature and the weather conditions. The pressure is an additional factor that



LITERATURE REVIEW

is used to accelerate the oxidation of bitumen in the laboratory, but it does not play a significant role in the pavement ageing. Simulation of ageing can be subdivided into short-term ageing and long-term ageing. Short-term ageing reflects the loss of volatiles that generally occurs during the hot phase of bituminous material preparation in the plant or during construction. Long-term ageing represents the oxidation process of a bituminous material during its lifetime. It appears to be difficult to simulate field ageing with laboratory ageing. However, a better field ageing simulation should represent long-term ageing in a relatively short testing time and should take into account the field microclimate. The durability of seals and bitumen was defined in Australia by Oliver (2004), Oliver and Boer (2008) and Oliver (2011) as the study of the life prediction of seals by means of correlation between bitumen hardening and factors such as bitumen viscosity, bitumen film thickness and seal aggregate size. These studies employed the Australian Road Research Board test method and modelled the prediction of seal life. In South Africa, research has been done on the durability of bitumen by modifying the Rolling Thin Film Oven Test (RTFOT) to simulate long-term ageing of bitumen (Muller and Jenkins, 2011).

5) *Rheological modelling of the linear visco-elastic properties of bituminous materials*: Essentially, this consists of the following:

- the construction of *master curves* using the thermorheologically simple behaviour of bituminous materials. Master curves are based on the Time Temperature Superposition Principle (TTSP) and are constructed by applying the shift factor methods and the empirical algebraic master curve equations of complex modulus and phase angles of bitumen (e.g. Christensen and Anderson model). The construction of master curves constitutes mathematical modelling.
- the use of *mechanical modelling*. Since visco-elastic materials show a combination of viscous and elastic behaviour, it is useful to consider the simple behaviour employed in analogue mechanical models constructed from linear springs and dashpots to describe the visco-elastic behaviour of bituminous materials. In the mechanical models, Hookean deformation is represented by a spring and Newtonian flow by a dashpot. The spring is an



LITERATURE REVIEW

element characterising a simple material in which the force is proportional to the extension, while the dashpot is an element describing a simple material in which the force is proportional to the rate of extension. The simplest combinations of springs and dashpots are the Maxwell and Kelvin-Voigt models. Complex materials are described by connecting the basic elements in series or in parallel. This creates generalisation of the Maxwell and Kelvin-Voigt models. The generalised Maxwell model is also known as Prony series. Di Benedetto *et al.* (2013) mention other analogically based models such as the Huet-Sayegh model and the 2S2P1D model (two springs, two parabolic elements and one dashpot), which is a generalisation of the Huet-Sayegh model.

- 6) *Cohesion and adhesion concepts*: Cohesion and adhesion failures depend on the physico-chemical and mechanical properties of the bonds within the bitumen and at the bitumen-aggregate interface. The physical contribution to adhesion is the aspect most reported in the literature and is based on the principle of surface energy from thermodynamic theory.
- 7) *Fatigue of bituminous materials*: Fatigue can be described as the phenomenon of fracture of a material under repeated or fluctuating stress having a maximum value generally less than the material's tensile strength. In the case of road pavements, which generally carry loads that are considerably lower than the load capacity, but in a cyclically repeatable way, it can be assumed that high cycle fatigue can occur. Cohesion and adhesion failure in the seal can be investigated in terms of fatigue.

From the literature review, the rheological response, the Cohesion Fatigue Damage (CFD) and Adhesion Fatigue Damage (AFD) appear to be fundamental in the investigation of bituminous seal materials performance.

The investigation into the rheological response, and the CFD and AFD of bituminous seal materials is subdivided into laboratory experiments, as described in Chapter 3, the interpretation of the test results, developed in Chapter 4, and the modelling itself, presented in Chapter 5. Chapter 6 discusses the bituminous material input parameters in the modelling of the seal system.



LITERATURE REVIEW

References

- Airey G. D., Liao M. C. and Thom N. H., 2006, Fatigue behaviour of bitumen-filler mastics, paper presented at the 10th International Conference on Asphalt Pavements, Quebec City, Canada, 12–17 August.
- Airey G., Rahimzadeh B. and Collop A., 2003, Visco-elastic linearity limits for bituminous materials, *Proceedings of the 6th International RILEM Symposium on Performance Testing and Evaluation of Bituminous Materials*, pp. 331–338, Zurich, Switzerland.
- Akzo Nobel, 2009, *Adhesion Promoters for Bitumen*, Technical bulletin, Amsterdam, Netherlands.
- Anderson D. A., Rowe G. M. and Christensen D. W., 2008, *Historical and current rheological binder characterization vs. binder performance*, paper presented at the Petersen Asphalt Research Conference, Laramie, WY, US.
- Anderson D. A., Christensen D. W. and Bahia H., 1991, Physical properties of asphalt cement and the development of performance-related specifications, *Journal of the Association of Asphalt Paving Technologists*, 60, 437–532.
- Anderson D. A., Christensen D. W., Bahia H. U., Dongré R., Sharma M. G, Antle C. E and Button J., 1994, *Binder Characterization and Evaluation, Vol. 3: Physical Characterization*, SHRP-A-369, National Research Council, Washington DC, US.
- Asphalt Academy, 2007, *The Use of Modified Bituminous Binders in Road Construction*, Technical Guideline 1 (TG1), 2nd ed., Asphalt Academy/CSIR Built Environment, Pretoria.
- ASTM (American Society for Testing and Materials International), 2002, *Standard Practice for Accelerated Weathering Test Conditions and Procedures for Bituminous Materials (Xenon-Arc Method)*, ASTM D4798-01, West Conshohocken, PA, US.
- ASTM (American Society for Testing and Materials International), 2013, *Standard Practice for Accelerated Aging of Asphalt Binder Using a Pressurized Aging Vessel (PAV)*, ASTM D6521-13, ASTM International, West Conshohocken, PA, US.
- ASTM D4798-01, see ASTM, 2002
- ASTM D6521-13, see ASTM, 2013
- Barnes H. A., Hutton J.F. and Walters K., 1993, *An Introduction to Rheology*, Vol. 3, Elsevier Science, Amsterdam, Netherlands.



LITERATURE REVIEW

- Bell C. A., 1989, *Aging of Asphalt-Aggregate Systems*, Summary Report SR-OSU-A-003A-89-2, Oregon State University, Corvallis, US.
- Bhasin A., 2006, *Development of methods to quantify bitumen-aggregate adhesion and loss of adhesion due to water*, PhD thesis, Texas A&M University, College Station, TX, US.
- Bonaquist R., 2008, *Refining the Simple Performance Tester for Use in Routine Practice*, Report 614, National Cooperative Highway Research Program (NCHRP), Transportation Research Board (TRB), Sterling, VA, US.
- Burnett D. J., Garcia A. R., Granier A., Pellegrin B. and Nguyen T., 2008, *Surface Energies as a Measure of the Interaction between Nanomaterials and Polymer Matrices*, Surface Measurement Systems Ltd, and National Institute of Standards and Technology, SAMPE 2008, Long Beach, CA, US.
- Caltrans (California Department of Transportation), 2003, *Maintenance Technical Advisory Guide (TAG), Chapter 5*, Caltrans Division of Maintenance.
- Chailleux E., Ramond G. and de la Roche C., 2006, A mathematical-based master curve construction method applied to complex modulus of bituminous materials, *Journal of Road Materials and Pavement Design*, 7, 75–92.
- Chipperfield E. H, Duthie J. L. and Girdler R. B., 1970, Asphalt characteristics in relation to road performance, *Proceedings of the American Association of Asphalt Paving Technologists*, 39, 575–613.
- Clyne T. R., Li X., Marasteanu M. O. and Skok E. L., 2003, *Dynamic and Resilient Modulus of MN/DOT Asphalt Mixtures*, MN/RC – 2003-09, Department of Civil Engineering, University of Minnesota, Minnesota Department of Transportation Office of Research Services, US.
- Cole K. S. and Cole, R. H., 1941, Dispersion and absorption in dielectrics. I. Alternating current characteristics, *Journal of Chemical Physics*, 9, 341–351.
- Cole K. S. and Cole, R. H., 1942, Dispersion and absorption in dielectrics. II. Direct current characteristics, *Journal of Chemical Physics*, 1, 98–105.
- Das B. M., 1990, *Principles of Geotechnical Engineering*, 2nd ed., PWS-Kent, Boston, MA, US.
- Dassault Systèmes, 2012, *Abaqus Theory Manual, 22.7.2 Frequency domain visco-elasticity*, Abaqus 6.2, available at:
http://www.maths.cam.ac.uk/computing/software/abaqus_docs/docs/v6.12/books/usb/default.htm?startat=pt05ch22s07abm13.html#usb-mat-cfreqvisco
- Department of the Army (US), 1952, *Geology and Its Military Applications*, TN5-545, p. 7, US.

LITERATURE REVIEW

- Desai C. S., 2002, *Mechanic pavement analysis and design using unified material and computer models*, paper presented at the Symposium on 3D Element Modelling of Pavement Structures, Amsterdam, Netherlands, 2–5 April.
- Di Benedetto H. and Corté J. F., 2005, *Matériaux routiers bitumineux. 2: Constitution et propriétés thermomécaniques des mélanges*, Hermes-Science, Lavoisier, France.
- Di Benedetto H., Delaporte B. and Sauzéat C., 2007, Three-dimensional linear behavior of bituminous materials: Experiments and modelling, *ASCE International Journal of Geomechanics*, 7(2), 149–157
- Di Benedetto H., Gabet T., Grenfell J., Perraton D. and Sauzéat C., Bodin D., 2013, *mechanical testing of bituminous mixtures*, Chapter 4, in *Advances in Interlaboratory Testing and Evaluation of Bituminous Materials*, RILEM State-of-the-art Reports, Vol. IX, Springer, Dordrecht, Netherlands.
- Di Benedetto H., Sauzeat C., Bilodeau K., Buannic M., Mangiafico S., Nguyen Q. T., Pouget S., Tapsoba N. and Van Rompu J., 2011, General overview of the time-temperature superposition principle validity for materials containing bituminous binder, *International Journal of Roads and Airports*, 1(1), 35–52.
- Domone P. and Illstone J. (Eds.), 2010, *Construction Materials: Their Nature and Behaviour*, 4th ed., Taylor & Francis, London.
- Dorn L., 1994, *Adhesive bonding – Terms and definitions, Lecture 4701, Basic level, Training in aluminium application technologies*, European Aluminium Association, Technische Universität, Berlin, Germany.
- Dougan C. E., Stephens J. E., Mahoney J. and Hansen G., 2003, *E* - Dynamic Modulus Test Protocol – Problems and Solutions*, Connecticut Department of Transportation Office of Research and Materials, US.
- Ferry J. D., 1980, *Visco-elastic Properties of Polymers*, John Wiley, New York.
- Flügge W. (Ed.), 1975, *Visco-elasticity*, 2nd ed., Springer-Verlag, Berlin, Heidelberg, New York.
- Garcia G. and Thompson M. R., 2007, *HMA Dynamic Modulus Predictive Models: A Review*, Research Report FHWA-ICT-07-2005, Illinois Centre for Transportation, Rantoul, IL, US.
- Hagos E. T., 2008, *The effect of aging on binder properties of porous asphalt concrete*, PhD thesis, Section of Road and Railway Engineering, Faculty of Civil Engineering and Geosciences, Delft University of Technology, Netherlands.

LITERATURE REVIEW

- Hanson F. M., 1935, Bituminous surface treatment on rural highways, *Proceedings of the New Zealand Society of Civil Engineers*, 21, 83.
- Hefer A. W., 2004, *Adhesion in bitumen-aggregate systems and quantification of the effects of water on the adhesive bond*, PhD thesis, Civil Engineering Department, Texas A&M University, College Station, TX, US.
- Hergt J. M., McDougall I., Banks M. R. and Green D. H., 1989, Igneous rocks. Jurassic dolerite, in: Burrett C. F. and Martin E. L. (Eds.), *Geology and Mineral Resources of Tasmania*, Special Publication of the Geological Society of Australia, 15: 375-381.
- Holtrop W., 2008, *Sprayed Sealing Practice in Australia*, Australian Asphalt Pavement Association, Australia.
- Hopman P.C., Kunst P.A.J.C. and Pronk, A.C., 1989, A renewed interpretation method for fatigue measurements – verification of Miner’s rule, in *Proceedings 4th Eurobitume Symposium*, Madrid, Spain.
- Howson J., Bhasin A., Masad E. A., Lytton L. and Little D., 2009, *Development of a Database for Surface Energy of Aggregates and Asphalt Binders*, Report 5-4524-01-1, Texas Transportation Institute, College Station, TX, US.
- Huurman, M., 2010, Developments in 3D surfacing seals FE modelling, *International Journal of Pavement Engineering*, 11(1), 1–12.
- Janisch D. W. and Gaillard FS, 1998, *Minnesota Seal Coat Handbook Final Report*, Minnesota Department of Transportation Office of Research Services, St. Paul, Minnesota
- Jansen K. M. B., 2006, *Thermomechanical modelling and characterization of polymers*, Lecture Notes, Delft University of Technology, Netherlands.
- Jooste F., 2004, *Re-evaluation of some aspects of the mechanistic-empirical design approach*, paper presented at the 8th Conference on Asphalt Pavements for Southern Africa, Sun City, South Africa.
- Kathirgamanathan P., Herrington P.R. and McIver I., 2012, *Chip seal finite element model*, paper presented at the 7th International Conference on Maintenance and Rehabilitation of Pavements and Technological Control, Auckland, New Zealand.
- King G., Anderson M., Hanson D. and Blankenship P., 2012, Using black space diagrams to predicts age-induced cracking, *Proceedings of the 7th RILEM International Conference on Cracking in Pavements*, pp. 453–463, A. Scarpas et al. (Eds.).
- Lakes R., 2009, *Visco-elastic Materials*, Cambridge University Press, New York, US.



LITERATURE REVIEW

- Leaman D. E., 1973, *The Engineering Properties of Tasmanian Dolerite, with Particular Reference to the Route of the Bell Bay Railway*, Technical Report, Department of Mines Tasmania, 16: 148–163.
- Li Q. and Kumar A, 2003, *National & International Practices in Decision Support Tools in Road Asset Management*, Project 2001-010-C/005, Final report, Queensland Department of Main Roads, Spring Hill, Queensland, Australia.
- Liao M.C, 2007, *Small and large strain rheological and fatigue characterisation of bitumen-filler mastics*, PhD Thesis, University of Nottingham, UK.
- Loulizi A., Flintsch G. W., Al-Qadi I. L. and Mokarem D., 2006, Comparing resilient modulus and dynamic modulus of hot-mix asphalt as material properties for flexible pavement design, Transportation Research Board Annual Meeting, *Transportation Research Record*, 1970(1), 161–170.
- Lurie J., 1984, *South African Geology for Mining, Metallurgical Hydrological and Civil Engineering*, 4th ed., McGraw-Hill, Johannesburg.
- Ma, L. X., Wu S. P., Huang J. F. and Li N., 2008, *Effect of UV aging on components, structure and properties of asphalt*, paper presented at the Second International Conference on Heterogeneous Material Mechanics (ICHMM-2008), Huangshan, China.
- Macosko C. W., 1994, *Rheology: Principles, Measurements, and Applications*, Wiley-VCH, Poughkeepsie, NY, US.
- Mangiafico S., 2014, *Linear Visco-Elastic Properties and Fatigue of Bituminous Mixtures Produced with Reclaimed Asphalt Pavement and Corresponding Binder Blends*, PhD thesis, l'École Nationale des Travaux Publics de l'État, France.
- Marais C. P., 1981, Rational Design of Single Surface Treatment Technique for Road Maintenance, *The Civil Engineer in South Africa*, August 1981.
- Maree, J.H. and Freeme, C.R., 1981, *The Mechanistic Design Method Used to Evaluate the Pavement Structures in the Catalogue of the Draft TRH 4 1980*, Technical Report RP/2/81, National Institute for Transport and Road Research, CSIR, Pretoria, South Africa
- McNaught, A. D. and Wilkinson, A., 1997, Shear modulus, in: *Compendium of Chemical Terminology*, (the "Gold Book"), 2nd ed., Blackwell Scientific Publications, Oxford.
- Medani T. O. and Huurman M., 2003, *Constructing the Stiffness Master Curves for Asphaltic Mixes*, Report 7-01-127-3, Delft University of Technology, Netherlands.
- Meyers M. A. and Chawla K. K., 1999, *Mechanical Behavior of Materials*, Prentice-Hall, Upper Saddle River, NJ, US.



LITERATURE REVIEW

- Milne T. I., 2004, *Towards a performance-related seal design method for bitumen and modified road seal binders*, PhD thesis, University of Stellenbosch, South Africa.
- Milne T. I., Huurman M., Van de Ven M. F. C., Jenkins K. J., Scarpas A. and Kasbergen C., 2004, *Toward mechanistic behaviour of flexible road surfacing seals using a prototype FEM model*, paper presented at 8th Conference on Asphalt Pavements for Southern Africa, Sun City, South Africa.
- Mohammad L. N., Wu Z., Myres L., Cooper S. and Abadie C. A., 2005, Practical look at simple performance tests: Louisiana's experience, *Journal of the Association of Asphalt Paving Technologists*, 74, 557–600.
- Molenaar A. A. A., 2010, *Road paving materials, Part III, Asphaltic materials*, Lecture Notes, CT 4880, Delft University of Technology, Netherlands.
- Muller J. and Jenkins K. J., 2011, *The use of an extended rolling thin film ageing method as an alternative to the pressurised ageing vessel method in the determination of bitumen durability*, paper presented at the 10th Conference on Asphalt Pavements for Southern Africa, KwaZulu-Natal, South Africa, 11–14 September 2011.
- NCHRP (National Cooperative Highway Research Program), 2004, *Guide for Mechanistic-Empirical Design of New and Rehabilitated Pavement Structures*, NCHRP Project 1-37A Available at: <http://www.trb.org/mepdg>.
- Newby B. Z., Chaudhury M. K. and Brown H. R., 1995, Macroscopic evidence of the effect of interfacial slippage on adhesion, *Science*, 269(5229), 1407–1409.
- Olard F. and Di Benedetto H., 2003, *General “2S2P1D” Model and Relation between the Linear Visco-elastic Behaviours of Bituminous Binders and Mixes*, Département Génie Civil et Bâtiment (URA CNRS), Ecole Nationale des TPE, France.
- Oliver J. W. H., 2004, *Prediction of the life of sprayed seals and the effect of climate, durability and seal size*, paper presented at the 6th International Conference on Managing Pavements, Brisbane, Australia.
- Oliver J. W. H., 2011, The effect of binder film thickness on asphalt cracking and ravelling, *Road & Transport Research*, 20(3).
- Oliver J. W. H. and Boer S., 2008, *Optimising sprayed seal life in response to global challenges*, paper presented at the 1st International Sprayed Sealing Conference ARRB Group, Adelaide, South Australia.
- Paterson W. D. O., 1987, *Road Deterioration and Maintenance Effects – Models for Planning and Management*, The World Bank and the Johns Hopkins University Press, Baltimore, MA, US.
- Pell P. S., McCarthy P. F. and Gardner R. R., 1961, Fatigue of bitumen and bituminous mixes, *International Journal of Mechanical Sciences*, 3(4), 247–267.

LITERATURE REVIEW

- Pellinen T. K. and Witczak M. W., 2002, Stress-dependent master curve construction for dynamic (complex) modulus, *Journal of the Association of Asphalt Paving Technologists*, 71, 281–309.
- Petrucci R. H., Harwood W. S., Herring G. F. and Madura J. D., 2007, *General Chemistry: Principles and Modern Applications*, AIE. Pearson/Prentice Hall, Upper Saddle River, NJ, US.
- Placet V., Passard J. and Perré P., 2009, *Visco-elastic properties of green wood across the grain measured by harmonic tests in the range of 0°C to 95°C - Hardwood vs. softwood and normal wood vs. reaction wood*, Laboratoire d'Etude et de Recherche sur le Matériau Bois, LERMAB-UMR INRA/ENGREF/UHP 1093, Nancy, France
- Pronk A.C., Kans L. and Gogh F., 1996, *Temperature increase in an asphalt beam during fatigue – theory and practice*, in: Road Research Workshop, CROW, Ede, Netherlands.
- Read J. and Whiteoak D., 2003, *The Shell Bitumen Handbook*, 5th ed., Shell UK Oil Products Limited, UK.
- Road Research Laboratory (UK), 1962, *Bituminous Materials in Road Construction*, Department of Scientific and Industrial Research, Her Majesty's Stationery Office, London.
- Rowe G.M. and Bouldin M.G., 2000, Improved techniques to evaluate the fatigue resistance of asphalt mixtures, in: *Proceedings of Euroasphalt & Eurobitume Congress*, Barcelona, Spain.
- Roylance D., 2001, *Engineering visco-elasticity – Polymer and composites*, Lecture Notes for 3.60s, Massachusetts Institute of Technology, Boston, MA, US.
- SABITA (Southern African Bitumen Association), 1993, *Appropriate Standards for Bituminous Surfacing*, Manual 10, Cape Town, South Africa.
- SABITA (Southern African Bitumen Association), 2007, *Bituminous Binders for Road Construction and Maintenance*, Manual 2, 4th ed., Cape Town, South Africa.
- SANRAL (South African National Roads Agency Limited), 2007, *Design and Construction of Surfacing Seals*, Technical Recommendations for Highways (TRH 3), Version 1.5, Pretoria, South Africa
- Schram S. and Abdelrahman M., 2009, Mechanistic-empirical modelling in network-level pavement management, *Journal of the Transportation Research Board*, No. 2093, pp. 76–83, Washington DC, US.
- Schultz J. and Nardin M., 1994, Theories and mechanisms of adhesion, in Pizzi A. and Mittal K. L. (Eds.), *Handbook of Adhesive Technology*, pp. 19–33, New York, Marcel Dekker.



LITERATURE REVIEW

- Semmelink C. J., 1987, A rational design approach for single and double surfacing seals based on the modified tray test, *Transportation Research Record*, 1106, 1, 202–207.
- Shuler S., Lord A., Epps-Martin A. and Hoyt D., 2011, *Manual for Emulsion-Based Chip Seals for Pavement Preservation*, NCRHP Report 680, Transportation Research Board (TRB), Washington DC, US.
- Soleimani A., 2009, *Use of dynamic phase angle and complex modulus for the low temperature performance grading of asphalt cements*, MSc thesis, Department of Chemistry, Queen's University, Kingston, Ontario, Canada.
- Sybilski D., Soenen H., Gajewski M., Chailleux E. and Bankowski W., 2013, Binder Testing, *Advances in Interlaboratory Testing and Evaluation of Bituminous Materials*, RILEM State-of-the-Art Report, Vol. IX, Springer, Dordrecht, Netherlands.
- Tarrer A. R. and Wagh V., 1993, *The Effect of the Physical and Chemical Characteristics of the Aggregate on Bonding*, Report SHRP-A/UIR-91-507, Strategic Highway Research Program, National Research Council, Washington DC, US.
- Theyse H. L., de Beer M. and Rust F. C., 1996, *Overview of the South African mechanistic pavement design analysis*, paper presented at the 75th Annual Transportation Research Board Meeting, Washington DC, US, 7–11 January 2011.
- Theyse H. L., Maina J. W. and Kannemeyer L., 2007, Revision of the South African flexible pavement design method; mechanistic-empirical components, *Proceedings of the 9th Conference on Asphalt Pavements for Southern Africa*, Gaborone, Botswana, 2–5 September 2007, pp. 256–292.
- Theyse H.L., de Beer M., Maina J. W. And Kannemeyer L., 2011, *Interim revision of the South African mechanistic-empirical pavement design method for flexible pavements*, paper presented at the 10th Conference on Asphalt Pavements for Southern Africa, KwaZulu-Natal, South Africa, 11–14 September 2011.
- Tran N. and Hall K. D., 2006, Evaluation of testing protocols for dynamic modulus of hot mix asphalt, *Transportation Research Record*, 1970.
- TRH 3, 2007, see SANRAL, 2007
- Vallerga B. A., 1981, Pavement deficiencies related to asphalt durability, *Proceedings of the Association of Asphalt Paving Technologists*, 50, 481–491.
- Van der Poel C. A., 1954, General system describing the visco-elastic properties of bitumens and its relation to routine test data, *Journal of Applied Chemistry*, 4, 231–236.
- Van Dijk W., 1975, Practical fatigue characterisation of bituminous mixes, *Proceedings of the Association of Asphalt Paving Technologists*, 44, 38–72.

LITERATURE REVIEW

- Van Lent D., 2008, *Aggregate characterisation in relation to bitumen-aggregate adhesion*, MSc thesis, Department of Road and Railway Engineering, Faculty of Civil Engineering and Geosciences, Delft University of Technology, Netherlands.
- Vert M., Doi Y., Hellwich K. H., Hess M., Hodge P., Kubisa P., Marguerite Rinaudo M. and Schué F., 2012, Terminology for biorelated polymers and applications, *Pure and Applied Chemistry*, 84(2), 377–410.
- Von Fraunhofer J.A., 2011, Adhesion and cohesion, Hindawi Publishing Corporation, *International Journal of Dentistry*, 2012, 1–7.
- Weinert H. H., 1980, *The Natural Road Construction Materials of Southern Africa*, H & R Academica, Cape Town.
- Williams M. L., Landel R. F. and Ferry J. D., 1955, *The Temperature Dependence of Relaxation Mechanisms in Amorphous Polymers and Other Glass-forming Liquids*, Department of Chemistry, University of Wisconsin, US.
- Woldekidan M. F., 2011, *Response modelling of bitumen, bituminous mastic and mortar*, PhD thesis, Department of Road and Railway Engineering, Faculty of Civil Engineering and Geosciences, Delft University of Technology, Netherlands.
- Woo W. J., Ofori-Abebresse E., Chowdhury A., Hilbrich J., Kraus Z., Martin A. E. and Glover C. J., 2007, *Polymer Modified Asphalt Durability in Pavements*, Texas Department of Transportation Research and Technology Implementation, Austin, TX, US.
- Xiang L., Tu J., Cheng J. and Que G., 2010, *Outdoor Aging of Road Asphalt and SBS Modified Asphalt*, Higher Education Press and Springer-Verlag, Berlin, Heidelberg.
- Yusoff N. I. M., 2012, *Modelling the linear visco-elastic rheological properties of bituminous binders*, PhD thesis, University of Nottingham, UK.
- Yusoff N. I. M., Shaw M. T. and Airey G. D., 2011, Modelling the linear visco-elastic rheological properties of bituminous binders, *Construction and Building Materials*, 25(5), 2171–2189.



3 EXPERIMENTAL PROGRAMME

3.1 Introduction

In an attempt to develop performance prediction for seal materials, it was decided that the following investigations, regarded as fundamentals, should be done:

- 1) *Rheological response modelling* of the bitumen under simulated traffic forces and environmental effects (ageing and water effect). It was proposed that the rheological modelling of bituminous binder behaviour should form part of the response model and should be constituted by:
 - the linear viscoelastic rheological models (Prony series, Huet-Sayegh and 2S2P1D) representing the complex modulus (G^*) and phase angle (δ) of four fresh bitumens from a plant and 49 bitumens recovered from a “field-aged” seal. The fresh bitumens from the plant were investigated in the following conditioning states or combinations of such states: fresh (Unaged); aged (by PAV method or by weatherometer (Q-SUN) method), or conditioned in water.
 - an ageing model based on the different ages of recovered bitumens from field-aged seals.
- 2) *Modelling of the damage mechanism* in the seal structure. Such damage could comprise two phenomena: Cohesion Fatigue Damage (CFD) and Adhesion Fatigue Damage (AFD). It was proposed to split the fatigue modelling into two components:
 - transfer function modelling, which would focus on the applied stress as a function of number of repetitions to failure – this is termed the “end-life fatigue damage”
 - fatigue damage modelling, which would represent the evolution of damage over the life of the seal. This damage is expressed as a function of parameters such as stress and temperature – this is termed the “accumulated fatigue damage”.
- 3) *The development of testing protocols* related to CFD and AFD.



LABORATORY EXPERIMENTS

Laboratory investigations were required in order to develop the behaviour response and the damage of the bituminous materials for later modelling.

The Dynamic Shear Rheometer (DSR) appeared to be a favourable choice for performing the three identified tests on bituminous materials, namely:

- the bitumen response test; modelling
- the Cohesion Fatigue Damage (CFD) test
- the Adhesion Fatigue Damage (AFD) test.

The traffic loading during the testing was simulated by the dynamic effect of the DSR. The environmental effect during the response test was replicated by varying the temperature, and by use of laboratory ageing of binder, recovered bitumen from field-aged seals, and bitumen conditioned in water. For the CFD and AFD tests, the environmental effect was replicated only by varying the temperature during the test.

Although, major tests were performed with DSR, a comprehensive bitumen specification tests were executed to confirm the quality of bitumen. Specification tests performed are listed in **Table 3-1**. Details on different type of bitumen specification tests performed are provided in Appendix D.

Table 3-1: Binders specification tests

	Type of binder	Test method
1	70/100 penetration grade (pen)	SANS 307:2005 (2005)
2	60% Cationic spray grade	SANS 307:2005 (2005)
3	SBS polymer modified (SE1)	TG 1 (2007)
4	Bitumen Rubber (SR1)	TG 1 (2007)

This laboratory experiment methodology lists the different materials used for the experiment, describes briefly the DSR equipment and its operation, presents the preparation and conditioning of samples, and the development of the testing procedures for CFD and AFD, and discusses the testing approach and protocols for CFD and AFD tests.

3.2 Bituminous Materials Used for the Experiment

The research considered specific types of bitumen and stone commonly used in South Africa. The following bituminous binders were selected and fresh samples collected from plant:

- Penetration bitumen (70/100): from TOSAS – sourced from Natref;
- Polymer modified bitumen (SE1): from COLAS (B/NKC, 53/12, NB 2)
- 60% Cationic spray grade emulsion, KRS 60, (SCE1): from TOSAS
- Rubber crumb ex tire, Bitumen Rubber, (SR1): from TOSAS

A verification of the type and the grade of all bitumens used in the research was performed. Related classification tests confirm the quality of these bitumens is presented in Appendix D.

All modified bitumen contained as base bitumen 70/100.

In addition to the fresh bituminous binders listed above, 28 samples of 70/100 and 21 samples of SE1 binders, recovered from different field aged seals across South Africa were used. The recovery process was performed according to BE-TM-BINDER-1-2006 (2014); this is a combination of parts of the following specifications and documents: TMH 1 C7 (b) (1986); ASTM D 1856 (2009); ASTM D 2172 (2011); van Assen (1997), and Mturi *et al.* (2013).

The stone used in the adhesion test was a basic aggregate, the dolerite (Dol): from Trichardt crushers in Trichardt, Mpumalanga, South Africa.

3.3 Basic description of the Dynamic Shear Rheometer (DSR)

According to the Asphalt Institute (1997), the ideal testing equipment for addressing both the loading time and temperature behaviour dependency of bituminous binders is the DSR. The DSR is adapted for use with bituminous binders to evaluate both time and temperature effects. When used to test bituminous binders, it measures the rheological properties (complex shear modulus and phase angle).

The DSR can accommodate the following accessories: a nitrogen vessel and a temperature test chamber to regulate the testing temperature; a compressor to

LABORATORY EXPERIMENTS

control the bearing system; and a computer with a software program. The test results of the DSR are available from software output files. The DSR and its essential accessories are shown in **Figure 3-1**.

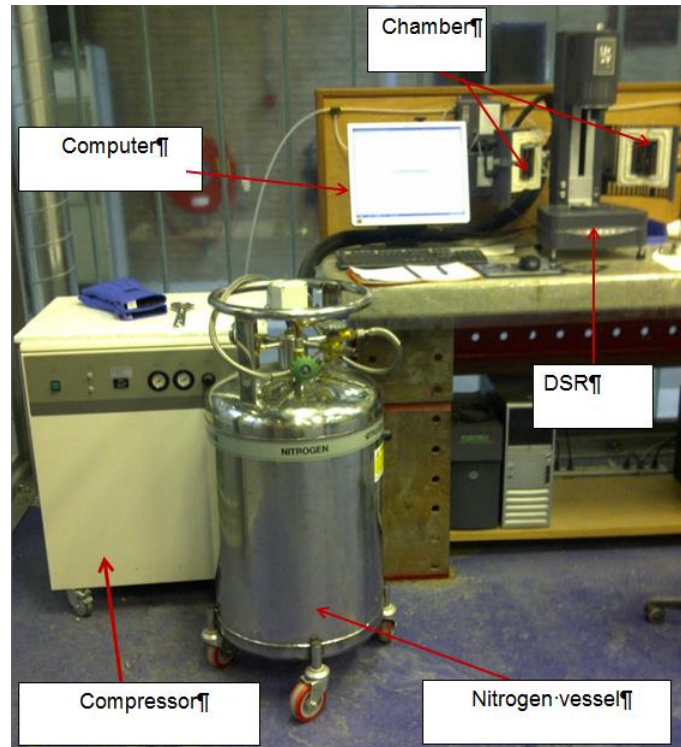


Figure 3-1: DSR and its accessories

The basic DSR operation consists of placing bitumen between two parallel plates, one that is fixed (stator) and the other that oscillates (rotor). The stator and the rotor are also called the “measuring system” or “geometry”.

Figure 3-2 represents the DSR operation schematically. The testing is carried out by oscillating the spindle about its own axis such that a radial line through point A moves to point B, then reverses direction and moves through point A to point C, followed by moving back from point C to point A. The procedure during DSR testing is that the responding strain/stress measurement is determined by applying a torque to a puck-shaped bituminous specimen in response to the applied stress-strain (Liao, 2007; Airey, 1997).

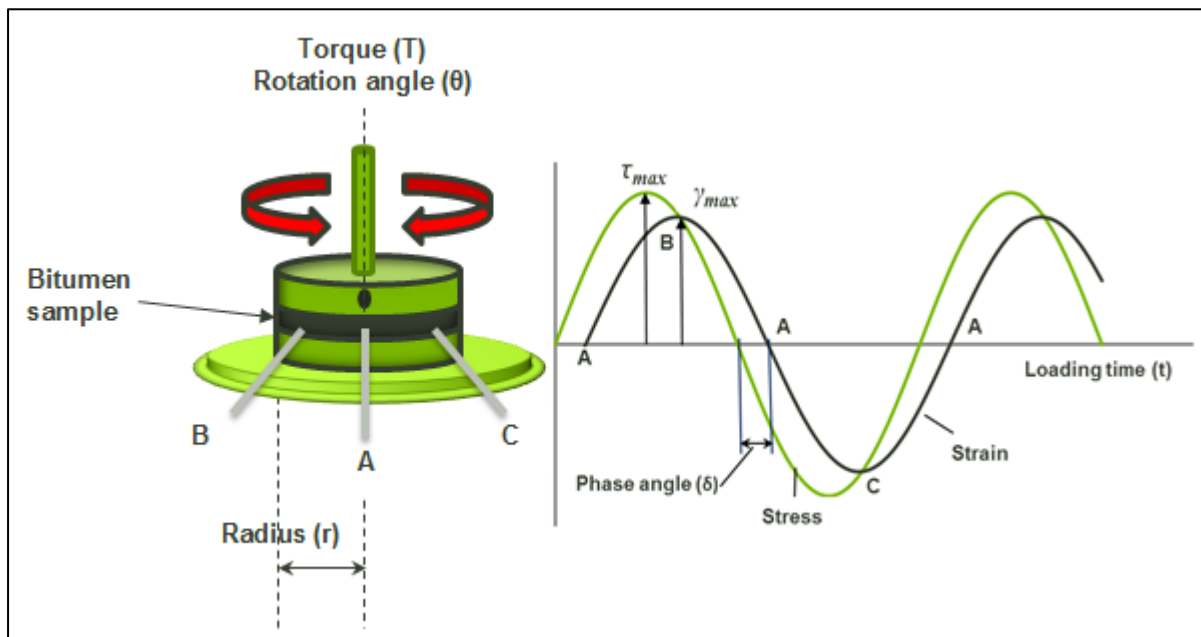


Figure 3-2: Schematic representation of DSR operation.

The latest DSR models are capable of handling many different types of measuring systems that allow for the testing of various types of sample. Common types of measuring systems are:

- parallel plate,
- cone and plate,
- concentric cylinders (single or double gap),
- solid torsional bar fixture.

For a specific test and/or sample, the geometry can be chosen to provide the optimum working ranges of strain or strain rate, and stress. [Figure 3-3](#) depicts the DSR testing setup of basic test (parallel plate configuration).

LABORATORY EXPERIMENTS

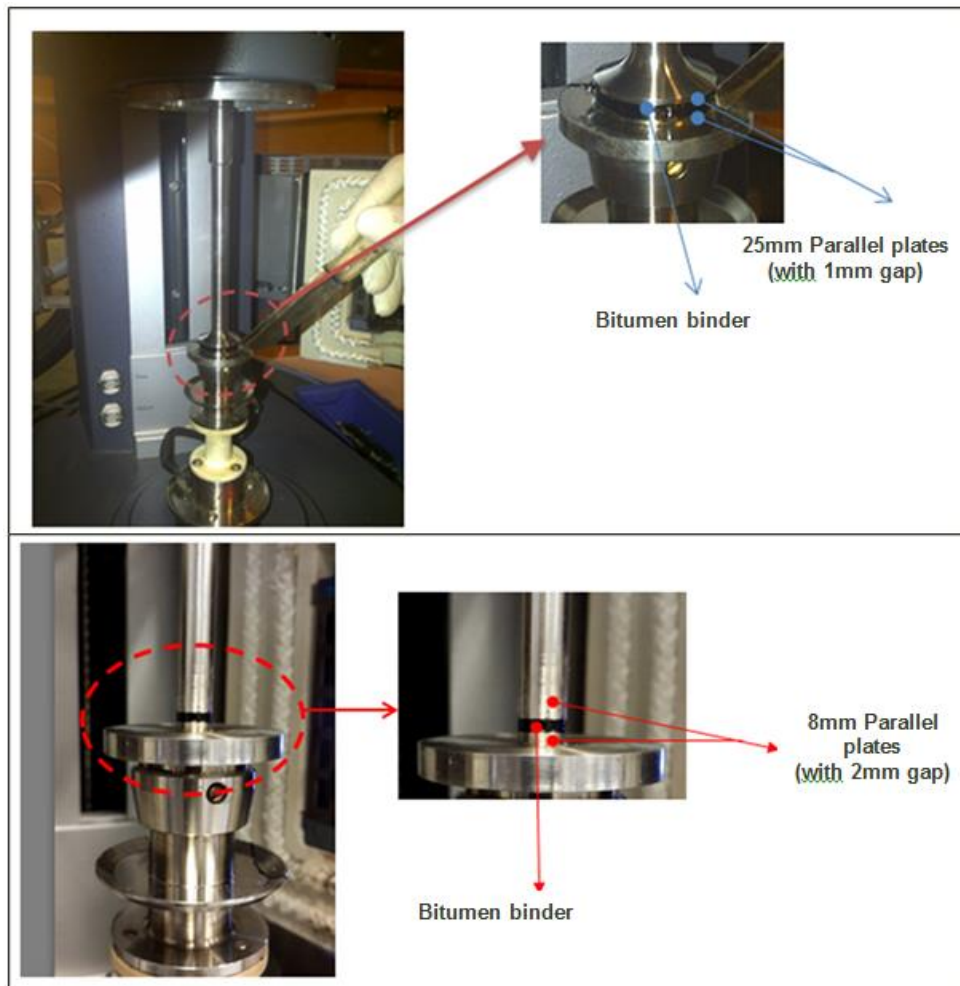


Figure 3-3: DSR Parallel plate configuration

Hagos (2008) and Mangiafico (2014) presented the development of the calculation of the shear stress and shear strain (see Figure 3-4 and Equation 3-1 to Equation 3-8).

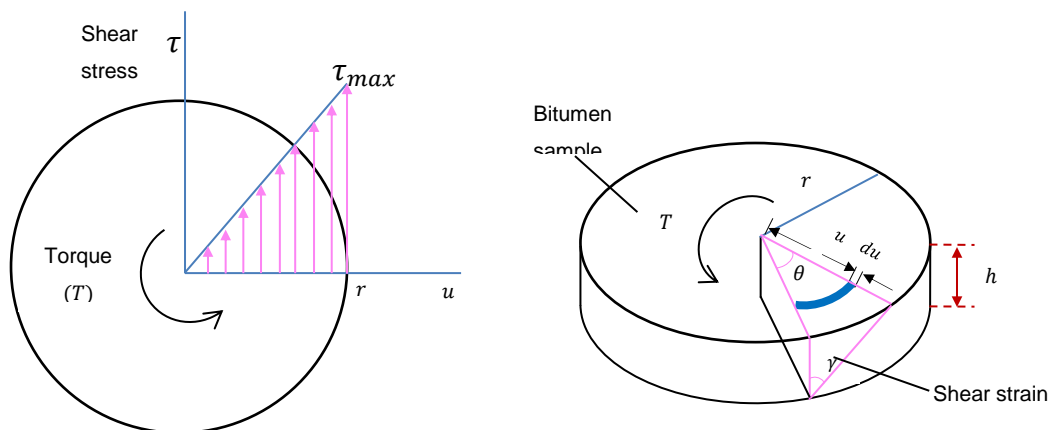


Figure 3-4 : Representation of Shear stress and strain in bitumen during DSR test.



LABORATORY EXPERIMENTS

$$\tau_{max} = \frac{T \cdot r}{I} \quad \text{Equation 3-1}$$

$$I = \int_0^r u^2 dA = \int_0^r u^2 (2\pi \cdot u du) = \frac{1}{2} \pi r^4 \quad \text{Equation 3-2}$$

$$\tau_{max} = \frac{2T}{\pi r^3} \quad \text{Equation 3-3}$$

$$\gamma = \frac{u}{h} \theta \quad \text{Equation 3-4}$$

$$\gamma_{max} = \frac{r}{h} \theta \quad \text{Equation 3-5}$$

$$G^* = \frac{\tau_{max} - \tau_{min}}{\gamma_{max} - \gamma_{min}} \quad \text{Equation 3-6}$$

$$\omega = \frac{1}{t} = 2\pi f \quad \text{Equation 3-7}$$

$$\delta = 2\pi f \cdot \Delta t = \omega \cdot \Delta t \quad \text{Equation 3-8}$$

where

I is the moment of inertia

τ is the shear stress [Pa]

T is the torque [mNm]

γ is the shear strain [%]

r is the radius of the sample [mm]



LABORATORY EXPERIMENTS

- h is the sample thickness [mm]
- θ is the deflection angle [rad]
- δ is the phase angle [$^{\circ}$]
- f is the frequency [Hz]
- ω is the radial frequency [rad/s]
- Δt is the time lag [s]
- G^* is the complex modulus [Pa]

3.3.1 Bitumen frequency sweep response test using the DSR

The bitumen frequency response test is a standard DSR test as described in standards such as AASHTO T315 (2005). This test often uses the parallel plate configuration. The purpose of this test is to provide visco-elastic response parameters such as G^* and δ at different temperatures and different frequencies for different bitumens. The test is generally performed as strain controlled, in sweep frequency mode. The bitumen film shear test uses the parallel plate measuring system. The diameter and the gap between the plates depend on the testing temperature. A guide to the choice of plate size and gap is given in Table 3-2.

Table 3-2: Guide to choice of plate size and gap as a function of testing temperature

Temperature range [$^{\circ}$ C]	Plate diameter [mm]	Gap [mm]
0- 30	8	2
>30	25	1

The DSR test can provide a range of data from the sample, among which can be listed: frequency, temperature, phase angle, complex modulus, deflection angle, normal force, normal stress, oscillation stress, strain, time, damping factor and torque.

3.3.2 DSR testing for cohesion fatigue damage and adhesion fatigue damage tests

In addition to the bitumen frequency sweep response test, the DSR was specially used to investigate CFD and AFD and failure in the seal system. This was an adaptation of work done on porous asphalt in the Netherlands (Huurman, 2007). The special DSR setups for CFD and AFD tests are presented respectively in Sections 3.3.3 and 3.3.4.

3.3.3 Special DSR setups for cohesion fatigue damage test

The CFD test was performed using a bitumen column 6 mm in diameter and 20 mm high, fitted with stainless steel rings 8 mm in diameter and 4 mm high at each end. A clamping system was mounted to the DSR to hold the two ends of the bitumen column via the stainless rings. The test was performed in time sweep regime. The bitumen column setup for the CFD test is shown in Figure 3-5.

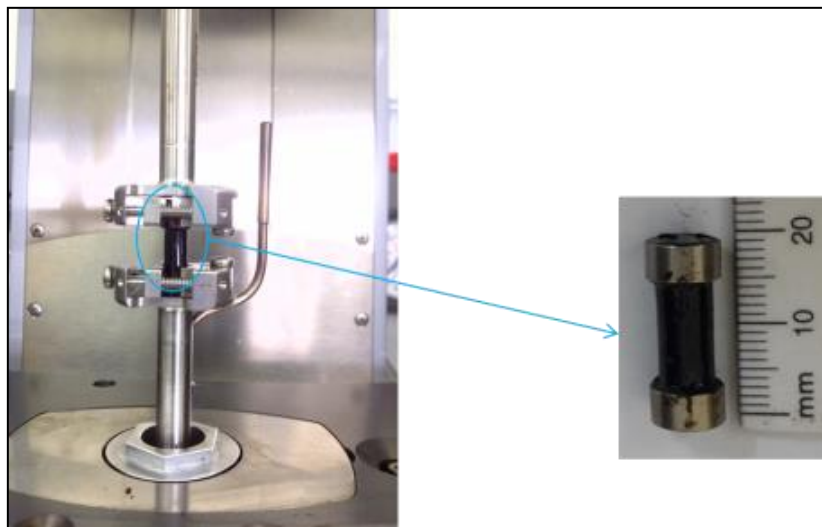


Figure 3-5: Bitumen column configuration for the DSR cohesion fatigue damage test

3.3.4 Special DSR setups for adhesion fatigue tests

The AFD tests were performed using stone columns 10.9 mm in diameter and 15 mm high, glued together by a bitumen film of not more than 100 μm . A clamping system was mounted to the DSR to hold the two ends of the bitumen column. The AFD test was also in time sweep regime. The stone column setup for the AFD test is shown in Figure 3-6.

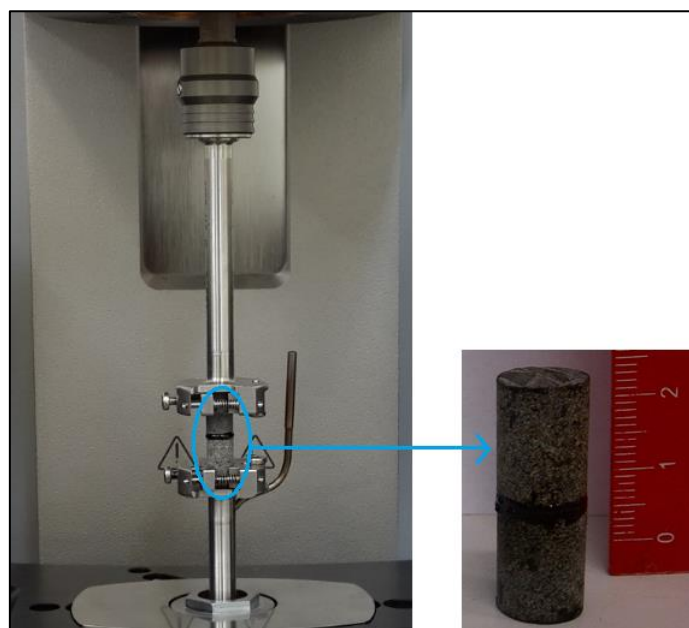


Figure 3-6: Stone column configuration for the DSR adhesion fatigue damage test

3.4 Sample Preparation and Conditioning

The samples prepared for the DSR tests consisted of a combination of dolomite stones and bitumen.

The stones were cored from dolomite rocks. In order to prepare stone-bitumen contact faces, stones were saw cut but not polished. The aim was to simulate the real surface texture as closely as possible at the stone-bitumen interface. In addition to stone columns 10.9 mm in diameter, further stone columns 6 mm in diameter and

10 mm high were used for supplementary tests. The two types of stone column are shown in Figure 3-7.



Figure 3-7: 10.9 mm and 6 mm stone columns

During the investigation, the bitumen was used in different conditioning states:

- fresh bitumen from plant (unaged and unconditioned)
- bitumen conditioned in water using a vacuum vessel (conditioned)
- bitumen aged by the Pressure Ageing Vessel (PAV) method (PAV aged)
- bitumen aged by the weatherometer (Q-SUN) method (Q-SUN aged)
- combined conditions as stated.

The PAV ageing was done according to method described by AASHTO R28-12 (2012). The water conditioning by vacuum vessel as adapted from Khedoe and Moraal (2007) is presented in Section 3.4.1, and the ageing using the Q-SUN weatherometer is described in Section 3.4.2.

3.4.1 Water conditioning by vacuum vessel

The vacuum vessel is placed at room temperature. The water conditioning is done by submerging the sample in demineralised water in the vacuum vessel and applying

LABORATORY EXPERIMENTS

the vacuum. The vacuum is applied at 0.9 bar below the atmospheric pressure for 90 minutes. The conditioning time is extended in three cycles of 30 minutes each. One cycle consists of 15 minutes of applying the vacuum and a 15-minute rest period. It should be noted that a “15-minute rest period” is dictated by the capacity of the supply pump. The conditioning by vacuum vessel is depicted in Figure 3-8.



Figure 3-8: Water conditioning by vacuum vessel

3.4.2 Ageing by Q-SUN

3.4.2.1 Q-SUN Apparatus and setup

The weatherometer used for ageing the bitumen was a Q-SUN apparatus from the Council for Scientific and Industrial Research (CSIR), Pretoria, South Africa. This apparatus and the setup for bitumen ageing are presented in Figure 3-9 to Figure 3-12.

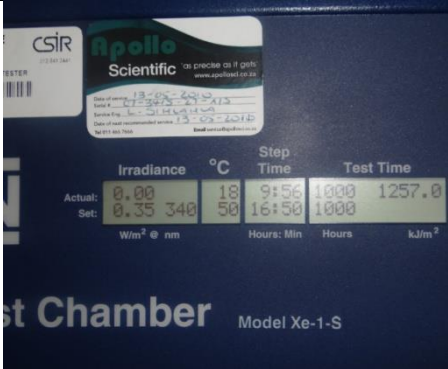



Figure 3-9: External view of the Q-SUN



Figure 3-10: Loading of bitumen

LABORATORY EXPERIMENTS

	samples
	
Figure 3-11: Q-SUN testing parameters	Figure 3-12: Samples after Q-SUN test

3.4.2.2 Q-SUN protocol

This protocol was established from ASTM standard D 4798-01 (2002), and the weatherometer ageing protocol as defined by Hagos (2008):

- Temperature: 50°C
- UV light (340 nm): 0.35 W/m²
- Ageing time: 1 000 hours (analysis time 1 000 hours) in the following hourly cycle: 51 minutes of light exposure, 9 minutes of light and water spray.

3.5 Development of Testing Procedures for Cohesion and Adhesion Fatigue Damage

Challenges were expected and experienced during the testing of the special CFD and AFD samples. In attempting to overcome these challenges, a testing procedure was developed, which led to the establishment of cohesion and adhesion testing protocols. The development of these sample preparation and testing protocols was based on the previous tests done at the Laboratory of Geoscience, Road and Railway Engineering, Delft University of Technology (Khedoe and Moraal, 2007).

The development of the testing procedure is discussed in this section, and the CFD and AFD testing protocols are presented in Section 3.7.

The following challenges were faced during the testing:



LABORATORY EXPERIMENTS

- The stabilisation of the testing temperature in the chamber: probably due to the use of the clamping system
- The choice of testing parameters, such as testing temperature, testing frequency, torque level, strain level, maximum testing time, etc.
- The choice of testing mode between strain-controlled and stress-controlled mode
- The impact of configuration changes to the DSR geometry on the test output (e.g. changing from parallel plate configuration to stone column configuration)
- The comparison between tests done in pure shear mode and tests done in combined shear and normal stress mode
- The influence of the binder film thickness between stones (in the AFD test) on the mode of failure (AFD failure or CFD failure)
- The verification of testing repeatability
- The binder fatigue related to changes in the sample radius
- The use of parallel plates for the CFD test.

3.5.1 Stabilisation of testing temperature in the chamber

The testing of visco-elastic material using the DSR requires high accuracy of the testing temperature (the tolerance used was within 0.1°C). It was noticed during the test that the use of the clamping system induced instability in the testing temperature in the chamber. After enquiries to the supplier, it was recommended to ensure that the clamping system is connected to the DSR operating system and that the link is maintained (e.g. by means of firmware control).

3.5.2 Choice of testing parameters

The testing parameters for the CFD and AFD tests are presented in Table 3-3.



Table 3-3: Testing parameters for cohesion fatigue damage and adhesion fatigue damage

Test type	Strain [%]	Torque [mNm]	Frequency [rad/s]	Max time [hours]	Temperature [°C]
CFD	2%	1 to 50	62.8	2	0;5; 10 ;15; 20; 23; 25
AFD	2%	50 to 200	62.8	2	10; 20; 23; 25

- *Testing temperature:* The temperature delimits the consistency of bitumen and has a major influence on the results. At lower temperatures the bitumen is stiffer than at high temperatures. In general, testing at a lower temperature was difficult to perform, especially for the adhesion test. Immediate failure of sample was often observed in the case of adhesion. This might explain the fact that adhesion in an adhesion test is not prone to fatigue. The test temperature ranged from 0 °C to 25 °C.
- *Testing frequency:* Happian-Smith (2000) mentioned two natural frequencies of an automobile: the lower frequency ranging from 1 to 2 Hz (6.28 to 12.56 rad/s) and another frequency around 10 to 11 Hz (62.83 to 69.12 rad/s). Hagos (2002) reported that the frequency equivalent to a moving vehicle at 80 km/h is 1.6 Hz (10.05 rad/s). González *et al.* (2008) mentioned frequencies of vehicle varying between 1 and 15 Hz (98.3 Hz). The selected frequency was 62.8 rad/s (10 Hz), as this frequency represents an acceptable value in the range of moving vehicles on the road. However, it was noted that increasing the frequency reduced the fatigue failure time of the sample.
- *Strain level:* A test done in the linear visco-elastic domain is defined by a specific range of strain. It appears that fatigue failure does not always occur in the visco-elastic range. This can also happen in the visco-plastic state of bitumen. Collop *et al.* (2003) highlighted the effect of visco-plastic components in the damage mechanism of bituminous materials. Thus, it was not necessary to determine this range in the CFD and AFD tests. However, the



LABORATORY EXPERIMENTS

value of strain was kept constant (2 per cent). An increase in the level of strain tends to reduce the failure time of the sample.

- *Torque level:* The choice of the torque level was crucial. An inappropriately high torque led to the sample experiencing immediate failure and a very low torque did not allow failure in the limited time available. The torque level is related to the height of the sample. The sample for CFD was 12mm high and the AFD sample was 100 μ m high. As the thickness reduces torque required to generate the set 2% strain increase. It should also be noted that the AFD test has a larger diameter requiring a higher torque. It was found that the AFD tests required higher torque (between 50 mNm and 175 mNm) than the CFD tests (in which torque was ranged between 1 mNm and 50 mNm).
- *Testing time:* Due to the time and cost constraints, the testing time was a parameter to be optimised taking into account the fact that the fatigue phenomenon is a relatively slow process which requires a stress or strain value below the inherent strength of the material. A testing time of two hours appeared to satisfy these constraints for CFD and AFD tests with 70/100 bitumen. It can be anticipated that for stiffer bitumens (such as modified bitumen and bitumen rubber) the testing time could be increased.

3.5.3 Choice of testing mode: strain controlled vs. stress controlled

Domone and Illstone (2010) reported that fatigue tests can be conducted in two different modes: constant stress or stress-controlled mode (in which the load is applied to the same level regardless of the resulting strain) and constant strain or strain-controlled mode (in which the strain developed in the sample remains constant regardless of the stress induced).

Both stress-controlled and strain-controlled tests were performed. A number of tests were initially done under strain-controlled mode. This was based on Monismith and Deacon (1969) that recommended strain control for thin layers (such as surfacing layers) and the use of stress control for thick structural layers. The results of the strain-controlled tests appeared to be inconsistent, as shown in Figure 3-13. Subsequent to the strain-controlled tests, stress-controlled tests were performed. These results displayed continuous reduction of G^* with time, and a clear failure time

LABORATORY EXPERIMENTS

was characterised by a sudden drop in the G^* value (i.e. an almost vertical drop) and a sudden increase in the deflection angle (θ). This might be explained by the “immediate and catastrophic failure” nature of stress-controlled test as described in Section 2.11.2. Figure 3-14 presents the outcome of the stress-controlled tests.

Stress-controlled mode was used for CFD and AFD tests.

The stress-controlled mode appeared to be the most reliable way of assessing the fatigue damage. In addition, it is suggested that the stress-controlled mode better reflects the interaction between a pavement and external forces. Pavements are often subjected to stress and react by means of deformation and strain. The opposite way – inducing the strain in the pavement to produce a stress – is unlikely to happen in reality.

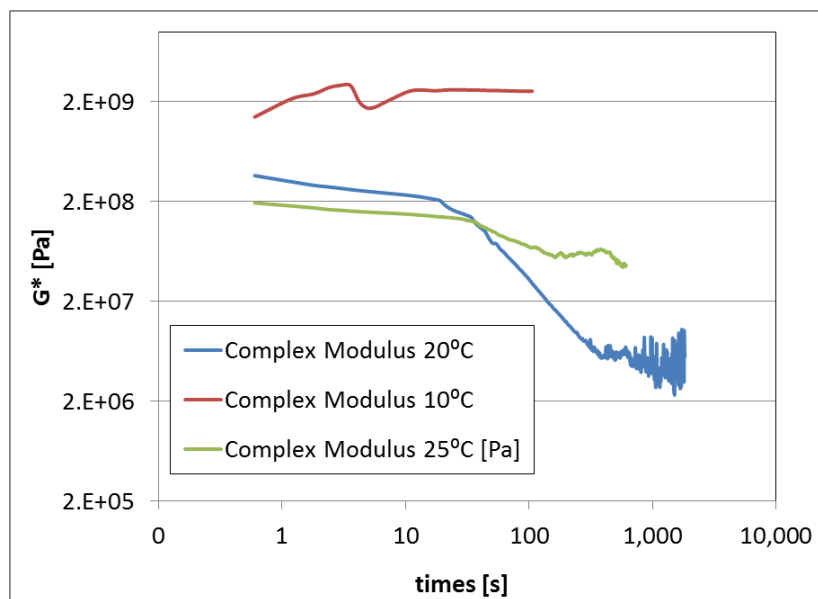


Figure 3-13: Complex modulus vs. time in strain-controlled mode at different temperatures for adhesion (DoI_70-100_Unaged-Cond_25C_0.75%_31.4_10.9)

LABORATORY EXPERIMENTS

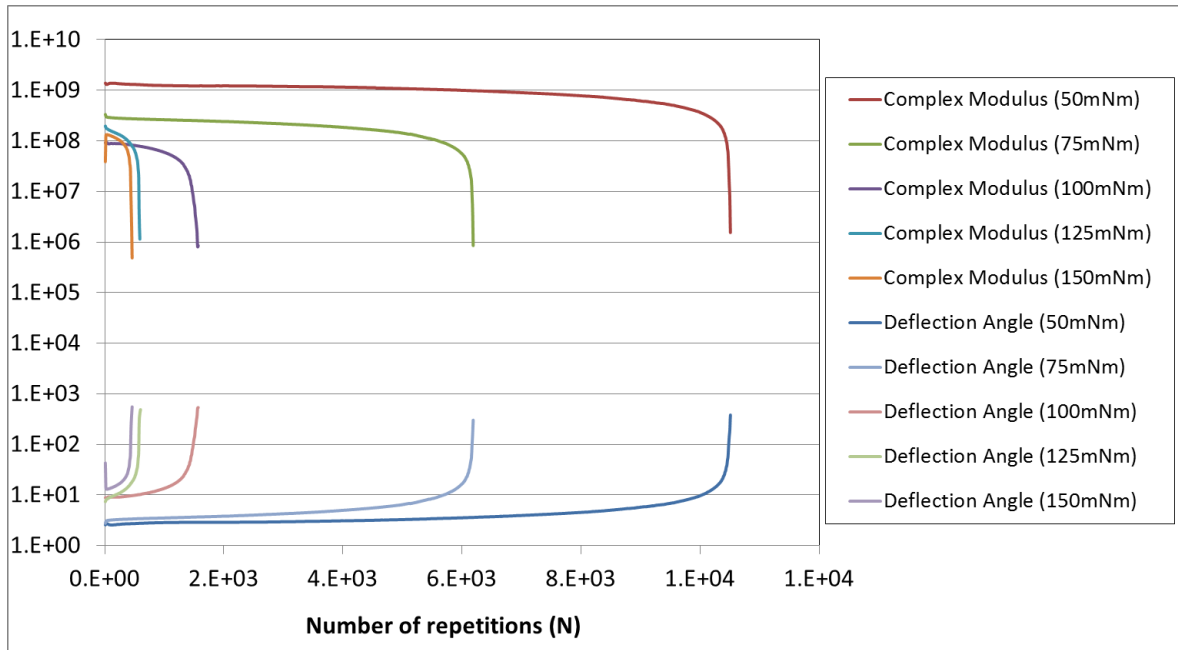


Figure 3-14: Complex modulus and deflection angle vs. time in stress-controlled mode at different temperatures for adhesion (DoI_70-100_Unaged_Uncond_25C_62.8_10.9_stress controlled)

3.5.4 Impact of changes in DSR geometry configuration on the test output

This impact was assessed by changing from parallel plate configuration to stone column configuration during the frequency sweep response test. The assessment consisted of comparing the complex modulus from different configurations. The change of gap between the stator and the rotor of DSR was used as comparison parameter.

In addition to the initial parallel plate tests, two test attempts were carried out using stone columns of 6 mm diameter and 10.9 mm diameter. All three tests setups are described in Table 3-4.

LABORATORY EXPERIMENTS

Table 3-4: Description of test setups for geometry configuration changes

Configuration	Bitumen	Rotor–stator gap [mm]	Type of test	DSR type and testing location
Parallel plate – 8mm diam.	70/100 – unaged-unconditioned	1	Frequency sweep	AR2000, TU Delft (Netherlands)
Dolerite stone column-6mm diam.	70/100 – unaged-unconditioned	11.93	Frequency sweep	AR2000, TU Delft (Netherlands)
Dolerite stone column-10.9mm diam.	70/100 – unaged-unconditioned	17	Frequency sweep	MCR302, SRT (South Africa)

The complex modulus master curves resulting from the tests are presented in Figure 3-15.

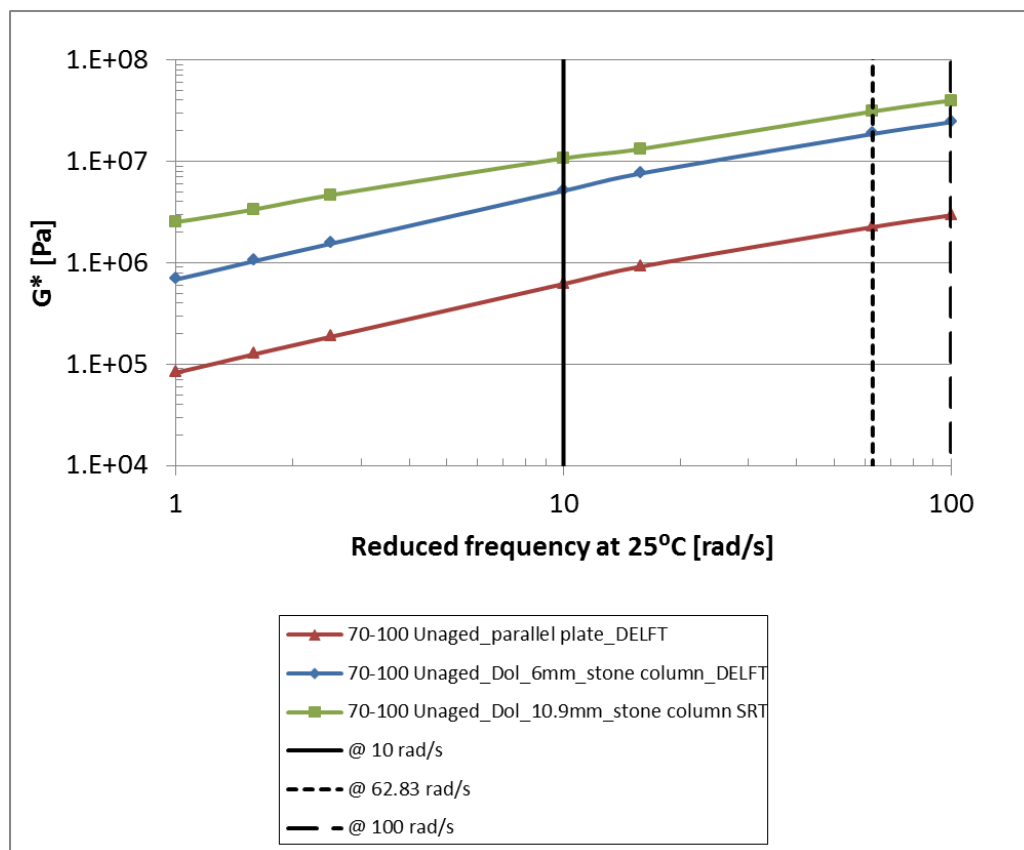


Figure 3-15: Comparison of parallel plate–stone column configurations based on the complex modulus



LABORATORY EXPERIMENTS

Based on this comparison, it appears that the gap between the top and bottom geometries of the DSR might influence the stiffness measured; the higher the gap, the higher the complex modulus. It should be noted that factors such as no linearity of viscoelastic range in the damage test and temperature equilibrium along the sample could also influence the variation of complex modulus as function of the gap. In the case of the no linearity of viscoelastic range, the shear rate across the sample would not be constant, thus the material is likely soft and trends to sag. Regarding the temperature equilibrium, the larger the sample the longer it will take to reach the equilibrium temperature.

From the tests conducted, the relationship between complex modulus and gap change could be expressed as an exponential function. Table 3-5 and Figure 3-16 represent this relationship. It should also be noted that sample diameter (which was not considered in the relationship) could affect the complex modulus results. It is advisable to confirm this relationship by increasing the number of tests and using a constant sample diameter for all the test configurations.

Further detailed research is recommended (such as torsion analysis, which can be conducted using classical torsion theory) to verify the influence of height (or gap) on the stiffness.

Table 3-5: Data for complex modulus – DSR–gap relationship

		70/100 Unaged_parallelplate_ DELFT	70/100 Unaged_DoI_6mm_stone column_DELFT	70/100 Unaged_DoI_10.9mm_stone column SRT
		G* [Pa]		
Gap [mm]		2	11.93	17
Frequency [rad/s]	at 15.8 rad/s	9.64E+05	7.67E+06	1.33E+07
	at 62.8 rad/s	2.57E+06	2.10E+07	3.10E+07
	at 100 rad/s	3.64E+06	2.88E+07	3.98E+07

LABORATORY EXPERIMENTS

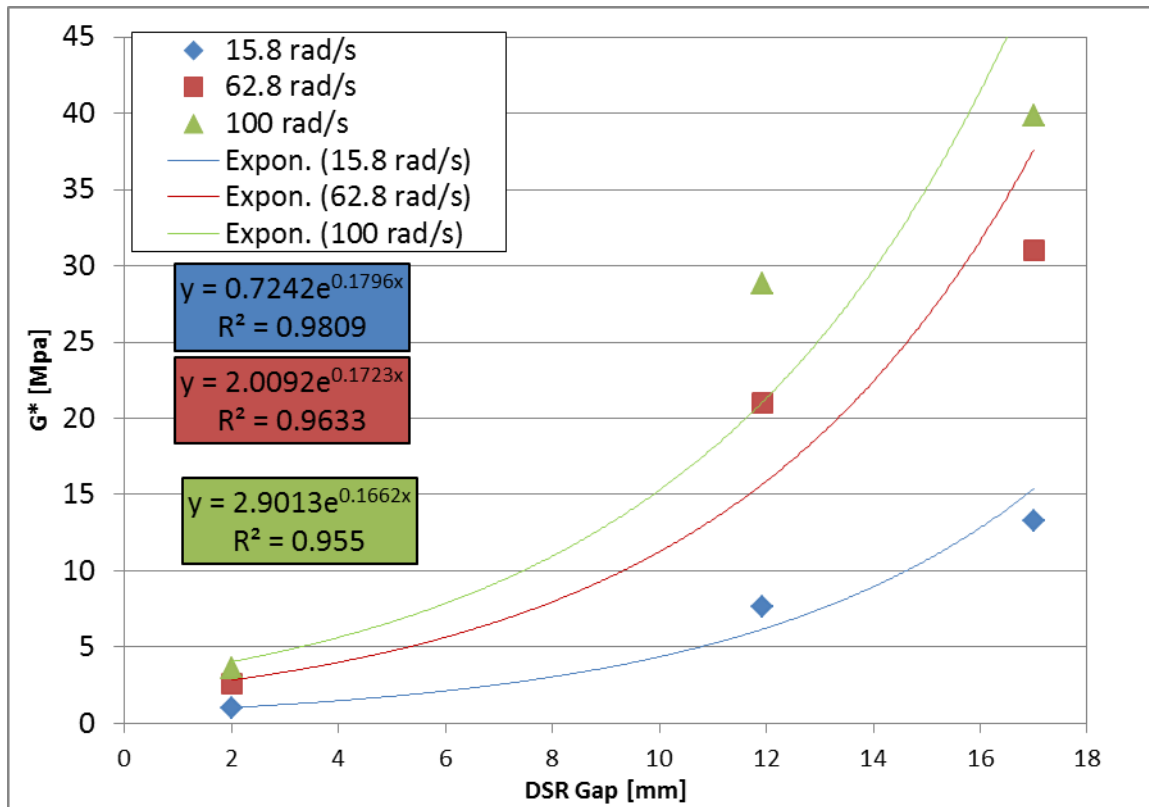


Figure 3-16: Complex modulus–DSR gap relationship

3.5.5 Pure shear test mode vs. combined shear and normal stress test mode

A given force applied to a material can generally be decomposed into a normal force and a transverse force. The normal force and the transverse force subject the material to a normal stress (σ) and a shear stress (τ). When the normal stress tends to reduce the length of the material under the stress, this is referred to as “compression”. When the length of the material is increased, the stress is called “tension”.

Liu (2007) reported that stress applied to a material is generally decomposed into normal and shear stresses. Mathematically, this can be represented by the Mohr’s circle equations. When a material is stressed to failure, normal stress and shear stress are used to determine the failure criteria of the material, such as the Mohr-Coulomb criterion. This criterion is represented in Figure 3-17 in which σ_1 , and σ_3 represent respectively the maximum stress and the minimum principal stress, ϕ is the angle of friction of the material and C is the cohesion of the material.

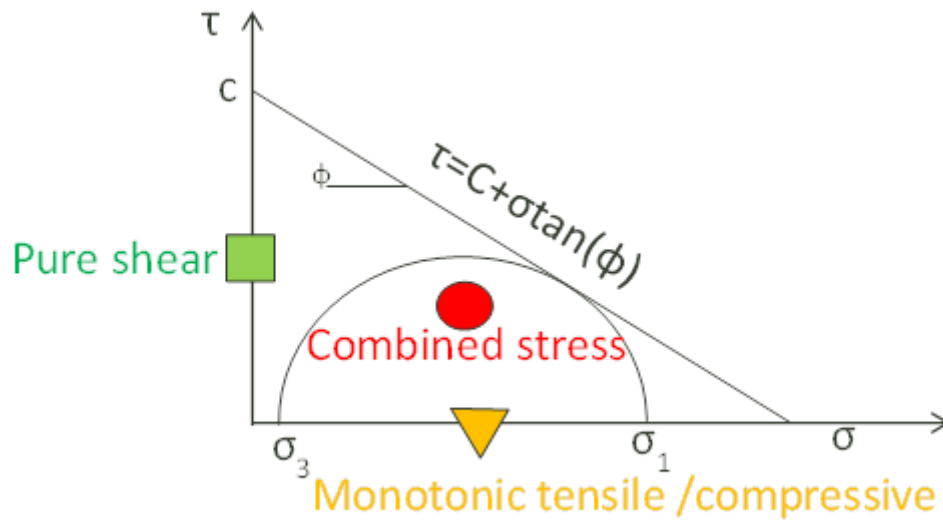


Figure 3-17: Presentation of shear and normal stress on a Mohr-Coulomb graph

Materials in a road pavement usually experience both shear stress and normal stress, as indicated by the red dot in the Mohr's circle presented in Figure 3-17. Normal DSR tests induce only pure shear stress (green square in Figure 3-17), while tensile or compressive monotonic tests induce pure normal stress (yellow triangle in Figure 3-17). In the DSR oscillatory testing, compression and tension in the sample are also induced. A limited normal force (less than 50 N) is provided on the DSR to maintain the gap constant and measure the change. Although the available DSR was not appropriated to carry out normal force tests, it was suggested that a trial be conducted during DSR testing which would incorporate the limited normal force. This was motivated by the fact that failure in combined shear and normal stresses appears to represent the reality of material failure better. The sign convention was defined as follows: negative (e.g. -10 N) means "tension", positive (e.g. +10 N) represents "compression" and zero normal force (i.e. 0 N) signifies pure shear.

Trial tests were performed for CFD and AFD at different temperatures and at following normal force levels: -10 N, 0 N and +10 N, as presented in Figure 3-18 to Figure 3-21.

LABORATORY EXPERIMENTS

In general, the tests performed under tension and those performed under pure shear showed the expected reduction of stiffness with time, with the shortest failure time being for tests done under tension. The behaviour in these two types of test appears to be logically correct as adding tension to the shear accelerates the failure of the sample. On the other hand, the tests performed under compression displayed a tendency for the sample to stiffen during the test before a possible decrease of stiffness with time. The tests performed under compression often did not display a specific failure time. This behaviour appears to be complex and might be due to the counter-effect of compression on the fracture phenomenon (compression force tends to mitigate the fracture of the material). This effect is significant in the adhesion tests, with no sign of stiffness reduction during the test.

This research thus focused only on tests performed under pure shear, as the introduction of compressive stress appears to be complex and the inclusion of normal force during tests with the currently available DSR has not yet been mastered.

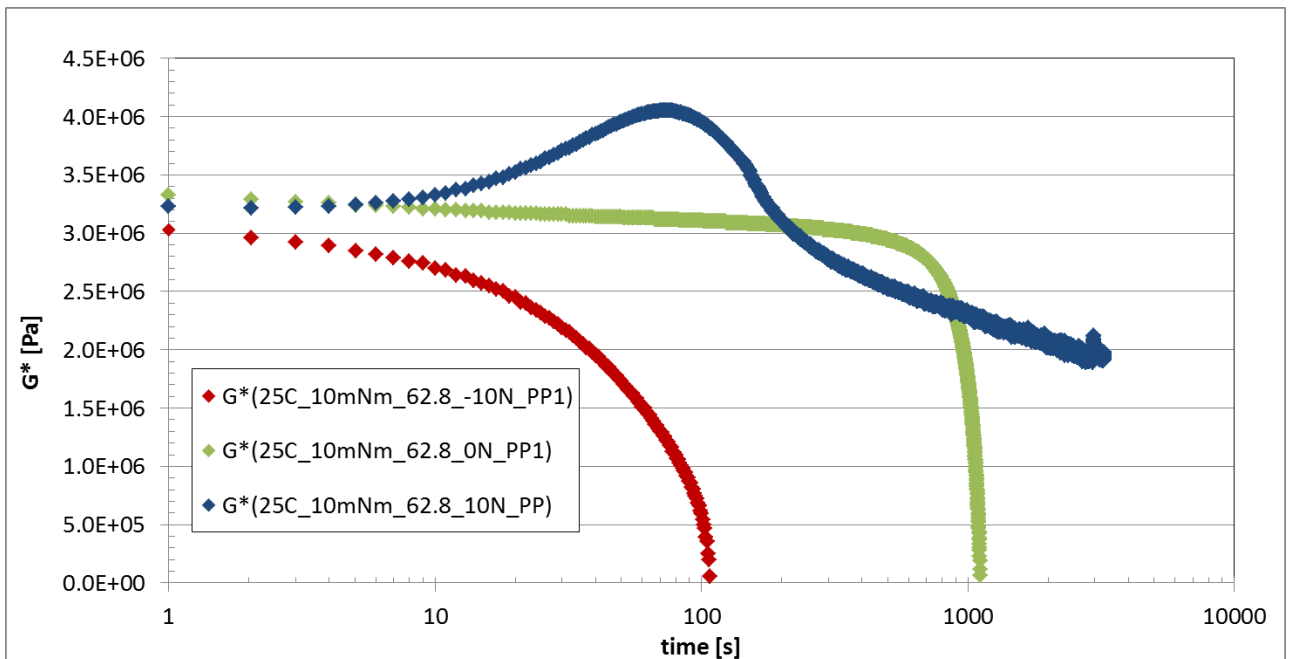


Figure 3-18: Comparison between pure shear and combined shear and normal force for DSR cohesion fatigue damage test at 25 °C

LABORATORY EXPERIMENTS

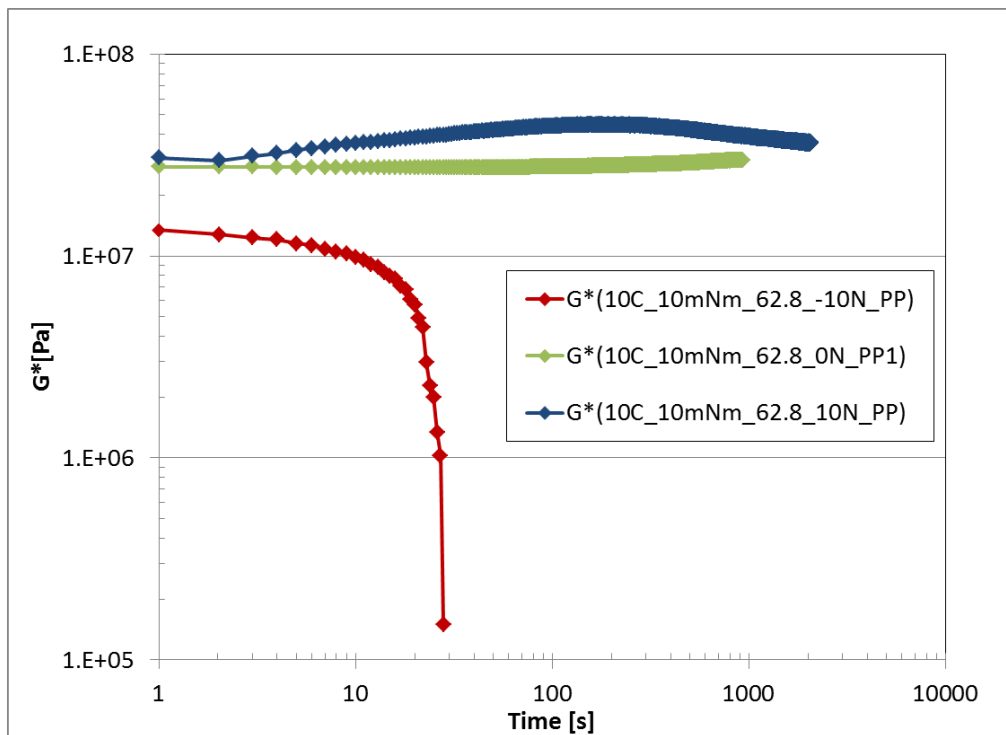


Figure 3-19: Comparison between pure shear and combined shear and normal force for DSR cohesion fatigue damage test at 10 °C

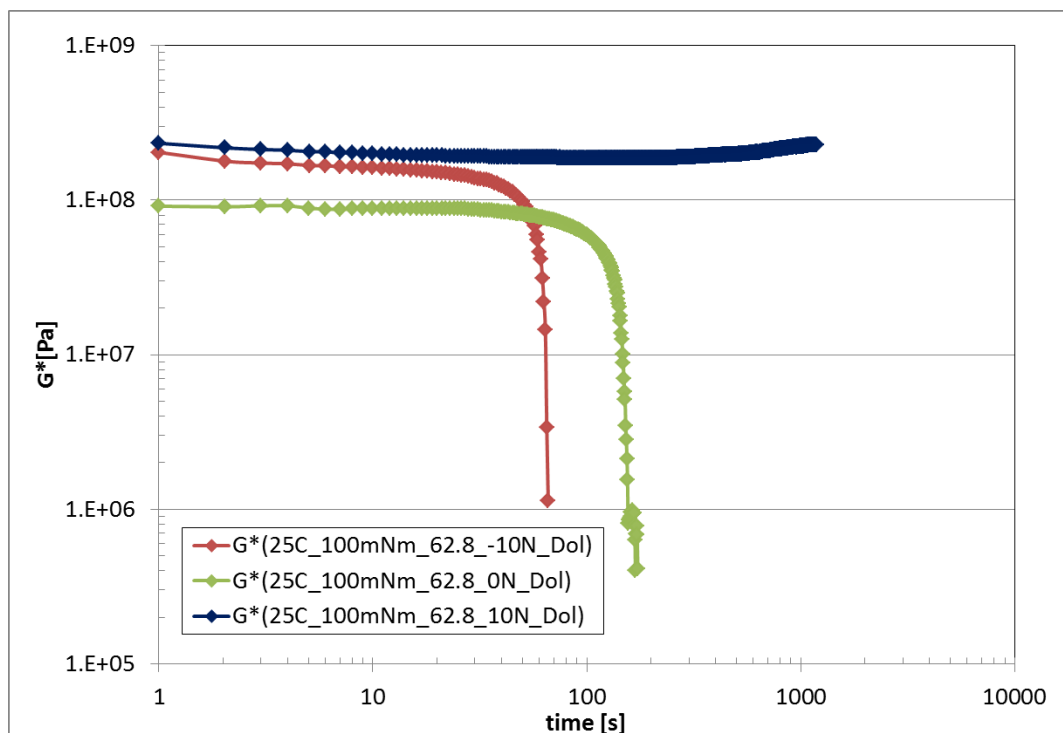


Figure 3-20: Comparison between pure shear and combined shear and normal force for DSR adhesion test at 25 °C

LABORATORY EXPERIMENTS

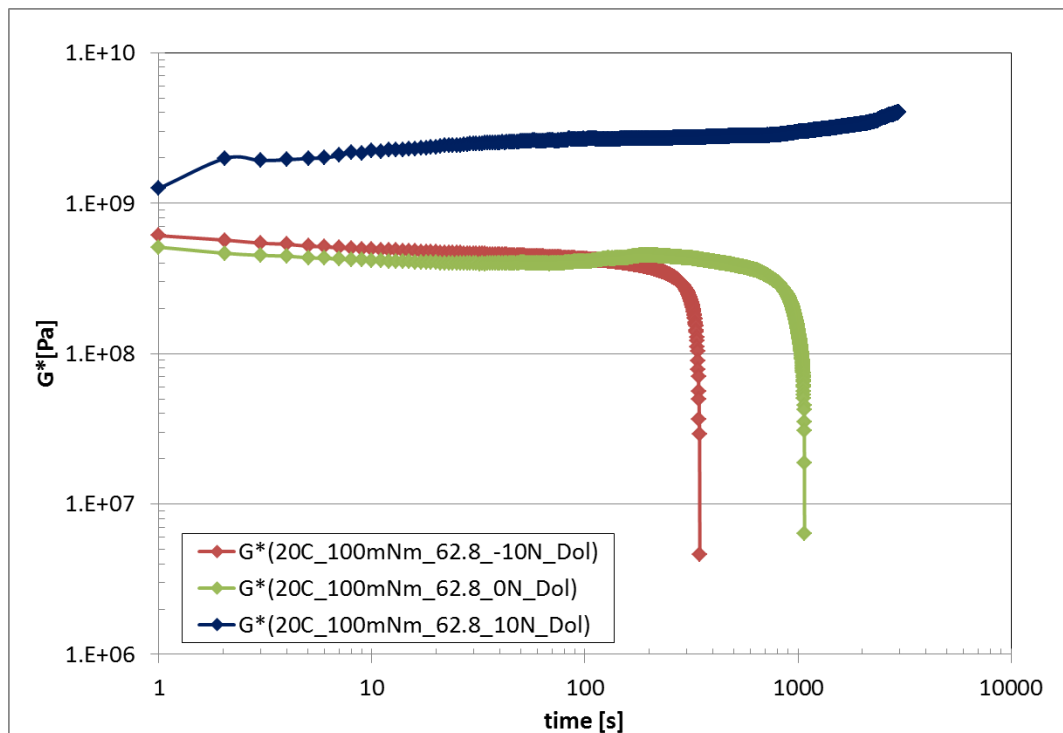


Figure 3-21: Comparison between pure shear and combine shear and normal force for DSR adhesion test at 20 °C

3.5.6 Choice of binder film thickness between stone columns in the adhesion test

Khedoe and Moraal (2007) and Huurman (2007) used a film thickness of 15 μm . As the stone columns were not polished as mentioned in Section 3.4, the cut face was not strictly flat and its texture was rough. For this reason the film thickness was set to 100 μm . In addition to this hypothesis of the reality, Mitton (2012) reported that the average film thickness of single seals varies between 1 mm and 2 mm.

It should be noted that the greater film thickness increased the probability of cohesion failure instead of adhesion failure. To confirm adhesion failure, the samples were visually inspected after the tests, as presented in Figure 3-22.



Figure 3-22: Example of visual inspection of adhesion failure

3.5.7 Repeatability of tests

The repeatability of a test in an investigation is crucial and impacts on the credibility of the investigation's outcomes.

In this research, tests were done in different laboratories using different models of the DSR equipment from different manufacturers. In addition, the fatigue tests performed were non-standard for the DSR. Therefore, some repeatability tests were undertaken to evaluate the reliability of the results.

The repeatability of the tests was assessed by comparing the results of similar samples using different DSR systems, and by comparing the results of similar samples from tests repeated on the same DSR.

The comparison based on different DSR systems was performed on the frequency sweep test using both the DSR (MCR302) from the CSIR, Pretoria, South Africa, and the DSR (AR 2000) from the Technical University of Delft, the Netherlands. As presented in Figure 3-23 and Figure 3-24, good correlation was found between the two DSRs.

LABORATORY EXPERIMENTS

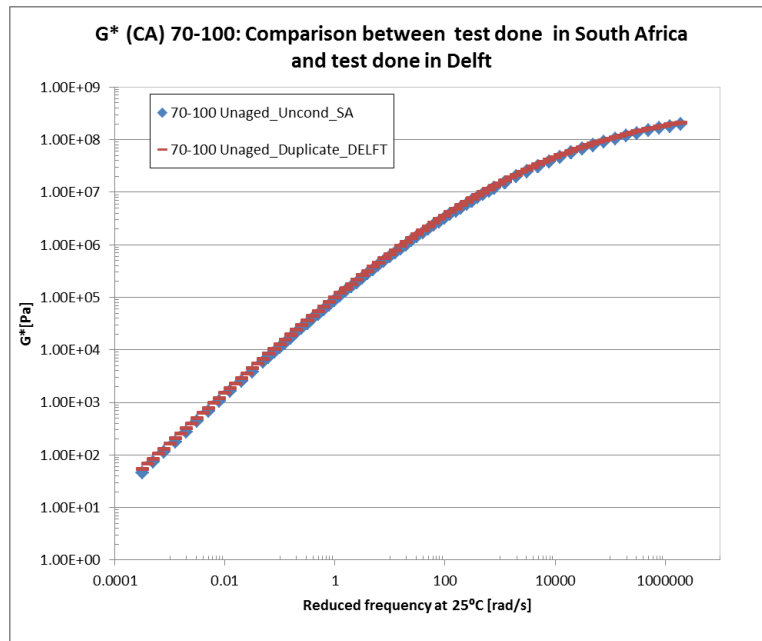


Figure 3-23: Frequency sweep comparison of CA complex modulus results between DSR-MCR302 (from the CSIR) DSR-AR 2000 (from TU Delft)

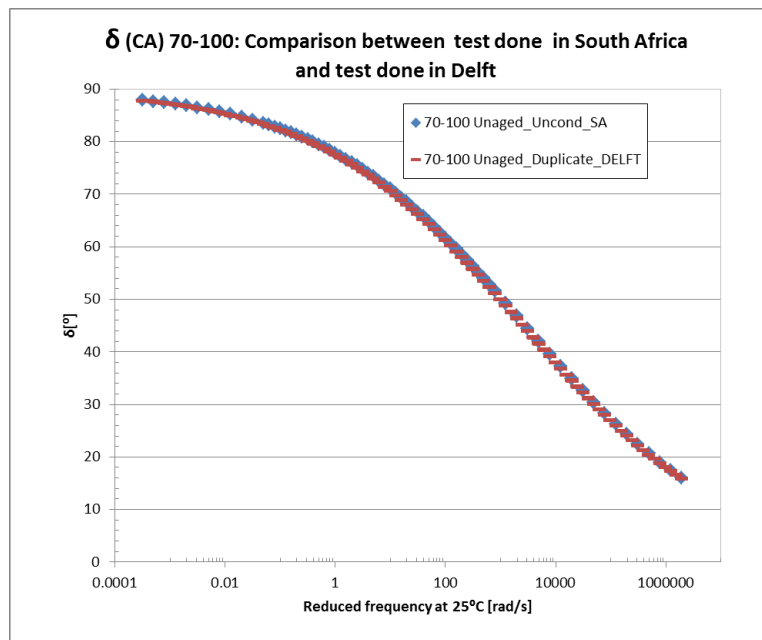


Figure 3-24: Frequency sweep comparison of CA phase angle results between DSR-MCR302 (from the CSIR) DSR-AR 2000 (from TU Delft)

LABORATORY EXPERIMENTS

The repeatability using the same machine was performed with MCR302 from the Specialised Road Technologies (SRT), Durban, South Africa. The results as presented in Figure 3-25 show that samples tested at a given torque level (e.g. 15 mNm) but for different times failed in the same range of time, and all the results were logical in terms of the level of torque compared with the time of failure (i.e. tests performed at 15 mNm failed earlier than tests performed at 10 mNm).

Therefore it can be concluded that the level of repeatability during this investigation was acceptable.

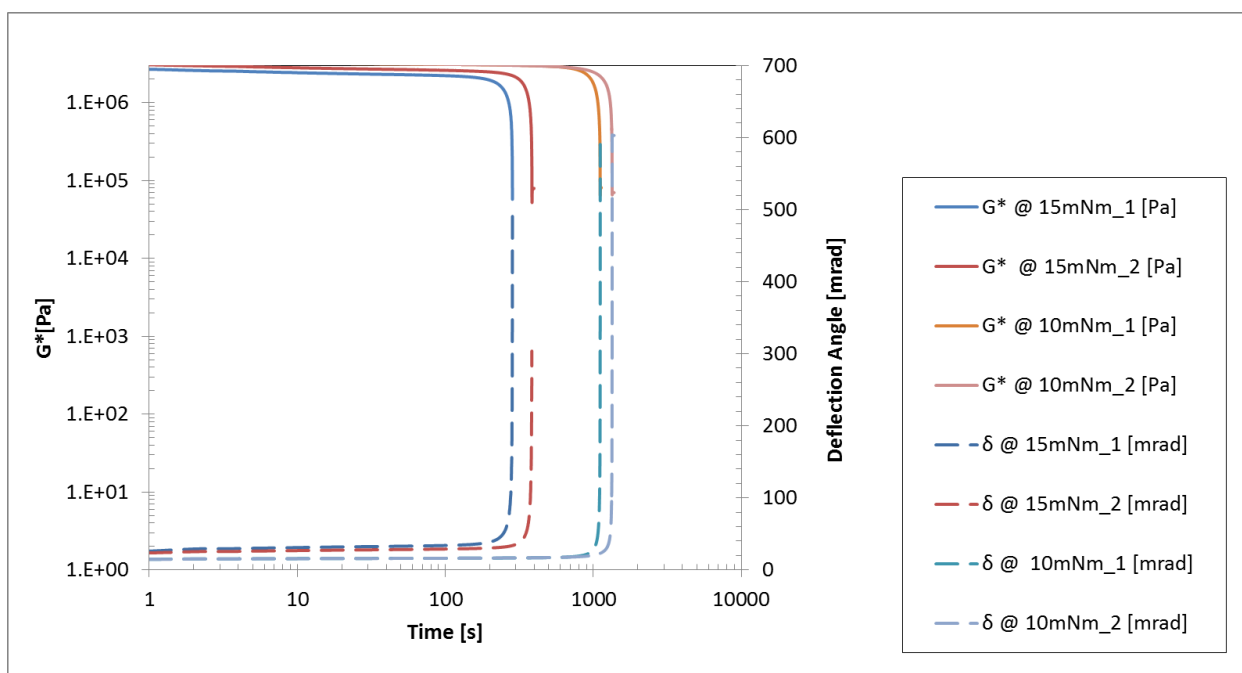


Figure 3-25: Example of repeatability of fatigue test performed on the same DSR

3.5.8 Binder fatigue related to change in sample radius

Sybilski et al. (2013) reported that a new definition of fatigue life should strictly be linked to material properties (not to sample geometry) and be method-independent. According to Hintz and Bahia (2013), during a DSR test, under cyclic torsional loading of a cylindrical sample, fracture manifests as a circumferential crack that starts at the periphery of a sample and propagates inwards, reducing the effective sample radius. Changes in the sample radius due to cracking contribute to the



fatigue damage during time sweep testing in the DSR. However, they concluded that the time sweep test is an appropriate test method for fatigue characterisation of bituminous binders using fracture mechanics.

It appears that fatigue damage during the time sweep test could be due to the combined effect of the visco-elastic properties of a material and a change in the radius of the sample. To account for the sample's radius change, it is suggested to monitor the rate of crack progression in the evaluation of the fatigue damage. Due to the anticipated complexity of a crack progression study, this investigation will assume that the fatigue damage is due only to the visco-elastic properties of the material. Planche *et al.* (2004) noted that for binder complex modulus below 10MPa the reduction in the outside edge of the sample is likely due to instability flow, which causes a necking down in the sample from viscous flow not fracture. Thus, for actual fatigue fracture, the modulus should be above 10MPa.

3.5.9 Use of parallel plates for cohesion fatigue damage test

During the investigation, the parallel plate configuration was used for the CFD tests. Compared with the bitumen column, poor response of the parallel plates was noticed, especially at low temperatures (0 °C to 10 °C). The bitumen tended to debond from the plates, demonstrating that the “fatigue work” takes place at the bitumen–plate interface (adhesion failure), instead of occurring within the bitumen.

A possible solution to address this issue is to manufacture parallel plates with rough surfaces to resist the debonding effect.

3.6 Testing Approach Adopted

Based on the discussion in Section 3.5, the following approach was adopted for the main investigation test procedures:

- Stress-controlled tests were used for both CFD and AFD.
- The tests were performed at several stress levels and at different temperatures (i.e. tests were performed at different stress levels for each given temperature).



LABORATORY EXPERIMENTS

- AFD tests were done using a stone column with a bitumen film thickness of 100 µm.
- CFD tests were performed using a bitumen column.
- All DSR fatigue tests were performed under pure shear stress (no normal force was included).

The procedures adopted form part of the testing protocols as presented in Section 3.7.

3.7 Testing Protocols

These protocols were based mainly on the Lifetime Optimisation Tool (LOT) research programme protocol from Delft University of Technology as reported by Khedoe and Moraal (2007).

3.7.1 Bitumen frequency sweep response protocol

In this research, the response test was performed using a parallel plate configuration of the DSR. This was done according to standard test AASHTO T315 (2005). However, the bitumen rubber test was performed using the CSIR's adjusted test method (GWDMS No 200726) as reported by Mturi *et al.* (2011). This adjustment was necessary due to the presence of crumb in the bitumen.

All the bitumens used in the test were prepared by heating them up to the temperatures as presented in Table 3-6. In addition, the bitumen emulsion (KRS 60) was distilled according to standard test ASTM D6997 (2012) prior to the response test. The distillation improved the consistency of the bitumen emulsion to avoid flow of bitumen between the parallel plates.

Table 3-6: Preparation temperature of bitumen for DSR test

Bitumen	Temp [°C]
70/100	180
SE1	200
KRS 60	60
SR1	200

The testing parameters are listed in Table 3-7.



LABORATORY EXPERIMENTS

Table 3-7: Test parameters for binder response

Temperature range [°C]	0*; 10; 25; 50
Frequency range [Hz]	0.01 to 100
Strain [%]	0.1
Normal force [N]	0

*: When recovered binders from field-aged seals were tested, 5 °C was used instead of 0 °C.

The value of frequencies used in the frequency test are presented in Table 3-8.

Table 3-8 : Values of frequencies (in Hz) used in frequency test

Frequency [Hz]		
0.0100	0.0158	0.0251
0.0398	0.0631	0.100
0.158	0.251	0.398
0.631	1.00	1.58
2.51	3.98	6.31
10.0	15.8	25.1
39.8	63.1	100

The proposed temperature regime for testing is: 0 °C, 10 °C, 25 °C and 50 °C. This choice is motivated by the temperature zone behaviour of bitumen as reported by Milne (2004):

- < 10 °C : Brittle (cold)
- 10 °C – 25 °C: Elastic (operational zone)
- 25 °C – 50 °C (to 60 °C): Visco-elastic (operational zone)
- 50 °C (to 60 °C) – 90 °C : Viscous (hot)

The matrix of testing for bitumen frequency sweep response which is constituted by the DSR 69 tests is presented in Table 3-9.

Table 3-9: Matrix for binder film shear response tests using the DSR

No.	Binder type	Water conditioning	Ageing	Temperature [°C]	Frequency [Hz]
1	70/100	Unconditioned	Unaged	0/10/25/50	0.01 to 100
2		Conditioned	Aged	0/10/25/50	0.01 to 100
3		Unconditioned	Unaged	0/10/25/50	0.01 to 100
4		Conditioned	Aged	0/10/25/50	0.01 to 100
5	SE1	Unconditioned	Unaged	0/10/25/50	0.01 to 100
6		Conditioned	Aged	0/10/25/50	0.01 to 100
7		Unconditioned	Unaged	0/10/25/50	0.01 to 100
8		Conditioned	Aged	0/10/25/50	0.01 to 100
9	KRS 60	Unconditioned	Unaged	0/10/25/50	0.01 to 100
10		Conditioned	Aged	0/10/25/50	0.01 to 100
11		Unconditioned	Unaged	0/10/25/50	0.01 to 100
12		Conditioned	Aged	0/10/25/50	0.01 to 100
13	SR1	Unconditioned	Unaged	0/10/25/50	0.01 to 100
14		Conditioned	Aged	0/10/25/50	0.01 to 100
15		Unconditioned	Unaged	0/10/25/50	0.01 to 100
16		Conditioned	Aged	0/10/25/50	0.01 to 100
17	70/100	Unconditioned	Q-SUN	0/5/10/25/50	0.01 to 100
18	SE1	Unconditioned	Q-SUN	0/5/10/25/50	0.01 to 100
19	SR1	Unconditioned	Q-SUN	0/105//25/50	0.01 to 100
47	28 samples 70/100 seals		Field aged	5/10/25/50	0.01 to 100
68	21 samples SE1 seals		Field aged	5/10/25/50	0.01 to 100

Notes:

- Conditioned: conditioned in water
- Aged: aged with PAV method
- Q-SUN: aged with Q-SUN weatherometer
- Unconditioned: not conditioned in water
- Unaged: not aged

3.7.2 Cohesion fatigue damage test protocol

As the bitumen column needed to be clamped into the DSR, two 304 stainless steel rings (outside diameter 8 mm, inside diameter 6 mm and height 4 mm) were mounted on both the top and bottom of the sample. These rings also ensured the correct transfer of the torque from the DSR to the sample.

To cast a bitumen column sample, a mould was necessary. A silicon split mould was used for casting five samples of 6 mm diameter. The mould is depicted in Figure 3-26. The bitumen column sample was mounted onto the DSR using the clamping system consisting of a stator (static part) and a rotor (moving part), as presented in Figure 3-27. Contact between the clamping system and the sample was realised via

LABORATORY EXPERIMENTS

the two stainless steel rings fitted as described above. These rings are shown in Figure 3-28. The height of the sample was 20 mm.



Figure 3-26: Three views of the split mould

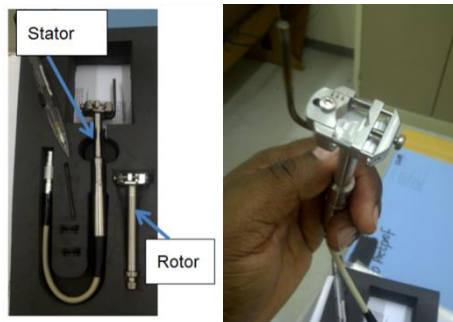


Figure 3-27: Two views of the clamping system

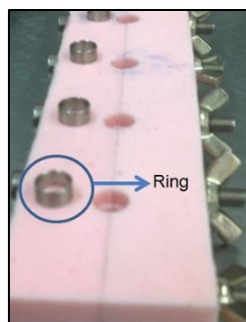


Figure 3-28: Illustration of rings

After the mould had been mounted, the sample was prepared as follows:

The bitumen was heated to a temperature of 140 °C. After the rings had been fitted to the mould, the mould was pre-heated to prevent unwanted cooling down of the bitumen during casting. When the mould was completely filled with hot bitumen

LABORATORY EXPERIMENTS

(Figure 3-29), it was placed in an oven at the same temperature used to heat the bitumen, for 5 minutes. This procedure reduced the amount of air voids in the sample. The mould was then taken out of the oven and allowed to cool down to ambient temperature for at least two hours.

After the slow cooling down, the mould was placed in a refrigerator at $-10\text{ }^{\circ}\text{C}$ for two hours before being split (Figure 3-30). The bitumen samples were carefully removed, avoiding damage. A visual inspection was done to select the best samples. The selection criteria were: air voids at the surface, damage the samples, under filling of the sample. The outer side of the rings was cleaned carefully to ensure a perfect fit in the DSR clamps. The clamping system was then mounted in the DSR and the sample was ready for bitumen column testing.

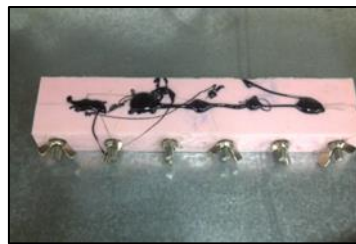


Figure 3-29: Bitumen poured into the mould



Figure 3-30: Bitumen column samples in the split mould

The test parameters for CFD are listed in Table 3-10.



Table 3-10: Test parameters for cohesion fatigue damage test

Bitumen type	70/100
Ageing	Unaged
Water conditioning	Unconditioned
Temperature range [°C]	0;5;10;15;20;23;25
Frequency range [Hz]	10
Strain [%]	2
Normal force [N]	0
Max. time [hour]	2
Torque [mNm]	5 to 40

Notes:

Unconditioned: not conditioned in water

Unaged : not aged

Thirty-one CFD tests were performed using these test parameters. The test was performed in duplicate, in the case of considerable deviation between the two tests, a third test was performed and most meaningful result was selected.

3.7.3 Adhesion fatigue damage test protocol

The stones were cored at 10.9 mm diameter from the rock and saw cut but the not polished, as explained in Section 3.4. Therefore, the cut face was not strictly flat and its texture was rough. For this reason the film thickness was arbitrarily set to 100 µm. The stone cores (columns) were cleaned in boiling water for 15 minutes to remove dirt (e.g. grease), after which the columns were ready for assembly.

The sample to be tested consisted of two stone columns glued together by a film interface layer of bitumen. For the assembly of these samples it was important for the two stone columns to be centred precisely. The DSR was an adequate tool for this purpose. The same clamps as for the bitumen columns (Figure 3-27) were used for mounting the stone columns. The upper, free rotating clamp held and kept the first (upper) stone column centred. The second (lower) stone column was tied firmly in the centre of the stator (Figure 3-31).

After the stone columns had been mounted and centred, the gap between the stone surfaces was set by moving the DSR drive shaft down in such a way as to allow contact between the two opposite faces of the top and bottom stone columns; this represents a “zero gap” between these stones columns (Figure 3-32). The

LABORATORY EXPERIMENTS

temperature in the DSR test chamber was set to 140 °C for 30 minutes. A small droplet of melted bitumen was placed on top of the bottom stone sample (Figure 3-33) and the temperature was brought down to around 30 °C, after which the gap was reduced gradually (by steps) to reach a 100 µm film thickness (Figure 3-34). This procedure was necessary to avoid the influence of the shrinking drive shaft at decreasing temperature on the interface layer thickness. The film of bitumen was trimmed to fit the stone column size (Figure 3-35). After cooling down at ambient temperature, the stone-binder sample was carefully removed from the clamps and stored at a temperature of 5 °C in a refrigerator before the test was started.



Figure 3-31: Fitting stones in the clamping system

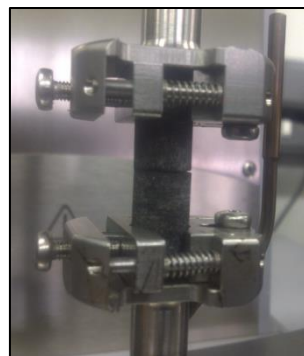


Figure 3-32: Zero gap between two stone columns

LABORATORY EXPERIMENTS

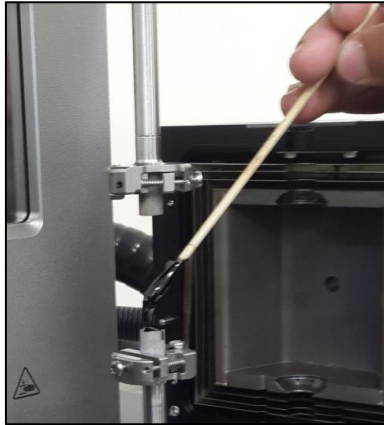


Figure 3-33: Placing a droplet of bitumen on the lower stone column

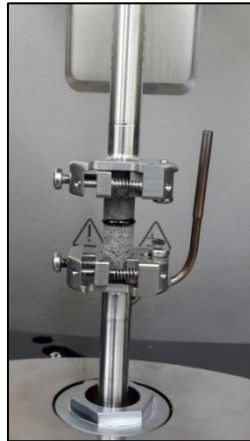


Figure 3-34: Joining the two stone columns together using the bitumen film



Figure 3-35: Trimming the bitumen film to fit the stone column



LABORATORY EXPERIMENTS

The test parameters for adhesion fatigue damage are listed in Table 3-11.

Table 3-11: Test parameters for cohesion fatigue damage test

Bitumen type	70/100
Ageing	Unaged
Water conditioning	Unconditioned
Temperature range [°C]	10; 20;23;25
Frequency range [Hz]	10
Strain [%]	2
Normal force [N]	0
Max. time [hour]	2
Torque [mNm]	50 to 200

Notes:

- Unconditioned: not conditioned in water
- Unaged: not aged

Twenty adhesion fatigue damage tests were performed using these test parameters. The test was performed in duplicate, in the case of considerable deviation between the two tests, a third test was performed and most meaningful result was selected.

3.8 Summary

The experimental programme for this investigation was subdivided into three main testing activities using the DSR equipment, namely:

- bitumen frequency sweep response test
- cohesion fatigue damage test (CFD)
- adhesion fatigue damage test (AFD).



LABORATORY EXPERIMENTS

The response tests were performed using the standard test method, whereas special protocols were developed for the CFD and AFD tests. These protocols were necessary owing to the challenges encountered during the preliminary testing.

The results and interpretation of the tests are presented in Chapter 4.

References

AASHTO (American Association of State and Transportation Officials) 2012, *Standard Practice for Accelerated Aging of Asphalt Binder Using a Pressurized Aging Vessel (PAV)*, AASHTO Designation: R 28-12, US.

AASHTO (American Association of State and Transportation Officials), 2005, *Determining the Rheological Properties of Asphalt Binder Using a Dynamic Shear Rheometer (DSR)*, AASHTO Designation: T 315-05, US.

AASHTO R 28-12, see AASHTO, 2012.

AASHTO T315-05, see AASHTO, 2005.

Airey G.D., 1997, *Rheological characteristics of polymer modified and aged bitumens*, PhD thesis, Department of Civil Engineering, University of Nottingham, UK.

Asphalt Academy, 2007, *The Use of Modified Bituminous Binders in Road Construction*, Technical Guideline(TG 1), 2nd ed., CSIR, Pretoria, South Africa.

Asphalt Institute, 1997, *Performance-graded Asphalt Binder Specification and Testing*, Superpave Series No. 1 (SP-1), Lexington, KY, US.

ASTM (American Society for Testing and Materials International), 2002, *Standard Practice for Accelerated Weathering Test Conditions and Procedures for Bituminous Materials (Xenon-Arc Method)*, ASTM D4798-01, West Conshohocken, PA, US.

ASTM (American Society for Testing and Materials), 2009, *Standard Test Method for Recovery of Asphalt from Solution by Abson Method*, ASTM D 1856-09, ASTM International, West Conshohocken, PA, US.

ASTM (American Society for Testing and Materials), 2011, *Standard Test Methods for Quantitative Extraction of Bitumen from Bituminous Paving Mixtures*, ASTM D 2172-11, ASTM International, West Conshohocken, PA, US.

ASTM (American Society for Testing and Materials), 2012, *Standard Test Method for Distillation of Emulsified Asphalt*, ASTM D6997-12, ASTM International, West Conshohocken, PA, US.

ASTM D 1856-09, see 2009.



LABORATORY EXPERIMENTS

ASTM D 2172-11, see ASTM, 2011.

ASTM D4798-01, see ASTM, 2002.

ASTM D6997-12, see ASTM, 2012.

BE-TM-BINDER-1-2006, see CSIR, 2014.

Collop A.C., Scarpas A.T., Kasbergen C. and de Bondt A, 2003, *Development and finite element implementation of a stress dependent elasto-visco-plastic constitutive model with damage for asphalt*, paper presented at the 82nd Transportation Research Board (TRB) Annual Meeting, Washington DC.

CSIR (Council for Scientific and Industrial Research), 2014, *Determination of Binder Content and Binder Recovery*, BE-TM-BINDER-1-2006, CSIR Internal Test Method, Revision 2, Pretoria, South Africa.

Domone P. and Illstone J. (Eds.), 2010, *Construction Materials: Their Nature and Behaviour*, 4th ed. Taylor & Francis, London

González A.; Covián E.; Madera, J., 2008, *Determination of Bridge Natural Frequencies Using a Moving Vehicle Instrumented with Accelerometers and GPS*, Civil-Comp Press, Dublin.

Hagos E. T., 2002, *Characterisation of polymer modified bitumen (PMB)*, Master's thesis, Section of Road and Railway Engineering, Faculty of Civil Engineering and Geosciences, Delft University of Technology, Netherlands.

Hagos E. T., 2008, *The effect of aging on binder properties of porous asphalt concrete*, PhD thesis, Section of Road and Railway Engineering, Faculty of Civil Engineering and Geosciences, Delft University of Technology, Netherlands.

Happian-Smith J., 2000, *Introduction to Modern Vehicle Design*, Transport Research Laboratory (TRL), Butterworth-Heinemann, UK.

Hintz C. and Bahia, H., 2013, *Understanding Mechanisms Leading to Asphalt Binder Fatigue in the Dynamic Shear Rheometer (DSR)*, *Road Materials and Pavement Design*, London, Taylor & Francis.

Huurman M., 2007, *Lifetime Optimisation Tool (LOT)*, Main report, Technical University of Delft, Netherlands.

Khedoe R.N. and Moraal J., 2007, *Sample preparation and laboratory testing for the LOT research program*, Report 7-07-170-4, Lifetime Optimisation Tool (LOT), Laboratory of Road and Railway Engineering, Delft University of Technology, Netherlands.

Liao M.C, 2007, *Small and large strain rheological and fatigue characterisation of bitumen-filler mastics*, PhD thesis, University of Nottingham, UK.

LABORATORY EXPERIMENTS

- Liu L., 2007, *Engineering properties of rocks, Rock Mechanics III*, Lecture notes, Department of Civil and Environmental Engineering, University of Connecticut, Mansfield, CT, US.
- Mangiafico S., 2014, *Linear visco-elastic properties and fatigue of bituminous mixtures produced with Reclaimed Asphalt Pavement and corresponding binder blends*, PhD thesis, l'École Nationale des Travaux Publics de l'État, France.
- Milne T. I., 2004, *Towards a performance-related seal design method for bitumen and modified road seal binders*, PhD thesis, University of Stellenbosch, South Africa.
- Mitton S., 2012, *Determining the bitumen thickness between aggregates of various surfacing seals*, Bachelor of Engineering project report (Civil Engineering), Faculty of Engineering, University of Pretoria, Pretoria, South Africa.
- Monismith C.L. and Deacon J.A., 1969, Fatigue of asphalt paving mixtures, *ASCE Journal of the Transport Engineering Division*, 95, 154–161.
- Mturi G.A. J., Mahlangu K., Conrad S. and Von Wissell M., 2013, *Asphalt Binder Extraction: Benzene Replacement in Test Method BE-TM-BINDER-1-2006*, CSIR Technical Report CSIR/BE/IE/IR/2012/0017/B, Pretoria, South Africa.
- Mturi G. A.J., Zoorob S. E., O'Connell J., Anochie-Boateng J. and Maina J., 2011, Rheological testing of crumb rubber modified bitumen, *Proceedings of the 7th International Conference on Road & Airfield Pavement Technology (ICPT)*, Paper P18, pp. 1316–1327, Bangkok, Thailand.
- NITRR (National Institute for Transport and Road Research), 1986, *The Determination of the Binder Content of a Bituminous Mixture (Indirect Method)*, Technical Methods for Highways (TMH 1 C7 (b)), pp. 193-194, CSIR, Pretoria, South Africa.
- Planche J. P., Anderson D. A., Gauthier G., Le Hir Y. M., Martin D., 2004, *Evaluation of fatigue properties of bituminous binders*, *Materials and Structures*, June 2004, Volume 37, Issue 5, pp 356-359.
- SABS South Africa Bureau of Standards, 2005, South African National Standard SANS 307:2005 *Penetration-grade Bitumens (includes Amendments 1–7)*, SABS Standards Division, Pretoria, South Africa.
- SANS 307:2005, 2005, see SABS, 2005
- Sybilski D., Soenen H., Gajewski M., Chailleux E. and Bankowski W., 2013, Binder Testing, *Advances in Interlaboratory Testing and Evaluation of Bituminous Materials*, RILEM State-of-the-Art Report, Vol. IX, Springer, Dordrecht, Netherlands.
- TG 1, 2007, see Asphalt Academy, 2007.



LABORATORY EXPERIMENTS

TMH 1C7(b), see NITRR, 1986.

Van Assen E., 1997, *Assessment of Binder Extraction Methodologies*, CSIR Contract Report CR-97/092, Pretoria, South Africa.



4 RESULTS, INTERPRETATION AND MODELLING CONCEPT OF COHESION AND ADHESION FATIGUE DAMAGE

4.1 Introduction

The results and interpretation of the different tests described in Chapter 1 are presented in this chapter. Different concepts which will constitute the basis of the modelling construction are also detailed.

The test outcomes and the development of modelling concepts are subdivided into three main parts:

- *Bitumen response*: developed from the testing matrix presented in Table 3-9
- *Cohesion fatigue damage (CFD)*: developed from the test set-up from Table 3-10
- *Adhesion fatigue damage (AFD)*: developed from the test set-up from Table 3-11.

4.2 Bitumen Response Outcome

In the bitumen response, the complex modulus (G^*) and the phase angle (δ) are reported as principal visco-elastic parameter results expressed as master curves.

Two types of test outcome are presented, namely the mathematical model and the mechanical model. For the sake of presenting the bitumen response outcome, only one type of bitumen conditioning state (i.e. 70/100-Unaged-Unconditioned) is detailed for both the mathematical and mechanical models. The remaining combinations of conditioning states for the different bitumen response (also called “case studies”) outcomes are presented in Appendix E. Fitting of the models to the data was assessed using the coefficient of determination (R^2).

4.2.1 Results of the mathematical models

Arrhenius and Williams Landel Ferry (WLF) shift factor methods were used in the construction of master curves (Section 2.9.1.7). These master curves were



RESULTS INTERPRETATIONS AND MODELLING CONCEPT

constructed based on TTSP by applying the CA formula. A testing temperature of 25 °C was selected as reference temperature in the master curves construction process. Graphs for the 70/100-Unaged-Unconditioned bitumen using Arrhenius and WLF shift factors are presented respectively in Figure 4-1 and Figure 4-2. The CA graphs for the remaining case studies are presented in Appendix E.1. The results of the four fresh bitumens (from plant) were modelled using both the Arrhenius and the WLF shift factor methods. As the objective of the response model was to reach at a mathematical model, it was decided to express the 49 field-aged recovered bitumens only in terms of the Arrhenius method to reduce the amount of data analysed. The initial DSR data, as processed by shift factor, form part of Appendix E.6.

The parameters of the shift factors and the model parameters derived from the CA mathematical formula for the 70/100-Unaged-Unconditioned bitumen are presented in Table 4-1. Full parameters for all the case studies are presented in Appendix E.2.

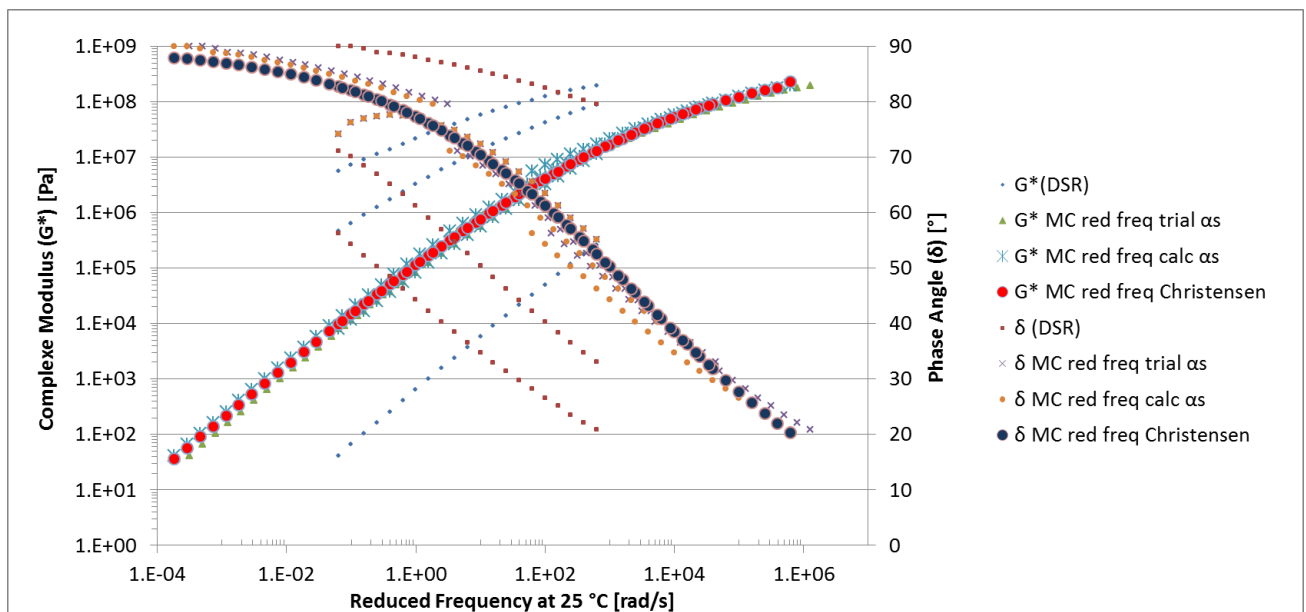


Figure 4-1: Complex modulus and phase angle master curves using the Arrhenius method and the CA formula

RESULTS INTERPRETATIONS AND MODELLING CONCEPT

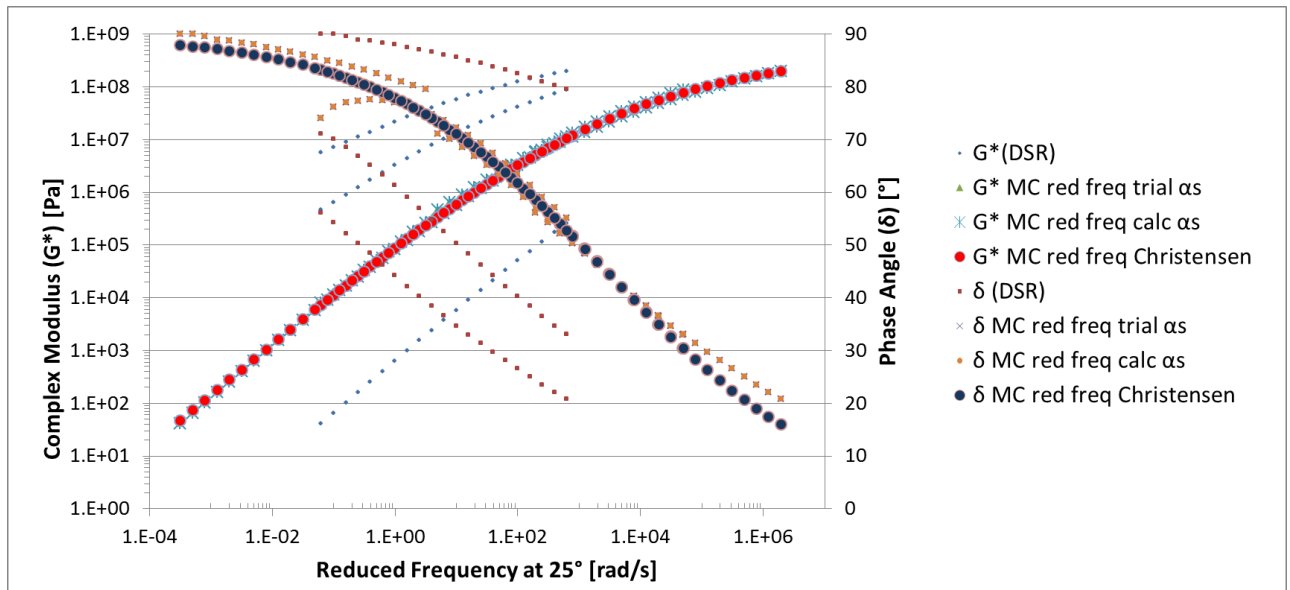


Figure 4-2: Complex modulus and phase angle master curves using the WLF method and the CA formula

Table 4-1: Shift factors and CA parameters for 70/100-Unaged-Unconditioned bitumen

Type of parameter		Value
Arrhenius parameters	ΔH	1.868E+05
WLF shift factor parameters	C_1	30.94
	C_2	121.21
CA parameters	$G_{glassy1}$	4.538E+08
	ω_{cross}	2.800E+03
	R	1.28



4.2.2 Mechanical model results

4.2.2.1 Prony series

Olard and Di Benedetto (2003) reported that generalised visco-elastic models with a finite number of elements (discrete model) are not accurate in describing the complex linear visco-elastic behaviour. Thus, it is necessary to increase the number of elements to enhance the modelled behaviour. In line with this principle, the Prony series used in this research was consisted of 10 elements. Figure 4-3 is a graphical representation of the Prony series for 70/100-Unaged-Unconditioned bitumen with the Prony series model parameters being presented in Table 4-2. The full Prony parameters for the cases studies are presented in Appendix E.3.

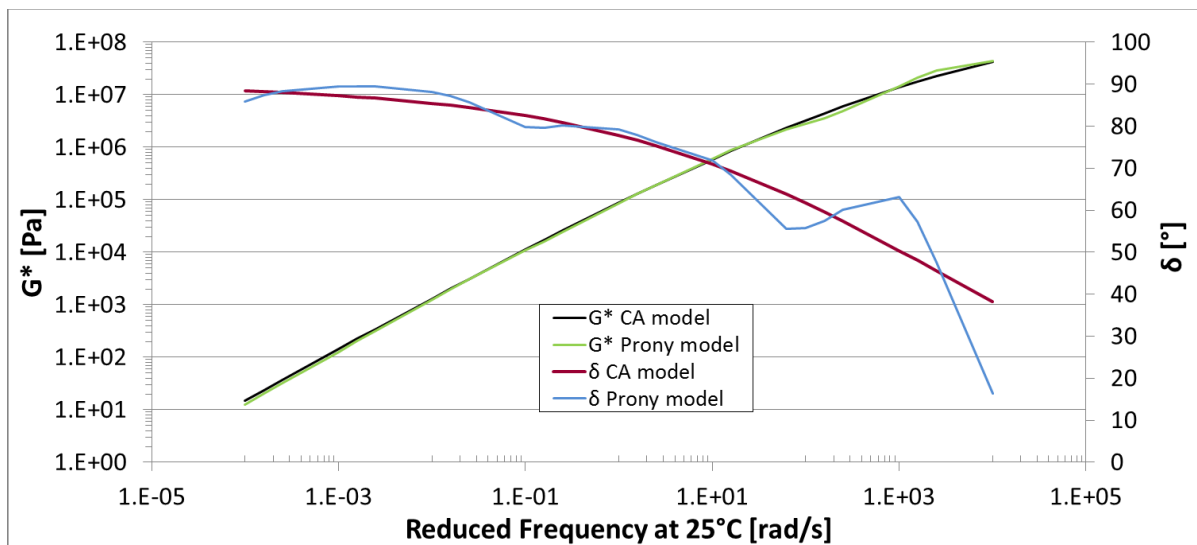


Figure 4-3: Mechanical model – Prony series

Table 4-2: Prony parameters for 70/100-Unaged-Unconditioned bitumen

Model parameters		α_j	τ_j
	Term 1	1.64E-03	1.01E-02
	Term 2	9.46E-01	3.19E-04
	Term 3	1.00E-08	1.86E-03
	Term 4	2.61E-02	3.07E-02
	Term 5	3.68E-05	6.48E-03
	Term 6	2.45E-02	5.99E-03
	Term 7	1.76E-04	1.41E+00
	Term 8	6.78E-05	1.09E+01
	Term 9	2.91E-05	8.83E-03
	Term 10 (residual)	1.65E-03	2.96E-01
G_0	4.62E+07		
R^2 for G^*		0.97	
R^2 for δ		0.84	

The Prony model's parameters for the different binders modelled are used as inputs in the development of the mechanistic analysis of seals. This analysis is based on the stress-strain principles and expressed as a finite element model of the seal (Milne, 2015; Mukandila *et al.*, 2015).

4.2.2.2 Huet-Sayegh model

The Huet-Sayegh (HS) model graph for 70/100-Unaged-Unconditioned bitumen is presented in Figure 4-4. The HS graphs of the remaining bitumens analysed using this model are presented as part of Appendix E.7. The HS model parameters for 70/100-Unaged-Unconditioned bitumen is presented in Table 4-3. Furthermore, the model parameters for all the bitumens analysed by the HS model are shown in Appendix E.4.

RESULTS INTERPRETATIONS AND MODELLING CONCEPT

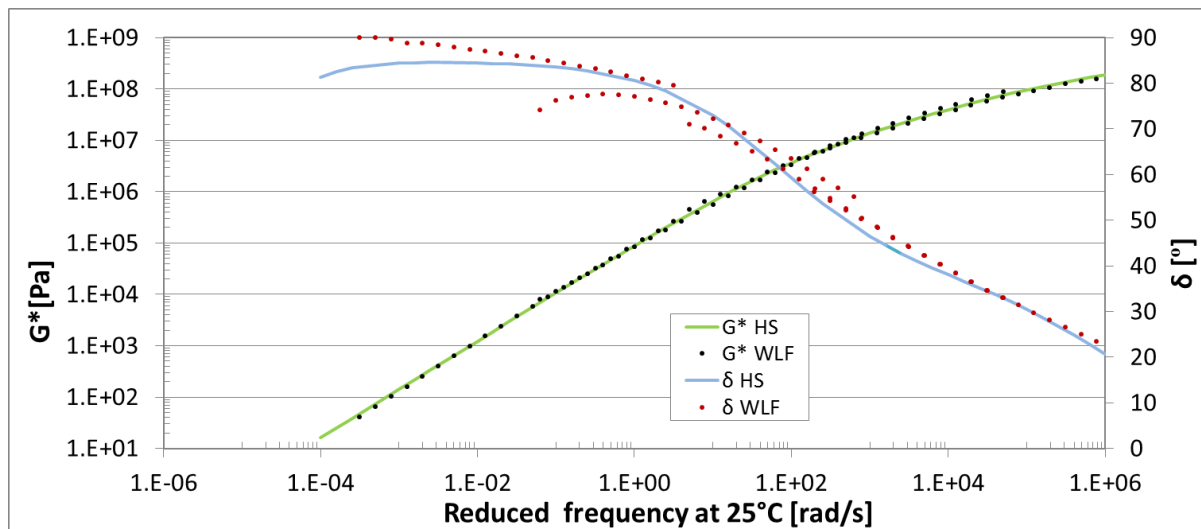


Figure 4-4: Mechanical model – HS model

Table 4-3: HS model parameters

Type of bitumen	Model parameters					
	G_0	G_∞	ζ (Zeta)	k	h	τ
70/100-Unaged-Unconditioned_25C	1	3.69E+08	9.87	0.43	0.94	2.53E-05

4.2.2.3 2S2P1D model

The 2S2P1D model for 70/100-Unaged-Unconditioned bitumen is presented graphically in Figure 4-5. The 2S2P1D graphs of the remaining bitumens analysed by this model are presented as part of Appendix E.7. The 2S2P1D model parameters for 70/100-Unaged-Unconditioned bitumen are presented in Table 4-4. The model parameters for all the bitumens analysed using the 2S2P1D model are shown in Appendix E.5.

RESULTS INTERPRETATIONS AND MODELLING CONCEPT

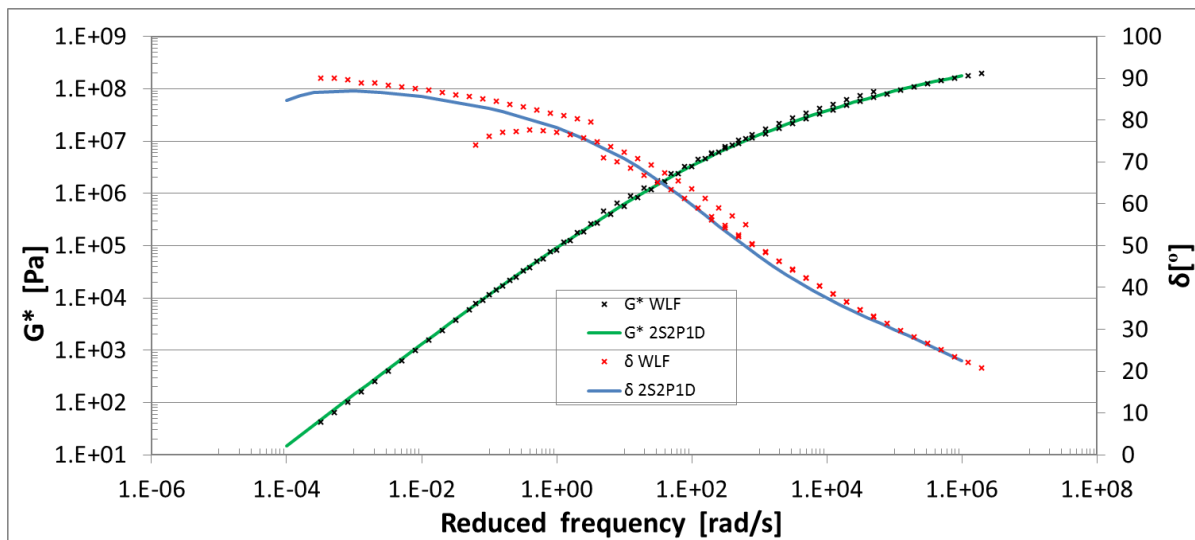


Figure 4-5: Mechanical model – 2S2P1D model

Table 4-4: 2S2P1D model parameters

Type of bitumen	Model parameters						
	G_0	G_∞	ζ (Zeta)	k	h	β	τ
70/100-Unaged-Unconditioned_25C	1	4.84E+08	6.58	0.37	0.75	9.78	5.4E-06

4.2.3 Comparison between different models

The complex moduli and phase angles obtained using the mathematical model and the three mechanical models were compared. The 70/100-Unaged-Unconditioned comparisons are presented respectively for the complex modulus and the phase angle in Figure 4-6 and Figure 4-7.

RESULTS INTERPRETATIONS AND MODELLING CONCEPT

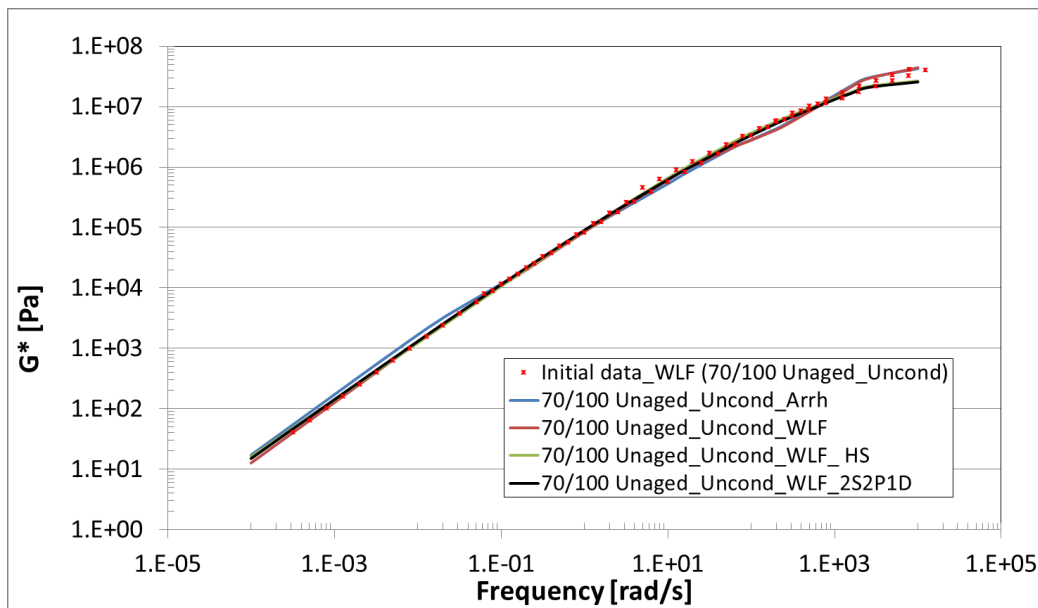


Figure 4-6: Complex moduli comparison for different models for 70/100-Unaged-Unconditioned bitumen

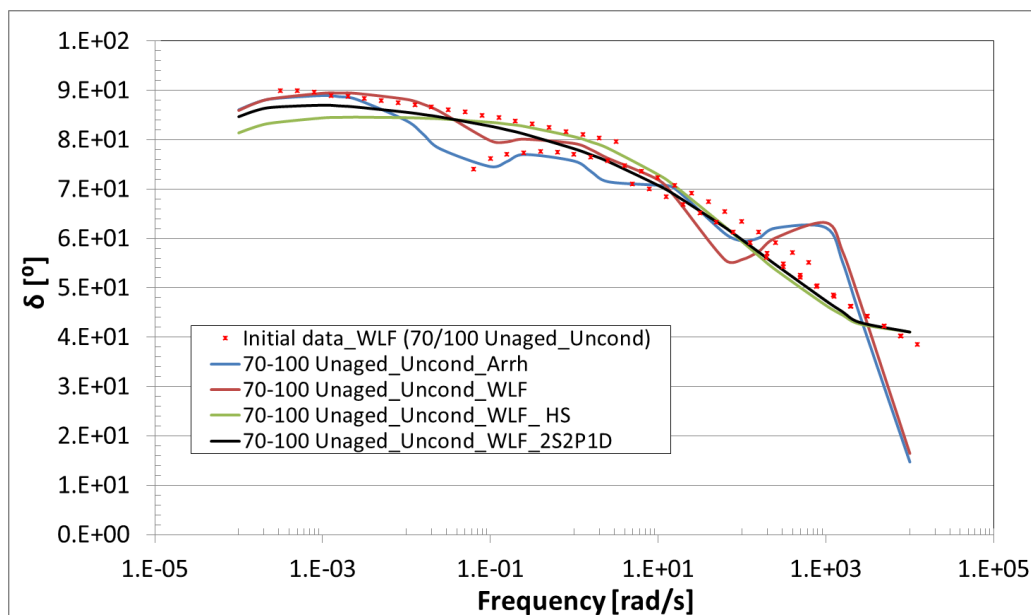


Figure 4-7: Phase angle comparison for different models for 70/100-Unaged-Unconditioned bitumen

Although the phase angles from the different models were in the same range, the complex moduli compared better than the phase angles. Prony's phase angle models for 70/100 bitumen displayed a poor fit at high frequency as presented in Figure 4-7. Unlike Prony's phase angle models, for modified binders (SE1, KRS 60

and SR1) the plot exhibited a better fit. Figure 4-8 shows the fit of Prony's phase angle in the case of bitumen rubber PAV aged and conditioned in water (SR1-PAV-Conditioned). In general, the phase angles from the HS and 2S2D1D models fit the initial data better than the equivalent phase angles from Prony series. The data of these models are presented in Appendix E.6, while the graphs are presented in Appendix E.7.

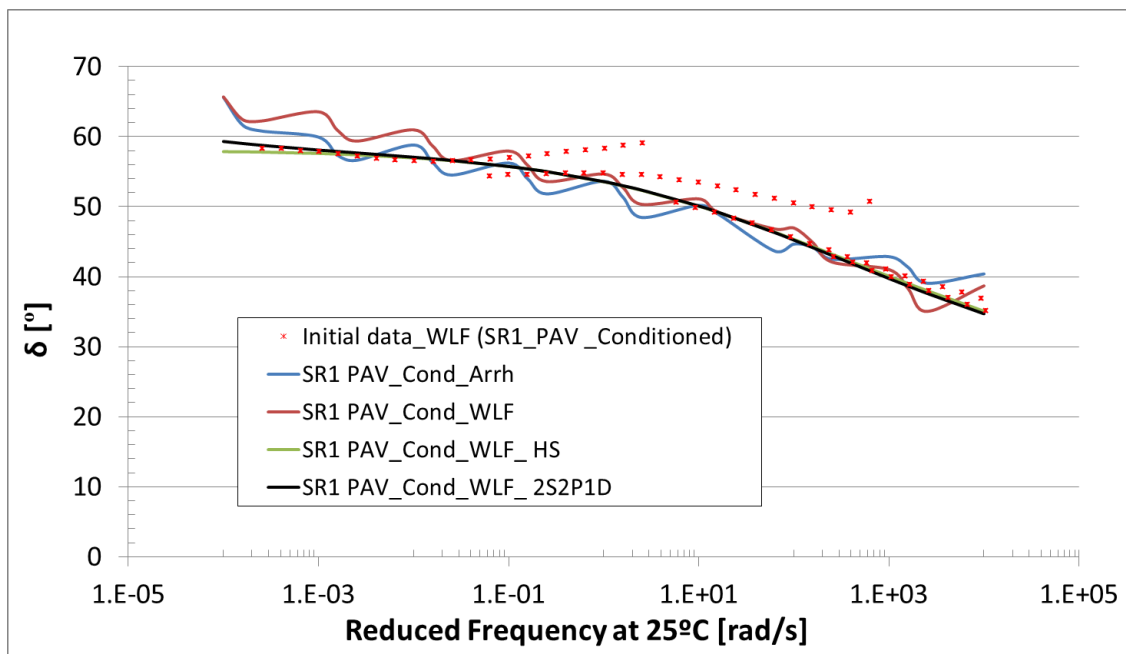


Figure 4-8: Phase angle comparison for different models for SR1-Unaged-Unconditioned bitumen

4.3 Cohesion and Adhesion Fatigue Damage Outcome

The cohesion and adhesion tests were performed as fatigue tests. The testing parameters for cohesion and adhesion are given in Table 4-5 and Table 4-6 respectively for cohesion and adhesion. As mentioned in Section 3.1, different torque levels simulate different traffic conditions and different temperatures represent different environmental conditions.



RESULTS INTERPRETATIONS AND MODELLING CONCEPT

Table 4-5: Testing parameters for cohesion damage

Angular frequency		62.83 [rad/s]				
Test temperature	Different torque levels tested for cohesion					
	[mNm]					
25 °C	25	20	15	10	5	
23 °C	25	20	15	10	5	
20 °C	25	20	15	10	5	
15 °C	25	20	15	10	-	
10 °C	25	20	15	10	-	
5 °C	40	35	30	25	-	
0 °C	40	35	30	25	-	

Table 4-6: Testing parameters for adhesion fatigue damage

Angular frequency		62.83 [rad/s]					
Test temperature	Different torque levels tested for adhesion						
	[mNm]						
25 °C	150	125	100	75	-	-	-
23 °C	175	140	125	110	100	75	50
20 °C	150	125	100	50	-	-	-
10 °C	200	150	-	-	-	-	-

Fatigue is the weakening of a material caused by repeatedly applied loads (Section 2.11 and Section 3.5.3). It is generally represented by the decrease in the material's stiffness. Thus, the outcome trend of the CFD or AFD test in stress mode is expressed graphically as a continuous reduction of G^* with a clear failure time. The characteristic of the failure time is the sudden drop in the G^* , coinciding with a sudden increase in the deflection angle (θ). Failure points (N_f) for different torque levels of test done at a given temperature are identified graphically. Figure 4-9 and

RESULTS INTERPRETATIONS AND MODELLING CONCEPT

Figure 4-10 illustrate respectively the typical output graphics of CFD and AFD tests. The full study cases are presented in Appendix F.

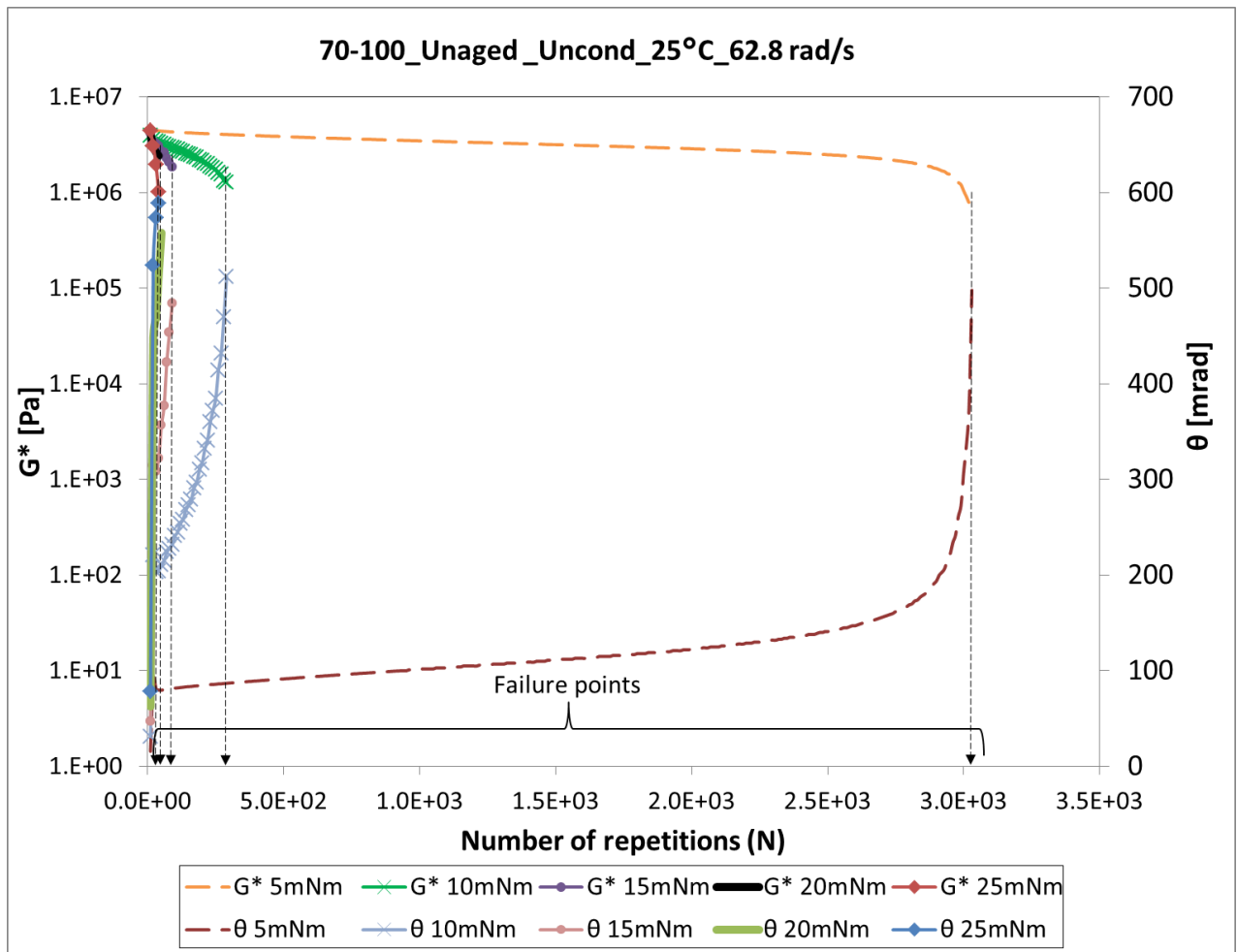


Figure 4-9: Complex modulus and deflection output of the cohesion fatigue damage test

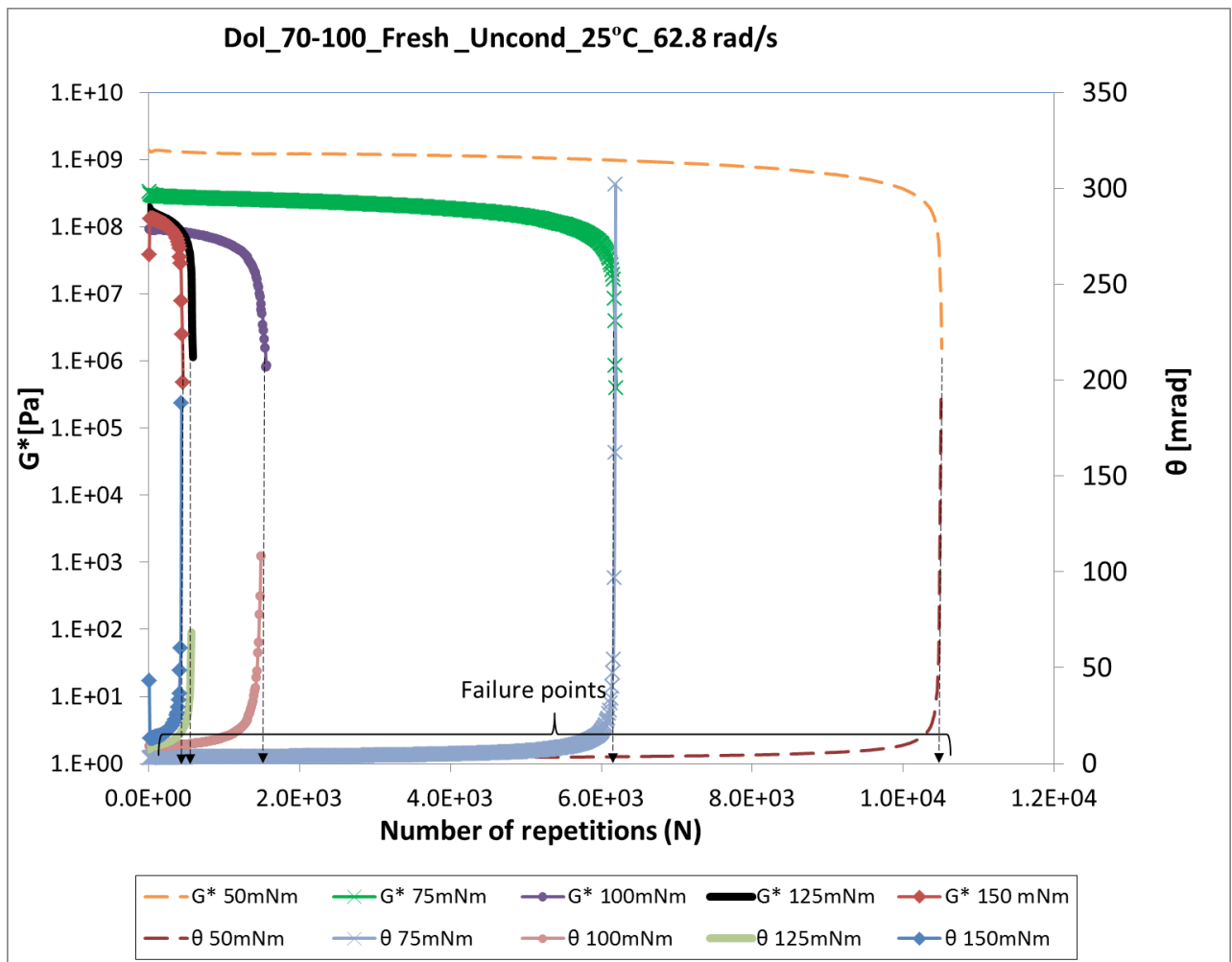


Figure 4-10: Complex modulus and deflection output of the adhesion fatigue damage test

4.4 End-life Damage Principle

The end-life damage principle is based on the determination of a transfer function by considering only the number of repetitions to failure at a specific stress level. The modelling process of end-life damage is presented as follows:

- 1) Collect the output results from the DSR fatigue tests done at different stress (torque) levels for a given temperature.
- 2) Determine the number of repetitions to failure, N_f , for each stress level at the given temperature.



RESULTS INTERPRETATIONS AND MODELLING CONCEPT

- 3) Express each stress level as a function of N_f (as presented in Equation 4-1) for each given temperature:

$$\tau = f(N_f) \qquad \text{Equation 4-1}$$

- 4) Obtain a fitting function of Equation 4-1 by regression.
- 5) Plot the isotherm of the fitting function.

The modelling of the “end-life damage” is presented in Section 5.3.2.

4.5 Principle of Accumulated Damage

Theyse and Van As (2010) reported that the current pavement design method used in South Africa estimates the structural capacity of a pavement from a condition of no distress to a condition of terminal distress, where terminal distress represents the level of distress for which the transfer functions were calibrated. No statement is made on how the terminal condition will be reached, but the classical methods estimate the number of axle loads that will result in the terminal condition. At best, a linear path can be assumed from zero distress to terminal distress. Some of the more modern ME pavement design methods use recursive simulation to simulate different periods of distress during the life-cycle of the pavement. The outcome from these methods is therefore not a linear progression of distress, but an incremental increase in distress until an unacceptable level of distress is reached.

This concept can be elaborated on by modelling the development of the distress or the damage during the life of the pavement material. In this regard, it was decided to model CFD and AFD as evolutions of the damage with time; this was called the “accumulated damage”. The damage is expressed by Equation 4-2.

$$D = 1 - \frac{G^* N}{G^*_0} \qquad \text{Equation 4-2}$$

where:

N is a given the number of load repetitions

D is the fatigue damage after N repetitions

RESULTS INTERPRETATIONS AND MODELLING CONCEPT

G^*_N is the complex modulus after N repetitions

G^*_0 is the initial complex modulus

At the beginning of the test (no damage condition), $G^*_N = G^*_0$, from Equation 4-2, $D = 0$. When failure occurs in the sample, the stiffness of the material at the failure position reduces significantly and the ratio $\frac{G^*_N}{G^*_0}$ tends to zero. Thus, from Equation 4-2, D trends to 1 ($D \approx 1$). It can be concluded that, theoretically, the damage is expressed as a number between 0 and 1, with:

- 0 representing the no-damage condition (material having its initial dynamic shear modulus)
- 1 representing failure condition

The steps in the modelling of the accumulated damage are as follows:

- 1) Collect the results output from the DSR fatigue tests done at different stress (torque) levels for a given temperature.
- 2) Represent the damage of the material as a change of G^* .
- 3) Calculate the damage (D) for each repetition of each stress level at the given temperature.
- 4) Express the damage as a function of the number of repetitions (N), (as presented in Equation 4-2), for each stress level for a given temperature.

$$D = f(N)$$

Equation 4-3

- 5) Obtain a fitting function of Equation 4-3 by regression.
- 6) Correlate the parameters of Equation 4-3 as functions of stress and temperature for each stress level and all temperatures.
- 7) Formulate a global equation for all stress levels and all temperatures with all parameters as functions of stress and/or temperature.



4.6 Summary

This chapter presents output data from DSR tests for response model and fatigue damage (cohesion and adhesion). In the response model, the Arrhenius and WLF equations were used for the shift factor. The mathematical model was based on the CA equation. The response model was further constructed using one mechanical discrete model (Prony series) and two mechanical continuous spectrum models (Huet-Sayegh and 2S2P1D). The Prony series, Huet-Sayegh and 2S2P1D model fitted data from the DSR test well. The mechanical model's parameters (especially the Prony model's parameters) for the different binders modelled are used as inputs in the development of a mechanistic analysis of seals. The end-life damage and the accumulated damage principles and data were presented.

References

- Milne T.I., 2015, Overview of enhancements to road surfacing seal design methodologies through seal system and materials modelling, *Proceedings of the 11th Conference on Asphalt Pavements for Southern Africa*, Sun City, South Africa, 16–19 August 2015, pp. 510–521.
- Mukandila E., Steyn W. J. vdM., Milne T. and Kannemeyer L., 2015, Rheological characteristics of South African bitumen, *Proceedings of the 11th Conference on Asphalt Pavements for Southern Africa*, Sun City, South Africa, 16–19 August 2015, pp. 401–411.
- Olard F. and Di Benedetto H., 2003, *General “2S2P1D” Model and Relation between the Linear Viscoelastic Behaviours of Bituminous Binders and Mixes*, Département Génie Civil et Bâtiment (URA CNRS), Ecole Nationale des TPE, France.
- Theyse H.L. and Van As C., 2010, *Stochastic Recursive Simulation, Preliminary System Design*, Version: 1st Draft, Draft Contract Report SANRAL-SAPDM-E3-2010-01, Revision of the South African Pavement Design Method, SANRAL, Pretoria, South Africa.



5 RHEOLOGICAL RESPONSE, COHESION AND ADHESION FATIGUE DAMAGE MODELS OF BITUMINOUS ROAD SEAL MATERIALS

5.1 Introduction

In this chapter models based on the response data and fatigue damage data presented in Chapter 4 are developed. The bitumen ageing model of the seal derived from the response data is detailed. In addition, the end-life damage and the accumulated damage modes are developed.

5.2 Models Based on Response Data

The rheological response is mainly constituted by the mathematical and mechanical model presented in Section 4.2. As mentioned in Section 3.2, 28 samples of 70/100 and 21 samples of SE1 binders, recovered from different field-aged seals across South Africa, were also modelled in terms of rheological response. This was considered as an opportunity to model the ageing of a seal's bitumen. The knowledge provided by the ageing model of a seal's bitumen should assist in the investigation of the seal's performance and with damage prediction over time.

The ageing model of the seal's bitumen was based on assessing G^* obtained from the Prony series of each recovered bitumen. In addition, laboratory ageing by Q-sun was performed for 70/100-Unaged-Unconditioned and SE1-Unaged-Unconditioned bitumens (Section 3.4.2.2). The principle of the ageing modelling is illustrated in Section 5.2.1, while the model is detailed in Section 5.2.2.

5.2.1 Principle of development of ageing model

In the model, the ageing was considered to be the stiffening of bitumen with time (stiffness being represented by G^*). The principle of development of the ageing model of a seal's bitumen is presented as follows:



- 1) All the extracted bitumens, fresh bitumens (Unaged-Unconditioned), and bitumens aged by the Q-SUN method were modelled using the Prony series method.
- 2) The data of G^* values for each specific bitumen type were combined and presented in a unique graph as functions of reduced frequency.
- 3) Three frequencies (i.e. 10 rad/s, 62.83 rad/s and 100 rad/s) were chosen as reference frequencies for the analysis of changing of G^* with the time. These frequencies were selected in a range reported as the “common moving vehicle frequency range” as reported in Section 3.5.2: automobile frequency ranging from 1 to 16 Hz (6.28 to 100.5 rad/s) (Happian-Smith, 2000) and Hagos, 2002).
- 4) Plot the value of G^* for each Prony series curve at the three given frequencies. These values of G^* are plotted as a function of time as expressed as in Equation 5-1.

$$G^* = f(t)$$

Equation 5-1

- 5) Obtain a fitting function of Equation 5-1 by regression.
- 6) Evaluate the simulated age of bitumen aged by the PAV and Q-SUN methods using the new formula obtained.

5.2.2 Ageing model of a seal's bitumen

Subsequent to the step-by-step principle set in Section 5.2.1, the development of a seal ageing model is detailed for 70/100 bitumen. Appendix G presents the full modelling information for both the 70/100 and SE1 ageing models.

The following details were used for model development:

- 1) The 49 field-aged bitumens were recovered from seals extracted at different locations in South Africa (Section 3.2). The locations and ages of the seals based on 70/100 and SE1 bitumens are presented respectively in Appendix G.1 and Appendix G.2. In this research, the age of the seal is the time (in years) counted from the construction of the seal. The age of the different extracted seals is a major input in the modelling.

RHEOLOGICAL RESPONSE, COHESION AND ADHESION FATIGUE DAMAGE OF BITUMINOUS ROAD SEAL MATERIALS

2) DSR tests were performed on the recovered bitumens and the Prony series master curves were constructed for each bitumen at different ages. The Prony series parameters for both 70/100 and SE1 bitumens are presented in Appendix G.3. The Prony series data for all 70/100 and SE1 bitumens are presented in respectively Appendix G.4 and Appendix G.5. Combined graphs for all G^* Prony series are presented in Appendix G.6 (for 70/100) and Appendix G.7 (for SE1). These graphs include the three reference frequencies. Figure 5-1 illustrates the combined graph for all 70/100 G^* Prony series.

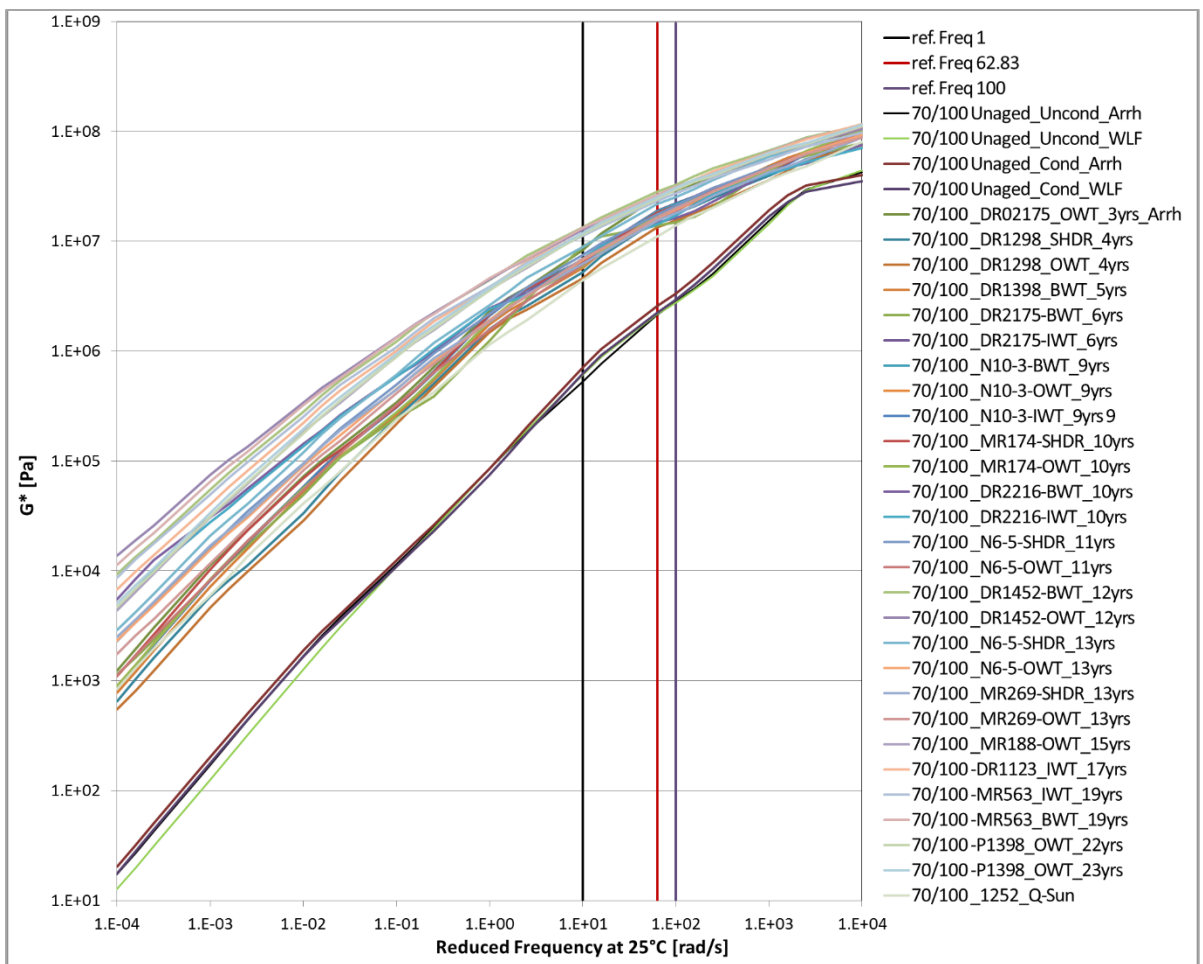


Figure 5-1: Combined graph for all 70/100 G^* Prony series

- 3) The data related to the change of G^* with time at the three reference frequencies were plotted. These data for 70/100 and SE1 are given respectively in Appendix G.8 and Appendix G.9.
- 4) The relationships between G^* and time were fitted using a “power”-type function referred to as the ageing model of a seal’s bitumen. The ageing model of a seal’s bitumen is presented in Equation 5-2. A typical plot of the ageing model is presented in Figure 5-2 for the case of 70/100 bitumen analysed at a frequency of 62.83 rad/s. The full ageing model data for 70/100 and SE1 bitumens are presented respectively in Appendix G.10 and Appendix G.11.

$$G^* = G^*_{t_0} + bt^c$$

Equation 5-2

where

t is the age (time) of the seal’s bitumen

$G^*_{t_0}$ is the initial complex modulus of a seal’s bitumen (complex modulus of the fresh bitumen).

G^* is the complex modulus of a seal’s bitumen at time t

b and c are constants

Values of $G^*_{t_0}$, b and c , as well as the coefficient of determination R^2 , for 70/100 and SE1 bitumens for the three reference frequencies are given in Table 5-1.

It should be noted that $G^*_{t_0}$ is assumed to be constant for the simplification purpose. In reality all binders do not have the same initial modulus.

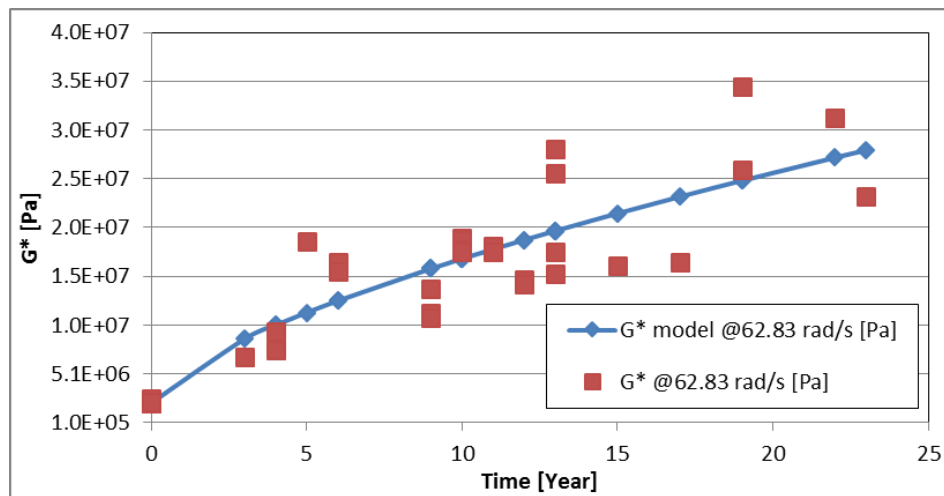


Figure 5-2: Relationship between G^* and time for 70/100 bitumen at 62.83 rad/s

Table 5-1: Values of constants of seal's bitumen ageing model for 70/100 and SE1

Type of bitumen	Frequency	10 rad/s	62.83 rad/s	100 rad/s
70/100	$G^*_{t_0}$	5.28E+05	2.14E+06	2.83E+06
	b	8.78E+05	3.13E+06	3.49E+06
	c	0.859	0.674	0.688
	R^2	0.73	0.74	0.75
SE1	$G^*_{t_0}$	8.13E+05	2.74E+06	3.63E+06
	b	1.63E+06	3.22E+06	4.64E+06
	c	0.828	0.843	0.759
	R^2	0.82	0.82	0.82

5) The graphs of the seal's bitumen ageing model for the three reference frequencies are illustrated in Figure 5-3 and Figure 5-5 respectively for 70/100 and SE1 bitumens.

Further, the relationship between modelled and Prony series G^* for the ageing is presented graphically in Figure 5-4 for 70/100 and in Figure 5-6 for SE1.



RHEOLOGICAL RESPONSE, COHESION AND ADHESION FATIGUE DAMAGE OF BITUMINOUS

ROAD SEAL MATERIALS

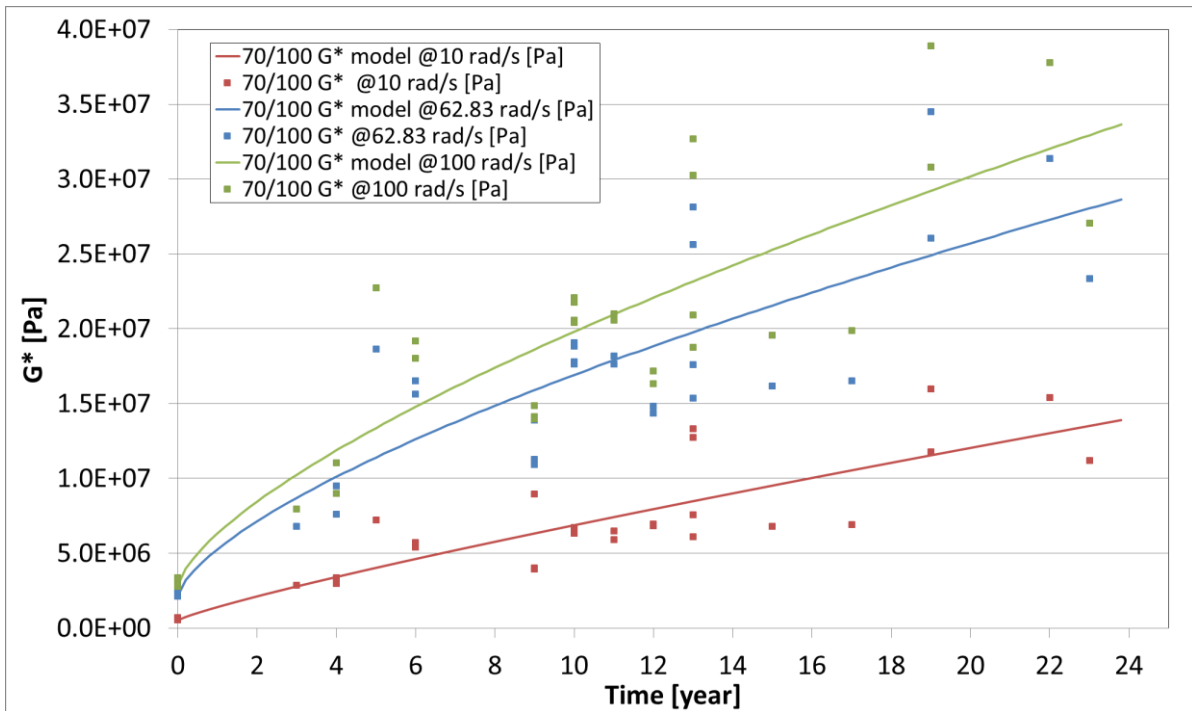


Figure 5-3: Combined graph of seal's bitumen ageing model for 70/100

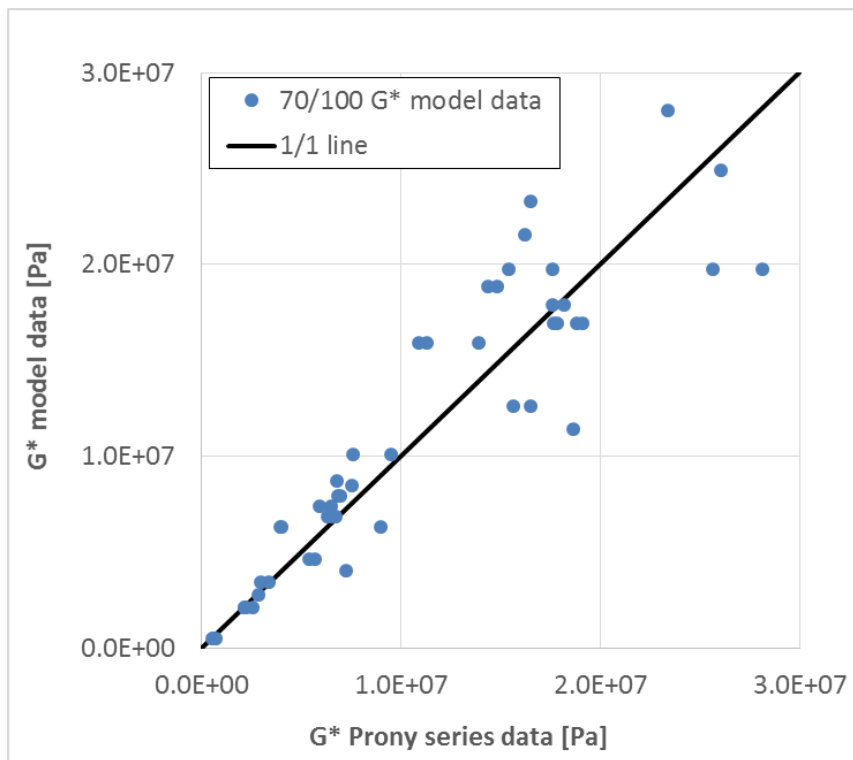


Figure 5-4: Relationship between modelled and Prony series G^* in the ageing model for 70/100



RHEOLOGICAL RESPONSE, COHESION AND ADHESION FATIGUE DAMAGE OF BITUMINOUS

ROAD SEAL MATERIALS

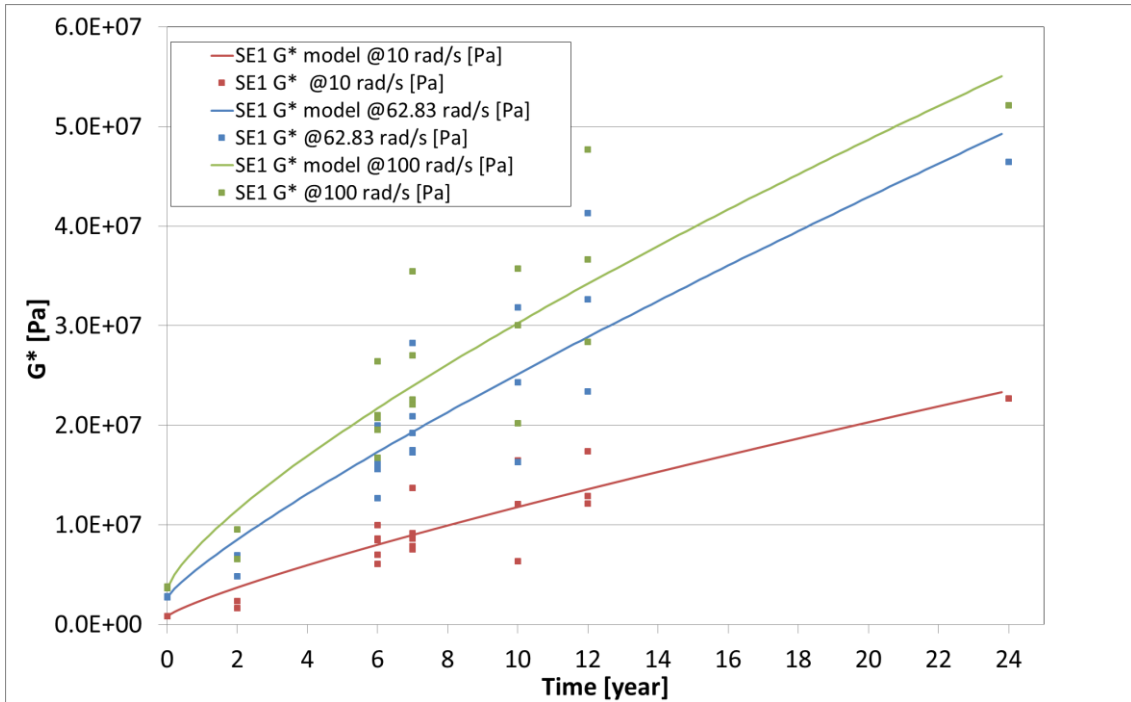


Figure 5-5: Combined graph of seal's bitumen ageing model for SE1

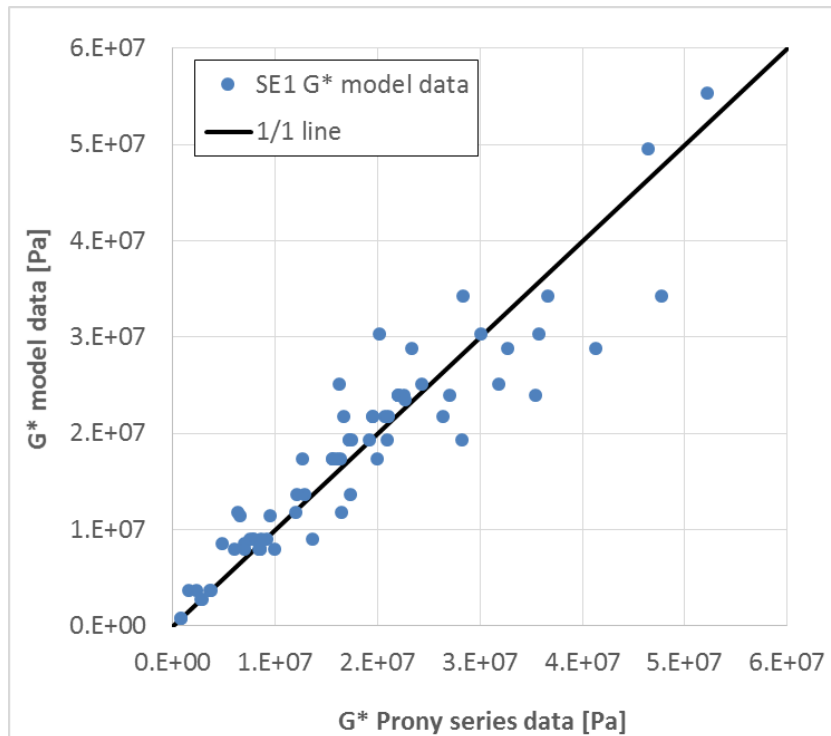


Figure 5-6: Relationship between modelled and Prony series G^* in the ageing model for SE1

6) G^* values collected from bitumen aged in the laboratory by the PAV and Q-SUN methods were plotted against the graph of the seal's bitumen ageing model. The aim was to assess the simulated ageing time on the field-aged model. G^* values for 70/100 and SE1 at the three reference frequencies are given in Table 5-2. The estimation of aged time of PAV and Q-SUN bitumens using the ageing model of a seal's bitumen is between 0.6 and 5.7 years, as indicated in Table 5-3. The Q-SUN method presents the highest aging simulation, with 5.7 years for SE1 at 10 rad/s.

Table 5-2: G^* values for 70/100 and SE1 at the three reference frequencies

Type of bitumen		G^* [Pa]		
		at 10 rad/s	at 62.83 rad/s	100 rad/s
70/100	70/100 PAV_Uncond_Arrh	3.38E+06	7.65E+06	8.83E+06
	70/100_1252_Q-Sun	4.42E+06	1.10E+07	1.40E+07
SE1	SE1 PAV_Uncond_Arrh	2.10E+06	6.06E+06	7.93E+06
	SE1 Q-SUN	1.83E+06	5.26E+06	6.84E+06

Table 5-3: Modelled aged time of PAV and Q-SUN for 70/100 and SE1 at the three reference frequencies

Type of bitumen		Modelled age time [year]		
		at 10 rad/s	at 62.83 rad/s	100 rad/s
70/100	70/100 PAV aged_Uncond_Arrh	3.9	2.3	2.2
	70/100_1252_Q-Sun	5.7	4.7	5.4
SE1	SE1 PAV_Uncond_Arrh	0.8	1.0	0.9
	SE1 Q-SUN	0.6	0.8	0.6



RHEOLOGICAL RESPONSE, COHESION AND ADHESION FATIGUE DAMAGE OF BITUMINOUS ROAD SEAL MATERIALS

7) The age for an average G^* in the common moving vehicle frequency range was assessed and is presented in Table 5-4. The related graphs for 70/100 and SE1 are respectively presented in Figure 5-7 and Figure 5-8.

Table 5-4: Data for average G^* and estimated aged time for PAV and Q-SUN aged bitumen

	Seal's bitumen ageing model constants			Average estimated aged time [year]	
	G^*_{t0}	b	c	70/100 PAV_Uncond_Arrh	70/100 _1252_Q-Sun
70/100	1.83E+06	2.47E+06	0.71	2.8	5.3
SE1	2.39E+06	3.15E+06	0.80	SE1 PAV_Uncond_Arrh 0.9	SE1 Q-SUN 0.6

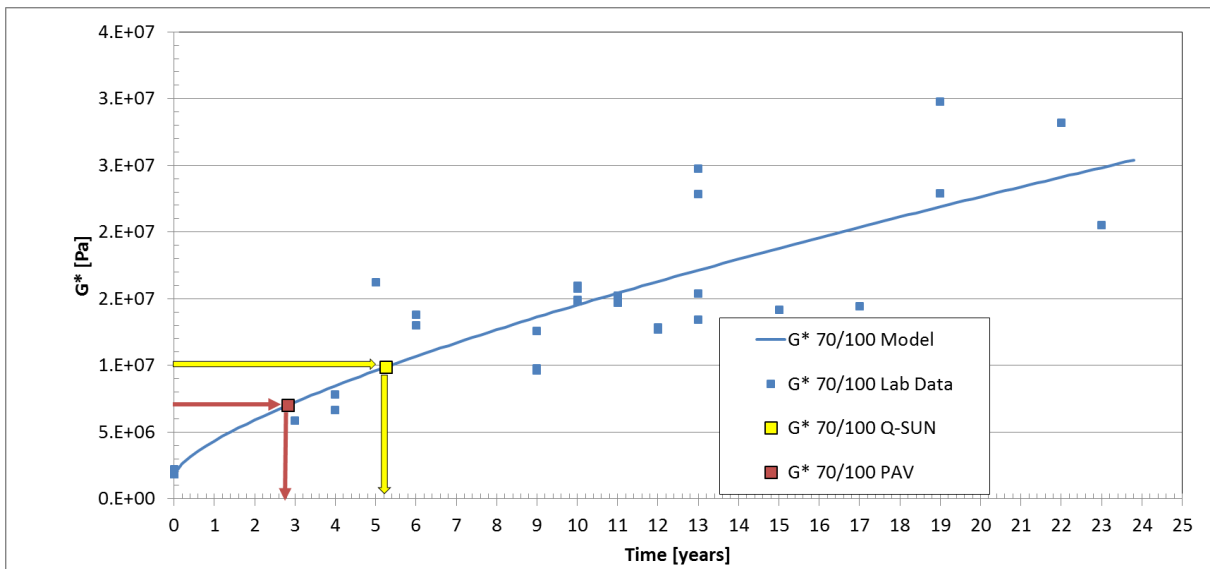


Figure 5-7: Graph of ageing model of 70/100 seal's bitumen based on average G^* from the three reference frequencies

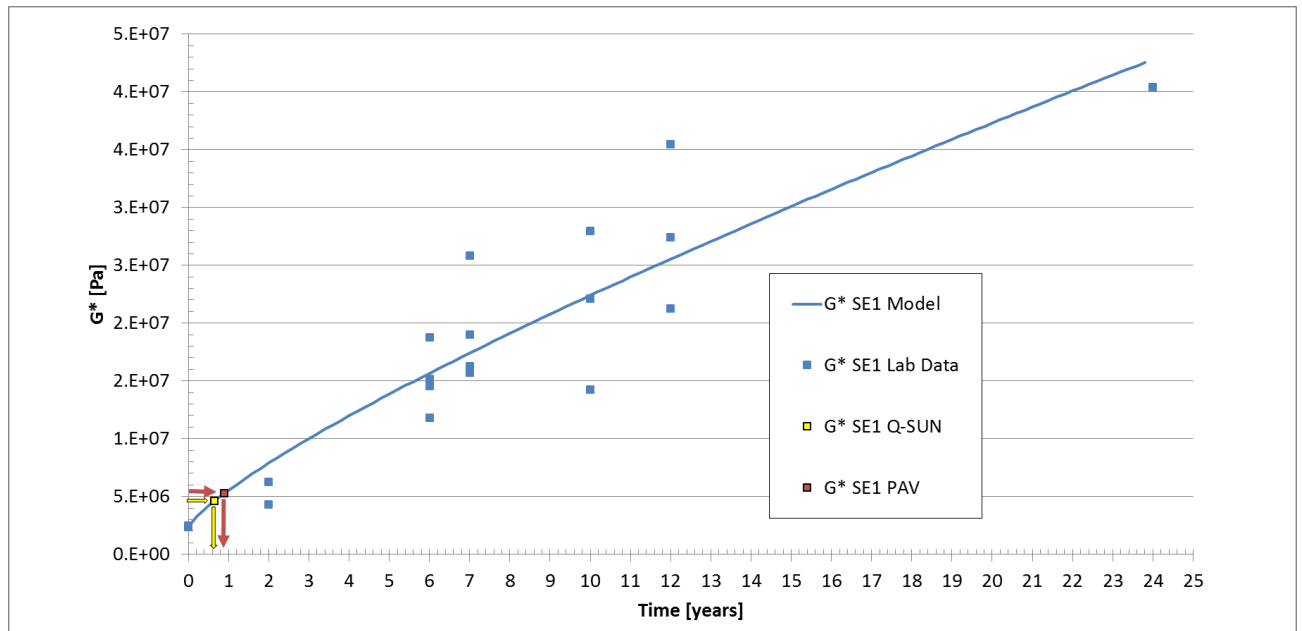


Figure 5-8: Graph of ageing model of SE1 seal's bitumen based on average G^* from the three reference frequencies

5.2.3 Discussion of the ageing model

The analysis of the 49 bitumens extracted from field-aged seals result in an ageing model for the seal's bitumen. This model, based on relative stiffening of G^* with time, is analysed for 70/100 and SE1 bitumens at three reference frequencies (10 rad/s, 62.83 rad/s and 100 rad/s).

Although Rowe *et al.* (2011) reported that the visco-elastic solid behaviour of modified binders cannot be modelled with some materials after ageing has occurred, the ageing model of a seal's bitumen developed appears to fit for both 70/100 and SE1. This model can be considered as a good attempt at a field-ageing simulation. However, the effect of different variabilities on this modelling attempt should be



noted. One of these variabilities is the change of bitumen consistency/stiffness due to:

- possible treatments undergone by the seal during its field exposure (e.g. rejuvenation)
- bitumen-recovery process in the laboratory
- differences in initial complex modulus
- change in ageing rate for different binders
- thickness of the seal

The ageing time simulations of the two laboratory ageing methods adopted (PAV and Q-SUN) were assessed based on the ageing model developed. From this assessment the following appears:

- On average, the PAV-aged bitumen can only simulate less than three years of 70/100 seal's bitumen.
- The Q-SUN method simulates on average just above five years for 70/100 seal's bitumen ageing.
- The simulation of SE1 ageing was found to be less than one year for both the PAV and Q-SUN methods. In this particular case, the PAV ageing time (0.9 years) is slightly higher than the Q-SUN ageing time (0.6 years).

A detailed investigation into the ageing model of both non-modified and modified bitumen is suggested. This investigation could compare laboratory ageing methods (Q-SUN and the PAV method) with field-aged binder recovered by a method that minimises the change in bitumen properties. The recovery process of bitumen requires more investigation which can be based on research reported in literature such as works performed by the Western Research Institute (WRI) (Burr,1993). In this regards, Steyn and Dednam (2014) and Kekana (2014) reported that mechanical methods of bitumen recovery (e.g. using centrifugal forces) appear to be promising compared with chemical methods.



5.3 Fatigue Damage Modelling

Fatigue damage modelling constituted the second part of the modelling following the ageing model based on response data. The fatigue modelling is based on the Cohesion Fatigue Damage (CFD) and Adhesion Fatigue Damage (AFD) data presented in Chapter 4. This modelling is developed in two components, namely end-life and accumulated damage. A background on fatigue life is presented prior to the development of the model.

5.3.1 Background to fatigue life

The fatigue mechanism approach in pavement bituminous materials has been investigated intensively in literature. Schapery (1981) investigated the constitutive equations for certain non-linear visco-elastic media and found that stresses and strains are pseudo-parameters in the form of convolution integrals. Galé (2000) validated this constitutive model equation by predicting the fatigue life for a continuously graded asphalt mix and produced a fatigue curve for use in the analytical design procedure for a continuously graded asphalt mix. A fatigue life investigation is also required for seal materials.

In this research fatigue damage of seal components was investigated in terms of adhesion and cohesion.

Huurman and Mo (2007) and Mo (2009) investigated the adhesion and cohesion of porous asphalt. The cohesion failure was characterised by means of laboratory testing on a binder column and modelled using a dissipated energy principle. The adhesion failure was characterised using a stone column laboratory test and modelled using the cumulative damage principle. This modelling approach for cohesion and adhesion damage is based on the determination of model parameters that are used as input into a predefined damage equation to determine the fatigue life or the damage. The determination of the model parameters is performed mainly by regression analyses. The approach for cohesion and the approach for adhesion are respectively detailed in Section 5.3.1.1 and Section 5.3.1.2.

5.3.1.1 Dissipated energy principle

The binder fatigue modelling was based on the dissipated energy principle as reported by Huurman and Mo (2007). The dissipated energy at repetition i (W_i) is calculated using Equation 5-3 to Equation 5-6.

$$W_i = \pi \tau_i \gamma_i \sin \delta_i \quad \text{Equation 5-3}$$

$$N_f = \left(\frac{W_0}{W_{initial}} \right)^n \quad \text{Equation 5-4}$$

where

W_i is the dissipated energy at i^{th} repetition

τ_i is the shear stress amplitude at i^{th} repetition

γ_i is the shear strain amplitude at i^{th} repetition

δ_i is the phase angle between maximum stress and strain

n is the material constant; n is expressed by Equation 5-5

N_f is the number of cycles to failure

W_0 is the reference energy; W_0 is expressed by Equation 5-6

$W_{initial}$ is the dissipated energy in the initial phase

$$n = a_1 + b_1 T \quad \text{Equation 5-5}$$

$$W_0 = a_2 + b_2 T \quad \text{Equation 5-6}$$

where

T is the temperature

a_1, b_1, a_2, b_2 are the model parameters

5.3.1.2 Cumulative damage principle

The adhesion modelling was based on the damage accumulation principle stated by Huurman and Mo (2007). This principle is described through Equation 5-7 to Equation 5-12.

$$D = \left(\frac{\sigma_{et}}{\sigma_0} \right)^{n_0} \quad \text{Equation 5-7}$$

Equation 5-7 is applicable for $\sigma_{et} > 0$; for $\sigma_{et} < 0$, D is considered to be zero.

with

$$\sigma_{et} = \sigma_n + \tau \cdot ctg\emptyset \quad \text{Equation 5-8}$$

where:

D is the rate of damage accumulation, $D = 1$ is failure of the adhesive zone

n_0 is a model parameter

σ_{et} is the equivalent tensile stress, i.e. tensile stress in the case of zero shear

σ_0 is the reference stress

σ_n is the adhesive zone normal stress

τ is the adhesive zone shear stress

\emptyset is the friction angle

$$N_f = \frac{1}{D_C} \quad \text{Equation 5-9}$$

where

N_f is the number of repetitions to failure

D_C is the damage accumulation in one repetition

$$n_0 = a_3 + b_3 T \quad \text{Equation 5-10}$$

$$\sigma_0 = a_4 + b_4 T \quad \text{Equation 5-11}$$

$$\Phi = a_5 + b_5 T \quad \text{Equation 5-12}$$

T is the temperature

$a_3, b_3, a_4, b_4, a_5,$ and b_5 are the model parameters

The output model parameters for the adhesion zone are: n_0, σ_0, Φ, D and N_f .

5.3.1.3 Establishment of modelling approach for cohesion and adhesion fatigue damage of bituminous seal materials

Instead of determining the model parameters of predefined damage equations, it was suggested in this research to monitor the change in stiffness of the bituminous seal materials. Therefore, G^* was monitored within the bitumen for CFD and at the stone-bitumen interface for AFD. Two components of this approach were suggested:

- 1) the expression of fatigue damage by monitoring ultimate G^* at failure of the material. This is a transfer function modelling, which expresses applied stress as a function of the number of repetitions to failure – it is termed the “end-life fatigue damage”
- 2) the monitoring of the G^* during the life period. This fatigue damage model represents the progression of damage over the life of the seal. This damage is expressed as a function of parameters such as stress and temperature – this is termed the “accumulated fatigue damage”.

The “accumulated fatigue damage” could be motivated by the “recursive simulation” models under development to be included in the SARDS. One of the ways used by SARDS to develop the recursive principle is the “memory-less” concept. The memory-less concept introduced by Theyse and van As (2010) is based on recent trends of mechanistic-empirical design method development towards modelling the incremental damage that occurs within recursive periods. Traffic loading,



environmental conditions and pavement characteristics remain consistent within each recursive period but vary from one recursive period to the next. Given the changing conditions from one recursive increment to the next, the damage incurred in successive recursive increments is not the same. The total damage is accumulated by the addition of the incremental damage from each recursive increment. Mechanistic-empirical design methods based on this approach are referred to as “recursive” mechanistic-empirical design methods. The incremental damage that occurs within a recursive analysis period may be modelled using a linear incremental damage model based on Miner’s Law or a non-linear incremental damage model. In the case of linear recursive mechanistic-empirical design methods, the damage models from classical mechanistic-empirical design methods may be used without modification. However, non-linear recursive methods require more advanced mathematical formulations of continuous damage models that capture the non-linear accumulation of damage. One of the tools used in the recursive mechanistic-empirical methods is the memory-less principle.

The memory-less principle used in the damage mechanism is borrowed from other fields such as probability and statistics. In probability distribution, the term "memory-less" refers to the properties of random variables in Markov processes that relate to the future and depend only on relevant information about the current time, not on information from further in the past (Feller, 1971; Theyse and Van As, 2010).

Theyse (2013) developed the memory-less principle (under the recursive simulation models) to predict the future damage and/or the failure of a material based only on the knowledge of current damage and the rate of the damage; therefore the damage history is not taken into account.

The implementation of the recursive simulation models requires knowledge of the characteristics of modelling parameters such as the stiffness of the material during the life period. This could be provided by the “accumulated fatigue damage” modelling of parameters such as G^* , as suggested in this research.



5.3.2 Fatigue damage model of cohesion and adhesion using the end-life principle

The end-life damage model was developed with 70/100 bitumen for CFD and AFD. The aggregate used for adhesion was dolorite (Dol).

5.3.2.1 Model development

The end-life model is based on the transfer function principle with the object of developing curves that present shear stress at the particular number of repetitions to failure (N_f). The model is developed using the criteria of a “sudden drop” in the G^* and the deflection angle (θ), as detailed in Section 3.5.2 and Section 4.3. The number of repetitions to failure (N_f) resulting from this criteria at different stress levels for a given temperature are recorded. These failure points are presented in Table 5-5 and Table 5-6 for cohesion and adhesion respectively. In these two tables, the torque is substituted by the equivalent shear stress using Equation 5-13 (as adapted from $\tau_{max} = \frac{2T}{\pi r^3}$ Equation 3-3).

$$\tau = K \frac{2M}{\pi r^3} \quad \text{Equation 5-13}$$

where

τ is the shear stress [Pa]

M is the torque [mNm]

r is the radius of the test sample; $r = 3$ mm for the bitumen column and $r = 5.45$ mm for the stone column

K is the conversion factor; $K = 1.00E+6$



Table 5-5: Number of repetitions to failure at different stress levels and temperatures for cohesion fatigue damage test

25 °C		23 °C		20 °C			
N_f	τ [Pa]	N_f	τ [Pa]	N_f	τ [Pa]		
40	5.97E+05	40	5.97E+05	70	5.97E+05		
50.4	4.77E+05	150	4.77E+05	130	4.77E+05		
90	3.58E+05	200	3.58E+05	350	3.58E+05		
290	2.39E+05	530	2.39E+05	730	2.39E+05		
3020	1.19E+05	5740	1.19E+05	15590	1.19E+05		
15 °C		10 °C		5 °C		0 °C	
N_f	τ [Pa]	N_f	τ [Pa]	N_f	τ [Pa]	N_f	τ [Pa]
330	5.97E+05	1270	5.97E+05	30	9.54E+05	3200	9.54E+05
450	4.77E+05	1980	4.77E+05	940	8.35E+05	7690	8.35E+05
590	3.58E+05	6430	3.58E+05	1540	7.16E+05	23580	7.16E+05
1210	2.39E+05	9070	2.39E+05	5620	5.97E+05	57220	5.97E+05

Table 5-6: Number of repetitions to failure at different stress levels and temperatures for adhesion fatigue damage test

25 °C		23 °C		20 °C		10 °C	
N_f	τ [Pa]	N_f	τ [Pa]	N_f	τ [Pa]	N_f	τ [Pa]
460	5.93E+05	690	6.92E+05	1 910	5.93E+05	8 900	7.90E+05
570	4.94E+05	2 790	5.53E+05	9 400	4.94E+05	40 700	5.93E+05
1 570	3.95E+05	3 450	4.94E+05	10 730	3.95E+05	-	-
6 190	2.96E+05	4 730	4.35E+05	38 320	1.98E+05	-	-
-	-	16 380	3.95E+05	-	-	-	-
-	-	43 160	296 418	-	-	-	-
-	-	48 970	197 612	-	-	-	-



transfer functions for cohesion within 70/100 bitumen and adhesion between dolomite and 70/100 bitumen are presented respectively in Figure 5-10 and Figure 5-11.

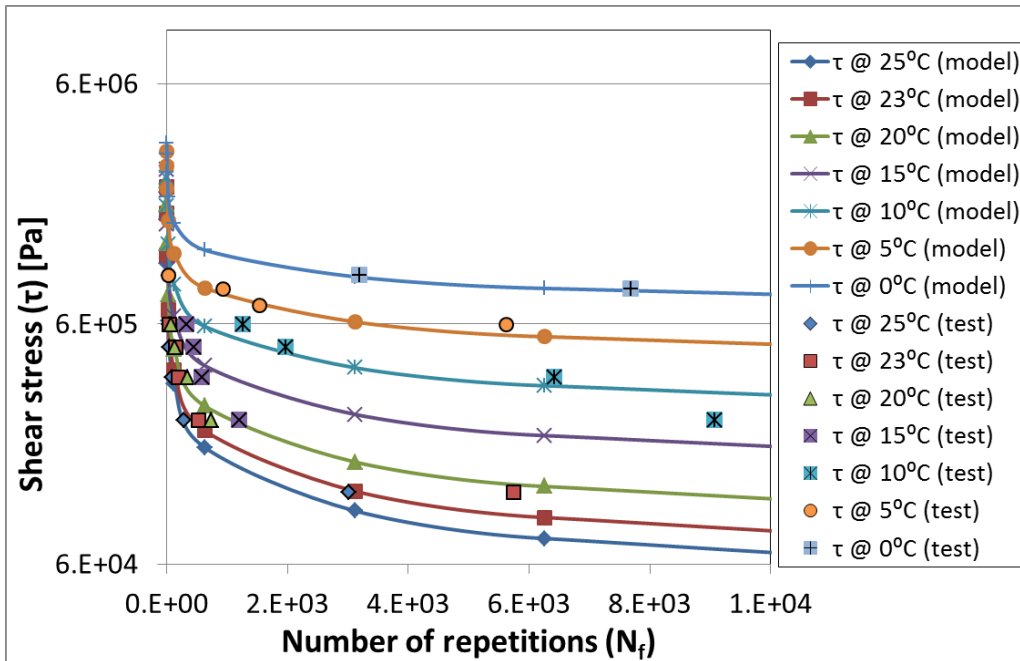
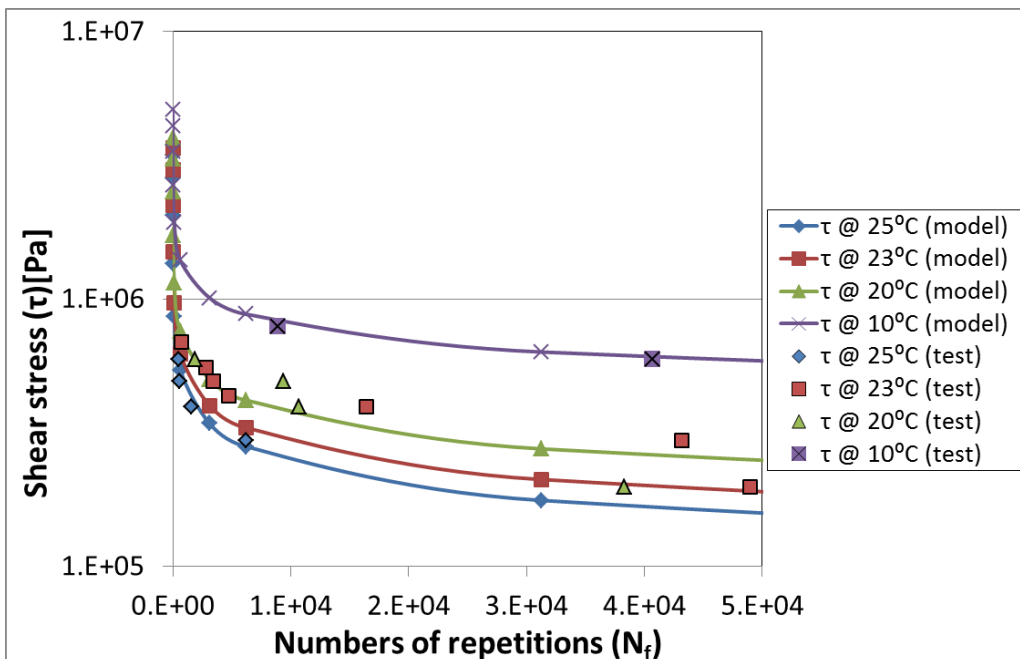


Figure 5-10: Cohesion fatigue damage transfer function for 70/100 bitumen



RHEOLOGICAL RESPONSE, COHESION AND ADHESION FATIGUE DAMAGE OF BITUMINOUS ROAD SEAL MATERIALS

Figure 5-11: Adhesion fatigue damage transfer function between dolorite and 70/100 bitumen

3) It was found that the coefficients a and b in Equation 5-14 could be expressed as functions of temperature. An example of this relationship is presented in Figure 5-12 for the case of coefficient a of the CFD. The full graphs of the relationship between the two coefficients (a and b) and the temperatures for the CFD and AFD are presented in Appendix H.

Both a and b were expressed as a linear relationship with the temperature. The coefficient a is presented in Equation 5-15, while the coefficient b is presented in Equation 5-16.

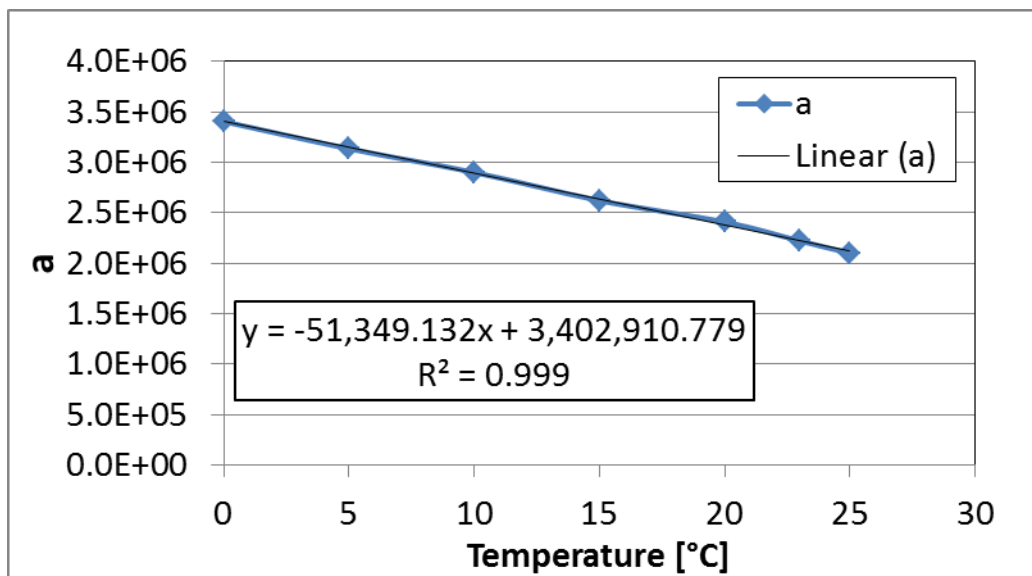


Figure 5-12: Relationship between coefficient “a” and the temperature for cohesion fatigue damage model with 70/100 bitumen binder

$$a = \alpha_1 T + \alpha_2$$

Equation 5-16

where:

α_1 and α_2 are constants

Values of α_1 and α_2 for the CFD model (of 70/100-Unaged-Unconditioned) and for the AFD model (between dolorite and 70/100-Unaged-Unconditioned) are given in Table 5-7.

$$b = \beta_1 T + \beta_2 \quad \text{Equation 5-17}$$

where

β_1 and β_2 are constants

Values of β_1 and β_2 for the CFD model (of 70/100-Unaged-Unconditioned) and for the AFD model (between dolorite and 70/100-Unaged-Unconditioned) are given in Table 5-7.

Using the relationship of coefficients a and b , Equation 5-14 can be written as presented in Equation 5-17.

$$\tau = (\alpha_1 T + \alpha_2)(1 + N_f)^{(\beta_1 T + \beta_2)} \quad \text{Equation 5-18}$$

Table 5-7: Values of model constants in the cohesion and adhesion fatigue damage models

Model description	α_1	α_2	β_1	β_2
Cohesion 70/100-Unaged-Unconditioned	-5.13E+04	3.40E+06	-0.01	-0.16
Adhesion Dol-70/100-Unaged-Unconditioned	-1.11E+06	6.23E+06	-0.06	-0.15

The correlation between the shear stress data from the laboratory tests and the modelled shear stress are given in Figure 5-13 and Figure 5-14 respectively for the



CFD model and the AFD model. It can be observed that the laboratory data and those from the model correlate well.

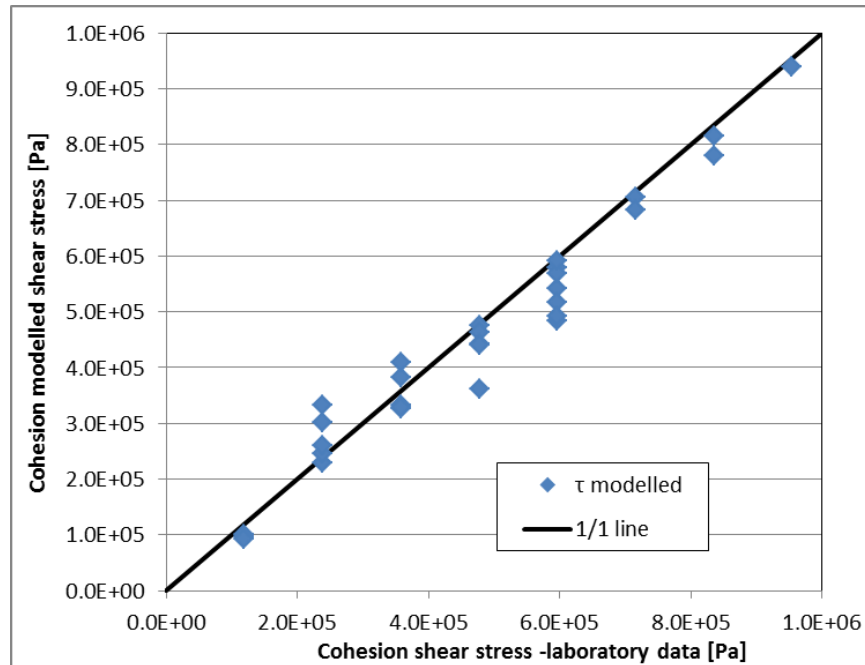


Figure 5-13: Correlation between modelled and laboratory-based shear stress in the case of cohesion fatigue damage

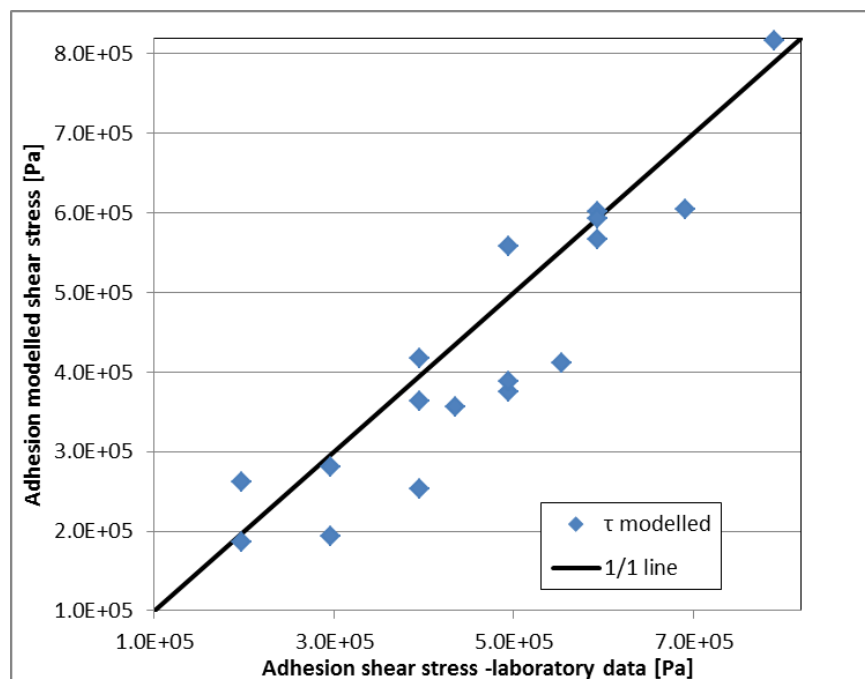


Figure 5-14: Correlation between modelled and laboratory-based shear stress in the case of adhesion fatigue damage

5.3.2.2 Discussion of end-life model

The end-life model defines transfer functions for CFD and AFD. These transfer functions allow the determination of the shear stress at failure as a function of the number of repetitions to failure and temperature. This model displayed a good fit to the laboratory data. The positions of the isotherms were consistent in increment compared with increments of the temperature (Figure 5-10 and Figure 5-11).

Considering the same number of repetitions to failure, the failure occurs at high shear stress for low temperature. Similarly, the failure occurs at low shear stress for high temperature. At the same shear stress, the failure occurs earlier at high temperature than at low temperature. The last observation appears to be counter-intuitive. This counter-intuitive observation has been mentioned in the literature such as in the book by Domone and Illstone (2010) in which it is reported that fatigue tests conducted under strain-controlled mode and stress-controlled mode produce reversed results. In a stress-controlled test, higher stiffness is related to longer life; conversely, in a strain-controlled test higher stiffness is related to shorter life, as presented in Figure 5-15. In this figure S1, S2, S3, S4 are stiffness of materials.

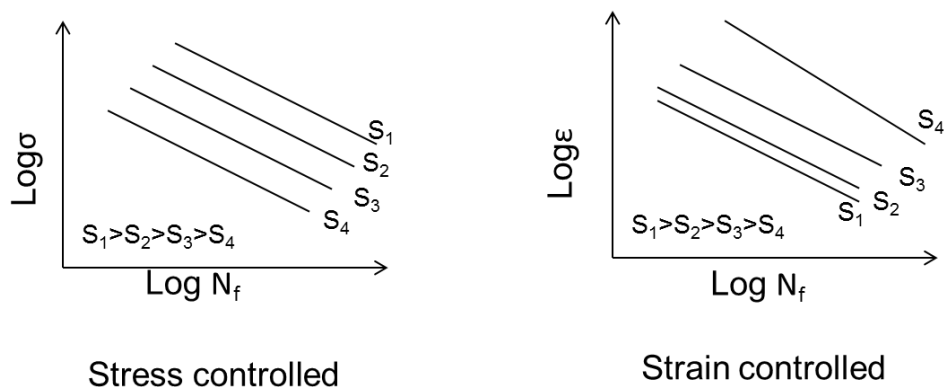


Figure 5-15: Reversed fatigue results under stress-controlled and strain-controlled conditions (after Domone and Illstone, 2010)

This counter-intuitive observation can be explained by the fact that bituminous the material at low temperature would be brittle and have a higher stiffness and therefore resulting to brittle and quick failure. Similarly, at high temperature the same material will be less stiff and display a creep-like behaviour carrying low stress, resulting in more deformation with possibility of “separation failure” occurring much later.

From the fatigue damage test results, it is noticed that at the same shear stress level, cohesion occurs earlier then adhesion as shown in Figure 5-16. This can be probably explained by fact that fatigue test does not suitably handle adhesion due to its requirement of low maximum stress value. In this case, the stiffer stone-column sample (for adhesion) might require more time to fail compare to the bitumen column sample (for cohesion). As a result of this observation it is suggested that it be investigated whether the adhesion phenomenon could be considered as a “non-fatigue” mechanism as discussed in Section 2.11.2. As the tensile is not well measured in a shear test, the adhesion can also be considered as a tensile fatigue test.

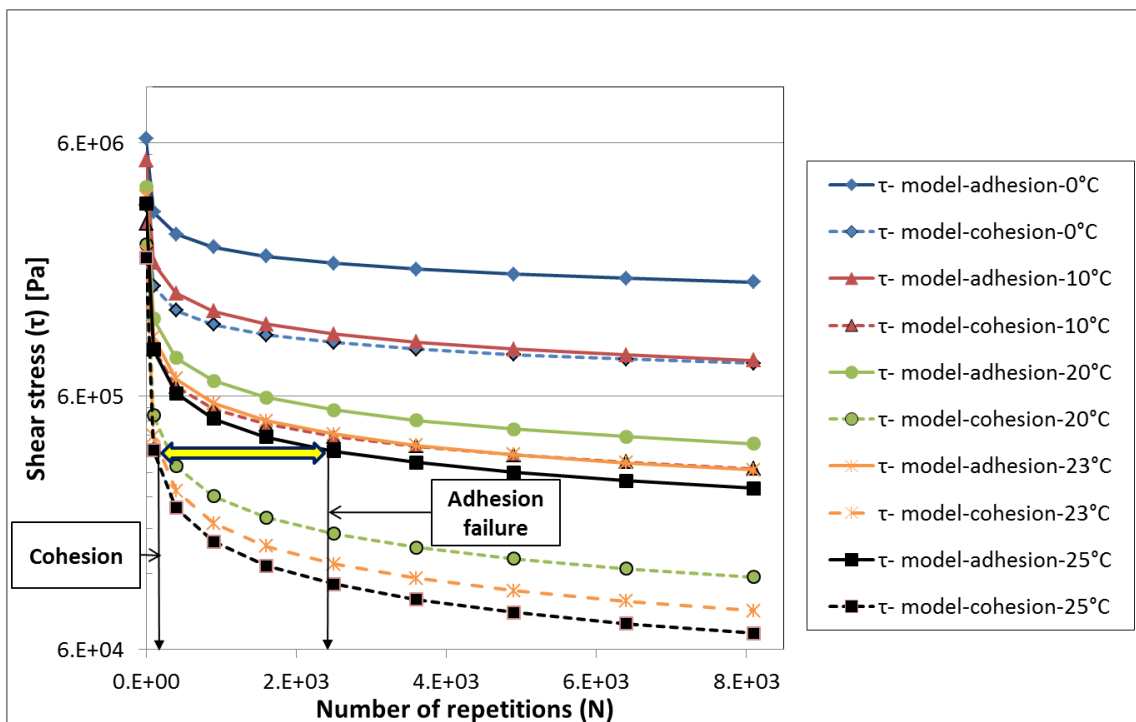


Figure 5-16: comparison cohesion-adhesion failure times



5.3.3 Accumulated fatigue damage model of cohesion and adhesion

The accumulated damage model was developed using the same materials and tests as the end-life damage model presented in Section 5.3.2.

5.3.3.1 Model development

Similarly to the end-life damage model, the model of accumulated damage is developed using the “sudden drop” principle. The sudden drop of G^* fixes the maximum damage to a value closer to one as mentioned in Section 4.5. The aim is to model the development of the damage during the seal’s life from a state of no damage (damage = 0) to the failure state (damage ≈ 1). The development of the accumulated damage model was based on the establishment of the fatigue damage (D) as a function of the number of repetitions (N), stress (τ) and temperature (T). Expressing the model in terms of stress and temperature accounted respectively for the traffic and the environmental effect.

For simplification reasons, the modelling was expressed in terms of the normalised number of repetitions (N_n), instead of the actual number of repetitions (N). The normalised number of repetitions (N_n) is presented in Equation 5-18. N_n also varies from zero to one.

$$N_n = \frac{N}{N_F} \quad \text{Equation 5-19}$$

where

N_n is the normalised number of repetitions

N is the number of repetitions at a given time

N_F is the number of repetitions to failure

The development of the accumulated modelling of CFD and AFD was done in two steps. In the initial step the damage at different torque levels for each separate temperature was modelled, and thereafter there was a generalised step in which all the models constructed at each temperature (isotherms) were combined into one global model. The global modelling consisted of adjustment of the model coefficients of the initial models.

The accumulated damage models of CFD and AFD were developed in the following steps to produce the final model:

- 1) The record of the variation of G^* with the number of repetitions (N) collected at different torque (stress) levels for a given temperature constitutes the major DSR testing outcome used in this modelling. Using the sudden drop principle, the complex modulus at failure ($G^*_{N_f}$) was determined for each stress level at a given temperature of the CFD and AFD tests.
- 2) The calculations of damage from the DSR results (D_X -calc) for CFD and AFD of each repetition were processed using Equation 4-2. The damage varied from zero (no damage) to one (failure state). In the symbol " D_X -calc", the subscript $X = C$ in the case of CFD and $X = A$ in the case of AFD.
- 3) Using Equation 5-18, the number of repetitions was normalised to range from zero to one.
- 4) The damage (D_X -calc) was expressed as a function of the normalised number of repetitions (N_n), $D_X = f(N_n)$, for each torque level for a given temperature. It was found that a rational function called the "Nelder" function provided the better fit for each stress level for a given temperature. This function is presented in Equation 5-19. In general, the Nelder function fitted both the CFD and AFD models well (as confirmed by coefficient of determination R^2 in Appendix I.3 and I.4).

$$D_X = \frac{N_n + a_X}{b_X + c_X(N_n + a_X) + w_X(N_n + a_X)^2} \quad \text{Equation 5-20}$$

where

D_X is the fatigue damage

N_n is the number of load repetitions

a_X, b_X, c_X and w are the model coefficients or Nelder coefficients

$X = C$ in the case of CFD and $X = A$ in the case of AFD.

5) In the initial stage of model development, Equation 5-19 was rewritten as expressed in Equation 5-20. The initial values of the Nelder coefficients (a'_X , b'_X , c'_X and w'_X) for each stress level for a given temperature were determined by a regression analysis. In the regression analysis, the modelled damage was fitted to the calculated damage from measured data by minimising the error between the two damages. A typical graph of damage as a function of the normalised number of repetitions is presented in Figure 5-17. Appendix I.1 and Appendix I.2 contain all the graphs of damage as a function of the normalised number of repetitions respectively for CFD and AFD. An example of initial Nelder coefficients in the case of CFD tested at 25 °C and at different stress levels is presented in Table 5-8. The entire set of initial Nelder coefficients for all CFD and AFD case tests are presented in Appendix I.3 and Appendix I.4 respectively.

$$D'_X = \frac{N_n + a'_X}{b'_X + c'_X(N_n + a'_X) + w'_X(N_n + a'_X)^2} \quad \text{Equation 5-21}$$

where

D'_X is the initial value of the fatigue damage

N_n is the number of load repetitions

a'_X , b'_X , c'_X and w'_X are the initial values of the model coefficients (or Nelder coefficients) determined at each torque level of each testing temperature of CFD and AFD.

RHEOLOGICAL RESPONSE, COHESION AND ADHESION FATIGUE DAMAGE OF BITUMINOUS ROAD SEAL MATERIALS

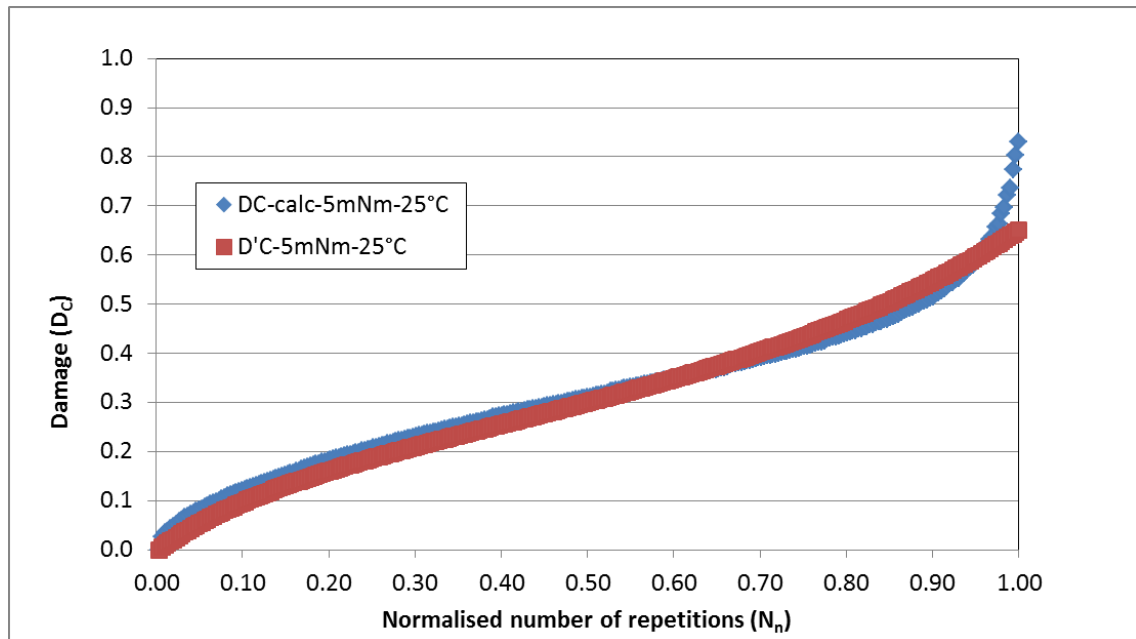


Figure 5-17: Damage calculated from DSR results (D_C -calc) and initial modelled damage (D'_C) vs. normalised number of repetitions at 5mNm – 25 °C

Table 5-8: Initial values of Nelder coefficients in the case of cohesion within 70/100 bitumen at 25 °C and at different stress levels

τ [Pa]	$a'_c(25\text{ }^\circ\text{C})$	$b'_c(25\text{ }^\circ\text{C})$	$c'_c(25\text{ }^\circ\text{C})$	$w'_c(25\text{ }^\circ\text{C})$
1.19E+05	-0.003	0.750	2.859	-2.082
2.39E+05	-0.044	0.811	1.445	-0.825
3.58E+05	-0.111	0.950	0.863	-0.121
4.77E+05	-0.200	1.150	-0.029	1.366
5.97E+05	-0.270	1.400	-2.308	2.324

6) A relationship between each initial value of the Nelder coefficient and the torque (stress) level could be observed at each temperature for both CFD and AFD. The relationship was developed by selecting an appropriate fitting function. These relationships for a'_x , b'_x , c'_x and w'_x are presented in Equation 5-21, Equation 5-22, Equation 5-23, and Equation 5-24 respectively. Graphs presenting the development of these equations are illustrated in Appendix I.5 and Appendix I.6 respectively for CFD and AFD.

$$a'_X = \alpha'_{X1}\tau + \alpha'_{X2} \quad \text{Equation 5-22}$$

$$b'_X = \beta'_{X1}e^{\beta'_{X2}\tau} \quad \text{Equation 5-23}$$

$$c'_X = \gamma'_{X1}\tau + \gamma'_{X2} \quad \text{Equation 5-24}$$

$$w'_X = \omega'_{X1}\tau + \omega'_{X2} \quad \text{Equation 5-25}$$

where

a'_X , b'_X , c'_X and w'_X are the initial Nelder coefficients for CFD and AFD as presented respectively in Appendix I.3 and Appendix I.4

α'_{X1} , α'_{X2} , β'_{X1} , β'_{X2} , γ'_{X1} , γ'_{X2} , ω'_{X1} and ω'_{X2} are the global model coefficients (global coefficients). These global model coefficients are determined for each testing temperature of CFD and AFD.

τ is the shear stress level calculated from the torque level using Equation 5-13
As an example of using the subscript X in the case of CFD, Equation 5-22 would be written as presented in Equation 5-25.

$$b'_C = \beta'_{C1}e^{\beta'_{C2}\tau} \quad \text{Equation 5-26}$$

The values of the global coefficients are presented in Table 5-9 in the case of CFD and in Table 5-10 in the case of AFD.

Table 5-9: Values of global coefficients for cohesion fatigue damage (CFD)

Initial Nelder coefficients for CFD	Temperature [°C]						
	0	5	10	15	20	23	25
α'_{C1}	-1.53E-08	-2.57E-09	-1.89E-08	-7.55E-08	-1.61E-07	-5.17E-07	-1.38E-02
α'_{C2}	1.1E-02	4.4E-04	3.6E-03	9.6E-03	2.28E-02	8.20E-02	8.09E-02
β'_{C1}	1.39E-03	1.00E-01	2.25E-01	3.40E-01	4.89E-01	5.74E-01	6.11E-01
β'_{C2}	5.98E-06	2.70E-06	2.10E-06	2.00E-06	1.40E-06	1.34E-06	1.34E-06
γ'_{C1}	-1.41E-05	-2.13E-06	-3.72E-06	-5.54E-06	-5.97E-06	-9.05E-06	-9.90E-06
γ'_{C2}	1.63E+01	4.17E+00	3.71E+00	3.87E+00	3.66E+00	3.65E+00	4.11E+00
ω'_{C1}	8.48E-06	2.80E-06	2.05E-06	4.49E-06	3.97E-06	7.40E-06	9.22E-06
ω'_{C2}	-1.02E+01	-4.09E+00	-2.30E+00	-2.89E+00	-2.42E+00	-2.63E+00	-3.17E+00



Table 5-10: Values of global coefficients for adhesion fatigue damage (AFD)

Initial Nelder coefficients for AFD	Temperature[°C]			
	10	20	23	25
α'_{A1}	-9.61E-09	-4.90E-08	-2.51E-08	-2.56E-08
α'_{A2}	5.70E-02	2.37E-02	8.23E-03	4.86E-03
β'_{A1}	4.23E+00	2.40E-01	2.87E-03	1.36E-03
β'_{A2}	5.2E-07	4.3E-06	5.2E-06	5.91E-06
γ'_{A1}	-0.0002	-1.36E-05	-7.02E-06	-1.07E-05
γ'_{A2}	117.18	7.81	7.27	9.12
ω'_{A1}	2.09E+00	7.20E-06	7.06E-06	1.06E-05
ω'_{A2}	5.35153	5.77	-6.21	-8.11

7) As discussed in Section 4.5 and in the introduction to this section (5.3.3.1), the ultimate aim of the accumulated modelling was to attempt to express the damage as a function of stress and temperature. Equation 5-21 to Equation 5-24 represented functions that connect the initial Nelder Coefficients to the stress levels at each tested temperature. The combination of each initial Nelder coefficient in one graph (as presented in Figure 5-18 for b'_c) allowed the assessment of a possible relationship linking the initial values of the Nelder coefficient to the temperature.

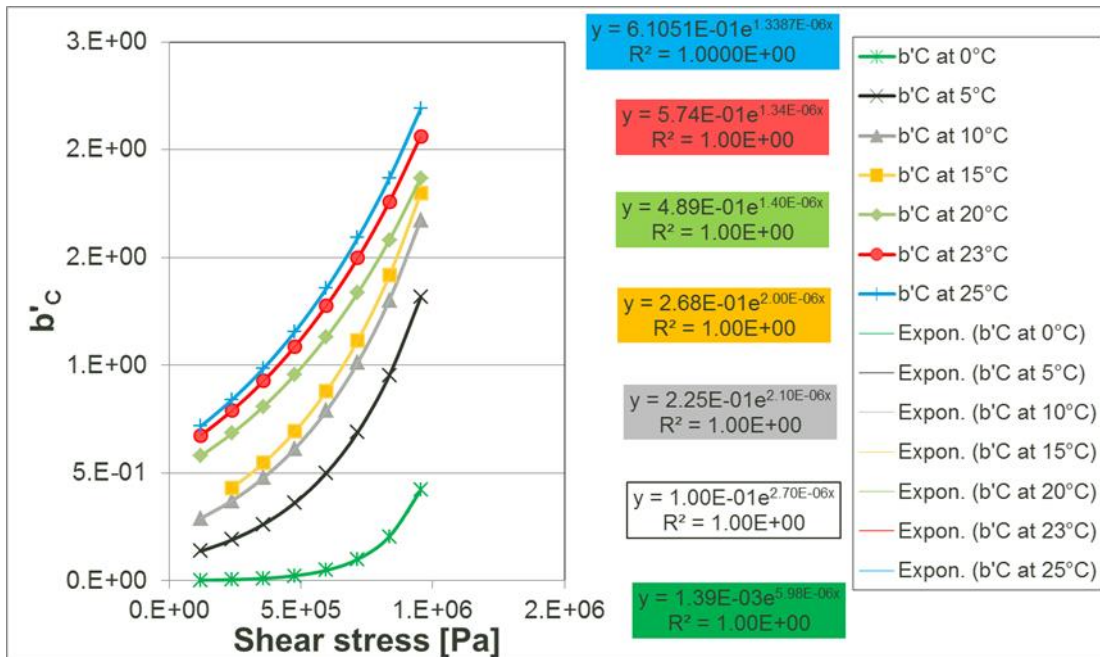


Figure 5-18: Combination of all Nelder Coefficients b'_c on a unique graph

The investigation of this relationship was based on the global model coefficients. In some cases, it was found that the global model coefficients could be expressed as a function of the stress level or of the temperature or of both of them. In the specific case of initial Nelder coefficient b'_c as expressed by Equation 5-25, it was observed that the global model coefficient β'_{c1} could be expressed as a linear function of temperature. This is presented in Figure 5-19 and expressed by Equation 5-26. No obvious relationship was found for β'_{c2} – neither with stress level, nor with temperature; thus β'_{c2} could be expressed as a constant.

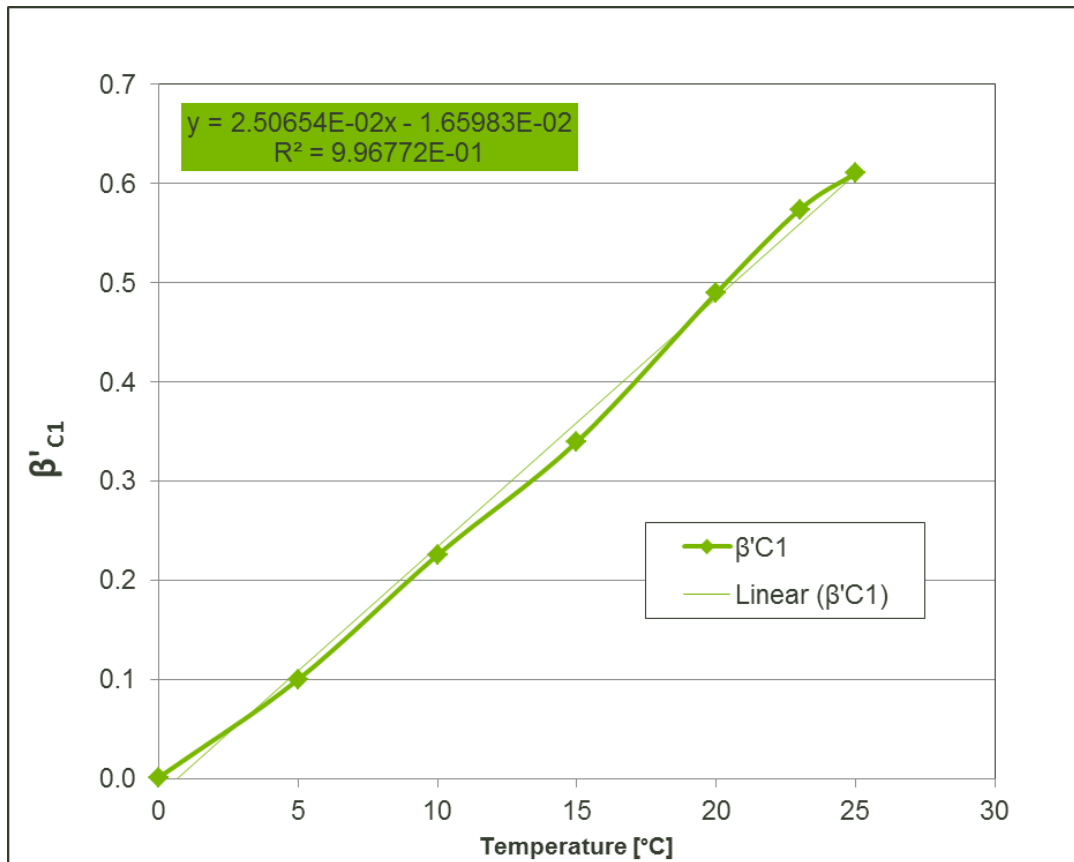


Figure 5-19: Relationship between β'_{C1} and temperature

Table 5-11 provides information on all global model coefficients in terms of their relationship with stress level and/or temperature. This information was based on the observed trends of the global model coefficients as a function of stress level and/or temperature.

$$\beta'_{C1} = \beta_{C1}T + \beta_{C2}$$

Equation 5-27

where

β'_{C1} is the global model coefficient

β_{C1} and β_{C2} are constants in the model

Table 5-11: Information on the relationship between global model coefficients and stress level and/or temperature, based on observed trends

Global model coefficients	Relationship with τ	Relationship with T	Observation
α'_{C1}	No	No	$\alpha'_{C1} = \text{Constant}$
α'_{C2}	No	No	$\alpha'_{C2} = \text{Constant}$
β'_{C1}	Yes	Yes	$\beta'_{C1} = f(\tau, T)$
β'_{C2}	No	No	$\beta'_{C2} = \text{Constant}$
γ'_{C1}	No	No	$\gamma'_{C1} = \text{Constant}$
γ'_{C2}	No	No	$\gamma'_{C2} = \text{Constant}$
ω'_{C1}	No	No	$\omega'_{C1} = \text{Constant}$
ω'_{C2}	No	No	$\omega'_{C2} = \text{Constant}$
α'_{A1}	Yes	Yes	$\alpha'_{A1} = f(\tau, T)$
α'_{A2}	No	No	$\alpha'_{A2} = \text{Constant}$
β'_{A1}	No	No	$\beta'_{A1} = \text{Constant}$
β'_{A2}	Yes	Yes	$\beta'_{A2} = f(\tau, T)$
γ'_{A1}	No	No	$\gamma'_{A1} = \text{Constant}$
γ'_{A2}	No	No	$\gamma'_{A2} = \text{Constant}$
ω'_{A1}	No	No	$\omega'_{A1} = \text{Constant}$
ω'_{A2}	No	No	$\omega'_{A2} = \text{Constant}$

By substituting Equation 5-26 in Equation 5-25, the adjusted model coefficient is obtained as represented in Equation 5-27. The adjusted model coefficient then replaces the initial Nelder coefficients.

$$b_C = (\beta_{C1}T + \beta_{C2})e^{\beta_{C3}\tau} \quad \text{Equation 5-28}$$

where

b_C is an adjusted model coefficient for CFD

β_{C1} , β_{C2} and β_{C3} are model constants for CFD

(It should be noted that $\beta_{C3} = \beta'_{C2}$, with β'_{C2} as presented in Equation 5-25)

T is the temperature

τ is the shear stress

Other adjusted model coefficients and global model coefficients were obtained in a similar manner and are presented in Equation 5-28 to Equation 5-34. The graphs representing the development of these coefficients and constants are presented in Appendix I.7 for CFD and Appendix I.8 for AFD.

$$a_c = \alpha_{c1}\tau + \alpha_{c2} \quad \text{Equation 5-29}$$

$$c_c = \gamma_{c1}\tau + \gamma_{c2} \quad \text{Equation 5-30}$$

$$w_c = \omega_{c1}\tau + \omega_{c2} \quad \text{Equation 5-31}$$

$$a_A = \alpha_{A1}\tau + \alpha_{A2}T + \alpha_{A3} \quad \text{Equation 5-32}$$

$$b_A = \beta_{A1}e^{(\beta_{A2}T + \beta_{A3})\tau} \quad \text{Equation 5-33}$$

$$c_A = \gamma_{A1}T + \gamma_{A2} \quad \text{Equation 5-34}$$

$$w_A = \omega_{A1}T + \omega_{A2} \quad \text{Equation 5-35}$$

where

a_c , c_c , and w_c are the adjusted model coefficients for CFD

a_A , b_A , c_A , and w_A are the adjusted model coefficients for AFD

α_{c1} , α_{c2} , γ_{c1} , γ_{c2} , ω_{c1} and ω_{c2} are model constants for CFD

α_{A1} , α_{A2} , α_{A3} , β_{A1} , β_{A2} , β_{A3} , γ_{A1} , γ_{A2} , ω_{A1} and ω_{A2} are model constants for AFD

T is the temperature

τ is the shear stress

- 8) The initial CFD and AFD models developed at each stress level and each temperature were generalised based on adjusted values of the model coefficients (a_x , b_x , c_x and w_x). The adjusted values of the model coefficients were included in Equation 5-19 to form the global damaged model at each level for each specific temperature. A typical plot of this global damage model

RHEOLOGICAL RESPONSE, COHESION AND ADHESION FATIGUE DAMAGE OF BITUMINOUS ROAD SEAL MATERIALS

for CFD in the case of the 70/100 bitumen modelled at the temperature of 25 °C is presented in Figure 5-20. The full set covering each specific graph for a different temperature is presented in Appendix I.9 for CFD and Appendix I.10 for AFD.

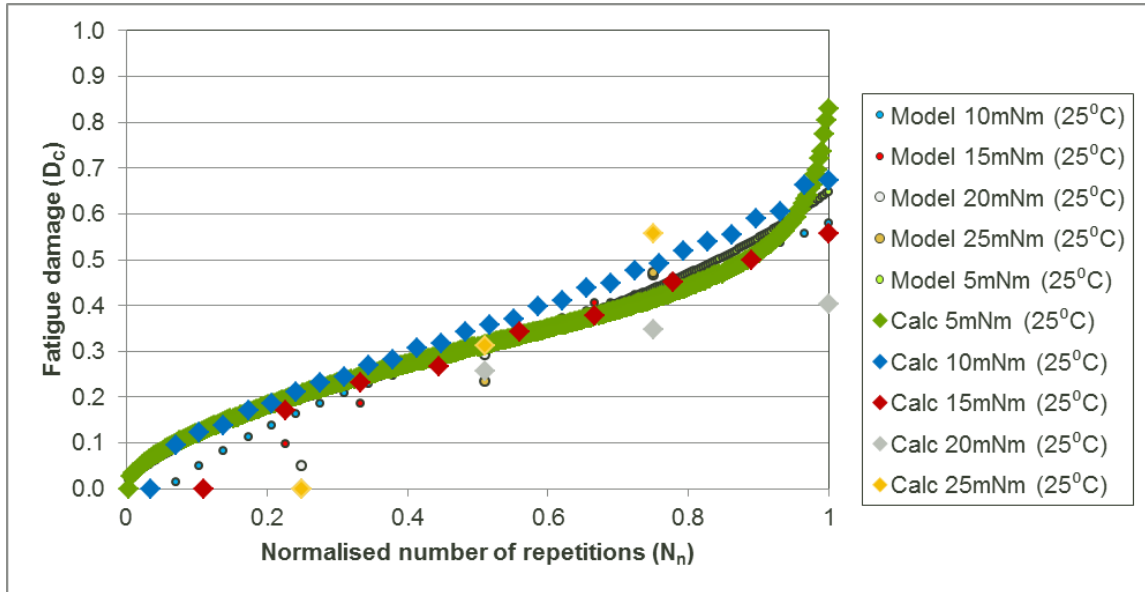


Figure 5-20: Plot of global damage model for CFD in the case of the 70/100 bitumen modelled at the temperature of 25 °C

The global damage model was generalised to include all temperatures and was symbolised by “ D_X -model”. D_X -model in the case of CFD is symbolised by “ D_C ” and D_X -model in the case of AFD is symbolised by “ D_A ”. These two models are respectively referred to as the CFD model within the seal’s bitumen and the AFD between seal stone and bitumen. The CFD model within the seal’s bitumen is presented in Equation 5-35 and shown graphically in Figure 5-21. Similarly, the adhesion between seal stone and bitumen is presented in Equation 5-36 and its graphic presentation is shown in Figure 5-22.

$$D_C = \frac{N_n + a_C}{b_C + c_C(N_n + a_C) + w_C(N_n + a_C)^2}$$

Equation 5-36



$$D_A = \frac{N_n + a_A}{b_A + c_A(N_n + a_A) + w_A(N_n + a_A)^2}$$

Equation 5-37

In these two equations, the adjusted model coefficients are as presented in Equation 5-27 to Equation 5-34 . An example of the values of adjusted model coefficients in the case of CFD tested at 25 °C and at different stress levels is presented in Table 5-12. The entire set of values of adjusted model coefficients for all CFD and AFD cases tested are presented in Appendix I.11 and Appendix I.12 respectively.

Table 5-12: Values of adjusted model coefficients in the case of cohesion fatigue damage tested at 25 °C and at different stress levels

τ [Pa]	a_c (25 °C)	b_c (25 °C)	c_c (25 °C)	w_c (25 °C)
1.193E+05	0.012	7.1567E-01	2.927	-2.068
2.386E+05	-0.057	8.3961E-01	1.747	-0.968
3.579E+05	-0.126	9.8500E-01	0.566	0.132
4.772E+05	-0.195	1.1556E+00	-0.615	1.233
5.965E+05	-0.264	1.3557E+00	-1.796	2.333

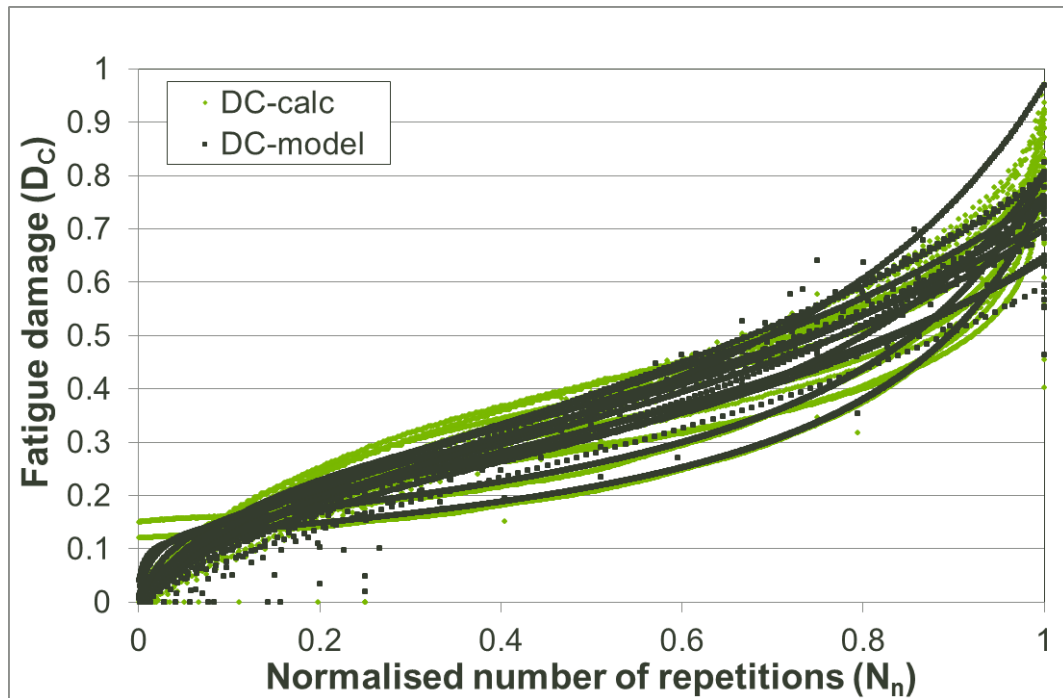


Figure 5-21: Normalised cohesion fatigue damage model during seal life

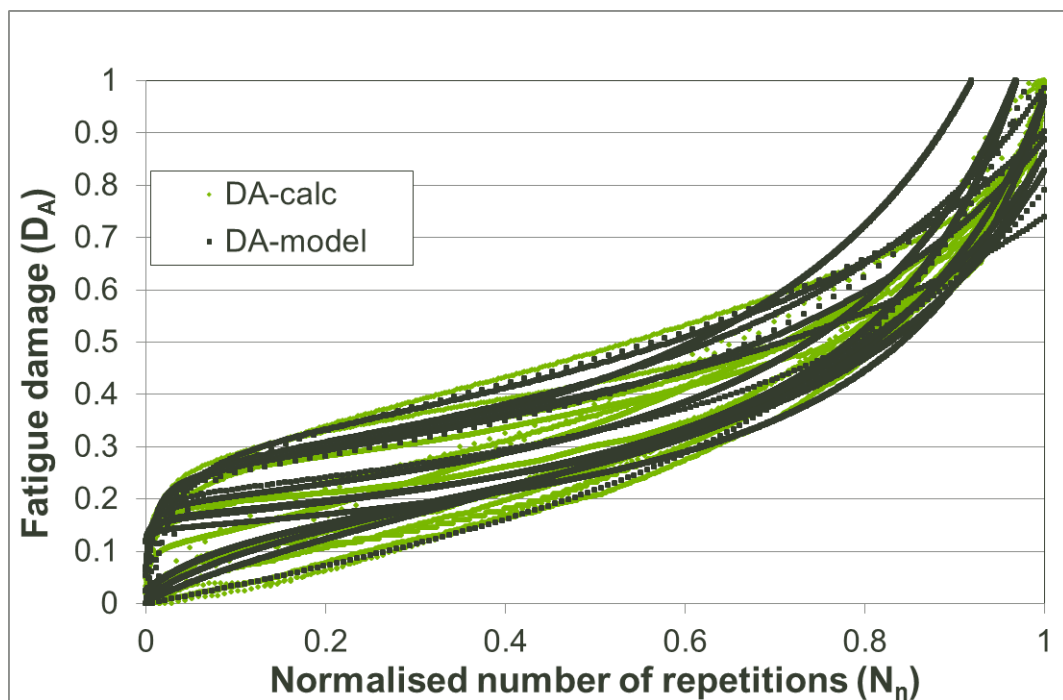


Figure 5-22: Normalised adhesion fatigue damage model during seal life

RHEOLOGICAL RESPONSE, COHESION AND ADHESION FATIGUE DAMAGE OF BITUMINOUS ROAD SEAL MATERIALS

The D_X -models (for CFD and AFD) were compared with the damage calculated (D_X -calc) from the DRS data. The coefficient of determination (R^2) and the Standard Error of Estimate (SEE) are presented in Table 5-13. In addition, the correlations between D_X -calc and D_X -model are given in Figure 5-23 and Figure 5-24 respectively for CFD and AFD. It can be concluded that there is an acceptable correlation between the damage calculated from laboratory data and from the model.

Table 5-13: coefficient of determination and Standard Error of Estimate for CFD and AFD

	CFD	AFD
R^2	0.98	0.97
SEE	0.04	0.08

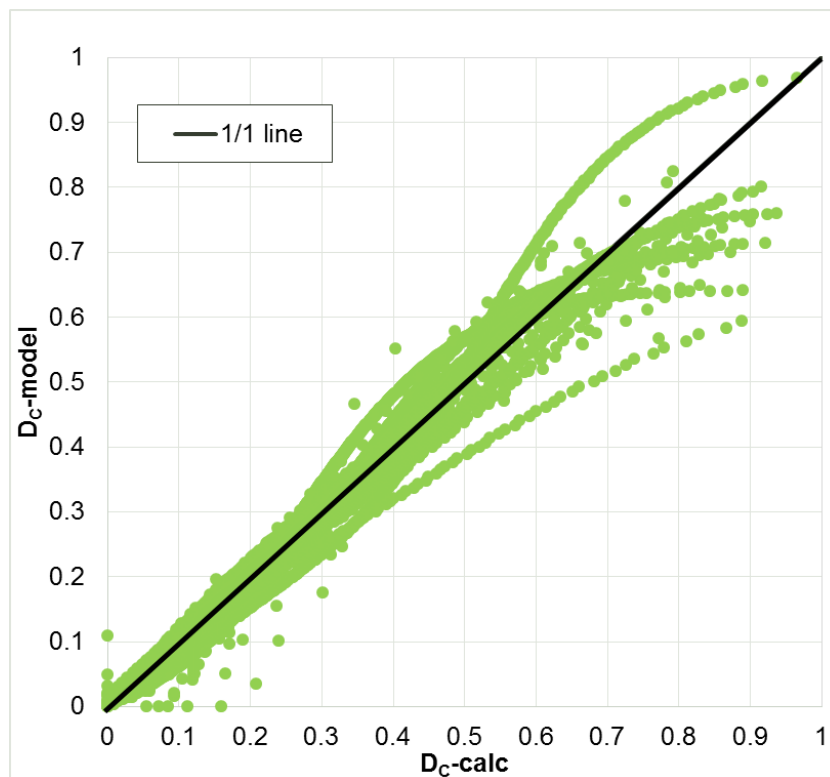


Figure 5-23: Correlation between damage calculated from laboratory data and modelled damage in the case of cohesion fatigue damage

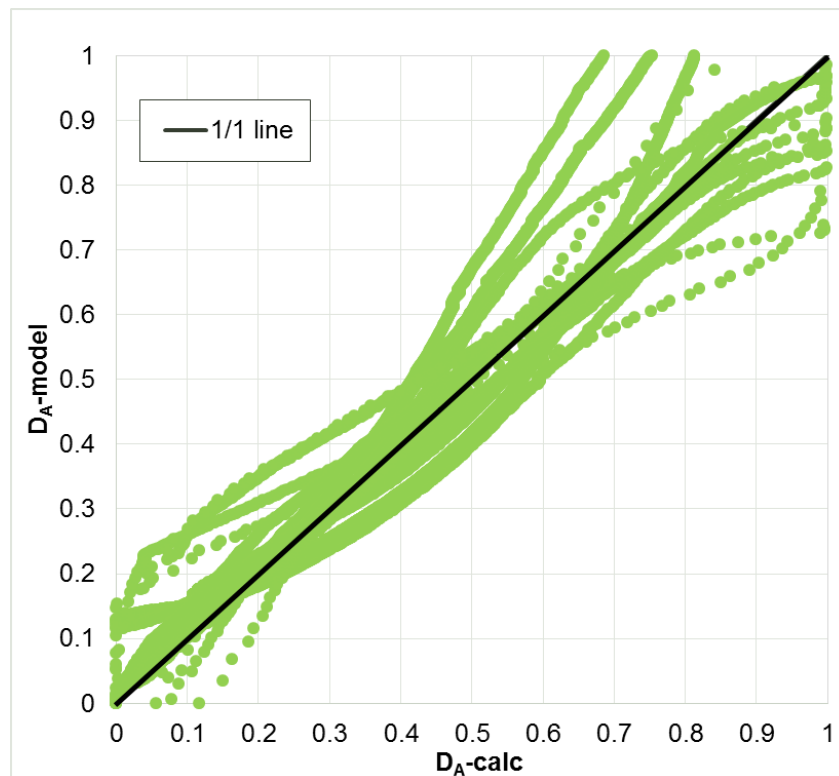


Figure 5-24: Correlation between damage calculated from laboratory data and modelled damage in the case of adhesion fatigue damage

5.3.3.2 Discussion of accumulated model

The development of the accumulated damage was based on the establishment of the fatigue damage as a function of number of repetitions, shear stress and temperature. In this process, the Nelder function was used as a model function for both CFD and AFD. The Nelder coefficients were used as initial model values. Possible relationships linking the Nelder coefficients to the shear stress and/or the temperature were investigated. In the case of confirmation, the relationships were expressed via the global model coefficients which were adjusted in the generalised and final CFD and AFD models.

Considering the adjusted coefficients as presented in Equation 5-27 to Equation 5-34, it appears that the adjusted coefficients for CFD could be easily



expressed as a function of the shear stress, while the adjusted coefficients for AFD tend to be expressed more easily as a function of temperature.

It can be concluded that the generalised model for CFD depends more on stress, whereas the generalised model for AFD appears to depend more on temperature. This observation seems to agree with the fact that adhesion damage is more sensitive to temperature change, while cohesion damage is more prone to be influenced by applied stress. As a result of this observation it is suggested that it be investigated whether the adhesion phenomenon could be considered as a “non-fatigue” mechanism as discussed in Section 2.11.2. The adhesion can also be considered as a tensile fatigue that is not well measured in a shear test.

5.4 Summary

The major response model developed was ageing, while the end-life model and accumulated model represented the development of CFD and AFD.

The ageing model was developed on the basis of G^* Prony series of recovered field-aged bitumens. The relationship between G^* and ageing time, considered at a fixed frequency, was fitted using a “power” type function. This model function is referred to as an ageing model of a seal’s bitumen. The ageing model of a seal’s bitumen developed appears to have a good fit for both 70/100 and SE1 bitumens and can be considered as a good attempt at simulating field ageing. However, different variabilities that could affect the model should be noted. One of these variabilities is the change in bitumen consistency/stiffness due to possible field treatment and the laboratory bitumen-recovery process. It was found that the Q-SUN method simulated higher field ageing than the PAV method in the case of 70/100; unlike in the case of SE1, the Q-SUN simulated less field ageing than the PAV method. Although the outcome from the ageing model appears to be conclusive, further investigation into laboratory ageing is required to elaborate on the relationship with field ageing. Such an investigation could also establish the influence of the modification of bitumen (e.g. with polymers) on the ageing process.



The end-life model defines transfer functions for CFD and AFD. The transfer function allows the determination of the shear stress at failure as a function of the number of repetitions to failure and temperature. The end-life model is presented as a “power” type function. This model displayed good fit to laboratory data. The positions of the isotherms were consistent in increment compared with the temperature increments. The apparent counter-intuitive position of the isotherm in this model was supported by the reverse of isotherms observed in the fatigue test performed in stress mode compared with the fatigue test performed in strain mode (Domone and Illstone, 2010). This counter-intuitive observation was substantiated by the fact that bituminous the material at low temperature would be brittle and have a higher stiffness and therefore resulting to brittle and quick failure. Similarly, at high temperature the same material will be less stiff and display a creep-like behaviour carrying low stress, resulting in more deformation with possibility of “separation failure” occurring much later”. It was also noticed that at the same shear stress level, cohesion occurs earlier than adhesion. This could be probably explained by fact that fatigue test does not suitably handle adhesion due to its requirement of low maximum stress value.

The aim of developing the accumulated damage model was to allow monitoring of the evolution of damage with time. This was based on the establishment of the fatigue damage as a function of the number of wheel load repetitions, shear stress and temperature. In this process, the Nelder function was used as a model function for both CFD and AFD. The Nelder coefficients were used as initial model coefficients values. Possible (obvious) relationships linking the Nelder coefficients to the shear stress and/or the temperature were investigated. For confirmation, the relationships were expressed via the global model coefficients, which were expressed as functions of shear stress and/or temperature. The global model coefficients were adjusted in the generalised and final CFD and AFD models. In this way the CFD model within the seal’s bitumen and AFD between seal stone and bitumen were obtained. It was observed that the generalised model for CFD depends more on stress, while the generalised model for AFD appears to depend more on temperature. This observation seems to agree with the fact that adhesion

damage is more sensitive to temperature change, whereas cohesion damage is more prone to be influenced by applied fatigue stress.

References

- Burr BL, Glover CJ, Davison RR, Bullin JA, 1993, *New Apparatus and Procedure for the Extraction And Recovery of Asphalt Binder from Pavement Mixtures*, Transportation Research Record, Issue 1391, 1993, p. 20-29.
- Domone P. and Illstone J. (Eds.), 2010, *Construction Materials: Their Nature and Behaviour*, 4th ed. Taylor & Francis, London.
- Feller W., 1971, *Introduction to Probability Theory and Its Applications*, Vol. II, 2nd ed., Wiley, USA.
- Galé N. E., 2000, *Fatigue characterisation of asphalt concrete using viscoelasticity and damage theory*, MEng thesis, University of Pretoria, South Africa.
- Hagos E. T., 2002, *Characterisation of polymer modified bitumen (PMB)*, Master's thesis, Section of Road and Railway Engineering, Faculty of Civil Engineering and Geosciences, International Institute for Infrastructural Hydraulic and Environmental Engineering (IHE), Delft, Netherlands.
- Happian-Smith J., 2000, *Introduction to Modern Vehicle Design*, Transport Research Laboratory (TRL), Butterworth-Heinemann, UK.
- Huurman M. and Mo L. T., 2007, *Fatigue in Mortar and Adhesive Zones: Measurements, Test Interpretation and Determination of Model Parameters*, Report 7-07-170-2, Lifetime Optimisation Tool (LOT), Laboratory of Road and Railway Engineering, Delft University of Technology, Netherlands.
- Kekane P., 2014, *The recovery of bituminous binder from asphalt at high centrifugal forces*, Bachelor of Engineering project report (Civil Engineering), Faculty of Engineering, University of Pretoria, Pretoria, South Africa.
- Mo L., 2009, *Damage development in the adhesive zone and mortar of porous asphalt concrete*, PhD thesis, Department of Road and Railway Engineering, Faculty of Civil Engineering and Geosciences, Delft University of Technology, Netherlands.
- Rowe G., Baumgardner G. and Sharrock M. J., 2011, *Application of Rheological Models to Modified Binders*, paper presented at the 48th Petersen Asphalt Research Conference, Western Research Institute, Laramie, Wyoming, USA.
- Schapery R. A., 1984, *Correspondence Principles and a Generalised Integral for Large Deformation and Fracture Analysis of Viscoelastic Media*, Civil Engineering Department, Texas A&M University, College Station, TX, USA.



Steyn W. J. vdM. and Dednam D., 2014, *Mechanical bitumen recovery from asphalt Samples*, paper presented at the 3rd International Conference on Transportation Infrastructure (ICTI 2014), Pisa, Italy.

Theyse H. L., 2013, *Revision of the South African Pavement Design Method*, SANRAL/SAPDM/B-4/2013-03 Report, SANRAL, Pretoria, South Africa.

Theyse H. L. and Van As C., 2010, *Stochastic Recursive Simulation. Preliminary System Design*, Version: 1st Draft, Draft Contract Report SANRAL-SAPDM-E3-2010-01, Revision of the South African Pavement Design Method, SANRAL, Pretoria, South Africa.



6 INPUT PARAMETERS FOR SEAL MODELLING AND SEAL DESIGN

6.1 Introduction

Stiffness and other road pavement material properties (e.g. Poisson ratio and the thickness) are necessary input parameters in the mechanistic evaluation of road performance and life. Knowledge of the stiffness of a bitumen is important in the assessment of the mechanistic response and performance of surfacings such as seals. The bitumen is a major component of the seal and the stiffness of the bitumen influences the response and damage mechanisms. These mechanisms dictate failures of the seal such as adhesion failure (stripping), fatigue cracking and low-temperature cracking. In this regard, the stiffness of the bitumen and bituminous seal materials within the binder, and between the stone and the binder, should be considered as major inputs in the mechanistic analysis of seals.

The response and fatigue damage models of bituminous seal materials developed in this research are required as input parameters into seal design.

6.2 Use of Rheological Response, Cohesion and Adhesion Fatigue Damage Parameters

The development of the response and fatigue damage models was based on the stiffness of bituminous materials. In the case of dynamic shear loading, the stiffness of the bituminous materials is represented by the complex modulus and the phase angle. These rheological parameters are used as inputs in the mechanistic analysis of seals. Gerber (2015) performed such an analysis through the finite element modelling of seals, based on the rheological and visco-elastic properties of the bitumen (in particular, Prony series parameters were used).

A field verification of the materials model and seal model is required for validation and calibration purposes. Field investigations for verification were reported by Van Zyl (2015). The cycling process representing the integration of seal modelling is presented in Figure 6-1.

INPUT PARAMETERS FOR SEAL MODELLING AND SEALS DESIGN

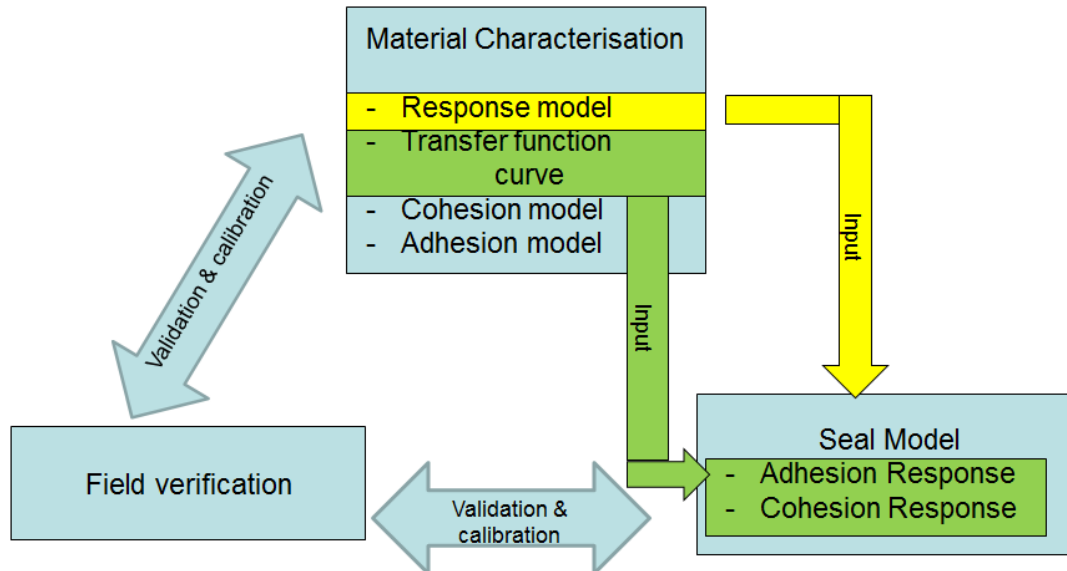


Figure 6-1: Cycling process representing the integration of seal modelling

Mukandila *et al.* (2015), Gerber (2015) and Milne (2015) recommended some materials parameters deriving from rheological response for use in CFD and AFD as seal modelling inputs. These parameters are presented in [Table 6-1](#).



INPUT PARAMETERS FOR SEAL MODELLING AND SEALS DESIGN

Table 6-1: Rheological response, cohesion and adhesion fatigue damage parameters used as inputs in seal modelling

Model type	Test configuration	Varying parameters	Constant parameters	Outputs
Binder response model	DSR Parallel plate test	<ul style="list-style-type: none"> - Binder type - Binder aged - Binder water conditioning - Temperature - Frequency 	<ul style="list-style-type: none"> - Strain 	<ul style="list-style-type: none"> - Christen – Anderson Master curves - Prony series parameters
CFD model	DSR bitumen column	<ul style="list-style-type: none"> - Binder type - Binder aged - Temperature 	<ul style="list-style-type: none"> - Strain, - Frequency 	<ul style="list-style-type: none"> - Transfer function formula and coefficients values
AFD model	DSR Stone column	<ul style="list-style-type: none"> - Binder type - Binder water conditioning - Stone type - Temperature 	<ul style="list-style-type: none"> - Strain - Frequency 	<ul style="list-style-type: none"> - Transfer function formula and coefficients values



6.3 Summary

Based on the integration process presented in Figure 6-1, the scope and the development of this research is summarised below.

The background to and principles of seal design and mechanistic design are presented in Chapter 2. The majority of the work focuses on the characterisation of bituminous seal materials in terms of response and damage; this is established through the modelling developed in Chapter 5. The modelling was based mainly on Dynamic Shear Rheometer (DSR) testing as developed in Chapter 3. Results from the testing programmes were interpreted and conceptualised for modelling in Chapter 4. The present chapter concludes the integration process by connecting output parameters from this research to seal modelling. The seal modelling is linked to the field performance of seals by the process of validation and calibration which should aim to calibrate the laboratory test outputs to fit site conditions.

References

- Gerber J.A.K., 2015, *Numerical modelling of performance and failure criteria for road seals*, PhD thesis, Department of Civil Engineering, University of Stellenbosch, South Africa, unpublished (submitted).
- Milne T. I., 2015, Overview of enhancements to road surfacing seal design methodologies through seal system and materials modelling, *Proceedings of the 11th Conference on Asphalt Pavements for Southern Africa*, Sun City, South Africa, 16–19 August 2015, pp. 510–521.
- Mukandila E., Steyn W. J. vdM., Milne T. and Kannemeyer L., 2015, Rheological characteristics of South African bitumen, *Proceedings of the 11th Conference on Asphalt Pavements for Southern Africa*, Sun City, South Africa, 16–19 August 2015, pp. 401–411.
- Van Zyl G., 2015, *Modelling of surfacing seal performance*, PhD thesis, Department of Civil Engineering, University of Stellenbosch, South Africa, unpublished.



CONCLUSION AND RECOMMENDATIONS

7 CONCLUSION AND RECOMMENDATIONS

7.1 Conclusion

Cohesion failure within the seal's bitumen and adhesion failure between the stone and bitumen are among the major failure modes of seals. Therefore, the performance prediction of seals requires investigation into the cohesion and adhesion. The evaluation of this performance was done at two levels: (i) response, which focuses on the bitumen's "working" characteristics; and (ii) damage assessment, which consists of investigations into the Cohesion Fatigue Damage (CFD) and Adhesion Fatigue Damage (AFD) of the seal materials.

The objectives of the investigation into rheological response, and cohesion and adhesion fatigue damage of bituminous road seal materials were:

- to present a seal's binder response model that could be used to characterise the different types of bitumen used in South African seals during early seal life and when the seal is aged
- to model the ageing of bitumen and explore ageing methods that could better simulate the field ageing of seal binders
- to develop the a cohesion fatigue damage (CFD) model within the binder and an adhesion fatigue damage (AFD) model between stone and binder

In this investigation, the response was based on the modelling of visco-elastic materials, while the fatigue damage was based on the principle of stiffness reduction of materials under the action of cyclic stress. The complex modulus and the phase angle represented the stiffness of the bituminous materials. A Dynamic Shear Rheometer (DSR) was the main laboratory device used to identify both response and damage with the aim of modelling these phenomena. The response test was performed using the standard DSR test, while the CFD and AFD tests required special test protocols. The development of these protocols was dictated mainly by the challenges encountered during the preliminary testing programme.



CONCLUSION AND RECOMMENDATIONS

In relation to the outcomes of the objectives of this investigation, the following can be noted:

- A seal's binder response model (during early seal life and when the seal is aged) was presented, using the rheological modelling of bituminous binder behaviour. This response model was constituted by the linear visco-elastic rheological models (Prony series, Huet-Sayegh and 2S2P1D) representing the complex modulus (G^*) and phase angle (δ) of four fresh bitumens (70/100, SE1, KRS 60 and SR1) from a plant. These bitumens were investigated in the following conditioning states or combinations of such states: fresh (unaged); aged (by PAV method or by weatherometer (Q-SUN) method); or conditioned in water.
- An ageing model was developed, which involved the rheological modelling of 49 bitumens (70/100 and SE1) recovered from "field-aged" seals for four different types of bitumen used in South African seals. This ageing model, based on the relative stiffening of the complex modulus, G^* , with time, was analysed for 70/100 and SE1 bitumens at three reference frequencies (10 rad/s, 62.83 rad/s and 100 rad/s). The ageing model of a seal's bitumen developed appears to fit for both 70/100 and SE1. This "power" type model function, referred to as the "ageing model of a seal's bitumen", can be considered as a good attempt at a field ageing simulation. It should be noted that unaged condition of bitumen (characterised by the initial complex modulus) was from the laboratory binder and did not represent the actual field materials. This important as all binders after ageing eventually end at about the same stiffness, but the start at very different initial complex modulus.
- However, the effect of different variabilities that could affect the model should be noted. One of these variabilities is the change of bitumen consistency/stiffness due to possible field treatment and the laboratory bitumen-recovery process. It was found that Q-SUN method simulated higher field ageing than the PAV method in the case of 70/100, unlike the Q-SUN method which simulated less field ageing than the PAV method. Although the outcome from the ageing model appears to be conclusive, further



CONCLUSION AND RECOMMENDATIONS

investigation into laboratory ageing is required to elaborate the relationship with field ageing.

- Regarding the modelling of the damage mechanism in the seal structure, it was found that this damage consisted of two phenomena, namely CFD and AFD and was divided into two components:
 - transfer function modelling, which focused on the applied stress as a function of the number of repetitions to failure – this was termed the “end-life fatigue damage”
 - fatigue damage modelling, which represented the evolution of damage over the life of the seal; this damage was expressed as a function of parameters such as stress and temperature – this is termed the “accumulated fatigue damage”

The end-life model defines transfer functions for CFD and AFD. The transfer function allows the determination of the shear stress at failure as a function of the number of repetitions to failure and as a function of temperature. The end-life model is presented as “power” type function. This model displayed good fit to the laboratory data. The positions of the isotherms were consistent in increment compared with the temperature increments. The apparent counter-intuitive position of the isotherm in this model was supported by the reverse of isotherms observed in the fatigue test performed in stress mode compared with the fatigue test performed in strain mode. This observation was substantiated by the fact that in a pavement, the material at low temperature would have a higher stiffness and therefore carry a higher stress, which will result in higher damage. Similarly, at high temperature the same material will be less stiff and carry low stress, resulting in less damage.

The aim of developing the accumulated damage model was to allow monitoring of the evolution of damage with time. This was based on the establishment of the fatigue damage as a function of the number of repetitions, shear stress and temperature. In this process, the Nelder function was used as a model function for both CFD and AFD. The Nelder coefficients were used as initial model coefficients values. Possible relationships linking the Nelder coefficients to the shear stress and/or the temperature were



CONCLUSION AND RECOMMENDATIONS

investigated. For model confirmation, the relationships were expressed via the global model coefficients, which were expressed as functions of shear stress and/or temperature. The global model coefficients were adjusted in the generalised and final CFD and AFD models. In this way the CFD model within the seal's bitumen and AFD between seal stone and bitumen were obtained. It was observed that the generalised model for CFD depends more on stress, while the generalised model for AFD appears to depend more on temperature. This observation seems to agree with the fact that adhesion damage is more sensitive to temperature change, while cohesion damage is more prone to be influenced by applied fatigue stress. From this observation, it is suggested to investigate whether the adhesion damage could be considered as a "non-fatigue" mechanism or investigate the cohesion using a tensile fatigue that is not well measured in a shear test.

The CFD and AFD models offer a practical advantage consisting of the possibility to be adapted and incorporated in the recursive simulation models as developed by South African Road Design System (SARDS). The CFD and AFD models provide an indication of non-linear development of the accumulated fatigue damage within bitumen and between bitumen and stone in the case of seal. This is represented by the modelling of the change of G^* , as suggested in this investigation.

It can be concluded that the ageing model and the fatigue damage models developed in this investigation can be considered as a major step in the understanding of the mechanistic behaviour of the seal.

7.2 Recommendations

As a step in the understanding of the mechanistic behaviour of the seal, this investigation requires more improvement and faced some limitations. The following are recommendations for further improvement:

- The damage investigation was performed on one type of bitumen (70/100) and in the case of AFD on only one type of aggregate (dolorite (Dol)). It is recommended to repeat the investigation with different types of bitumen (such as the four bitumens used in the response) and different types of aggregate



CONCLUSION AND RECOMMENDATIONS

(typical aggregates used in South Africa such as quartzite and granite). By using different bitumens for CFD, the CFD damage model could be expressed as a function of bitumen type. On the other hand, the different combinations of bitumen and aggregate will afford the opportunity to express AFD as a function of different types of adhesion zone. These adhesion zones depend mostly on the surface texture of the aggregate.

- Further detailed research is recommended to assess the impact of using special DSR setups (bitumen column and stone column) on the DSR geometry configuration on the test output. Tests such as torsion analysis, which can be conducted using classical torsion theory, should be conducted to verify the influence of height (or gap) on the stiffness.
- Materials in a road pavement usually experience both shear stress and normal stress. In this investigation, the introduction of normal force was abandoned. With the rapid improvement of DSR equipment, it is recommended to consider the influence of normal force on the fatigue damage.
- It is recommended to monitor the progress of cracking in the sample under cyclic torsional loading during the DSR test. Such an investigation could clarify the contribution to fatigue damage due to radius change, as well as the contribution to fatigue due to the visco-elastic properties of bitumen.
- It is also recommended to correlate the CFD and AFD models to actual field performance.

In this investigation, it has been reported that fatigue is more likely to occur in the form of ductile fracture than brittle fracture, and that fatigue is frequently correlated with a high number of applied stress cycles (more than 1 000). It was also mentioned that the adhesion of a visco-elastic adhesive might be controlled by the interfacial slippage, which can be considered as a brittle fracture. This implies that adhesion might be considered as a “non-fatigue” mechanism. In addition, the investigation of the accumulated fatigue damage model reveals that adhesion damage is more sensitive to temperature change than applied fatigue stress when compared with cohesion damage. Adhesion failure could be due to an instantaneous force that is



CONCLUSION AND RECOMMENDATIONS

higher than the adhesion bond. It is suggested to investigate whether the adhesion damage could be considered as a “non-fatigue” mechanism or a tensile fatigue that is not well measured in a shear test.



REFERENCES

- AASHTO (American Association of State and Transportation Officials) 2012, *Standard Practice for Accelerated Aging of Asphalt Binder Using a Pressurized Aging Vessel (PAV)*, AASHTO Designation: R 28-12, US.
- AASHTO (American Association of State and Transportation Officials), 2005, *Determining the Rheological Properties of Asphalt Binder Using a Dynamic Shear Rheometer (DSR)*, AASHTO Designation: T 315-05, US.
- AASHTO R 28-12, see AASHTO, 2012.
- AASHTO T315-05, see AASHTO, 2005.
- Airey G. D., 1997, *Rheological characteristics of polymer modified and aged bitumens*, PhD thesis, Department of Civil Engineering, University of Nottingham, UK.
- Airey G. D., Liao M. C. and Thom N. H., 2006, *Fatigue behaviour of bitumen-filler mastics*, paper presented at the 10th International Conference on Asphalt Pavements, Quebec City, Canada, 12–17 August.
- Airey G., Rahimzadeh B. and Collop A., 2003, Visco-elastic linearity limits for bituminous materials, *Proceedings of the 6th International RILEM Symposium on Performance Testing and Evaluation of Bituminous Materials*, pp. 331–338, Zurich, Switzerland.
- Akzo Nobel, 2009, *Adhesion Promoters For Bitumen*, Technical bulletin, Amsterdam, Netherlands.
- Anderson D. A., Rowe G. M. and Christensen D. W., 2008, *Historical and current rheological binder characterization vs. binder performance*, paper presented at the Petersen Asphalt Research Conference, Laramie, WY, US.
- Anderson D. A., Christensen D. W. and Bahia H., 1991, Physical properties of asphalt cement and the development of performance-related specifications, *Journal of the Association of Asphalt Paving Technologists*, 60, 437–532.
- Anderson D. A., Christensen D. W., Bahia H. U., Dongré R., Sharma M. G, Antle C. E and Button J., 1994, *Binder Characterization and Evaluation, Vol. 3: Physical Characterization*, SHRP-A-369, National Research Council, Washington DC, US.
- Asphalt Academy, 2007, *The Use of Modified Bituminous Binders in Road Construction*, Technical Guideline 1 (TG1), 2nd ed., Asphalt Academy/ CSIR Built Environment, Pretoria.



INPUT PARAMETERS FOR SEAL MODELLING AND SEALS DESIGN

Asphalt Institute, 1997, Performance-graded Asphalt Binder Specification and Testing, Superpave Series No. 1 (SP-1), Lexington, KY, US.

ASTM (American Society for Testing and Materials International), 2002, *Standard Practice for Accelerated Weathering Test Conditions and Procedures for Bituminous Materials (Xenon-Arc Method)*, ASTM D4798-01, West Conshohocken, PA, US.

ASTM (American Society for Testing and Materials), 2009, *Standard Test Method for Recovery of Asphalt from Solution by Absorption Method*, ASTM D 1856-09, ASTM International, West Conshohocken, PA, US.

ASTM (American Society for Testing and Materials), 2011, *Standard Test Methods for Quantitative Extraction of Bitumen from Bituminous Paving Mixtures*, ASTM D 2172-11, ASTM International, West Conshohocken, PA, US.

ASTM (American Society for Testing and Materials), 2012, *Standard Test Method for Distillation of Emulsified Asphalt*, ASTM D6997-12, ASTM International, West Conshohocken, PA, US.

ASTM (American Society for Testing and Materials International), 2013, *Standard Practice for Accelerated Aging of Asphalt Binder Using a Pressurized Aging Vessel (PAV)*, ASTM D6521-13, ASTM International, West Conshohocken, PA, US.

ASTM D4798-01, see ASTM, 2002.

ASTM D 1856-09, see 2009.

ASTM D 2172-11, see ASTM, 2011.

ASTM D6997-12, see ASTM, 2012.

ASTM D6521-13, see ASTM, 2013.

Barnes H. A., Hutton J.F. and Walters K., 1993, *An Introduction to Rheology*, Vol. 3, Elsevier Science, Amsterdam, the Netherlands.

Bell C. A., 1989, *Aging of Asphalt-Aggregate Systems*, Summary Report SR-OSU-A-003A-89-2, Oregon State University, Corvallis, US.

BE-TM-BINDER-1-2006, see CSIR, 2014.

Bhasin A., 2006, *Development of methods to quantify bitumen-aggregate adhesion and loss of adhesion due to water*, PhD thesis, Texas A&M University, College Station, TX, US.



INPUT PARAMETERS FOR SEAL MODELLING AND SEALS DESIGN

- Bonaquist R., 2008, *Refining the Simple Performance Tester for Use in Routine Practice*, Report 614, National Cooperative Highway Research Program (NCHRP), Transportation Research Board (TRB), Sterling, VA, US.
- Burnett D. J., Garcia A. R., Granier A., Pellegrin B. and Nguyen T., 2008, *Surface Energies as a Measure of the Interaction Between Nanomaterials and Polymer Matrices*, Surface Measurement Systems Ltd, and National Institute of Standards and Technology, SAMPE 2008, Long Beach, CA, US.
- Burr BL, Glover CJ, Davison RR, Bullin JA, 1993, *New Apparatus and Procedure for the Extraction And Recovery of Asphalt Binder from Pavement Mixtures*, Transportation Research Record, Issue 1391, 1993, p. 20-29.
- Caltrans (California Department of Transportation), 2003, *Maintenance Technical Advisory Guide (TAG), Chapter 5*, Caltrans Division of Maintenance.
- Chailleux E., Ramond G. and de la Roche C., 2006, A mathematical-based master curve construction method applied to complex modulus of bituminous materials, *Journal of Road Materials and Pavement Design*, 7, 75–92.
- Chipperfield E. H, Duthie J. L. and Girdler R. B., 1970, Asphalt characteristics in relation to road performance, *Proceedings of the American Association of Asphalt Paving Technologists*, 39, 575–613.
- Clyne T. R., Li X., Marasteanu M. O. and Skok E. L., 2003, *Dynamic and Resilient Modulus of MN/DOT Asphalt Mixtures*, MN/RC – 2003-09, Department of Civil Engineering, University of Minnesota, Minnesota Department of Transportation Office of Research Services, US.
- Cole K. S. and Cole, R. H., 1941, Dispersion and absorption in dielectrics. I. Alternating current characteristics, *Journal of Chemical Physics*, 9, 341–351.
- Cole K. S. and Cole, R. H., 1942, Dispersion and absorption in dielectrics. II. Direct current characteristics, *Journal of Chemical Physics*, 1, 98–105.
- Collop A. C., Scarpas A. T., Kasbergen C. and de Bondt A, 2003, *Development and finite element implementation of a stress dependent elasto-visco-plastic constitutive model with damage for asphalt*, paper presented at the 82nd Transportation Research Board (TRB) Annual Meeting, Washington DC, US.
- CSIR (Council for Scientific and Industrial Research), 2014, *Determination of Binder Content and Binder Recovery*, BE-TM-BINDER-1-2006, CSIR Internal Test Method, Revision 2, Pretoria, South Africa.
- Das B. M., 1990, *Principles of Geotechnical Engineering*, 2nd ed., PWS-Kent, Boston, MA, US.



INPUT PARAMETERS FOR SEAL MODELLING AND SEALS DESIGN

- Dassault Systèmes, 2012, Abaqus Theory Manual, 22.7.2 Frequency domain viscoelasticity, Abaqus 6.2, available at: http://www.maths.cam.ac.uk/computing/software/abaqus_docs/docs/v6.12/books/usb/default.htm?startat=pt05ch22s07abm13.html#usb-mat-cfreqvisco
- Department of the Army (US), 1952, *Geology and Its Military Applications*, TN5-545, p. 7, US.
- Desai C. S., 2002, *Mechanic pavement analysis and design using unified material and computer models*, paper presented at the Symposium on 3D Element Modelling of Pavement Structures, Amsterdam, Netherlands, 2–5 April.
- Di Benedetto H. and Corté J. F., 2005, *Matériaux routiers bitumineux. 2: Constitution et propriétés thermomécaniques des mélanges*, Hermes-Science, Lavoisier, France.
- Di Benedetto H., Delaporte B. and Sauzéat C., 2007, Three-dimensional linear behavior of bituminous materials: Experiments and modelling, *ASCE International Journal of Geomechanics*, 7(2), 149–157
- Di Benedetto H., Gabet T., Grenfell J., Perraton D. and Sauzéat C., Bodin D., 2013, *mechanical testing of bituminous mixtures*, Chapter 4, in *Advances in Interlaboratory Testing and Evaluation of Bituminous Materials*, RILEM State-of-the-art Reports, Vol. IX, Springer, Dordrecht, Netherlands.
- Di Benedetto H., Sauzeat C., Bilodeau K., Buannic M., Mangiafico S., Nguyen Q. T., Pouget S., Tapsoba N. and Van Rompu J., 2011, General overview of the time-temperature superposition principle validity for materials containing bituminous binder, *International Journal of Roads and Airports*, 1(1), 35–52.
- Domone P. and Illstone J. (Eds.), 2010, *Construction Materials: Their Nature and Behaviour*, 4th ed., Taylor & Francis, London.
- Dorn L., 1994, *Adhesive bonding – Terms and definitions, Lecture 4701, Basic level, Training in aluminium application technologies*, European Aluminium Association, Technische Universität, Berlin, Germany.
- Dougan C. E., Stephens J. E., Mahoney J. and Hansen G., 2003, *E* - Dynamic Modulus Test Protocol – Problems and Solutions*, Connecticut Department of Transportation Office of Research and Materials, US.
- Feller W., 1971, *Introduction to Probability Theory and Its Applications*, Vol II, 2nd ed., Wiley, New York, USA.
- Ferry J. D., 1980, *Visco-elastic Properties of Polymers*, Wiley, New York.
- Flügge W. (Ed.), 1975, *Visco-elasticity*, 2nd ed., Springer-Verlag, Berlin, Heidelberg, New York.

INPUT PARAMETERS FOR SEAL MODELLING AND SEALS DESIGN

- Galé N. E., 2000, *Fatigue characterisation of asphalt concrete using viscoelasticity and damage theory*. MEng thesis, University of Pretoria, South Africa.
- Garcia G. and Thompson M. R., 2007, *HMA Dynamic Modulus Predictive Models: A Review*, Research Report FHWA-ICT-07-2005, Illinois Centre for Transportation, Rantoul, IL, US.
- Gerber J.A.K., 2015, *Numerical modelling of performance and failure criteria for road seals*, PhD thesis, Department of Civil Engineering, University of Stellenbosch, South Africa, unpublished (submitted).
- González A.; Covián E.; Madera, J., 2008, *Determination of Bridge Natural Frequencies Using a Moving Vehicle Instrumented with Accelerometers and GPS*, Civil-Comp Press, Dublin.
- Hagos E. T., 2008, *The effect of aging on binder properties of porous asphalt concrete*, PhD thesis, Section of Road and Railway Engineering, Faculty of Civil Engineering and Geosciences, Delft University of Technology, Netherlands.
- Hagos E. T., 2002, *Characterisation of polymer modified bitumen (PMB)*, Master's thesis, Section of Road and Railway Engineering, Faculty of Civil Engineering and Geosciences, Delft University of Technology, Netherlands.
- Hanson F. M., 1935, Bituminous surface treatment on rural highways, *Proceedings of the New Zealand Society of Civil Engineers*, 21, 83.
- Happian-Smith J., 2000, *Introduction to Modern Vehicle Design*, Transport Research Laboratory (TRL), Butterworth Heinemann, UK.
- Hefer A. W., 2004, *Adhesion in bitumen-aggregate systems and quantification of the effects of water on the adhesive bond*, PhD thesis, Civil Engineering Department, Texas A&M University, College Station, TX, US.
- Hergt J. M., McDougall I., Banks M. R. and Green D. H., 1989, Igneous rocks. Jurassic dolerite, in: Burrett C. F. and Martin E. L. (Eds.), *Geology and Mineral Resources of Tasmania*, Special Publication of the Geological Society of Australia, 15, 375–381.
- Hintz C. and Bahia, H., 2013, *Understanding Mechanisms Leading to Asphalt Binder Fatigue in the Dynamic Shear Rheometer (DSR)*, *Road Materials and Pavement Design*, London, Taylor & Francis.
- Holtrop W., 2008, *Sprayed Sealing Practice in Australia*, Australian Asphalt Pavement Association, Australia.

INPUT PARAMETERS FOR SEAL MODELLING AND SEALS DESIGN

- Hopman P.C., Kunst P.A.J.C. and Pronk, A.C., 1989, A renewed interpretation method for fatigue measurements – verification of Miner’s rule, in: *Proceedings 4th Eurobitume Symposium*, Madrid, Spain.
- Howson J., Bhasin A., Masad E. A., Lytton L. and Little D., 2009, *Development of a Database for Surface Energy of Aggregates and Asphalt Binders*, Report 5-4524-01-1, Texas Transportation Institute, College Station, TX, US.
- Huurman, M., 2010, Developments in 3D surfacing seals FE modelling, *International Journal of Pavement Engineering*, 11(1), 1–12.
- Huurman M., 2007, *Lifetime Optimisation Tool (LOT)*, Main report, Technical University of Delft, Netherlands.
- Huurman M. and Mo L. T., 2007, *Fatigue in mortar and adhesive zones; Measurements, test interpretation and determination of model parameters*, Report 7-07-170-2, Lifetime Optimisation Tool (LOT), Laboratory of Road and Railway Engineering, Delft University of Technology, Netherlands.
- Janisch D. W. and Gaillard FS, 1998, *Minnesota Seal Coat Handbook Final Report*, Minnesota Department of Transportation Office of Research Services, St. Paul, Minnesota, US.
- Jansen K. M. B., 2006, *Thermomechanical modelling and characterization of polymers*, Lecture Notes, Delft University of Technology, Netherlands.
- Jooste F., 2004, *Re-evaluation of some aspects of the mechanistic-empirical design approach*, paper presented at the 8th Conference on Asphalt Pavements for Southern Africa, Sun City, South Africa.
- Kathirgamanathan P., Herrington P.R. and McIver I., 2012, *Chip seal finite element model*, paper presented at the 7th International Conference on Maintenance and Rehabilitation of Pavements and Technological Control, Auckland, New Zealand.
- Kekane P., 2014, *The recovery of bituminous binder from asphalt at high centrifugal forces*, Bachelor of Engineering project report (Civil Engineering), Faculty of Engineering, University of Pretoria, Pretoria, South Africa.
- Khedoe R.N. and Moraal J., 2007, *Sample preparation and laboratory testing for the LOT research program*, Report 7-07-170-4, Lifetime Optimisation Tool (LOT), Laboratory of Road and Railway Engineering, Delft University of Technology, Netherlands.
- King G., Anderson M., Hanson D. and Blankenship P., 2012, Using black space diagrams to predict age-induced cracking, *Proceedings of the 7th RILEM International Conference on Cracking in Pavements*, pp. 453–463, A. Scarpas et al. (Eds.).
- Lakes R., 2009, *Visco-elastic Materials*, Cambridge University Press, New York, US.



INPUT PARAMETERS FOR SEAL MODELLING AND SEALS DESIGN

- Leaman D. E., 1973, *The Engineering Properties of Tasmanian Dolerite, with Particular Reference to the Route of the Bell Bay Railway*, Technical Report, Department of Mines, Tasmania, 16, 148–163.
- Li Q. and Kumar A, 2003, *National & International Practices in Decision Support Tools in Road Asset Management*, Project 2001-010-C/005, Final report, Queensland Department of Main Roads, Spring Hill, Queensland, Australia.
- Liao M.C, 2007, *Small and large strain rheological and fatigue characterisation of bitumen-filler mastics*, PhD thesis, University of Nottingham, UK.
- Liu L., 2007, *Engineering properties of rocks, Rock Mechanics III*, Lecture notes, Department of Civil and Environmental Engineering, University of Connecticut, Mansfield, CT, US.
- Lombard L., 2013, expanded range of binder-types, testing temperatures (not lower temperatures) and curing regimes. MSc Eng. dissertation, Department of Civil Engineering, University of Stellenbosch, South Africa.
- Loulizi A., Flintsch G. W., Al-Qadi I. L. and Mokarem D., 2006, Comparing resilient modulus and dynamic modulus of hot-mix asphalt as material properties for flexible pavement design, Transportation Research Board Annual Meeting, *Transportation Research Record*, 1970(1), 161–170.
- Lurie J., 1984, *South African Geology for Mining, Metallurgical Hydrological and Civil Engineering*, 4th ed., McGraw-Hill, Johannesburg.
- Ma, L. X., Wu S. P., Huang J. F. and Li N., 2008, *Effect of UV aging on components, structure and properties of asphalt*, paper presented at the 2nd International Conference on Heterogeneous Material Mechanics (ICHMM-2008), Huangshan, China.
- Macosko C. W., 1994, *Rheology: Principles, Measurements, and Applications*, Wiley-VCH, Poughkeepsie, NY, US.
- Mangiafico S., 2014, *Linear visco-elastic properties and fatigue of bituminous mixtures produced with Reclaimed Asphalt Pavement and corresponding binder blends*, PhD thesis, l'École Nationale des Travaux Publics de l'État, France.
- Marais C. P., 1981, Rational design of single surface treatment technique for road maintenance, *The Civil Engineer in South Africa*, August 1981.
- Maree, J.H. and Freeme, C.R., 1981, *The Mechanistic Design Method Used to Evaluate the Pavement Structures in the Catalogue of the Draft TRH 4 1980*, Technical Report RP/2/81, National Institute for Transport and Road Research, CSIR, Pretoria, South Africa.
- McNaught, A. D. and Wilkinson, A., 1997, Shear modulus, in: *Compendium of Chemical Terminology*, (the "Gold Book"), 2nd ed., Blackwell Scientific Publications, Oxford.



INPUT PARAMETERS FOR SEAL MODELLING AND SEALS DESIGN

- Medani T. O. And Huurman M., 2003, *Constructing the Stiffness Master Curves for Asphaltic Mixes*, Report 7-01-127-3, Delft University of Technology, Netherlands.
- Meyers M. A. and Chawla K. K., 1999, *Mechanical Behavior of Materials*, Prentice-Hall, Upper Saddle River, NJ, US.
- Milne T. I., 2004, *Towards a performance-related seal design method for bitumen and modified road seal binders*, PhD thesis, University of Stellenbosch, South Africa.
- Milne T. I., Huurman M., Van de Ven M. F. C., Jenkins K. J., Scarpas A. and Kasbergen C., 2004, *Toward mechanistic behaviour of flexible road surfacing seals using a prototype FEM model*, paper presented at 8th Conference on Asphalt Pavements for Southern Africa, Sun City, South Africa.
- Milne T.I., 2015, Overview of Enhancements to Road Surfacing Seal Design Methodologies through Seal System and Materials Modelling, *Proceedings of the 11th Conference on Asphalt Pavements for Southern Africa*, Sun City, South Africa, 16–19 August 2015, pp. 510–521.
- Mitton S., 2012, *Determining the bitumen thickness between aggregates of various surfacing seals*, Bachelor of Engineering project report (Civil Engineering), Faculty of Engineering, University of Pretoria, Pretoria, South Africa.
- Mo L., 2009, *Damage development in the adhesive zone and mortar of porous asphalt concrete*, PhD thesis, Department of Road and Railway Engineering, Faculty of Civil Engineering and Geosciences, Delft University of Technology, Netherlands.
- Moraes R., Velasquez R. and Hussain B., 2011, *Measuring effect of moisture on asphalt-aggregate bond with the bitumen bond strength test*, Transportation Research Board Annual Meeting, Washington, DC, US.
- Mohammad L. N., Wu Z., Myres L., Cooper S. and Abadie C. A., 2005, Practical look at simple performance tests: Louisiana's experience, *Journal of the Association of Asphalt Paving Technologists*, 74, 557–600.
- Molenaar A. A. A., 2010, *Road paving materials, Part III, Asphaltic materials*, Lecture Notes, CT 4880, Delft University of Technology, Netherlands.
- Mturi G. A. J., Mahlangu K., Conrad S. and Von Wissell M., 2013, *Asphalt Binder Extraction: Benzene Replacement in Test Method BE-TM-BINDER-1-2006*, CSIR Technical Report CSIR/BE/IE/IR/2012/0017/B, Pretoria, South Africa.
- Mturi G. A. J., Zoorob S. E., O'Connell J., Anochie-Boateng J. and Maina J., 2011, Rheological testing of crumb rubber modified bitumen, *Proceedings of the 7th International Conference on Road & Airfield Pavement Technology (ICPT)*, Paper P18, pp. 1316–1327, Bangkok, Thailand.



INPUT PARAMETERS FOR SEAL MODELLING AND SEALS DESIGN

- Muller J. and Jenkins K. J., 2011, *The use of an extended rolling thin film ageing method as an alternative to the pressurised ageing vessel method in the determination of bitumen durability*, paper presented at the 10th Conference on Asphalt Pavements for Southern Africa, KwaZulu-Natal, South Africa, 11–14 September 2011.
- Mukandila E., Steyn W. J. vdM., Milne T. and Kannemeyer L., 2015, Rheological characteristics of South African bitumen, *Proceedings of the 11th Conference on Asphalt Pavements for Southern Africa*, Suncity, South Africa, 16–19 August 2015, pp. 401–411.
- NCHRP (National Cooperative Highway Research Program), 2004, *Guide for Mechanistic-Empirical Design of New and Rehabilitated Pavement Structures*, NCHRP Project 1-37A. Available at: <http://www.trb.org/mepdg>.
- Newby B. Z., Chaudhury M. K. and Brown H. R., 1995, Macroscopic evidence of the effect of interfacial slippage on adhesion, *Science*, 269 (5229), 1407–1409.
- Olard F. and Di Benedetto H., 2003, *General “2S2P1D” Model and Relation between the Linear Visco-elastic Behaviours of Bituminous Binders and Mixes*, Département Génie Civil et Bâtiment (URA CNRS), Ecole Nationale des TPE, France.
- Oliver J. W. H., 2004, *Prediction of the life of sprayed seals and the effect of climate, durability and seal size*, paper presented at the 6th International Conference on Managing Pavements, Brisbane, Australia.
- Oliver J. W. H., 2011, The effect of binder film thickness on asphalt cracking and ravelling, *Road & Transport Research*, 20(3).
- Oliver J. W. H. and Boer S., 2008, *Optimising sprayed seal life in response to global challenges*, paper presented at the 1st International Sprayed Sealing Conference, ARRB Group, Adelaide, South Australia.
- Paterson W. D. O., 1987, *Road Deterioration and Maintenance Effects – Models for Planning and Management*, The World Bank and the Johns Hopkins University Press, Baltimore, MA, US.
- Pell P. S., McCarthy P. F. and Gardner R. R., 1961, Fatigue of bitumen and bituminous mixes, *International Journal of Mechanical Sciences*, 3(4), 247–267.
- Pellinen T. K. and Witczak M. W., 2002, Stress dependent master curve construction for dynamic (complex) modulus, *Journal of the Association of Asphalt Paving Technologists*, 71, 281–309.
- Petrucci R. H., Harwood W. S., Herring G. F. and Madura J. D., 2007, *General Chemistry: Principles and Modern Applications*, AIE, Pearson/Prentice Hall, Upper Saddle River, NJ, US.
- Placet V., Passard J. and Perré P., 2009, *Visco-elastic properties of green wood across the grain measured by harmonic tests in the range of 0°C to 95°C* -



INPUT PARAMETERS FOR SEAL MODELLING AND SEALS DESIGN

Hardwood vs. softwood and normal wood vs. reaction wood, Laboratoire d'Etude et de Recherche sur le Matériau Bois, LERMAB-UMR INRA/ENGREF/UHP 1093, Nancy, France

Planche J. P., Anderson D. A., Gauthier G., Le Hir Y. M., Martin D., 2004, *Evaluation of fatigue properties of bituminous binders*, *Materials and Structures*, June 2004, Volume 37, Issue 5, pp 356-359.

Pronk A.C., Kans L. and Gogh F., 1996, Temperature increase in an asphalt beam during fatigue – theory and practice, in: Road Research Workshop, CROW, Ede, Netherlands.

Read J. and Whiteoak D., 2003, *The Shell Bitumen Handbook*, 5th ed., Shell UK Oil Products Limited, UK.

Road Research Laboratory (UK), 1962, *Bituminous Materials in Road Construction*, Department of Scientific and Industrial Research, Her Majesty's Stationery Office, London.

Rowe G.M. and Bouldin M.G., 2000, Improved techniques to evaluate the fatigue resistance of asphalt mixtures, in: *Proceedings of Euroasphalt & Eurobitume Congress*, Barcelona, Spain.

Rowe G, Baumgardner G and Sharrock M. J., 2011, *Application of rheological models to modified binders*, paper presented at the 48th Petersen Asphalt Research Conference, Western Research Institute, Laramie, Wyoming, USA.

Roylance D., 2001, *Engineering visco-elasticity – Polymer and composites*, Lecture Notes for 3.60s, Massachusetts Institute of Technology, Boston, MA, US.

SABITA (Southern African Bitumen Association), 1993, *Appropriate Standards for Bituminous Surfacing*, Manual 10, Cape Town, South Africa.

SABITA (Southern African Bitumen Association), 2007, *Bituminous Binders for Road Construction and Maintenance*, Manual 2, 4th ed., Cape Town, South Africa.

SABS (South Africa Bureau of Standards), 2005, *South African National Standard SANS 307:2005 Penetration-grade Bitumens* (includes Amendments 1–7), SABS Standards Division, Pretoria, South Africa.

SANRAL (South African National Roads Agency Limited), 2007, *Design and Construction of Surfacing Seals*, Technical Recommendations for Highways (TRH 3), Version 1.5, Pretoria, South Africa

SANS 307:2005, 2005, see SABS, 2005.

Schapery R. A., 1984, *Correspondence principles and a generalised integral for large deformation and fracture analysis of viscoelastic media*. Civil Engineering Department, Texas A&M University, College Station, TX, US.

INPUT PARAMETERS FOR SEAL MODELLING AND SEALS DESIGN

- Schram S. and Abdelrahman M., 2009, Mechanistic-empirical modelling in network-level pavement management, *Journal of the Transportation Research Board*, No. 2093, pp. 76–83, Washington DC, US.
- Schultz J. and Nardin M., 1994, Theories and mechanisms of adhesion, in Pizzi A. and Mittal K. L. (Eds.), *Handbook of Adhesive Technology*, pp. 19–33, New York, Marcel Dekker.
- Semmelink C. J., 1987, A rational design approach for single and double surfacing seals based on the modified tray test, *Transportation Research Record*, 1106, 1, 202–207.
- Shuler S., Lord A., Epps-Martin A. and Hoyt D., 2011, *Manual for Emulsion-Based Chip Seals for Pavement Preservation*, NCRHP Report 680, Transportation Research Board (TRB), Washington DC, US.
- Soleimani A., 2009, *Use of dynamic phase angle and complex modulus for the low temperature performance grading of asphalt cements*, MSc thesis, Department of Chemistry, Queen's University, Kingston, Ontario, Canada.
- Steyn W.J. vdM. and Dednam D., 2014, *Mechanical bitumen recovery from asphalt samples*, paper presented at the 3rd International Conference on Transportation Infrastructure (ICTI 2014) Pisa, Italy.
- Sybilski D., Soenen H., Gajewski M., Chailleux E. and Bankowski W., 2013, Binder Testing, *Advances in Interlaboratory Testing and Evaluation of Bituminous Materials*, RILEM State-of-the-Art Report, Vol. IX, Springer, Dordrecht, Netherlands.
- Tarrer A. R. and Wagh V., 1993, *The Effect of the Physical and Chemical Characteristics of the Aggregate on Bonding*, Report SHRP-A/UIR-91-507, Strategic Highway Research Program, National Research Council, Washington DC, US.
- TG 1, 2007, see Asphalt Academy, 2007.
- Theyse H. L., de Beer M. and Rust F. C., 1996, *Overview of the South African mechanistic pavement design analysis*, paper presented at the 75th Annual Transportation Research Board Meeting, Washington DC, US, 7–11 January 2011.
- Theyse H. L., Maina J. W. and Kannemeyer L., 2007, Revision of the South African flexible pavement design method; mechanistic-empirical components, *Proceedings of the 9th Conference on Asphalt Pavements for Southern Africa*, Gaborone, Botswana, 2–5 September 2007, pp. 256–292.
- Theyse H.L. and Van As. C., 2010, *Stochastic Recursive Simulation, Preliminary System Design*, Version: 1st Draft, Draft Contract Report SANRAL-SAPDM-E3-2010-01, Revision of the South African Pavement Design Method, SANRAL South Africa.



INPUT PARAMETERS FOR SEAL MODELLING AND SEALS DESIGN

- Theyse H.L., de Beer M., Maina J. W. and Kannemeyer L., 2011, *Interim revision of the South African mechanistic-empirical pavement design method for flexible pavements*, paper presented at the 10th Conference on Asphalt Pavements for Southern Africa, KwaZulu-Natal, South Africa, 11–14 September 2011.
- Theyse H.L., 2013, *Revision of the South African Pavement Design Method*, SANRAL/SAPDM/B-4/2013-03 report, SANRAL South Africa.
- TMH 1 C7(b), see NITRR, 1986.
- Tran N. and Hall K. D., 2006, Evaluation of testing protocols for dynamic modulus of hot mix asphalt, *Transportation Research Record*, 1970.
- TRH 3, 2007, see SANRAL, 2007.
- Vallerga B. A., 1981, Pavement deficiencies related to asphalt durability, *Proceedings of the Association of Asphalt Paving Technologists*, 50, 481–491.
- Van Assen E., 1997, *Assessment of Binder Extraction Methodologies*, CSIR Contract Report CR-97/092, Pretoria, South Africa.
- Van der Poel C. A., 1954, General system describing the visco-elastic properties of bitumens and its relation to routine test data, *Journal of Applied Chemistry*, 4, 231–236.
- Van Dijk W., 1975, Practical fatigue characterisation of bituminous mixes. *Proceedings of the Association of Asphalt Paving Technologists*, 44, 38–72.
- Van Lent D., 2008, *Aggregate characterisation in relation to bitumen-aggregate adhesion*, MSc thesis, Department of Road and Railway Engineering, Faculty of Civil Engineering and Geosciences, Delft University of Technology, Netherlands.
- Van Zyl G., 2015, *Modelling of Surfacing Seal Performance*, PhD thesis, Department of Civil Engineering, University of Stellenbosch, South Africa, unpublished.
- Vert M., Doi Y., Hellwich K. H., Hess M., Hodge P., Kubisa P., Marguerite Rinaudo M. and Schué F., 2012, Terminology for biorelated polymers and applications, *Pure and Applied Chemistry*, 84(2), 377–410.
- Von Fraunhofer J.A., 2011, Adhesion and cohesion, Hindawi Publishing Corporation, *International Journal of Dentistry*, 2012, 1–7.
- Weinert H. H., 1980, *The Natural Road Construction Materials of Southern Africa*, H & R Academica, Cape Town.
- Williams M. L., Landel R. F. and Ferry J. D., 1955, *The Temperature Dependence of Relaxation Mechanisms in Amorphous Polymers and Other Glass-forming Liquids*¹, Department of Chemistry, University of Wisconsin, Madison, WI, US.



- Woldekidan M. F., 2011, *Response modelling of bitumen, bituminous mastic and mortar*, PhD thesis, Department of Road and Railway Engineering, Faculty of Civil Engineering and Geosciences, Delft University of Technology, Netherlands.
- Woo W. J., Ofori-Abebresse E., Chowdhury A., Hilbrich J., Kraus Z., Martin A. E. and Glover C. J., 2007, *Polymer Modified Asphalt Durability in Pavements*, Texas Department of Transportation Research and Technology Implementation, Austin, TX, US.
- Xiang L., Tu J., Cheng J. and Que G., 2010, *Outdoor Aging of Road Asphalt and SBS Modified Asphalt*, Higher Education Press and Springer-Verlag, Berlin, Heidelberg.
- Yusoff N. I. M., 2012, *Modelling the linear visco-elastic rheological properties of bituminous binders*, PhD thesis, University of Nottingham, UK.
- Yusoff N. I. M., Shaw M. T. and Airey G. D., 2011, Modelling the linear visco-elastic rheological properties of bituminous binders, *Construction and Building Materials*, 25(5), 2171–2189.



APPENDICES

APPENDICES

A OVERVIEW OF SEAL DESIGN

A.1 Introduction

Seal designs, as used worldwide, are based on volumetric principles.

Semmelink (1987) drew attention to the fact that a certain amount of empty space is present in a single or double seal layer. Some of these voids are lost during the life of the seal because of the effects of traffic on the embedment of the aggregate at the bottom of the layer and the wear of the aggregate at the top of the seal layer. A portion of the voids must be left unfilled with binder to ensure good skid resistance. This concept represents the base of most of the seal designs. TRH 3 (2007) schematised the concept as presented in Figure A-1.

The volumetric principle in seal design focuses on the application rates of binder, spread rates of aggregate and void content within the seal.

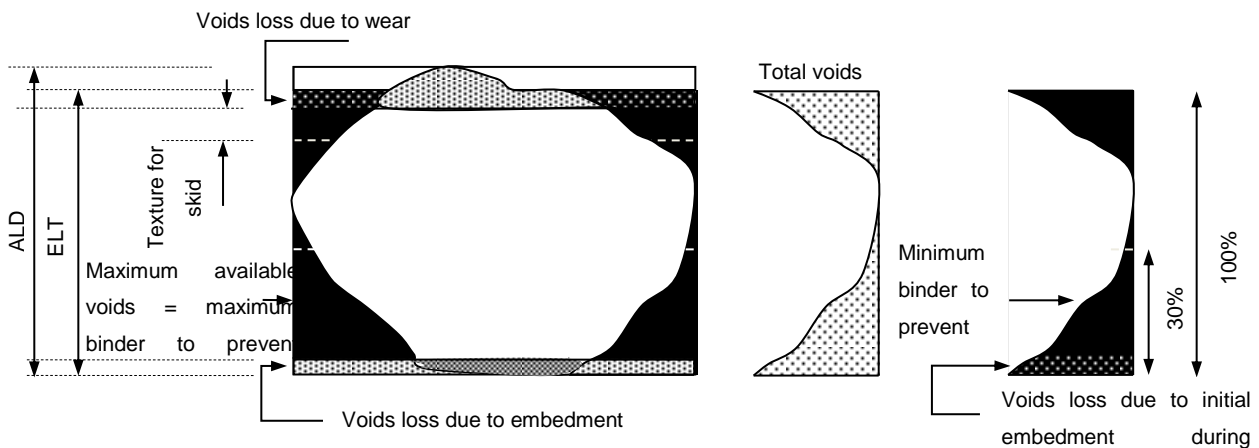


Figure A-1: Principles applied for design of the binder application rate (after TRH 3, 2007)

The practical spread rate of stone and the bulk voids can be determined by the modified tray test (see Figure A-2 and Equation A-1 to Equation A-3) as described by Semmelink (1987).

APPENDIX A

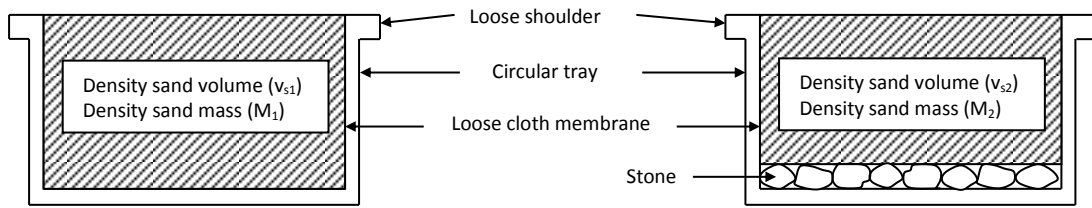


Figure A-2: Schematic illustration of the modified tray test

The void space that is occupied by the aggregate sample and the voids in the layer, in the modified tray test, is determined as shown in Equation A-1.

$$v_t = v_{s1} - v_{s2} = \frac{(M_1 - M_2)}{RD_s} \quad \text{Equation A-1}$$

where

v_t is the volume of the aggregate plus the voids between the aggregates (ml)

v_{s1} is the volume of the density sand required to fill the tray without aggregate (ml)

v_{s2} is the volume of the density sand required to fill the tray with aggregate (ml)

M_1 is the mass of the density sand required to fill the tray without aggregate sample (g)

M_2 is the mass of the density sand required to fill the tray with aggregate sample (g)

RD_s is the bulk relative density of the density sand (g/ml)

The Effective Layer Thickness (ELT) in millimetres, as described in Figure A-2 and determined by the modified tray test, is expressed as in Equation A-2.

$$ELT = \frac{10 v_t}{\Omega} \quad \text{Equation A-2}$$

where

Ω is the area of the tray [cm^2]



The layer voids (Z_l) in the modified tray test are determined as in Equation A-3.

$$Z_l = \frac{(v_t - v_a)}{v_t} 100\% = \frac{v_t - \left(\frac{M_a}{RD_a}\right)}{v_t} 100\% \quad \text{Equation A-3}$$

where

v_a is the volume of the aggregate sample required to cover the tray area [ml]

M_a is the mass of the aggregate sample required to cover the area [ml]

RD_a is the relative density of the aggregate sample

Semmelink (1987) pointed out that the use of the ELT as a design parameter was preferable to the Average Least Dimension (ALD) because the ELT gives a better average value for the layer thickness of aggregate, since with the ALD only the highest points of the least dimension of aggregate particles are measured.

Although the principles applied to the design of the binder application rate use the same concept, they vary from one seal design to another. A brief description of some seal design approaches (namely the South African, McLeod, Australian and New Zealand approaches) are presented in the following paragraphs.

A.2 Seal Design Approach in South Africa

Among the seals commonly used in South Africa are the sand seal, slurry seal, single seal, double seal and Cape seal. TRH 3 (2007) states that the sand seal did not have a specific design method, while the slurry seal was based on experience or on a semi-empirical method using the hot-mix Marshall design procedure. The single seal and the double seal used a rational design, on which the Cape seal was also based.

The principle of calculation in the rational design approach is practically the same for the single seal and double seal layers. The single seal layer design approach will be



APPENDIX A

emphasised, although this principle is also applicable to multiple seal layers such as the double seal and Cape seal.

A.2.1 Calculation of application rate of binder

According to Marais (1981), in the calculation of the available voids to be filled with binder, the investigation of the change of the voids due to embedment on the underside of the stone mat and the degradation and wear taking place on top of the stone mat is expressed as a percentage of volume, also called the “fractional void volume” (Z). This calculation of available voids should also take into account the following:

- the voids necessary to accommodate the minimum binder that could prevent stone loss, and
- the minimum voids required for skid resistance.

Marais (1981) also noted that research into seal design methods tended to agree on the assumption that the volume of voids in a single layer of aggregate follows a curvilinear relationship. This curvilinear relationship comes from the assumption that the distribution of voids in single layer aggregates should be the same as that in a layer of spheres tightly packed. The fractional void volume (Z) can be expressed as a function of the depth (D) of the layer of spheres, as in Equation A-4:

$$Z = 2.528D - 4.578D^2 + 3.058D^3 \quad \text{Equation A-4}$$

From all the above, the principle of seal design, as set out by Semmelink (1987), Marais (1981) and TRH 3 (2007), can be summarised as follows:

A.2.2 Calculation of different void fractions necessary for the design

- *Fractional void loss due to embedment and wear (Z_1) as a decimal*

If D_1 and D_2 are respectively embedment and wear expressed as decimal fractions of the ELT, then using Equation A-4, the Z_1 can be expressed as in Equation A-5.



APPENDIX A

$$Z_1 = 2.528(D_1 + D_2) - 4.578(D_1^2 + D_2^2) + 3.058(D_1^3 + D_2^3) \quad \text{Equation A-5}$$

Note that the potential embedment of the base or the existing surface is evaluated using a test called the “Ball penetration test for surface treatment design”, as described by the CSRA (Committee of State Road Authorities) (1984) and TRH 3 (2007).

- *Fractional void loss due to demand for skid resistance (Z_2) as a decimal*

Marais (1981) reported that a minimum texture depth of 0.64 mm is recommended for skid resistance when the stone size is greater than 7 mm. in the case of a stone size less than 6.4 mm, 10% of ALD should be allowed for texture depth.

The texture depth is generally assessed using the Sand Patch Test as described in ASTM method E965 (American Society for Testing and Materials (ASTM), 2002b).

Using a minimum texture depth of 0.7, Z_2 is as expressed as in Equation A-6:

$$Z_2 = \frac{0.7}{Z_l \times ELT} \quad \text{Equation A-6}$$

where

Z_l is the layer void content as measured with the modified tray test

- *Available void fraction that may be filled with binder for a normal life expectancy (Z_3)*

This is the total voids (expressed as a fraction). It is equal to 1 minus the sum of fractional void loss due to embedment and wear, and fractional void loss due to skid resistance demand ($Z_1 + Z_2$). Z_3 and is as expressed in Equation A-7.

$$Z_3 = 1 - (Z_1 + Z_2) \quad \text{Equation A-7}$$



APPENDIX A

- *Minimum void fraction to ensure that there is no aggregate loss (Z_5)*

Semmelink (1987) indicated that to ensure no aggregate loss, the aggregate needs to be at least half covered with binder. This means that 50 per cent of the voids should be filled. He excluded from the 50 per cent of the voids the initial embedment due to construction rolling.

Using Equation A-4, the fraction of void loss due to rolling embedment (Z_4) is expressed as in Equation A-8.

$$Z_4 = 2.528D_3 - 4.578D_3^2 + 3.058D_3^3 \quad \text{Equation A-8}$$

where

D_3 is the embedment due to rolling expressed as a decimal fraction of the ELT

Consequently, the minimum void fraction to ensure that there is no aggregate loss (Z_5) is as expressed in Equation A-9.

$$Z_5 = 0.5 - Z_4 \quad \text{Equation A-9}$$

It should be noted that TRH 3 (2007) prescribes a minimum amount of voids to be filled with binder to prevent stone loss, when there is no embedment, of 42% for single seals and 55% for double seals.

If the available void fraction Z_3 is greater than the minimum void fraction Z_5 , the seal will have a normal life expectancy. Otherwise (if Z_3 is smaller than Z_5), the seal will have a reduced life expectancy.

A.2.3 Determination of binder application rate

By using void fractions Z_3 and Z_5 , the binder application rate can be calculated as a function of the layer volume (Z_l) and the ELT.



APPENDIX A

The maximum nominal cold binder application rate (B_{max}) and the minimum nominal cold binder application rate (B_{min}) for single seals are expressed respectively by Equation A-10 and Equation A-11.

$$B_{max} = Z_3 \times Z_l \times ELT \quad \text{Equation A-10}$$

$$B_{min} = Z_5 \times Z_l \times ELT \quad \text{Equation A-11}$$

Note that B_{max} is only applicable in the case where Z_3 is greater than Z_5 .

For practical reasons, during construction, it is required to convert the cold binder application rate to the hot spray rate. The conversion factors from cold residual binder to hot spray rates, for some binders, are reported in different literature sources, such as TRH 3 (2007).

A.2.4 Calculation of spread rate of aggregate

Semmelink (1987) stated that, theoretically, the number of square metres that should be covered by 1 m³ of loose aggregate, A , is equal to the volume of solids in 1 m³ of aggregate divided by the volume of solids in 1 m² of aggregate.

This means that if the fractional void volume in the loose aggregate is equal to Z_b , then the fractional volume of stone particles will be equal to $100 - Z_b$; and the fractional volume of stone in the layer will be equal to $100 - Z_l$, with Z_l being the fractional void content in a single layer.

Therefore, A , can be represented by Equation A-12.

$$A = \frac{1000(100-Z_b)}{ELT(100-Z_l)} \pi r^2 \quad \text{Equation A-12}$$

The number 1 000 appearing on the numerator of the expression of A represents the conversion of ELT from millimetres to metres.



APPENDIX A

The spread rate, Q , expressed in m^3/m^2 , is then the inverse of A , and is expressed as in Equation A-13.

$$Q = \frac{ELT(100-Z_l)}{1000(100-Z_b)} \pi r^2$$

Equation A-13

Note that the aggregate spread rate is influenced by the flakiness of the aggregate.

Marais (1981) noted that the more flaky the stone, the greater the volume of voids in the loose bulk aggregate. TRH 3 (2007) paraphrased this by saying that the more flaky the aggregate, the less aggregate is required per unit area to obtain a “shoulder to shoulder” pattern, and flaky aggregate could reduce voids available to accommodate the binder.

A.2.5 Other aspects considered in the seal design process

In South Africa some recommended values are applied during the design of single seals and double seals, as presented in Table A-1.

The South African seal design also makes provision for the adjustment of certain design parameters, such as existing texture, climate, steep gradients and slow speed, aggregate spread rate, porous surfaces, fatty surfaces and construction traffic. The traffic is generally expressed in terms of Equivalent Light Vehicles (ELVs).

APPENDIX A

Table A-1: Recommended values applied in single seal and double seal design

Design principles	Value		Comment	Source
	Single seal	Double seal		
Minimum amount of voids to be filled with binder to prevent stone loss	42% of voids	55% of voids	Volume excluding embedment and representing 30% wetting of aggregate height	TRH 3 (2007)
	50%	-	-	Marais (1981) and Semmelink (1987)
Amount of void loss due to traffic wear	Min 210 kN (10% FACT)		-	TRH 3 (2007)
Required texture depth to provide adequate skid resistance	0.64 mm for ALD > 0.7 mm; 0.4 mm for ALD < 0.64 mm		-	Marais (1981)
	0.7 mm for high ALD ; 0.3 mm – 0.5 mm (for low ALD)		-	TRH 3 (2007)
Amount of embedment during construction	90% of total embedment		-	Semmelink (1987)
	50% of total embedment		-	TRH 3 (2007)
Total embedment potential	Less than 3 mm		Determined by ball-penetration test	TRH 3 (2007)
Flakiness Index (FI)	15%		Reference value	TRH 3 (2007)
Effective Least Thickness (ELT)	$ELT = 0.85679 * ALD + 0.46715$	$ELT_d = 0.86028 * (ELT_1 + ELT_2) + 0.19188$	ELT _d refers to double seal ELT ₁ refers to 1 st layer of seal ELT ₂ refers to 2 nd layer of seal	Semmelink (1987) and TRH 3 (2007)
Percentage void content in aggregate layer	$45.3333 - 0.333 * ELT$	$63.01263 + 0.04743 * ELT_d^2 - 2.41172 * ELT_d$	ELT _d refers to double seal	Semmelink (1987) and TRH 3 (2007)
	$67(0.8 - e^{-0.16ALD})$	-	-	Marais (1981)
Void content in loose stone	$0.22FI + 42.1$		FI: Flakiness Index	Marais (1981)
Equivalent Light Vehicles (ELVs)	$ELVs / \text{lane/day} = \text{Nbre light vehicles} + (\text{Nbre heavy vehicles} * 40)$		-	TRH 3 (2007)



A.3 McLeod Seal Design Approach

The McLeod seal design is also based on the calculation of the binder application rate and aggregate spreading rate.

Janisch and Gaillard (1998) and Einarsson (2009) reported that the McLeod seal design method is based on two principles:

The aggregate spreading rate is determined for a single seal, and the amount of aggregate remains constant, regardless of the binder type or pavement condition. However, during seal design, the traffic volume is considered in addition to some aggregate factors, specifically:

- *Aggregate grading*: The more graded the aggregate is, the closer the particles will be to each other within the seal layer; this leaves very little room for the binder. The best grading for a seal is single-sized aggregate.
- *Particle shape*: Particles can be round or angular, flat or cubical. Their shape will determine how they lock together in the seal layer. The more they lock together, the better the seal is able to withstand external forces such as turning and stopping of vehicles.
- *Specific gravity of aggregate*: This plays a role in determining the aggregate spreading rate.
- *Aggregate absorption*: The binder application rate needs to be compensated for the absorption capacity of the aggregate.

The voids in the aggregate layer need to be 70% filled with binder for good performance of a moderately trafficked seal – 70% refers to cold residual binder (binder after curing).

The McLeod seal design process can be summarised as follows (Wood *et al.*, 2006; Caltrans, 2003):



APPENDICES A

- *Determination of ALD (as per Equation A-14)*

$$ALD = \frac{P_{50\%}}{1.139285} + (0.011506) * FI \quad \text{Equation A-14}$$

where

ALD is the average least dimension [mm]

FI is the Flakiness Index [%]

*P*_{50%} is the median particle size [mm]

The median particle size is determined from the grading chart. It is the theoretical sieve size through which 50 per cent of the material passes (50 per cent passing size).

- *Voids in the loose aggregate (V), as expressed in Equation A-15*

$$V = 1 - \frac{BRD}{1000G} \quad \text{Equation A-15}$$

where

V is the voids in the loose aggregate [%]

BRD is the loose bulk relative density of the cover aggregate [kg/m³]

G is the bulk specific gravity of the aggregate

Wood *et al.* (2006) and Caltrans (2003) reported some of the parameters affecting the MacLeod seal design where correction factors need to be considered. Among these are aggregate absorption, traffic volume, traffic whip-off (due to the passing of vehicles as the fresh seal coat is curing), and existing condition of the pavement (its absorption ability).



APPENDICES A

- *Aggregate design equation*

The aggregate application rate is determined from Equation A-16.

$$Q = (1 - 0.4V) * ALD * G * E \quad \text{Equation A-16}$$

where

Q is the cover aggregate application rate [kg/m²]

V is the void in the loose aggregate [%] as per Equation A-15

ALD is the average least dimension [mm]

G is the bulk specific gravity of the aggregate

E is the wastage factor for traffic whip-off

- *Binder design equation*

The binder application rate is calculated according to Equation.

$$B = \frac{(0.40 * ALD * T * V) + S + A_a + P}{R} \quad \text{Equation A-17}$$

where

B : is the binder application rate [l/m²]

T : is the traffic factor (based on expected vehicles per day)

V : is the voids in the loose aggregate [%]

S : is the surface condition factor [l/m²] (based on existing surface)

A_a : is the aggregate absorption factor [l/m²]

P : is the surface hardness correction for soft pavement [l/m²]

R : is the residual asphalt content of the binder [%]



- *Aggregate application*

Caltrans (2003) states that the calculation of the design aggregate application rate is based on determining the amount of aggregate needed to create an even, single coat of stones on the pavement surface. The amount of cover aggregate required can be determined using Equation A-18.

$$C = (1 - 0.4V) * ALD * G * E \quad \text{Equation A-18}$$

where

C : is the cover aggregate (kg/m^2)

V is the void in the loose aggregate (%)

ALD : is the average least dimension [mm]

G is the bulk specific gravity

E : is the wastage factor (%)

The wastage factor (E) is needed to account for whip-off and handling and is normally estimated by the designer based on experience with local conditions.

A.4 Austroads Seal Design Approach

The Australian seal design approach is similar to the South African design approach.

Holtrop (2008) lists some essential points of the Australian single seal design as the following:

- The application rate of binder and the aggregate spread rate are key parameters in the seal design philosophy in Australia.



APPENDICES A

- The ALD and the Flakiness Index (FI) are two major aggregate parameters in the design. The aggregate is expected to have between 15 and 25% flaky particles; if the FI is outside this range, an adjustment for aggregate shape has to be done.
- The design traffic, expressed in vehicles/lane/day, based on the Average Annual Daily Traffic (AADT), is also considered in the design. The design makes provision for a traffic volume with 5 to 15% of heavy vehicles. If the percentage of heavy vehicles is outside this range, an adjustment for heavy vehicles has to be made. It should be noted that in the design, the truck is considered as the “standard vehicle” and all other types and classes of vehicle are expressed to that standard in terms of their effect on seal performance. Thus, the concept of Equivalent Heavy Vehicles (EHVs) is used, with Large Heavy Vehicles (LHVs) with seven axles and more estimated to have three times the effect of EHVs.
- The amount of binder required depends on the void space in the aggregate seal layer. In general, a single layer of aggregate particles settles with 40 to 60% voids after orientation and packing of aggregate by rolling and trafficking. The estimate of this void is known as the “Basic Voids Factor” (BVF). If the binder is a polymer-modified binder or an emulsion, specified factors for each binder, such as the Polymer Factor (PF), have been developed to determine a modified basic binder rate.
- After initial rolling, the binder is expected to rise, at least, up to 30 to 40% of the height of the aggregate particle, and about two years after construction, the binder rise could increase to 50 to 65%.
- The portion of voids to be filled is a function of requirements such as minimum surface texture for skid resistance and maximum seal life.
- The design binder application rate is calculated from the BVF with due consideration of all adjustments (for aggregate shape and effect of heavy vehicles) and all necessary allowances (surface texture of existing layer and embedment into the pavement surface).



APPENDICES A

- The aggregate spread rate is based on the ALD, with some adjustments for traffic volume, aggregate shape, type of binder and type of treatment.

The Austroads Sprayed Seal Design Project Group (ASSDPG) (2001) schematised the Australian seal design process as presented in Figure A-3.



APPENDICES A

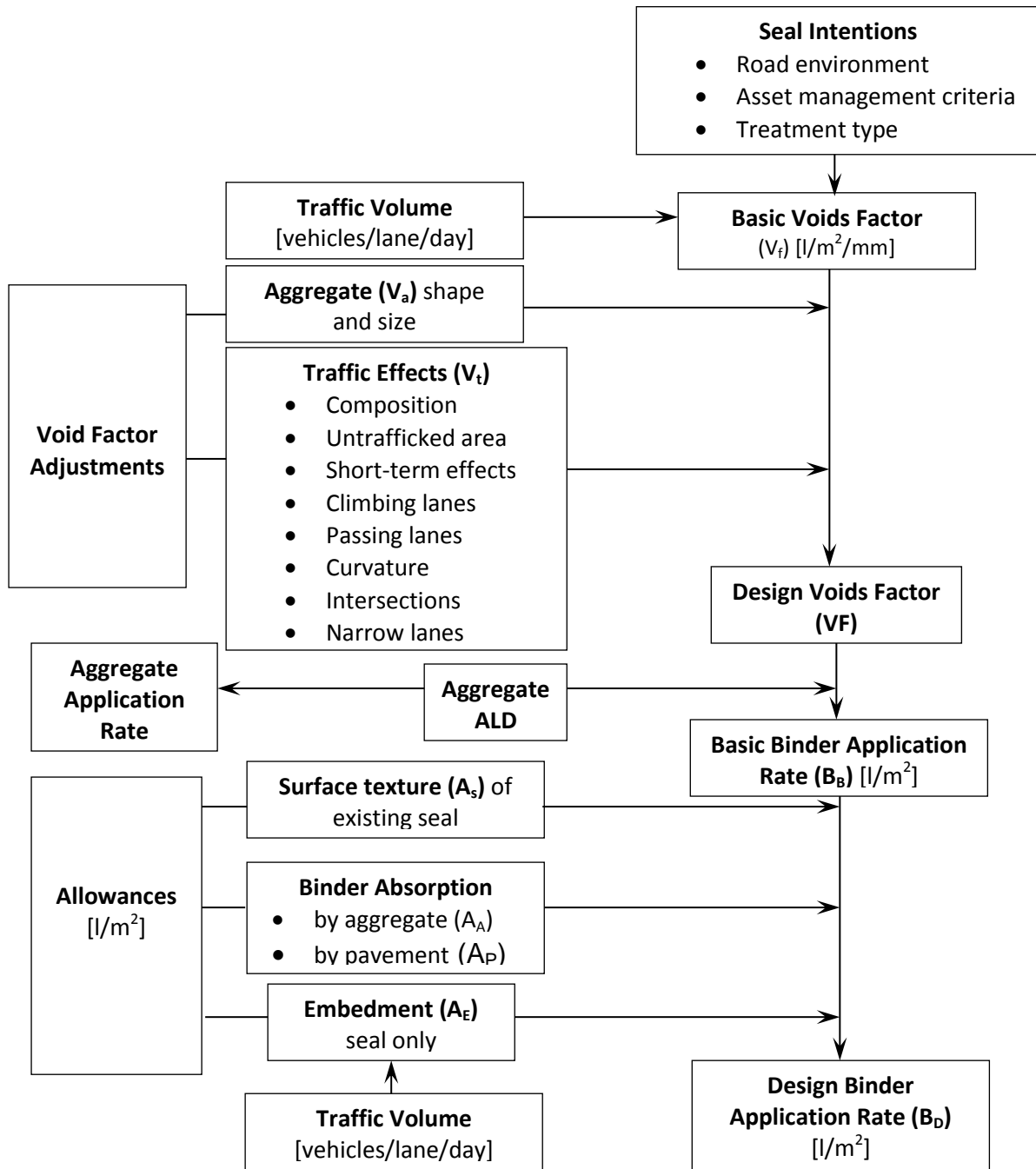


Figure A-3: Flowchart for design of aggregate and binder application rates for seals (adapted from ASSDPG, 2001)



APPENDICES A

References

- ASTM (American Society for Testing and Materials International), 2002, *Standard Test Method for Measuring Pavement Macrotexture Depth Using a Volumetric Technique*, ASTM E965-96, Annual Book of Standards, Vol. 4.03, West Conshohocken, US.
- ASSDPG (Austroads Sprayed Seal Design Project Group), 2001, *Austroads Provisional Sprayed Seal Design Method Revision 2000*, First edition, Austroads Incorporated, Sydney, Australia.
- Caltrans (California Department of Transportation), 2003, *Maintenance Technical Advisory Guide (TAG), Chapter 5*, Caltrans Division of Maintenance.
- CSRA (Committee of State Road Authorities), 1984, *Special Methods for Testing Roads, Technical Methods for Highways (TMH 6)*, National Institute for Transport and Road Research, CSIR, Pretoria, South Africa.
- Einarsson I. T., 2009, *Chip seals: Examination of design and construction in two countries*, Master's thesis, Department of Civil and Environmental Engineering, University of Washington, US.
- Holtrop W., 2008, *Sprayed Sealing Practice in Australia*, Australian Asphalt Pavement Association, Australia.
- Janisch D. W., Gaillard F. S., 1998, *Minnesota Seal Coat Handbook, Final Report*, Minnesota Department of Transportation, Office of Research Services, St. Paul, MN, US.
- Marais C. P., 1981, Rational design of single surface treatment technique for road maintenance, *The Civil Engineer in South Africa*, August 1981
- SANRAL (South African National Roads Agency Limited), 2007, *Design and Construction of Surfacing Seals*, Technical Recommendations for Highways (TRH 3), Version 1.5, May 2007, Pretoria, South Africa.
- Semmelink C. J., 1987, A rational design approach for single and double surfacing seals based on the Modified Tray Test, *Transportation Research Record* 1106(1), 202–207.
- TRH 3, 2007, see SANRAL (South African National Roads Agency Limited), 2007.
- Wood T. J., Janisch D. W., Gaillard F.S., 2006, *Minnesota Seal Coat Handbook*, revised in 2006, Minnesota Department of Transportation, Office of Research Services, St. Paul, MN, US.



B FORMULAE OF SOME MATHEMATICAL VISCO-ELASTIC MODELS

The mathematical formulae presented below are based mainly on work done by Anderson *et al.* (1994), Yusoff *et al.* (2011) and Yusoff (2012).

B.1 Modified Van der Poel's nomograph

The concept of expressing bituminous material characteristics (such as stiffness) as functions of temperature and time started with empirical and semi-empirical relationships, such as the modified Van der Poel's nomograph developed by Heukelom and Klomp (1964). The modified Van der Poel's relationship is presented in Equation B-1.

$$S_m = S \left[1 + \left(\frac{2.5}{n} \right) \left(\frac{C_v}{1-C_v} \right) \right]^n \quad \text{Equation B-1}$$

where

S_m is the asphalt mixture stiffness

S is the bitumen stiffness

C_v is the volume concentration of aggregates

n is a parameter dependant of S

B.2 Jongepier and Kuilman's Model

Jongepier and Kuilman developed an empirical algebraic model, suggesting that the relaxation spectrum of bitumen is approximately log normal in shape, as presented in Equation B-2 to Equation B-5:

$$G'(x) = \frac{G_g}{\beta\sqrt{\pi}} e^{\left\{ \left(\frac{\beta(x-\frac{1}{2})}{2} \right) \right\}^2} \times \int_0^\infty e^{\left(\frac{u}{\beta} \right)^2} \times \frac{\cosh(x+\frac{1}{2})u}{\cosh u} du \quad \text{Equation B-2}$$

$$G''(x) = \frac{G_g}{\beta\sqrt{\pi}} e^{\left\{ \left(\frac{\beta(x-\frac{1}{2})}{2} \right) \right\}^2} \times \int_0^\infty e^{\left(\frac{u}{\beta} \right)^2} \times \frac{\cosh(x-\frac{1}{2})u}{\cosh u} du \quad \text{Equation B-3}$$



APPENDIX B

with

$$u = \ln \omega_r \tau$$

Equation B-4

$$x = \frac{2}{\beta^2} \ln \omega_r$$

Equation B-5

where

ω is

ω_r is the reduced frequency [rad/s]

τ is the relaxation time [s]

G_g is the glassy modulus [Pa]

β is the width parameter

B.3 Dobson's Model

This is a mathematical model developed for describing the master curve, based upon empirical relationships between the phase angle and the modulus for bitumen. The equation expressed the modulus in terms of frequency reverse as presented in **Equation B-6**.

$$\log \omega_r^{-b} = \log(G_r^{-b} - 1) + \frac{20.5 - G_r^{-b}}{230.3}$$

Equation B-6

where

ω_r^{-b} is a unique function of G_r^{-b}

b is a parameter describing the width of the relaxation spectrum



B.4 Dickinson and Witt's Model

In this model the master curve of the complex modulus is mathematically treated as a hyperbola. The Dickinson and Witt's model is presented in **Equation B-7** to **Equation B-10**.

$$\log|G_r^*(\omega)| = 0.5 \{ \log \omega_r - [(\log \omega_r)^2 + (2\beta)^2]^{0.5} \} \quad \text{Equation B-7}$$

$$\delta(\omega) = \delta' + 0.25(\pi - 2\delta') \{ \log \omega_r - [(\log \omega_r)^2 + (2\beta)^2]^{-0.5} \} \quad \text{Equation B-8}$$

with

$$|G_r^*(\omega)| = \frac{|G^*(\omega)|}{G_g} \quad \text{Equation B-9}$$

$$\omega_r = \frac{\omega \eta_0 a(T)}{G_g} \quad \text{Equation B-10}$$

where

$|G^*(\omega)|$ is complex modulus at frequency ω

$|G_r^*(\omega)|$ is the relative complex modulus at frequency ω

$\delta(\omega)$ is the phase angle at frequency ω

δ' is the limiting phase angle at infinite frequency

G_g is the glassy modulus

η_0 is the Newtonian viscosity

$a(T)$ is the shift factor at temperature T relative to the selected reference temperature

β is a "shear susceptibility" parameter, which is defined as the distance on a log-log scale between the glassy modulus and the modulus at $\omega_r = 1$



APPENDIX B

B.5 Christensen and Anderson (CA) Model

This is a mathematically simple model to allow direct engineering calculations. The model is presented in **Equation B-11** to **Equation B-13**.

$$G^* = G_{glassy} \left[1 + \left\{ \frac{\omega}{\omega_{cross}} \right\}^{\left(\frac{\log 2}{R} \right)} \right]^{-\frac{R}{\log 2}} \quad \text{Equation B-11}$$

$$\delta = \frac{90}{\left[1 + \left\{ \frac{\omega}{\omega_{cross}} \right\}^{\frac{\log 2}{R}} \right]} \quad \text{Equation B-12}$$

$$R = \frac{\log 2 \left\{ \log \left(\frac{G^*}{G_{glassy}} \right) \right\}}{\log \left(1 - \frac{\delta}{90} \right)} \quad \text{Equation B-13}$$

where

G^* is the measured complex modulus

G_{glassy} is the glassy modulus

R is the Rheological Index (shape factor)

ω is the test frequency

ω_{cross} is the crossover frequency (location parameter)

δ is the measured phase angle

B.6 Fractional Model

The Fractional Model is used to describe the LVE behaviour of unmodified bitumens and polymer-modified binders. The Fractional Model equation for the complex modulus and the phase angle equation are respectively given in Equation B-14 and Equation B-15.

$$|G^*| = \eta_0 \omega \left[\frac{\prod_1^m (1 + (\mu_k \omega)^2)}{\prod_1^n (1 + (\lambda_k \omega)^2)} \right]^{\frac{1}{2(n-m)}} \quad \text{Equation B-14}$$



$$\delta = \frac{\pi}{2} + \frac{1}{(n-m)} [\sum_1^m \text{atan}(\mu_k \omega) - \sum_1^n \text{atan}(\lambda_k \omega)] \quad \text{Equation B-15}$$

where

μ_k and λ_k are the relaxation time $\mu_k > 0, \lambda_k > 0$

m and n are the numbers of relaxation time ($n > m$)

B.7 Christensen, Anderson and Marasteanu (CAM) Model

This model was developed by modifying the Christensen Anderson (CA) Model to improve the fitting, particularly in the lower and higher zones of the frequency range of bitumens. The Christensen Anderson and Marasteanu model (CAM) attempts to improve the descriptions of both unmodified and modified bitumen and is described by Equation B-16 and Equation B-18.

$$|G^*| = G_g \left[1 + \left(\frac{\omega_c}{\omega} \right)^v \right]^{-\frac{w}{v}} \quad \text{Equation B-16}$$

$$\delta = \frac{90w}{\left[1 + \left(\frac{\omega_c}{\omega} \right)^v \right]} \quad \text{Equation B-17}$$

with

$$v = \log \frac{2}{R} \quad \text{Equation B-18}$$

where

$|G^*|$ is the complex modulus

G_{glassy} is the glassy modulus

R is the Rheological Index (shape factor)

ω is the test frequency

ω_{cross} is the crossover frequency (location parameter)



APPENDIX B

δ is the measured phase angle

w is a parameter addressing the issue of how fast or how slow the $|G^*|$ data converge into the two asymptotes (the 45 °C asymptote and the G_g asymptote) as the frequency goes to zero or infinity.

B.8 Bahia and Co-workers' Model

This model uses mathematical equations to characterise the unmodified and modified bitumen and asphalt mixture with bitumen modification under dynamic shear loading over a wide range of frequencies, temperatures and strains. Bahia and Co-workers' Model is described by Equation B-19 and Equation B-20

$$|G^*| = G_e + \frac{G_g - G_e}{\left[1 + \left(\frac{f_c}{f'}\right)^k\right]^{\frac{m_e}{k}}} \quad \text{Equation B-19}$$

$$R = \log \frac{2^{\frac{m_e}{k}}}{1 + \left(2^{\frac{m_e}{k}} - 1\right) \frac{G_e}{G_g}} \quad \text{Equation B-20}$$

where

G_e is the equilibrium modulus

$G_e = |G^*|$, G_e is a horizontal asymptote when f approaches zero. $G_e = 0$ for bitumen

G_g is the glassy modulus

$G_g = |G^*|(f \rightarrow \infty)$, G_g is a horizontal asymptote when f approaches infinity

f_c is the crossover frequency (location parameter)

f' is the reduced frequency function of both temperature and strain

k and m_e are shape parameters

B.9 Al-Qadi and Co-workers' Model

The complex modulus of this model is based on the Havriliak and Negami function. Al-Qadi and Co-workers's Model is presented in Equation B-21 and Equation B-22.



APPENDIX B

$$|G^*| = G_g \left[1 - \frac{1}{\left[1 + \left(\frac{\omega}{\omega_0} \right)^v \right]^w} \right] \quad \text{Equation B-21}$$

$$\delta = \frac{90}{\left[1 + \left(\frac{\omega}{\omega_0} \right)^v \right]^w} \quad \text{Equation B-22}$$

where

ω_0 is the scale parameter that defines the location of the transition along the frequency axis

v and w are the dimensionless model parameters

B.10 Polynomial Model

This is simpler polynomial function used to express the $|G^*|$ master curve constructed from a dynamic modulus test. It is also used for describing the complex modulus for bituminous binders. The Polynomial Model is presented in Equation B-23.

$$\log |G^*| = A(\log f)^3 + B(\log f)^2 + C(\log f) \quad \text{Equation B-23}$$

where

f is reduced frequency

A , B and C are the shape parameters

B.11 Sigmoidal Model

The Sigmoidal Model was introduced the by National Cooperative Highway Research Program (NCHRP) and applied in the Mechanistic-Empirical Pavement Design Guide (ME PDG) developed in the United States of America. The Sigmoidal



APPENDIX B

Model is used to describe the rate dependency of the modulus master curve. It is presented in Equation B-24.

$$\log|G^*| = v + \frac{\alpha}{1+e^{\beta+\gamma\{\log(\omega)\}}} \quad \text{Equation B-24}$$

where

$\log(\omega)$ is the log reduced frequency

v is the lower asymptote

α is the difference between the values of the upper and lower asymptote

β and γ define the shape between the asymptotes and the location of the inflection point (inflection point obtained from $10^{\left(\frac{\beta}{\gamma}\right)}$)

B.12 The LCPC Master Curve Construction Method

The Laboratoire Central des Ponts et Chaussées (LCPC) Method is a mathematical equation that uses the Kramers-Kronig to express curves from complex modulus measurements. This model is presented in Equation B-25 and Equation B-26.

$$\log|G^*(\omega)| - \log|G^*(\infty)| = -\frac{2}{\pi} \int_0^\infty \frac{u \delta(u) - \omega \delta(\omega)}{u^2 - \omega^2} du \quad \text{Equation B-25}$$

$$\delta = \frac{2\omega}{\pi} \int_0^\infty \frac{\log|G^*(u)| - \log|G^*(\omega)|}{u^2 - \omega^2} du \quad \text{Equation B-26}$$

B.13 Generalised Logistic Sigmoidal Model

The generalisation of the Sigmoidal Model, also called the Generalised Logistic Sigmoidal Model (or Richards Model) describes the stiffness of an asphalt mixture. This model is given by Equation B-27.

$$\log|G^*| = v + \frac{\alpha}{[1+\lambda e^{(\beta+\gamma\{\log(\omega)\})}]^{\frac{1}{\lambda}}} \quad \text{Equation B-27}$$



APPENDIX B

The λ parameter allows the curve to take a non-symmetrical shape for the master curve. When λ reduces to one, Equation B-27 reduces to the standard sigmoidal function as represented in Equation B-24.

B.14 New Complex Modulus and Phase Angle Predictive Model

This model was developed based on a database containing data points from different unmodified and modified bitumens investigated. The equations for $|G^*|$ and δ are respectively shown in Equation B-28 and

Equation **B-29** $|G^*| = 0.0051 f_s \eta_{f_s,T} (\sin \delta) 7.1542 - 0.4929 f_s + 0.0211 f_s^2$

Equation B-28

$$\delta = 90 + (b_1 + b_2 VTS') \times \log(f_s \times \eta_{f_s,T}) + (b_3 + b_4 VTS') \times \{\log(f_s, \eta_{f_s,T})\}^2$$

Equation B-29

References

Anderson D.A., Christensen D.W., Bahia H.U, Dongré, R., Sharma M.G, Antle C.E and Button, J., 1994, *Binder Characterization and Evaluation*, Volume 3: Physical Characterization. SHRP-A-369. National Research Council, Washington D.C., USA.

Yusoff N. I. M., 2012, *Modelling the Linear Visco-elastic Rheological Properties of Bituminous Binders*, PhD thesis, University of Nottingham, UK.

Yusoff N. I. M., Shaw M. T., Airey G. D., 2011, Modelling the linear visco-elastic rheological properties of bituminous binders, *Construction and Building Materials*, Science Direct, Elsevier.

C DEVELOPMENT OF MECHANICAL MODEL

The development of mechanical models is based on the Lecture Notes on Engineering Visco-elasticity by Roylance (2001).

The linear models are constructed from Hookean springs and Newtonian dashpots as defined by Equation C-1 and Equation C-2 respectively; they are presented in Figure C-1 and Figure C-2 respectively.

$$\sigma = E \varepsilon_s \quad \text{Equation C-1}$$

$$\sigma = \eta \dot{\varepsilon}_d \quad \text{Equation C-2}$$

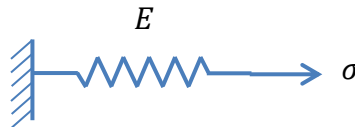


Figure C-1: Hookean spring model

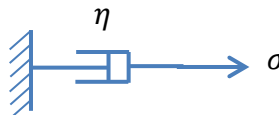


Figure C-2: Newtonian dashpot model

The following should be noted:

- The subscripts “s” and “d” in the equations refer to the spring and dashpot elements respectively.
- The dot is used to indicate time differentiation, e.g. $\dot{\varepsilon}_d = \frac{\partial \varepsilon_d}{\partial t}$.

C.1 Maxwell Model and Generalised Maxwell Model

The Maxwell model is a spring and dashpot in series as presented in Figure C-3.

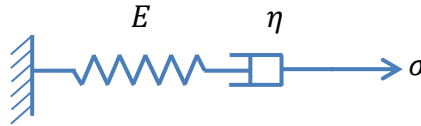


Figure C-3: Maxwell model

The applied stress in the Maxwell system is the same as the stress borne by the spring and the stress experienced in the dashpot. This is presented in Equation C-3. On the other hand, the strain created by the applied stress is equal to the sum of the strains induced in the spring and in the dashpot. Equation C-4 expresses this relationship.

$$\sigma = \sigma_s = \sigma_d \quad \text{Equation C-3}$$

$$\varepsilon = \varepsilon_s + \varepsilon_d \quad \text{Equation C-4}$$

By differentiation, Equation C-4 is expressed as Equation C-5:

$$\dot{\varepsilon} = \dot{\varepsilon}_s + \dot{\varepsilon}_d \quad \text{Equation C-5}$$

By transforming Equation C-1 and Equation C-2 and substituting $\dot{\varepsilon}_s$ and $\dot{\varepsilon}_d$ into Equation C-5, the time-dependent stress–strain relation is developed as per Equation C-6.

$$\dot{\varepsilon} = \frac{\dot{\sigma}}{E} + \frac{\sigma}{\eta} \quad \text{Equation C-6}$$



APPENDIX C

By solving the differential equation considering a stress-relaxation condition (i.e. $\varepsilon(t) = \varepsilon_0 = \text{constant}$), Equation C-6 is written as Equation C-7.

$$\frac{1}{E} \frac{d\sigma}{dt} = -\frac{1}{\eta} \sigma \quad \text{Equation C-7}$$

By integrating Equation C-7 (see Equation C-8), Equation C-9 is obtained.

$$\int_{\sigma_0}^{\sigma} \frac{d\sigma}{\sigma} = -\frac{E}{\eta} \int_0^t dt \quad \text{Equation C-8}$$

$$\sigma = \sigma_0 e^{\left(-\frac{t}{\tau}\right)} \quad \text{Equation C-9}$$

where:

$$\tau = \frac{\eta}{E} \quad \text{Equation C-10}$$

with:

τ being the relaxation time (characteristic parameter with units of time)

The relaxation modulus (E_{rel}) may be obtained from Equation C-9, noting that the initial stress is just that needed to stretch the spring to a strain ε_0 . This relaxation modulus is given by Equation C-11.

$$E_{rel}(t) = \frac{\sigma(t)}{\varepsilon_0} = \frac{\sigma_0}{\varepsilon_0} e^{\left(-\frac{t}{\tau}\right)} = E e^{\left(-\frac{t}{\tau}\right)} \quad \text{Equation C-11}$$

The Maxwell model permitted the unrestricted flow that many materials (such as most of the polymers) do not exhibit. This deficiency in the model can be remedied by placing a spring (called the equilibrium spring) in parallel with the Maxwell unit to give a useful model known as the “standard linear solid” as presented in Figure C-4. The differential constitutive law for this model is developed as per Equation C-12 to Equation C-24.

APPENDIX C

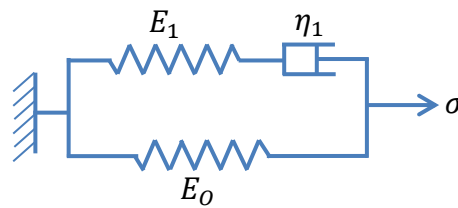


Figure C-4: Standard linear solid model

$$\sigma = \sigma_1 + \sigma_0 \quad \text{Equation C-12}$$

$$\varepsilon = \varepsilon_1 = \varepsilon_0 \quad \text{Equation C-13}$$

The strain in the first arm of Figure C-4 is given by Equation C-14.

$$\varepsilon_1 = \varepsilon_{s1} + \varepsilon_{d1} \quad \text{Equation C-14}$$

Letting $D = \frac{\partial}{\partial t}$ be the time-derivative operator, the stress in the dashpot of the first arm can be written as per Equation C-15.

$$\sigma_1 = \eta_1 D \varepsilon_{d1} \quad \text{Equation C-15}$$

Thus the strain in the dashpot of the first arm can be expressed as per Equation C-16.

$$\varepsilon_{d1} = \frac{\sigma_1}{\eta_1 D} \quad \text{Equation C-16}$$

The strain in the spring of the first arm is expressed as per Equation C-17.

$$\varepsilon_{s1} = \frac{\sigma_1}{E_1} \quad \text{Equation C-17}$$

By substituting Equation C-16 and Equation C-17 in Equation C-14 and using Equation C-13, Equation C-18 is obtained.

$$\varepsilon_1 = \varepsilon = \frac{\sigma_1}{E_1} + \frac{\sigma_1}{\eta_1 D} \quad \text{Equation C-18}$$



APPENDIX C

From Equation C-18, the stress in the first arm (σ_1) can be isolated as per Equation C-19.

$$\sigma_1 = \frac{E_1 \eta_1 D \varepsilon}{E_1 + \eta_1 D} \quad \text{Equation C-19}$$

By dividing the numerator and the denominator of the second member of Equation C-19 by E_1 , and taking in account Equation C-10, Equation C-20 is obtained.

$$\sigma_1 = \frac{E_1 D \varepsilon}{\frac{1}{\tau_1} + D} \quad \text{Equation C-20}$$

Taking into account Equation C-13, the stress in the second arm of Figure C-4 is expressed as per Equation C-21.

$$\sigma_0 = \varepsilon E_0 \quad \text{Equation C-21}$$

Thus, by substituting Equation C-20 and Equation C-21 in Equation C-12, the stress in the standard linear solid model is expressed as Equation C-22.

$$\sigma = \frac{E_1 D \varepsilon}{\frac{1}{\tau_1} + D} + \varepsilon E_0 \quad \text{Equation C-22}$$

Equation C-22 can be written as

$$D\sigma + \frac{\sigma}{\tau_1} = D\varepsilon(E_1 + E_0) + \frac{\varepsilon E_0}{\tau_1} \quad \text{Equation C-23}$$

Since $D\sigma = \dot{\sigma}$ and $D\varepsilon = \dot{\varepsilon}$, Equation C-23 can be written as per Equation C-24

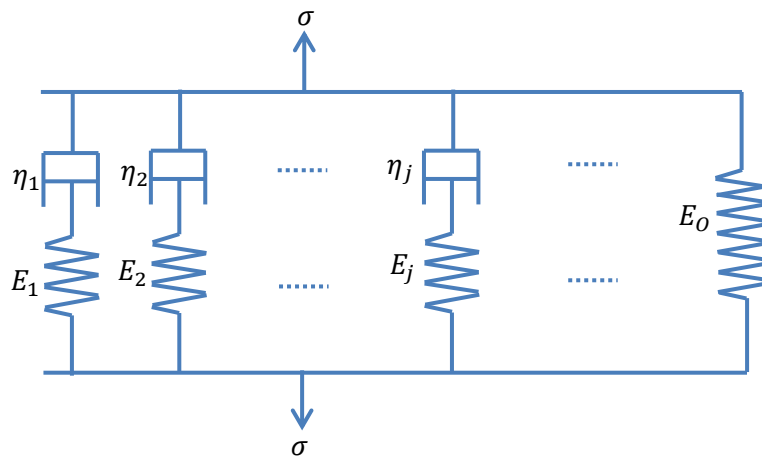
$$(E_1 + E_0)\dot{\varepsilon} + \frac{E_0}{\tau_1}\varepsilon = \dot{\sigma} + \frac{1}{\tau_1}\sigma \quad \text{Equation C-24}$$

Equation C-24 is the constitutive law for the standard linear solid model.

In the case where an improved fit to experimental data is necessary, additional spring and dashpot elements may be used in the linear solid model. Two general

APPENDIX C

spring-dashpot models are encountered frequently: the Wiechert model, also known as Prony series, which is an array of Maxwell units in parallel as presented in FigureC-5; and the Kelvin model, which is a series arrangement. Prony series is suitable for describing the stress resulting from an imposed strain, whereas the Kelvin model is convenient for the situation where strain results from imposed stress. The Kelvin model can also be generalised. More details on Prony series are provided in this section, and the Kelvin model will be dealt with in a separate section (see 0).



FigureC-5: Prony series

The stress transmitted by the j^{th} arm in the Prony model, as per Equation C-20, is expressed in Equation C-25.

$$\sigma_j = \frac{E_j D \varepsilon}{\frac{1}{\tau_j} + D} \quad \text{Equation C-25}$$

The total stress transmitted by the model is the sum of all the “ σ_j ”, plus the stress in the equilibrium spring. This is given in Equation C-26 and Equation C-27.

$$\sigma = E_0 \varepsilon + \sum_j \sigma_j \quad \text{Equation C-26}$$



APPENDIX C

$$\sigma = \left(E_0 + \sum_j \frac{E_j D}{\tau_j + D} \right) \varepsilon \quad \text{Equation C-27}$$

In the case of the dynamic response, the time dependency of both the stress and the strain are of the form $e^{(i\omega t)}$. All time derivatives will therefore contain the expression $(i\omega)e^{(i\omega t)}$, so Equation C-27 can be presented as in Equation C-28 and in Equation C-29.

$$\sigma_0^* e^{i\omega t} = \left(E_0 + \sum_j \frac{E_j(i\omega)}{\left(i\omega + \frac{1}{\tau_j}\right)} \right) \varepsilon_0^* e^{i\omega t} \quad \text{Equation C-28}$$

$$E^* = \frac{\sigma_0^*}{\varepsilon_0^*} = E_0 + \sum_j \frac{E_j(i\omega)}{\left(i\omega + \frac{1}{\tau_j}\right)} \quad \text{Equation C-29}$$

Equation C-29 can be manipulated algebraically to yield the forms presented in Equation C-30 and Equation C-31. These equations represent the Prony series model.

$$E^* = E_0 + \sum_j E_j - \sum_j \frac{E_j}{1 + (i\omega\tau_j)} \quad \text{Equation C-30}$$

$$E^* = E_0 + \sum_j \frac{E_j \omega^2 \tau_j^2}{1 + \omega^2 \tau_j^2} + i \sum_j \frac{E_j \omega \tau_j}{1 + \omega^2 \tau_j^2} \quad \text{Equation C-31}$$

According to Huurman and Woldekidan (2007) and Dassault Systèmes (2012), in FE packages such as ABAQUS, the Prony series is incorporated as the primary linear visco-elasticity model. The Prony series model is implemented on the basis of the bulk and shear moduli, K and G .



APPENDIX C

The initial response is defined by the initial elastic modulus (E_0) and the initial Poisson's ratio (ν_0). These inputs are translated to K_0 and G_0 via Equation C-32 to Equation C-35.

$$G_0 = \frac{E_0}{2(1+\nu_0)} \quad \text{Equation C-32}$$

$$K_0 = \frac{E_0}{3(1+\nu_0)} \quad \text{Equation C-33}$$

$$\nu_0 = \frac{3K_0 - 2G_0}{6K_0 + 2G_0} \quad \text{Equation C-34}$$

$$E_0 = \frac{9K_0G_0}{3K_0 + G_0} \quad \text{Equation C-35}$$

Huurman and Woldekidan (2007) and Dassault Systèmes (2012) report that for dynamic data obtained in the frequency domain (e.g. data from a Dynamic Shear Rheometer (DSR)), a transformation from the time domain to the frequency domain in a Prony series formulation is required. Using Fourier transforms, the expression for the time-dependent shear modulus can be written in the frequency domain as per Equation C-36 and Equation C-37.

$$G'(\omega) = G_0 \left[1 - \sum_{j=1}^N \frac{\alpha_j \tau_j^2 \omega^2}{1 + \tau_j^2 \omega^2} \right] \quad \text{Equation C-36}$$

$$G''(\omega) = G_0 \left[\sum_{j=1}^N \frac{\alpha_j \tau_j \omega}{1 + \tau_j^2 \omega^2} \right] \quad \text{Equation C-37}$$

where

G' is the storage modulus

G'' is the loss modulus

ω is the angular frequency

N is the number of terms in the Prony series

α_j is the stiffness reduction ratio for the j^{th} Prony element (without unit)

C.2 Kelvin-Voigt model and generalised Kelvin-Voigt model

The Maxwell model is suitable for the relaxation loading type but it simulates creep loading poorly. The Kelvin model is appropriated for creep.

The Kelvin model is presented in Figure C-7 and its constitutive law is developed in Equation C-38 to Equation C-48.

The stress applied in the Kelvin-Voigt model and the strain generated (as represented in Figure C-6) are presented in Equation C-38 and Equation C-33.

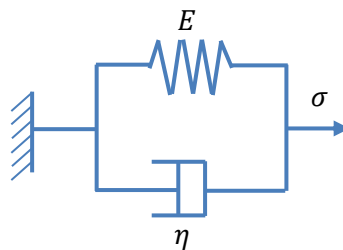


Figure C-6: Kelvin-Voigt model

$$\sigma = \sigma_s + \sigma_d$$

Equation C-38

$$\varepsilon = \varepsilon_s = \varepsilon_d$$

Equation C-39



APPENDIX C

By substituting Equation C-1 and Equation C-2 in Equation C-38, Equation C-40 is obtained.

$$\sigma = E\varepsilon_s + \eta D\varepsilon_d \quad \text{Equation C-40}$$

Using Equation C-10, Equation C-40 can be rewritten as Equation C-41.

$$\varepsilon(t) = \frac{\sigma(t)}{\tau E \left(\frac{1}{\tau} + D\right)} \quad \text{Equation C-41}$$

For creep, $\sigma(t)$ is a constant as presented in Equation C-42.

$$\sigma(t) = R \quad \text{Equation C-42}$$

From basic Laplace transforms, Equation C-43, Equation C-44, Equation C-45 can be defined.

$$\mathcal{L}f(t) = \bar{f}(P) = \int_0^{\infty} f(t)e^{-Pt} dt \quad \text{Equation C-43}$$

$$\Delta(t) = \frac{1}{P} \quad \text{Equation C-44}$$

$$\frac{1}{\tau} \left(1 - e^{-\frac{t}{\tau}}\right) = \frac{1}{P \left(P + \frac{1}{\tau}\right)} \quad \text{Equation C-45}$$

Using Equation C-44, the derivative of Equation C-42 can be written as Equation C-46.

$$\bar{\sigma}(P) = \frac{R}{P} \quad \text{Equation C-46}$$

APPENDIX C

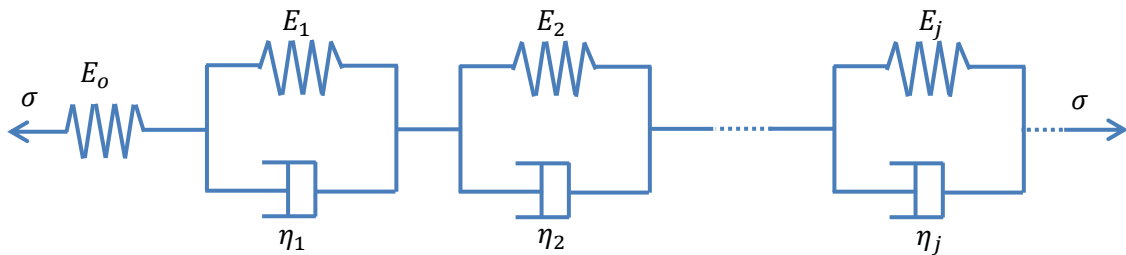
Using Laplace transforms, the derivative of Equation C-41 can be expressed as Equation C-49.

$$\bar{\varepsilon}(P) = \frac{R}{E\tau P\left(P + \frac{1}{\tau_j}\right)} \quad \text{Equation C-47}$$

By integrating Equation C-47 and incorporating Equation C-45, Equation C-48 is obtained.

$$\frac{\varepsilon(t)}{R} = \frac{R\left(1 - e^{-\frac{t}{\tau}}\right)}{E} \quad \text{Equation C-48}$$

The Kelvin-Voigt Model can be generalised as presented in FigureC-7 and its constitutive law is developed in Equation C-49 to Equation C-53.



FigureC-7: Generalised Kelvin-Voigt model

$$\varepsilon = \varepsilon_0 + \sum_j \varepsilon_j \quad \text{Equation C-49}$$

$$\frac{\varepsilon(t)}{\sigma(t)} = \frac{\varepsilon_0}{\sigma_0} + \sum_j \frac{\varepsilon_j}{\sigma_j} \quad \text{Equation C-50}$$



APPENDIX C

By replacing Equation C-41 in Equation C-50 and after manipulation, Equation C-51 is obtained.

$$\varepsilon(t) = \left(\frac{1}{E_0} + \sum_j \frac{1}{\tau_j E_j \left(\frac{1}{\tau_j} + D \right)} \right) \sigma(t) \quad \text{Equation C-51}$$

Using Laplace transforms, the derivative of Equation C-51 can be expressed as Equation C-52.

$$\bar{\varepsilon}(P) = \left(\frac{1}{E_0} + \sum_j \frac{1}{E_j \tau_j \left(P + \frac{1}{\tau_j} \right)} \right) \frac{R}{P} = \frac{R}{P E_0} + \sum_j \frac{R}{E_j \tau_j P \left(P + \frac{1}{\tau_j} \right)} \quad \text{Equation C-52}$$

By integrating Equation C-52 and incorporating Equation C-45, Equation C-53 is obtained.

$$\frac{\varepsilon(t)}{R} = \frac{1}{E_0} + \sum_j \frac{1}{E_j} \left(1 - e^{-\frac{t}{\tau_j}} \right) \quad \text{Equation C-53}$$

References

- Dassault Systèmes, 2012, *Abaqus Theory Manual*, 22.7.2 Frequency domain visco-elasticity, Abaqus 6.2, Available at:
http://www.maths.cam.ac.uk/computing/software/abaqus_docs/docs/v6.12/books/usb/default.htm?startat=pt05ch22s07abm13.html#usb-mat-cfreqvisco
- Huurman M. and Woldekidan M. F., 2007, *Mortar response: Measurements, test interpretation and determination of model parameters*, Lifetime Optimisation Tool (LOT), Report 7-07-170-3, Laboratory of Road and Railway Engineering, Delft University of Technology, Netherlands.
- Roylance D., 2001, *Engineering Visco-elasticity – Polymers and composites*, Lecture Notes for 3.60s, Massachusetts Institute of Technology, Boston, MA, US.



D BITUMEN CLASSICATION TEST RESULTS

Note:

- The bitumen class “80/100” as referred to in the following document is equivalent to bitumen class “70/100” in the research. This difference is due to the change in the grading classification of penetration grade bitumen in the South African industry that has occurred recently.



APPENDIX D



ROAD MATERIALS TESTING LABORATORY

BUILT ENVIRONMENT UNIT CSIR

(A SANAS Accredited Testing Laboratory: T0325)

P O BOX 395, PRETORIA, 0001

Contact: G Mturi Telephone: +27 12 841-2234
Email: gmturi@csir.co.za Fax: +27 12 841-2690

TEST REPORT NO: JR 5004	
Status: FINAL	Date of Issue: 31st January 2012

Client Details:

Client/Requestor	Address	Client details
Estimé Mukandila Aurecon South Africa (Pty) Ltd	Aurecon Centre, Lynnwood Bridge Office Park, 4 Daventry Str, Lynnwood Manor, 0081, Tshwane, South Africa	Tel: +27 12 427-2842 Fax: +27 86 608-0371 Cell: +27 76 873-9814 Email: Estime.Mukandila@aurecongroup.com

Sample Details:

Sample description		Binder and Emulsion samples				
Sample no	Client	80/100	S-E1	S-R1 (BR)	KRS 60	KRS 60/3
	CSIR	12152	12153	12154	12155	12156
Date sample received		15 th December 2012				
Sample condition		All samples were received in good condition without any visible traces of foreign material.				
Testing	Accredited	Softening Point (ASTM D36), Penetration (ASTM D5), Viscosity @60°C, 135°C and 165°C (ASTM D4402), RTFOT (ASTM D2872), Ductility (ASTM D113)				
	Non accredited	Spot Test (AASHTO T102), Elastic Recovery (MB-4), Force Ductility (EN 13703), Flash Point (ASTM D93), Viscosity S-R1 (MB-13), Compression Recovery (MB-11), Resilience (MB-10), Flow (MB-12), Binder Content (MB-22), Residue on Sieving (MB-23), Saybolt Furol Viscosity (MB-21), Particle Charge (MB-24), Sedimentation (SANS 309)				
Sample preparation		As per test method				
Comments / Remarks						

Authorized Signatory: G.A.J. MTURI Signature:

Name: DR VENTURA Signature:
Group Leader Date: 31/01/2012

This report relates only to the samples actually supplied to CSIR Built Environment. Residual material will be stored for 3 months unless otherwise requested by client. This certificate shall not be reproduced except in full without the written approval of the Director of CSIR Built Environment.

SANAS Disclaimer:

Test marked "*" in this Report are not include in the SANAS Schedule of Accreditation for this laboratory.
Opinions and interpretations expressed herein are outside the scope of SANAS accreditation.

Form no: R10a	Revision no: 7	Date: 28/01/2011
---------------	----------------	------------------



APPENDIX D

TEST REPORT
NO: JR5004
Status: Final

RESULTS

Table 1: Test results for the 80/100pen grade bitumen as per SANS 307 specifications

Test	Test Results	80/100pen Specification Requirements	Test Method
Penetration (10 ⁻¹ mm)	84	80 – 100	ASTM D5
Softening Point (°C)	46.6	42 – 51	ASTM D36
Viscosity @ 60°C (Pa.s)	119	75 – 150	ASTM D4402
Viscosity @ 135°C (Pa.s)	0.308	0.15 – 0.40	ASTM D4402
Spot Test (% Xylene)	Negative	30 Max	AASHTO T102
After Ageing (RTFOT)			
Mass Change (%m/m)	+ 0.077	0.3 max	ASTM D2872
(Viscosity @ 60°C, (Pa.s)) % of original	(226) 190	300 max	ASTM D4402
Softening Point (°C)	50.4	44 min	ASTM D36
Increase in Softening Point (°C)	3.8	7 max	ASTM D36
(Retained Penetration (10 ⁻¹ mm)) % of Original	(61) 73	50 min	ASTM D5

Table 2: Test results for the S-E1 modified binder as per TG-1 guideline requirements

Test	Test Results	S-E1 Specification Requirements	Test Method
Softening Point (°C)	54.6	50 – 60	MB-17
Elastic Recovery (%)	40	> 50	MB-4
Ductility – Tenacity < E ₂₀₀ (N.mm)	299	Report only*	EN 13589 / EN 13703
Force Ductility [#] E ₄₀₀ -E ₂₀₀ @ 5°C (N)	73		
Viscosity @ 165°C (Pa.s)	0.160	≤ 0.55	MB-18
Stability @ 160°C (°C)	0.2	≤ 5	MB-6
Flash Point (°C)	352	≥ 230	ASTM D93
After Ageing (RTFOT)			
Mass Change (%m/m)	+ 0.066	≤ 1.0	MB-3
Difference in Softening Point (°C)	+5	-2 to +8	MB-17
Elastic Recovery (%)	Failed elongation**	> 40	MB-4

* The values for force ductility test are expressed as the difference of conventional energy corresponding to two elongation points (200mm and 400mm)

* No values provided but the test can be used to rank various binders according to their low temperature cohesion properties

** Failed elongation at 95mm

Form no: R10a	Revision no: 7	Date: 28/01/2011
---------------	----------------	------------------



APPENDIX D

TEST REPORT
NO: JR5004
Status: Final

Table 3: Test results for the S-R1 modified binder as per TG-1 guideline requirements

Test	Test Results	S-R1 Specification Requirements	Test Method
Softening Point (°C)	60.0	55 – 62	MB-17
Viscosity @ 190°C (dPa.s)	35	20 – 40	MB-13
Compression Recovery (%)	5 mins	> 70	MB-11
	1 hour	> 70	
	4 days	> 25	
Resilience @ 25°C (%)	25	13 – 35	MB-10
Flow (mm)	14	15 – 70	MB-12

Table 4: Test results for the KRS 60 cationic spray grade emulsion as per SANS 548 specifications

Test	Test Results	Spray type 60 Specification Requirements	Test Method
Saybolt Furol Viscosity @ 50°C, (seconds)	33	20 – 50	ASTM D 244
Binder content (%m/m)	63.1	60 – 63	*
Fluxing agent content [#] (%m/m of binder)	2.8	5 max.	ASTM D 244
Residue on sieving (g/100 mL, max.)	0.01 (710µm sieve) 0.05 (150µm sieve)	0.25	SANS 309
Particle charge (Modified procedure)	Positive	Positive	SABS 548
Binder deposit on the cathode after 30 min (g, min.)	2.42	1.0	SABS 548
Sedimentation after 60 complete rotations	Sedimentation observed even after 150 rotations	Nil	SABS 309/548

In ASTM D 244 "Fluxing agent" is referred to as "oil distillate".

* By difference from water content determined in accordance with method ASTM D 244.

Form no: R10a	Revision no: 7	Date: 28/01/2011
---------------	----------------	------------------

Page 3 of 4

This is not a controlled document once printed



APPENDIX D

TEST REPORT
NO: JR5004
Status: Final

Table 5: Test results for the KRS 60/3 cationic spray grade (SC-E1) emulsion as per TG-1 guideline requirements

Test	Test Results	SC-E1 Specification Requirements		Test Method
Binder content (%m/m)	60.2	65-68	70-73	MB-22
Saybolt Furol Viscosity @ 50°C (seconds)	21	51-200	51-400	MB-21
Residue on sieving (g)	710µm sieve	0.02	≤ 0.1	MB-23
	150µm sieve	0.04	≤ 0.5	
Particle charge (Modified procedure)	Positive	Positive		MB-24
Sedimentation after 60 complete rotations	Sedimentation observed even after 150 rotations	Nil		SANS 309
Recovered binder residue				MB-20
Softening Point (°C)	48.8	≥ 48		MB-17
Elastic Recovery @ 15°C (%)	53	≥ 50		MB-4
Ductility – Tenacity < E ₂₀₀ (N.mm)	2278	Report only*		EN 13589 / EN 13703
Force Ductility [#] E ₄₀₀ -E ₂₀₀ @ 5°C (N)	2298			

* No values provided but the test can be used to rank various binders according to their low temperature cohesion properties

The values for force ductility test are expressed as the difference of conventional energy corresponding to two elongation points (200mm and 400mm)





Form no: R10a Revision no: 7 Date: 28/01/2011

Page 4 of 4

This is not a controlled document once printed



APPENDIX D

 <p>our future through science</p>	ROAD MATERIALS TESTING LABORATORY BUILT ENVIRONMENT UNIT CSIR		 T0325																																																								
	(A SANAS Accredited Testing Laboratory: T0325) P O BOX 395, PRETORIA, 0001																																																										
Contact: Email:	G Mturi gmturi@csir.co.za	Telephone: +27 12 841-2234 Fax: +27 12 841-2690																																																									
TEST REPORT NO: JR 5004-2																																																											
Status: FINAL		Date of issue: 18th May 2012																																																									
Client Details:																																																											
<table border="1"> <tr> <th>Client/Requestor</th> <th>Address</th> <th>Client details</th> </tr> <tr> <td>Estimé Mukandila Aurecon South Africa (Pty) Ltd</td> <td>Aurecon Centre, Lynnwood Bridge Office Park, 4 Davenry Str, Lynnwood Manor, 0081, Tshwane, South Africa</td> <td>Tel: +27 12 427-2842 Fax: +27 86 608-0371 Cell: +27 76 873-9814 Email: Estime.Mukandila@aurecongroup.com</td> </tr> </table>	Client/Requestor	Address	Client details	Estimé Mukandila Aurecon South Africa (Pty) Ltd	Aurecon Centre, Lynnwood Bridge Office Park, 4 Davenry Str, Lynnwood Manor, 0081, Tshwane, South Africa	Tel: +27 12 427-2842 Fax: +27 86 608-0371 Cell: +27 76 873-9814 Email: Estime.Mukandila@aurecongroup.com																																																					
Client/Requestor	Address	Client details																																																									
Estimé Mukandila Aurecon South Africa (Pty) Ltd	Aurecon Centre, Lynnwood Bridge Office Park, 4 Davenry Str, Lynnwood Manor, 0081, Tshwane, South Africa	Tel: +27 12 427-2842 Fax: +27 86 608-0371 Cell: +27 76 873-9814 Email: Estime.Mukandila@aurecongroup.com																																																									
Sample Details:																																																											
<table border="1"> <tr> <th>Sample description</th> <td colspan="5">Binder and Emulsion samples</td> </tr> <tr> <th rowspan="2">Sample no</th> <th>Client</th> <td>80/100</td> <td>S-E1</td> <td>S-R1 (BR)</td> <td>KRS 60</td> <td>KRS 60/3</td> </tr> <tr> <th>CSIR</th> <td>12152</td> <td>12347</td> <td>12154</td> <td>12155</td> <td>12156</td> </tr> <tr> <th>Date sample received</th> <td colspan="5">15th December 2012 (18th April 2012 for the S-E1 sample)</td> </tr> <tr> <th>Sample condition</th> <td colspan="5">All samples were received in good condition without any visible traces of foreign material.</td> </tr> <tr> <th rowspan="2">Testing</th> <th>Accredited</th> <td colspan="4">Softening Point (ASTM D36), Viscosity @ 165°C (ASTM D4402)</td> </tr> <tr> <th>Non accredited</th> <td colspan="4">Elastic Recovery (MB-4), Force Ductility (EN 13703), Flash Point (ASTM D93), RTFOT (MB-3), Stability (MB-6), Frequency Sweeps (AASHTO T315)</td> </tr> <tr> <th>Sample preparation</th> <td colspan="5">As per test methods</td> </tr> <tr> <th>Comments / Remarks</th> <td colspan="5"></td> </tr> </table>	Sample description	Binder and Emulsion samples					Sample no	Client	80/100	S-E1	S-R1 (BR)	KRS 60	KRS 60/3	CSIR	12152	12347	12154	12155	12156	Date sample received	15 th December 2012 (18 th April 2012 for the S-E1 sample)					Sample condition	All samples were received in good condition without any visible traces of foreign material.					Testing	Accredited	Softening Point (ASTM D36), Viscosity @ 165°C (ASTM D4402)				Non accredited	Elastic Recovery (MB-4), Force Ductility (EN 13703), Flash Point (ASTM D93), RTFOT (MB-3), Stability (MB-6), Frequency Sweeps (AASHTO T315)				Sample preparation	As per test methods					Comments / Remarks										
Sample description	Binder and Emulsion samples																																																										
Sample no	Client	80/100	S-E1	S-R1 (BR)	KRS 60	KRS 60/3																																																					
	CSIR	12152	12347	12154	12155	12156																																																					
Date sample received	15 th December 2012 (18 th April 2012 for the S-E1 sample)																																																										
Sample condition	All samples were received in good condition without any visible traces of foreign material.																																																										
Testing	Accredited	Softening Point (ASTM D36), Viscosity @ 165°C (ASTM D4402)																																																									
	Non accredited	Elastic Recovery (MB-4), Force Ductility (EN 13703), Flash Point (ASTM D93), RTFOT (MB-3), Stability (MB-6), Frequency Sweeps (AASHTO T315)																																																									
Sample preparation	As per test methods																																																										
Comments / Remarks																																																											
Authorized Signatory: <u>G.A.J. Mturi</u> Signature: 																																																											
Name: <u>DFC VENTURA</u> Signature: 																																																											
Group Leader Date: <u>18/05/2012</u>																																																											
This report relates only to the samples actually supplied to CSIR Built Environment. Residual material will be stored for 3 months unless otherwise requested by client. This certificate shall not be reproduced except in full without the written approval of the Director of CSIR Built Environment.																																																											
SANAS Disclaimer: Test marked "*" in this Report are not include in the SANAS Schedule of Accreditation for this laboratory. Opinions and interpretations expressed herein are outside the scope of SANAS accreditation.																																																											
Form no: R10a		Revision no: 8		Date: 25/04/2012																																																							
Page 1 of 2																																																											
This is not a controlled document once printed																																																											



APPENDIX D

TEST REPORT
NO: JR5004:2
Status: Final

RESULTS

Table 1: Test results for the S-E1 modified binder as per TG-1 guideline requirements

Test	Test Results	S-E1 Specification Requirements	Test Method
Softening Point (°C)	55.0	50 – 60	MB-17
Elastic Recovery (%)	83	> 50	MB-4
Ductility – Tenacity < E ₂₀₀ (N.mm) @ 5°C (N)	1739	Report only*	EN 13589 / EN 13703
Force Ductility* E ₄₀₀ -E ₂₀₀ @ 5°C (N)	1591		
Ductility – Tenacity < E ₂₀₀ (N.mm) @ 15°C (N)	129	Report only*	EN 13589 / EN 13703
Force Ductility* E ₄₀₀ -E ₂₀₀ @ 15°C (N)	114		
Viscosity @ 165°C (Pa.s)	0.215	≤ 0.55	MB-18
Stability @ 160°C (°C)	1.0	≤ 5	MB-6
Flash Point (°C)	341	≥ 230	ASTM D93
After Ageing (RTFOT)			
Mass Change (%m/m)	+ 0.074	≤ 1.0	MB-3
Difference in Softening Point (°C)	+ 2.6	-2 to +8	MB-17
Elastic Recovery (%)	80	> 40	MB-4

* The values for force ductility test are expressed as the difference of conventional energy corresponding to two elongation points (200mm and 400mm)

* No values provided but the test can be used to rank various binders according to their low temperature cohesion properties

Please note: all other test results (as per the quotation dated: 26 April 2012) will be included in an excel spreadsheet labelled, DSR binder test results (parallel-plate configuration).

Form no: R10a	Revision no: 8	Date: 25/04/2012
---------------	----------------	------------------

Page 2 of 2

This is not a controlled document once printed

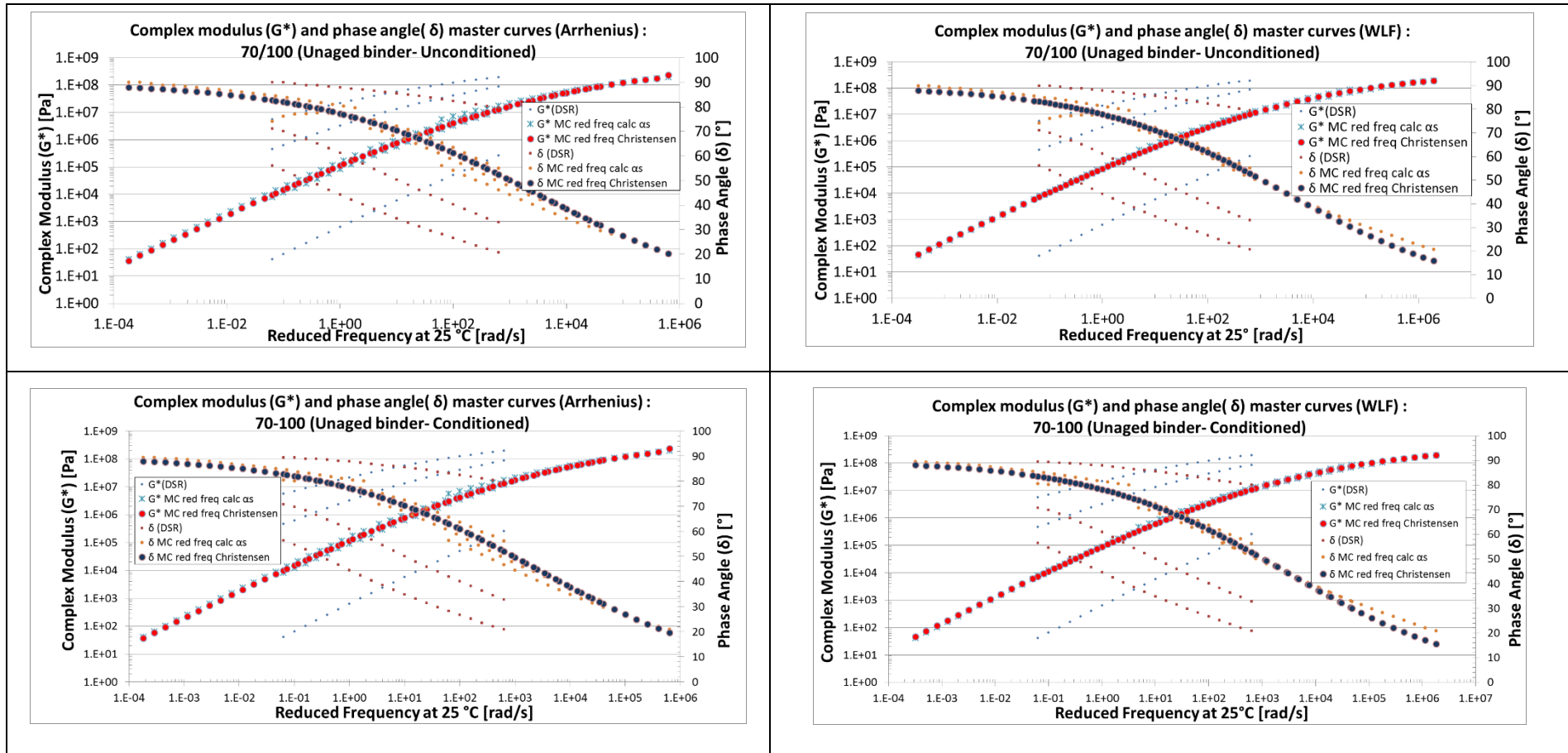


E BITUMEN RESPONSE DATA

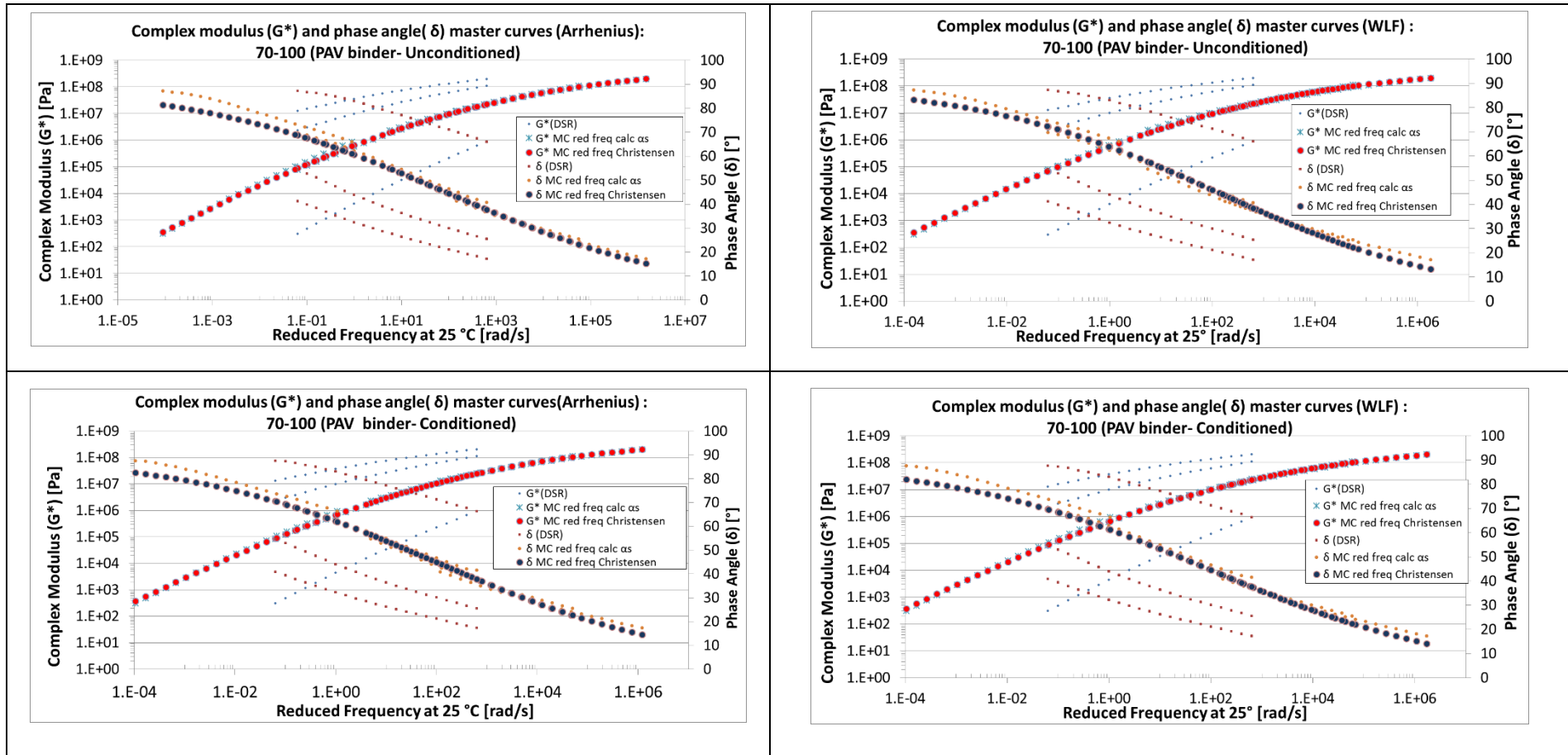
APPENDIX E

E.1 Arrhenius and WLF graphs

70/100

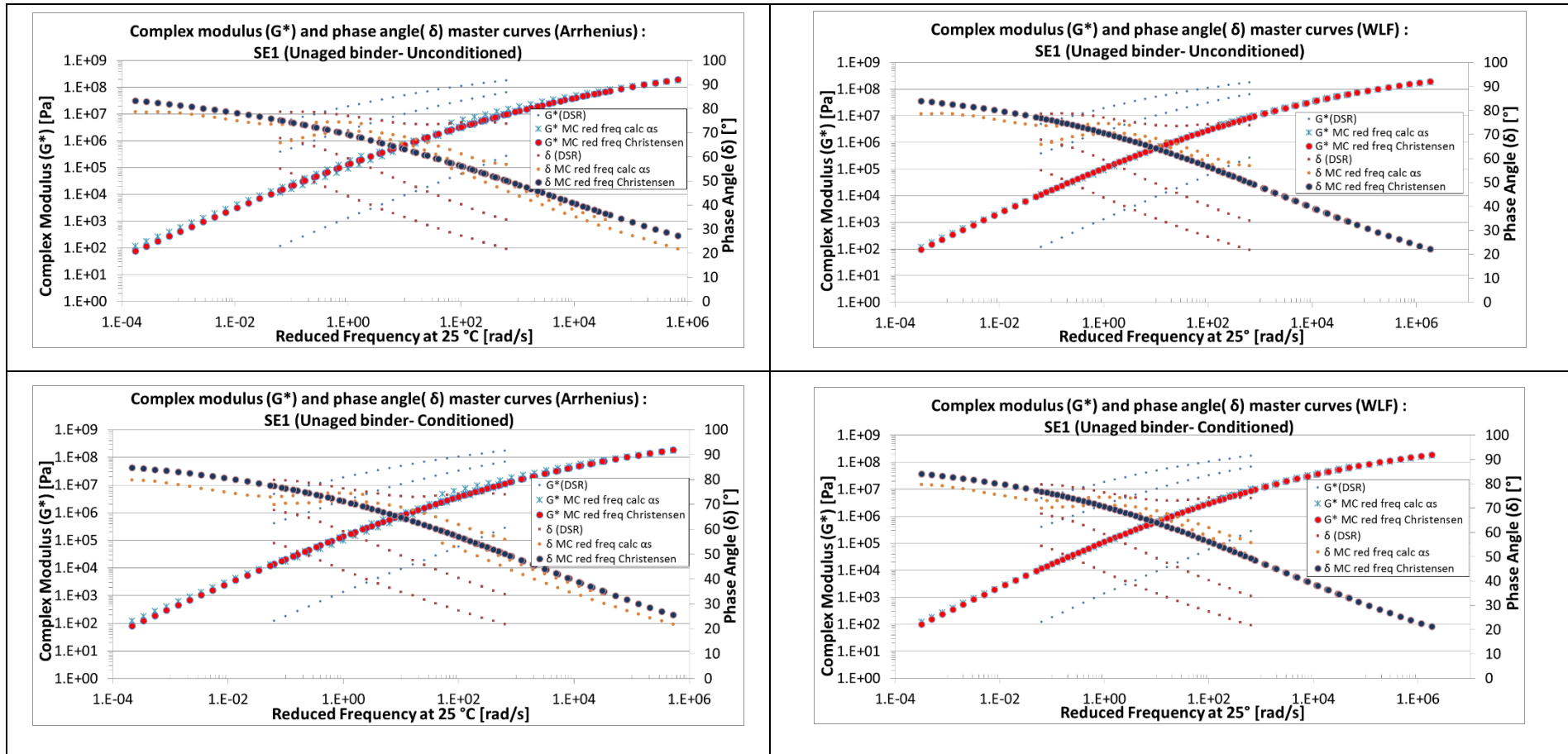


APPENDIX E

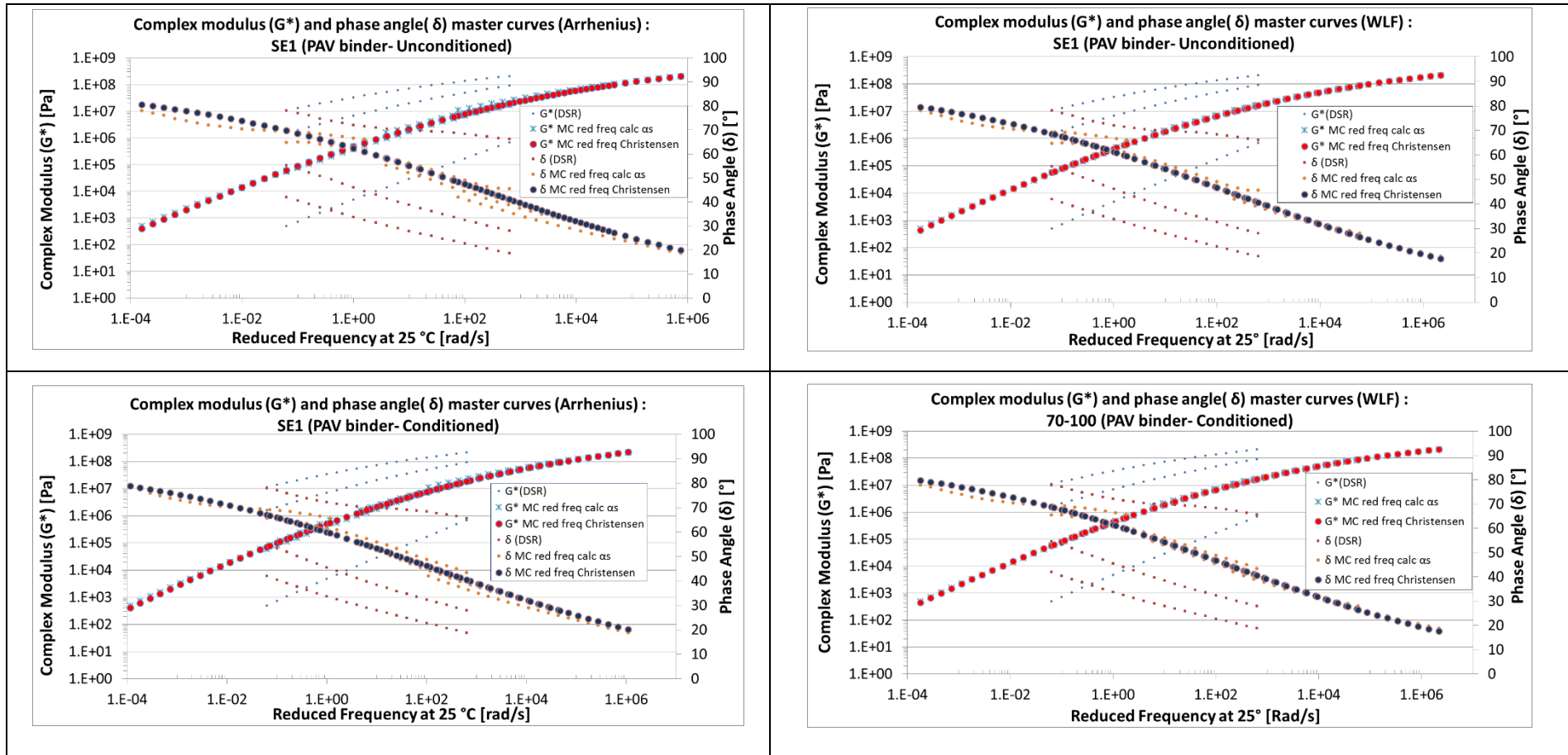


APPENDIX E

SE1

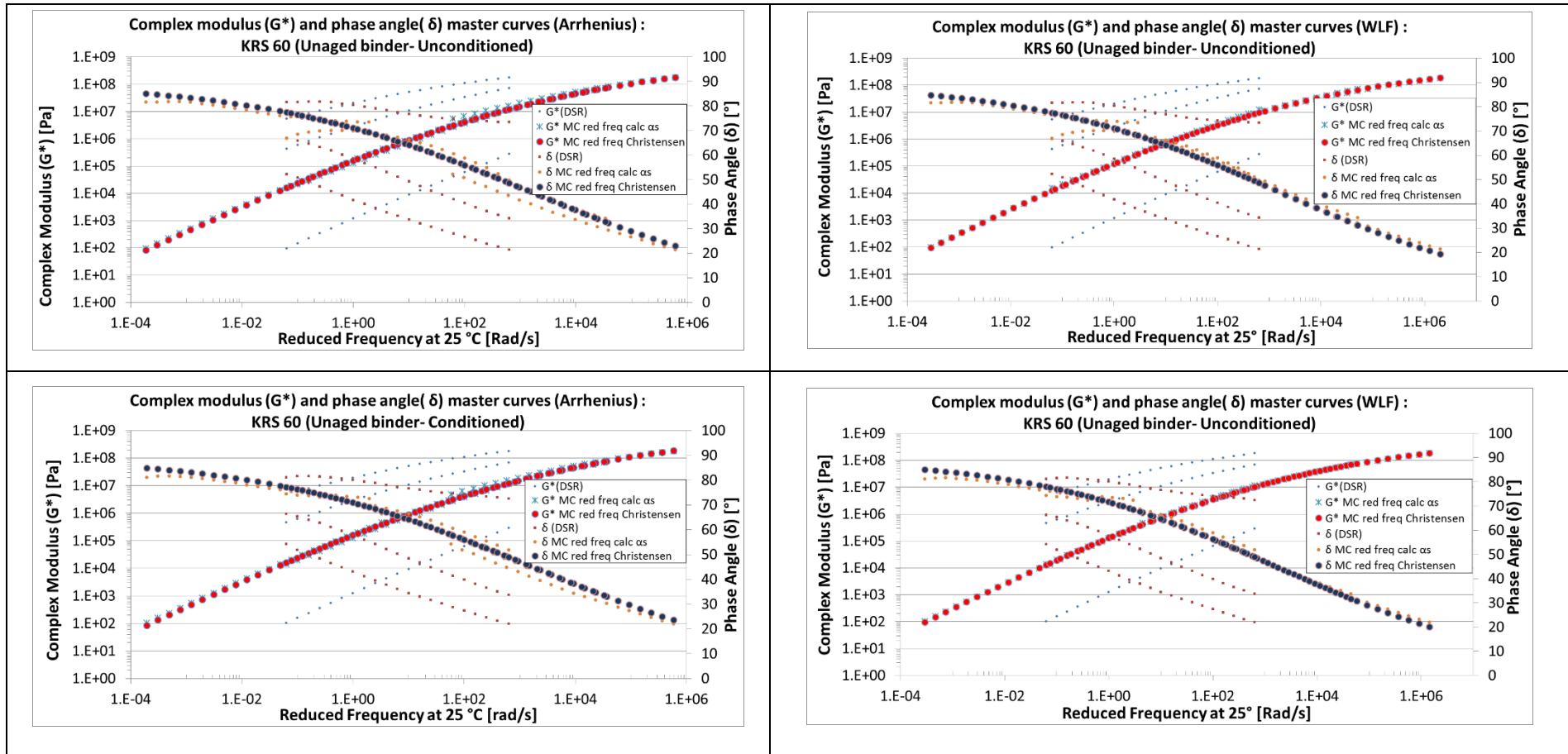


APPENDIX E

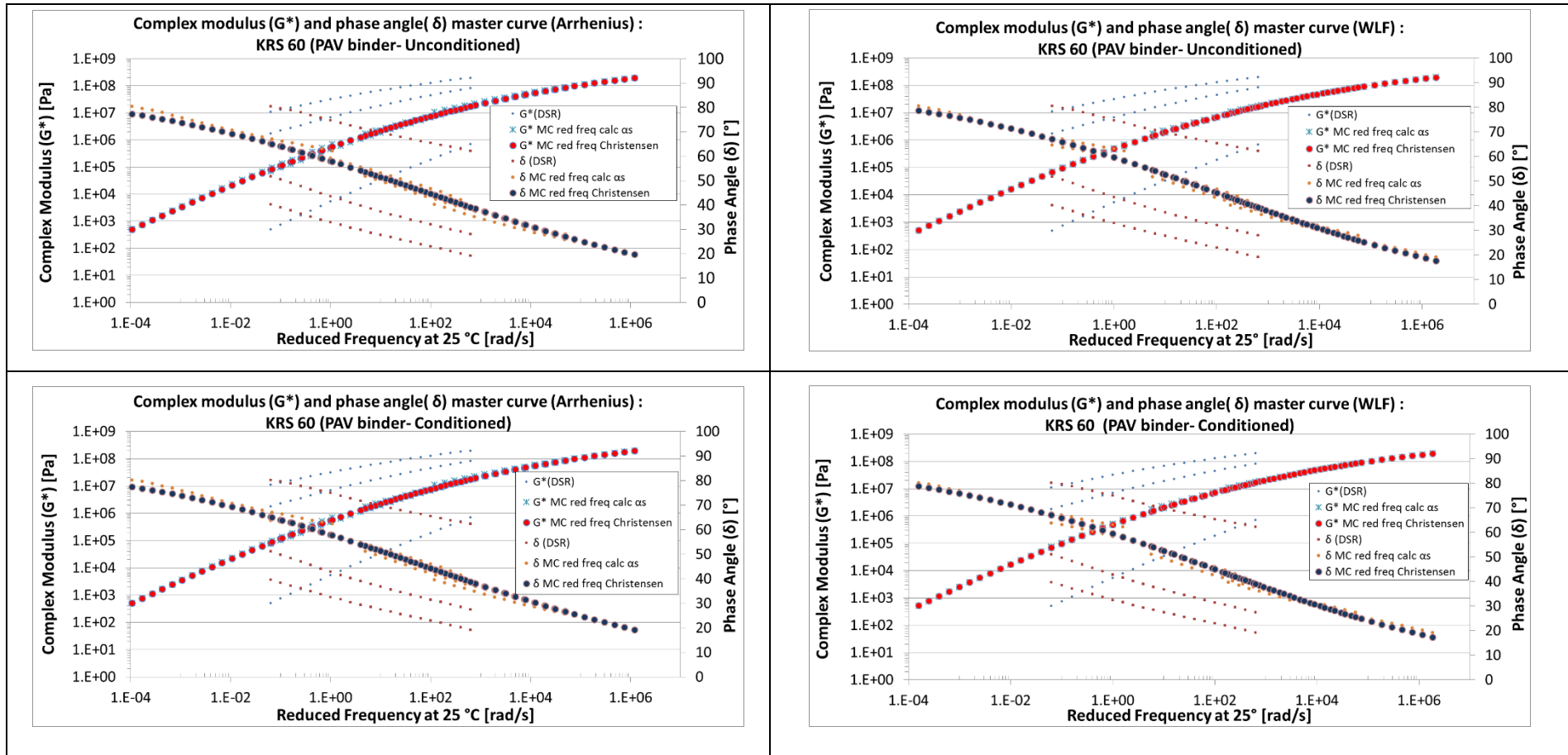


APPENDIX E

KRS 60

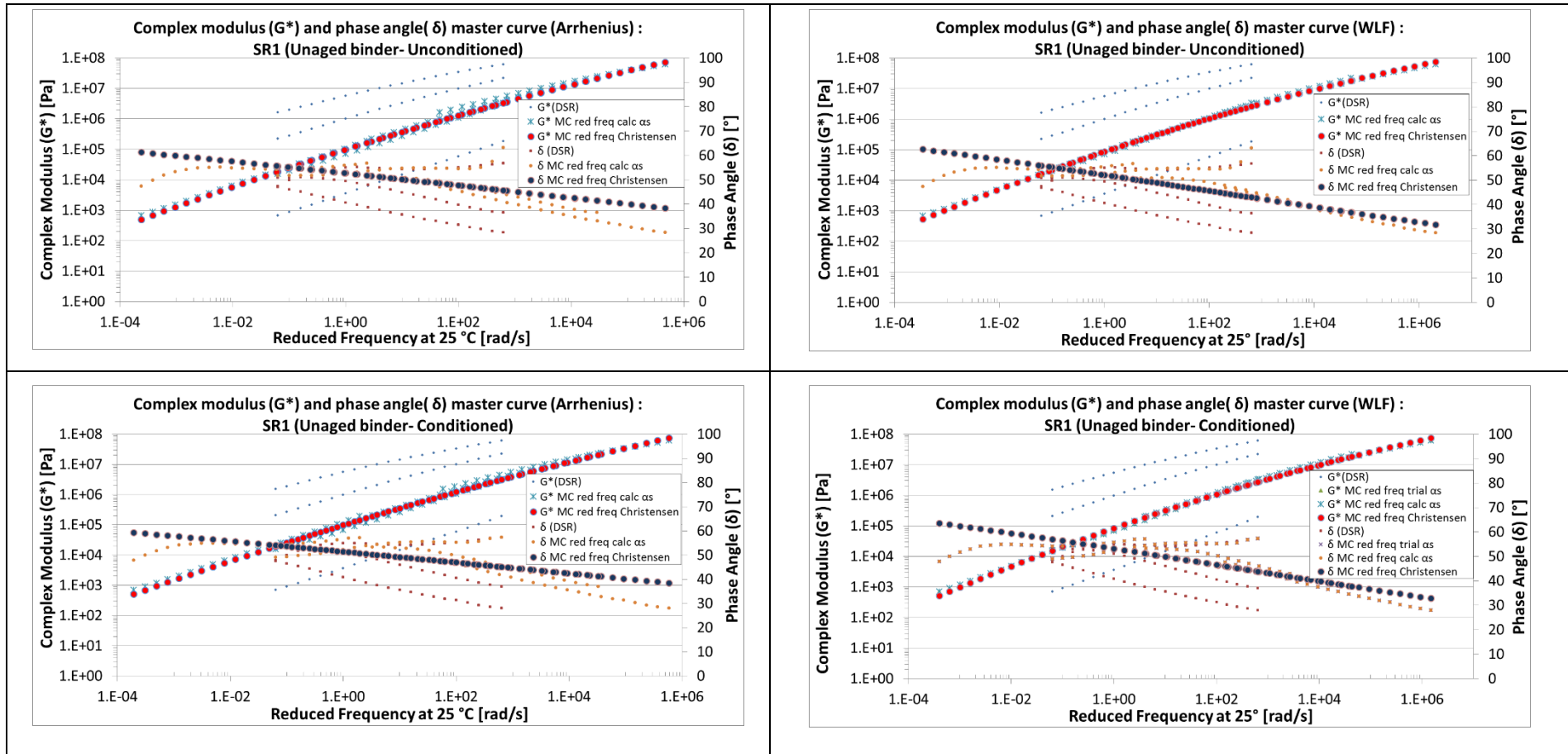


APPENDIX E

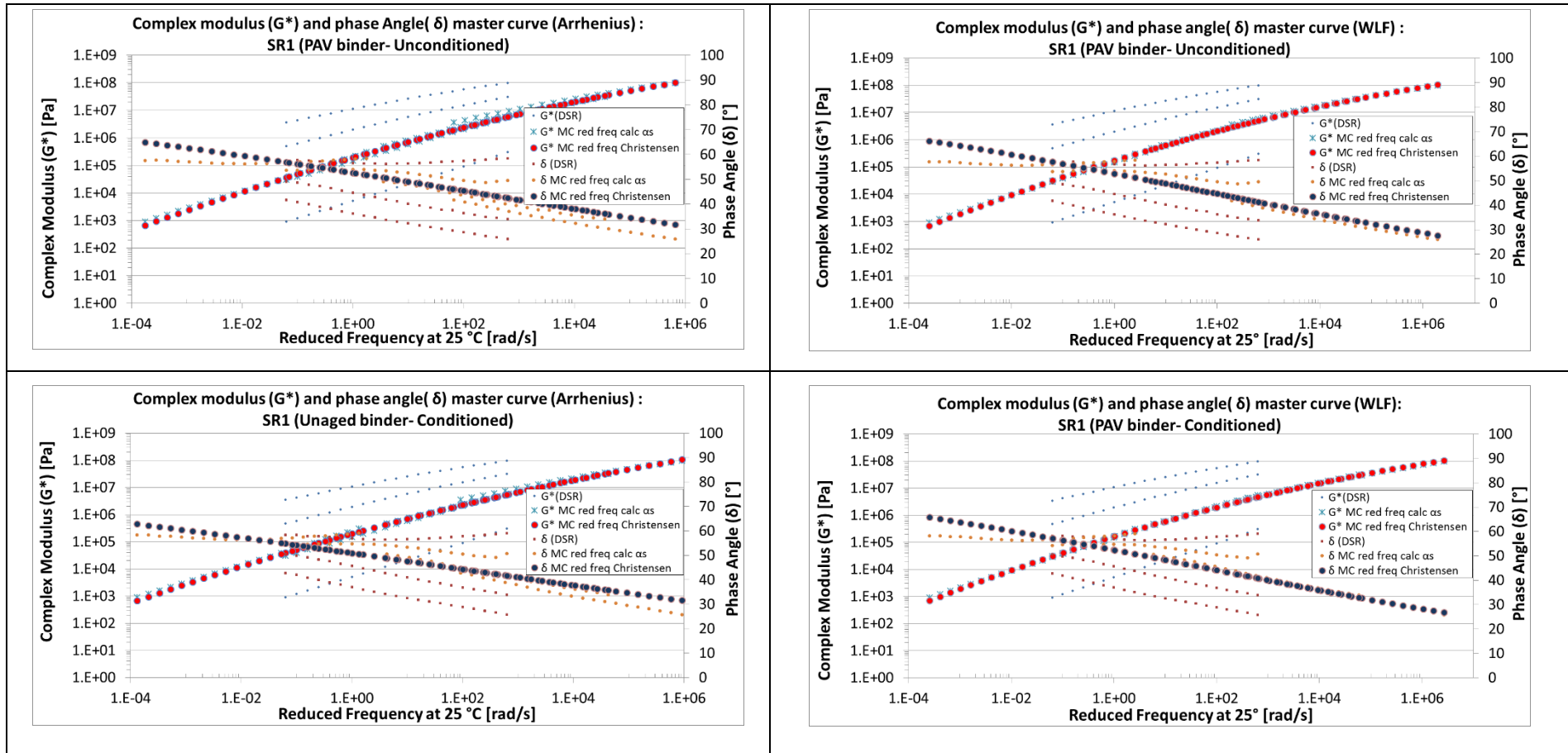


APPENDIX E

SR1



APPENDIX E



APPENDIX E

E.2 Shift factor parameters (Arrhenius and WLF) and CA model parameters

Type of Bitumen	Arrhenius: ΔH	WLF: C1	WLF: C2	G_{glassy}	ω_{cross}	R	R^2 for G^*	R^2 for δ
70/100 Unaged Unconditioned	186798	30.94	121.2	4.54E+08	2.80E+03	1.28	0.99	0.98
70/100 Unaged Conditioned	187010.5	31.35	123.5	4.32E+08	2.69E+03	1.26	1.00	0.98
70/100 Aged Unconditioned	209892	49.5	180.7	4.69E+08	1.29E+02	1.64	1.00	0.98
70/100 Aged Conditioned	204252.1	66.84	236.1	5.59E+08	8.92E+01	1.77	1.00	0.98
SE1 Unaged Unconditioned	188871.9	31.52	123.8	1.06E+09	2.32E+03	1.8	1.00	0.96
SE1 Unaged Conditioned	181840.5	31.51	123.7	9.24E+08	1.96E+03	1.76	1.00	0.99
SE1 Aged Unconditioned	191788.2	41.78	153.2	9.56E+08	1.67E+02	2.04	1.00	0.99
SE1 Aged Conditioned	201714.6	41.78	153.2	9.36E+08	1.70E+02	2.02	1.00	0.99
KRS 60 Unaged Unconditioned	185952	32.57	126	7.12E+08	1.55E+03	1.67	1.00	0.98
KRS 60 Unaged Conditioned	184835.7	34.91	137.8	7.39E+08	1.65E+03	1.64	1.00	0.99
KRS 60 Aged Unconditioned	204133.3	47.97	175.1	9.06E+08	1.09E+02	2.09	1.00	0.99
KRS 60 Aged Conditioned	204133.3	47.97	175.1	8.48E+08	1.01E+02	2.07	1.00	0.99
SR1 Unaged Unconditioned	178600.7	29.21	115.3	7.14E+10	1.59E+02	4.73	0.97	0.62
SR1 Unaged Conditioned	184835.7	29.18	119	8.18E+10	2.94E+02	4.64	1.00	0.99
SR1 Aged Unconditioned	188243.5	35.46	135.5	1.02E+10	8.17E+01	3.73	1.00	0.99
SR1 Aged Conditioned	197320.6	32.2	121.4	8.49E+09	6.33E+01	3.73	1.00	0.99
70/100_DR02175_OWT_3yrs_Arrh	212032.5	-	-	7.55E+08	2.95E+01	1.72	1.00	0.98
70/100_DR1298_SHDR_4yrs	214057.1	-	-	4.70E+08	4.26E+01	1.62	0.99	0.97
70/100_DR1298_OWT_4yrs	212032.5	-	-	4.51E+08	5.49E+01	1.59	0.99	0.96
70/100_DR1398_BWT_5yrs	210024.7	-	-	4.93E+08	3.25E+01	1.65	0.99	0.97
70/100_DR1398_IWT_5yrs	211072.4	-	-	5.66E+08	4.45E+01	1.73	0.99	0.97

APPENDIX E

70/100_DR2175-BWT_6yrs	205513.3	-	-	3.42E+08	1.64E+01	1.71	0.99	0.96
70/100_DR2175-IWT_6yrs	200000.6	-	-	4.65E+08	2.88E+01	1.59	0.99	0.96
70/100_N10-3-BWT_9yrs	201164.3	-	-	5.04E+08	2.93E+01	1.65	0.98	0.98
70/100_N10-3-OWT_9yrs	203432.4	-	-	4.83E+08	2.61E+01	1.68	0.98	0.98
70/100_N10-3-IWT_9yrs	200000.6	-	-	4.76E+08	2.66E+01	1.65	0.98	0.98
70/100_MR174-SHDR_10yrs	209726.2	-	-	683531840	2.59E+01	1.81	1.00	0.97
70/100_MR174-OWT_10yrs	203432.4	-	-	4.83E+08	2.61E+01	1.68	0.99	0.95
70/100_DR2216-BWT_10yrs	219492.4	-	-	7.63E+08	1.84E+00	2.4	1.00	0.96
70/100_DR2216-IWT_10yrs	206242.2	-	-	6.13E+08	2.53E+00	2.23	0.99	0.97
70/100_N6-5-SHDR_11yrs	207649.7	-	-	4.27E+08	8.22E+00	1.79	1.00	0.97
70/100_N6-5-OWT_11yrs	214119.2	-	-	5.37E+08	2.63E+01	1.72	0.99	0.97
70/100_DR1452-BWT_12yrs	208577.6	-	-	5.97E+08	1.57E+00	2.02	0.99	0.98
70/100_DR1452-OWT_12yrs	214271.1	-	-	6.37E+08	6.28E-01	2.25	0.99	0.96
70/100_N6-5-SHDR_13yrs	208169.0	-	-	5.54E+08	8.02E+00	1.83	1.00	0.98
70/100_N6-5-OWT_13yrs	217054.6	-	-	8.12E+08	1.11E+01	2.06	1.00	0.96
70/100_MR269-SHDR_13yrs	219776.6	-	-	6.19E+08	2.04E+00	2.04	1.00	0.95
70/100_MR269-OWT_13yrs	204989.7	-	-	4.86E+08	1.31E+01	1.80	0.99	0.97
70/100_MR188-OWT_15yrs	218153.7	-	-	5.19E+08	5.19E+08	1.82	1.00	0.98
70/100-DR1123_IWT_17yrs	230327.6	-	-	6.45E+08	2.59E+00	2.01	1.00	0.97
70/100-MR563_IWT_19yrs	210536.3	-	-	4.92E+08	1.22E+00	2.06	1.00	0.97
70/100-MR563_BWT_19yrs	208563.1	-	-	5.24E+08	9.13E-01	2.08	0.99	0.97
70/100-P1398_OWT_22yrs	209089.6	-	-	4.14E+08	3.64E+00	1.77	1.00	0.97
70/100-P1398_OWT_23yrs	208242.6	-	-	4.07E+08	3.24E+00	1.76	0.99	0.97
70/100 Q-SUN	194907.9	-	-	5.87E+08	3.74E+01	1.83	0.99	0.96

APPENDIX E

SE1_N2-32_OWT_2yrs_Arrh	183413.3	-	-	6.48E+08	7.34E+02	1.50	0.99	0.90
SE1_N2-32_SHDR_2yrs_Arrh	187725.5	-	-	5.97E+08	3.42E+02	1.48	0.99	0.94
SE1_N2-32_OWT_6yrs_Arrh	194940.5	-	-	5.56E+08	6.23E+01	1.59	0.99	0.97
SE1_N2-32_SHDR_6yrs_Arrh	199424.4	-	-	4.98E+08	2.92E+01	1.53	0.99	0.98
SE1_N6-4_OWT_6yrs_Arrh	213539.7	-	-	8.27E+08	6.10E+00	2.21	1.00	0.97
SE1_N6-4_SHDR_6yrs_Arrh	207712.9	-	-	7.60E+08	1.04E+01	2.11	1.00	0.97
SE1_N1-29_OWT_6yrs_Arrh	213539.7	-	-	5.28E+08	2.97E+00	2.06	1.00	0.97
SE1_N1-29_SHDR_6yrs_Arrh	217415.5	-	-	5.57E+08	8.25E+00	1.96	1.00	0.96
SE1_N2-31_OWT_7yrs_Arrh	206626.5	-	-	4.84E+08	5.21E+00	1.70	1.00	0.98
SE1_N2-31_SHDR_7yrs_Arrh	208003.3	-	-	5.02E+08	8.49E-01	1.97	1.00	0.98
SE1_N8-8_OWT_7yrs_Arrh	207712.9	-	-	6.58E+08	2.50E+01	1.84	1.00	0.97
SE1_N8-8_SHDR_7yrs_Arrh	202499.9	-	-	6.13E+08	2.13E+01	1.80	1.00	0.97
SE1_N2-31_Pongola_BWT_7yrs_Arrh	202918.7	-	-	6.64E+08	2.73E-01	2.12	0.99	0.98
SE1_N2-31_OWT_Pongola_7yrs_Arrh	207712.9	-	-	6.24E+08	1.77E-01	2.13	1.00	0.98
SE1_N10-2_OWT_7yrs_Arrh	205134.9	-	-	5.49E+08	21.610796	1.68	0.99	0.98
SE1_N10-2_SHDR_7yrs_Arrh	204671.1	-	-	5.50E+08	1.71E+01	1.72	0.99	0.98
SE1_N6-4_OWT_10yrs_Arrh	206307.5	-	-	6.36E+08	4.52E+00	1.92	1.00	0.98
SE1_N2-31_SHDR_12yrs_Arrh	207712.9	-	-	5.31E+08	4.77E+00	1.64	1.00	0.98
SE1_N2-31_OWT_12yrs_Arrh	207712.9	-	-	4.93E+08	2.26E+00	1.66	1.00	0.98
SE1_N2-31_S_SHDR_12yrs_Arrh	207712.9	-	-	5.25E+08	6.11E+00	1.69	1.00	0.98
SE1_N2-31_S_OWT_12yrs_Arrh	207712.9	-	-	4.44E+08	3.08E+00	1.85	1.00	0.98
SE1_N10-3_OWT_24yrs_Arrh	218765.6	-	-	6.63E+08	4.90E-01	2.04	1.00	0.98
SE1 Q-SUN	192875.0	-	-	8.63E+08	2.80E+02	1.91	0.99	0.94

APPENDIX E

E.3 Prony series model parameters

APPENDIX E

Prony parameters for 70/100 bitumen

Type of bitumen	model parameters (70/100)											
	G_0		term1	term2	term3	term4	term5	term6	term7	term8	term9	term10 (residual)
70/100 Unaged Unconditioned_25C	4.62E+07	α_j	1.64E-03	9.46E-01	1.00E-08	2.61E-02	3.68E-05	2.45E-02	1.76E-04	6.78E-05	2.91E-05	1.65E-03
		τ_j	1.01E-02	3.19E-04	1.86E-03	3.07E-02	6.48E-03	5.99E-03	1.41E+00	1.09E+01	8.83E-03	2.96E-01
70/100 Unaged Conditioned_25C	3.56E+07	α_j	1.53E-03	9.26E-01	1.00E-08	3.48E-02	3.67E-05	3.54E-02	1.74E-04	6.76E-05	2.91E-05	1.53E-03
		τ_j	1.57E-02	5.19E-04	1.86E-03	3.07E-02	5.01E+01	3.99E-03	3.40E+00	7.90E+00	8.83E-02	2.00E-01
70/100 PAV_Uncond_25C	6.06E+07	α_j	1.61E-03	4.48E-01	4.53E-01	5.74E-02	3.61E-05	3.84E-02	1.76E-04	6.78E-05	2.91E-05	1.71E-03
		τ_j	8.92E+00	1.11E-04	1.29E-03	2.77E-02	1.06E-03	9.03E-02	1.09E+00	1.21E+02	3.00E+00	2.00E+00
70/100 PAV Conditioned_25C	6.49E+07	α_j	1.12E-03	4.16E-01	4.84E-01	5.44E-02	3.62E-05	4.23E-02	1.77E-04	6.53E-05	2.91E-05	1.77E-03
		τ_j	2.12E+01	1.12E-04	1.42E-03	2.90E-02	1.06E-03	1.03E-01	1.09E+00	1.18E+02	2.99E+00	1.87E+00

Prony parameters for SE1 bitumen

Type of bitumen	model parameters											
	G_0		term1	term2	term3	term4	term5	term6	term7	term8	term9	term10 (residual)
SE1 Unaged Unconditioned_25C	2.40E+07	α_j	6.16E-05	6.92E-02	1.38E-04	9.09E-04	8.50E-01	6.01E-02	6.50E-04	1.84E-02	1.81E-04	2.00E-04
		τ_j	2.91E-03	1.18E-02	1.07E-04	1.76E-03	3.81E-04	7.41E-03	7.88E-03	1.77E-01	5.19E+00	3.54E+01
SE1 Unaged Conditioned_25C	2.55E+07	α_j	6.16E-05	6.92E-02	1.38E-04	9.09E-04	8.50E-01	6.01E-02	6.50E-04	1.84E-02	1.81E-04	2.00E-04
		τ_j	2.91E-03	1.16E-02	1.07E-04	1.78E-03	3.70E-04	7.41E-03	7.88E-03	1.70E-01	5.19E+00	3.09E+01
SE1 PAV Unconditioned_25C	6.86E+07	α_j	6.15E-05	6.52E-02	1.38E-04	8.93E-04	8.51E-01	5.91E-02	6.41E-04	2.27E-02	2.07E-04	2.64E-04
		τ_j	3.81E-03	1.17E-02	1.07E-04	1.97E-03	2.07E-04	7.18E-03	7.87E-03	2.74E-01	5.64E+00	7.55E+01
SE1 PAV Conditioned_25C	6.86E+07	α_j	6.15E-05	6.52E-02	1.38E-04	8.93E-04	8.51E-01	5.91E-02	6.41E-04	2.27E-02	2.07E-04	2.64E-04
		τ_j	3.81E-03	1.17E-02	1.07E-04	1.97E-03	2.07E-04	7.18E-03	7.87E-03	2.74E-01	5.64E+00	7.55E+01

APPENDIX E

Prony parameters for KRS 60 bitumen

	model parameters											
Type of bitumen	G_0		term1	term2	term3	term4	term5	term6	term7	term8	term9	term10 (residual)
KRS 60 Unaged Unconditioned	6.48E+07	α_j	4.37E-04	2.68E-03	6.45E-02	3.15E-06	1.39E-02	3.96E-04	5.27E-05	8.00E-08	7.46E-01	1.73E-01
		τ_j	1.83E-03	2.98E-01	4.71E-03	4.30E+02	3.93E-02	2.25E+00	2.07E+01	8.66E+03	7.38E-05	6.71E-04
KRS 60 Unaged Conditioned	6.48E+07	α_j	4.37E-04	2.68E-03	6.45E-02	3.15E-06	1.39E-02	3.96E-04	5.27E-05	8.00E-08	7.46E-01	1.73E-01
		τ_j	1.83E-03	2.98E-01	4.71E-03	4.30E+02	3.93E-02	2.25E+00	2.07E+01	8.66E+03	7.38E-05	6.71E-04
KRS 60 PAV Unconditioned	1.60E+08	α_j	4.61E-04	4.34E-03	6.50E-02	2.27E-05	3.20E-02	5.72E-04	6.46E-05	1.00E-08	8.98E-01	3.83E-09
		τ_j	1.55E+00	5.11E-01	2.07E-03	5.12E+02	1.40E-02	2.83E+00	4.32E+01	1.25E+03	3.70E-05	7.05E-04
KRS 60 PAV Conditioned	1.60E+08	α_j	4.61E-04	4.34E-03	6.50E-02	2.27E-05	3.20E-02	5.72E-04	6.46E-05	1.00E-08	8.98E-01	3.83E-09
		τ_j	5.95E+00	5.11E-01	2.07E-03	5.12E+02	1.40E-02	2.83E+00	4.32E+01	1.25E+03	3.70E-05	7.05E-04

Prony parameters for SR1 bitumen

	model parameters											
Type of bitumen	G_0		term1	term2	term3	term4	term5	term6	term7	term8	term9	term10 (residual)
SR1 Unaged Unconditioned	1.75E+07	α_j	4.34E-04	5.23E-03	5.87E-02	5.97E-05	1.85E-02	1.33E-03	3.00E-04	1.09E-05	7.48E-01	1.67E-01
		τ_j	1.82E-03	5.36E-01	5.82E-03	6.31E+02	5.51E-02	5.36E+00	5.60E+01	8.92E+03	5.41E-05	6.29E-04
SR1 Unaged Conditioned	1.92E+07	α_j	4.37E-04	4.74E-03	5.61E-02	4.93E-05	1.72E-02	1.17E-03	2.56E-04	8.30E-06	7.56E-01	1.64E-01
		τ_j	1.83E-03	5.25E-01	5.72E-03	6.15E+02	5.41E-02	5.24E+00	5.47E+01	8.66E+03	5.29E-05	6.18E-04
SR1 PAV Unconditioned	3.52E+07	α_j	4.37E-04	4.74E-03	5.61E-02	4.93E-05	1.72E-02	1.17E-03	2.56E-04	8.30E-06	7.56E-01	1.64E-01
		τ_j	1.83E-03	5.25E-01	5.72E-03	6.15E+02	5.41E-02	5.24E+00	5.47E+01	8.66E+03	5.29E-05	6.18E-04
SR1 PAV Conditioned	3.52E+07	α_j	4.37E-04	4.74E-03	5.61E-02	4.93E-05	1.72E-02	1.17E-03	2.56E-04	8.63E-06	7.56E-01	1.64E-01
		τ_j	1.83E-03	5.25E-01	5.72E-03	6.15E+02	5.41E-02	5.24E+00	5.47E+01	8.66E+03	3.29E-05	6.18E-04

APPENDIX E

E.4 Huet-Sayegh model parameters

Type of Bitumen	Model parameters					
	G_0	G_∞	ζ (Zeta)	k	h	τ
70/100 Unaged Unconditioned_25C	1	3.69E+08	9.8717	0.4343	0.9440	2.53E-05
70/100 Unaged Conditioned_25C	1	3.67E+08	10.4503	0.4370	0.9549	2.92E-05
70/100 Unaged Conditioned_25C	1	2.23E+08	10.8547	0.4236	0.9037	0.000178
70/100 PAV Conditioned_25C	1	3.43E+08	12.8344	0.3877	0.8650	0.000196
SE1 Unaged Unconditioned_25C	1	5.27E+08	6.9743	0.3457	0.7845	3.5E-06
SE1 Unaged Conditioned_25C	1	4.36E+08	7.5628	0.3872	0.8301	7.02E-06
SE1 PAV Conditioned_25C	1	4.31E+08	9.4612	0.3631	0.7898	3.02E-05
SE1 PAV Conditioned_25C	1	4.4E+08	9.8384	0.3643	0.7954	3.22E-05
SCE1 Unaged Unconditioned_25C	1	3.59E+08	9.7313	0.4180	0.8736	1.92E-05
SCE1 Unaged Conditioned_25C	1	3.84E+08	9.3667	0.4172	0.8750	1.87E-05
SCE1 PAV Conditioned_25C	1	3.81E+08	11.3546	0.3802	0.8051	5.87E-05
SCE1 PAV Conditioned_25C	1	3.82E+08	11.8623	0.3786	0.8096	6.53E-05
SR1 Unaged Unconditioned_25C	220	3.07E+08	8.5642	0.3834	0.6574	9.08E-07
SR1 Unaged Conditioned_25C	220	3.07E+08	8.5642	0.3834	0.6574	9.08E-07
SR1 PAV Conditioned_25C	1	3.92E+08	6.8316	0.3279	0.6431	1.06E-06
SR1 PAV Conditioned_25C	1	3.00E+08	6.8285	0.3436	0.6477	1.79E-06

APPENDIX E

E.5 2S2P1D model parameters

Type of Bitumen	Model parameters						
	G_0	G_∞	ζ (Zeta)	k	h	β	τ
70/100 Unaged Unconditioned_25C	1	4.84E+08	6.5779	0.3670	0.7488	9.7800	5.4E-06
70/100 Unaged Conditioned_25C	1	2.48E+08	8.6052	0.4663	0.9651	3.916E+07	5E-05
70/100 Unaged Conditioned_25C	1	2.23E+08	10.8547	0.4236	0.9037	3.916E+07	0.00038
70/100 PAV Conditioned_25C	10	3.43E+08	12.8767	0.3881	0.8657	3.916E+07	0.0002
SE1 Unaged Unconditioned_25C	1	5.27E+08	6.9743	0.3457	0.7845	76.4766	3.5E-06
SE1 Unaged Conditioned_25C	1	4.25E+08	7.1172	0.3745	0.8078	71.6794	6.6E-06
SE1 PAV Conditioned_25C	1	4.33E+08	7.4985	0.3416	0.7436	138.5175	1.8E-05
SE1 PAV Conditioned_25C	1	5.22E+08	8.1654	0.3339	0.7372	130.0579	1.3E-05
SCE1 Unaged Unconditioned_25C	6	3.31E+08	5.9223	0.3830	0.7791	23.6613	9.2E-06
SCE1 Unaged Conditioned_25C	1	4.11E+08	6.9966	0.3759	0.7915	23.2825	9E-06
SCE1 PAV Conditioned_25C	7	5.5E+08	7.3239	0.3168	0.6849	162.5106	7.8E-06
SCE1 PAV Conditioned_25C	7	5.5E+08	7.3269	0.3166	0.6847	162.4829	8.1E-06
SR1 Unaged Unconditioned_25C	501	3.39E+08	13.0074	0.4044	0.6797	220.5315	1.8E-06
SR1 Unaged Conditioned_25C	603	3.3E+08	12.7706	0.4105	0.6800	222.5369	1.9E-06
SR1 PAV Conditioned_25C	2	1.65E+08	4.8136	0.3876	0.6587	1.9384E+04	6.4E-06
SR1 PAV Conditioned_25C	1	4.25E+08	8.1705	0.3282	0.6426	3.1050E+04	9.3E-07



APPENDIX E

E.6 Complex moduli and phase angle data for different models



APPENDIX E

Initial data_WLF (70/100 Unaged Unconditioned)		
Reduced	G*	δ
[rad/s]	[Pa]	[°]
0.000316	4.16E+01	90.00
0.000502	6.54E+01	90.00
0.000796	1.03E+02	89.60
0.001260	1.62E+02	88.90
0.001996	2.57E+02	88.80
0.003165	4.05E+02	88.40
0.005020	6.35E+02	88.00
0.007963	9.92E+02	87.50
0.012599	1.55E+03	87.10
0.019958	2.42E+03	86.60
0.031650	3.76E+03	86.10
0.050196	5.84E+03	85.60
0.062800	7.98E+03	74.10
0.079629	9.04E+03	85.00
0.099600	1.16E+04	76.20
0.125995	1.40E+04	84.50
0.158000	1.70E+04	77.00
0.199576	2.15E+04	83.80
0.250000	2.53E+04	77.30
0.316499	3.30E+04	83.20
0.396000	3.76E+04	77.60
0.501963	5.04E+04	82.50
0.628000	5.62E+04	77.50
0.796286	7.67E+04	81.70
0.996000	8.35E+04	77.10
1.259946	1.16E+05	81.00
1.580000	1.24E+05	76.50
1.995755	1.76E+05	80.30
2.500000	1.82E+05	75.70
3.164985	2.63E+05	79.60
3.960000	2.69E+05	74.80
4.962588	4.62E+05	71.10
6.280000	3.93E+05	73.60
7.870602	6.39E+05	70.10
9.960000	5.72E+05	72.30
12.485493	8.97E+05	68.50
15.800000	8.27E+05	70.80
19.755527	1.25E+06	66.90
25.000000	1.19E+06	69.20
31.292755	1.73E+06	65.20
39.600000	1.68E+06	67.40
49.625884	2.39E+06	63.30
62.800000	2.37E+06	65.50
78.706019	3.26E+06	61.30
99.600000	3.30E+06	63.50
124.854930	4.41E+06	59.10
158.000000	4.56E+06	61.30
194.821169	5.64E+06	56.20
197.555269	5.91E+06	57.00
250.000000	6.23E+06	59.10
308.983892	7.17E+06	54.30
312.927546	7.82E+06	54.80
396.000000	8.45E+06	57.10
490.155171	9.03E+06	52.20
496.258835	1.03E+07	52.60
628.000000	1.13E+07	55.10
775.561979	1.14E+07	50.30
787.060191	1.33E+07	50.40
1228.490174	1.39E+07	48.50
1248.549299	1.71E+07	48.30
1948.211690	1.75E+07	46.30
1975.552688	2.17E+07	46.20
3089.838923	2.17E+07	44.30
3129.275457	2.73E+07	44.20
4901.551705	2.69E+07	42.20
4962.588351	3.39E+07	42.20
7755.619787	3.29E+07	40.30
7870.601907	4.17E+07	40.30
12284.901742	3.99E+07	38.50

	Modelled data (70/100 Unaged Unconditioned)							
	Arrh Prony		WLF Prony		WLF HS		WLF 2S2P1D	
	G*	δ	G*	δ	G*	δ	G*	δ
R ² CA	0.99	0.98	0.99	0.98				
R ² Mec.	0.97	0.83	0.97	0.84	1.00	1.00	0.99	0.98
Reduced	G*	δ	G*	δ	G*	δ	G*	δ
[rad/s]	[Pa]	[°]	[Pa]	[°]	[Pa]	[°]	[Pa]	[°]
0.0001	1.73E+01	86.07	1.27E+01	85.94	1.62E+01	81.39	1.50E+01	84.67
0.000158489	2.73E+01	87.45	2.01E+01	87.42	2.49E+01	82.61	2.36E+01	85.88
0.000251189	4.33E+01	88.29	3.19E+01	88.34	3.84E+01	83.41	3.70E+01	86.57
0.001	1.72E+02	88.96	1.27E+02	89.42	1.41E+02	84.42	1.42E+02	87.00
0.001584893	2.73E+02	88.72	2.01E+02	89.46	2.17E+02	84.52	2.23E+02	86.85
0.002511886	4.32E+02	88.21	3.18E+02	89.39	3.36E+02	84.57	3.48E+02	86.62
0.01	1.68E+03	83.85	1.26E+03	88.18	1.23E+03	84.47	1.31E+03	85.57
0.015848932	2.58E+03	81.11	2.00E+03	87.19	1.90E+03	84.37	2.03E+03	85.12
0.025118864	3.85E+03	78.18	3.13E+03	85.70	2.92E+03	84.23	3.13E+03	84.61
0.1	1.17E+04	74.56	1.10E+04	79.81	1.06E+04	83.54	1.14E+04	82.75
0.158489319	1.69E+04	75.61	1.62E+04	79.58	1.63E+04	83.17	1.74E+04	82.00
0.251188643	2.51E+04	77.02	2.43E+04	80.12	2.50E+04	82.72	2.64E+04	81.17
1	8.57E+04	75.66	8.49E+04	79.24	8.86E+04	80.60	9.03E+04	78.16
1.584893192	1.26E+05	73.56	1.28E+05	77.99	1.34E+05	79.55	1.35E+05	76.95
2.511886432	1.81E+05	71.51	1.91E+05	76.27	2.02E+05	78.29	1.99E+05	75.61
10	5.28E+05	70.76	6.07E+05	71.88	6.55E+05	72.94	6.19E+05	70.76
15.84893192	7.72E+05	70.07	8.93E+05	68.42	9.51E+05	70.61	8.88E+05	68.83
62.83185	2.14E+06	60.96	2.16E+06	55.64	2.66E+06	62.36	2.44E+06	62.20
100	2.83E+06	59.53	2.77E+06	55.73	3.64E+06	59.37	3.35E+06	59.74
158.4893192	3.74E+06	60.11	3.62E+06	57.39	4.89E+06	56.45	4.52E+06	57.23
251.1886432	5.05E+06	62.11	4.83E+06	60.12	6.47E+06	53.65	6.02E+06	54.70
1000	1.53E+07	62.17	1.45E+07	63.19	1.37E+07	46.44	1.31E+07	47.37
1584.893192	2.21E+07	55.14	2.11E+07	57.29	1.73E+07	44.47	1.66E+07	45.13
2511.886432	2.97E+07	44.62	2.91E+07	47.53	2.15E+07	42.68	2.07E+07	43.01
10000	4.26E+07	14.71	4.41E+07	16.44	2.66E+07	41.04	2.56E+07	41.04



APPENDIX E

Initial data_WLF (70/100 Unaged_Unconditioned)		
Reduced [rad/s]	G* [Pa]	δ [°]
0.000316	4.16E+01	90.00
0.000502	6.54E+01	90.00
0.000796	1.03E+02	89.60
0.001260	1.62E+02	88.90
0.001996	2.57E+02	88.80
0.003165	4.05E+02	88.40
0.005020	6.35E+02	88.00
0.007963	9.92E+02	87.50
0.012599	1.55E+03	87.10
0.019958	2.42E+03	86.60
0.031650	3.76E+03	86.10
0.050196	5.84E+03	85.60
0.062800	7.98E+03	85.10
0.079629	9.04E+03	85.00
0.099600	1.16E+04	84.50
0.125995	1.40E+04	84.50
0.158000	1.70E+04	84.50
0.199576	2.15E+04	83.80
0.250000	2.53E+04	83.20
0.316499	3.30E+04	83.20
0.396000	3.76E+04	82.50
0.501963	5.04E+04	82.50
0.628000	5.62E+04	82.50
0.796286	7.67E+04	81.70
0.996000	8.35E+04	81.00
1.259946	1.16E+05	81.00
1.580000	1.24E+05	76.50
1.995755	1.76E+05	80.30
2.500000	1.82E+05	75.70
3.164985	2.63E+05	79.60
3.960000	2.69E+05	74.80
4.962588	4.62E+05	71.10
6.280000	3.93E+05	73.60
7.870602	6.39E+05	70.10
9.960000	5.72E+05	72.30
12.485493	8.97E+05	68.50
15.800000	8.27E+05	70.80
19.755527	1.25E+06	66.90
25.000000	1.19E+06	69.20
31.292755	1.73E+06	65.20
39.600000	1.68E+06	67.40
49.625884	2.39E+06	63.30
62.800000	2.37E+06	65.50
78.706019	3.26E+06	61.30
99.600000	3.30E+06	63.50
124.854930	4.41E+06	59.10
158.000000	4.56E+06	61.30
194.821169	5.64E+06	56.20
197.555269	5.91E+06	57.00
250.000000	6.23E+06	59.10
308.983892	7.17E+06	54.30
312.927546	7.82E+06	54.80
396.000000	8.45E+06	57.10
490.155171	9.03E+06	52.20
496.258835	1.03E+07	52.60
628.000000	1.13E+07	55.10
775.561979	1.14E+07	50.30
787.060191	1.33E+07	50.40
1228.490174	1.39E+07	48.50
1248.549299	1.71E+07	48.30
1948.211690	1.75E+07	46.30
1975.552688	2.17E+07	46.20
3089.838923	2.17E+07	44.30
3129.275457	2.73E+07	44.20
4901.551705	2.69E+07	42.20
4962.588351	3.39E+07	42.20
7755.619787	3.29E+07	40.30
7870.601907	4.17E+07	40.30
12284.901742	3.99E+07	38.50

	Modelled data (70/100 Unaged_Unconditioned)							
	Arrh Prony		WLF Prony		WLF HS		WLF 2S2P1D	
	G*	δ	G*	δ	G*	δ	G*	δ
R ² CA	0.99	0.98	0.99	0.98				
R ² Mec.	0.97	0.83	0.97	0.84	1.00	1.00	0.99	0.98
Reduced [rad/s]	G*	δ	G*	δ	G*	δ	G*	δ
0.0001	1.73E+01	86.07	1.27E+01	85.94	1.62E+01	81.39	1.50E+01	84.67
0.000158489	2.73E+01	87.45	2.01E+01	87.42	2.49E+01	82.61	2.36E+01	85.88
0.000251189	4.33E+01	88.29	3.19E+01	88.34	3.84E+01	83.41	3.70E+01	86.57
0.001	1.72E+02	88.96	1.27E+02	89.42	1.41E+02	84.42	1.42E+02	87.00
0.001584893	2.73E+02	88.72	2.01E+02	89.46	2.17E+02	84.52	2.23E+02	86.85
0.002511886	4.32E+02	88.21	3.18E+02	89.39	3.36E+02	84.57	3.48E+02	86.62
0.01	1.68E+03	83.85	1.26E+03	88.18	1.23E+03	84.47	1.31E+03	85.57
0.015848932	2.58E+03	81.11	2.00E+03	87.19	1.90E+03	84.37	2.03E+03	85.12
0.025118864	3.85E+03	78.18	3.13E+03	85.70	2.92E+03	84.23	3.13E+03	84.61
0.1	1.17E+04	74.56	1.10E+04	79.81	1.06E+04	83.54	1.14E+04	82.75
0.158489319	1.69E+04	75.61	1.62E+04	79.58	1.63E+04	83.17	1.74E+04	82.00
0.251188643	2.51E+04	77.02	2.43E+04	80.12	2.50E+04	82.72	2.64E+04	81.17
1	8.57E+04	75.66	8.49E+04	79.24	8.86E+04	80.60	9.03E+04	78.16
1.584893192	1.26E+05	73.56	1.28E+05	77.99	1.34E+05	79.55	1.35E+05	76.95
2.511886432	1.81E+05	71.51	1.91E+05	76.27	2.02E+05	78.29	1.99E+05	75.61
10	5.28E+05	70.76	6.07E+05	71.88	6.55E+05	72.94	6.19E+05	70.76
15.84893192	7.72E+05	70.07	8.93E+05	68.42	9.51E+05	70.61	8.88E+05	68.83
62.83185	2.14E+06	60.96	2.16E+06	55.64	2.66E+06	62.36	2.44E+06	62.20
100	2.83E+06	59.53	2.77E+06	55.73	3.64E+06	59.37	3.35E+06	59.74
158.4893192	3.74E+06	60.11	3.62E+06	57.39	4.89E+06	56.45	4.52E+06	57.23
251.1886432	5.05E+06	62.11	4.83E+06	60.12	6.47E+06	53.65	6.02E+06	54.70
1000	1.53E+07	62.17	1.45E+07	63.19	1.37E+07	46.44	1.31E+07	47.37
1584.893192	2.21E+07	55.14	2.11E+07	57.29	1.73E+07	44.47	1.66E+07	45.13
2511.886432	2.97E+07	44.62	2.91E+07	47.53	2.15E+07	42.68	2.07E+07	43.01
10000	4.26E+07	14.71	4.41E+07	16.44	2.66E+07	41.04	2.56E+07	41.04



APPENDIX E

Initial data_WLF (70/100 Unaged_Conditioned)		
Reduced [rad/s]	G* [Pa]	δ [°]
0.000320	4.13E+0	89.5
0.000507	6.52E+0	89.4
0.000805	1.03E+0	89.0
0.001273	1.63E+0	88.9
0.002017	2.57E+0	88.6
0.003198	4.06E+0	88.2
0.005072	6.36E+0	87.9
0.008046	9.94E+0	87.5
0.012732	1.55E+0	87.0
0.020167	2.42E+0	86.5
0.031982	3.76E+0	86.1
0.050722	5.83E+0	85.6
0.062800	8.26E+0	80.5
0.080463	9.03E+0	85.0
0.099600	1.23E+0	80.2
0.127315	1.40E+0	84.5
0.158000	1.81E+0	80.3
0.201668	2.15E+0	83.8
0.250000	2.70E+0	80.1
0.319816	3.29E+0	83.2
0.396000	4.04E+0	79.5
0.507225	5.03E+0	82.5
0.628000	6.05E+0	78.8
0.804633	7.66E+0	81.8
0.996000	9.00E+0	78.0
1.273154	1.16E+0	81.2
1.580000	1.33E+0	77.2
2.016676	1.75E+0	80.5
2.500000	1.97E+0	76.2
3.198163	2.62E+0	80.1
3.960000	2.90E+0	75.1
4.800106	4.66E+0	70.8
6.280000	4.24E+0	73.8
7.612908	6.34E+0	69.9
9.960000	6.17E+0	72.5
12.076701	8.87E+0	68.4
15.800000	8.90E+0	71.0
19.108704	1.26E+0	66.6
25.000000	1.27E+0	69.3
30.268187	1.75E+0	64.8
39.600000	1.81E+0	67.6
48.001064	2.41E+0	62.9
62.800000	2.53E+0	65.7
76.129075	3.27E+0	61.0
99.600000	3.51E+0	63.8
120.767007	4.40E+0	58.9
158.000000	4.81E+0	61.8
180.137033	5.63E+0	56.5
191.087037	5.91E+0	56.7
250.000000	6.51E+0	59.9
285.695040	7.07E+0	54.7
302.681866	7.83E+0	54.5
396.000000	8.76E+0	58.3
453.211007	8.89E+0	52.8
480.010636	1.03E+0	52.3
628.000000	1.18E+0	56.3
717.106024	1.11E+0	50.8
761.290753	1.33E+0	50.1
1135.895942	1.40E+0	48.8
1207.670071	1.70E+0	48.0
1801.370333	1.75E+0	46.7
1910.870365	2.16E+0	46.0
2856.950400	2.19E+0	44.6
3026.818658	2.70E+0	44.0
4532.110073	2.70E+0	42.5
4800.106357	3.37E+0	42.0
7171.060242	3.31E+0	40.5
7612.907535	4.15E+0	40.1
11358.95942	4.01E+0	38.6

	Modelled data (70/100 Unaged_Conditioned)							
	Arrh Prony		WLF Prony		WLF HS		WLF 2S2P1D	
	G*	δ	G*	δ	G*	δ	G*	δ
R ² CA	0.99	0.98	0.99	0.99				
R ² Mec. Model	0.94	0.76	0.95	0.76	1.00	1.00	0.99	0.98
Reduced [rad/s]	G*	δ	G*	δ	G*	δ	G*	δ
0.0001	2.03E+0	87.41	1.78E+0	88.53	1.51E+0	82.12	1.44E+0	82.83
0.000158489	3.21E+0	88.26	2.82E+0	88.97	2.34E+0	83.45	2.25E+0	84.23
0.000251189	5.09E+0	88.73	4.46E+0	89.18	3.63E+0	84.30	3.50E+0	85.12
0.001	2.03E+0	88.62	1.78E+0	88.74	1.35E+0	85.38	1.32E+0	86.23
0.001584893	3.21E+0	88.06	2.81E+0	88.13	2.10E+0	85.49	2.06E+0	86.33
0.002511886	5.07E+0	87.09	4.44E+0	87.13	3.26E+0	85.54	3.21E+0	86.36
0.01	1.90E+0	80.15	1.67E+0	80.16	1.21E+0	85.43	1.21E+0	86.19
0.015848932	2.82E+0	76.87	2.47E+0	76.87	1.88E+0	85.32	1.88E+0	86.05
0.025118864	4.06E+0	74.69	3.56E+0	74.69	2.91E+0	85.18	2.93E+0	85.86
0.1	1.24E+0	74.78	1.09E+0	74.80	1.07E+0	84.44	1.07E+0	84.93
0.158489319	1.82E+0	74.55	1.59E+0	74.57	1.66E+0	84.05	1.69E+0	84.46
0.251188643	2.63E+0	74.76	2.30E+0	74.78	2.55E+0	83.56	2.60E+0	83.87
1	8.52E+0	80.22	7.47E+0	80.22	9.14E+0	81.27	9.35E+0	81.21
1.584893192	1.31E+0	81.15	1.15E+0	81.15	1.39E+0	80.14	1.42E+0	79.94
2.511886432	2.03E+0	80.81	1.78E+0	80.81	2.09E+0	78.77	2.14E+0	78.43
10	7.10E+0	74.63	6.23E+0	74.63	6.84E+0	72.99	6.92E+0	72.35
15.84893192	1.05E+0	70.45	9.21E+0	70.45	9.93E+0	70.50	9.99E+0	69.84
62.83185	2.56E+0	58.34	2.25E+0	58.34	2.76E+0	61.82	2.74E+0	61.50
100	3.35E+0	59.62	2.94E+0	59.62	3.76E+0	58.75	3.74E+0	58.66
158.4893192	4.57E+0	61.93	4.00E+0	61.93	5.03E+0	55.79	5.00E+0	55.94
251.1886432	6.42E+0	63.42	5.63E+0	63.42	6.63E+0	52.99	6.59E+0	53.37
1000	1.92E+0	55.38	1.68E+0	55.38	1.39E+0	45.95	1.41E+0	46.74
1584.893192	2.61E+0	45.88	2.29E+0	45.88	1.75E+0	44.05	1.77E+0	44.84
2511.886432	3.24E+0	34.49	2.84E+0	34.49	2.17E+0	42.35	2.22E+0	43.04
10000	3.99E+0	10.14	3.50E+0	10.14	2.68E+0	40.78	2.75E+0	41.30



APPENDIX E

Initial data_WLF (70/100 PAV Unconditioned)		
Reduced [rad/s]	G* [Pa]	δ [°]
0.000153	3.04E+0	87.2
0.000243	4.72E+0	86.8
0.000385	7.35E+0	86.3
0.000609	1.14E+0	85.7
0.000965	1.77E+0	84.9
0.001530	2.72E+0	84.0
0.002427	4.18E+0	83.0
0.003850	6.37E+0	81.9
0.006092	9.67E+0	80.7
0.009650	1.46E+0	79.5
0.015304	2.18E+0	78.3
0.024272	3.25E+0	77.1
0.038504	4.80E+0	75.9
0.060925	7.05E+0	74.7
0.062800	7.85E+0	69.7
0.096505	1.03E+0	73.5
0.099600	1.11E+0	68.8
0.153043	1.50E+0	72.3
0.158000	1.55E+0	67.7
0.242724	2.16E+0	71.2
0.250000	2.17E+0	66.6
0.385043	3.10E+0	70.0
0.396000	3.01E+0	65.3
0.609246	4.43E+0	68.7
0.628000	4.18E+0	63.9
0.965045	6.29E+0	67.4
0.996000	5.75E+0	62.4
1.530425	8.87E+0	66.0
1.580000	7.87E+0	60.9
2.500000	1.07E+0	59.4
3.960000	1.44E+0	57.8
5.551029	2.35E+0	54.6
6.280000	1.93E+0	56.2
8.803861	3.04E+0	52.8
9.960000	2.56E+0	54.5
13.965964	3.91E+0	51.1
15.800000	3.36E+0	52.9
22.098045	4.98E+0	49.3
25.000000	4.38E+0	51.2
35.003303	6.32E+0	47.4
39.600000	5.67E+0	49.6
55.510289	7.94E+0	45.6
62.800000	7.27E+0	48.0
88.038611	9.89E+0	44.0
99.600000	9.24E+0	46.4
139.659645	1.23E+0	42.3
158.000000	1.17E+0	44.9
177.973440	1.29E+0	41.2
220.980450	1.51E+0	40.7
250.000000	1.46E+0	43.3
282.263609	1.52E+0	39.9
350.033034	1.85E+0	39.1
396.000000	1.82E+0	41.9
447.767573	1.81E+0	38.4
555.102892	2.24E+0	37.7
628.000000	2.25E+0	40.7
708.492995	2.16E+0	36.9
880.386115	2.71E+0	36.3
1122.252904	2.57E+0	35.3
1396.596447	3.23E+0	34.9
1779.734404	3.03E+0	33.9
2209.804505	3.85E+0	33.6
2822.636093	3.59E+0	32.5
3500.330336	4.54E+0	32.4
4477.675730	4.20E+0	31.2
5551.028916	5.33E+0	31.2
7084.929952	4.88E+0	29.9
8803.861147	6.22E+0	30.0
11222.52904	5.64E+0	28.7

	Modelled data (70/100 PAV Unconditioned)							
	Arrh Prony		WLF Prony		WLF HS		WLF 2S2P1D	
	G*	δ	G*	δ	G*	δ	G*	δ
R ² CA	1.00	0.98	0.99	0.99				
R ² Mec.	0.99	0.76	0.98	0.86	1.00	0.99	0.99	0.98
Reduced [rad/s]	G*	δ	G*	δ	G*	δ	G*	δ
[rad/s]	[Pa]	[°]	[Pa]	[°]	[Pa]	[°]	[Pa]	[°]
0.0001	3.16E+0	86.67	2.05E+0	70.66	2.43E+0	79.19	2.30E+0	80.81
0.00015848	5.01E+0	87.72	3.15E+0	77.33	3.64E+0	79.22	3.48E+0	80.82
0.00025118	7.93E+0	88.28	4.92E+0	81.62	5.47E+0	79.22	5.26E+0	80.79
0.001	3.15E+0	87.85	1.93E+0	86.00	1.85E+0	79.02	1.82E+0	80.47
0.00158489	4.97E+0	86.93	3.05E+0	85.61	2.77E+0	78.89	2.75E+0	80.27
0.00251188	7.82E+0	85.45	4.78E+0	84.40	4.14E+0	78.72	4.14E+0	80.03
0.01	2.83E+0	77.80	1.67E+0	78.50	1.39E+0	77.91	1.41E+0	78.88
0.01584893	4.25E+0	74.47	2.48E+0	77.60	2.07E+0	77.49	2.12E+0	78.31
0.02511886	6.30E+0	69.74	3.73E+0	76.48	3.07E+0	76.97	3.16E+0	77.61
0.1	1.50E+0	51.19	1.17E+0	63.70	9.95E+0	74.60	1.03E+0	74.56
0.15848931	1.83E+0	50.31	1.55E+0	59.08	1.46E+0	73.45	1.51E+0	73.15
0.25118864	2.30E+0	52.40	2.01E+0	57.02	2.13E+0	72.08	2.19E+0	71.51
1	5.35E+0	61.99	4.54E+0	62.09	6.27E+0	66.47	6.36E+0	65.28
1.58489319	7.55E+0	65.92	6.36E+0	65.98	8.79E+0	64.09	8.85E+0	62.83
2.51188643	1.11E+0	68.07	9.32E+0	68.39	1.22E+0	61.52	1.21E+0	60.28
10	3.38E+0	56.62	2.87E+0	58.19	2.94E+0	53.22	2.88E+0	52.65
15.8489319	4.42E+0	49.93	3.80E+0	51.73	3.83E+0	50.52	3.73E+0	50.31
62.83185	7.65E+0	37.44	6.80E+0	39.21	7.75E+0	43.54	7.61E+0	44.38
100	8.83E+0	38.70	7.94E+0	40.40	9.61E+0	41.64	9.50E+0	42.73
158.489319	1.07E+0	42.83	9.70E+0	44.26	1.18E+0	39.97	1.18E+0	41.24
251.188643	1.38E+0	46.79	1.27E+0	47.60	1.44E+0	38.50	1.44E+0	39.87
1000	3.16E+0	36.00	2.86E+0	34.97	2.50E+0	34.93	2.58E+0	36.10
1584.89319	3.67E+0	29.15	3.29E+0	28.24	2.98E+0	33.91	3.10E+0	34.85
2511.88643	4.06E+0	24.77	3.62E+0	24.15	3.54E+0	32.94	3.69E+0	33.55
10000	5.69E+0	17.97	5.07E+0	17.96	4.18E+0	31.97	4.37E+0	32.18



APPENDIX E

Initial data_WLF (70/100 PAV Conditioned)		
Reduced [rad/s]	G* [Pa]	δ [°]
0.000104	3.12E+0	87.6
0.000166	4.87E+0	87.3
0.000263	7.59E+0	86.7
0.000416	1.18E+0	85.8
0.000658	1.84E+0	85.0
0.001044	2.85E+0	84.0
0.001656	4.37E+0	83.1
0.002627	6.69E+0	81.9
0.004156	1.01E+0	80.8
0.006583	1.53E+0	79.6
0.010440	2.29E+0	78.4
0.016558	3.40E+0	77.2
0.026267	5.02E+0	76.0
0.041562	7.38E+0	74.9
0.062800	8.58E+0	70.3
0.065835	1.08E+0	73.7
0.099600	1.21E+0	69.4
0.104405	1.57E+0	72.5
0.158000	1.69E+0	68.3
0.165584	2.26E+0	71.3
0.250000	2.37E+0	67.1
0.262674	3.25E+0	70.1
0.396000	3.31E+0	65.8
0.415623	4.64E+0	68.9
0.628000	4.60E+0	64.4
0.658347	6.59E+0	67.7
0.996000	6.34E+0	62.9
1.044046	9.30E+0	66.4
1.580000	8.70E+0	61.4
2.500000	1.18E+0	59.8
3.960000	1.60E+0	58.2
5.850023	2.33E+0	54.7
6.280000	2.14E+0	56.6
9.278062	3.01E+0	53.0
9.960000	2.85E+0	54.9
14.718211	3.85E+0	51.2
15.800000	3.76E+0	53.2
23.288309	4.92E+0	49.4
25.000000	4.91E+0	51.6
36.888682	6.28E+0	47.6
39.600000	6.35E+0	49.9
58.500233	7.92E+0	45.8
62.800000	8.15E+0	48.3
92.780624	9.90E+0	44.1
99.600000	1.04E+0	46.7
147.182115	1.23E+0	42.4
158.000000	1.31E+0	45.1
171.954089	1.31E+0	40.9
232.883093	1.52E+0	40.8
250.000000	1.64E+0	43.6
272.716995	1.60E+0	39.5
368.886820	1.86E+0	39.3
396.000000	2.04E+0	42.2
432.623346	1.90E+0	37.9
585.002330	2.25E+0	37.8
628.000000	2.51E+0	41.5
684.530610	2.26E+0	36.4
927.806243	2.71E+0	36.4
1084.296486	2.67E+0	35.0
1471.821149	3.25E+0	35.0
1719.540893	3.15E+0	33.6
2328.830932	3.87E+0	33.7
2727.169951	3.70E+0	32.3
3688.868196	4.57E+0	32.5
4326.233456	4.32E+0	31.0
5850.023301	5.38E+0	31.3
6845.306101	5.03E+0	29.7
9278.062433	6.28E+0	30.1
10842.96486	5.81E+0	28.5

	Modelled data (70/100 PAV Conditioned)								
	Arrh Prony			WLF Prony		WLF HS		WLF 2S2P1D	
	G*	δ	τ	G*	δ	G*	δ	G*	δ
R ² CA	1.00	0.98		1.00	0.98				
R ² Mec.	0.96	0.83		0.98	0.79	1.00	0.99	0.99	0.97
Reduced [rad/s]	G* [Pa]	δ [°]	G* [Pa]	δ [°]	G* [Pa]	δ [°]	G* [Pa]	δ [°]	
0.0001	3.09E+0	75.59	2.71E+0	89.81	3.61E+0	77.45	3.62E+0	76.12	
0.00015848	4.82E+0	79.74	4.29E+0	89.69	5.37E+0	77.44	5.37E+0	76.56	
0.00025118	7.57E+0	81.80	6.81E+0	89.51	7.99E+0	77.39	7.98E+0	76.82	
0.001	2.84E+0	78.39	2.70E+0	88.07	2.62E+0	77.08	2.62E+0	76.95	
0.00158489	4.21E+0	74.96	4.27E+0	86.97	3.89E+0	76.91	3.88E+0	76.84	
0.00251188	5.98E+0	72.24	6.72E+0	85.31	5.77E+0	76.69	5.76E+0	76.66	
0.01	1.74E+0	77.31	2.42E+0	76.51	1.87E+0	75.67	1.87E+0	75.69	
0.01584893	2.65E+0	79.21	3.60E+0	72.51	2.75E+0	75.16	2.75E+0	75.19	
0.02511886	4.07E+0	79.56	5.23E+0	67.26	4.04E+0	74.54	4.05E+0	74.57	
0.1	1.37E+0	75.46	1.16E+0	54.06	1.26E+0	71.80	1.26E+0	71.83	
0.15848931	2.02E+0	74.76	1.47E+0	56.26	1.82E+0	70.53	1.82E+0	70.55	
0.25118864	3.02E+0	73.37	1.97E+0	59.81	2.61E+0	69.04	2.61E+0	69.05	
1	8.93E+0	56.54	5.29E+0	67.05	7.31E+0	63.26	7.32E+0	63.24	
1.58489319	1.12E+0	50.32	7.65E+0	69.37	1.01E+0	60.94	1.01E+0	60.92	
2.51188643	1.34E+0	48.21	1.14E+0	69.96	1.37E+0	58.48	1.37E+0	58.46	
10	2.98E+0	58.71	3.38E+0	55.89	3.17E+0	50.94	3.17E+0	50.91	
15.8489319	4.28E+0	58.21	4.36E+0	49.56	4.08E+0	48.58	4.08E+0	48.55	
62.83185	9.50E+0	40.89	7.61E+0	39.80	8.08E+0	42.54	8.08E+0	42.53	
100	1.10E+0	38.37	9.01E+0	41.95	9.99E+0	40.90	9.99E+0	40.89	
158.489319	1.31E+0	39.21	1.13E+0	45.98	1.22E+0	39.44	1.22E+0	39.44	
251.188643	1.62E+0	40.63	1.51E+0	48.50	1.49E+0	38.14	1.49E+0	38.14	
1000	3.11E+0	31.44	3.31E+0	32.80	2.59E+0	34.88	2.59E+0	34.89	
1584.89319	3.63E+0	27.17	3.73E+0	26.05	3.09E+0	33.92	3.08E+0	33.93	
2511.88643	4.17E+0	22.31	4.05E+0	22.09	3.66E+0	32.97	3.66E+0	32.98	
10000	5.02E+0	7.59	5.50E+0	16.50	4.33E+0	32.01	4.32E+0	32.02	



APPENDIX E

Initial data_WLF (SE1 Unaged Unconditioned)		
Reduced [rad/s]	G* [Pa]	δ [°]
0.000314	1.19E+0	78.7
0.000499	1.78E+0	78.6
0.000791	2.67E+0	78.8
0.001252	3.99E+0	78.6
0.001983	5.98E+0	78.2
0.003144	8.95E+0	77.7
0.004986	1.33E+0	77.0
0.007910	1.97E+0	76.4
0.012516	2.91E+0	75.7
0.019825	4.27E+0	75.0
0.031440	6.25E+0	74.4
0.049863	9.10E+0	73.9
0.062800	1.14E+0	65.9
0.079100	1.32E+0	73.6
0.099600	1.58E+0	66.8
0.125158	1.92E+0	73.5
0.158000	2.21E+0	68.0
0.198251	2.79E+0	73.7
0.250000	3.11E+0	69.0
0.314397	4.06E+0	74.0
0.396000	4.42E+0	69.7
0.498630	5.93E+0	74.3
0.628000	6.33E+0	70.2
0.791000	8.69E+0	74.5
0.996000	9.09E+0	70.5
1.251582	1.28E+0	74.6
1.580000	1.30E+0	70.6
1.982506	1.88E+0	74.4
2.500000	1.88E+0	70.4
3.143974	2.76E+0	73.8
3.960000	2.69E+0	70.0
4.850628	3.92E+0	67.8
6.280000	3.86E+0	69.3
7.693035	5.39E+0	67.1
9.960000	5.51E+0	68.4
12.203810	7.42E+0	65.7
15.800000	7.81E+0	67.3
19.309826	1.02E+0	64.4
25.000000	1.10E+0	66.0
30.586764	1.40E+0	62.9
39.600000	1.54E+0	64.5
48.506283	1.91E+0	61.2
62.800000	2.13E+0	63.0
76.930347	2.58E+0	59.4
99.600000	2.93E+0	61.3
122.038100	3.45E+0	57.5
158.000000	3.98E+0	59.7
183.181235	4.95E+0	55.1
193.098260	4.60E+0	55.5
250.000000	5.34E+0	58.4
290.523106	6.27E+0	53.2
305.867643	6.06E+0	53.4
396.000000	7.07E+0	57.4
460.869987	7.90E+0	51.5
485.062828	7.89E+0	51.4
628.000000	9.31E+0	57.0
729.224663	9.96E+0	49.6
769.303467	1.02E+0	49.5
1155.091867	1.25E+0	47.6
1220.381001	1.30E+0	47.5
1831.812354	1.57E+0	45.6
1930.982597	1.64E+0	45.6
2905.231059	1.95E+0	43.7
3058.676434	2.06E+0	43.8
4608.699872	2.40E+0	41.9
4850.628284	2.56E+0	41.9
7292.246633	2.94E+0	40.1
7693.034667	3.15E+0	40.3
11550.91866	3.57E+0	38.3

	Modelled data (SE1 Unaged Unconditioned)							
	Arrh Prony		WLF Prony		WLF HS		WLF 2S2P1D	
	G*	δ	G*	δ	G*	δ	G*	δ
R ² CA	0.99	0.94	1.00	0.96				
R ² Mec.	0.93	0.62	0.92	0.68	1.00	1.00	1.00	0.98
Reduced [rad/s]	G* [Pa]	δ [°]	G* [Pa]	δ [°]	G* [Pa]	δ [°]	G* [Pa]	δ [°]
0.0001	3.80E+0	76.57	3.18E+0	76.57	5.07E+0	73.56	4.43E+0	78.80
0.00015848	5.92E+0	81.33	4.95E+0	81.33	7.41E+0	73.90	6.65E+0	78.74
0.00025118	9.32E+0	84.33	7.80E+0	84.33	1.09E+0	74.12	9.98E+0	78.53
0.001	3.69E+0	87.50	3.09E+0	87.50	3.41E+0	74.40	3.32E+0	77.49
0.00158489	5.85E+0	87.34	4.89E+0	87.34	4.99E+0	74.41	4.93E+0	77.07
0.00251188	9.25E+0	86.60	7.74E+0	86.60	7.30E+0	74.41	7.30E+0	76.65
0.01	3.53E+0	79.15	2.95E+0	79.15	2.29E+0	74.26	2.35E+0	75.39
0.01584893	5.27E+0	74.34	4.41E+0	74.34	3.35E+0	74.18	3.45E+0	74.97
0.02511886	7.49E+0	69.34	6.26E+0	69.34	4.89E+0	74.07	5.05E+0	74.55
0.1	1.87E+0	69.36	1.57E+0	69.36	1.52E+0	73.55	1.57E+0	73.28
0.15848931	2.68E+0	72.42	2.24E+0	72.42	2.22E+0	73.30	2.29E+0	72.84
0.25118864	3.93E+0	75.24	3.29E+0	75.24	3.23E+0	73.00	3.32E+0	72.38
1	1.40E+0	78.81	1.17E+0	78.81	9.87E+0	71.64	9.98E+0	70.77
1.58489319	2.16E+0	76.54	1.81E+0	76.54	1.42E+0	71.00	1.43E+0	70.13
2.51188643	3.26E+0	72.11	2.73E+0	72.11	2.05E+0	70.24	2.05E+0	69.40
10	8.13E+0	56.58	6.80E+0	56.58	5.95E+0	67.06	5.88E+0	66.59
15.8489319	1.04E+0	56.91	8.73E+0	56.91	8.38E+0	65.66	8.26E+0	65.39
62.8318530	2.74E+0	55.26	2.29E+0	55.26	2.22E+0	60.41	2.20E+0	60.77
100	3.63E+0	49.84	3.04E+0	49.84	3.03E+0	58.33	3.00E+0	58.87
158.489319	4.50E+0	45.02	3.76E+0	45.02	4.07E+0	56.15	4.05E+0	56.82
251.188643	5.35E+0	43.25	4.48E+0	43.25	5.40E+0	53.90	5.39E+0	54.63
1000	1.13E+0	49.31	9.42E+0	49.31	1.17E+0	47.22	1.19E+0	47.68
1584.89319	1.55E+0	45.69	1.29E+0	45.69	1.48E+0	45.14	1.50E+0	45.37
2511.88643	2.02E+0	37.74	1.69E+0	37.74	1.85E+0	43.17	1.88E+0	43.15
10000	2.78E+0	12.53	2.32E+0	12.53	3.42E+0	37.97	3.45E+0	37.20



APPENDIX E

Initial data_WLF (SE1 Unaged Conditioned)		
Reduced [rad/s]	G* [Pa]	δ [°]
0.000315	1.23E+0	79.8
0.000499	1.85E+0	79.6
0.000792	2.78E+0	79.3
0.001252	4.17E+0	78.6
0.001984	6.25E+0	78.0
0.003146	9.33E+0	77.3
0.004990	1.38E+0	76.5
0.007916	2.04E+0	75.8
0.012525	3.00E+0	75.0
0.019840	4.37E+0	74.3
0.031463	6.36E+0	73.7
0.049900	9.24E+0	73.3
0.062800	1.21E+0	70.0
0.079158	1.34E+0	73.1
0.099600	1.70E+0	70.4
0.125250	1.93E+0	73.2
0.158000	2.40E+0	70.5
0.198396	2.81E+0	73.5
0.250000	3.40E+0	70.7
0.314628	4.08E+0	73.9
0.396000	4.84E+0	71.1
0.498995	5.97E+0	74.3
0.628000	6.95E+0	71.3
0.791579	8.76E+0	74.5
0.996000	9.97E+0	71.4
1.252499	1.29E+0	74.6
1.580000	1.43E+0	71.3
1.983958	1.90E+0	74.4
2.500000	2.06E+0	71.0
3.146276	2.81E+0	74.1
3.960000	2.95E+0	70.5
4.849939	4.13E+0	67.8
6.280000	4.23E+0	69.8
7.691941	5.70E+0	66.7
9.960000	6.04E+0	68.9
12.202075	7.75E+0	65.8
15.800000	8.57E+0	67.7
19.307080	1.05E+0	64.6
25.000000	1.21E+0	66.4
30.582415	1.45E+0	63.0
39.600000	1.69E+0	65.0
48.499386	2.02E+0	61.1
62.800000	2.33E+0	63.5
76.919409	2.72E+0	59.3
99.600000	3.20E+0	61.9
122.020749	3.65E+0	57.4
158.000000	4.34E+0	60.2
183.191499	4.79E+0	54.5
193.070805	4.85E+0	55.4
250.000000	5.82E+0	58.7
290.539384	6.10E+0	53.1
305.824155	6.38E+0	53.5
396.000000	7.77E+0	57.4
460.895811	7.67E+0	51.2
484.993861	8.30E+0	51.5
628.000000	1.04E+0	55.9
729.265523	9.60E+0	49.3
769.194086	1.07E+0	49.5
1155.156588	1.20E+0	47.5
1220.207485	1.37E+0	47.6
1831.914994	1.48E+0	45.6
1930.708046	1.73E+0	45.7
2905.393844	1.87E+0	43.6
3058.241545	2.17E+0	43.9
4608.958105	2.31E+0	41.8
4849.938612	2.68E+0	42.1
7292.655230	2.83E+0	40.0
7691.940856	3.30E+0	40.4
11551.56588	3.43E+0	38.2

	Modelled data (SE1 Unaged Conditioned)							
	Arrh Prony		WLF Prony		WLF HS		WLF 2S2P1D	
	G*	δ	G*	δ	G*	δ	G*	δ
R ² CA	0.99	0.94	0.99	0.96				
R ² Mec.	0.92	0.60	0.94	0.56	1.00	1.00	1.00	0.98
Reduced [rad/s]	G* [Pa]	δ [°]	G* [Pa]	δ [°]	G* [Pa]	δ [°]	G* [Pa]	δ [°]
0.0001	3.90E+0	65.72	3.48E+0	59.91	5.07E+0	73.56	4.65E+0	77.71
0.00015848	5.86E+0	74.03	5.09E+0	69.84	7.41E+0	73.90	6.95E+0	77.75
0.00025118	9.07E+0	79.62	7.77E+0	76.82	1.09E+0	74.12	1.04E+0	77.66
0.001	3.56E+0	86.47	3.02E+0	85.74	3.41E+0	74.40	3.41E+0	77.02
0.00158489	5.63E+0	86.86	4.78E+0	86.40	4.99E+0	74.41	5.06E+0	76.74
0.00251188	8.91E+0	86.58	7.56E+0	86.29	7.30E+0	74.41	7.49E+0	76.46
0.01	3.43E+0	80.66	2.91E+0	80.59	2.29E+0	74.26	2.41E+0	75.56
0.01584893	5.20E+0	76.40	4.41E+0	76.37	3.35E+0	74.18	3.54E+0	75.25
0.02511886	7.54E+0	71.57	6.40E+0	71.56	4.89E+0	74.07	5.20E+0	74.93
0.1	1.93E+0	69.42	1.64E+0	69.44	1.52E+0	73.55	1.63E+0	73.87
0.15848931	2.75E+0	72.20	2.33E+0	72.21	2.22E+0	73.00	2.38E+0	73.47
0.25118864	4.01E+0	74.99	3.40E+0	74.99	3.23E+0	73.00	3.47E+0	73.02
1	1.42E+0	78.99	1.21E+0	78.98	9.87E+0	71.64	1.05E+0	71.32
1.58489319	2.20E+0	76.94	1.87E+0	76.92	1.42E+0	71.00	1.52E+0	70.59
2.51188643	3.33E+0	72.73	2.83E+0	72.71	2.05E+0	70.24	2.18E+0	69.76
10	8.44E+0	57.10	7.16E+0	57.03	5.95E+0	67.06	6.27E+0	66.46
15.8489319	1.09E+0	57.15	9.21E+0	57.07	8.38E+0	65.66	8.81E+0	65.05
62.8318530	2.84E+0	55.43	2.41E+0	55.31	2.22E+0	60.41	2.32E+0	59.82
100	3.78E+0	49.99	3.20E+0	49.83	3.03E+0	58.33	3.14E+0	57.75
158.489319	4.69E+0	45.08	3.97E+0	44.87	4.07E+0	56.15	4.21E+0	55.59
251.188643	5.57E+0	43.22	4.71E+0	42.95	5.40E+0	53.90	5.57E+0	53.35
1000	1.17E+0	49.33	9.80E+0	49.33	1.17E+0	47.22	1.20E+0	46.64
1584.89319	1.60E+0	45.83	1.35E+0	46.05	1.48E+0	45.14	1.51E+0	44.53
2511.88643	2.10E+0	37.96	1.77E+0	38.33	1.85E+0	43.17	1.88E+0	42.52
10000	2.90E+0	12.66	2.46E+0	12.88	3.42E+0	37.97	3.44E+0	37.20



APPENDIX E

Initial data WLF (SE1 PAV Unconditioned)		
Reduced [rad/s]	G* [Pa]	δ [°]
0.000179	5.00E+0	78.1
0.000284	7.37E+0	77.1
0.000450	1.08E+0	76.1
0.000713	1.59E+0	74.8
0.001129	2.33E+0	73.8
0.001790	3.39E+0	72.9
0.002839	4.89E+0	72.1
0.004504	7.02E+0	71.5
0.007126	1.01E+0	71.0
0.011287	1.44E+0	70.5
0.017900	2.06E+0	70.2
0.028390	2.95E+0	70.0
0.045036	4.21E+0	69.7
0.062800	5.55E+0	64.8
0.071259	6.02E+0	69.5
0.099600	7.64E+0	65.0
0.112874	8.58E+0	69.2
0.158000	1.06E+0	64.8
0.179002	1.22E+0	68.9
0.250000	1.47E+0	64.1
0.283895	1.74E+0	68.4
0.396000	2.03E+0	63.6
0.450356	2.47E+0	67.9
0.628000	2.82E+0	62.9
0.712589	3.49E+0	67.4
0.996000	3.88E+0	62.1
1.128741	4.92E+0	66.7
1.580000	5.32E+0	61.2
1.790024	6.90E+0	66.2
2.500000	7.26E+0	60.1
3.960000	9.86E+0	58.9
5.846627	1.58E+0	55.3
6.280000	1.33E+0	57.6
9.272677	2.01E+0	54.1
9.960000	1.79E+0	56.3
14.709668	2.61E+0	52.4
15.800000	2.38E+0	54.9
23.274791	3.36E+0	50.9
25.000000	3.15E+0	53.5
36.867268	4.30E+0	49.4
39.600000	4.11E+0	52.0
58.466274	5.45E+0	47.8
62.800000	5.33E+0	50.5
92.726766	6.88E+0	46.2
99.600000	6.88E+0	49.1
147.096677	8.69E+0	44.6
158.000000	8.78E+0	47.8
216.494290	1.12E+0	42.1
232.747907	1.08E+0	43.1
250.000000	1.11E+0	46.5
343.357186	1.35E+0	40.7
368.672685	1.34E+0	41.6
396.000000	1.39E+0	45.7
544.683086	1.63E+0	39.2
584.662743	1.65E+0	40.2
628.000000	1.70E+0	45.6
861.840326	1.96E+0	37.9
927.267662	2.01E+0	38.8
1365.155077	2.35E+0	36.5
1470.966773	2.44E+0	37.5
2164.942900	2.81E+0	35.1
2327.479072	2.94E+0	36.2
3433.571860	3.34E+0	33.8
3686.726850	3.52E+0	35.0
5446.830862	3.94E+0	32.6
5846.627428	4.18E+0	33.8
8618.403263	4.62E+0	31.4
9272.676622	4.94E+0	32.6
13651.55076	5.40E+0	30.2

	Modelled data (SE1 PAV Unconditioned)							
	Arrh Prony		WLF Prony		WLF HS		WLF 2S2P1D	
	G*	δ	G*	δ	G*	δ	G*	δ
R ² CA	1.00	0.97	1.00	0.98				
R ² Mec.	0.99	0.56	0.96	0.62	1.00	1.00	1.00	0.99
Reduced [rad/s]	G* [Pa]	δ [°]	G* [Pa]	δ [°]	G* [Pa]	δ [°]	G* [Pa]	δ [°]
0.0001	2.54E+0	55.74	2.29E+0	59.49	3.43E+0	70.75	3.06E+0	76.76
0.00015848	3.62E+0	66.48	3.34E+0	69.35	4.93E+0	70.76	4.52E+0	76.12
0.00025118	5.47E+0	74.18	5.09E+0	76.19	7.08E+0	70.75	6.67E+0	75.46
0.001	2.10E+0	82.87	1.97E+0	83.65	2.10E+0	70.60	2.09E+0	73.51
0.00158489	3.31E+0	82.40	3.11E+0	83.13	3.01E+0	70.51	3.04E+0	72.88
0.00251188	5.19E+0	80.35	4.89E+0	81.20	4.32E+0	70.40	4.41E+0	72.25
0.01	1.69E+0	63.75	1.62E+0	65.38	1.27E+0	69.89	1.32E+0	70.43
0.01584893	2.20E+0	57.84	2.14E+0	59.36	1.82E+0	69.64	1.89E+0	69.83
0.02511886	2.73E+0	55.90	2.69E+0	57.00	2.60E+0	69.34	2.69E+0	69.22
0.1	6.55E+0	69.46	6.46E+0	69.59	7.50E+0	68.03	7.69E+0	67.25
0.15848931	9.65E+0	73.20	9.51E+0	73.27	1.06E+0	67.42	1.08E+0	66.51
0.25118864	1.45E+0	75.72	1.43E+0	75.75	1.50E+0	66.71	1.52E+0	65.72
1	5.22E+0	74.00	5.14E+0	74.00	4.13E+0	63.77	4.11E+0	62.87
1.58489319	7.86E+0	68.65	7.74E+0	68.65	5.72E+0	62.49	5.67E+0	61.72
2.51188643	1.12E+0	60.85	1.11E+0	60.84	7.87E+0	61.05	7.77E+0	60.45
10	2.10E+0	43.95	2.07E+0	43.91	1.95E+0	55.85	1.91E+0	55.90
15.8489319	2.53E+0	46.39	2.49E+0	46.36	2.58E+0	53.88	2.54E+0	54.16
62.8318530	6.06E+0	49.53	5.96E+0	49.55	5.63E+0	47.79	5.59E+0	48.51
100	7.93E+0	44.10	7.81E+0	44.12	7.15E+0	45.79	7.15E+0	46.55
158.489319	9.63E+0	38.27	9.49E+0	38.27	8.98E+0	43.90	9.02E+0	44.64
251.188643	1.10E+0	34.79	1.09E+0	34.75	1.12E+0	42.11	1.13E+0	42.77
1000	1.81E+0	45.20	1.78E+0	45.14	2.04E+0	37.47	2.08E+0	37.67
1584.89319	2.44E+0	48.50	2.40E+0	48.49	2.46E+0	36.15	2.50E+0	36.16
2511.88643	3.39E+0	46.95	3.33E+0	47.00	2.94E+0	34.92	2.99E+0	34.75
10000	6.30E+0	21.62	6.20E+0	21.71	4.89E+0	31.60	4.94E+0	30.95



APPENDIX E

Initial data WLF (SE1 PAV Conditioned)		
Reduced [rad/s]	G* [Pa]	δ [°]
0.000179	4.89E+0	77.9
0.000284	7.23E+0	77.1
0.000450	1.07E+0	75.9
0.000713	1.56E+0	74.8
0.001129	2.29E+0	73.9
0.001790	3.33E+0	73.0
0.002839	4.80E+0	72.2
0.004503	6.90E+0	71.5
0.007126	9.91E+0	71.0
0.011287	1.42E+0	70.5
0.017899	2.03E+0	70.2
0.028388	2.90E+0	69.9
0.045033	4.14E+0	69.7
0.062800	5.86E+0	65.6
0.071255	5.91E+0	69.4
0.099600	8.05E+0	65.6
0.112869	8.42E+0	69.2
0.158000	1.11E+0	64.9
0.178994	1.20E+0	68.8
0.250000	1.54E+0	64.3
0.283882	1.70E+0	68.4
0.396000	2.12E+0	63.6
0.450335	2.42E+0	67.8
0.628000	2.94E+0	62.8
0.712555	3.42E+0	67.2
0.996000	4.03E+0	61.9
1.128687	4.83E+0	66.5
1.580000	5.50E+0	60.9
1.789937	6.79E+0	65.7
2.500000	7.49E+0	59.8
3.960000	1.01E+0	58.6
5.846879	1.63E+0	54.6
6.280000	1.36E+0	57.3
9.273076	2.10E+0	53.3
9.960000	1.82E+0	56.0
14.710301	2.69E+0	51.9
15.800000	2.42E+0	54.7
23.275793	3.46E+0	50.2
25.000000	3.20E+0	53.3
36.868856	4.42E+0	48.7
39.600000	4.16E+0	51.8
58.468792	5.62E+0	47.1
62.800000	5.40E+0	50.3
92.730760	7.08E+0	45.6
99.600000	6.95E+0	48.9
147.103012	8.86E+0	44.1
158.000000	8.87E+0	47.6
216.511819	1.14E+0	42.0
232.757931	1.10E+0	42.7
250.000000	1.13E+0	46.3
343.384987	1.38E+0	40.5
368.688562	1.36E+0	41.2
396.000000	1.41E+0	45.1
544.727189	1.65E+0	39.1
584.687922	1.67E+0	39.8
628.000000	1.76E+0	43.5
861.910109	1.97E+0	37.8
927.307596	2.03E+0	38.5
1365.265612	2.39E+0	36.4
1471.030122	2.46E+0	37.2
2165.118193	2.86E+0	35.0
2327.579306	2.96E+0	35.9
3433.849873	3.39E+0	33.8
3686.885621	3.54E+0	34.7
5447.271887	4.01E+0	32.5
5846.879218	4.21E+0	33.6
8619.101088	4.71E+0	31.3
9273.075957	4.98E+0	32.4
13652.65612	5.49E+0	30.2

	Modelled data (SE1 PAV Conditioned)							
	Arrh Prony		WLF Prony		WLF HS		WLF 2S2P1D	
	G*	δ	G*	δ	G*	δ	G*	δ
R ² CA	1.00	0.98	1.00	0.99				
R ² Mec.	0.95	0.60	0.96	0.63	1.00	1.00	1.00	0.99
Reduced [rad/s]	G* [Pa]	δ [°]	G* [Pa]	δ [°]	G* [Pa]	δ [°]	G* [Pa]	δ [°]
0.0001	2.95E+0	66.99	2.29E+0	59.49	3.33E+0	71.26	2.93E+0	78.01
0.00015848	4.46E+0	74.63	3.34E+0	69.35	4.80E+0	71.27	4.36E+0	77.32
0.00025118	6.93E+0	79.54	5.09E+0	76.19	6.91E+0	71.26	6.46E+0	76.61
0.001	2.71E+0	83.44	1.97E+0	83.65	2.07E+0	71.11	2.06E+0	74.44
0.00158489	4.27E+0	81.91	3.11E+0	83.13	2.97E+0	71.02	3.01E+0	73.73
0.00251188	6.66E+0	78.77	4.89E+0	81.20	4.28E+0	70.90	4.38E+0	73.02
0.01	2.01E+0	59.08	1.62E+0	65.38	1.27E+0	70.38	1.32E+0	70.95
0.01584893	2.52E+0	53.65	2.14E+0	59.36	1.82E+0	70.12	1.90E+0	70.27
0.02511886	3.06E+0	53.05	2.69E+0	57.00	2.60E+0	69.81	2.71E+0	69.59
0.1	7.31E+0	69.14	6.46E+0	69.59	7.57E+0	68.46	7.78E+0	67.44
0.15848931	1.08E+0	73.02	9.51E+0	73.27	1.07E+0	67.83	1.10E+0	66.66
0.25118864	1.62E+0	75.58	1.43E+0	75.75	1.52E+0	67.09	1.54E+0	65.83
1	5.84E+0	73.85	5.14E+0	74.00	4.21E+0	64.04	4.17E+0	62.90
1.58489319	8.79E+0	68.44	7.74E+0	68.65	5.84E+0	62.71	5.74E+0	61.74
2.51188643	1.26E+0	60.54	1.11E+0	60.84	8.04E+0	61.21	7.87E+0	60.46
10	2.33E+0	42.93	2.07E+0	43.91	1.99E+0	55.83	1.94E+0	55.91
15.8489319	2.78E+0	45.09	2.49E+0	46.36	2.64E+0	53.81	2.57E+0	54.17
62.8318530	6.42E+0	48.46	5.96E+0	49.55	5.74E+0	47.61	5.67E+0	48.50
100	8.32E+0	44.14	7.81E+0	44.12	7.29E+0	45.60	7.24E+0	46.53
158.489319	1.02E+0	39.71	9.49E+0	38.27	9.14E+0	43.70	9.14E+0	44.60
251.188643	1.19E+0	36.79	1.09E+0	34.75	1.13E+0	41.92	1.14E+0	42.72
1000	2.00E+0	45.26	1.78E+0	45.14	2.07E+0	37.34	2.10E+0	37.61
1584.89319	2.68E+0	48.60	2.40E+0	48.49	2.49E+0	36.05	2.53E+0	36.11
2511.88643	3.72E+0	47.41	3.33E+0	47.00	2.98E+0	34.85	3.03E+0	34.72
10000	7.06E+0	22.40	6.20E+0	21.71	4.95E+0	31.60	4.99E+0	31.06



APPENDIX E

Initial data WLF (KRS 60 Unaged Unconditioned)		
Reduced [rad/s]	G* [Pa]	δ [°]
0.000285	9.70E+0	81.7
0.000452	1.48E+0	81.7
0.000717	2.26E+0	81.9
0.001135	3.43E+0	81.9
0.001798	5.23E+0	81.6
0.0029	7.96E+0	81.0
0.0045	1.20E+0	80.5
0.0072	1.81E+0	79.8
0.0113	2.71E+0	79.0
0.0180	4.05E+0	78.3
0.0285	6.03E+0	77.6
0.0452	8.94E+0	76.9
0.0628	1.54E+0	67.0
0.0717	1.32E+0	76.2
0.0996	2.16E+0	68.6
0.1135	1.94E+0	75.6
0.1580	3.06E+0	69.4
0.1798	2.85E+0	75.1
0.2500	4.36E+0	69.9
0.2851	4.18E+0	74.7
0.3960	6.24E+0	70.1
0.4522	6.10E+0	74.4
0.6280	8.94E+0	70.1
0.7173	8.92E+0	74.1
0.9960	1.28E+0	69.9
1.1350	1.30E+0	73.9
1.5800	1.82E+0	69.5
1.7978	1.90E+0	73.6
2.5000	2.60E+0	69.0
2.8510	2.78E+0	73.5
3.9600	3.69E+0	68.2
5.1350	4.32E+0	66.8
6.2800	5.23E+0	67.3
8.1440	6.03E+0	66.0
9.9600	7.37E+0	66.3
12.9192	8.29E+0	64.8
15.8000	1.03E+0	65.1
20.4418	1.13E+0	63.3
25.0000	1.44E+0	63.8
32.3799	1.54E+0	61.9
39.6000	1.99E+0	62.3
51.3499	2.10E+0	60.3
62.8000	2.73E+0	60.6
81.4403	2.83E+0	58.6
99.6000	3.72E+0	58.9
129.1924	3.78E+0	56.8
158.0000	5.03E+0	56.9
200.1464	5.53E+0	52.3
204.4184	4.99E+0	55.0
250.0000	6.76E+0	54.8
317.4297	6.92E+0	50.9
323.7988	6.59E+0	53.1
396.0000	9.13E+0	52.5
503.5532	8.65E+0	48.9
513.4990	8.58E+0	51.2
628.0000	1.24E+0	49.8
796.7613	1.08E+0	47.2
814.4029	1.11E+0	49.3
1262.0699	1.34E+0	45.4
1291.9243	1.41E+0	47.5
2001.4644	1.65E+0	43.7
2044.1841	1.79E+0	45.6
3174.2971	2.06E+0	41.8
3237.9876	2.24E+0	43.9
5035.5315	2.50E+0	40.1
5134.9904	2.78E+0	42.1
7967.6132	3.05E+0	38.4
8144.0294	3.42E+0	40.5
12620.699	3.68E+0	36.8

	Modelled data (KRS 60 Unaged Unconditioned)							
	Arrh Prony		WLF Prony		WLF HS		WLF 2S2P1D	
	G*	δ	G*	δ	G*	δ	G*	δ
R ² CA	1.00	0.97	0.98	0.98				
R ² Mec.	1.00	0.99	0.98	0.99	1.00	1.00	1.00	0.98
Reduced [rad/s]	G* [Pa]	δ [°]	G* [Pa]	δ [°]	G* [Pa]	δ [°]	G* [Pa]	δ [°]
0.0001	4.18E+0	83.07	3.62E+0	83.07	4.36E+0	77.24	3.46E+0	75.62
0.00015848	6.42E+0	83.68	5.56E+0	83.68	6.50E+0	77.65	5.28E+0	78.37
0.00025118	9.92E+0	84.34	8.60E+0	84.34	9.71E+0	77.91	8.07E+0	80.00
0.001	3.73E+0	82.84	3.23E+0	82.84	3.23E+0	78.19	2.88E+0	81.38
0.00158489	5.67E+0	81.14	4.91E+0	81.14	4.83E+0	78.19	4.38E+0	81.24
0.00251188	8.43E+0	80.00	7.31E+0	80.00	7.21E+0	78.16	6.65E+0	80.95
0.01	2.89E+0	81.83	2.50E+0	81.83	2.39E+0	77.87	2.29E+0	79.56
0.01584893	4.46E+0	81.44	3.86E+0	81.44	3.57E+0	77.71	3.44E+0	78.99
0.02511886	6.82E+0	79.98	5.91E+0	79.98	5.31E+0	77.52	5.15E+0	78.39
0.1	2.21E+0	76.74	1.91E+0	76.74	1.74E+0	76.60	1.69E+0	76.38
0.15848931	3.29E+0	76.50	2.85E+0	76.50	2.58E+0	76.15	2.50E+0	75.63
0.25118864	4.91E+0	75.31	4.25E+0	75.31	3.81E+0	75.61	3.68E+0	74.85
1	1.50E+0	71.73	1.30E+0	71.73	1.21E+0	73.26	1.14E+0	72.15
1.58489319	2.18E+0	70.61	1.89E+0	70.61	1.75E+0	72.18	1.65E+0	71.10
2.51188643	3.14E+0	68.41	2.72E+0	68.41	2.54E+0	70.91	2.37E+0	69.96
10	8.51E+0	64.72	7.37E+0	64.72	7.36E+0	65.97	6.79E+0	65.87
15.8489319	1.20E+0	63.05	1.04E+0	63.05	1.03E+0	63.95	9.49E+0	64.26
62.8318530	2.93E+0	58.32	2.53E+0	58.32	2.62E+0	57.21	2.45E+0	58.71
100	4.01E+0	57.70	3.48E+0	57.70	3.49E+0	54.86	3.31E+0	56.64
158.489319	5.48E+0	55.19	4.74E+0	55.19	4.59E+0	52.57	4.40E+0	54.53
251.188643	7.19E+0	51.71	6.23E+0	51.71	5.96E+0	50.37	5.78E+0	52.39
1000	1.51E+0	47.32	1.31E+0	47.32	1.22E+0	44.56	1.23E+0	46.05
1584.89319	1.92E+0	44.78	1.66E+0	44.78	1.53E+0	42.91	1.54E+0	44.05
2511.88643	2.37E+0	42.59	2.06E+0	42.59	1.89E+0	41.39	1.92E+0	42.13
10000	4.79E+0	36.71	4.15E+0	36.71	3.44E+0	37.32	3.51E+0	36.82



APPENDIX E

Initial data WLF (KRS 60 Unaged Conditioned)		
Reduced	G*	δ
[rad/s]	[Pa]	[°]
0.0002952	1.04E+0	81.20
0.0004681	1.59E+0	81.60
0.0007426	2.42E+0	81.70
0.0011750	3.67E+0	81.40
0.0018612	5.59E+0	81.10
0.0029516	8.52E+0	80.70
0.0046812	1.28E+0	80.10
0.007	1.93E+0	79.50
0.012	2.90E+0	78.90
0.019	4.33E+0	78.10
0.030	6.44E+0	77.40
0.047	9.54E+0	76.70
0.06	1.39E+0	74.40
0.074	1.41E+0	76.10
0.10	2.01E+0	73.90
0.117	2.07E+0	75.50
0.16	2.92E+0	73.70
0.19	3.03E+0	75.00
0.25	4.23E+0	73.10
0.30	4.44E+0	74.60
0.40	6.13E+0	72.50
0.47	6.49E+0	74.20
0.63	8.88E+0	71.90
0.74	9.48E+0	73.90
1.00	1.28E+0	71.20
1.17	1.38E+0	73.50
1.58	1.83E+0	70.50
1.86	2.02E+0	73.10
2.50	2.63E+0	69.70
2.95	2.95E+0	72.50
3.96	3.75E+0	68.70
4.46	4.62E+0	66.40
6.28	5.31E+0	67.70
7.08	6.22E+0	65.40
9.96	7.50E+0	66.50
11.23	8.33E+0	64.10
15.80	1.05E+0	65.20
17.77	1.15E+0	62.80
25.00	1.47E+0	63.80
28.14	1.60E+0	61.20
39.60	2.03E+0	62.30
44.63	2.18E+0	59.60
62.80	2.78E+0	60.60
70.78	2.92E+0	57.80
99.60	3.77E+0	59.00
112.29	3.88E+0	56.00
143.77	4.85E+0	54.30
158.00	5.08E+0	57.20
177.67	5.10E+0	54.20
228.01	6.49E+0	51.90
250.00	6.79E+0	55.50
281.43	6.64E+0	52.30
361.70	8.03E+0	50.40
396.00	8.98E+0	53.80
446.31	8.63E+0	50.40
572.32	1.03E+0	48.40
628.00	1.19E+0	51.90
707.84	1.11E+0	48.50
906.55	1.28E+0	46.60
1122.88	1.42E+0	46.70
1437.66	1.57E+0	44.90
1776.70	1.78E+0	44.90
2280.11	1.93E+0	43.20
2814.30	2.21E+0	43.20
3617.05	2.40E+0	41.30
4463.08	2.74E+0	41.50
5723.17	2.98E+0	39.50
7078.39	3.35E+0	39.90
9065.51	3.56E+0	37.90
11228.76	4.10E+0	38.20

	Modelled data (KRS 60 Unaged Conditioned)							
	Arrh Prony		WLF Prony		WLF HS		WLF 2S2P1D	
	G*	δ	G*	δ	G*	δ	G*	δ
R ² CA	1.00	0.98	1.00	0.99				
R ² Mec.	0.99	0.99	1.00	0.99	1.00	1.00	1.00	0.99
Reduced	G*	δ	G*	δ	G*	δ	G*	δ
[rad/s]	[Pa]	[°]	[Pa]	[°]	[Pa]	[°]	[Pa]	[°]
0.0001	3.63E+0	83.09	3.62E+0	83.07	4.44E+0	77.40	3.80E+0	82.72
0.00015848	5.58E+0	83.70	5.56E+0	83.68	6.63E+0	77.80	5.84E+0	82.84
0.00025118	8.62E+0	84.35	8.60E+0	84.34	9.90E+0	78.05	8.95E+0	82.76
0.001	3.24E+0	82.86	3.23E+0	82.84	3.30E+0	78.34	3.19E+0	81.87
0.00158489	4.92E+0	81.16	4.91E+0	81.14	4.94E+0	78.34	4.84E+0	81.45
0.00251188	7.33E+0	80.02	7.31E+0	80.00	7.37E+0	78.31	7.34E+0	81.00
0.01	2.51E+0	81.86	2.50E+0	81.83	2.45E+0	78.05	2.52E+0	79.50
0.01584893	3.87E+0	81.46	3.86E+0	81.44	3.66E+0	77.90	3.78E+0	78.96
0.02511886	5.93E+0	80.01	5.91E+0	79.98	5.45E+0	77.72	5.66E+0	78.39
0.1	1.92E+0	76.79	1.91E+0	76.74	1.79E+0	76.86	1.86E+0	76.55
0.15848931	2.86E+0	76.55	2.85E+0	76.50	2.66E+0	76.43	2.75E+0	75.87
0.25118864	4.27E+0	75.38	4.25E+0	75.31	3.94E+0	75.92	4.06E+0	75.14
1	1.30E+0	71.83	1.30E+0	71.73	1.25E+0	73.69	1.27E+0	72.57
1.58489319	1.90E+0	70.73	1.89E+0	70.61	1.83E+0	72.65	1.84E+0	71.54
2.51188643	2.73E+0	68.56	2.72E+0	68.41	2.65E+0	71.43	2.65E+0	70.40
10	7.44E+0	64.98	7.37E+0	64.72	7.75E+0	66.62	7.63E+0	66.21
15.8489319	1.05E+0	63.36	1.04E+0	63.05	1.09E+0	64.63	1.07E+0	64.51
62.8318530	2.58E+0	58.88	2.53E+0	58.32	2.80E+0	57.89	2.77E+0	58.60
100	3.54E+0	58.35	3.48E+0	57.70	3.75E+0	55.50	3.73E+0	56.38
158.489319	4.85E+0	55.99	4.74E+0	55.19	4.95E+0	53.16	4.95E+0	54.12
251.188643	6.39E+0	52.73	6.23E+0	51.71	6.44E+0	50.90	6.49E+0	51.84
1000	1.37E+0	49.09	1.31E+0	47.32	1.33E+0	44.88	1.36E+0	45.25
1584.89319	1.77E+0	46.76	1.66E+0	44.78	1.66E+0	43.16	1.70E+0	43.24
2511.88643	2.23E+0	44.56	2.06E+0	42.59	2.06E+0	41.57	2.11E+0	41.33
10000	4.57E+0	34.25	4.15E+0	36.71	3.76E+0	37.34	3.80E+0	36.27



APPENDIX E

Initial data_WLF (KRS 60_PAV Unconditioned)		
Reduced	G*	δ
[rad/s]	[Pa]	[°]
0.0001570	4.98E+0	80.50
0.0002490	7.45E+0	79.70
0.00040	1.11E+0	79.00
0.00063	1.66E+0	78.00
0.00099	2.47E+0	76.90
0.00157	3.66E+0	75.90
0.00249	5.37E+0	74.80
0.00395	7.84E+0	73.80
0.00625	1.14E+0	72.70
0.00990	1.65E+0	71.70
0.02	2.37E+0	70.70
0.02	3.39E+0	69.70
0.04	4.82E+0	68.80
0.06	6.83E+0	67.90
0.06	7.00E+0	64.70
0.10	9.63E+0	67.10
0.10	9.63E+0	63.70
0.16	1.35E+0	66.30
0.16	1.32E+0	63.20
0.25	1.90E+0	65.50
0.25	1.80E+0	62.40
0.40	2.64E+0	64.70
0.40	2.46E+0	61.30
0.63	3.67E+0	63.90
0.63	3.35E+0	60.20
0.99	5.08E+0	63.10
1.00	4.53E+0	59.20
1.57	7.01E+0	62.30
1.58	6.10E+0	58.00
2.50	8.17E+0	56.90
3.96	1.09E+0	55.70
5.61	1.75E+0	51.80
6.28	1.44E+0	54.50
8.90	2.22E+0	50.60
9.96	1.90E+0	53.20
14.12	2.79E+0	49.20
15.80	2.49E+0	52.00
22.34	3.53E+0	47.70
25.00	3.24E+0	50.80
35.39	4.42E+0	46.30
39.60	4.17E+0	49.40
56.12	5.56E+0	44.90
62.80	5.34E+0	48.10
89.01	6.91E+0	43.60
99.60	6.82E+0	46.80
141.20	8.53E+0	42.30
158.00	8.66E+0	45.50
184.73	1.12E+0	40.30
223.43	1.05E+0	41.00
250.00	1.10E+0	44.00
292.98	1.34E+0	39.00
353.91	1.29E+0	39.70
396.00	1.39E+0	42.20
464.77	1.60E+0	37.80
561.24	1.58E+0	38.50
628.00	1.78E+0	39.70
735.39	1.91E+0	36.50
890.13	1.91E+0	37.40
1164.86	2.28E+0	35.30
1412.05	2.30E+0	36.20
1847.30	2.71E+0	34.10
2234.25	2.75E+0	35.20
2929.79	3.20E+0	33.00
3539.06	3.28E+0	34.10
4647.66	3.76E+0	31.90
5612.44	3.89E+0	33.10
7353.89	4.41E+0	30.80
8901.26	4.58E+0	32.10
11648.57	5.13E+0	29.80

	Modelled data (KRS 60_PAV Unconditioned)							
	Arrh Prony		WLF Prony		WLF HS		WLF 2S2P1D	
	G*	δ	G*	δ	G*	δ	G*	δ
R ² CA	1.00	0.99	1.00	0.99				
R ² Mec.	0.99	0.76	0.99	0.78	1.00	1.00	1.00	0.99
Reduced	G*	δ	G*	δ	G*	δ	G*	δ
[rad/s]	[Pa]	[°]	[Pa]	[°]	[Pa]	[°]	[Pa]	[°]
0.0001	4.65E+0	71.11	3.22E+0	76.69	3.93E+0	72.04	3.25E+0	80.84
0.00015848	6.86E+0	74.72	5.04E+0	79.84	5.69E+0	72.02	4.93E+0	80.36
0.00025118	1.04E+0	77.30	7.91E+0	80.90	8.22E+0	71.98	7.46E+0	79.67
0.001	3.77E+0	73.00	2.88E+0	72.98	2.48E+0	71.70	2.50E+0	76.89
0.00158489	5.48E+0	67.50	4.11E+0	67.65	3.58E+0	71.55	3.70E+0	75.82
0.00251188	7.45E+0	61.85	5.53E+0	63.58	5.17E+0	71.37	5.44E+0	74.71
0.01	1.62E+0	65.97	1.38E+0	67.36	1.54E+0	70.55	1.67E+0	71.28
0.01584893	2.32E+0	71.61	1.97E+0	68.52	2.21E+0	70.16	2.40E+0	70.14
0.02511886	3.47E+0	75.73	2.80E+0	69.16	3.17E+0	69.70	3.42E+0	69.00
0.1	1.24E+0	78.55	8.62E+0	73.91	9.18E+0	67.74	9.61E+0	65.65
0.15848931	1.89E+0	77.04	1.30E+0	73.03	1.30E+0	66.85	1.34E+0	64.54
0.25118864	2.83E+0	74.48	1.93E+0	70.10	1.83E+0	65.82	1.86E+0	63.42
1	8.46E+0	61.94	5.31E+0	56.54	4.92E+0	61.82	4.80E+0	59.93
1.58489319	1.13E+0	57.08	6.99E+0	50.72	6.74E+0	60.19	6.51E+0	58.69
2.51188643	1.47E+0	54.02	8.68E+0	45.09	9.15E+0	58.42	8.78E+0	57.39
10	3.28E+0	42.32	1.46E+0	49.38	2.15E+0	52.59	2.06E+0	53.11
15.8489319	3.90E+0	36.64	1.95E+0	55.06	2.81E+0	50.59	2.69E+0	51.56
62.8318530	5.95E+0	38.29	5.35E+0	52.21	5.80E+0	44.96	5.72E+0	46.62
100	7.45E+0	40.90	6.88E+0	47.03	7.26E+0	43.27	7.25E+0	44.92
158.489319	9.41E+0	41.18	8.48E+0	43.61	9.00E+0	41.72	9.08E+0	43.23
251.188643	1.16E+0	40.65	1.05E+0	41.57	1.11E+0	40.29	1.13E+0	41.58
1000	2.31E+0	41.33	1.76E+0	33.74	1.99E+0	36.67	2.05E+0	36.94
1584.89319	2.91E+0	37.25	1.97E+0	35.78	2.39E+0	35.63	2.46E+0	35.53
2511.88643	3.45E+0	32.20	2.31E+0	41.58	2.85E+0	34.63	2.94E+0	34.20
10000	5.08E+0	30.39	5.80E+0	54.55	4.75E+0	31.75	4.82E+0	30.63



APPENDIX E

Initial data_WLF (KRS 60_PAV _Conditioned)		
Reduced	G*	δ
[rad/s]	[Pa]	[°]
0.00016	5.07E+0	80.2
0.00025	7.55E+0	79.7
0.00040	1.13E+0	78.8
0.00063	1.70E+0	77.8
0.00099	2.52E+0	76.9
0.00157	3.72E+0	75.9
0.00249	5.45E+0	75.0
0.00395	7.95E+0	73.9
0.0063	1.16E+0	72.9
0.0099	1.67E+0	71.8
0.0157	2.40E+0	70.8
0.0249	3.44E+0	69.9
0.0395	4.90E+0	68.9
0.0625	6.94E+0	68.0
0.0628	7.63E+0	63.9
0.0990	9.79E+0	67.2
0.0996	1.04E+0	63.2
0.1570	1.38E+0	66.4
0.1580	1.41E+0	62.3
0.2490	1.93E+0	65.5
0.2500	1.93E+0	61.5
0.395	2.69E+0	64.7
0.396	2.62E+0	60.5
0.625	3.73E+0	63.9
0.628	3.55E+0	59.5
0.990	5.17E+0	63.1
1.00	4.79E+0	58.4
1.57	7.13E+0	62.4
1.58	6.42E+0	57.3
2.50	8.57E+0	56.1
3.96	1.14E+0	54.9
5.61	1.82E+0	51.2
6.28	1.50E+0	53.7
8.90	2.30E+0	49.8
9.96	1.97E+0	52.5
14.12	2.89E+0	48.4
15.80	2.57E+0	51.2
22.34	3.64E+0	47.0
25.00	3.33E+0	50.0
35.39	4.56E+0	45.6
39.60	4.27E+0	48.7
56.12	5.72E+0	44.2
62.80	5.46E+0	47.4
89.01	7.10E+0	42.9
99.60	6.94E+0	46.1
141.20	8.77E+0	41.6
158.00	8.78E+0	44.8
184.73	1.13E+0	39.7
223.43	1.08E+0	40.3
250.00	1.11E+0	43.2
292.98	1.34E+0	38.5
353.91	1.31E+0	39.1
396.00	1.41E+0	41.5
464.77	1.62E+0	37.2
561.24	1.60E+0	37.9
628.00	1.80E+0	39.4
735.39	1.91E+0	36.2
890.13	1.93E+0	36.8
1164.86	2.31E+0	34.9
1412.05	2.31E+0	35.6
1847.30	2.74E+0	33.7
2234.25	2.77E+0	34.6
2929.79	3.23E+0	32.6
3539.06	3.29E+0	33.5
4647.66	3.79E+0	31.6
5612.44	3.89E+0	32.5
7353.89	4.44E+0	30.5
8901.26	4.57E+0	31.5
11648.57	5.15E+0	29.5

	Modelled data (KRS 60_PAV Conditioned)							
	Arrh Prony		WLF Prony		WLF HS		WLF 2S2P1D	
	G*	δ	G*	δ	G*	δ	G*	δ
R ² CA	1.00	0.99	1.00	0.99				
R ² Mec.	0.96	0.77	0.96	0.81	1.00	0.99	1.00	0.99
Reduced	G*	δ	G*	δ	G*	δ	G*	δ
[rad/s]	[Pa]	[°]	[Pa]	[°]	[Pa]	[°]	[Pa]	[°]
0.0001	3.84E+0	64.20	3.54E+0	77.90	3.97E+0	72.45	3.37E+0	80.83
0.00015848	5.77E+0	71.61	5.54E+0	80.77	5.75E+0	72.43	5.11E+0	80.33
0.00025118	8.90E+0	75.80	8.72E+0	81.74	8.34E+0	72.39	7.72E+0	79.63
0.001	3.21E+0	73.05	3.19E+0	74.65	2.53E+0	72.11	2.58E+0	76.83
0.00158489	4.62E+0	68.93	4.59E+0	70.02	3.66E+0	71.95	3.82E+0	75.75
0.00251188	6.31E+0	65.99	6.28E+0	66.77	5.30E+0	71.76	5.62E+0	74.64
0.01	1.69E+0	70.53	1.69E+0	70.82	1.59E+0	70.92	1.72E+0	71.20
0.01584893	2.48E+0	71.33	2.47E+0	71.53	2.29E+0	70.52	2.47E+0	70.05
0.02511886	3.60E+0	71.27	3.60E+0	71.41	3.28E+0	70.03	3.53E+0	68.91
0.1	1.12E+0	68.24	1.12E+0	68.29	9.54E+0	67.97	9.89E+0	65.55
0.15848931	1.60E+0	64.55	1.60E+0	64.58	1.35E+0	67.04	1.38E+0	64.44
0.25118864	2.19E+0	60.70	2.19E+0	60.72	1.91E+0	65.96	1.91E+0	63.32
1	5.25E+0	53.44	5.24E+0	53.45	5.13E+0	61.76	4.93E+0	59.81
1.58489319	6.92E+0	49.15	6.92E+0	49.16	7.03E+0	60.04	6.69E+0	58.57
2.51188643	8.62E+0	44.29	8.62E+0	44.29	9.54E+0	58.20	9.00E+0	57.26
10	1.46E+0	49.28	1.46E+0	49.28	2.23E+0	52.15	2.11E+0	52.96
15.8489319	1.94E+0	55.01	1.94E+0	55.02	2.90E+0	50.11	2.76E+0	51.40
62.8318530	5.35E+0	52.21	5.35E+0	52.21	5.94E+0	44.42	5.84E+0	46.46
100	6.88E+0	47.02	6.88E+0	47.02	7.41E+0	42.73	7.39E+0	44.75
158.489319	8.48E+0	43.61	8.48E+0	43.61	9.17E+0	41.20	9.25E+0	43.07
251.188643	1.05E+0	41.56	1.05E+0	41.57	1.12E+0	39.79	1.15E+0	41.42
1000	1.76E+0	33.74	1.76E+0	33.74	2.00E+0	36.26	2.08E+0	36.80
1584.89319	1.97E+0	35.78	1.97E+0	35.78	2.40E+0	35.25	2.50E+0	35.40
2511.88643	2.31E+0	41.58	2.31E+0	41.58	2.87E+0	34.29	2.98E+0	34.07
10000	5.80E+0	54.55	5.80E+0	54.55	4.75E+0	31.50	4.88E+0	30.52



APPENDIX E

Initial data_WLF (SR1_Unaged _Unconditioned)		
Reduced [rad/s]	G* [Pa]	δ [°]
0.000345	6.87E+0	47.5
0.000548	8.84E+0	49.8
0.000869	1.16E+0	51.9
0.001375	1.53E+0	53.3
0.002178	2.04E+0	54.3
0.003454	2.72E+0	55.0
0.005477	3.63E+0	55.1
0.008689	4.82E+0	55.2
0.013748	6.41E+0	55.0
0.021777	8.48E+0	54.8
0.034536	1.12E+0	54.5
0.054774	1.48E+0	54.4
0.062800	1.59E+0	51.8
0.086890	1.95E+0	54.3
0.099600	2.02E+0	51.8
0.137484	2.57E+0	54.4
0.158000	2.57E+0	51.8
0.217775	3.38E+0	54.5
0.250000	3.30E+0	51.8
0.345360	4.47E+0	54.7
0.396000	4.24E+0	52.0
0.547736	5.90E+0	55.1
0.628000	5.49E+0	52.4
0.868899	7.84E+0	55.5
0.996000	7.11E+0	52.8
1.374840	1.04E+0	55.9
1.580000	9.25E+0	53.2
2.177747	1.40E+0	56.3
2.500000	1.21E+0	53.7
3.453599	1.88E+0	56.9
3.960000	1.58E+0	54.1
4.946141	2.27E+0	51.0
6.280000	2.08E+0	54.5
7.844516	2.87E+0	50.9
9.960000	2.75E+0	54.8
12.444112	3.68E+0	51.1
15.800000	3.62E+0	54.9
19.690051	4.74E+0	51.0
25.000000	4.78E+0	54.9
31.189041	6.10E+0	50.6
39.600000	6.30E+0	54.8
49.461409	7.88E+0	50.1
62.800000	8.25E+0	54.8
78.445164	1.01E+0	49.5
99.600000	1.09E+0	54.5
124.441124	1.30E+0	48.7
158.000000	1.43E+0	54.5
196.900513	1.66E+0	47.9
203.386530	1.63E+0	47.0
250.000000	1.87E+0	55.1
311.890412	2.11E+0	46.9
322.568446	2.01E+0	46.1
396.000000	2.49E+0	57.5
494.614088	2.68E+0	46.0
511.704965	2.47E+0	45.2
628.000000	3.38E+0	63.3
784.451642	3.38E+0	44.9
809.659755	3.06E+0	44.0
1244.411240	4.24E+0	43.9
1282.501052	3.78E+0	42.9
1969.005126	5.29E+0	42.9
2033.865305	4.66E+0	41.8
3118.904119	6.57E+0	42.0
3225.684464	5.71E+0	40.7
4946.140876	8.08E+0	40.9
5117.049652	6.97E+0	39.7
7844.516422	9.92E+0	39.8
8096.597551	8.47E+0	38.7
12444.11239	1.21E+0	38.8

	Modelled data (SR1_Unaged_Unconditioned)								
	Arrh Prony			WLF Prony		WLF HS		WLF 2S2P1D	
	G*	δ	τ	G*	δ	G*	δ	G*	δ
R ² CA	0.98	0.56	0.97	0.62					
R ² Mec.	1.00	0.87	1.00	0.97	1.00	0.96	0.97	0.31	
Reduced [rad/s]	G*	δ	τ	G*	δ	G*	δ	G*	δ
0.0001	3.10E+0	65.02	2.30E+0	66.31	4.12E+0	31.46	5.13E+0	7.39	
0.00015848	4.17E+0	61.26	3.07E+0	62.54	4.92E+0	36.09	5.25E+0	11.06	
0.00025118	5.49E+0	60.30	4.04E+0	62.07	6.04E+0	40.32	5.46E+0	16.22	
0.001	1.44E+0	58.64	1.11E+0	62.81	1.25E+0	49.51	8.00E+0	39.94	
0.00158489	1.92E+0	55.40	1.52E+0	60.03	1.64E+0	51.41	1.02E+0	47.91	
0.00251188	2.44E+0	54.05	2.01E+0	58.45	2.16E+0	52.84	1.37E+0	54.29	
0.01	5.87E+0	58.28	5.08E+0	60.02	5.04E+0	55.10	3.72E+0	63.27	
0.01584893	8.01E+0	56.52	6.95E+0	57.64	6.71E+0	55.39	5.24E+0	63.91	
0.02511886	1.05E+0	54.70	9.12E+0	55.55	8.94E+0	55.51	7.36E+0	63.89	
0.1	2.47E+0	57.01	2.17E+0	56.98	2.11E+0	55.21	1.97E+0	61.64	
0.15848931	3.35E+0	55.28	2.93E+0	54.90	2.80E+0	54.94	2.70E+0	60.52	
0.25118864	4.38E+0	53.05	3.81E+0	52.60	3.71E+0	54.60	3.67E+0	59.33	
1	9.86E+0	54.35	8.54E+0	53.79	8.51E+0	53.22	8.87E+0	55.62	
1.58489319	1.32E+0	52.66	1.14E+0	51.89	1.12E+0	52.66	1.17E+0	54.39	
2.51188643	1.71E+0	50.36	1.46E+0	49.50	1.46E+0	52.06	1.55E+0	53.19	
10	3.66E+0	51.95	3.11E+0	50.49	3.21E+0	50.00	3.40E+0	49.77	
15.8489319	4.87E+0	50.47	4.09E+0	48.66	4.14E+0	49.25	4.37E+0	48.72	
62.8318530	9.76E+0	48.87	8.00E+0	46.79	8.64E+0	46.87	8.98E+0	45.83	
100	1.29E+0	49.87	1.04E+0	47.10	1.10E+0	46.05	1.13E+0	44.95	
158.489319	1.70E+0	48.56	1.34E+0	45.28	1.39E+0	45.23	1.42E+0	44.12	
251.188643	2.17E+0	45.94	1.67E+0	42.96	1.74E+0	44.41	1.78E+0	43.35	
1000	4.24E+0	44.26	3.21E+0	43.60	3.38E+0	42.03	3.39E+0	41.27	
1584.89319	5.35E+0	42.56	4.06E+0	41.71	4.19E+0	41.26	4.18E+0	40.65	
2511.88643	6.57E+0	40.94	4.95E+0	39.57	5.16E+0	40.51	5.14E+0	40.06	
10000	1.31E+0	37.68	9.44E+0	39.18	9.45E+0	38.34	9.38E+0	38.41	



APPENDIX E

Initial data_WLF (SR1 Unaged _Conditioned)		
Reduced [rad/s]	G* [Pa]	δ [°]
0.000396	7.16E+0	48.0
0.000628	9.21E+0	50.0
0.000997	1.20E+0	51.8
0.001577	1.57E+0	53.1
0.002499	2.09E+0	54.2
0.003963	2.79E+0	54.6
0.006285	3.70E+0	54.9
0.009970	4.91E+0	54.9
0.015775	6.52E+0	54.8
0.024987	8.62E+0	54.6
0.039626	1.14E+0	54.4
0.062800	1.56E+0	49.1
0.062847	1.50E+0	54.3
0.099600	1.98E+0	49.3
0.099696	1.97E+0	54.3
0.157747	2.60E+0	54.4
0.158000	2.51E+0	49.8
0.249872	3.43E+0	54.6
0.250000	3.20E+0	50.2
0.396000	4.11E+0	50.8
0.396261	4.53E+0	54.9
0.628000	5.30E+0	51.6
0.628465	5.99E+0	55.3
0.996000	6.86E+0	52.3
0.996963	7.95E+0	55.8
1.577473	1.06E+0	56.4
1.580000	8.92E+0	53.1
2.498717	1.43E+0	57.0
2.500000	1.17E+0	53.9
3.960000	1.53E+0	54.4
3.962612	1.96E+0	57.2
4.221910	2.11E+0	53.3
6.280000	2.02E+0	54.9
6.695895	2.71E+0	53.4
9.960000	2.67E+0	55.3
10.622002	3.50E+0	53.0
15.800000	3.53E+0	55.5
16.806965	4.52E+0	52.9
25.000000	4.66E+0	55.6
26.622233	5.88E+0	52.5
39.600000	6.15E+0	55.5
42.219096	7.63E+0	51.9
62.800000	8.07E+0	55.5
66.958949	9.88E+0	51.1
99.600000	1.06E+0	55.3
106.220020	1.27E+0	50.2
147.170434	1.53E+0	47.6
158.000000	1.40E+0	55.3
168.069651	1.64E+0	49.2
233.410433	1.91E+0	46.6
250.000000	1.83E+0	55.7
266.222327	2.10E+0	48.2
370.269562	2.38E+0	45.4
396.000000	2.45E+0	56.8
422.190964	2.67E+0	47.1
585.869560	2.96E+0	44.4
628.000000	3.28E+0	57.4
669.589490	3.38E+0	46.0
928.017383	3.67E+0	43.2
1062.200195	4.26E+0	44.9
1471.704335	4.54E+0	42.0
1680.696511	5.35E+0	43.8
2334.104328	5.58E+0	40.9
2662.223274	6.66E+0	42.9
3702.695620	6.83E+0	39.7
4221.909636	8.23E+0	41.7
5858.695602	8.32E+0	38.6
6695.894900	1.01E+0	40.6
9280.173833	1.01E+0	37.6
10622.00195	1.24E+0	39.6

	Modelled data (SR1 Unaged Conditioned)								
	Arrh Prony			WLF Prony		WLF HS		WLF 2S2P1D	
	G*	δ	τ	G*	δ	G*	δ	G*	δ
R ² CA	0.97	0.56	0.97	0.60					
R ² Mec.	0.99	0.81	1.00	0.98	1.00	0.96	0.98	0.28	
Reduced [rad/s]	G*	δ	τ	G*	δ	G*	δ	G*	δ
0.0001	3.51E+0	61.24	2.00E+0	66.09	4.12E+0	31.46	6.15E+0	6.23	
0.00015848	4.56E+0	55.83	2.70E+0	62.99	4.92E+0	36.09	6.26E+0	9.35	
0.00025118	5.70E+0	54.05	3.59E+0	62.84	6.04E+0	40.32	6.46E+0	13.78	
0.001	1.35E+0	58.37	1.00E+0	63.87	1.25E+0	49.51	8.84E+0	35.64	
0.00158489	1.83E+0	57.09	1.38E+0	61.15	1.64E+0	51.41	1.10E+0	43.81	
0.00251188	2.40E+0	56.45	1.84E+0	59.55	2.16E+0	52.84	1.44E+0	50.73	
0.01	6.04E+0	59.78	4.73E+0	61.06	5.04E+0	55.10	3.76E+0	61.49	
0.01584893	8.28E+0	57.83	6.51E+0	58.74	6.71E+0	55.39	5.26E+0	62.50	
0.02511886	1.09E+0	55.96	8.59E+0	56.64	8.94E+0	55.51	7.34E+0	62.76	
0.1	2.62E+0	57.71	2.07E+0	58.00	2.11E+0	55.21	1.94E+0	60.98	
0.15848931	3.56E+0	55.76	2.82E+0	55.97	2.80E+0	54.94	2.65E+0	59.96	
0.25118864	4.65E+0	53.51	3.68E+0	53.66	3.71E+0	54.60	3.60E+0	58.84	
1	1.06E+0	54.71	8.38E+0	54.78	8.51E+0	53.22	8.67E+0	55.31	
1.58489319	1.42E+0	52.86	1.13E+0	52.91	1.12E+0	52.66	1.15E+0	54.13	
2.51188643	1.83E+0	50.48	1.45E+0	50.52	1.46E+0	52.06	1.51E+0	52.98	
10	3.94E+0	51.43	3.13E+0	51.44	3.21E+0	50.00	3.31E+0	49.72	
15.8489319	5.21E+0	49.63	4.13E+0	49.64	4.14E+0	49.25	4.25E+0	48.72	
62.8318530	1.03E+0	47.68	8.21E+0	47.68	8.64E+0	46.87	8.74E+0	45.97	
100	1.35E+0	48.01	1.07E+0	48.01	1.10E+0	46.05	1.10E+0	45.14	
158.489319	1.76E+0	46.20	1.39E+0	46.20	1.39E+0	45.23	1.39E+0	44.35	
251.188643	2.19E+0	43.85	1.74E+0	43.85	1.74E+0	44.41	1.74E+0	43.62	
1000	4.26E+0	44.44	3.38E+0	44.44	3.38E+0	42.03	3.33E+0	41.64	
1584.89319	5.42E+0	42.56	4.30E+0	42.56	4.19E+0	41.26	4.12E+0	41.04	
2511.88643	6.63E+0	40.37	5.26E+0	40.37	5.16E+0	40.51	5.07E+0	40.47	
10000	1.28E+0	39.94	1.01E+0	39.96	9.45E+0	38.34	9.31E+0	38.86	



APPENDIX E

Initial data_WLF (SR1_PAV Unconditioned)		
Reduced [rad/s]	G* [Pa]	δ [°]
0.000251	9.19E+0	57.6
0.000398	1.23E+0	57.7
0.000631	1.64E+0	57.6
0.000998	2.20E+0	57.3
0.001581	2.94E+0	57.0
0.002507	3.94E+0	56.8
0.003977	5.24E+0	56.6
0.006308	6.97E+0	56.4
0.009981	9.27E+0	56.3
0.015810	1.23E+0	56.2
0.025073	1.64E+0	56.3
0.039766	2.18E+0	56.4
0.062800	3.05E+0	53.7
0.063082	2.91E+0	56.5
0.099600	3.93E+0	53.7
0.099813	3.88E+0	56.7
0.158000	5.10E+0	53.9
0.158104	5.18E+0	57.0
0.250000	6.65E+0	54.0
0.250730	6.92E+0	57.2
0.396000	8.70E+0	54.0
0.397655	9.26E+0	57.4
0.628000	1.14E+0	54.0
0.630819	1.24E+0	57.7
0.996000	1.50E+0	54.0
0.998131	1.67E+0	57.9
1.580000	1.97E+0	53.9
1.581039	2.26E+0	58.2
2.500000	2.58E+0	53.7
2.507304	3.09E+0	58.4
3.960000	3.39E+0	53.4
5.186938	4.98E+0	49.0
6.280000	4.44E+0	53.0
8.226418	6.20E+0	48.6
9.960000	5.81E+0	52.6
13.049939	7.92E+0	47.8
15.800000	7.57E+0	52.0
20.648638	1.00E+0	47.3
25.000000	9.84E+0	51.4
32.707443	1.26E+0	46.4
39.600000	1.27E+0	50.8
51.869379	1.59E+0	45.5
62.800000	1.64E+0	50.1
82.264175	1.99E+0	44.6
99.600000	2.11E+0	49.5
130.499394	2.48E+0	43.7
158.000000	2.70E+0	49.0
191.413243	3.68E+0	41.7
206.486383	3.09E+0	42.8
250.000000	3.46E+0	48.7
303.578965	4.44E+0	40.8
327.074431	3.82E+0	41.9
396.000000	4.44E+0	49.1
481.581089	5.35E+0	39.9
518.693794	4.71E+0	41.1
628.000000	5.73E+0	49.5
761.995393	6.44E+0	38.9
822.641750	5.79E+0	40.2
1207.000703	7.80E+0	38.0
1304.993941	7.09E+0	39.4
1914.132428	9.43E+0	37.1
2064.863831	8.64E+0	38.6
3035.789647	1.13E+0	36.2
3270.744309	1.05E+0	37.8
4815.810885	1.35E+0	35.4
5186.937945	1.27E+0	37.5
7619.953932	1.61E+0	34.6
8226.417504	1.53E+0	36.3
12070.00702	1.91E+0	33.7

	Modelled data (SR1_PAV Unconditioned)							
	Arrh Prony		WLF Prony		WLF HS		WLF 2S2P1D	
	G*	δ	G*	δ	G*	δ	G*	δ
R ² CA	0.99	0.83	1.00	0.88				
R ² Mec.	1.00	0.96	0.99	0.94	1.00	0.99	0.99	0.92
Reduced [rad/s]	G*	δ	G*	δ	G*	δ	G*	δ
	[Pa]	[°]	[Pa]	[°]	[Pa]	[°]	[Pa]	[°]
0.0001	4.19E+0	66.09	3.67E+0	66.09	4.89E+0	57.54	4.62E+0	59.58
0.00015848	5.65E+0	62.99	4.95E+0	62.99	6.57E+0	57.53	6.27E+0	59.40
0.00025118	7.51E+0	62.84	6.58E+0	62.84	8.82E+0	57.51	8.49E+0	59.22
0.001	2.10E+0	63.87	1.84E+0	63.87	2.13E+0	57.37	2.10E+0	58.66
0.00158489	2.90E+0	61.15	2.54E+0	61.15	2.86E+0	57.30	2.83E+0	58.46
0.00251188	3.85E+0	59.55	3.37E+0	59.55	3.84E+0	57.22	3.82E+0	58.25
0.01	9.90E+0	61.06	8.67E+0	61.06	9.22E+0	56.88	9.30E+0	57.55
0.01584893	1.36E+0	58.74	1.19E+0	58.74	1.23E+0	56.74	1.25E+0	57.28
0.02511886	1.80E+0	56.64	1.57E+0	56.64	1.65E+0	56.57	1.67E+0	56.99
0.1	4.33E+0	58.00	3.79E+0	58.00	3.92E+0	55.90	3.99E+0	55.96
0.15848931	5.90E+0	55.97	5.16E+0	55.97	5.21E+0	55.61	5.31E+0	55.55
0.25118864	7.71E+0	53.66	6.75E+0	53.66	6.93E+0	55.29	7.05E+0	55.12
1	1.75E+0	54.78	1.54E+0	54.78	1.61E+0	54.05	1.63E+0	53.58
1.58489319	2.36E+0	52.91	2.06E+0	52.91	2.12E+0	53.53	2.14E+0	52.99
2.51188643	3.04E+0	50.52	2.66E+0	50.52	2.79E+0	52.96	2.80E+0	52.36
10	6.55E+0	51.44	5.73E+0	51.44	6.22E+0	50.87	6.18E+0	50.24
15.8489319	8.65E+0	49.64	7.57E+0	49.64	8.06E+0	50.05	7.98E+0	49.46
62.8318530	1.72E+0	47.68	1.50E+0	47.68	1.70E+0	47.25	1.67E+0	46.96
100	2.25E+0	48.01	1.97E+0	48.01	2.17E+0	46.20	2.13E+0	46.07
158.489319	2.91E+0	46.20	2.55E+0	46.20	2.74E+0	45.12	2.69E+0	45.17
251.188643	3.64E+0	43.85	3.18E+0	43.85	3.45E+0	44.01	3.38E+0	44.25
1000	7.08E+0	44.44	6.20E+0	44.44	6.60E+0	40.60	6.53E+0	41.37
1584.89319	9.00E+0	42.56	7.88E+0	42.56	8.10E+0	39.47	8.05E+0	40.37
2511.88643	1.10E+0	40.37	9.65E+0	40.37	9.88E+0	38.35	9.88E+0	39.33
10000	2.12E+0	39.96	1.86E+0	39.96	1.73E+0	35.14	1.77E+0	35.98



APPENDIX E

Initial data WLF (SR1_PAV Conditioned)		
Reduced [rad/s]	G* [Pa]	δ [°]
0.000257	9.00E+0	58.30
0.000408	1.21E+0	58.30
0.000647	1.61E+0	57.90
0.001024	2.16E+0	57.80
0.001622	2.89E+0	57.50
0.002573	3.87E+0	57.20
0.004080	5.15E+0	56.90
0.006473	6.86E+0	56.60
0.010242	9.13E+0	56.50
0.016223	1.21E+0	56.40
0.025727	1.61E+0	56.50
0.040803	2.15E+0	56.60
0.062800	3.11E+0	54.30
0.064728	2.87E+0	56.70
0.099600	4.00E+0	54.50
0.102418	3.83E+0	57.00
0.158000	5.18E+0	54.60
0.162230	5.12E+0	57.20
0.250000	6.74E+0	54.70
0.257274	6.85E+0	57.50
0.396000	8.81E+0	54.80
0.408033	9.18E+0	57.80
0.628000	1.15E+0	54.80
0.647282	1.23E+0	58.10
0.996000	1.51E+0	54.80
1.024180	1.66E+0	58.30
1.580000	1.98E+0	54.60
1.622302	2.25E+0	58.70
2.500000	2.60E+0	54.50
2.572741	3.06E+0	59.10
3.960000	3.42E+0	54.20
5.874510	4.69E+0	50.60
6.280000	4.48E+0	53.80
9.316898	5.90E+0	49.80
9.960000	5.87E+0	53.40
14.779819	7.51E+0	49.20
15.800000	7.67E+0	52.90
23.385789	9.54E+0	48.30
25.000000	9.98E+0	52.30
37.043090	1.21E+0	47.60
39.600000	1.29E+0	51.70
58.745103	1.53E+0	46.60
62.800000	1.67E+0	51.10
93.168985	1.94E+0	45.70
99.600000	2.15E+0	50.50
147.79818	2.43E+0	44.70
158.00000	2.75E+0	49.90
233.85789	3.03E+0	43.80
250.00000	3.50E+0	49.50
265.2757	3.50E+0	42.80
370.43090	3.78E+0	42.80
396.00000	4.43E+0	49.20
420.7239	4.22E+0	42.00
587.45102	4.69E+0	41.90
628.00000	5.53E+0	50.70
667.4134	5.11E+0	40.80
931.68984	5.79E+0	41.00
1056.0339	6.16E+0	40.00
1477.9818	7.11E+0	40.10
1672.7578	7.45E+0	38.90
2338.5789	8.68E+0	39.30
2652.7572	8.99E+0	38.00
3704.3090	1.06E+0	38.50
4207.2392	1.08E+0	37.00
5874.5102	1.28E+0	37.70
6674.1345	1.29E+0	36.00
9316.8984	1.54E+0	36.90
10560.339	1.54E+0	35.10

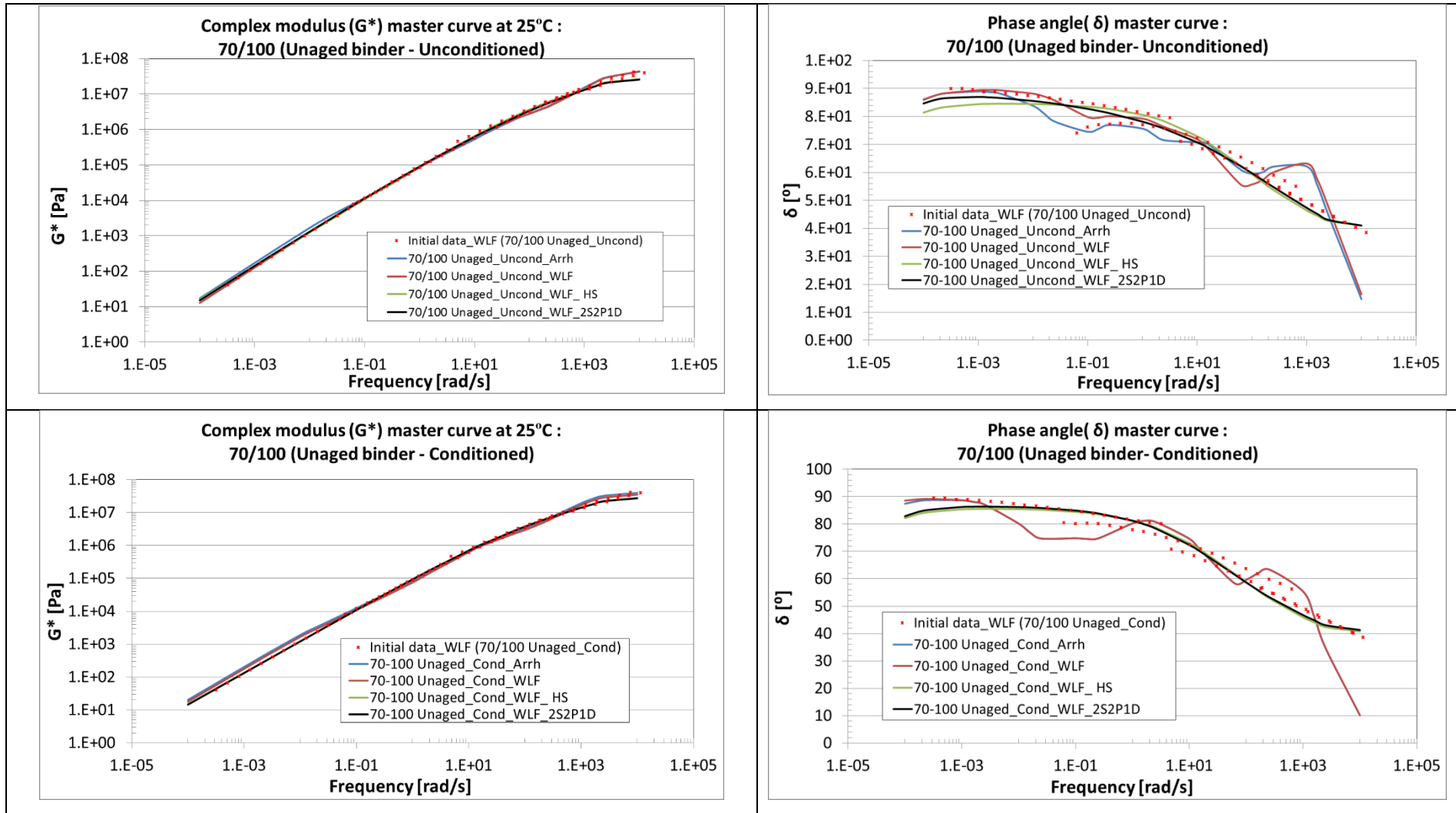
	Modelled data (SR1_PAV Conditioned)							
	Arrh Prony		WLF Prony		WLF HS		WLF 2S2P1D	
	G*	δ	G*	δ	G*	δ	G*	δ
R ² CA	0.99	0.84	0.99	0.87				
R ² Mec.	1.00	0.96	1.00	0.95	1.00	0.99	1.00	0.93
Reduced [rad/s]	G* [Pa]	δ [°]	G* [Pa]	δ [°]	G* [Pa]	δ [°]	G* [Pa]	δ [°]
0.0001	6.00E+0	65.62	3.75E+0	65.68	4.75E+0	57.85	4.67E+0	59.31
0.0001584	8.03E+0	61.67	5.03E+0	62.45	6.38E+0	57.83	6.31E+0	59.03
0.0002511	1.06E+0	60.80	6.66E+0	62.23	8.58E+0	57.79	8.53E+0	58.77
0.001	2.79E+0	59.93	1.85E+0	63.55	2.08E+0	57.60	2.09E+0	58.09
0.0015848	3.73E+0	57.35	2.54E+0	60.91	2.80E+0	57.50	2.81E+0	57.88
0.0025118	4.83E+0	56.62	3.37E+0	59.37	3.75E+0	57.40	3.78E+0	57.68
0.01	1.22E+0	58.80	8.67E+0	60.98	9.04E+0	56.96	9.12E+0	57.06
0.0158489	1.65E+0	56.30	1.19E+0	58.67	1.21E+0	56.77	1.22E+0	56.84
0.0251188	2.15E+0	54.51	1.57E+0	56.57	1.62E+0	56.56	1.63E+0	56.60
0.1	5.09E+0	56.23	3.79E+0	57.94	3.84E+0	55.74	3.87E+0	55.74
0.1584893	6.84E+0	53.97	5.16E+0	55.91	5.11E+0	55.39	5.15E+0	55.39
0.2511886	8.82E+0	51.82	6.74E+0	53.59	6.78E+0	55.00	6.84E+0	55.00
1	1.98E+0	53.62	1.53E+0	54.66	1.57E+0	53.55	1.58E+0	53.58
1.5848931	2.65E+0	51.40	2.06E+0	52.77	2.06E+0	52.96	2.08E+0	53.00
2.5118864	3.39E+0	48.46	2.65E+0	50.33	2.70E+0	52.32	2.72E+0	52.36
10	6.95E+0	50.19	5.69E+0	51.11	5.94E+0	50.06	6.00E+0	50.09
15.848931	9.25E+0	48.97	7.51E+0	49.23	7.67E+0	49.20	7.75E+0	49.22
62.831853	1.78E+0	43.66	1.48E+0	46.81	1.60E+0	46.36	1.61E+0	46.30
100	2.24E+0	44.66	1.93E+0	46.96	2.02E+0	45.33	2.05E+0	45.23
158.48931	2.86E+0	44.23	2.49E+0	44.87	2.55E+0	44.29	2.57E+0	44.14
251.18864	3.59E+0	42.49	3.09E+0	42.10	3.19E+0	43.23	3.22E+0	43.04
1000	6.79E+0	42.86	5.80E+0	41.02	6.04E+0	40.07	6.07E+0	39.74
1584.8931	8.59E+0	41.36	7.25E+0	38.32	7.39E+0	39.04	7.41E+0	38.67
2511.8864	1.05E+0	39.08	8.63E+0	35.05	9.00E+0	38.02	9.00E+0	37.63
10000	1.93E+0	40.39	1.41E+0	38.69	1.58E+0	35.07	1.56E+0	34.70

APPENDIX E

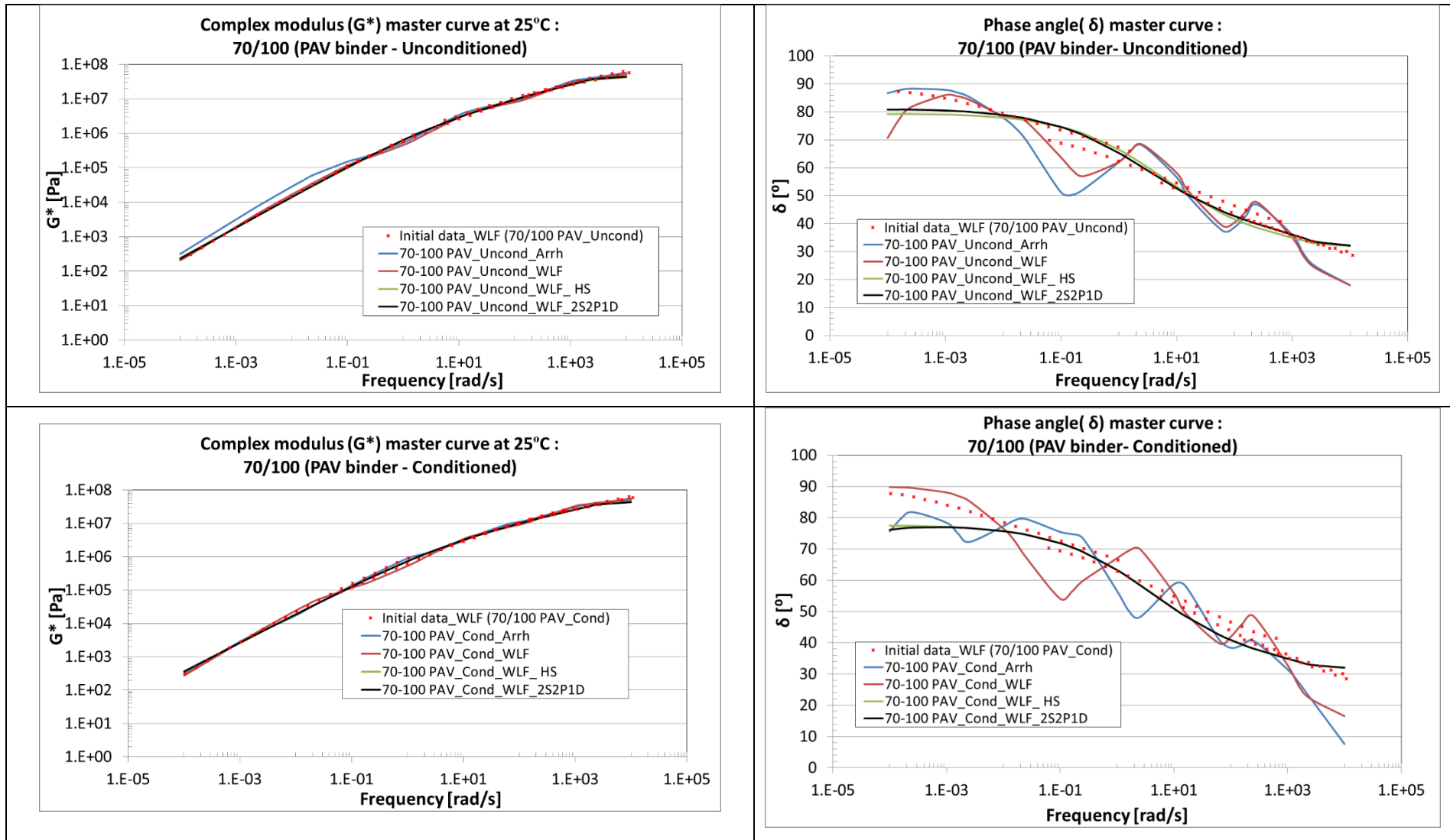
E.7 Complex moduli and phase angle graphs for different models

APPENDIX E

70/100

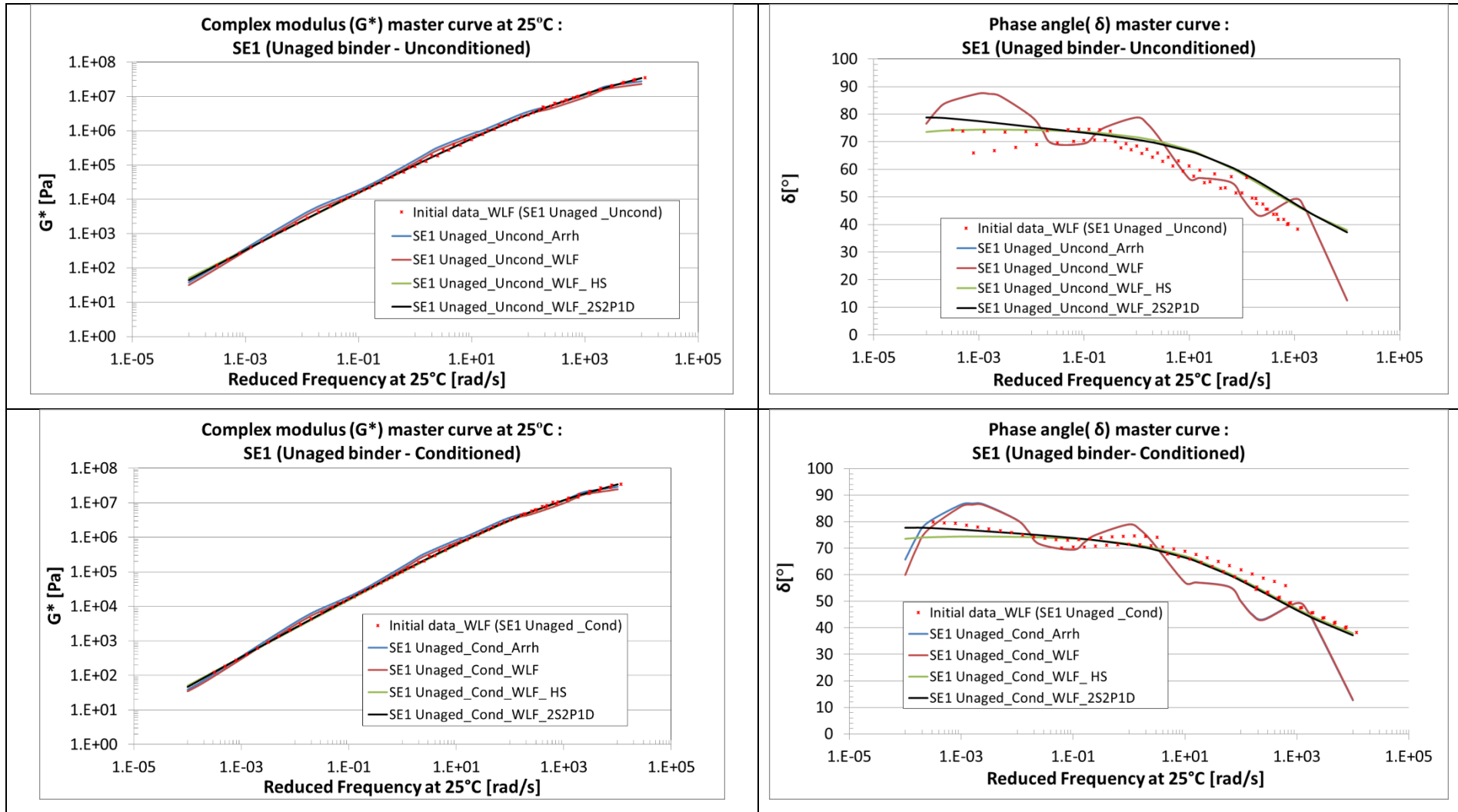


APPENDIX E

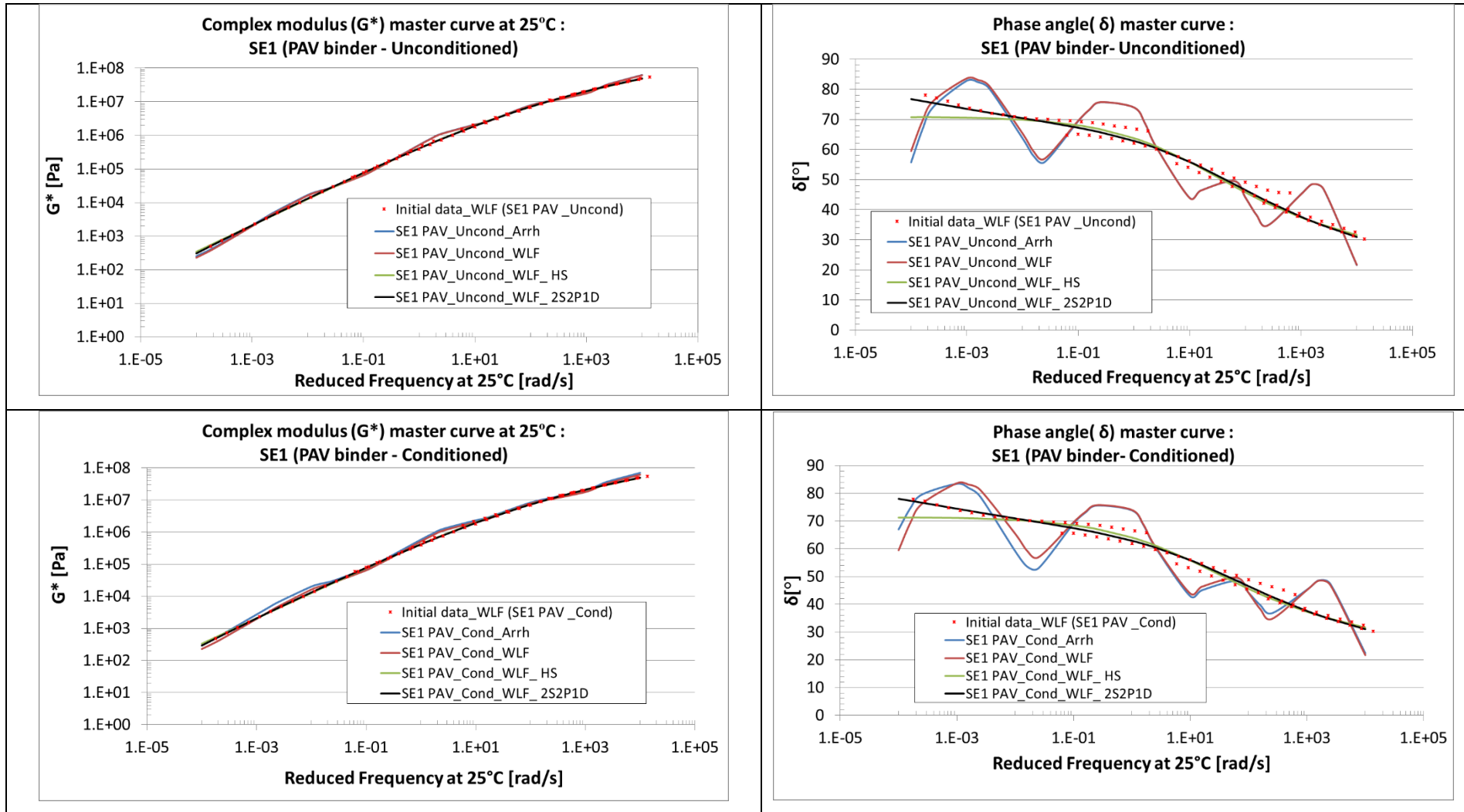


APPENDIX E

SE1

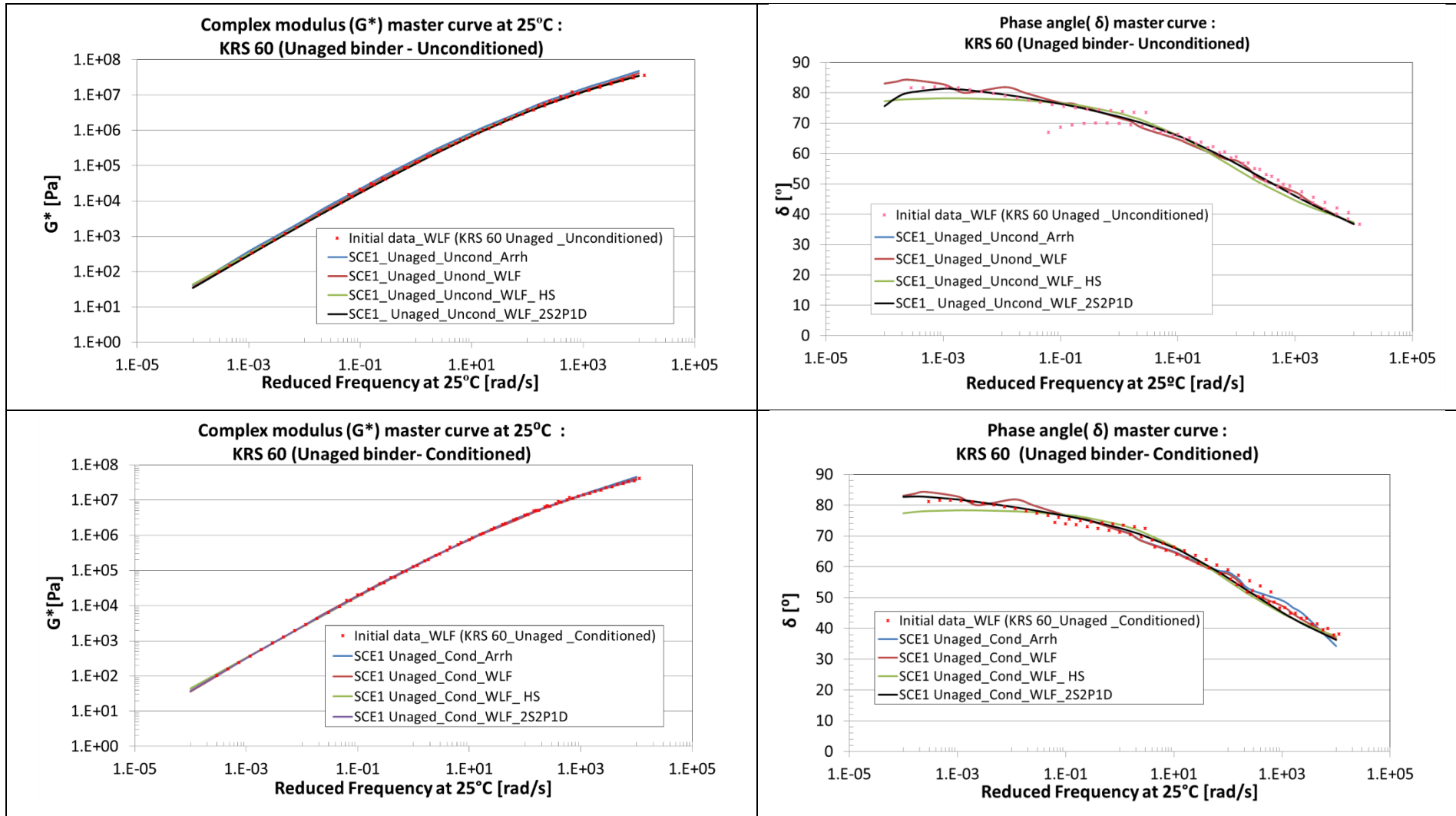


APPENDIX E

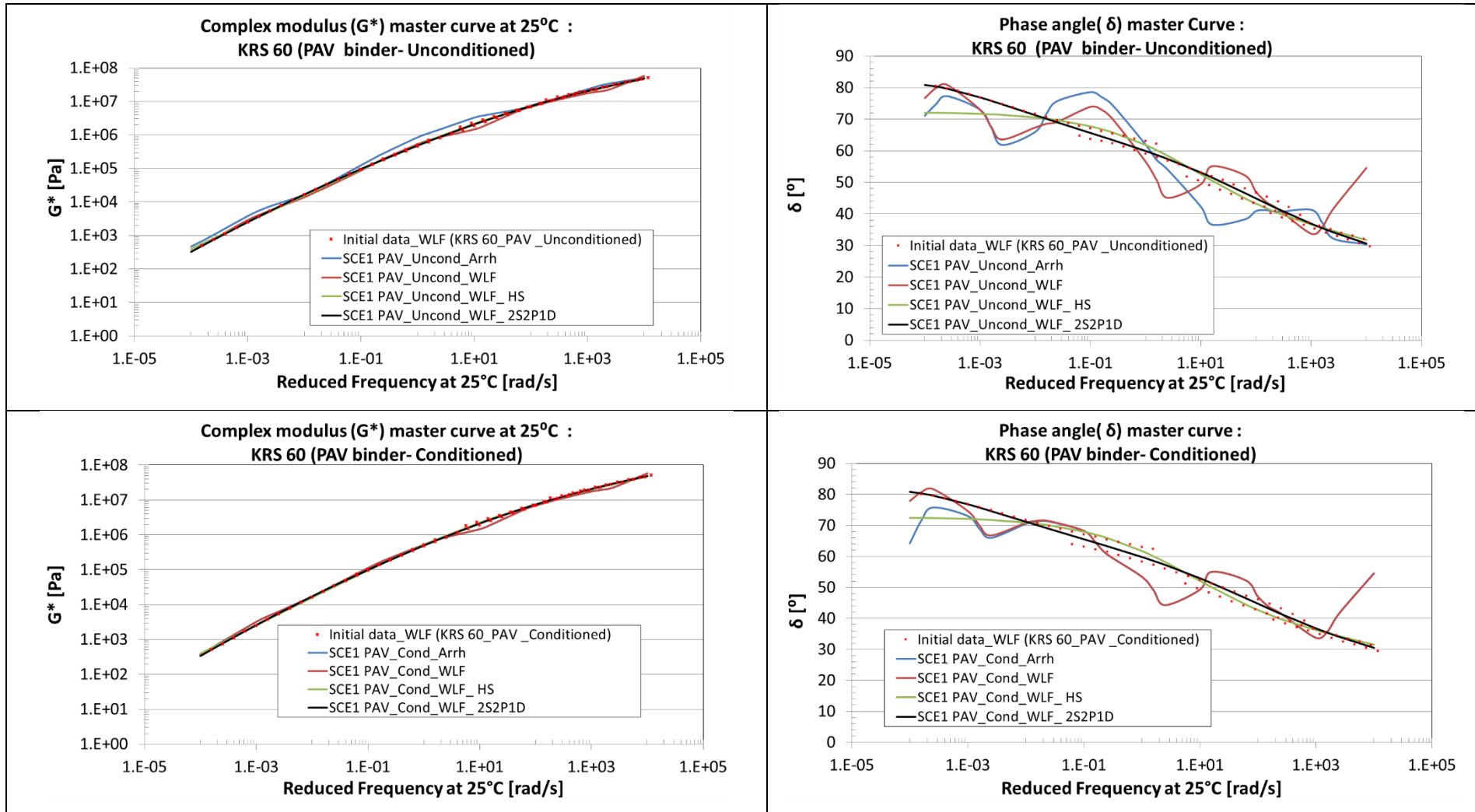


APPENDIX E

KRS 60

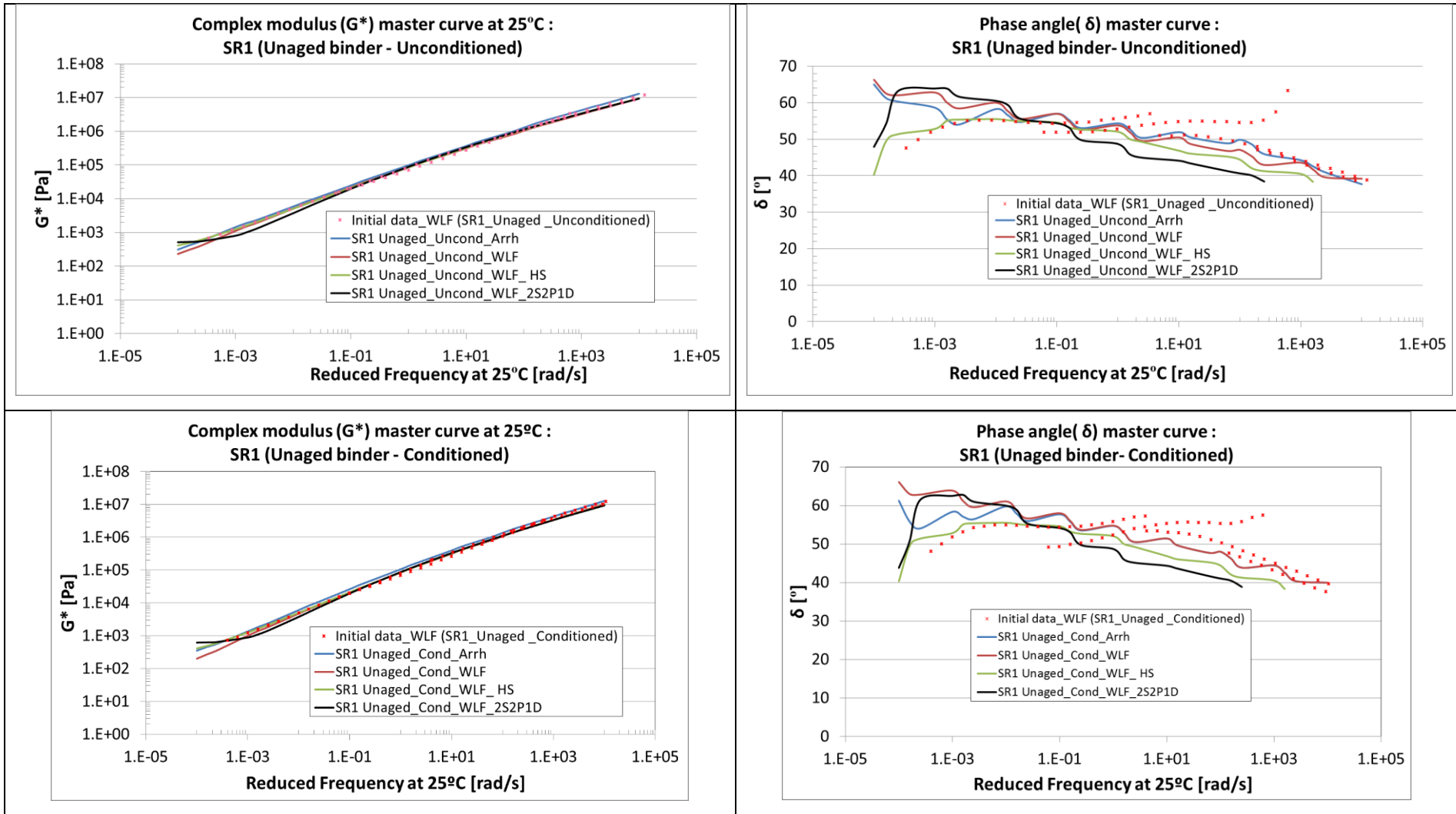


APPENDIX E

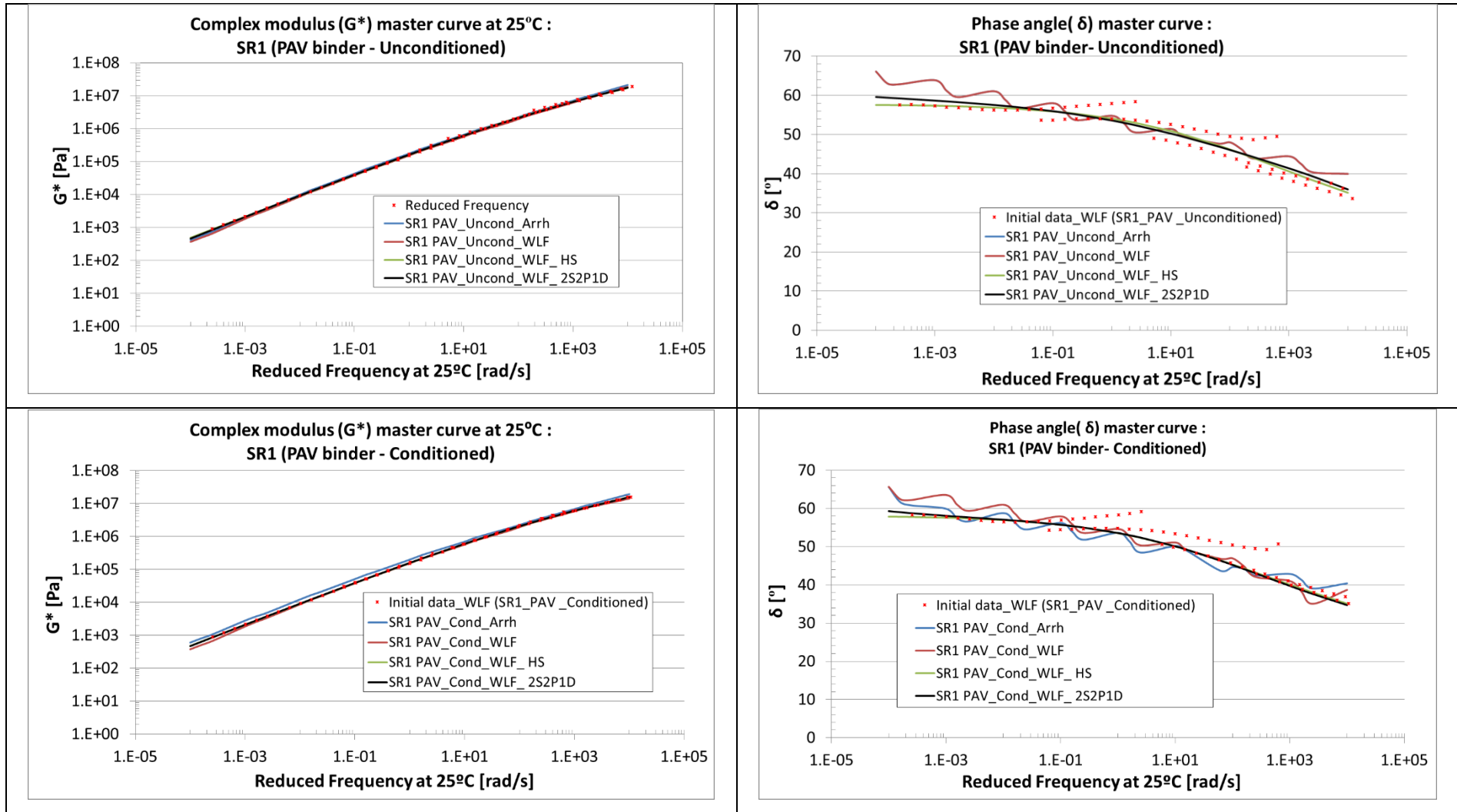


APPENDIX E

SR1



APPENDIX E





APPENDIX F

F COHESION AND ADHESION FATIGUE DAMAGE TESTING DATA

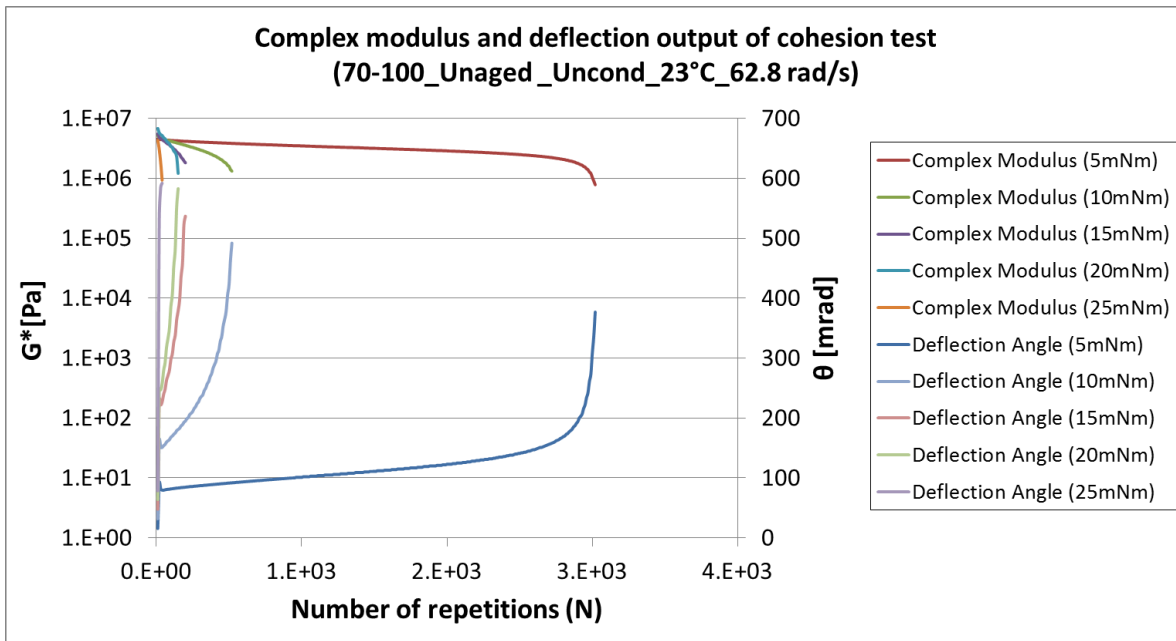
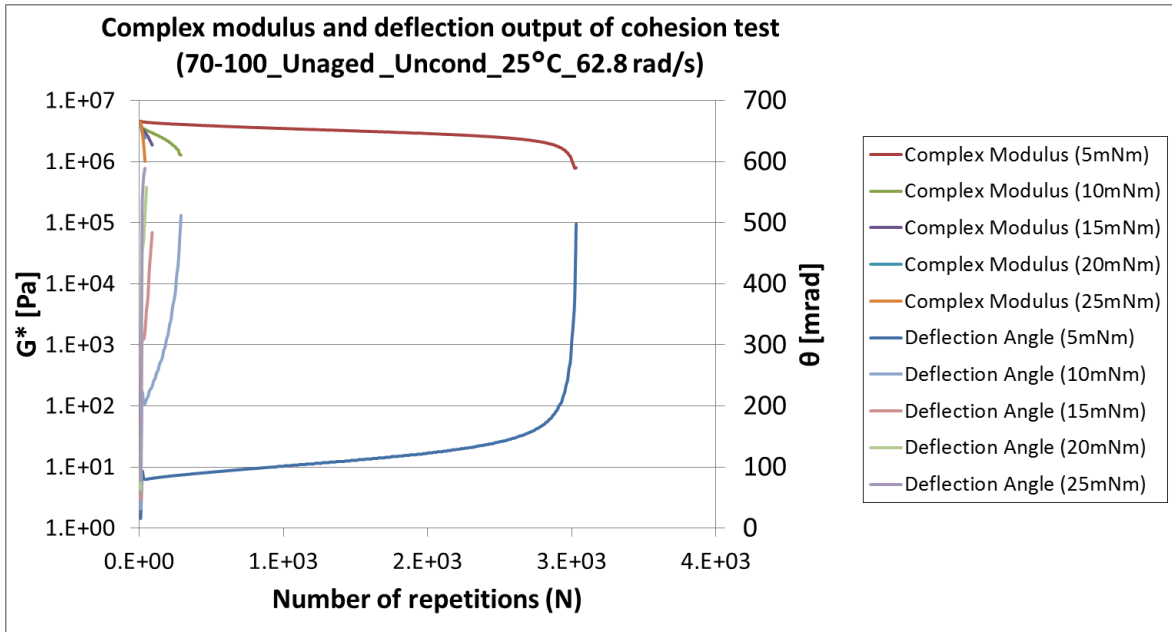
F.1 Complex modulus and deflection output data of cohesion fatigue tests:

Due to the size, the data are provided in a soft copy (see attached soft copy)



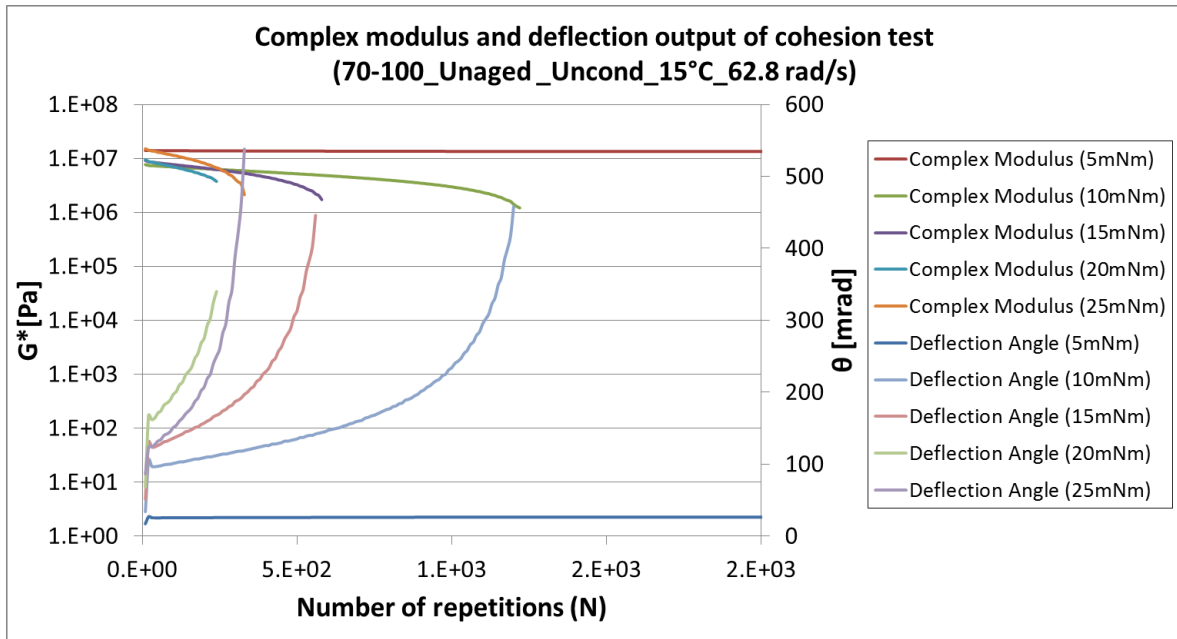
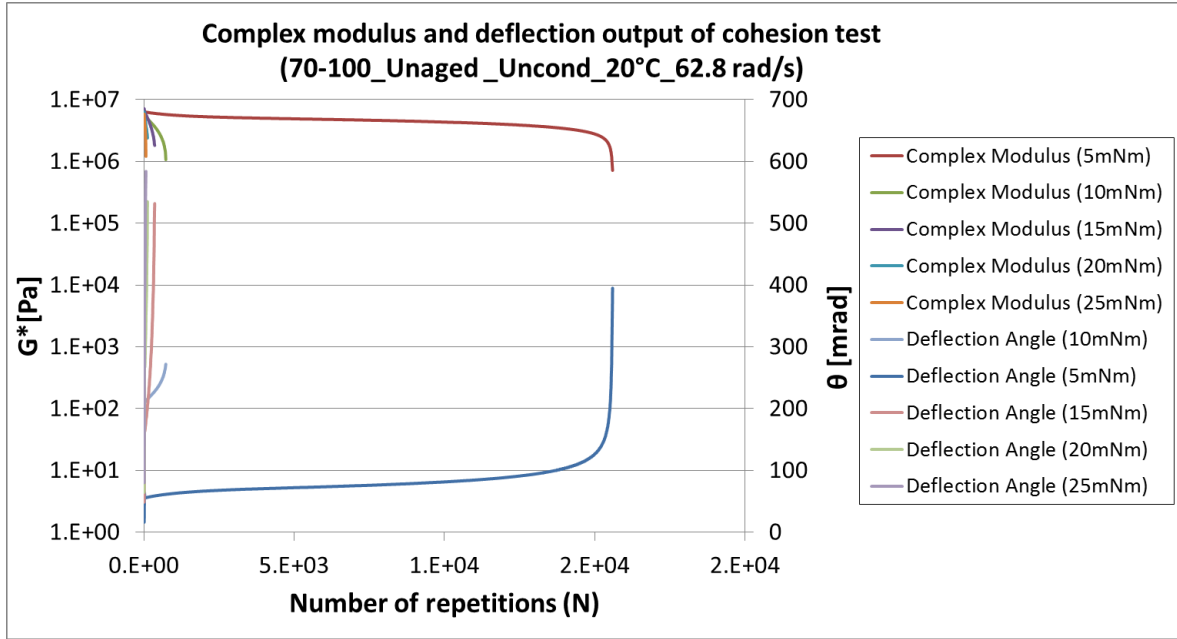
APPENDIX F

F.2 Complex modulus and deflection output graph of cohesion fatigue tests



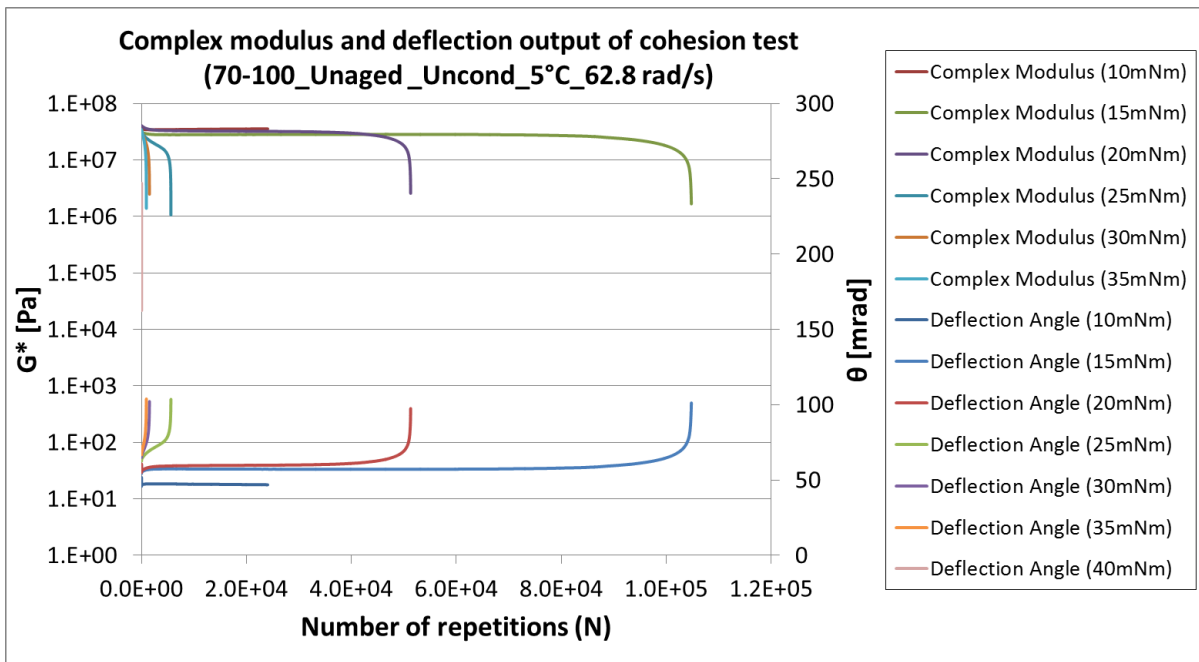
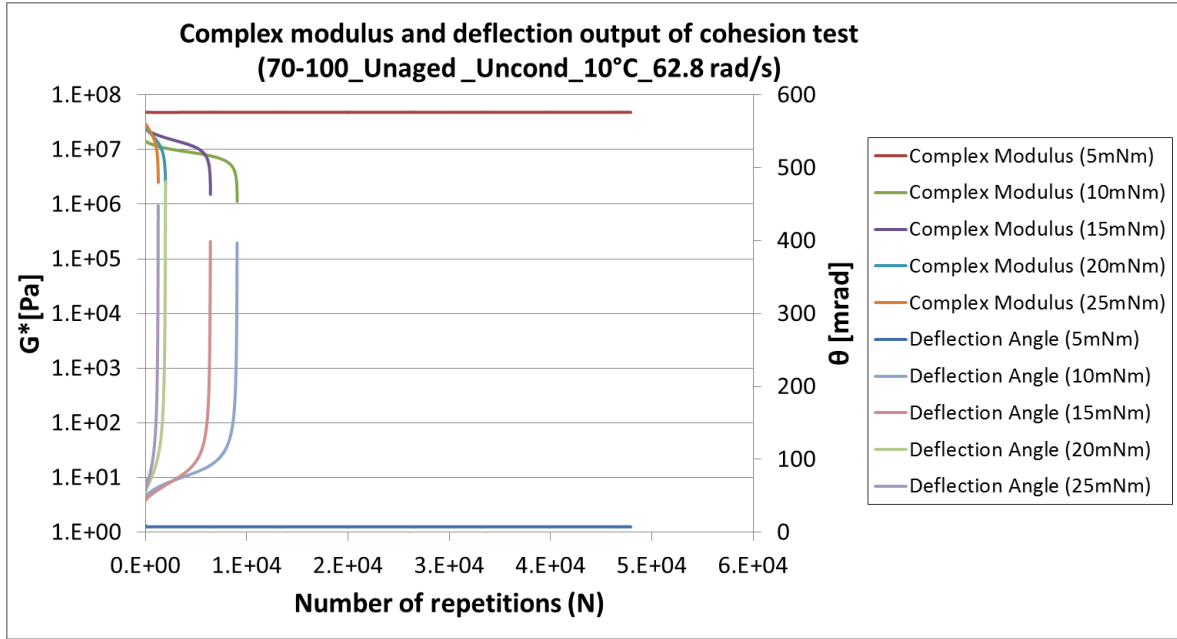


APPENDIX F



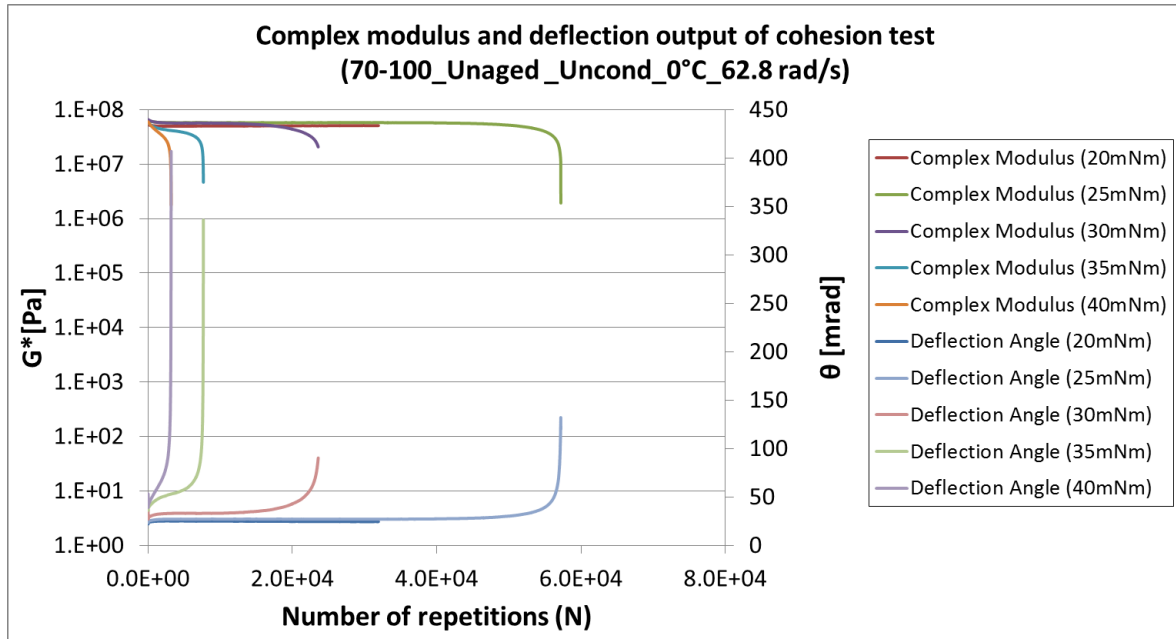


APPENDIX F





APPENDIX F



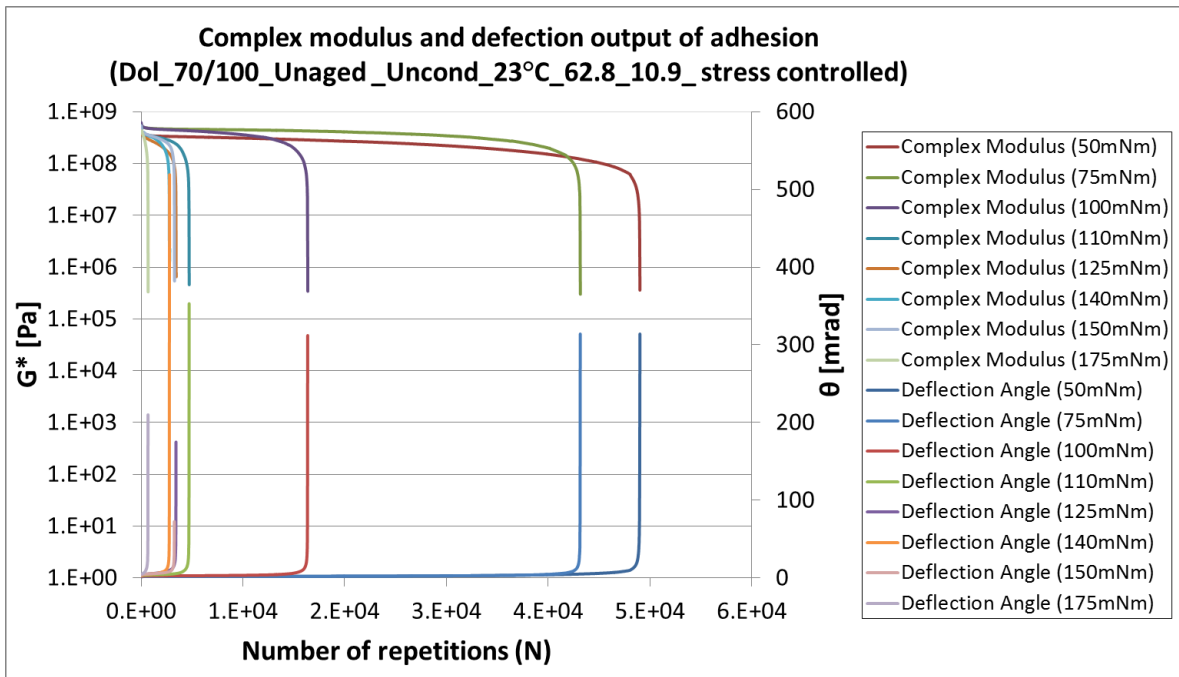
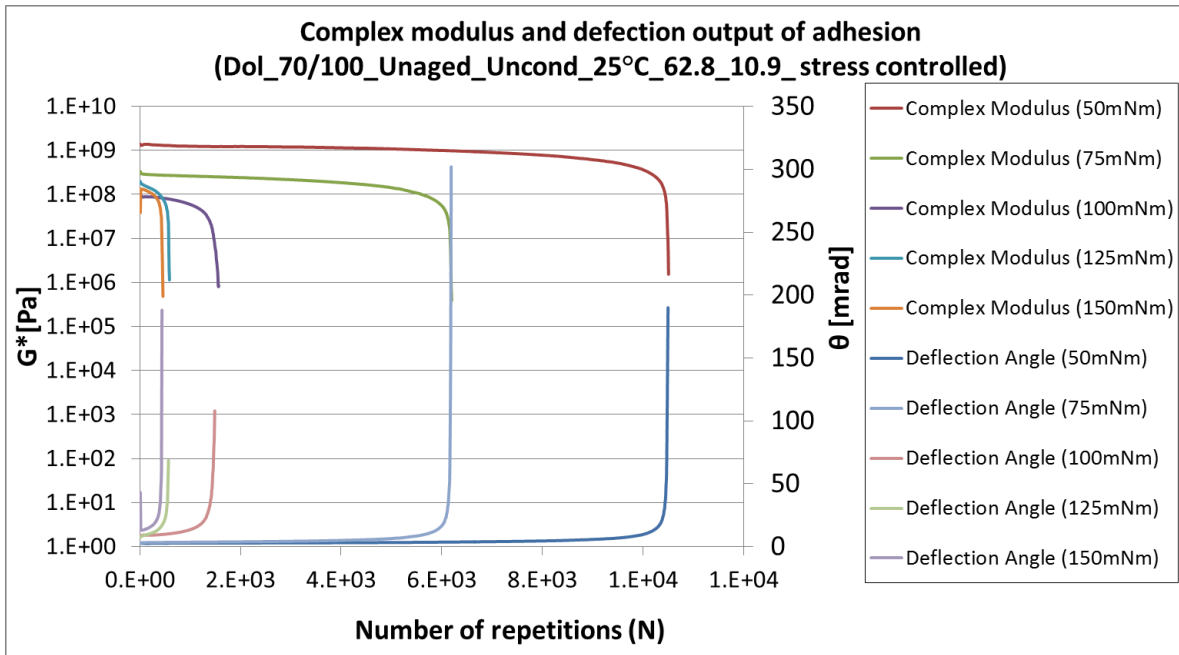
F.3 Complex modulus and deflection output data of adhesion fatigue damage tests

Due to the size, the data are provided in a soft copy (see attached soft copy)



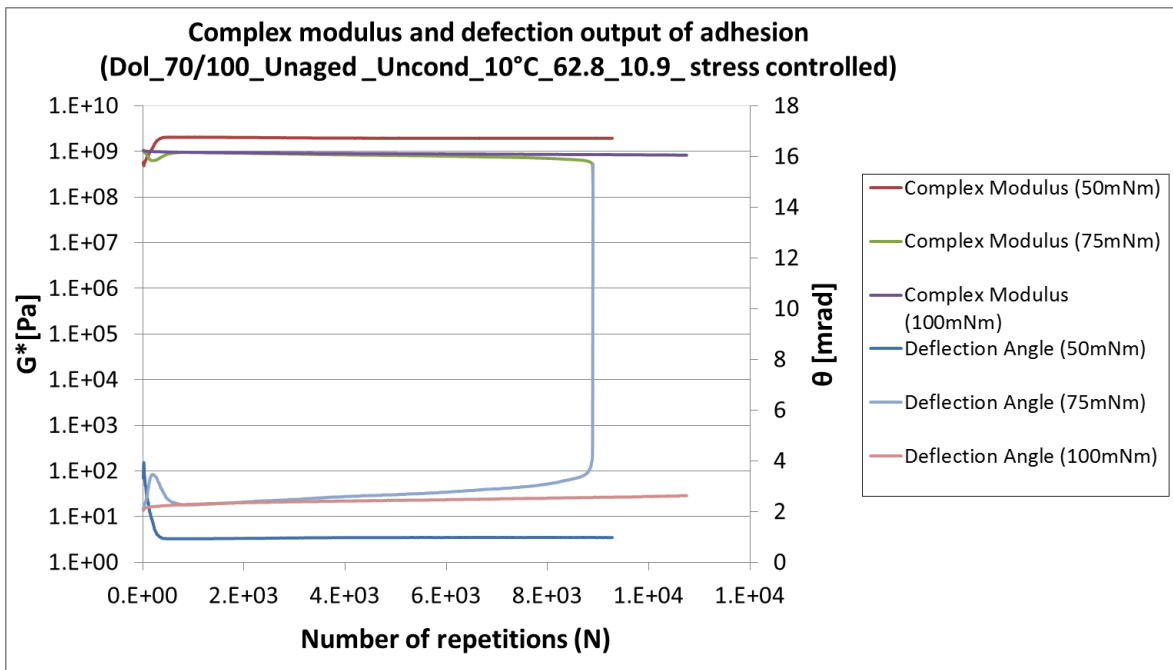
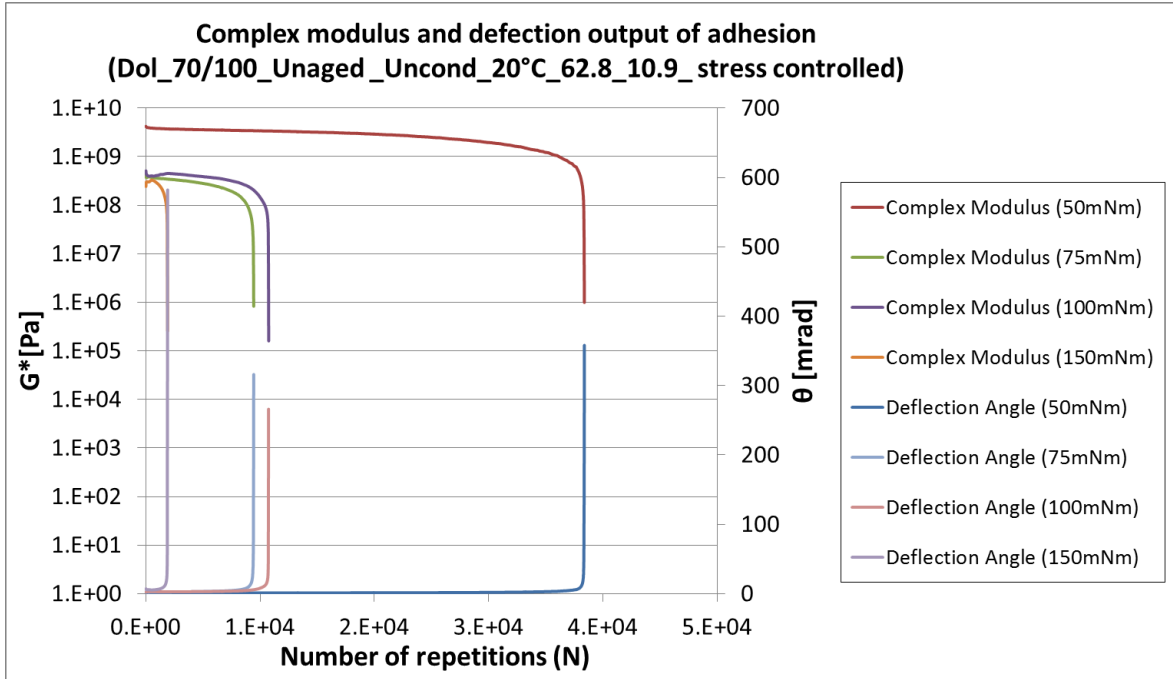
APPENDIX F

F.4 Complex modulus and deflection output graph of adhesion fatigue damage tests





APPENDIX F





G DATA ON AGEING MODEL OF SEAL'S BITUMEN

APPENDIX G

G.1 Initial information on the 70/100 bitumen recovered

Initial No	Province	Location	ROAD NO	Position sampled	Seal type	Age (Years)	Binder type	
							GPS X	GPS Y
								Cat 65% tack
								Cat 65% tack + Cat 65% Fog
								70/100
								70/100 + Cat 65% Fog
								Slurry for Cape Seals = Anionic 60%
DR 02175-OWT-3Yrs	WC	Kardoesie - Piekenierskloof	DR 02175	OWT	13mm + 7mm Double Seal	3	S32°34'46.2"	E018°55'17.8"
DR 1298-OWT-4Yrs	WC	Genadendal	DR 1298	OWT	13mm Cape Seal	4	S34°03'00.2"	E019°31'09.9"
DR 1298-SHDR-4Yrs	WC	Genadendal	DR 1298	SHDR	13mm Cape Seal	4	S34°03'00.2"	E019°31'09.9"
DR 1398-BWT-5Yrs	WC	Slanghoek	DR 1398	BWT	13mm + 7mm Double Seal	5	S33°32'41.3"	E019°12'21.5"
DR 1398-IWT-5Yrs	WC	Slanghoek	DR 1398	IWT	13mm + 7mm Double Seal	5	S33°32'41.3"	E019°12'21.5"
DR 02175-BWT-6Yrs	WC	Kardoesie - Piekenierskloof	DR 02175	BWT	13mm + 7mm Double Seal	6	S32°36'12.2"	E018°56'04.2"
DR 02175-IWT-6Yrs	WC	Kardoesie - Piekenierskloof	DR 02175	IWT	13mm + 7mm Double Seal	6	S32°36'12.2"	E018°56'04.2"
N 10/3-BWT-9Yrs	EC	Cradock-Cookhouse	N 10/3	BWT	19mm Cape Seal	9	S32°37'13.6"	E025°53'33.9"
N 10/3-IWT-9Yrs	EC	Cradock-Cookhouse	N 10/3	IWT	19mm Cape Seal	9	S32°37'13.6"	E025°53'33.9"
N 10/3-OWT-9Yrs	EC	Cradock-Cookhouse	N 10/3	OWT	19mm Cape Seal	9	S32°37'13.6"	E025°53'33.9"
DR 2216-BWT-10Yrs	WC	Vredendal na Strandfontein	DR 2216	BWT	13mm Single Seal	10	S31°36'56.8"	E018°15'31.4"
DR 2216-IWT-10Yrs	WC	Vredendal na Strandfontein	DR 2216	IWT	13mm Single Seal	10	S31°36'56.8"	E018°15'31.4"
MR 174-OWT-10Yrs	WC	Malmesbury	MR 174	OWT	19mm Cape Seal	10	S33°30'35.7"	E018°44'04.8"
MR 174-SHDR-10Yrs	WC	Malmesbury	MR 174	SHDR	19mm Cape Seal	10	S33°30'35.7"	E018°44'04.8"
N 6/5-OWT-11Yrs	EC	Aliwal Noord 2	N 6/5	OWT	19mm Cape Seal	11	S30°46'11.9"	E026°44'54.8"
N 6/5-SHDR-11Yrs	EC	Aliwal Noord 2	N 6/5	SHDR	19mm Cape Seal	11	S30°46'11.9"	E026°44'54.8"
DR 1452 -BWT-12Yrs	WC	Kersieplaas Lakenvlei	DR 1452	BWT	13mm Single Seal	12	S33°20'14.6"	E019°33'02.5"
DR 1452 -OWT-12Yrs	WC	Kersieplaas Lakenvlei	DR 1452	OWT	13mm Single Seal	12	S33°20'14.6"	E019°33'02.5"
MR 269-OWT-13Yrs	WC	Hemel en Aarde- Hermanus	MR 269	OWT	13mm + 7mm Double Seal	13	S34°23'12.5"	E019°15'11.0"
N 6/5-OWT-13Yrs	EC	Aliwal Noord	N 6/5	OWT	19mm Cape Seal	13	S30°43'03.9"	E026°42'29.3"
MR 269-SHDR-13Yrs	WC	Hemel en Aarde- Hermanus	MR 269	SHDR	13mm + 7mm Double Seal	13	S34°23'12.5"	E019°15'11.0"
N 6/5-SHDR-13Yrs	EC	Aliwal Noord	N 6/5	SHDR	19mm Cape Seal	13	S30°43'03.9"	E026°42'29.3"
MR 188-OWT-15Yrs	WC	Durbanville	MR 188	OWT	19mm Cape Seal	15	S33°43'26.8"	E018°41'47.7"
DR 1123-IWT-17Yrs	WC	Klipheuwel	DR 1123	IWT	13mm + 7mm Double Seal	17	S33°41'48.7"	E018°32'32.3"
MR 536 -BWT-19Yrs	WC	Eendekuiipad na Kruiwapad	MR 536	BWT	9mm Single Seal	19	S32°41'45.6"	E018°52'54.6"
MR 536 -IWT-19Yrs	WC	Eendekuiipad na Kruiwapad	MR 536	IWT	9mm Single Seal	19	S32°41'45.6"	E018°52'54.6"
P 1398-OWT-22Yrs	WC	Rawsonville	P 1398	OWT	13mm + 7mm Double Seal	22	S33°40'52.3"	E019°17'32.9"
P 1398-OWT-23Yrs	WC	Rawsonville	P 1398	OWT	19mm Cape Seal	23	S33°41'04.3"	E19°18'06.6"

APPENDIX G

G.2 Initial information on the SE1 bitumen recovered

Initial No	Province	Location	ROAD NO	Position sample	Seal type	Age (Years)	Binder type	
							GPS X	GPS Y
	KZN:	Kwazulu Natal		IWT	Inner Wheel Track		Binder type	Cat 65% tack
	EC:	Eastern Cap		OWT	Outer Wheel Track			Cat 65% tack + Cat 65% Fog
	NC	Northern Cap		BWT	Between Wheel Track			70/100
				SHDR	Shoulder			70/100 + Cat 65% Fog
								Slurry for Cape Seals = Anionic 60%
Initial No	Province	Location	ROAD NO	Position sample	Seal type	Age (Years)	GPS X	GPS Y
N 2/32-OWT-2Yrs	KZN	Mbekakanye	N 2/32	OWT	13mm + 7mm Double Seal	2	S27°21'44.6"	E031°31'11.6"
N 2/32-SHDR-2Yrs	KZN	Mbekakanye	N 2/32	SHDR	13mm + 7mm Double Seal	2	S27°21'44.6"	E031°31'11.6"
N 1/29-OWT-6Yrs	Limpopo	Beitbridge	N 1/29	OWT	19mm+6mm+6mm Multiple	6	S22°16'8.64"	E29°59'46.13"
N 2/32-OWT-6Yrs	KZN	Pongola	N 2/32	OWT	13mm + 7mm Double Seal	6	S27°21'20.7"	E031°40'22.4"
N 6/4-OWT-6Yrs	EC	Sterkstroom-Aliwal Noord	N 6/4	OWT	19mm+6mm+6mm Multiple	6	S31°16'13.6"	E026°44'02.7"
N 1/29-SHDR-6Yrs	Limpopo	Beitbridge	N 1/29	SHDR	19mm+6mm+6mm Multiple	6	S22°16'8.64"	E29°59'46.13"
N 2/32-SHDR-6Yrs	KZN	Pongola	N 2/32	SHDR	13mm + 7mm Double Seal	6	S27°21'20.7"	E031°40'22.4"
N 6/4-SHDR-6Yrs	EC	Sterkstroom-Aliwal Noord	N 6/4	SHDR	19mm+6mm+6mm Multiple	6	S31°16'13.6"	E026°44'02.7"
N 2/31-BWT-7Yrs	KZN	Pongola dam 1	N 2/31	BWT	19mm+6mm+6mm Multiple	7	S27°24'31.8"	E031°51'03.6"
N 10/2-OWT-7Yrs	EC	Golden Valley	N 10/2	OWT	19mm+6mm+6mm Multiple	7	S32°51'41.0"	E025°47'31.8"
N 2/31-OWT-7Yrs	KZN	Pongola dam 1	N 2/31	OWT	19mm+6mm+6mm Multiple	7	S27°24'31.8"	E031°51'03.6"
N 8/8-OWT-7Yrs	NC	Kimberley	N 8/8	OWT	19mm+9mm Double seal	7	S28°48'34.0"	E24°48'38.4"
N 10/2-SHDR-7Yrs	EC	Golden Valley	N 10/2	SHDR	19mm+6mm+6mm Multiple	7	S32°51'41.0"	E025°47'31.8"
N 8/8-SHDR-7Yrs	NC	Kimberley	N 8/8	SHDR	19mm+9mm Double seal	7	S28°48'34.0"	E24°48'38.4"
N 6/4-OWT-10Yrs	EC	Queenstown	N 6/4	OWT	19mm+6mm+6mm Multiple	10	S31°53'01.1"	E026°47'42.8"
N 6/4-SHDR-10Yrs	EC	Queenstown	N 6/4	SHDR	19mm+6mm+6mm Multiple	10	S31°53'01.1"	E026°47'42.8"
N 1/29-OWT-10Yrs	Limpopo	Musina	N 1/29	OWT	19mm+6mm+6mm Multiple	10	S22°26'38.4"	E030°00'00.8"
N 2/31-OWT-12Yrs	KZN	St Lucia	N 2/31	OWT	13mm + 7mm Double Seal	12	S27°50'32.38"	E032°12'26.68"
N 2/31-SHDR-12Yrs	KZN	St Lucia	N 2/31	SHDR	13mm + 7mm Double Seal	12	S27°50'32.38"	E032°12'26.68"
N 2/31-SHDR-12Yrs	KZN	St Lucia	N 2/31	SHDR	13mm + 7mm Double Seal	12	S27°50'32.38"	E032°12'26.68"
N10/3-OWT-24Yrs	EC	DaggaBoer	N10/3	OWT	19mm+6mm+6mm Multiple	24	S32°31'32.2"	E025°50'10.0"

APPENDIX G

G.3 Prony series parameters for recovered bitumen from field-aged seals
Prony parameters for recovered bitumen from 70/100 field-aged seals

model parameters (70/100) recovered from 28 field-aged seals (Part 1)												
Type of bitumen	G_0		term1	term2	term3	term4	term5	term6	term7	term8	term9	term10 (residual)
DR 02175-OWT-3Yrs	1.05E+08	α_j	6.01E-04	4.99E-01	2.67E-01	2.06E-01	3.96E-05	2.65E-02	2.26E-04	6.75E-05	3.22E-05	7.37E-04
		τ_j	6.19E+01	3.20E-04	2.79E-03	2.81E-02	1.06E-03	6.97E-01	1.42E+00	6.15E+02	3.35E+00	1.45E+01
DR 1298-OWT-4Yrs	7.86E+07	α_j	5.99E-04	6.60E-01	1.75E-01	1.39E-01	3.96E-05	2.45E-02	2.26E-04	6.74E-05	3.22E-05	7.36E-04
		τ_j	2.84E+00	3.20E-04	2.78E-03	2.79E-02	1.06E-03	6.94E-01	5.07E-01	4.00E+02	7.48E-01	1.45E+01
DR 1298-SHDR-4Yrs	7.86E+07	α_j	6.00E-04	5.93E-01	2.15E-01	1.65E-01	3.96E-05	2.54E-02	2.26E-04	6.74E-05	3.22E-05	7.37E-04
		τ_j	1.18E+01	3.20E-04	2.78E-03	2.79E-02	1.06E-03	6.94E-01	1.42E+00	6.14E+02	3.35E+00	1.45E+01
DR 1398-BWT-5Yrs	7.51E+07	α_j	6.58E-04	5.74E-01	2.21E-01	1.71E-01	3.99E-05	3.11E-02	2.32E-04	6.37E-05	3.23E-05	1.36E-03
		τ_j	3.53E+00	6.04E-04	3.04E-03	2.88E-02	1.06E-03	6.38E-01	5.00E-01	4.79E+02	7.48E-01	3.05E+01
DR 1398-IWT-5Yrs	9.17E+07	α_j	6.03E-04	6.52E-01	1.83E-01	1.37E-01	3.96E-05	2.58E-02	2.26E-04	7.09E-05	3.22E-05	7.63E-04
		τ_j	2.86E+00	2.93E-04	2.79E-03	2.79E-02	1.06E-03	7.25E-01	5.07E-01	4.17E+02	7.49E-01	1.50E+01
DR 02175-BWT-6Yrs	1.24E+08	α_j	6.75E-04	5.16E-01	3.80E-01	3.04E-03	3.96E-05	9.99E-02	2.28E-04	7.14E-05	3.22E-05	7.97E-04
		τ_j	2.09E+01	5.00E-05	1.04E-03	3.01E-02	1.06E-03	9.06E-02	5.04E-01	4.12E+02	9.96E-01	1.63E+01
DR 02175-IWT-6Yrs	1.14E+08	α_j	5.15E-04	6.45E-01	1.91E-01	1.33E-01	3.96E-05	3.00E-02	2.27E-04	6.38E-05	3.22E-05	7.01E-04
		τ_j	3.47E+01	2.03E-04	2.79E-03	2.60E-02	1.06E-03	5.64E-01	5.06E-01	3.90E+02	7.98E-01	1.38E+01
N 10/3-BWT-9Yrs	1.14E+08	α_j	5.16E-04	6.51E-01	1.88E-01	1.31E-01	3.96E-05	2.98E-02	2.27E-04	6.39E-05	3.22E-05	7.01E-04
		τ_j	3.77E+01	2.03E-04	2.79E-03	2.60E-02	1.06E-03	5.65E-01	5.06E-01	3.90E+02	7.98E-01	1.38E+01
N 10/3-IWT-9Yrs	1.13E+08	α_j	5.16E-04	6.74E-01	1.72E-01	1.22E-01	3.96E-05	2.93E-02	2.27E-04	6.39E-05	3.22E-05	7.01E-04
		τ_j	3.97E+01	2.03E-04	2.79E-03	2.60E-02	1.06E-03	5.65E-01	5.06E-01	3.90E+02	7.98E-01	1.38E+01
N 10/3-OWT-9Yrs	1.14E+08	α_j	5.16E-04	6.74E-01	1.72E-01	1.22E-01	3.96E-05	2.93E-02	2.27E-04	6.39E-05	3.22E-05	7.01E-04
		τ_j	3.97E+01	2.03E-04	2.79E-03	2.60E-02	1.06E-03	5.65E-01	5.06E-01	3.90E+02	7.98E-01	1.38E+01
DR 2216-BWT-10Yrs	8.91E+07	α_j	7.63E-04	4.94E-01	3.51E-01	1.24E-01	3.98E-05	2.56E-02	2.56E-04	1.80E-04	3.26E-05	3.87E-03
		τ_j	1.62E+02	1.20E-04	1.71E-03	4.60E-02	1.06E-03	1.10E+00	4.73E-01	2.12E+03	7.88E-01	1.78E+01
DR 2216-IWT-10Yrs	7.44E+07	α_j	8.06E-04	4.99E-01	3.49E-01	1.19E-01	3.98E-05	2.77E-02	2.56E-04	1.75E-04	3.26E-05	4.00E-03
		τ_j	1.66E+02	2.64E-04	3.38E-03	6.00E-02	1.06E-03	1.40E+00	4.74E-01	1.81E+03	7.88E-01	1.95E+01
MR 174-OWT-10Yrs	1.10E+08	α_j	4.27E-04	6.74E-01	1.67E-01	1.30E-01	3.96E-05	2.68E-02	2.27E-04	6.19E-05	3.22E-05	7.04E-04
		τ_j	5.92E+01	2.40E-04	2.85E-03	2.42E-02	1.06E-03	5.55E-01	5.06E-01	4.04E+02	7.98E-01	1.29E+01
MR 174-SHDR-10Yrs	1.15E+08	α_j	5.16E-04	6.70E-01	1.75E-01	1.24E-01	3.96E-05	2.94E-02	2.27E-04	6.39E-05	3.22E-05	7.01E-04
		τ_j	6.98E+01	2.03E-04	2.79E-03	2.60E-02	1.06E-03	5.65E-01	5.06E-01	3.90E+02	7.98E-01	1.38E+01
N 6/5-OWT-11Yrs	8.97E+08	α_j	3.14E-03	9.24E-03	6.97E-02	7.80E-04	1.33E-04	3.61E-02	2.07E-02	1.48E-01	1.45E-05	9.84E-07
		τ_j	2.43E-01	3.22E-02	8.28E-05	2.03E+00	1.99E+01	6.41E-04	4.47E-03	1.61E-06	2.44E+02	4.00E+03

APPENDIX G

model parameters (70/100) recovered from 28 field-aged seals (Part 2)												
Type of bitumen	G_0		term1	term2	term3	term4	term5	term6	term7	term8	term9	term10 (residual)
N 6/5-SHDR-11Yrs	6.65E+08	α_j	1.58E-03	5.47E-03	4.56E-02	2.89E-04	3.76E-05	2.88E-02	1.49E-02	8.27E-02	1.19E-01	2.59E-06
		τ_j	2.20E+00	2.64E-01	6.11E-04	2.41E+01	3.02E+02	4.29E-03	3.28E-02	7.45E-05	2.64E-07	4.92E+03
DR 1452 -BWT-12Yrs	9.32E+08	α_j	2.26E-03	7.09E-03	5.13E-02	4.60E-04	6.90E-05	3.15E-02	1.65E-02	9.59E-02	3.75E-01	8.69E-06
		τ_j	3.25E+00	3.17E-01	4.52E-04	3.80E+01	4.51E+02	4.15E-03	3.58E-02	3.04E-05	5.05E-07	5.97E+03
DR 1452 -OWT-12Yrs	1.67E+09	α_j	8.28E-04	5.04E-03	2.79E-02	2.28E-04	4.39E-05	1.73E-02	1.03E-02	3.87E-01	6.33E-06	2.16E-03
		τ_j	5.75E+00	1.04E-01	2.25E-04	5.52E+01	6.33E+02	1.80E-03	1.40E-02	2.34E-06	7.89E+03	7.44E-01
MR 269-OWT-13Yrs	1.36E+09	α_j	2.79E-04	3.28E-03	2.52E-02	5.68E-05	3.22E-06	1.48E-02	7.74E-03	4.88E-02	9.16E-07	1.08E-03
		τ_j	5.74E+00	1.15E-01	4.21E-04	6.44E+01	6.30E+02	2.81E-03	1.77E-02	4.49E-05	5.78E+03	7.86E-01
N 6/5-OWT-13Yrs	1.43E+09	α_j	2.93E-04	3.08E-03	2.53E-02	5.90E-05	8.41E-06	1.42E-02	7.23E-03	5.31E-02	9.16E-07	1.06E-03
		τ_j	6.12E+00	1.13E-01	4.06E-04	5.66E+01	6.09E+02	2.73E-03	1.71E-02	4.65E-05	7.41E+03	7.86E-01
MR 269-SHDR-13Yrs	3.71E+08	α_j	2.18E-03	9.07E-03	1.47E-01	4.04E-04	3.98E-05	7.02E-02	2.91E-02	4.05E-01	1.82E-01	3.22E-06
		τ_j	2.96E+00	2.79E-01	1.64E-04	3.68E+01	6.37E+02	2.14E-03	2.47E-02	2.54E-06	7.61E-06	9.67E+03
N 6/5-SHDR-13Yrs	4.76E+08	α_j	2.29E-03	9.80E-03	1.46E-01	4.02E-04	3.74E-05	7.50E-02	3.20E-02	4.04E-01	1.81E-01	2.38E-06
		τ_j	2.98E+00	2.92E-01	1.64E-04	3.53E+01	6.12E+02	2.25E-03	2.57E-02	3.65E-06	1.92E-06	9.71E+03
MR 188-OWT-15Yrs	2.11E+09	α_j	3.67E-04	3.55E-03	2.08E-02	7.20E-05	9.33E-06	1.34E-02	7.67E-03	3.87E-02	9.99E-07	1.28E-03
		τ_j	7.30E+00	1.26E-01	4.11E-04	6.90E+01	6.93E+02	2.80E-03	1.85E-02	3.89E-05	6.25E+03	9.06E-01
DR 1123-IWT-17Yrs	1.81E+09	α_j	3.42E-03	8.09E-03	4.15E-02	9.89E-04	2.02E-04	2.31E-02	1.40E-02	1.11E-01	2.48E-05	3.71E-06
		τ_j	2.96E-01	3.18E-02	6.11E-05	3.03E+00	3.50E+01	5.71E-04	4.25E-03	1.10E-11	4.19E+02	5.01E+03
MR 536 -BWT-19Yrs	1.12E+09	α_j	1.06E-03	3.27E-03	2.79E-02	2.77E-04	5.20E-05	1.65E-02	8.05E-03	4.93E-02	3.73E-01	7.91E-06
		τ_j	7.12E+00	8.64E-01	1.65E-03	6.31E+01	6.11E+02	1.37E-02	1.10E-01	1.66E-04	1.94E-06	7.00E+03
MR 536 -IWT-19Yrs	1.66E+09	α_j	3.46E-03	7.61E-03	3.50E-02	1.16E-03	2.44E-04	2.08E-02	1.32E-02	6.65E-01	3.45E-05	5.70E-06
		τ_j	3.04E-01	3.38E-02	6.00E-05	3.15E+00	3.68E+01	5.63E-04	4.26E-03	2.60E-10	4.29E+02	4.83E+03
P 1398-OWT-22Yrs	3.50E+09	α_j	1.07E-03	2.78E-03	1.86E-02	3.03E-04	6.28E-05	9.86E-03	5.72E-03	9.43E-01	9.39E-06	9.90E-07
		τ_j	5.62E-01	7.19E-02	1.15E-04	4.67E+00	4.20E+01	1.20E-03	9.49E-03	1.50E-10	4.24E+02	5.41E+03
P 1398-OWT-23Yrs	3.67E+09	α_j	1.07E-03	2.77E-03	1.81E-02	3.09E-04	6.50E-05	9.61E-03	5.63E-03	9.43E-01	9.45E-06	9.90E-07
		τ_j	5.66E-01	7.22E-02	1.14E-04	4.76E+00	4.34E+01	1.20E-03	9.50E-03	1.50E-10	4.39E+02	5.46E+03

APPENDIX G

Prony parameters for recovered bitumen from SE1 field-aged seals

model parameters(SE1) recovered from 21 field-aged seals (Part 1)												
Type of bitumen	G_0		term1	term2	term3	term4	term5	term6	term7	term8	term9	term10 (residual)
N 2/32-OWT-2Yrs	6.90E+07	α_j	6.18E-05	6.95E-02	1.38E-04	9.09E-04	8.50E-01	6.03E-02	6.50E-04	1.84E-02	1.81E-04	1.00E-06
		τ_j	1.00E+02	8.77E-03	1.07E-04	9.86E-03	2.01E-04	4.21E-03	9.98E-03	1.57E-01	5.39E+00	3.24E+01
N 2/32-SHDR-2Yrs	1.00E+08	α_j	6.18E-05	6.95E-02	1.38E-04	9.09E-04	8.50E-01	6.03E-02	6.50E-04	1.84E-02	1.81E-04	1.00E-06
		τ_j	1.00E+02	8.77E-03	1.07E-04	9.86E-03	2.01E-04	4.21E-03	9.98E-03	1.57E-01	5.39E+00	3.54E+01
N 1/29-OWT-6Yrs	7.70E+07	α_j	6.96E-05	2.06E-01	1.40E-04	9.89E-04	5.15E-01	2.00E-01	6.91E-04	7.41E-02	1.91E-04	2.24E-03
		τ_j	9.63E-05	7.54E-03	1.07E-04	2.59E-02	3.81E-04	1.35E-03	9.99E-03	1.65E-01	5.44E+00	2.03E+01
N 2/32-OWT-6Yrs	1.09E+08	α_j	2.72E-04	2.19E-01	1.39E-04	4.67E-02	4.59E-01	2.01E-01	3.86E-04	6.58E-02	6.49E-04	6.65E-03
		τ_j	8.41E+02	4.39E-05	1.07E-04	1.12E-02	3.06E-04	5.40E-03	1.02E-02	2.63E-01	4.11E+00	1.37E+01
N 6/4-OWT-6Yrs	1.03E+08	α_j	2.43E-04	2.23E-01	1.53E-04	1.66E-03	4.83E-01	2.02E-01	1.02E-03	8.83E-02	3.41E-04	8.41E-03
		τ_j	6.21E+02	8.49E-05	1.07E-04	1.01E-02	2.57E-04	5.98E-03	1.02E-02	1.14E-01	5.30E+00	6.74E+00
N 1/29-SHDR-6Yrs	7.83E+07	α_j	1.87E-04	2.35E-01	1.38E-04	2.62E-02	4.49E-01	2.12E-01	3.78E-04	7.07E-02	5.44E-04	5.74E-03
		τ_j	9.54E+02	1.91E-04	1.07E-04	1.02E-02	7.61E-04	1.11E-02	1.02E-02	2.65E-01	4.28E+00	1.38E+01
N 2/32-SHDR-6Yrs	1.07E+08	α_j	6.96E-05	2.20E-01	1.40E-04	9.90E-04	4.82E-01	2.08E-01	6.91E-04	8.68E-02	1.91E-04	2.33E-03
		τ_j	1.99E+00	7.55E-03	1.07E-04	9.87E-03	2.12E-04	2.38E-03	9.99E-03	1.99E-01	5.44E+00	2.56E+01
N 6/4-SHDR-6Yrs	1.03E+08	α_j	2.43E-04	2.23E-01	1.53E-04	1.66E-03	4.83E-01	2.02E-01	1.02E-03	8.83E-02	3.41E-04	8.41E-03
		τ_j	6.21E+02	8.49E-05	1.07E-04	1.01E-02	2.57E-04	5.98E-03	1.02E-02	1.14E-01	5.30E+00	6.74E+00
N 2/31-BWT-7Yrs	1.69E+08	α_j	7.85E-04	1.86E-01	1.58E-04	1.00E-01	4.67E-01	2.04E-01	5.54E-04	3.38E-02	1.92E-03	6.61E-03
		τ_j	4.42E+02	4.52E-05	1.07E-04	7.82E-02	2.94E-04	5.78E-03	1.03E-02	9.93E-01	3.92E+00	1.98E+01
N 10/2-OWT-7Yrs	1.13E+08	α_j	2.65E-04	2.17E-01	1.58E-04	6.74E-02	4.58E-01	1.80E-01	5.40E-04	7.22E-02	9.64E-04	4.79E-03
		τ_j	2.27E+02	9.66E-05	1.07E-04	9.54E-03	4.57E-04	8.43E-03	1.02E-02	1.48E-01	3.41E+00	7.60E+00

APPENDIX G

model parameters(SE1) recovered from 21 field-aged seals (Part 2)												
Type of bitumen	G_0		term1	term2	term3	term4	term5	term6	term7	term8	term9	term10 (residual)
N 2/31-OWT-7Yrs	1.43E+08	α_j	2.79E-04	2.10E-01	1.58E-04	5.47E-02	4.72E-01	1.75E-01	5.37E-04	7.98E-02	9.83E-04	6.47E-03
		τ_j	5.62E+02	4.85E-05	1.07E-04	1.56E-02	5.82E-04	8.62E-03	1.02E-02	2.60E-01	3.48E+00	1.26E+01
N 8/8-OWT-7Yrs	1.21E+08	α_j	1.64E-04	2.50E-01	1.57E-04	4.67E-02	4.54E-01	1.75E-01	5.21E-04	6.58E-02	1.00E-03	6.65E-03
		τ_j	3.78E+02	6.11E-05	1.07E-04	1.21E-02	3.27E-04	5.22E-03	1.02E-02	1.00E-01	3.86E+00	3.78E+00
N 10/2-SHDR-7Yrs	9.33E+07	α_j	2.43E-04	2.15E-01	1.58E-04	6.04E-02	4.58E-01	1.79E-01	5.38E-04	7.99E-02	9.78E-04	5.59E-03
		τ_j	5.01E+02	1.00E-04	1.07E-04	9.50E-03	5.42E-04	8.37E-03	1.02E-02	2.37E-01	3.46E+00	1.11E+01
N 8/8-SHDR-7Yrs	1.21E+08	α_j	1.64E-04	2.50E-01	1.57E-04	4.67E-02	4.54E-01	1.75E-01	5.21E-04	6.58E-02	1.00E-03	6.65E-03
		τ_j	3.78E+02	6.11E-05	1.07E-04	1.21E-02	3.27E-04	5.22E-03	1.02E-02	1.00E-01	3.86E+00	3.78E+00
N 6/4-OWT-10Yrs	1.30E+08	α_j	4.04E-03	1.90E-02	2.75E-01	8.84E-04	1.44E-04	1.56E-01	7.71E-02	2.54E-01	2.13E-01	4.62E-05
		τ_j	1.11E+01	1.29E+00	3.21E-04	7.03E+01	8.16E+02	1.04E-02	1.17E-01	1.11E-04	1.83E-03	1.19E+03
N 6/4-SHDR-10Yrs	9.03E+07	α_j	1.49E-04	1.84E-01	1.60E-04	1.83E-01	1.36E-01	4.39E-01	5.95E-04	5.18E-02	1.73E-03	3.62E-03
		τ_j	4.64E+02	1.13E-04	1.07E-04	1.30E-02	1.88E-03	4.16E-04	1.03E-02	2.11E-01	4.27E+00	8.75E+00
N 1/29-OWT-10Yrs	1.09E+08	α_j	1.03E-02	3.03E-02	2.39E-01	3.05E-03	7.68E-04	1.69E-01	8.37E-02	2.37E-01	2.27E-01	1.57E-04
		τ_j	1.96E+01	2.47E+00	3.96E-04	1.51E+02	1.18E+03	2.64E-02	2.67E-01	1.21E-04	3.28E-03	1.24E+04
N 2/31-OWT-12Yrs	1.86E+08	α_j	7.70E-03	4.04E-02	2.01E-01	1.10E-03	1.86E-04	1.96E-01	1.55E-01	1.98E-01	2.00E-01	2.07E-05
		τ_j	1.12E+01	8.75E-01	9.98E-04	1.03E+02	9.73E+02	5.09E-03	5.03E-02	9.78E-05	2.23E-04	1.74E+04
N 2/31-SHDR-12Yrs	1.59E+08	α_j	7.79E-03	6.55E-02	2.02E-01	8.92E-04	1.39E-04	1.94E-01	1.73E-01	1.71E-01	1.85E-01	1.89E-05
		τ_j	8.06E+00	3.65E-01	1.09E-03	8.31E+01	7.87E+02	4.04E-03	2.75E-02	1.14E-04	2.65E-04	6.01E+03
N 2/31-S-SHDR-12Yrs	1.45E+08	α_j	6.07E-03	3.24E-02	2.07E-01	8.41E-04	1.20E-04	1.81E-01	1.75E-01	1.95E-01	2.02E-01	9.42E-06
		τ_j	7.82E+00	6.64E-01	7.42E-04	7.76E+01	7.75E+02	3.27E-03	3.49E-02	1.47E-04	3.21E-04	9.52E+03
N10/3-OWT-24Yrs	1.75E+08	α_j	1.55E-02	8.45E-02	1.85E-01	1.91E-03	3.48E-04	1.77E-01	1.66E-01	1.84E-01	1.86E-01	2.49E-05
		τ_j	1.20E+01	4.57E-01	7.65E-04	1.63E+02	1.68E+03	3.50E-03	2.77E-02	1.02E-04	1.67E-04	1.01E+04

APPENDIX G

G.4 Complex modulus Prony data for all 70/100 bitumens

APPENDIX G

	70/100 Unaged_Uncond_Arrh	70/100 Unaged_Uncond_WLF	70/100 Unaged_Cond_Arrh	70/100 Unaged_Cond_WLF	70/100 _DR02175_OWT_3yrs_Arrh	70/100 _DR1298_SHDR_4yrs	70/100 _DR1298_OWT_4yrs	70/100 _DR1398_BWT_5yrs
age [yrs]	0	0	0	0	3	4	4	5
Reduced Frequency	G* model	G* model	G* model	G* model	G* model	G* model	G* model	G* model
[rad/s]	[Pa]	[Pa]	[Pa]	[Pa]	[Pa]	[Pa]	[Pa]	[Pa]
0.0001	1.73E+01	1.27E+01	2.03E+01	1.78E+01	1.25E+03	6.55E+02	5.51E+02	7.77E+02
0.0001585	2.73E+01	2.01E+01	3.21E+01	2.82E+01	1.94E+03	1.03E+03	8.11E+02	1.21E+03
0.0002512	4.33E+01	3.19E+01	5.09E+01	4.46E+01	3.05E+03	1.62E+03	1.24E+03	1.90E+03
0.001	1.72E+02	1.27E+02	2.03E+02	1.78E+02	1.12E+04	5.81E+03	4.61E+03	7.19E+03
0.0015849	2.73E+02	2.01E+02	3.21E+02	2.81E+02	1.63E+04	8.24E+03	6.88E+03	1.08E+04
0.0025119	4.32E+02	3.18E+02	5.07E+02	4.44E+02	2.35E+04	1.13E+04	9.84E+03	1.59E+04
0.01	1.68E+03	1.26E+03	1.90E+03	1.67E+03	7.24E+04	3.38E+04	2.86E+04	5.24E+04
0.0158489	2.58E+03	2.00E+03	2.82E+03	2.47E+03	1.01E+05	5.19E+04	4.35E+04	7.82E+04
0.0251189	3.85E+03	3.13E+03	4.06E+03	3.56E+03	1.37E+05	7.98E+04	6.66E+04	1.12E+05
0.1	1.17E+04	1.10E+04	1.24E+04	1.09E+04	3.43E+05	2.48E+05	2.17E+05	2.65E+05
0.1584893	1.69E+04	1.62E+04	1.82E+04	1.59E+04	4.88E+05	3.50E+05	3.18E+05	3.74E+05
0.2511886	2.51E+04	2.43E+04	2.63E+04	2.30E+04	7.21E+05	5.07E+05	4.75E+05	5.50E+05
1	8.57E+04	8.49E+04	8.52E+04	7.47E+04	2.31E+06	1.58E+06	1.49E+06	1.75E+06
1.5848932	1.26E+05	1.28E+05	1.31E+05	1.15E+05	3.06E+06	2.09E+06	1.95E+06	2.34E+06
2.5118864	1.81E+05	1.91E+05	2.03E+05	1.78E+05	3.81E+06	2.57E+06	2.39E+06	2.90E+06
10	5.28E+05	6.07E+05	7.10E+05	6.23E+05	8.32E+06	5.24E+06	4.61E+06	5.70E+06
15.848932	7.72E+05	8.93E+05	1.05E+06	9.21E+05	1.18E+07	7.34E+06	6.38E+06	7.88E+06
62.83185	2.14E+06	2.16E+06	2.56E+06	2.25E+06	2.53E+07	1.56E+07	1.34E+07	1.65E+07
100	2.83E+06	2.77E+06	3.35E+06	2.94E+06	2.90E+07	1.80E+07	1.55E+07	1.92E+07
158.48932	3.74E+06	3.62E+06	4.57E+06	4.00E+06	3.34E+07	2.08E+07	1.79E+07	2.26E+07
251.18864	5.05E+06	4.83E+06	6.42E+06	5.63E+06	3.95E+07	2.47E+07	2.14E+07	2.75E+07
1000	1.53E+07	1.45E+07	1.92E+07	1.68E+07	5.98E+07	3.95E+07	3.59E+07	4.85E+07
1584.8932	2.21E+07	2.11E+07	2.61E+07	2.29E+07	6.80E+07	4.66E+07	4.39E+07	5.77E+07
2511.8864	2.97E+07	2.91E+07	3.24E+07	2.84E+07	7.87E+07	5.60E+07	5.42E+07	6.56E+07
10000	4.26E+07	4.41E+07	3.99E+07	3.50E+07	1.02E+08	7.57E+07	7.55E+07	7.43E+07

APPENDIX G

	70/100 _DR1398_IWT_5yrs	70/100_DR2175- BWT_6yrs	70/100_DR2175- IWT_6yrs	70/100_N10-3- BWT_9yrs	70/100_N10-3- OWT_9yrs	70/100_N10-3- IWT_9yrs	70/100_MR174- SHDR_10yrs	70/100_MR174- OWT_10yrs
age [yrs]	5	6	6	9	9	9	10	10
Reduced Frequency	G* model	G* model	G* model	G* model	G* model	G* model	G* model	G* model
[rad/s]	[Pa]	[Pa]	[Pa]	[Pa]	[Pa]	[Pa]	[Pa]	[Pa]
0.0001	6.25E+02	1.15E+03	8.79E+02	8.84E+02	8.97E+02	8.88E+02	1.10E+03	8.96E+02
0.0001585	9.74E+02	1.62E+03	1.36E+03	1.38E+03	1.39E+03	1.38E+03	1.70E+03	1.39E+03
0.0002512	1.53E+03	2.37E+03	2.13E+03	2.16E+03	2.18E+03	2.16E+03	2.66E+03	2.18E+03
0.001	5.77E+03	8.13E+03	8.12E+03	8.28E+03	8.35E+03	8.28E+03	1.02E+04	8.35E+03
0.0015849	8.57E+03	1.20E+04	1.23E+04	1.26E+04	1.27E+04	1.26E+04	1.56E+04	1.27E+04
0.0025119	1.22E+04	1.70E+04	1.81E+04	1.85E+04	1.87E+04	1.85E+04	2.33E+04	1.86E+04
0.01	3.56E+04	4.91E+04	5.69E+04	5.82E+04	5.86E+04	5.81E+04	7.03E+04	5.66E+04
0.0158489	5.42E+04	7.35E+04	8.47E+04	8.60E+04	8.62E+04	8.54E+04	9.60E+04	7.96E+04
0.0251189	8.31E+04	1.09E+05	1.23E+05	1.23E+05	1.23E+05	1.22E+05	1.27E+05	1.08E+05
0.1	2.70E+05	2.48E+05	3.20E+05	3.18E+05	3.12E+05	3.09E+05	3.12E+05	2.76E+05
0.1584893	3.96E+05	3.03E+05	4.49E+05	4.46E+05	4.37E+05	4.34E+05	4.40E+05	3.89E+05
0.2511886	5.92E+05	3.90E+05	6.58E+05	6.54E+05	6.40E+05	6.34E+05	6.46E+05	5.68E+05
1	1.84E+06	1.24E+06	2.19E+06	2.17E+06	2.12E+06	2.10E+06	2.15E+06	1.89E+06
1.5848932	2.39E+06	1.92E+06	2.99E+06	2.97E+06	2.90E+06	2.87E+06	2.94E+06	2.59E+06
2.5118864	2.89E+06	2.98E+06	3.76E+06	3.73E+06	3.64E+06	3.61E+06	3.69E+06	3.28E+06
10	5.42E+06	8.96E+06	6.73E+06	6.65E+06	6.38E+06	6.32E+06	6.49E+06	5.93E+06
15.848932	7.45E+06	1.10E+07	9.01E+06	8.90E+06	8.48E+06	8.41E+06	8.64E+06	7.99E+06
62.83185	1.57E+07	1.39E+07	1.91E+07	1.88E+07	1.78E+07	1.77E+07	1.82E+07	1.76E+07
100	1.80E+07	1.49E+07	2.21E+07	2.18E+07	2.06E+07	2.04E+07	2.10E+07	2.06E+07
158.48932	2.09E+07	1.68E+07	2.56E+07	2.53E+07	2.39E+07	2.36E+07	2.43E+07	2.39E+07
251.18864	2.50E+07	2.05E+07	3.04E+07	3.00E+07	2.83E+07	2.81E+07	2.89E+07	2.83E+07
1000	4.10E+07	4.61E+07	4.64E+07	4.58E+07	4.38E+07	4.34E+07	4.45E+07	4.45E+07
1584.8932	4.95E+07	5.44E+07	5.34E+07	5.29E+07	5.11E+07	5.07E+07	5.19E+07	5.31E+07
2511.8864	6.11E+07	5.99E+07	6.43E+07	6.40E+07	6.27E+07	6.22E+07	6.35E+07	6.59E+07
10000	8.75E+07	7.84E+07	1.04E+08	1.04E+08	1.04E+08	1.03E+08	1.05E+08	1.03E+08

APPENDIX G

	70/100_DR2216- BWT_10yrs	70/100_DR2216- IWT_10yrs	70/100_N6-5- SHDR_11yrs	70/100_N6-5- OWT_11yrs	70/100_DR1452- BWT_12yrs	70/100_DR1452- OWT_12yrs	70/100_N6-5- SHDR_13yrs	70/100_N6-5- OWT_13yrs
age [yrs]	10	10	11	11	12	12	13	13
Reduced Frequency	G* model	G* model	G* model	G* model	G* model	G* model	G* model	G* model
[rad/s]	[Pa]	[Pa]	[Pa]	[Pa]	[Pa]	[Pa]	[Pa]	[Pa]
0.0001	5.51E+03	4.42E+03	2.30E+03	1.12E+03	9.34E+03	1.38E+04	2.90E+03	2.34E+03
0.0001585	8.45E+03	6.80E+03	3.43E+03	1.69E+03	1.34E+04	1.91E+04	4.21E+03	3.38E+03
0.0002512	1.26E+04	1.03E+04	4.97E+03	2.51E+03	1.86E+04	2.61E+04	6.20E+03	4.85E+03
0.001	3.06E+04	2.76E+04	1.61E+04	8.22E+03	5.49E+04	7.49E+04	2.08E+04	1.55E+04
0.0015849	4.07E+04	3.75E+04	2.41E+04	1.25E+04	7.88E+04	1.03E+05	2.95E+04	2.22E+04
0.0025119	5.65E+04	5.27E+04	3.51E+04	1.87E+04	1.09E+05	1.35E+05	4.07E+04	3.08E+04
0.01	1.44E+05	1.37E+05	9.52E+04	5.49E+04	2.82E+05	3.40E+05	1.21E+05	9.01E+04
0.0158489	1.92E+05	1.85E+05	1.38E+05	8.05E+04	4.00E+05	4.63E+05	1.77E+05	1.27E+05
0.0251189	2.63E+05	2.56E+05	1.99E+05	1.19E+05	5.45E+05	6.02E+05	2.49E+05	1.72E+05
0.1	5.91E+05	5.86E+05	4.93E+05	3.22E+05	1.21E+06	1.33E+06	6.06E+05	4.51E+05
0.1584893	7.46E+05	7.66E+05	6.80E+05	4.49E+05	1.66E+06	1.76E+06	8.52E+05	6.15E+05
0.2511886	9.91E+05	1.05E+06	9.54E+05	6.38E+05	2.25E+06	2.23E+06	1.18E+06	8.10E+05
1	2.43E+06	2.40E+06	2.19E+06	1.56E+06	4.42E+06	4.48E+06	2.59E+06	1.92E+06
1.5848932	2.92E+06	2.81E+06	2.86E+06	2.09E+06	5.71E+06	5.62E+06	3.47E+06	2.50E+06
2.5118864	3.39E+06	3.26E+06	3.80E+06	2.84E+06	7.41E+06	6.85E+06	4.65E+06	3.18E+06
10	6.84E+06	6.96E+06	7.55E+06	6.08E+06	1.33E+07	1.27E+07	8.84E+06	6.79E+06
15.848932	9.15E+06	9.04E+06	9.52E+06	7.83E+06	1.64E+07	1.52E+07	1.11E+07	8.40E+06
62.83185	1.48E+07	1.44E+07	1.76E+07	1.54E+07	2.81E+07	2.56E+07	2.18E+07	1.62E+07
100	1.63E+07	1.72E+07	2.09E+07	1.88E+07	3.27E+07	3.02E+07	2.53E+07	1.96E+07
158.48932	1.88E+07	2.16E+07	2.53E+07	2.33E+07	3.89E+07	3.46E+07	2.96E+07	2.34E+07
251.18864	2.31E+07	2.74E+07	3.04E+07	2.85E+07	4.62E+07	3.96E+07	3.61E+07	2.83E+07
1000	4.23E+07	4.10E+07	4.71E+07	4.64E+07	6.67E+07	6.08E+07	5.88E+07	4.62E+07
1584.8932	4.67E+07	4.57E+07	5.48E+07	5.50E+07	7.67E+07	6.77E+07	6.50E+07	5.41E+07
2511.8864	5.09E+07	5.23E+07	6.25E+07	6.35E+07	8.80E+07	7.63E+07	7.37E+07	6.36E+07
10000	7.48E+07	7.10E+07	8.91E+07	9.55E+07	1.14E+08	1.05E+08	1.15E+08	9.28E+07

APPENDIX G

	70/100_MR269-SHDR_13yrs	70/100_MR269-OWT_13yrs	70/100_MR188-OWT_15yrs	70/100-DR1123_IWT_17yrs	70/100-MR563_IWT_19yrs	70/100-MR563_BWT_19yrs	70/100-P1398_OWT_22yrs	70/100-P1398_OWT_23yrs	70/100_1252_Q-Sun
age [yrs]	13	13	15	17	19	19	22	23	
Reduced Frequency	G* model	G* model	G* model	G* model	G* model	G* model	G* model	G* model	G* model
[rad/s]	[Pa]	[Pa]	[Pa]	[Pa]	[Pa]	[Pa]	[Pa]	[Pa]	[Pa]
0.0001	2.53E+03	1.76E+03	4.36E+03	6.79E+03	8.69E+03	1.14E+04	4.65E+03	5.03E+03	8.41E+02
0.0001585	3.61E+03	2.57E+03	6.48E+03	9.93E+03	1.27E+04	1.61E+04	6.84E+03	7.41E+03	1.30E+03
0.0002512	5.22E+03	3.68E+03	9.53E+03	1.39E+04	1.77E+04	2.23E+04	9.81E+03	1.06E+04	1.97E+03
0.001	1.70E+04	1.16E+04	3.09E+04	4.03E+04	4.94E+04	6.51E+04	3.09E+04	3.37E+04	5.98E+03
0.0015849	2.38E+04	1.72E+04	4.40E+04	5.84E+04	7.07E+04	9.07E+04	4.53E+04	4.93E+04	8.94E+03
0.0025119	3.24E+04	2.54E+04	6.19E+04	8.17E+04	9.77E+04	1.22E+05	6.42E+04	6.97E+04	1.35E+04
0.01	9.39E+04	8.25E+04	1.84E+05	2.22E+05	2.54E+05	3.22E+05	1.80E+05	1.96E+05	4.10E+04
0.0158489	1.37E+05	1.15E+05	2.54E+05	3.19E+05	3.61E+05	4.36E+05	2.57E+05	2.80E+05	5.68E+04
0.0251189	1.90E+05	1.54E+05	3.41E+05	4.42E+05	4.93E+05	5.68E+05	3.54E+05	3.83E+05	8.10E+04
0.1	4.45E+05	4.12E+05	8.98E+05	1.00E+06	1.08E+06	1.33E+06	8.83E+05	9.47E+05	2.39E+05
0.1584893	6.22E+05	5.72E+05	1.20E+06	1.37E+06	1.47E+06	1.73E+06	1.21E+06	1.30E+06	3.19E+05
0.2511886	8.60E+05	7.69E+05	1.55E+06	1.87E+06	1.99E+06	2.18E+06	1.61E+06	1.71E+06	4.26E+05
1	1.85E+06	1.89E+06	3.60E+06	3.81E+06	3.84E+06	4.61E+06	3.54E+06	3.74E+06	1.14E+06
1.5848932	2.45E+06	2.48E+06	4.59E+06	4.95E+06	4.90E+06	5.75E+06	4.64E+06	4.90E+06	1.49E+06
2.5118864	3.29E+06	3.18E+06	5.76E+06	6.49E+06	6.33E+06	6.97E+06	5.85E+06	6.16E+06	1.90E+06
10	6.27E+06	6.91E+06	1.18E+07	1.19E+07	1.12E+07	1.32E+07	1.14E+07	1.19E+07	4.42E+06
15.848932	7.85E+06	8.56E+06	1.43E+07	1.46E+07	1.36E+07	1.57E+07	1.42E+07	1.48E+07	5.62E+06
62.83185	1.55E+07	1.65E+07	2.61E+07	2.61E+07	2.34E+07	2.66E+07	2.43E+07	2.52E+07	1.10E+07
100	1.79E+07	1.99E+07	3.08E+07	3.05E+07	2.70E+07	3.14E+07	2.95E+07	3.06E+07	1.40E+07
158.48932	2.11E+07	2.37E+07	3.60E+07	3.62E+07	3.19E+07	3.58E+07	3.47E+07	3.59E+07	1.71E+07
251.18864	2.57E+07	2.86E+07	4.27E+07	4.30E+07	3.77E+07	4.07E+07	3.97E+07	4.10E+07	2.02E+07
1000	4.29E+07	4.59E+07	6.55E+07	6.44E+07	5.53E+07	6.24E+07	6.19E+07	6.36E+07	3.61E+07
1584.8932	4.79E+07	5.34E+07	7.49E+07	7.46E+07	6.36E+07	6.89E+07	6.95E+07	7.13E+07	4.22E+07
2511.8864	5.49E+07	6.22E+07	8.58E+07	8.49E+07	7.21E+07	7.65E+07	7.65E+07	7.84E+07	4.81E+07
10000	8.83E+07	8.74E+07	1.15E+08	1.17E+08	9.70E+07	1.10E+08	1.12E+08	1.14E+08	8.01E+07

APPENDIX G

G.5 Complex modulus Prony data for all SE1 bitumens

APPENDIX G

	SE1 Unaged_Uncond_Arrh	SE1 Unaged_Cond_Arrh	SE1_N2- 32_OWT_2yrs_Arrh	SE1_N2- 32_SHDR_2yrs_Arrh	SE1_N2- 32_OWT_6yrs_Arrh	SE1_N2- 32_SHDR_6yrs_Arrh	SE1_N1- 29_OWT_6yrs_Arrh	SE1_N1- 29_SHDR_6yrs_Arrh
age [yrs]	0	0	2	2	6	6	6	6
Reduced Frequency	G* model	G* model	G* model	G* model	G* model	G* model	G* model	G* model
[rad/s]	[Pa]	[Pa]	[Pa]	[Pa]	[Pa]	[Pa]	[Pa]	[Pa]
0.0001	3.80E+01	3.90E+01	8.03E+01	1.16E+02	4.87E+02	8.74E+02	3.99E+03	2.25E+03
0.0001585	5.92E+01	5.86E+01	1.24E+02	1.80E+02	7.54E+02	1.37E+03	6.12E+03	3.52E+03
0.0002512	9.32E+01	9.07E+01	1.95E+02	2.82E+02	1.18E+03	2.17E+03	9.47E+03	5.48E+03
0.001	3.69E+02	3.56E+02	7.67E+02	1.11E+03	4.68E+03	8.60E+03	3.03E+04	1.71E+04
0.0015849	5.85E+02	5.63E+02	1.21E+03	1.75E+03	7.42E+03	1.36E+04	3.96E+04	2.23E+04
0.0025119	9.25E+02	8.91E+02	1.89E+03	2.74E+03	1.18E+04	2.16E+04	5.00E+04	2.88E+04
0.01	3.53E+03	3.43E+03	5.96E+03	8.65E+03	4.60E+04	8.35E+04	1.33E+05	8.45E+04
0.0158489	5.27E+03	5.20E+03	7.98E+03	1.16E+04	7.09E+04	1.27E+05	2.01E+05	1.30E+05
0.0251189	7.49E+03	7.54E+03	1.07E+04	1.56E+04	1.06E+05	1.84E+05	3.05E+05	1.98E+05
0.1	1.87E+04	1.93E+04	3.37E+04	4.88E+04	2.34E+05	3.78E+05	7.80E+05	5.12E+05
0.1584893	2.68E+04	2.75E+04	5.06E+04	7.33E+04	2.85E+05	4.75E+05	9.23E+05	6.16E+05
0.2511886	3.93E+04	4.01E+04	7.58E+04	1.10E+05	3.67E+05	6.41E+05	1.08E+06	7.42E+05
1	1.40E+05	1.42E+05	2.74E+05	3.96E+05	1.14E+06	2.14E+06	2.41E+06	1.86E+06
1.5848932	2.16E+05	2.20E+05	4.24E+05	6.15E+05	1.75E+06	3.27E+06	3.47E+06	2.73E+06
2.5118864	3.26E+05	3.33E+05	6.45E+05	9.35E+05	2.64E+06	4.84E+06	4.88E+06	3.87E+06
10	8.13E+05	8.44E+05	1.62E+06	2.34E+06	6.06E+06	9.97E+06	8.44E+06	6.97E+06
15.848932	1.04E+06	1.09E+06	1.99E+06	2.89E+06	6.96E+06	1.12E+07	9.22E+06	7.98E+06
62.831853	2.74E+06	2.84E+06	4.80E+06	6.96E+06	1.27E+07	2.00E+07	1.60E+07	1.64E+07
100	3.63E+06	3.78E+06	6.59E+06	9.54E+06	1.67E+07	2.64E+07	2.10E+07	2.07E+07
158.48932	4.50E+06	4.69E+06	8.50E+06	1.23E+07	2.11E+07	3.37E+07	2.66E+07	2.44E+07
251.18864	5.35E+06	5.57E+06	1.03E+07	1.50E+07	2.54E+07	4.08E+07	3.17E+07	2.74E+07
1000	1.13E+07	1.17E+07	1.78E+07	2.58E+07	4.31E+07	5.81E+07	4.35E+07	4.41E+07
1584.8932	1.55E+07	1.60E+07	2.38E+07	3.45E+07	5.14E+07	6.34E+07	5.08E+07	5.26E+07
2511.8864	2.02E+07	2.10E+07	3.29E+07	4.77E+07	6.04E+07	7.12E+07	6.12E+07	6.01E+07
10000	2.78E+07	2.90E+07	6.20E+07	8.99E+07	7.52E+07	9.99E+07	8.79E+07	7.48E+07

APPENDIX G

	SE1_N6- 4_OWT_6yrs_Arrh	SE1_N6- 4_SHDR_6yrs_Arrh	SE1_N2- 31_OWT_7yrs_Arrh	SE1_N8- 8_OWT_7yrs_Arrh	SE1_N8- 8_SHDR_7yrs_Arrh	SE1_N2- 31_BWT_7yrs_Arrh	SE1_N10- 2_OWT_7yrs_Arrh	SE1_N10- 2_SHDR_7yrs_Arrh
age [yrs]	6	6	7	7	7	7	7	7
Reduced Frequency	G* model	G* model	G* model	G* model	G* model	G* model	G* model	G* model
[rad/s]	[Pa]	[Pa]	[Pa]	[Pa]	[Pa]	[Pa]	[Pa]	[Pa]
0.0001	2.54E+03	2.32E+03	3.91E+03	1.22E+03	1.24E+03	2.03E+03	1.31E+03	1.95E+03
0.0001585	3.81E+03	3.64E+03	6.09E+03	1.92E+03	1.93E+03	3.21E+03	2.05E+03	3.08E+03
0.0002512	5.87E+03	5.72E+03	9.55E+03	3.02E+03	3.03E+03	5.07E+03	3.23E+03	4.86E+03
0.001	2.02E+04	1.99E+04	3.42E+04	1.14E+04	1.14E+04	1.88E+04	1.26E+04	1.78E+04
0.0015849	2.76E+04	2.72E+04	4.82E+04	1.68E+04	1.68E+04	2.70E+04	1.94E+04	2.55E+04
0.0025119	3.52E+04	3.48E+04	6.42E+04	2.33E+04	2.34E+04	3.61E+04	2.90E+04	3.45E+04
0.01	8.16E+04	8.14E+04	1.69E+05	5.38E+04	5.39E+04	6.79E+04	7.61E+04	8.92E+04
0.0158489	1.22E+05	1.21E+05	2.54E+05	7.79E+04	7.80E+04	9.23E+04	1.08E+05	1.34E+05
0.0251189	1.86E+05	1.86E+05	3.86E+05	1.18E+05	1.18E+05	1.33E+05	1.59E+05	2.04E+05
0.1	6.19E+05	6.18E+05	1.04E+06	4.30E+05	4.30E+05	3.99E+05	5.05E+05	5.85E+05
0.1584893	8.17E+05	8.16E+05	1.27E+06	6.28E+05	6.28E+05	5.55E+05	6.66E+05	7.31E+05
0.2511886	9.88E+05	9.88E+05	1.54E+06	8.52E+05	8.52E+05	7.88E+05	8.26E+05	8.98E+05
1	1.66E+06	1.66E+06	3.74E+06	1.56E+06	1.56E+06	2.16E+06	1.76E+06	2.22E+06
1.5848932	2.27E+06	2.27E+06	5.45E+06	2.04E+06	2.04E+06	2.68E+06	2.56E+06	3.25E+06
2.5118864	3.27E+06	3.27E+06	7.70E+06	2.86E+06	2.86E+06	3.24E+06	3.78E+06	4.65E+06
10	8.59E+06	8.59E+06	1.37E+07	7.86E+06	7.86E+06	7.54E+06	9.17E+06	8.63E+06
15.848932	1.02E+07	1.02E+07	1.53E+07	9.71E+06	9.71E+06	1.05E+07	1.08E+07	9.59E+06
62.831853	1.56E+07	1.56E+07	2.83E+07	1.73E+07	1.73E+07	1.92E+07	2.09E+07	1.75E+07
100	1.95E+07	1.95E+07	3.55E+07	2.21E+07	2.21E+07	2.21E+07	2.70E+07	2.26E+07
158.48932	2.43E+07	2.43E+07	4.20E+07	2.75E+07	2.75E+07	2.64E+07	3.27E+07	2.74E+07
251.18864	2.86E+07	2.86E+07	4.72E+07	3.27E+07	3.27E+07	3.26E+07	3.69E+07	3.11E+07
1000	3.82E+07	3.82E+07	7.10E+07	4.63E+07	4.63E+07	5.26E+07	5.21E+07	4.60E+07
1584.8932	4.48E+07	4.48E+07	8.54E+07	5.52E+07	5.52E+07	6.18E+07	6.28E+07	5.54E+07
2511.8864	5.51E+07	5.51E+07	9.87E+07	6.73E+07	6.73E+07	7.56E+07	7.49E+07	6.49E+07
10000	8.91E+07	8.91E+07	1.19E+08	9.87E+07	9.87E+07	1.22E+08	1.01E+08	8.38E+07

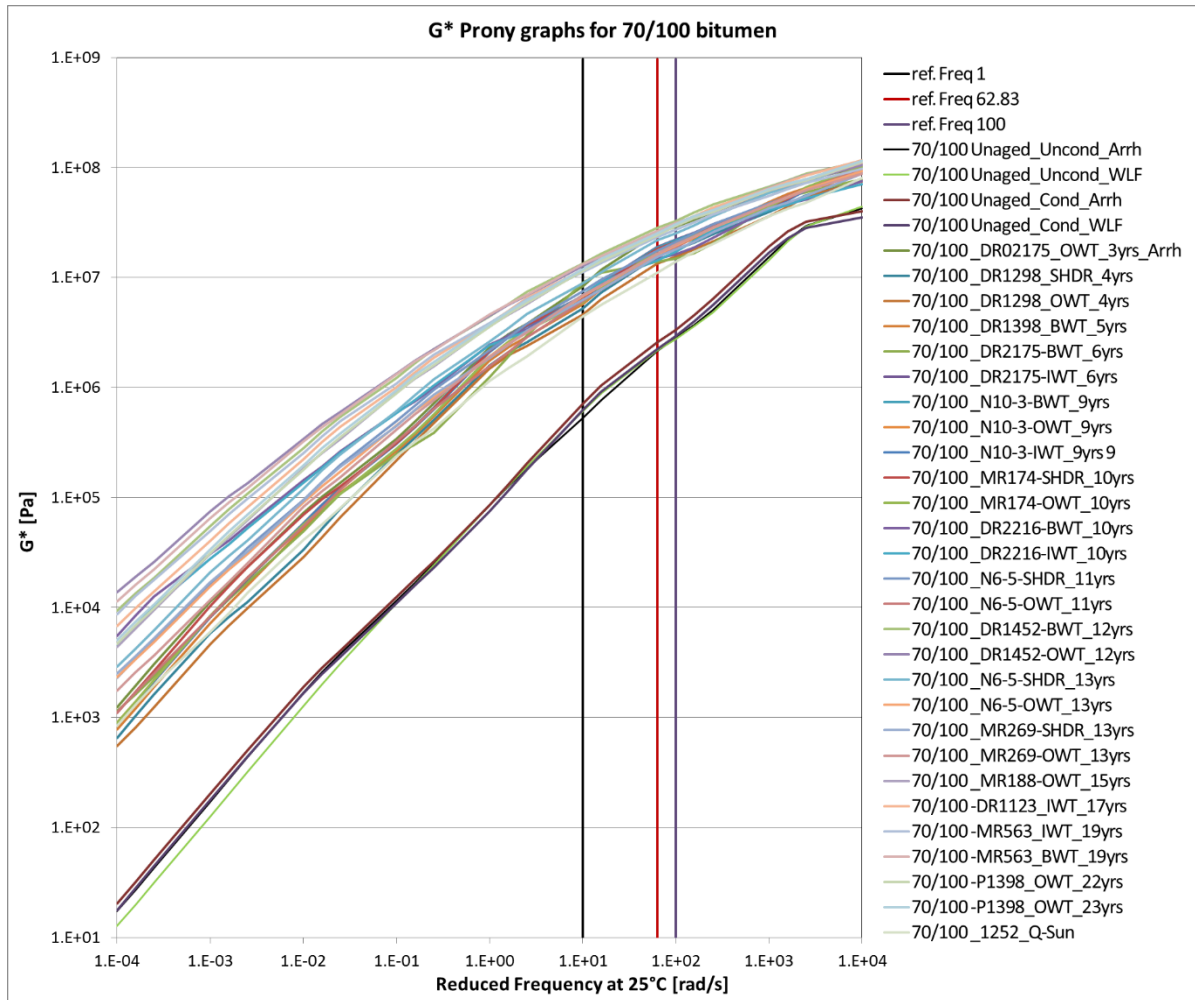
APPENDIX G

	SE1_N6- 4_OWT_10yrs_Arrh	SE1_N6- 4_SHDR_10yrs_Arrh	SE1_N1- 29_OWT_10yrs	SE1_N2- 31_SHDR_12yrs_Arrh	SE1_N2- 31_S_SHDR_12yrs_Arrh	SE1_N2- 31_S_OWT_12yrs_Arrh	SE1_N10- 3_OWT_24yrs_Arrh	SE1 Q-SUN
age [yrs]	10	10	10	12	12	12	24	
Reduced Frequency	G* model	G* model	G* model	G* model	G* model	G* model	G* model	G* model
[rad/s]	[Pa]	[Pa]	[Pa]	[Pa]	[Pa]	[Pa]	[Pa]	[Pa]
0.0001	4.27E+03	1.12E+03	2.92E+04	5.79E+03	4.15E+03	5.40E+03	2.31E+04	1.46E+02
0.0001585	6.59E+03	1.76E+03	3.92E+04	8.61E+03	6.12E+03	7.57E+03	3.41E+04	2.26E+02
0.0002512	1.02E+04	2.77E+03	5.39E+04	1.26E+04	9.09E+03	1.11E+04	5.02E+04	3.55E+02
0.001	3.30E+04	1.03E+04	1.45E+05	3.97E+04	3.03E+04	3.57E+04	1.36E+05	1.40E+03
0.0015849	4.49E+04	1.49E+04	1.92E+05	5.61E+04	4.31E+04	4.97E+04	1.85E+05	2.21E+03
0.0025119	6.05E+04	2.03E+04	2.58E+05	7.92E+04	6.10E+04	6.85E+04	2.59E+05	3.47E+03
0.01	1.75E+05	5.27E+04	6.11E+05	2.37E+05	1.84E+05	1.92E+05	6.52E+05	1.19E+04
0.0158489	2.45E+05	7.92E+04	7.85E+05	3.30E+05	2.56E+05	2.63E+05	8.63E+05	1.67E+04
0.0251189	3.38E+05	1.21E+05	1.03E+06	4.58E+05	3.53E+05	3.62E+05	1.19E+06	2.26E+04
0.1	8.70E+05	3.88E+05	2.16E+06	1.28E+06	9.85E+05	9.28E+05	2.94E+06	5.27E+04
0.1584893	1.14E+06	5.10E+05	2.71E+06	1.67E+06	1.31E+06	1.21E+06	3.50E+06	7.44E+04
0.2511886	1.51E+06	6.39E+05	3.47E+06	2.10E+06	1.68E+06	1.61E+06	4.08E+06	1.08E+05
1	3.55E+06	1.45E+06	6.42E+06	5.17E+06	4.11E+06	3.71E+06	8.82E+06	3.82E+05
1.5848932	4.41E+06	2.10E+06	7.85E+06	7.33E+06	5.36E+06	4.46E+06	1.20E+07	5.83E+05
2.5118864	5.55E+06	3.03E+06	9.85E+06	9.86E+06	6.57E+06	5.40E+06	1.52E+07	8.60E+05
10	1.21E+07	6.33E+06	1.65E+07	1.74E+07	1.29E+07	1.21E+07	2.27E+07	1.83E+06
15.848932	1.43E+07	7.56E+06	1.92E+07	2.17E+07	1.76E+07	1.51E+07	2.69E+07	2.23E+06
62.831853	2.43E+07	1.63E+07	3.18E+07	4.13E+07	3.27E+07	2.34E+07	4.64E+07	5.26E+06
100	3.01E+07	2.02E+07	3.57E+07	4.77E+07	3.67E+07	2.83E+07	5.22E+07	6.84E+06
158.48932	3.58E+07	2.36E+07	4.02E+07	5.53E+07	4.19E+07	3.45E+07	5.87E+07	8.40E+06
251.18864	4.18E+07	2.69E+07	4.59E+07	6.46E+07	4.91E+07	4.03E+07	6.69E+07	1.00E+07
1000	6.45E+07	4.34E+07	6.19E+07	9.49E+07	7.74E+07	5.78E+07	9.46E+07	1.69E+07
1584.8932	7.28E+07	5.20E+07	6.78E+07	1.05E+08	8.97E+07	6.60E+07	1.05E+08	2.20E+07
2511.8864	8.29E+07	6.17E+07	7.54E+07	1.15E+08	1.03E+08	7.45E+07	1.16E+08	3.02E+07
10000	1.15E+08	8.28E+07	9.86E+07	1.46E+08	1.35E+08	9.88E+07	1.54E+08	6.33E+07



APPENDIX G

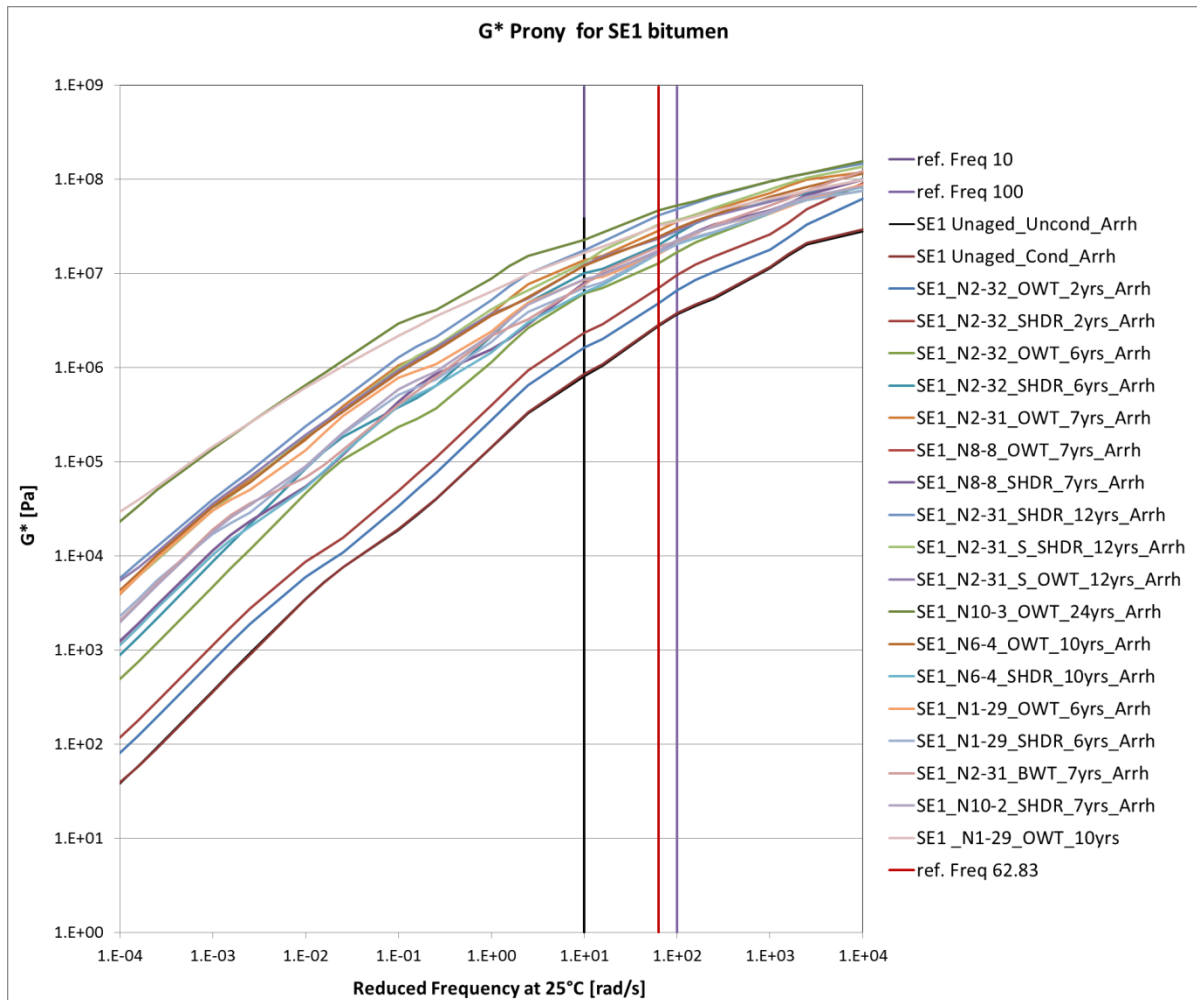
G.6 Combined graph for all 70/100 G* Prony series bitumens





APPENDIX G

G.7 Combined graph for all SE1 G^* Prony series bitumens





APPENDIX G

G.8 Complex modulus Prony data of all 70/100 bitumen case studies at 10, 62.83 and 100 rad/s

Type binder	Time [Yrs.]	G* model @10 rad/s [Pa]	G* model @100 rad/s [Pa]	G* model @100 rad/s [Pa]
70/100 Unaged_Uncond_Arrh	0	626438	2356415	3170673
70/100 Unaged_Uncond_WLF	0	526179.2	1979281	2663220
70/100 Unaged_Cond_Arrh	0	710030	2560339	3351876
70/100 Unaged_Cond_WLF	0	622614.9	2245122	2939208
70/100_DR02175_OWT_3yrs_Arrh	3	8315969	25282272	28975440
70/100_DR1298_SHDR_4yrs	4	5238997	15626608	17953097
70/100_DR1298_OWT_4yrs	4	4611136	13443750	15451623
70/100_DR1398_BWT_5yrs	5	5703772	16506877	19165600
70/100_DR1398_IWT_5yrs	5	5415055	15650924	18014066
70/100_DR2175-BWT_6yrs	6	8963054	13883229	14857809
70/100_DR2175-IWT_6yrs	6	6725734	19083774	22078451
70/100_N10-3-BWT_9yrs	9	6650268	18818718	21770713
70/100_N10-3-OWT_9yrs	9	6376328	17812456	20583092
70/100_N10-3-IWT_9yrs	9	6320486	17656444	20402808
70/100_MR174-SHDR_10yrs	10	6487782	18166081	20994840
70/100_MR174-OWT_10yrs	10	5926489	17620831	20553691
70/100_DR2216-BWT_10yrs	10	6839367	14811565	16334000
70/100_DR2216-IWT_10yrs	10	6957618	14354910	17182536
70/100_N6-5-SHDR_11yrs	11	7551224	17611583	20909719
70/100_N6-5-OWT_11yrs	11	6084019	15375699	18773156
70/100_DR1452-BWT_12yrs	12	13322417	28146462	32700631
70/100_DR1452-OWT_12yrs	12	12736499	25620606	30239500
70/100_N6-5-SHDR_13yrs	13	8839405	21801116	25262401
70/100_N6-5-OWT_13yrs	13	6788520	16185012	19570283
70/100_MR269-SHDR_13yrs	13	6267990	15452184	17949665
70/100_MR269-OWT_13yrs	13	6905008	16511545	19879309
70/100_MR188-OWT_15yrs	15	11777010	26062664	30795181
70/100-DR1123_IWT_17yrs	17	11851153	26111532	30509827
70/100-MR563_IWT_19yrs	19	11184800	23353430	27039647
70/100-MR563_BWT_19yrs	19	13219017	26554328	31388522
70/100-P1398_OWT_22yrs	22	11406677	24284318	29501300
70/100-P1398_OWT_23yrs	23	11931493	25206775	30566670
70/100 PAVaged_Uncond_Arrh	2	3379591	7650750	8831783
70/100_1252_Q-Sun		4423886	10977402	14001770



APPENDIX G

G.9 Complex modulus Prony data of all SE1 bitumen case studies at 10, 62.83 and 100 rad/s

Type binder	Time [Yrs.]	G* model @10 rad/s [Pa]	G* model @62.83 rad/s [Pa]	G* model @100 rad/s [Pa]
SE1 Unaged_Uncond_Arrh	1E-13	812560.7	2738070	3633008
SE1 Unaged_Cond_Arrh	1E-13	844148.5	2844697	3781132
SE1_N2-32_OWT_2yrs_Arrh	2	1616478	4803193	6585136
SE1_N2-32_SHDR_2yrs_Arrh	2	2342699	6961084	9543587
SE1_N2-32_OWT_6yrs_Arrh	6	6064171	12692512	16716513
SE1_N2-32_SHDR_6yrs_Arrh	6	9971937	19966854	26423486
SE1_N1-29_OWT_6yrs_Arrh	6	8441568	16026794	21003414
SE1_N1-29_SHDR_6yrs_Arrh	6	6967679	16378954	20712332
SE1_N6-4_OWT_6yrs_Arrh	6	8589712	15582319	19530389
SE1_N6-4_SHDR_6yrs_Arrh	6	8589312	15581979	19530124
SE1_N2-31_OWT_7yrs_Arrh	7	13696982	28287197	35470215
SE1_N8-8_OWT_7yrs_Arrh	7	7858991	17288304	22066017
SE1_N8-8_SHDR_7yrs_Arrh	7	7859041	17288358	22066069
SE1_N2-31_BWT_7yrs_Arrh	7	7544594	19205645	22088481
SE1_N10-2_OWT_7yrs_Arrh	7	9174675	20901598	27001787
SE1_N10-2_SHDR_7yrs_Arrh	7	8627034	17499395	22565638
SE1_N6-4_OWT_10yrs_Arrh	10	12056224	24329774	30052810
SE1_N6-4_SHDR_10yrs_Arrh	10	6327749	16282117	20211563
SE1_N1-29_OWT_10yrs	10	16451402	31811802	35729768
SE1_N2-31_SHDR_12yrs_Arrh	12	17392653	41316937	47709376
SE1_N2-31_S_SHDR_12yrs_Arrh	12	12905531	32669392	36652758
SE1_N2-31_S_OWT_12yrs_Arrh	12	12146031	23363829	28348863
SE1_N10-3_OWT_24yrs_Arrh	24	22709632	46436389	52151510
SE1 PAVaged_Uncond_Arrh	2	2102751	6055382	7929793
SE1 Q-SUN		1831228	5262442	6837445



APPENDIX G

G.10 70/100 seal's ageing model data at 10, 62.83 and 100 rad/s

		G* at 10 rad/s				Calculation of G* standard error of Estimate (SEE)	
		Σ Error	Sserr	2.13E+14	Σ (y-y) ²	1.80E+03	
			mean	6.83E+06		N	32
		4.31	Stot	5.4.E+14	SEE	7.51	
			R ²	0.61			
type binder	time [Yrs]	G* @10 rad/s [Pa]	G* model @10 rad/s [Pa]	Error	error G*	Stot G*	(y-y) ²
70-100 Unaged_Uncond_Arrh	0	5.28E+05	528134	3.38E-11	9.424298928	4.E+13	2.73E-01
70-100 Unaged_Uncond_WLF	0	607486.316	528134	2.26E-02	6296795549	4.E+13	2.73E-01
70-100 Unaged_Cond_Arrh	0	710029.993	528134	1.19E-01	33086164776	4.E+13	2.71E-01
70-100 Unaged_Cond_WLF	0	622614.877	528134	3.20E-02	8926642684	4.E+13	2.72E-01
70-100_DR02175_OWT_3yrs_Arrh	3	2874076.84	3445218	2.75E-02	3.26202E+11	2.E+13	1.17E+01
70-100_DR1298_SHDR_4yrs	4	2976781.15	4101292	7.52E-02	1.26453E+12	1.E+13	1.66E+01
70-100_DR1298_OWT_4yrs	4	3381283.68	4101292	3.08E-02	5.18413E+11	1.E+13	1.65E+01
70-100_DR1398_BWT_5yrs	5	13166530.1	4710196	3.22E+00	7.15096E+13	4.E+13	2.10E+01
70-100_DR1398_IWT_5yrs	5	7240294.58	4710196	2.89E-01	6.4014E+12	2.E+11	2.15E+01
70-100_DR2175-BWT_6yrs	6	5703772.14	5283970	6.31E-03	1.76233E+11	1.E+12	2.73E+01
70-100_DR2175-IWT_6yrs	6	5415054.99	5283970	6.15E-04	17183144917	2.E+12	2.74E+01
70-100_N10-3-BWT_9yrs	9	3931864.21	6858102	1.82E-01	8.56287E+12	8.E+12	4.65E+01
70-100_N10-3-OWT_9yrs	9	4021694.03	6858102	1.71E-01	8.04521E+12	8.E+12	4.65E+01
70-100_N10-3-IWT_9yrs	9	8963053.81	6858102	9.42E-02	4.43082E+12	5.E+12	4.58E+01
70-100_MR174-SHDR_10yrs	10	6725733.52	7346314	7.14E-03	3.8512E+11	1.E+10	5.30E+01
70-100_MR174-OWT_10yrs	10	6650267.66	7346314	8.98E-03	4.8448E+11	3.E+10	5.30E+01
70-100_DR2216-BWT_10yrs	10	6376328.44	7346314	1.74E-02	9.40871E+11	2.E+11	5.30E+01
70-100_DR2216-IWT_10yrs	10	6320486.27	7346314	1.95E-02	1.05232E+12	3.E+11	5.30E+01
70-100_N6-5-SHDR_11yrs	11	6487782	7820314	2.90E-02	1.77564E+12	1.E+11	6.01E+01
70-100_N6-5-OWT_11yrs	11	5926489.04	7820314	5.86E-02	3.58657E+12	8.E+11	6.02E+01
70-100_DR1452-BWT_12yrs	12	6839367.35	8281759	3.03E-02	2.0805E+12	7.E+07	6.75E+01
70-100_DR1452-OWT_12yrs	12	6957618	8281759	2.56E-02	1.75335E+12	2.E+10	6.74E+01
70-100_N6-5-SHDR_13yrs	13	7551223.64	8731991	1.83E-02	1.39421E+12	5.E+11	7.49E+01
70-100_N6-5-OWT_13yrs	13	6084019.46	8731991	9.20E-02	7.01175E+12	6.E+11	7.52E+01
70-100_MR269-SHDR_13yrs	13	13322417.4	8731991	2.76E-01	2.1072E+13	4.E+13	7.39E+01
70-100_MR269-OWT_13yrs	13	12736499.1	8731991	2.10E-01	1.60361E+13	3.E+13	7.40E+01
70-100_MR188-OWT_15yrs	15	6788520.03	9603059	8.59E-02	7.92163E+12	2.E+09	9.09E+01
70-100-DR1123_IWT_17yrs	17	6905007.77	10440436	1.15E-01	1.24993E+13	5.E+09	1.08E+02
70-100-MR536_IWT_19yrs	19	15975218.7	11249191	1.77E-01	2.23353E+13	8.E+13	1.23E+02
70-100-MR536_BWT_19yrs	19	11777009.7	11249191	2.20E-03	2.78592E+11	2.E+13	1.24E+02
70-100-P1398_OWT_22yrs	22	15387967.3	12416858	5.73E-02	8.82749E+12	7.E+13	1.50E+02
70-100-P1398_OWT_23yrs	23	11184800	12795426	1.58E-02	2.59412E+12	2.E+13	1.61E+02
70-100 PAVaged_Uncond_Arrh	3	3379591.42					
70-100_1252_Q-Sun	5	4423885.93					



APPENDIX G

		G* at 62.83 rad/s				Calculation of G* standard error of Estimate (SEE)	
		Σ Error	Sserr	8.05E+14			
		2.42	mean	1.63E+07	$\Sigma (y-y)^2$	9.70E+03	
			Stot	2.2.E+15	N	32	
			R ²	0.63	SEE	17.41	
type binder	time [Yrs]	G* @62.83 rad/s [Pa]	G* model @62.83 rad/s [Pa]	Error	error G*	Stot G*	(y-y) ²
70-100 Unaged_Uncond_Arrh	0	2141172.48	2141365	8.10E-09	37140.27009	2.E+14	4.49E+00
70-100 Unaged_Uncond_WLF	0	2159154.29	2141365	6.90E-05	316451583.6	2.E+14	4.49E+00
70-100 Unaged_Cond_Arrh	0	2560338.63	2141365	3.83E-02	1.75539E+11	2.E+14	4.48E+00
70-100 Unaged_Cond_WLF	0	2245121.78	2141365	2.35E-03	10765426873	2.E+14	4.49E+00
70-100_DR02175_OWT_3yrs_Arrh	3	6799831.4	10248297	1.13E-01	1.18919E+13	9.E+13	1.04E+02
70-100_DR1298_SHDR_4yrs	4	9497124.99	11625709	3.35E-02	4.53087E+12	5.E+13	1.33E+02
70-100_DR1298_OWT_4yrs	4	7611675.13	11625709	1.19E-01	1.61125E+13	7.E+13	1.33E+02
70-100_DR1398_BWT_5yrs	5	29032411.3	12853327	1.58E+00	2.61763E+14	2.E+14	1.58E+02
70-100_DR1398_IWT_5yrs	5	18644497.1	12853327	2.03E-01	3.35377E+13	6.E+12	1.60E+02
70-100_DR2175-BWT_6yrs	6	16506877.1	13973417	3.29E-02	6.41842E+12	6.E+10	1.91E+02
70-100_DR2175-IWT_6yrs	6	15650923.7	13973417	1.44E-02	2.81403E+12	4.E+11	1.91E+02
70-100_N10-3-BWT_9yrs	9	11285385.9	16902254	1.10E-01	3.15492E+13	2.E+13	2.82E+02
70-100_N10-3-OWT_9yrs	9	10918295.9	16902254	1.25E-01	3.58077E+13	3.E+13	2.82E+02
70-100_N10-3-IWT_9yrs	9	13883228.8	16902254	3.19E-02	9.11451E+12	6.E+12	2.81E+02
70-100_MR174-SHDR_10yrs	10	19083773.7	17775425	5.42E-03	1.71178E+12	8.E+12	3.09E+02
70-100_MR174-OWT_10yrs	10	18818718.2	17775425	3.44E-03	1.08846E+12	7.E+12	3.09E+02
70-100_DR2216-BWT_10yrs	10	17812456.2	17775425	4.34E-06	1371319656	2.E+12	3.10E+02
70-100_DR2216-IWT_10yrs	10	17656443.8	17775425	4.48E-05	14156490230	2.E+12	3.10E+02
70-100_N6-5-SHDR_11yrs	11	18166081.2	18609718	5.68E-04	1.96814E+11	4.E+12	3.40E+02
70-100_N6-5-OWT_11yrs	11	17620830.9	18609718	2.82E-03	9.77897E+11	2.E+12	3.40E+02
70-100_DR1452-BWT_12yrs	12	14811564.9	19410183	5.61E-02	2.11473E+13	2.E+12	3.71E+02
70-100_DR1452-OWT_12yrs	12	14354910.4	19410183	6.78E-02	2.55558E+13	4.E+12	3.71E+02
70-100_N6-5-SHDR_13yrs	13	17611582.9	20180853	1.62E-02	6.60115E+12	2.E+12	4.00E+02
70-100_N6-5-OWT_13yrs	13	15375699	20180853	5.67E-02	2.30895E+13	8.E+11	4.01E+02
70-100_MR269-SHDR_13yrs	13	28146461.8	20180853	1.56E-01	6.34509E+13	1.E+14	3.96E+02
70-100_MR269-OWT_13yrs	13	25620605.9	20180853	7.27E-02	2.95909E+13	9.E+13	3.97E+02
70-100_MR188-OWT_15yrs	15	16185011.9	21645373	6.36E-02	2.98155E+13	7.E+09	4.62E+02
70-100-DR1123_IWT_17yrs	17	16511545	23023464	8.00E-02	4.24051E+13	6.E+10	5.23E+02
70-100-MR536_IWT_19yrs	19	34518293.1	24329599	1.75E-01	1.03809E+14	3.E+14	5.75E+02
70-100-MR536_BWT_19yrs	19	26062663.9	24329599	5.07E-03	3.00351E+12	1.E+14	5.79E+02
70-100-P1398_OWT_22yrs	22	31372590.4	26176805	3.94E-02	2.69962E+13	2.E+14	6.69E+02
70-100-P1398_OWT_23yrs	23	23353430.1	26766713	1.63E-02	1.16505E+13	5.E+13	7.04E+02
70-100 PAVaged_Uncond_Arrh	1	7650750					
70-100_1252_Q-Sun	4	10977402.4					



APPENDIX G

		G* at 100 rad/s			Calculation of G* standard error of Estimate (SEE)		
		Σ Error	Sserr	1.09E+15	Σ (y-y) ²	1.34E+04	
			mean	1.91E+07		N	32
		2.52	Stot	2.9.E+15	SEE	20.43	
		R ²	0.63				
type binder	time [Yrs]	G* @100 rad/s [Pa]	G* model @100 rad/s [Pa]	Error	error G*	Stot G*	(y-y) ²
70-100 Unaged_Uncond_Arrh	0	2829662.39	2829856	4.67E-09	37401.3477	3.E+14	7.85E+00
70-100 Unaged_Uncond_WLF	0	2771994.77	2829856	4.18E-04	3347896215	3.E+14	7.85E+00
70-100 Unaged_Cond_Arrh	0	3351875.56	2829856	3.40E-02	2.72505E+11	2.E+14	7.82E+00
70-100 Unaged_Cond_WLF	0	2939208.42	2829856	1.49E-03	11957999924	3.E+14	7.84E+00
70-100_DR02175_OWT_3yrs_Arrh	3	7938568.08	12102471	1.18E-01	1.73381E+13	1.E+14	1.45E+02
70-100_DR1298_SHDR_4yrs	4	11047957.6	13698875	3.74E-02	7.02736E+12	7.E+13	1.85E+02
70-100_DR1298_OWT_4yrs	4	9011256.46	13698875	1.17E-01	2.19738E+13	1.E+14	1.85E+02
70-100_DR1398_BWT_5yrs	5	34711135	15124092	1.68E+00	3.83652E+14	2.E+14	2.18E+02
70-100_DR1398_IWT_5yrs	5	22735859.7	15124092	2.53E-01	5.7939E+13	1.E+13	2.22E+02
70-100_DR2175-BWT_6yrs	6	19165599.8	16426236	2.78E-02	7.50412E+12	1.E+09	2.64E+02
70-100_DR2175-IWT_6yrs	6	18014066.3	16426236	9.34E-03	2.52121E+12	1.E+12	2.64E+02
70-100_N10-3-BWT_9yrs	9	14131096.6	19837960	8.28E-02	3.25683E+13	3.E+13	3.88E+02
70-100_N10-3-OWT_9yrs	9	13960699.9	19837960	8.78E-02	3.45422E+13	3.E+13	3.88E+02
70-100_N10-3-IWT_9yrs	9	14857809.2	19837960	6.30E-02	2.48019E+13	2.E+13	3.88E+02
70-100_MR174-SHDR_10yrs	10	22078451.1	20856790	3.43E-03	1.49246E+12	9.E+12	4.26E+02
70-100_MR174-OWT_10yrs	10	21770712.8	20856790	1.92E-03	8.35255E+11	7.E+12	4.26E+02
70-100_DR2216-BWT_10yrs	10	20583091.6	20856790	1.72E-04	74910756659	2.E+12	4.26E+02
70-100_DR2216-IWT_10yrs	10	20402808.3	20856790	4.74E-04	2.06099E+11	2.E+12	4.27E+02
70-100_N6-5-SHDR_11yrs	11	20994840.4	21830910	1.47E-03	6.99012E+11	3.E+12	4.67E+02
70-100_N6-5-OWT_11yrs	11	20553690.8	21830910	3.42E-03	1.63129E+12	2.E+12	4.68E+02
70-100_DR1452-BWT_12yrs	12	16334000.4	22766103	7.98E-02	4.13719E+13	8.E+12	5.11E+02
70-100_DR1452-OWT_12yrs	12	17182535.7	22766103	6.02E-02	3.11762E+13	4.E+12	5.11E+02
70-100_N6-5-SHDR_13yrs	13	20909719.2	23666991	1.36E-02	7.60255E+12	3.E+12	5.50E+02
70-100_N6-5-OWT_13yrs	13	18773155.5	23666991	4.28E-02	2.39496E+13	1.E+11	5.51E+02
70-100_MR269-SHDR_13yrs	13	32700631.2	23666991	1.46E-01	8.16067E+13	2.E+14	5.45E+02
70-100_MR269-OWT_13yrs	13	30239499.6	23666991	7.71E-02	4.31979E+13	1.E+14	5.46E+02
70-100_MR188-OWT_15yrs	15	19570283.1	25380253	5.24E-02	3.37557E+13	2.E+11	6.34E+02
70-100-DR1123_IWT_17yrs	17	19879308.5	26993856	6.95E-02	5.06168E+13	6.E+11	7.18E+02
70-100-MR536_IWT_19yrs	19	38902413.8	28524415	1.32E-01	1.07703E+14	4.E+14	7.92E+02
70-100-MR536_BWT_19yrs	19	30795180.9	28524415	6.34E-03	5.15638E+12	1.E+14	7.96E+02
70-100-P1398_OWT_22yrs	22	37775692.3	30690891	5.33E-02	5.01944E+13	3.E+14	9.19E+02
70-100-P1398_OWT_23yrs	23	27039647.2	31383198	1.92E-02	1.88664E+13	6.E+13	9.68E+02
70-100 PAVaged_Uncond_Arrh	1	8831782.94					
70-100_1252_Q-Sun	4	14001769.7					



APPENDIX G

G.11 SE1 seal's ageing model data at 10, 62.83 and 100 rad/s

		G* at 10 rad/s				Calculation of G* standard error of Estimate (SEE)	
		Σ Error	Sserr	1.12E+14	Σ (y-y) ²	2.37E+03	
			mean	9.15E+06		N	23
		1.40	Stot	6.3.E+14	SEE	10.15	
			R ²	0.8219			
Type binder	Time [Yrs]	G* @10 rad/s [Pa]	G* model @10 rad/s [Pa]	Error	error G*	Stot G*	(y-y) ²
SE1 Unaged_Uncond_Arrh	0	812560.655	812561	1.17E-21	7.74134E-10	7.E+13	6.47E-01
SE1 Unaged_Cond_Arrh	0	844148.541	812561	1.51E-03	997794532.1	7.E+13	6.47E-01
SE1_N2-32_OWT_2yrs_Arrh	2	1616477.58	3706747	3.18E-01	4.36923E+12	6.E+13	1.36E+01
SE1_N2-32_SHDR_2yrs_Arrh	2	2342699.31	3706747	1.35E-01	1.86063E+12	5.E+13	1.36E+01
SE1_N2-32_OWT_6yrs_Arrh	6	6064171.17	8002438	5.87E-02	3.75688E+12	1.E+13	6.31E+01
SE1_N2-32_SHDR_6yrs_Arrh	6	9971937.1	8002438	6.06E-02	3.87893E+12	7.E+11	6.25E+01
SE1_N1-29_OWT_6yrs_Arrh	6	8441568.36	8002438	3.01E-03	1.92836E+11	5.E+11	6.27E+01
SE1_N1-29_SHDR_6yrs_Arrh	6	6967678.68	8002438	1.67E-02	1.07073E+12	5.E+12	6.29E+01
SE1_N6-4_OWT_6yrs_Arrh	6	8589711.71	8002438	5.39E-03	3.44891E+11	3.E+11	6.27E+01
SE1_N6-4_SHDR_6yrs_Arrh	6	8589312.26	8002438	5.38E-03	3.44422E+11	3.E+11	6.27E+01
SE1_N2-31_OWT_7yrs_Arrh	7	13696981.8	8981635	2.76E-01	2.22345E+13	2.E+13	7.82E+01
SE1_N8-8_OWT_7yrs_Arrh	7	7858990.52	8981635	1.56E-02	1.26033E+12	2.E+12	7.93E+01
SE1_N8-8_SHDR_7yrs_Arrh	7	7859040.5	8981635	1.56E-02	1.26022E+12	2.E+12	7.93E+01
SE1_N2-31_BWT_7yrs_Arrh	7	7544594.3	8981635	2.56E-02	2.06509E+12	3.E+12	7.93E+01
SE1_N10-2_OWT_7yrs_Arrh	7	9174675.35	8981635	4.62E-04	37264664053	5.E+08	7.90E+01
SE1_N10-2_SHDR_7yrs_Arrh	7	8627033.74	8981635	1.56E-03	1.25742E+11	3.E+11	7.91E+01
SE1_N6-4_OWT_10yrs_Arrh	10	12056224.2	11789383	5.12E-04	71204256032	8.E+12	1.36E+02
SE1_N6-4_SHDR_10yrs_Arrh	10	6327749.44	11789383	2.15E-01	2.98294E+13	8.E+12	1.38E+02
SE1_N1-29_OWT_10yrs	10	16451401.9	11789383	1.56E-01	2.17344E+13	5.E+13	1.35E+02
SE1_N2-31_SHDR_12yrs_Arrh	12	17392652.6	13578762	7.89E-02	1.45458E+13	7.E+13	1.80E+02
SE1_N2-31_S_SHDR_12yrs_Arrh	12	12905530.9	13578762	2.46E-03	4.5324E+11	1.E+13	1.81E+02
SE1_N2-31_S_OWT_12yrs_Arrh	12	12146031.3	13578762	1.11E-02	2.05272E+12	9.E+12	1.81E+02
SE1_N10-3_OWT_24yrs_Arrh	24	22709632.1	23479972	1.08E-03	5.93424E+11	2.E+14	5.41E+02
SE1 Q-SUN	0.57	1831227.84					
SE1 PAVaged_Uncond_Arrh	0.75	2102751					



APPENDIX G

		G* at 62.83 rad/s				Calculation of G* standard error of Estimate (SEE)	
		Σ Error	Sserr	4.81E+14	Σ (y-y') ²	1.08E+04	
			mean	1.97E+07		N	23
		1.04	Stot	2.7.E+15	SEE	21.70	
			R ²	0.8219			
Type binder	Time [Yrs]	G* @62.83 rad/s [Pa]	G* model @62.83 rad/s [Pa]	Error	error G*	Stot G*	(y-y') ²
SE1 Unaged_Uncond_Arrh	0	2738070.41	2738070	1.67E-22	1.25554E-09	3.E+14	7.35E+00
SE1 Unaged_Cond_Arrh	0	2844696.81	2738070	1.52E-03	11369189584	3.E+14	7.34E+00
SE1_N2-32_OWT_2yrs_Arrh	2	4803192.58	8507517	1.90E-01	1.3722E+13	2.E+14	7.16E+01
SE1_N2-32_SHDR_2yrs_Arrh	2	6961083.89	8507517	3.30E-02	2.39145E+12	2.E+14	7.12E+01
SE1_N2-32_OWT_6yrs_Arrh	6	12692512.4	17303081	7.10E-02	2.12573E+13	5.E+13	2.95E+02
SE1_N2-32_SHDR_6yrs_Arrh	6	19966854.1	17303081	2.37E-02	7.09569E+12	5.E+10	2.93E+02
SE1_N1-29_OWT_6yrs_Arrh	6	16026793.7	17303081	5.44E-03	1.62891E+12	1.E+13	2.94E+02
SE1_N1-29_SHDR_6yrs_Arrh	6	16378954.2	17303081	2.85E-03	8.5401E+11	1.E+13	2.94E+02
SE1_N6-4_OWT_6yrs_Arrh	6	15582319.4	17303081	9.89E-03	2.96102E+12	2.E+13	2.94E+02
SE1_N6-4_SHDR_6yrs_Arrh	6	15581979	17303081	9.89E-03	2.96219E+12	2.E+13	2.94E+02
SE1_N2-31_OWT_7yrs_Arrh	7	28287196.7	19324076	2.15E-01	8.03375E+13	7.E+13	3.63E+02
SE1_N8-8_OWT_7yrs_Arrh	7	17288304.4	19324076	1.11E-02	4.14437E+12	6.E+12	3.67E+02
SE1_N8-8_SHDR_7yrs_Arrh	7	17288358	19324076	1.11E-02	4.14415E+12	6.E+12	3.67E+02
SE1_N2-31_BWT_7yrs_Arrh	7	19205645.2	19324076	3.76E-05	14025844273	3.E+11	3.66E+02
SE1_N10-2_OWT_7yrs_Arrh	7	20901597.6	19324076	6.66E-03	2.48857E+12	1.E+12	3.65E+02
SE1_N10-2_SHDR_7yrs_Arrh	7	17499394.7	19324076	8.92E-03	3.32946E+12	5.E+12	3.67E+02
SE1_N6-4_OWT_10yrs_Arrh	10	24329773.6	25141386	1.04E-03	6.58714E+11	2.E+13	6.20E+02
SE1_N6-4_SHDR_10yrs_Arrh	10	16282116.8	25141386	1.24E-01	7.84866E+13	1.E+13	6.24E+02
SE1_N1-29_OWT_10yrs	10	31811802.2	25141386	7.04E-02	4.44945E+13	1.E+14	6.16E+02
SE1_N2-31_SHDR_12yrs_Arrh	12	41316936.9	28863053	1.86E-01	1.55099E+14	5.E+14	8.09E+02
SE1_N2-31_S_SHDR_12yrs_Arrh	12	32669392.2	28863053	1.74E-02	1.44882E+13	2.E+14	8.14E+02
SE1_N2-31_S_OWT_12yrs_Arrh	12	23363829.3	28863053	3.63E-02	3.02415E+13	1.E+13	8.20E+02
SE1_N10-3_OWT_24yrs_Arrh	24	46436389.3	49597956	4.06E-03	9.99551E+12	7.E+14	2.41E+03
SE1 Q-SUN	0.75	5262442.13					
SE1 PAVaged_Uncond_Arrh	1.04	6055381.99					



APPENDIX G

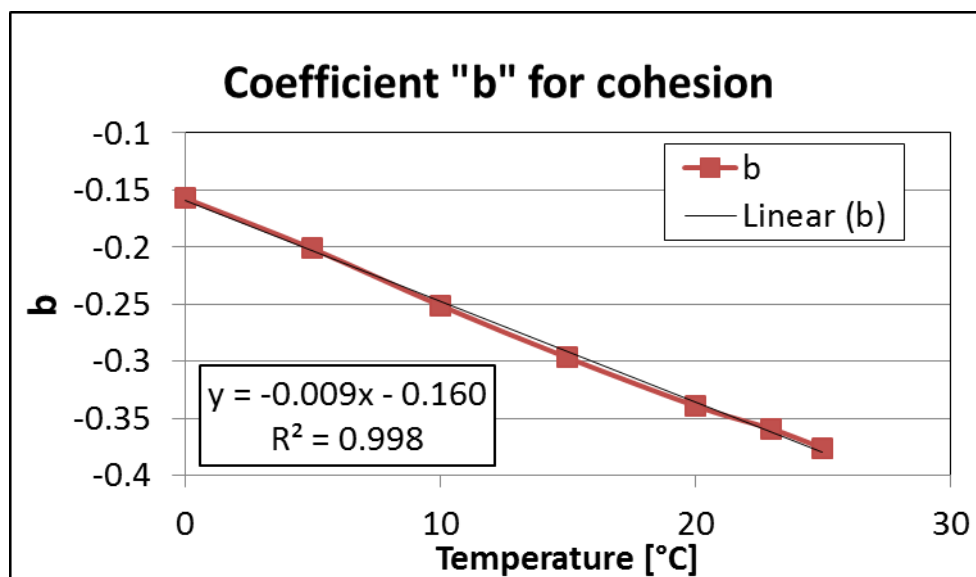
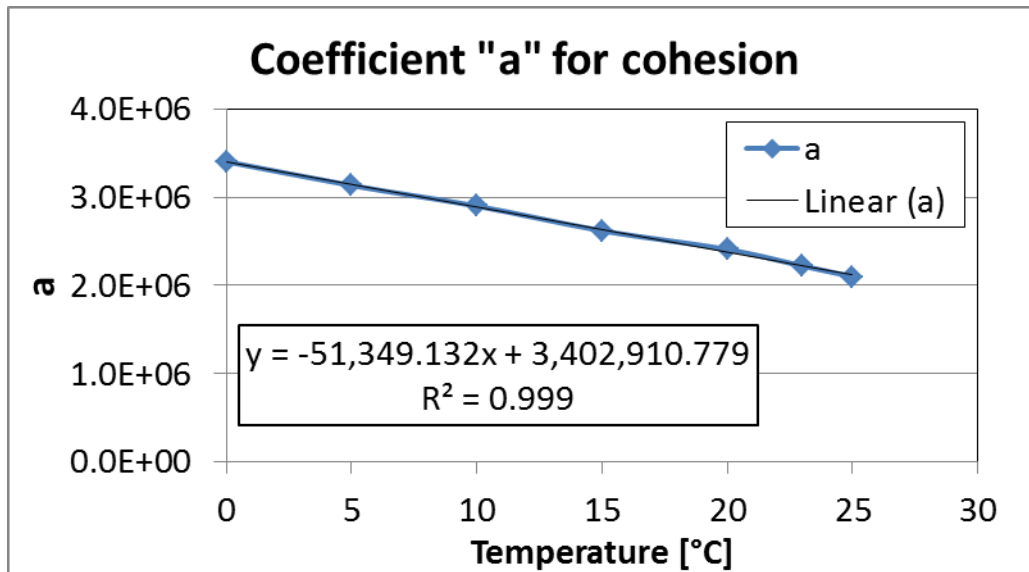
		G* at 100 rad/s				Calculation of G* standard error of Estimate (SEE)	
		Σ Error	Sserr	6.04E+14			
		0.94	mean	2.40E+07	$\Sigma (y-y)^2$	1.56E+04	
			Stot	3.3.E+15	N	23	
			R ²	0.8186	SEE	26.02	
Type binder	Time [Yrs]	G* @100 rad/s [Pa]	G* model @100 rad/s [Pa]	Error	error G*	Stot G*	(y-y) ²
SE1 Unaged_Uncond_Arrh	0	3633007.99	3633008	3.05E-20	4.02111E-07	4.E+14	1.29E+01
SE1 Unaged_Cond_Arrh	0	3781132.4	3633008	1.66E-03	21940838421	4.E+14	1.29E+01
SE1_N2-32_OWT_2yrs_Arrh	2	6585136.35	11484605	1.82E-01	2.40048E+13	3.E+14	1.30E+02
SE1_N2-32_SHDR_2yrs_Arrh	2	9543587.05	11484605	2.86E-02	3.76755E+12	2.E+14	1.30E+02
SE1_N2-32_OWT_6yrs_Arrh	6	16716513.4	21704600	5.28E-02	2.4881E+13	5.E+13	4.64E+02
SE1_N2-32_SHDR_6yrs_Arrh	6	26423485.9	21704600	4.73E-02	2.22679E+13	6.E+12	4.60E+02
SE1_N1-29_OWT_6yrs_Arrh	6	21003414.5	21704600	1.04E-03	4.91661E+11	9.E+12	4.62E+02
SE1_N1-29_SHDR_6yrs_Arrh	6	20712332.2	21704600	2.09E-03	9.84595E+11	1.E+13	4.62E+02
SE1_N6-4_OWT_6yrs_Arrh	6	19530388.6	21704600	1.00E-02	4.7272E+12	2.E+13	4.63E+02
SE1_N6-4_SHDR_6yrs_Arrh	6	19530124.3	21704600	1.00E-02	4.72834E+12	2.E+13	4.63E+02
SE1_N2-31_OWT_7yrs_Arrh	7	35470214.9	23947009	2.32E-01	1.32784E+14	1.E+14	5.57E+02
SE1_N8-8_OWT_7yrs_Arrh	7	22066016.7	23947009	6.17E-03	3.53813E+12	4.E+12	5.63E+02
SE1_N8-8_SHDR_7yrs_Arrh	7	22066068.9	23947009	6.17E-03	3.53794E+12	4.E+12	5.63E+02
SE1_N2-31_BWT_7yrs_Arrh	7	22088481.3	23947009	6.02E-03	3.45413E+12	4.E+12	5.63E+02
SE1_N10-2_OWT_7yrs_Arrh	7	27001787.2	23947009	1.63E-02	9.33167E+12	9.E+12	5.61E+02
SE1_N10-2_SHDR_7yrs_Arrh	7	22565637.8	23947009	3.33E-03	1.90819E+12	2.E+12	5.63E+02
SE1_N6-4_OWT_10yrs_Arrh	10	30052810.1	30260771	4.72E-05	43247901622	4.E+13	8.98E+02
SE1_N6-4_SHDR_10yrs_Arrh	10	20211562.8	30260771	1.10E-01	1.00987E+14	1.E+13	9.04E+02
SE1_N1-29_OWT_10yrs	10	35729767.7	30260771	3.27E-02	2.99099E+13	1.E+14	8.94E+02
SE1_N2-31_SHDR_12yrs_Arrh	12	47709375.9	34211582	1.56E-01	1.8219E+14	6.E+14	1.14E+03
SE1_N2-31_S_SHDR_12yrs_Arrh	12	36652758	34211582	5.09E-03	5.95934E+12	2.E+14	1.15E+03
SE1_N2-31_S_OWT_12yrs_Arrh	12	28348863.1	34211582	2.94E-02	3.43715E+13	2.E+13	1.15E+03
SE1_N10-3_OWT_24yrs_Arrh	24	52151509.8	55374391	3.39E-03	1.0387E+13	8.E+14	3.01E+03
SE1 Q-SUN	0.61	6837444.88					
SE1 PAVaged_Uncond_Arrh	0.90	7929793.13					



APPENDIX H

H END-LIFE DAMAGE MODEL DATA OF BITUMINOUS SEAL MATERIALS

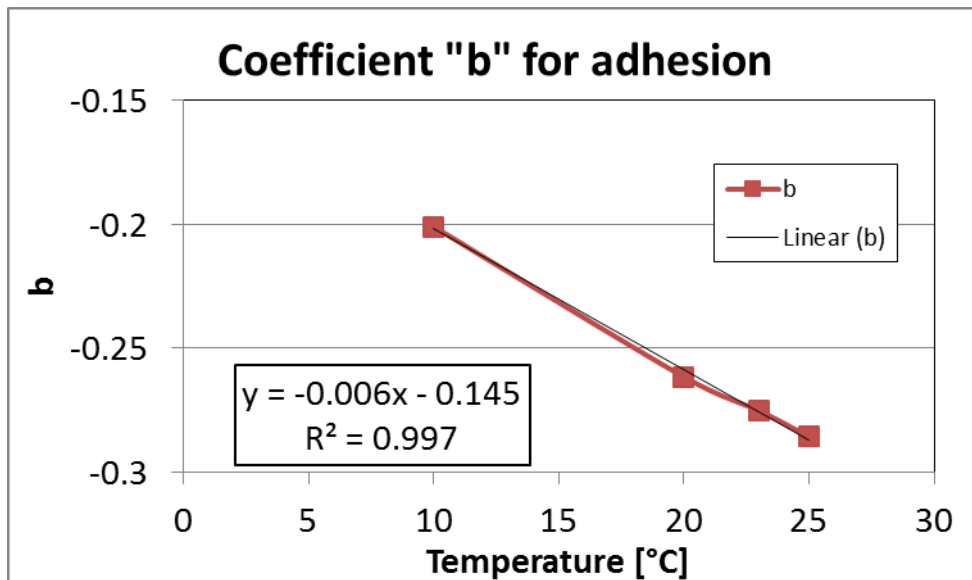
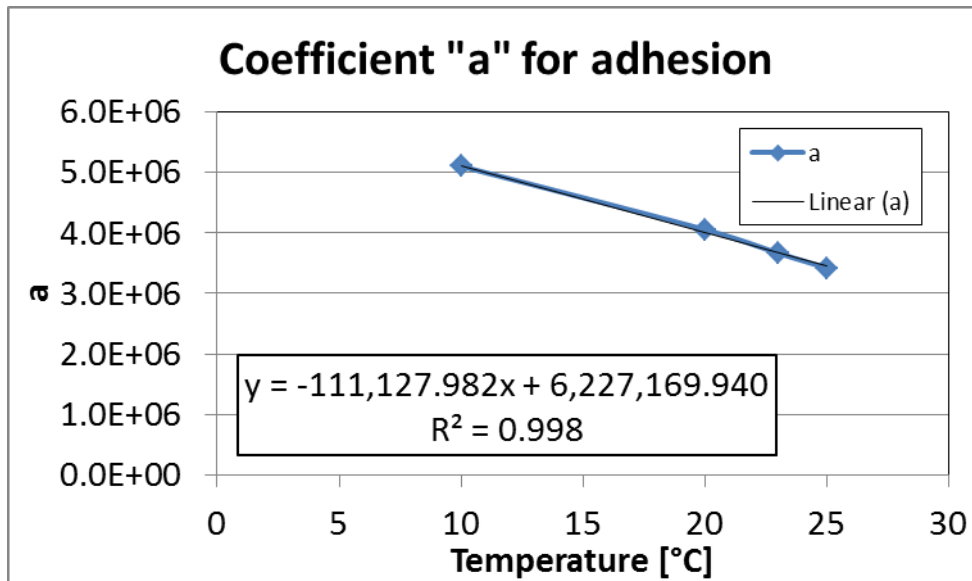
H.1 Graphs of coefficients "a" and "b" for cohesion fatigue damage model





APPENDIX H

H.2 Graphs of coefficients "a" and "b" for adhesion fatigue damage model



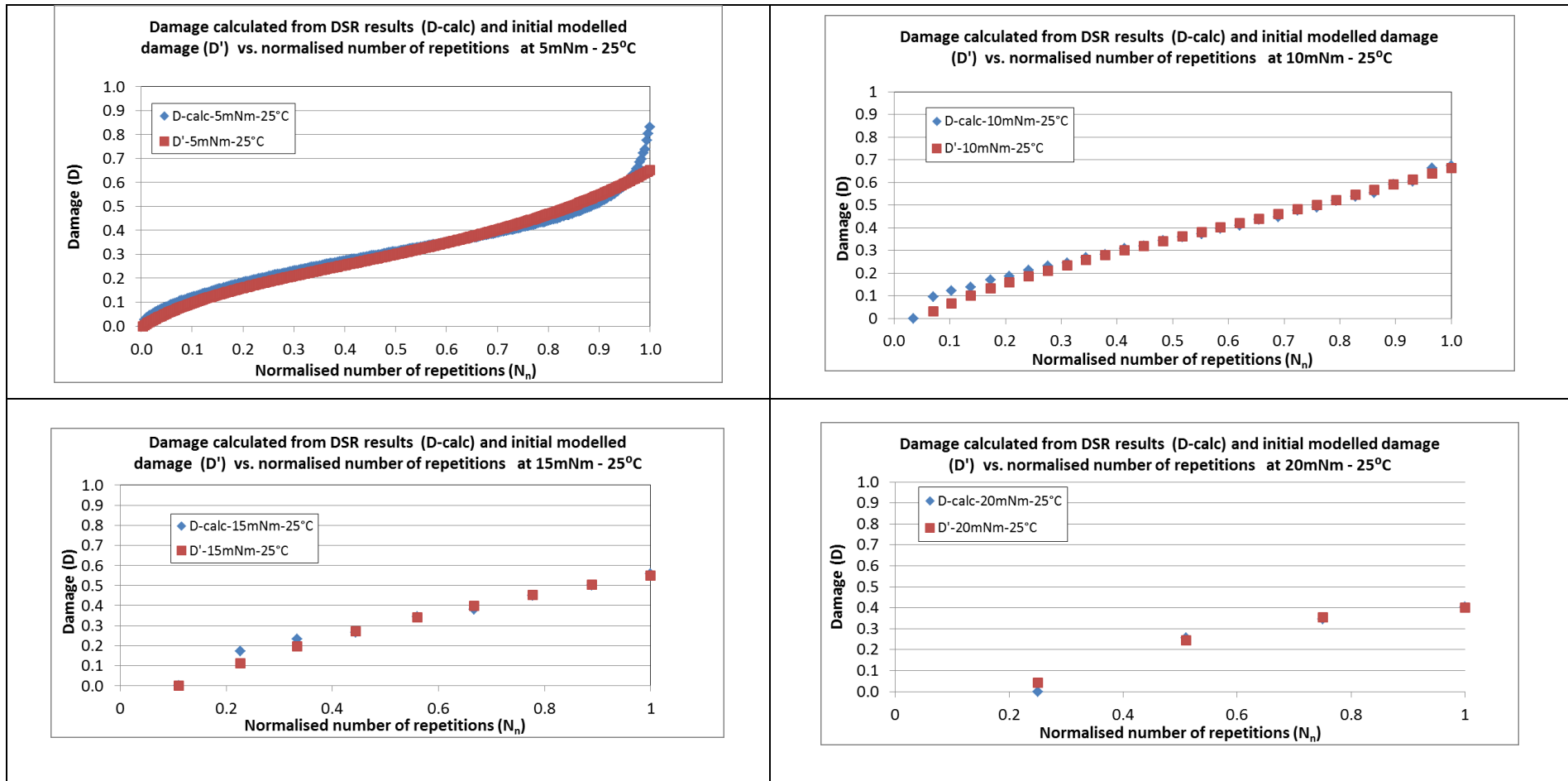


APPENDIX I

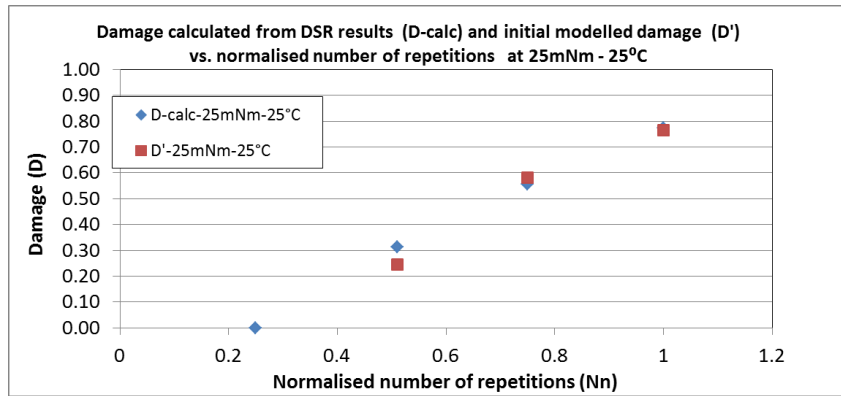
**I DATA OF ACCUMULATED DAMAGE MODEL OF
BITUMINOUS SEAL MATERIALS**

APPENDIX I

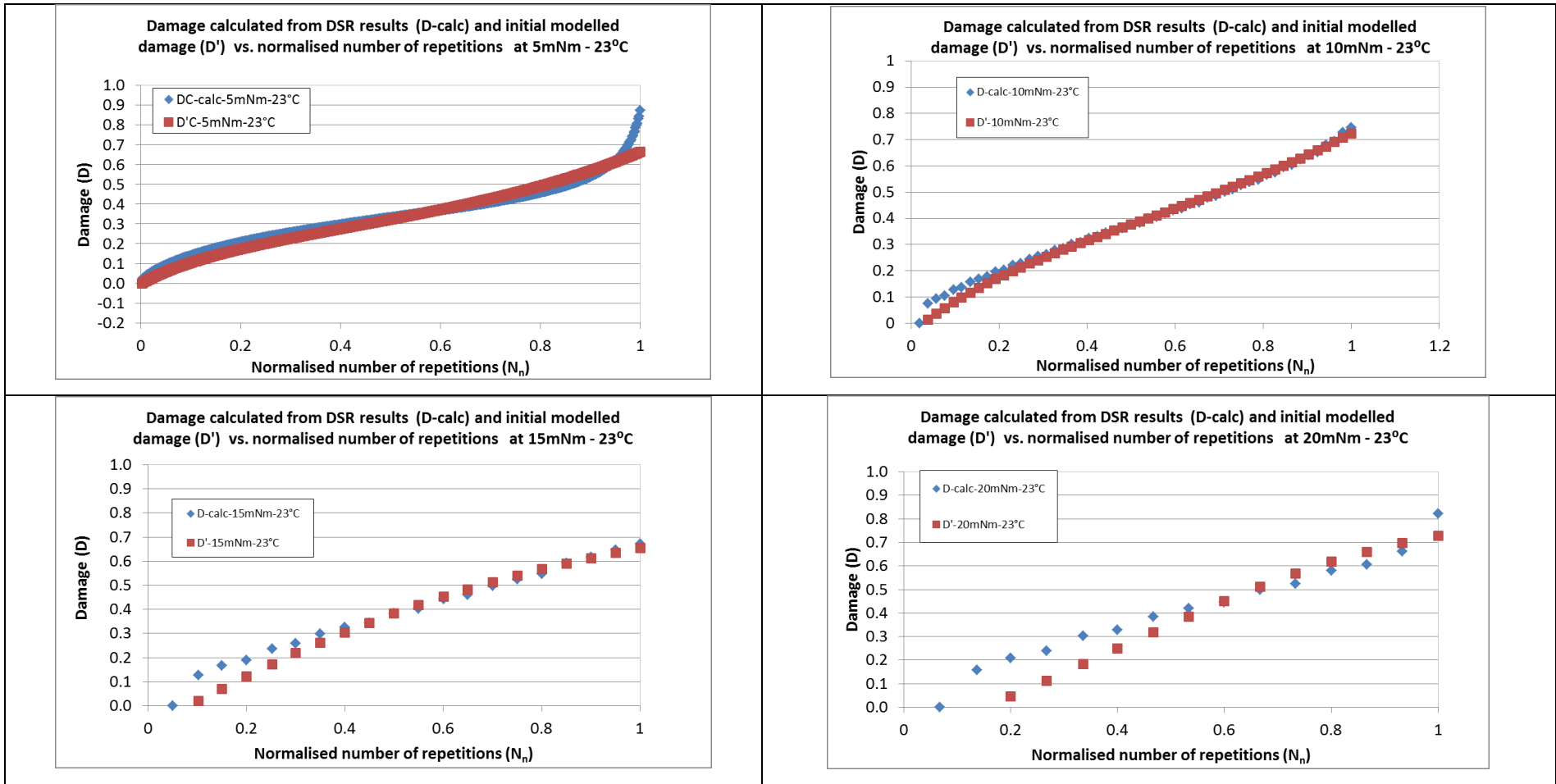
I.1 Graphs of damage as function of normalised number of repetitions for cohesion fatigue damage



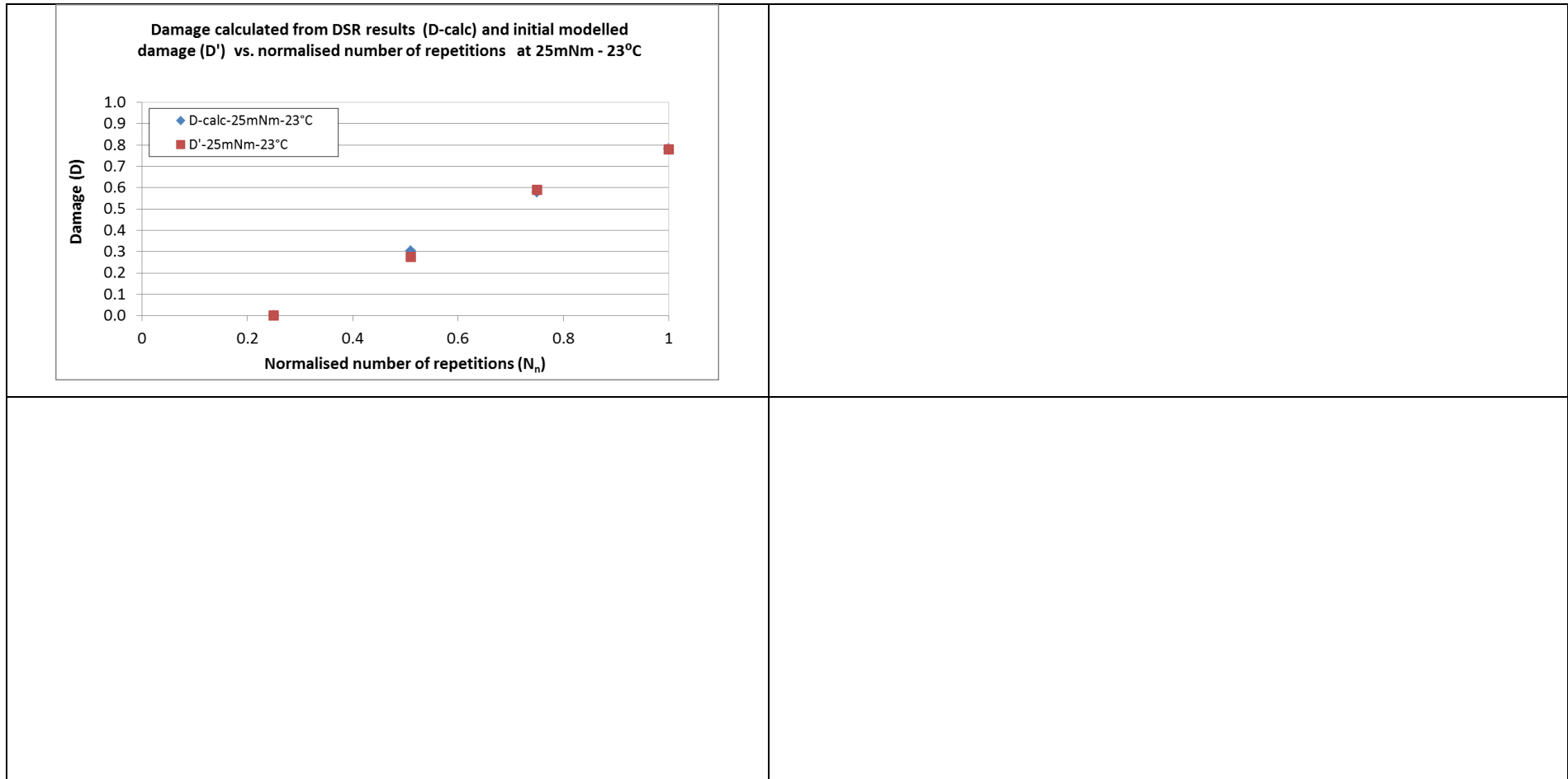
APPENDIX I



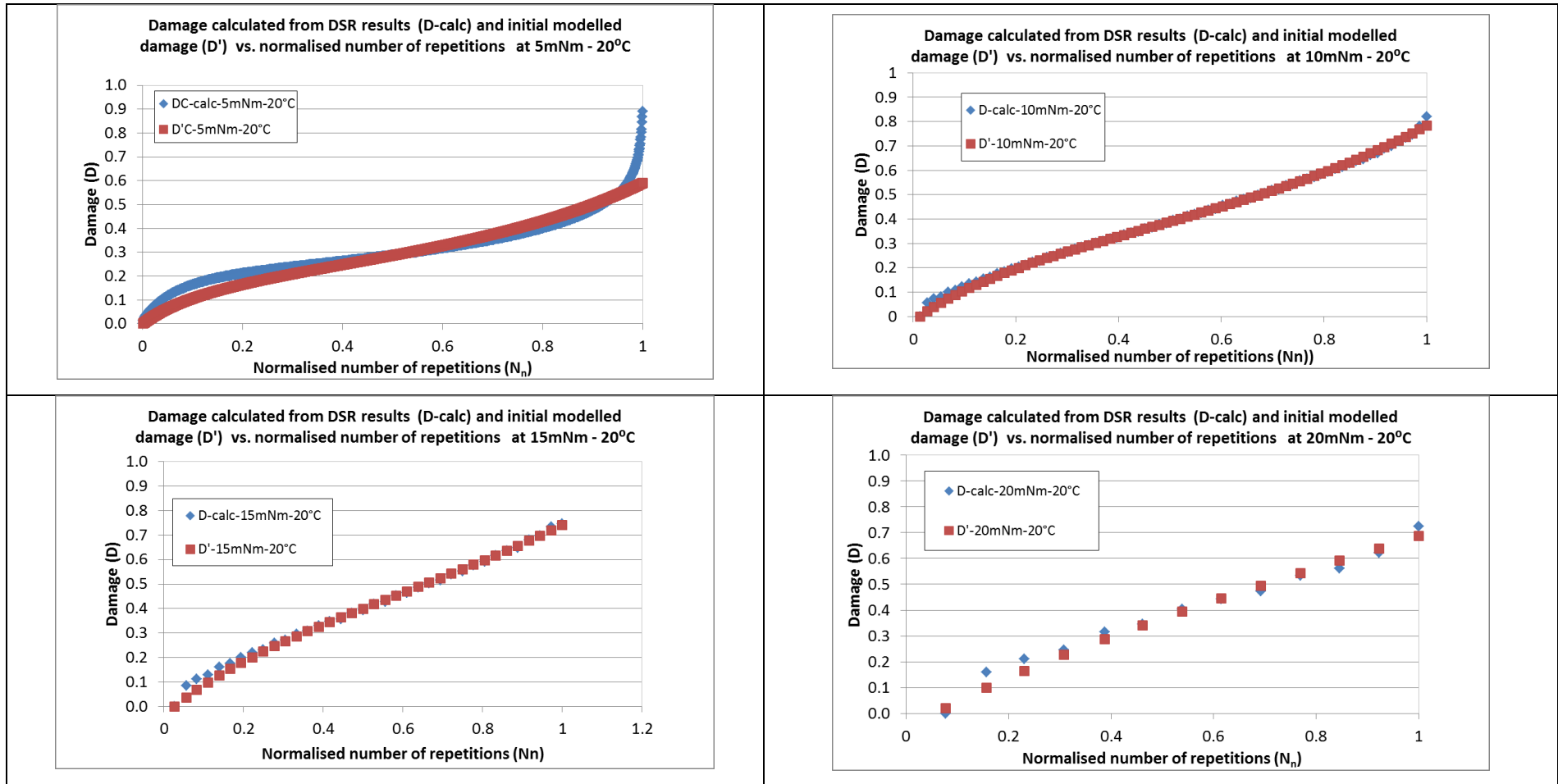
APPENDIX I



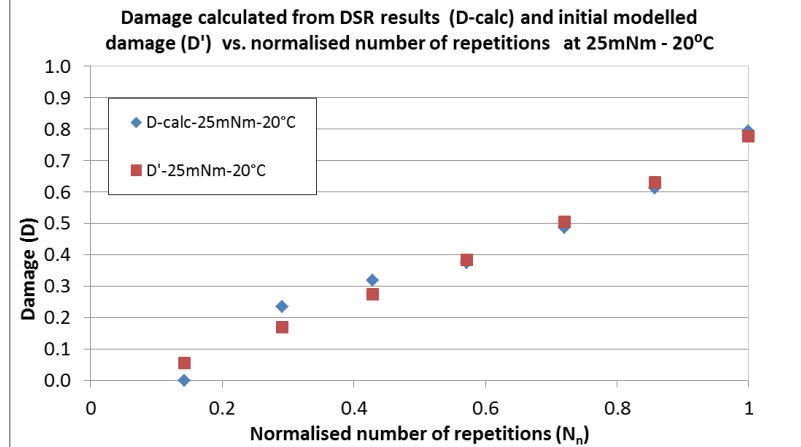
APPENDIX I



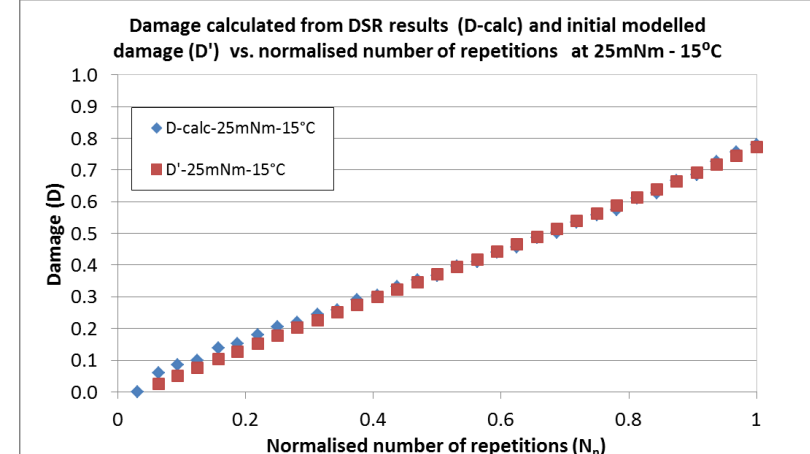
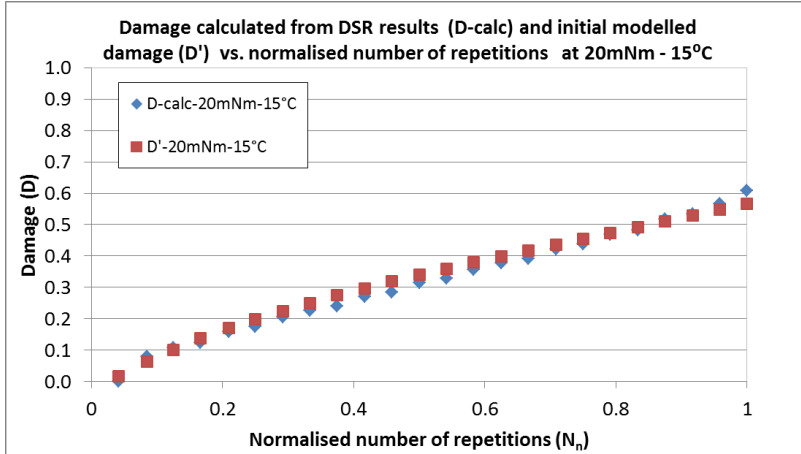
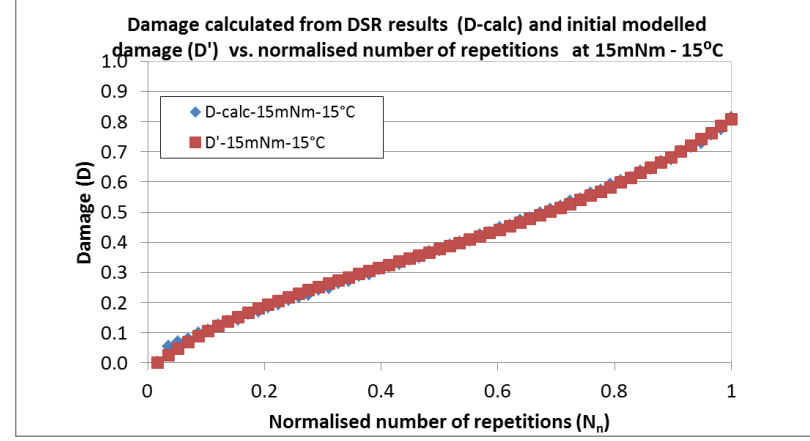
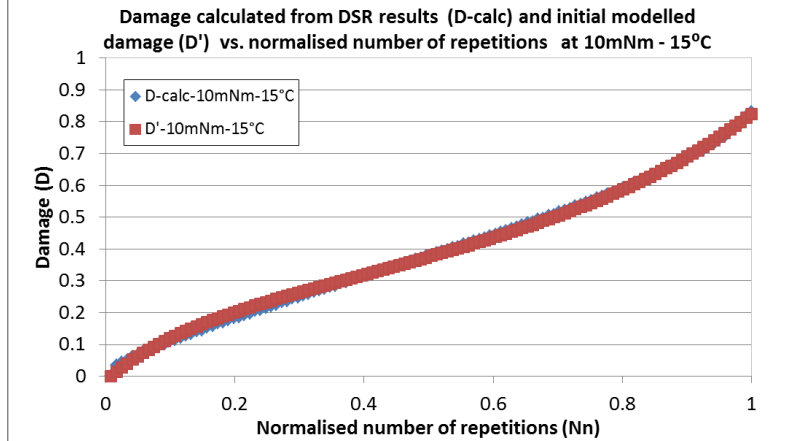
APPENDIX I



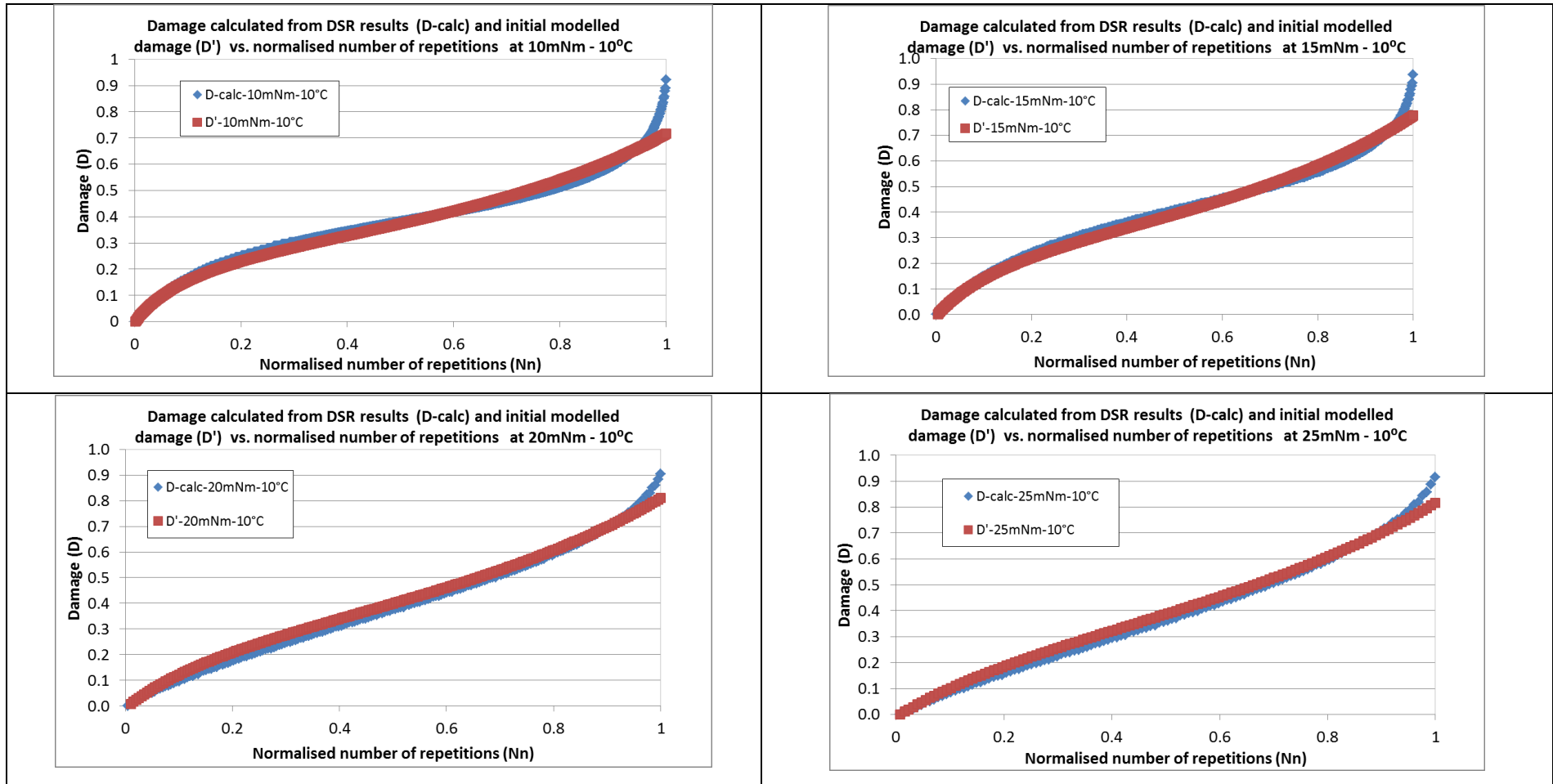
APPENDIX I



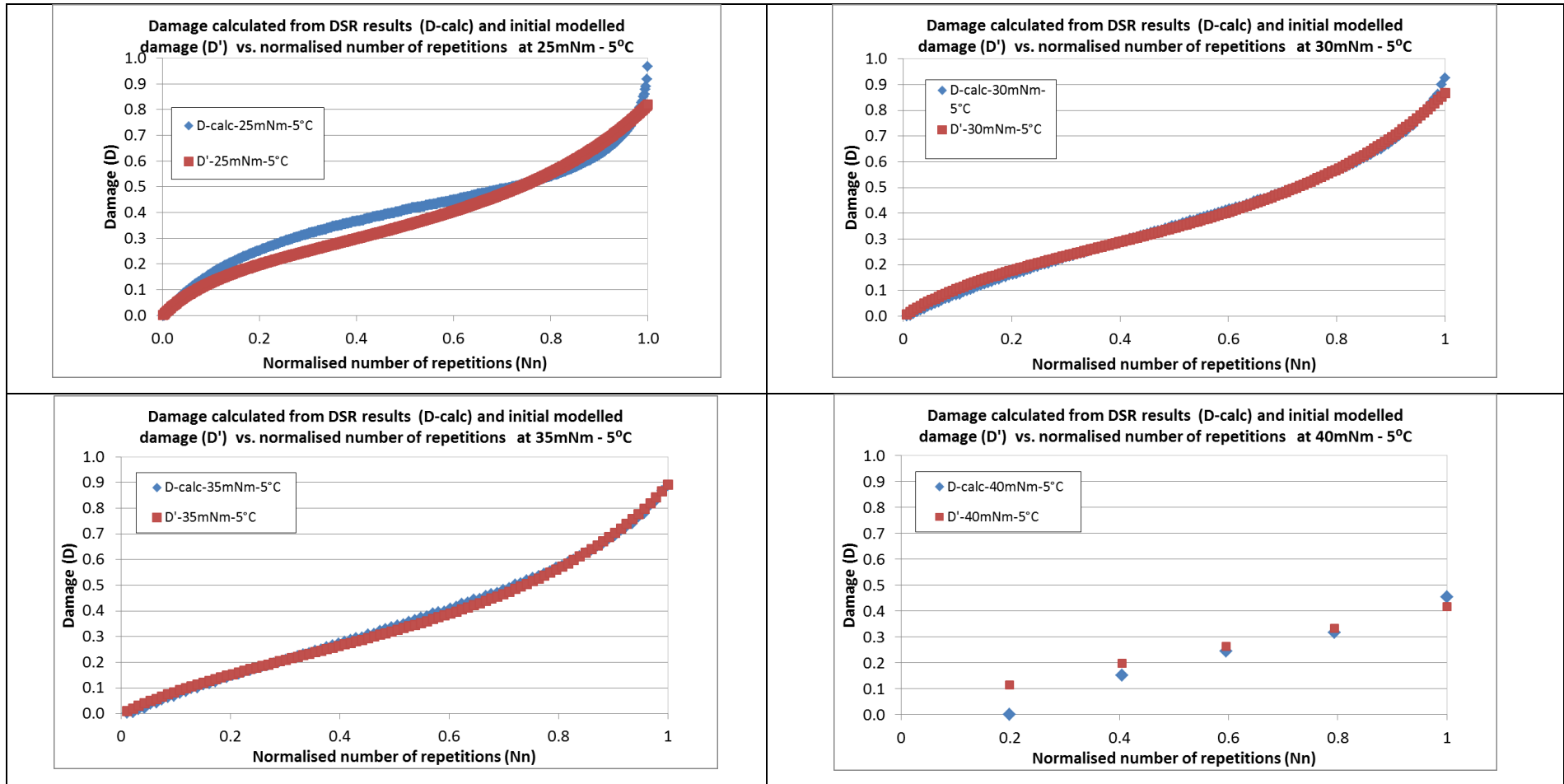
APPENDIX I



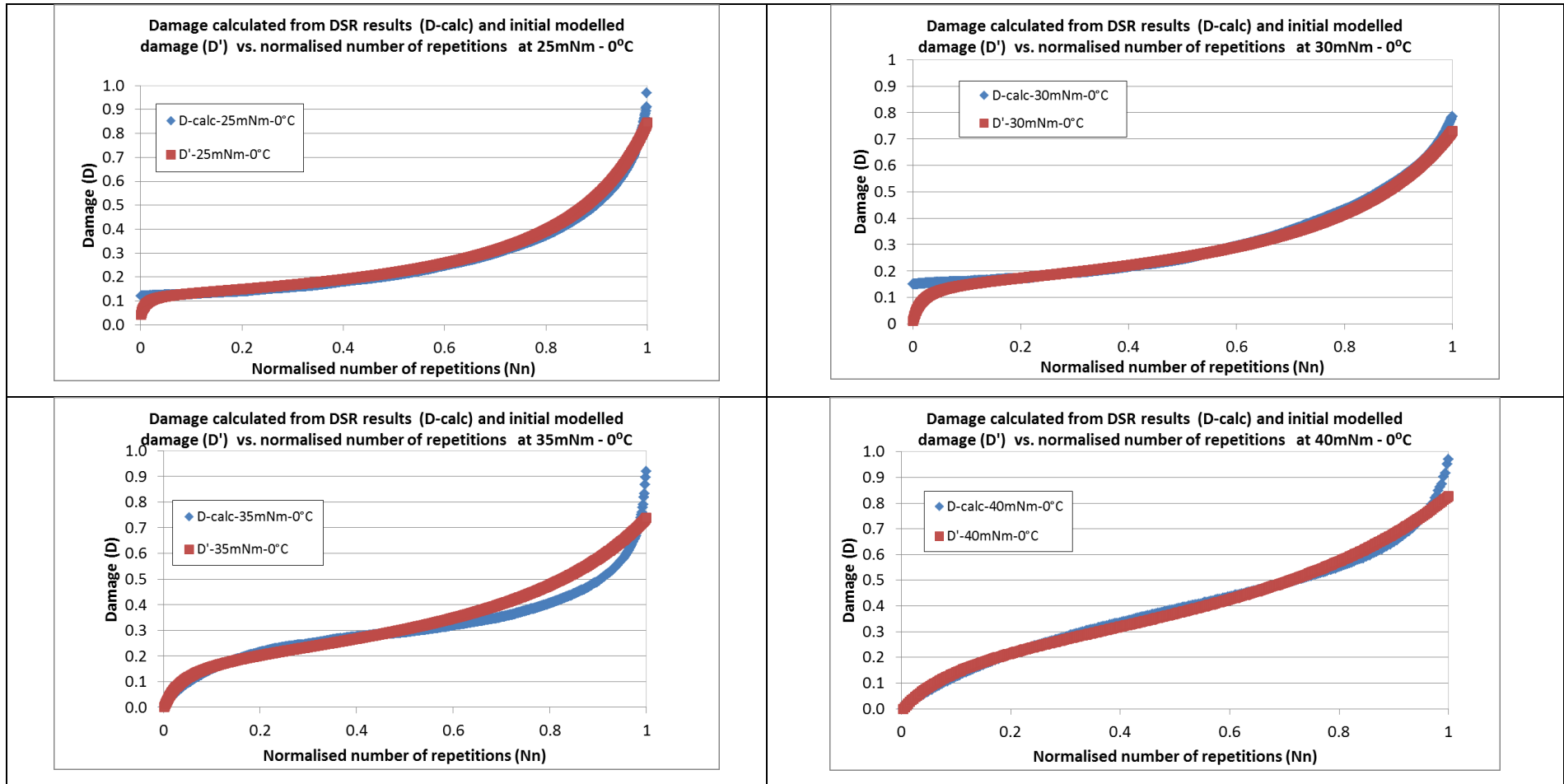
APPENDIX I



APPENDIX I

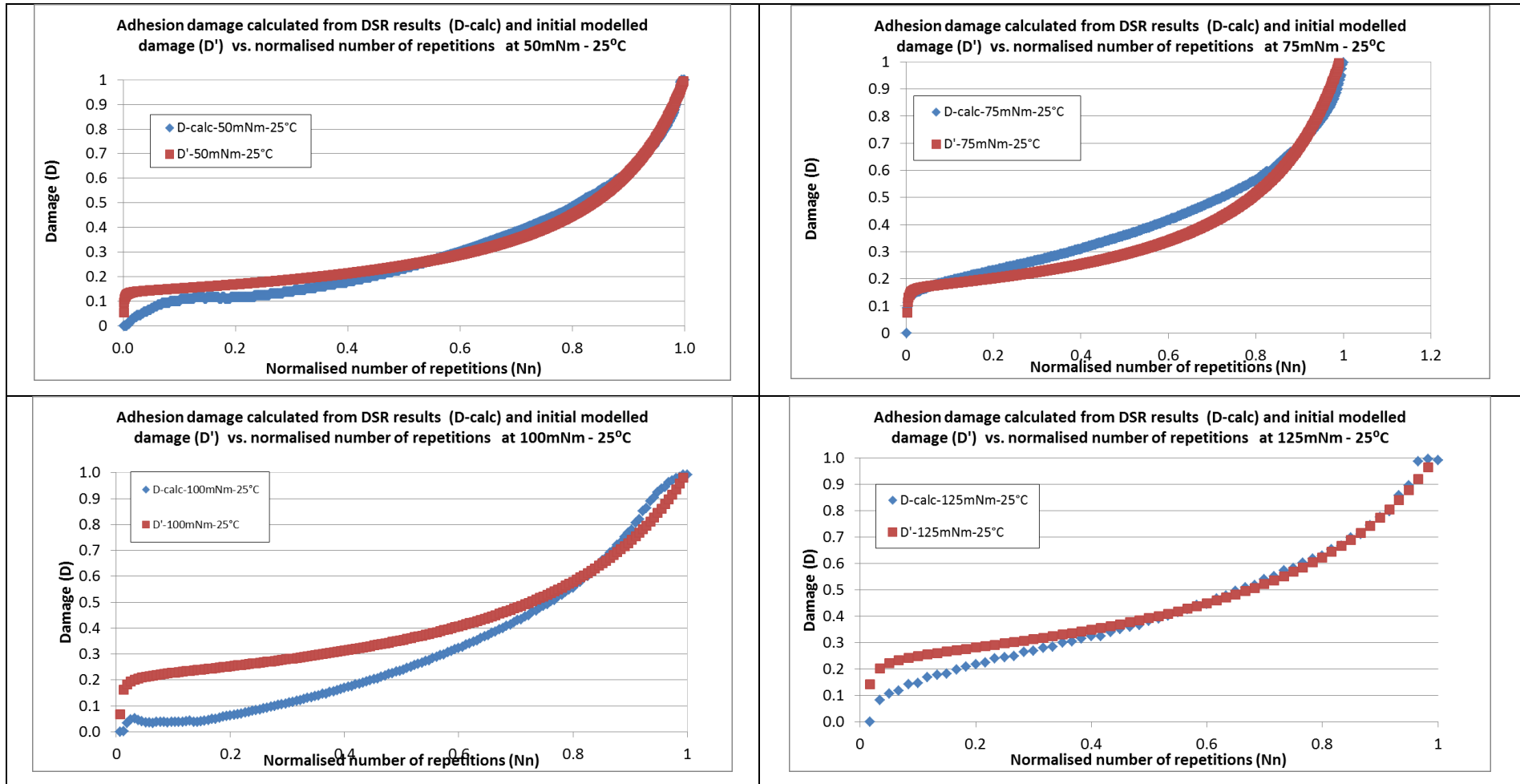


APPENDIX I

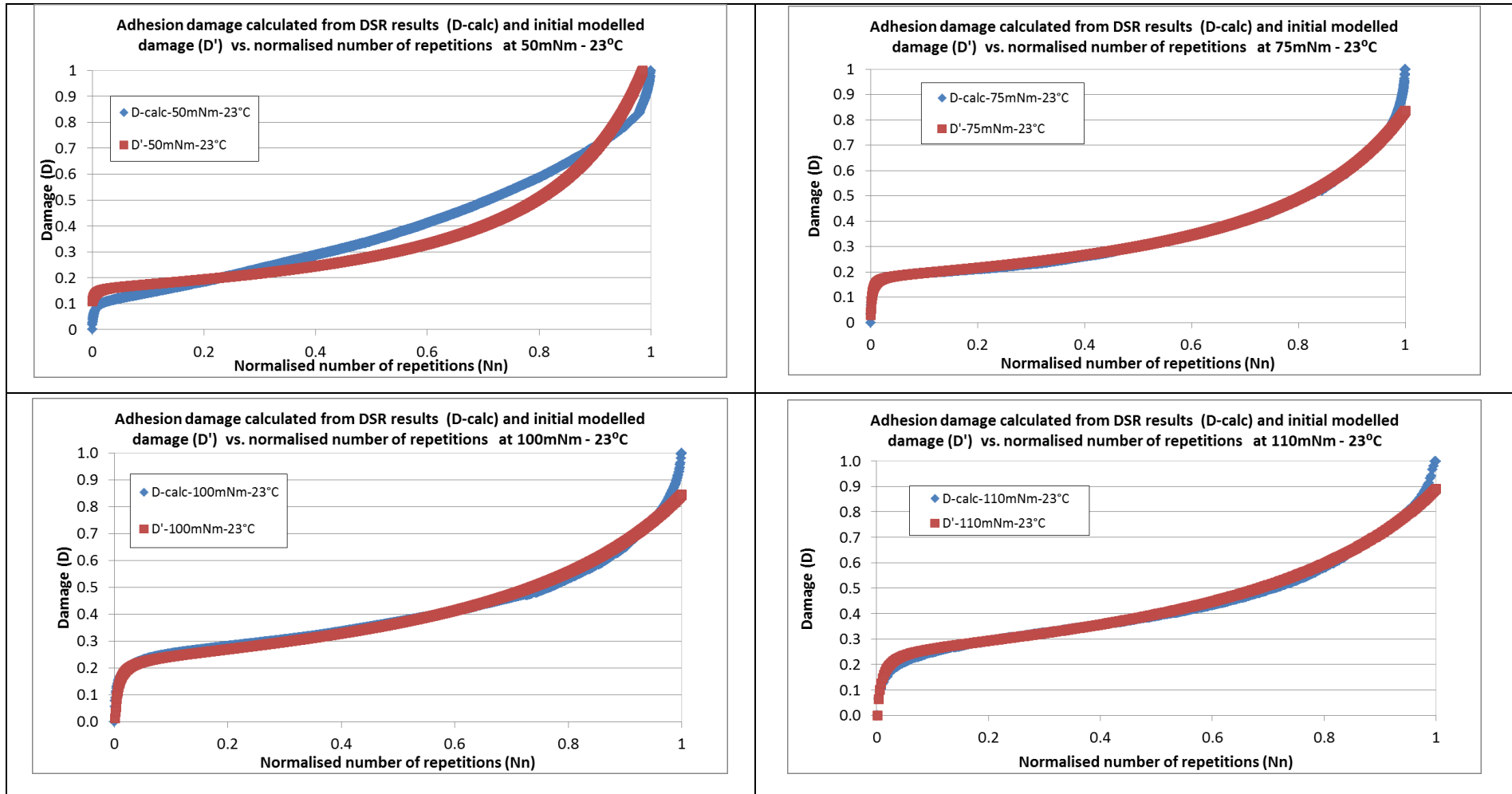


APPENDIX I

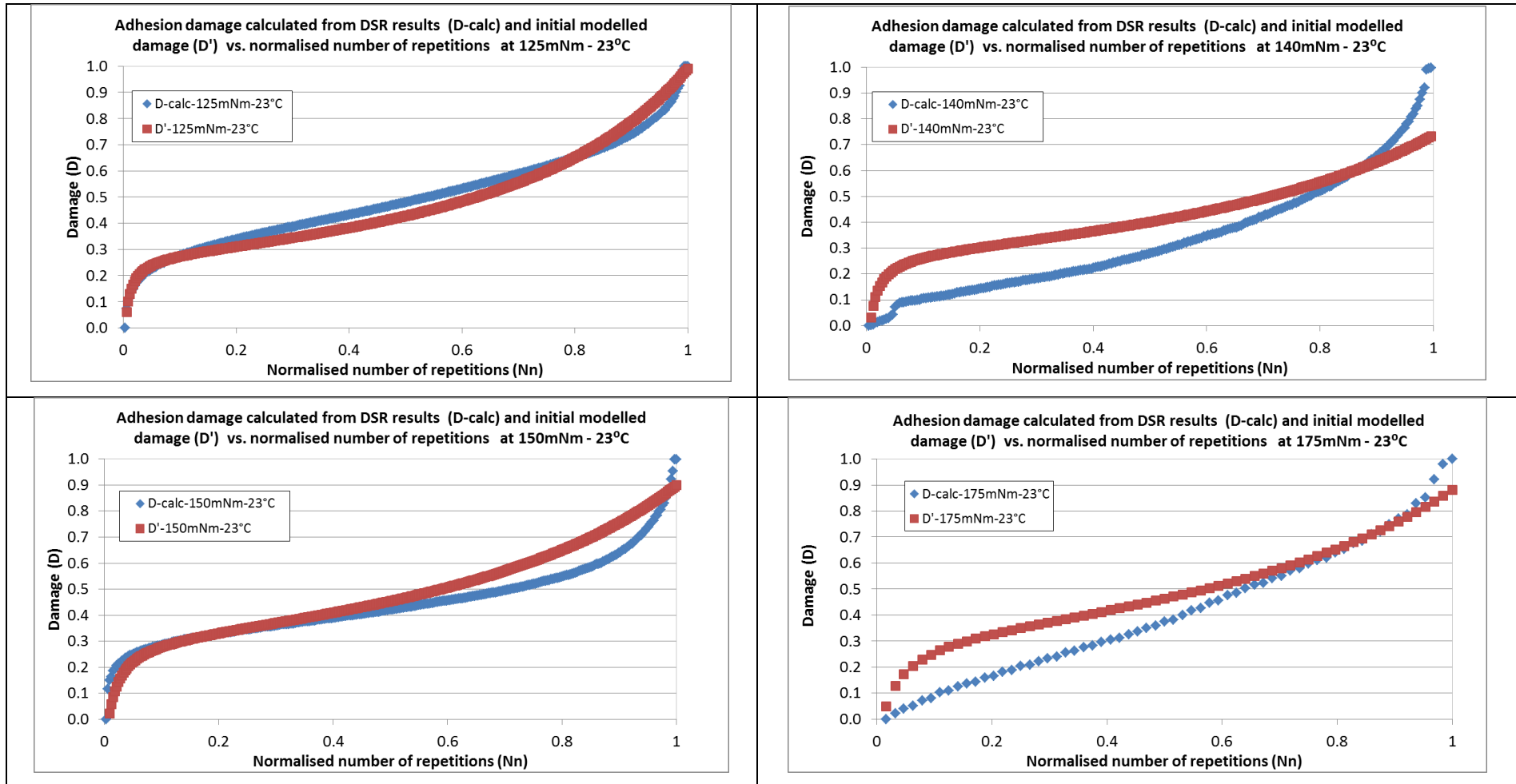
I.2 Graphs of damage as function of normalised number of repetitions for adhesion fatigue damage



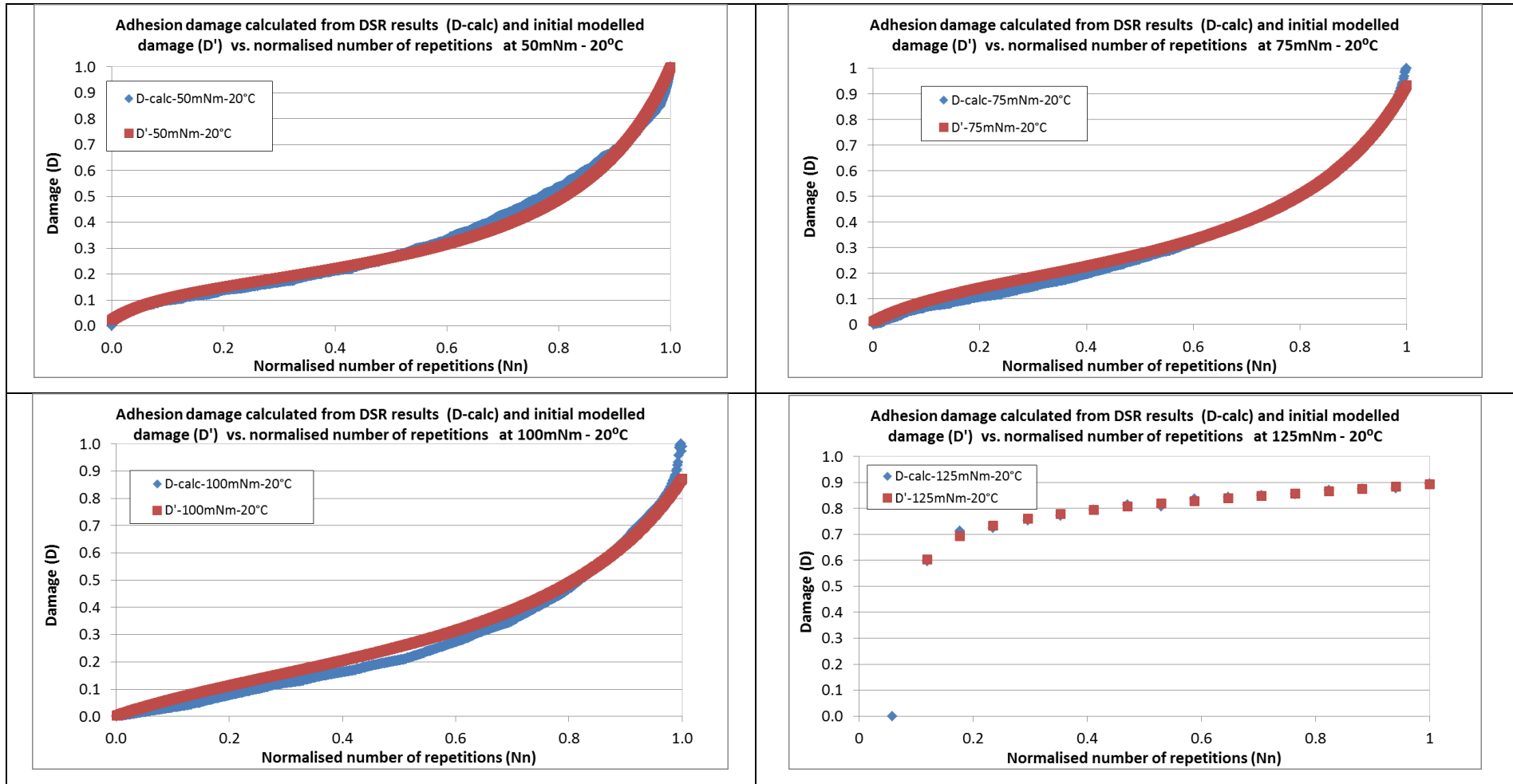
APPENDIX I



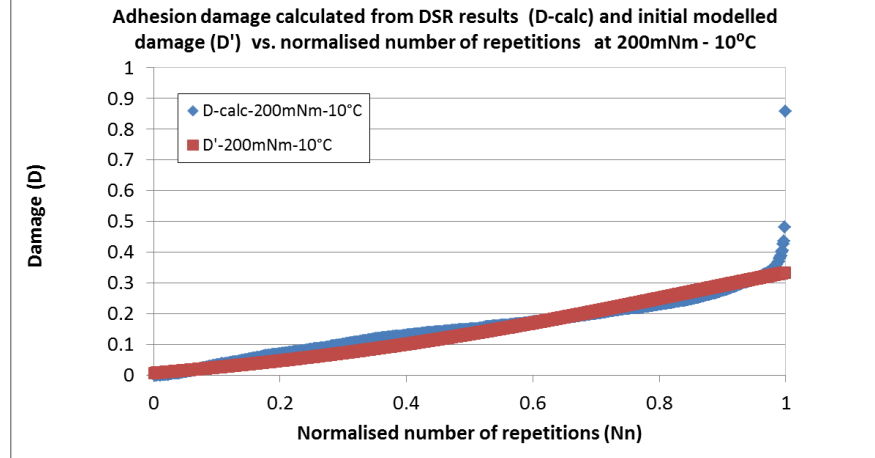
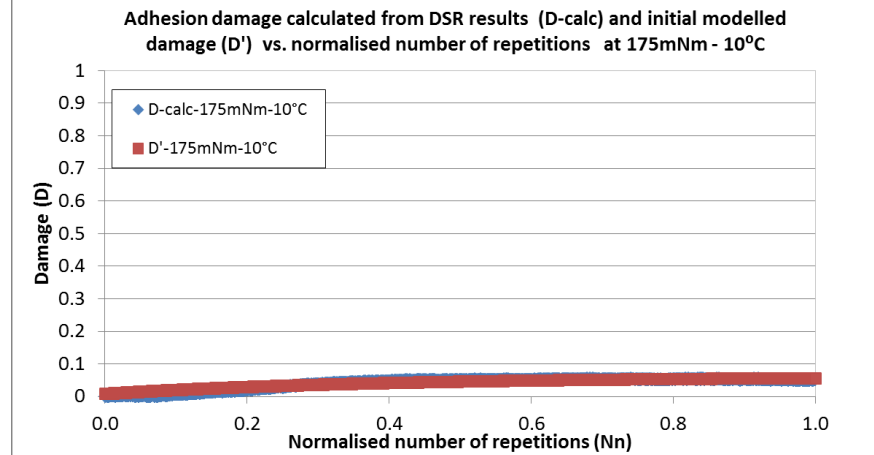
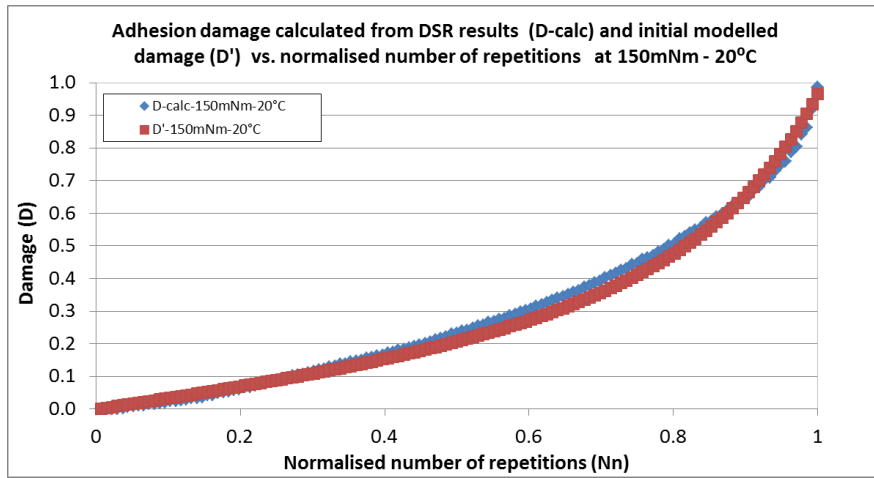
APPENDIX I



APPENDIX I



APPENDIX I





APPENDIX I

I.3 Initial Nelder coefficients for cohesion fatigue damage

τ [Pa]	M [mNm]	Initial Nelder Model Coefficients for Cohesion(25°C)				R^2
		$a'_c(25^\circ\text{C})$	$b'_c(25^\circ\text{C})$	$c'_c(25^\circ\text{C})$	$w'_c(25^\circ\text{C})$	
1.19E+05	5	-0.003	0.750	2.859	-2.082	0.98
2.39E+05	10	-0.044	0.811	1.445	-0.825	1.00
3.58E+05	15	-0.111	0.950	0.863	-0.121	1.00
4.77E+05	20	-0.200	1.150	-0.029	1.366	1.00
5.97E+05	25	-0.270	1.400	-2.308	2.324	1.00

τ [Pa]	M [mNm]	Initial Nelder Model Coefficients for Cohesion (23°C)				R^2
		$a'_c(23^\circ\text{C})$	$b'_c(23^\circ\text{C})$	$c'_c(23^\circ\text{C})$	$w'_c(23^\circ\text{C})$	
1.19E+05	5	-0.002	0.706	2.570	-1.773	0.97
2.39E+05	10	-0.029	0.755	1.480	-0.901	1.00
3.58E+05	15	-0.085	0.900	0.365	0.199	1.00
4.77E+05	20	-0.150	1.100	-0.566	0.761	0.99
5.97E+05	25	-0.250	1.300	-1.809	1.810	1.00

τ [Pa]	M [mNm]	Initial Nelder Model Coefficients for Cohesion (20°C)				R^2
		$a'_c(20^\circ\text{C})$	$b'_c(20^\circ\text{C})$	$c'_c(20^\circ\text{C})$	$w'_c(20^\circ\text{C})$	
1.19E+05	5	-0.001	0.619	3.431	-2.358	0.96
2.39E+05	10	-0.014	0.660	1.816	-1.224	1.00
3.58E+05	15	-0.028	0.753	1.227	-0.671	1.00
4.77E+05	20	-0.057	0.938	0.730	-0.287	1.00
5.97E+05	25	-0.075	1.200	0.411	-0.458	1.00

τ [Pa]	M [mNm]	Initial Nelder Model Coefficients for Cohesion (15°C)				R^2
		$a'_c(15^\circ\text{C})$	$b'_c(15^\circ\text{C})$	$c'_c(15^\circ\text{C})$	$w'_c(15^\circ\text{C})$	
2.39E+05	10	-0.008	0.560	2.386	-1.752	1.00
3.58E+05	15	-0.017	0.655	2.002	-1.457	1.00
4.77E+05	20	-0.027	0.830	1.460	-0.562	1.00
5.97E+05	25	-0.035	1.144	0.363	-0.263	1.00



APPENDIX I

τ [Pa]	M [mNm]	Initial Nelder Model Coefficients for Cohesion (10°C)				R^2
		$a'_c(10^\circ\text{C})$	$b'_c(10^\circ\text{C})$	$c'_c(10^\circ\text{C})$	$w'_c(10^\circ\text{C})$	
2.39E+05	10	-0.001	0.372	2.843	-1.822	0.98
3.58E+05	15	-0.003	0.478	2.374	-1.571	0.99
4.77E+05	20	-0.005	0.614	1.903	-1.293	1.00
5.97E+05	25	-0.008	0.789	1.522	-1.100	1.00

τ [Pa]	M [mNm]	Initial Nelder Model Coefficients for Cohesion (5°C)				R^2
		$a'_c(5^\circ\text{C})$	$b'_c(5^\circ\text{C})$	$c'_c(5^\circ\text{C})$	$w'_c(5^\circ\text{C})$	
5.97E+05	25	-0.001	0.501	3.000	-2.283	0.98
7.16E+05	30	-0.001	0.691	2.590	-2.133	0.99
8.35E+05	35	-0.002	0.953	2.200	-2.036	1.00
9.54E+05	40	-0.002	1.316	2.282	-1.200	1.00

τ [Pa]	M [mNm]	Initial Nelder Model Coefficients for Cohesion (0°C)				R^2
		$a'_c(0^\circ\text{C})$	$b'_c(0^\circ\text{C})$	$c'_c(0^\circ\text{C})$	$w'_c(0^\circ\text{C})$	
5.97E+05	25	0.002	0.049	7.800	-6.650	0.41
7.16E+05	30	0.001	0.100	6.274	-5.000	0.08
8.35E+05	35	-0.001	0.206	4.596	-3.451	0.94
9.54E+05	40	-0.003	0.421	2.918	-2.140	0.99



APPENDIX I

I.4 Initial Nelder coefficients for adhesion fatigue damage

τ [Pa]	M [mNm]	Initial Nelder Model Coefficients for Adhesion (25°C)				R^2
		a'_A (25°C)	b'_A (25°C)	c'_A (25°C)	w'_A (25°C)	
197,612	50	-0.001	0.005	7.115	-6.129	0.96
296,418	75	-0.002	0.008	5.885	-4.947	0.92
395,224	100	-0.005	0.013	4.591	-3.625	0.82
494,030	125	-0.008	0.027	4.008	-3.077	0.96

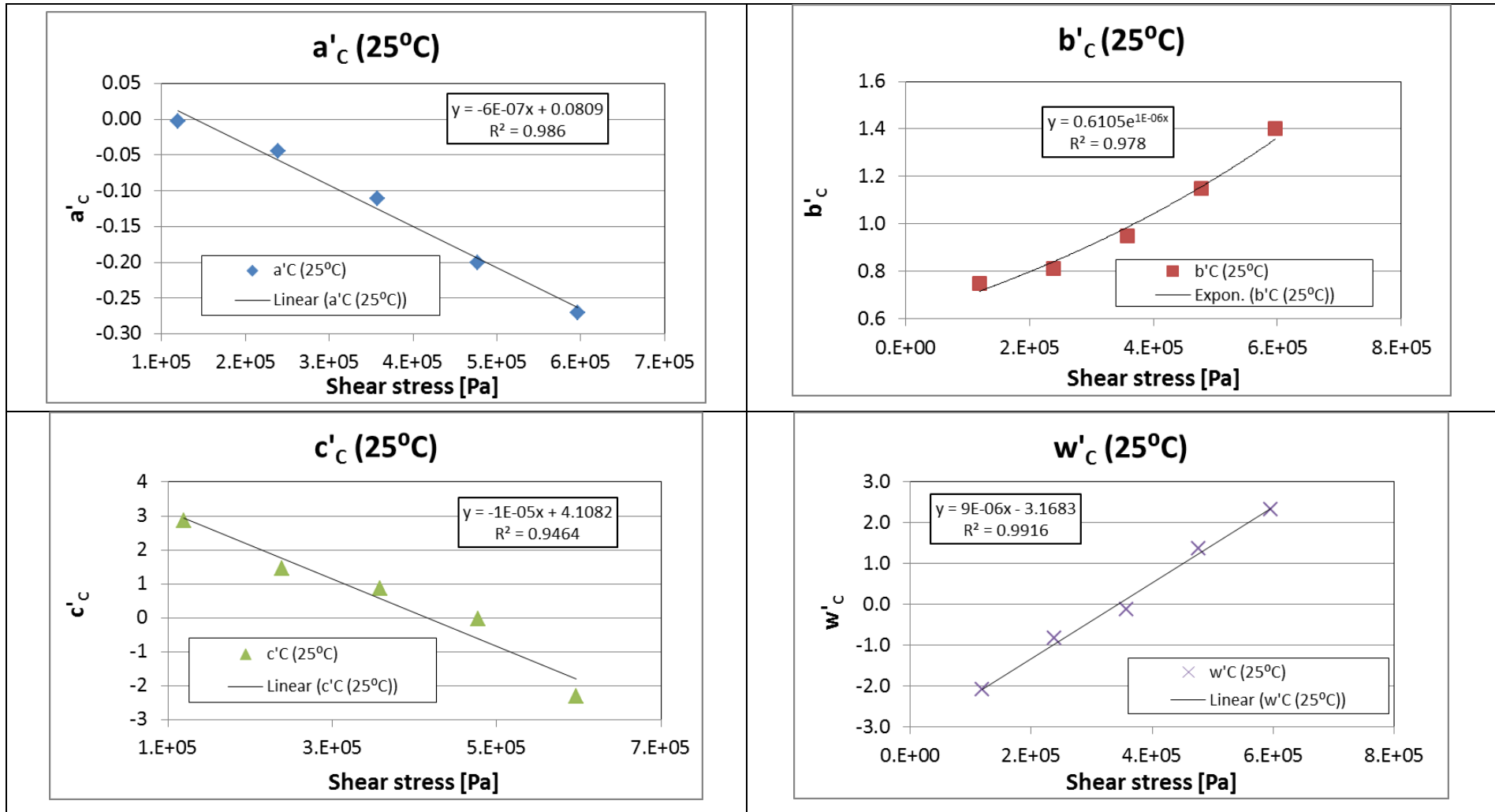
τ [Pa]	M [mNm]	Initial Nelder Model Coefficients for Adhesion (23°C)				R^2
		a'_A (23°C)	b'_A (23°C)	c'_A (23°C)	w'_A (23°C)	
1.98E+05	50	0.003	0.010	6.179	-5.248	0.92
2.96E+05	75	0.000	0.011	5.416	-4.231	0.99
3.95E+05	100	-0.002	0.021	4.200	-3.043	0.99
4.35E+05	110	-0.002	0.026	3.818	-2.726	0.99
4.94E+05	125	-0.003	0.036	3.558	-2.593	0.95
5.53E+05	140	-0.006	0.055	3.450	-2.162	0.69
5.93E+05	150	-0.008	0.067	3.071	-2.042	0.83
6.92E+05	175	-0.009	0.117	2.814	-1.814	0.84

τ [Pa]	M [mNm]	Initial Nelder Model Coefficients for Adhesion (20°C)				R^2
		a'_A (20°C)	b'_A (20°C)	c'_A (20°C)	w'_A (20°C)	
2.96E+05	75	0.009	0.820	3.838	-3.549	0.99
3.95E+05	100	0.004	1.406	2.499	-2.743	0.98
5.93E+05	150	-0.005	2.956	-0.329	-1.615	0.99

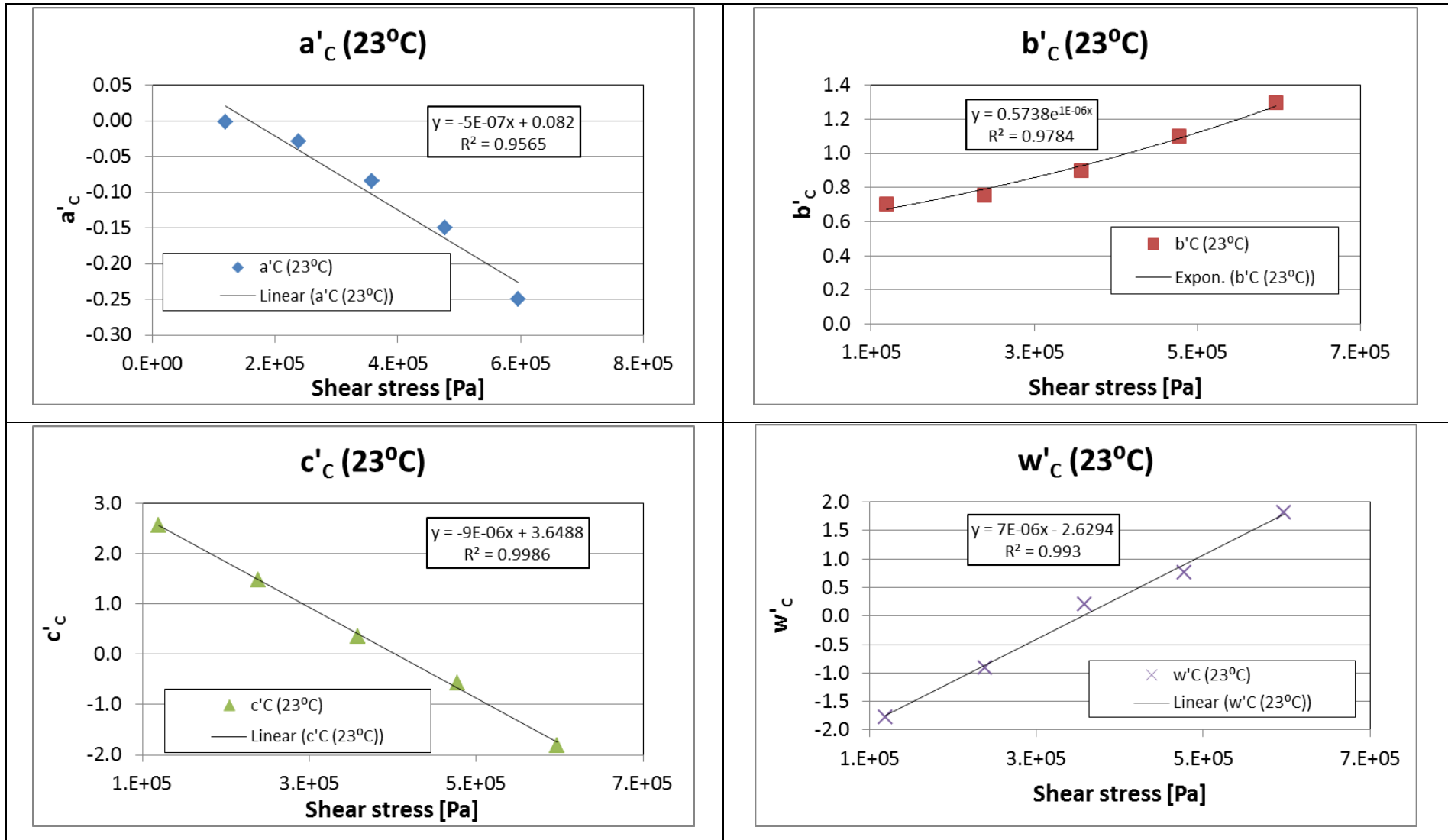
τ [Pa]	M [mNm]	Initial Nelder Model Coefficients for Adhesion (10°C)				R^2
		a'_A (10°C)	b'_A (10°C)	c'_A (10°C)	w'_A (10°C)	
6.92E+05	175	0.050	6.061	9.929	1.983	0.86
7.90E+05	200	0.049	6.379	-5.392	2.189	0.95

APPENDIX I

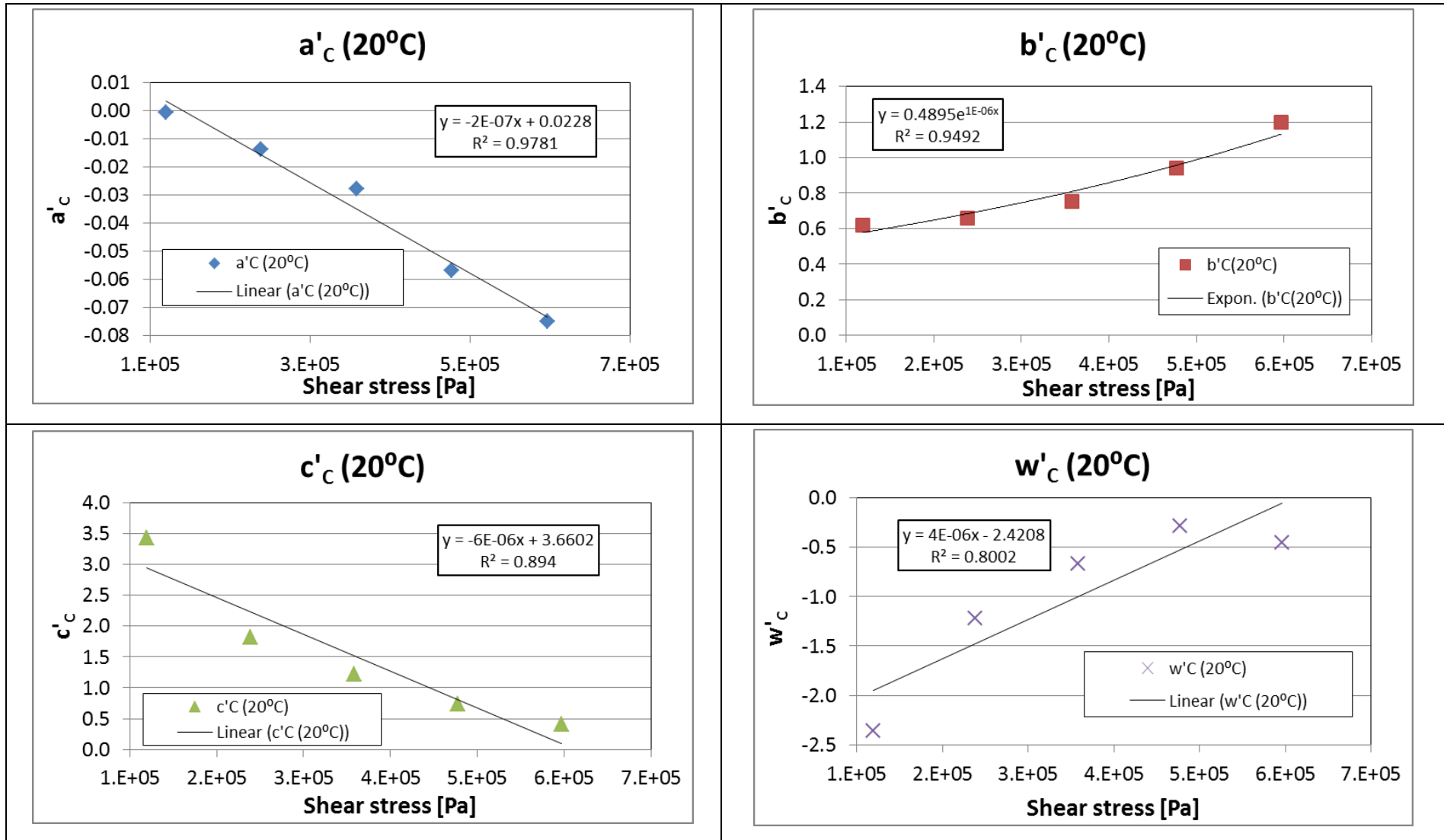
I.5 Graphic development of relationship between the initial Nelder coefficients and stress level for cohesion fatigue damage



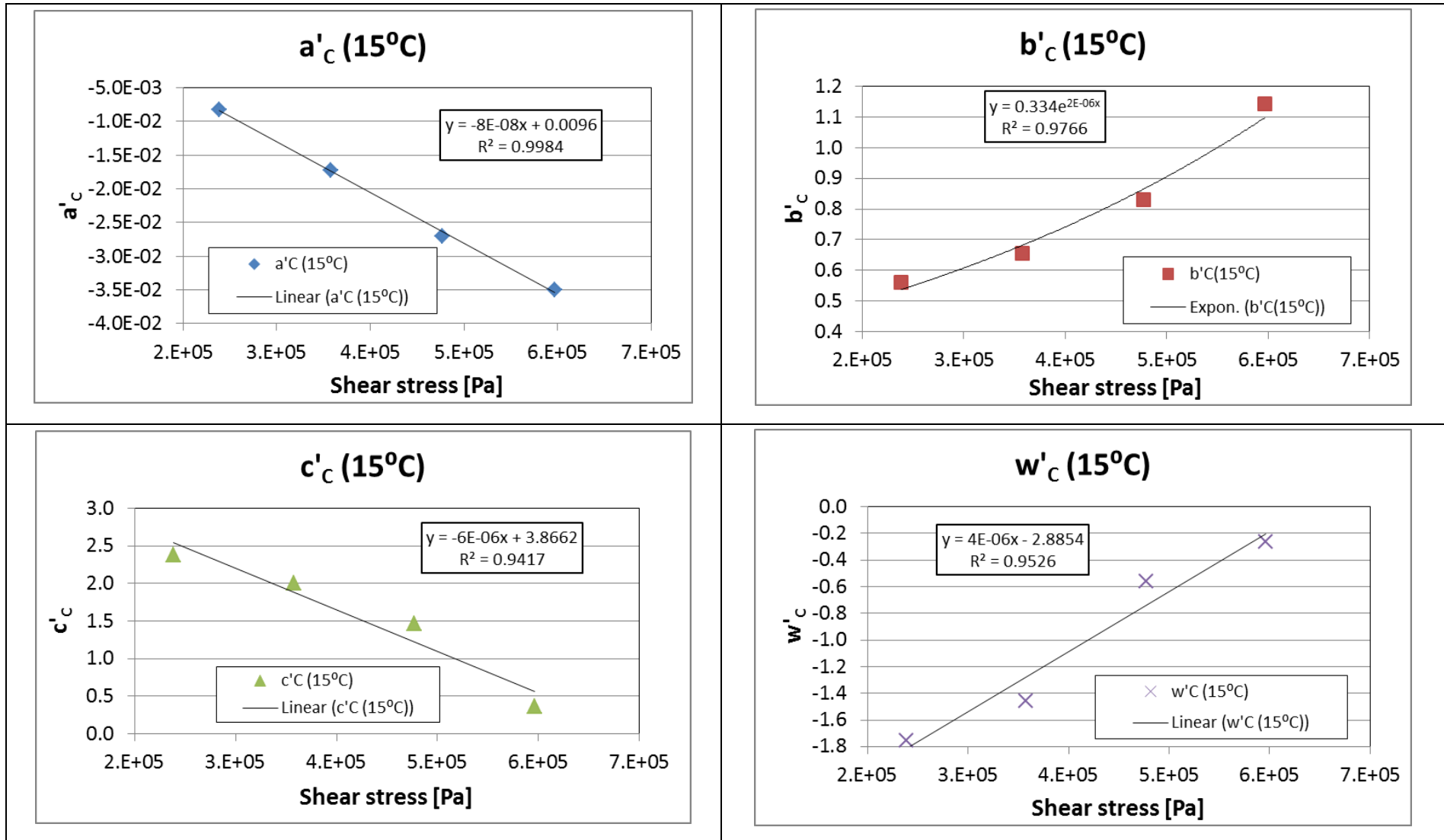
APPENDIX I



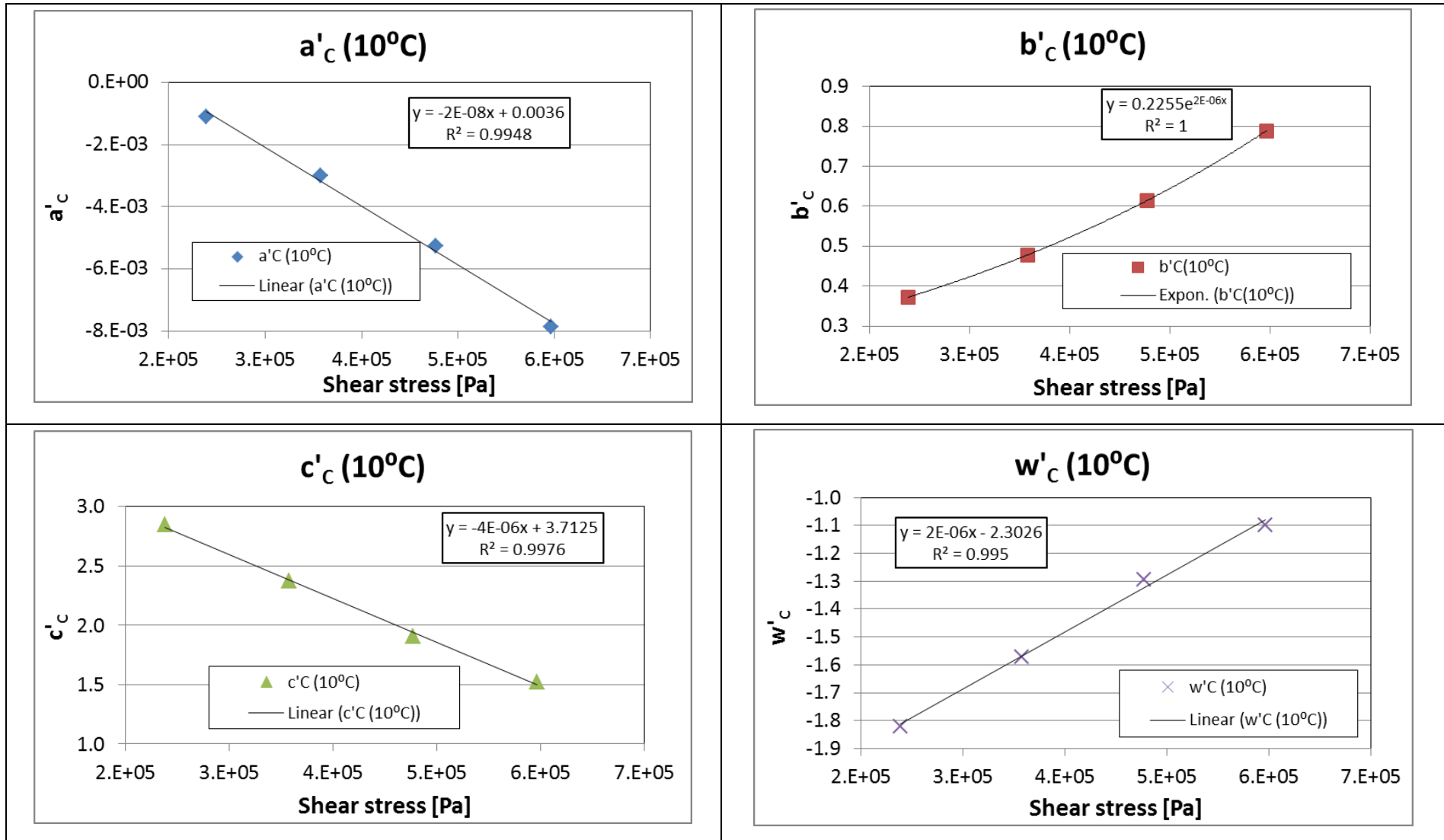
APPENDIX I



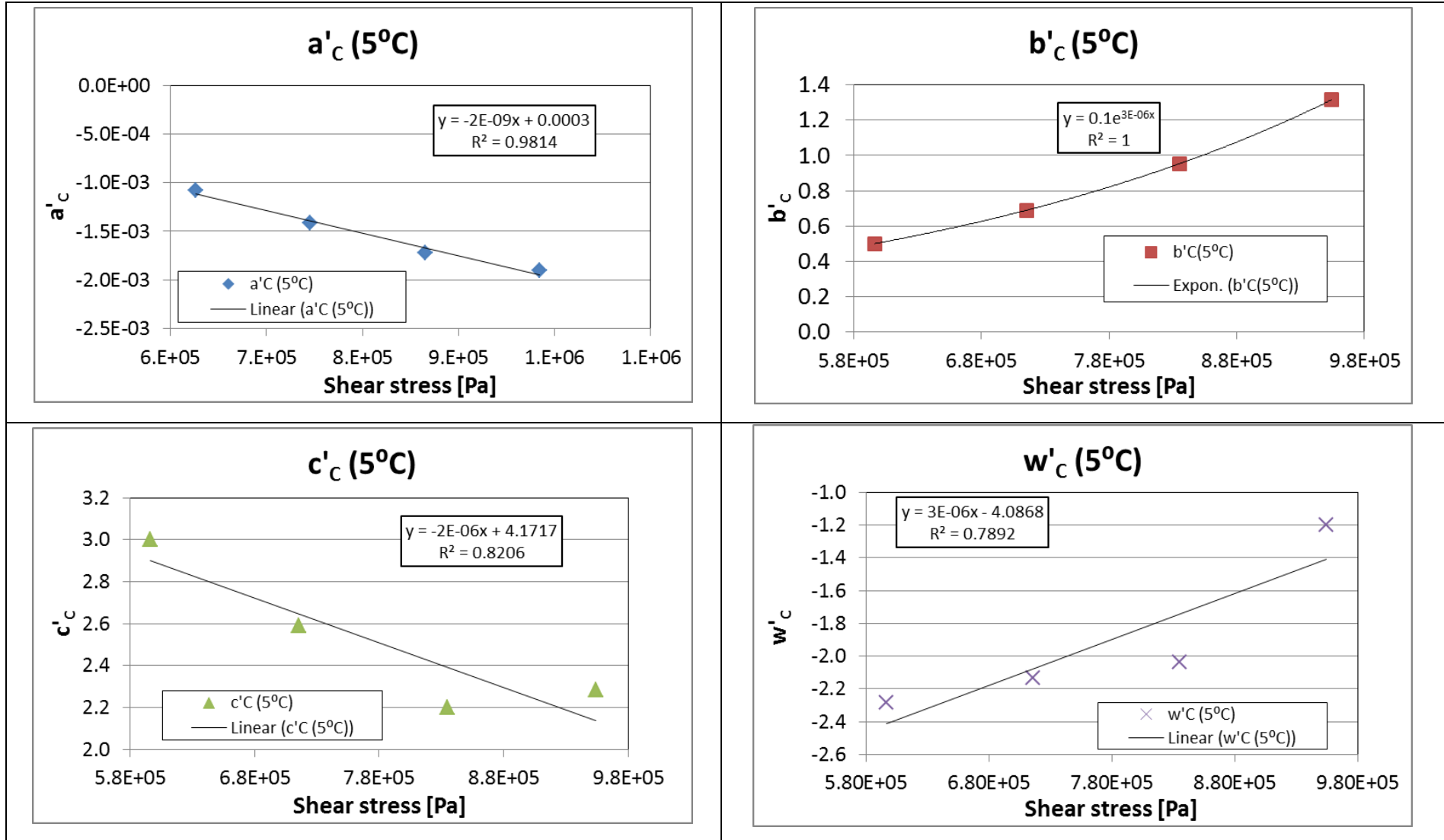
APPENDIX I



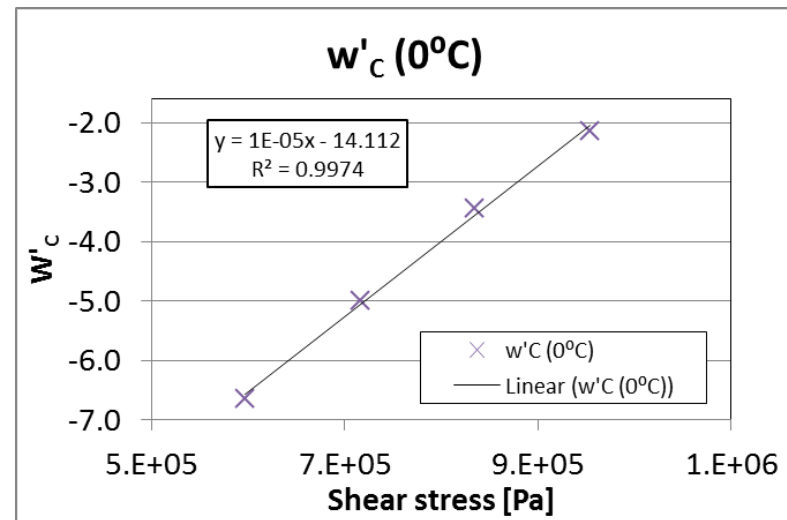
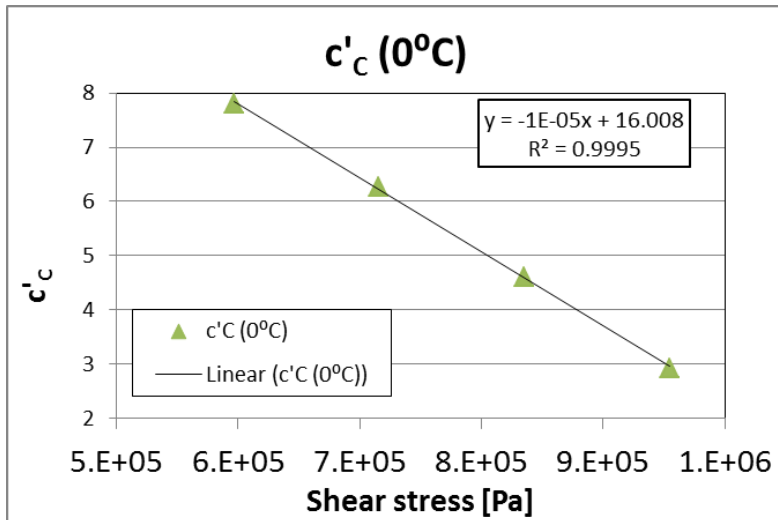
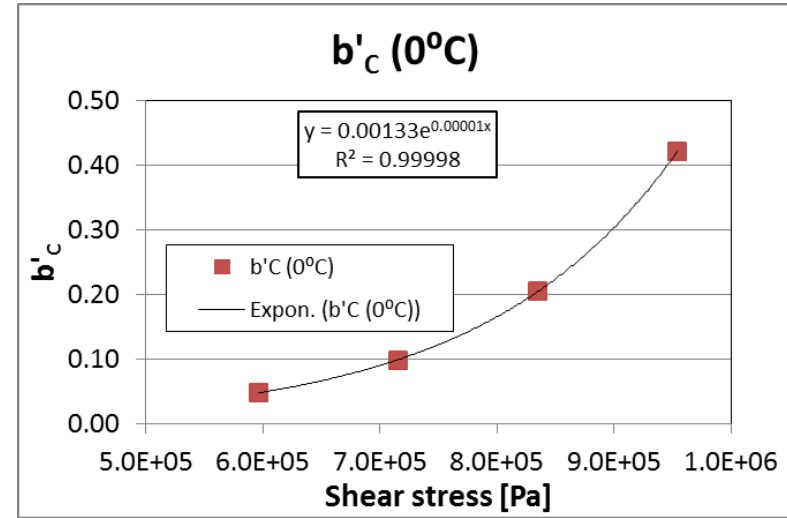
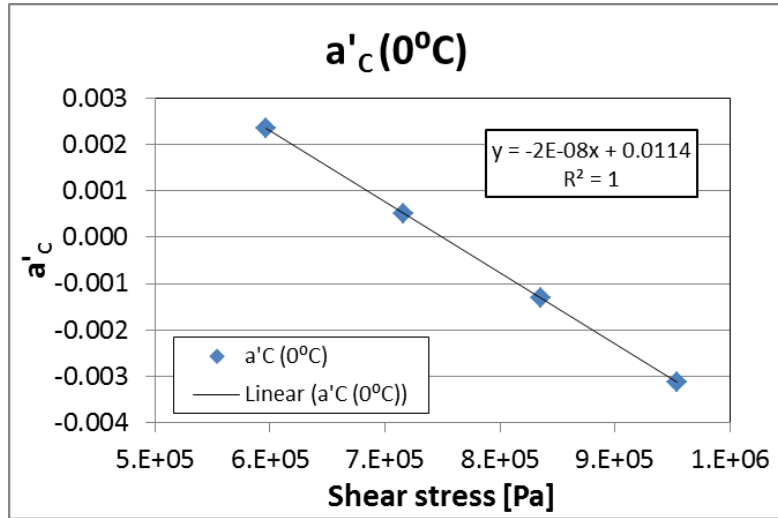
APPENDIX I



APPENDIX I

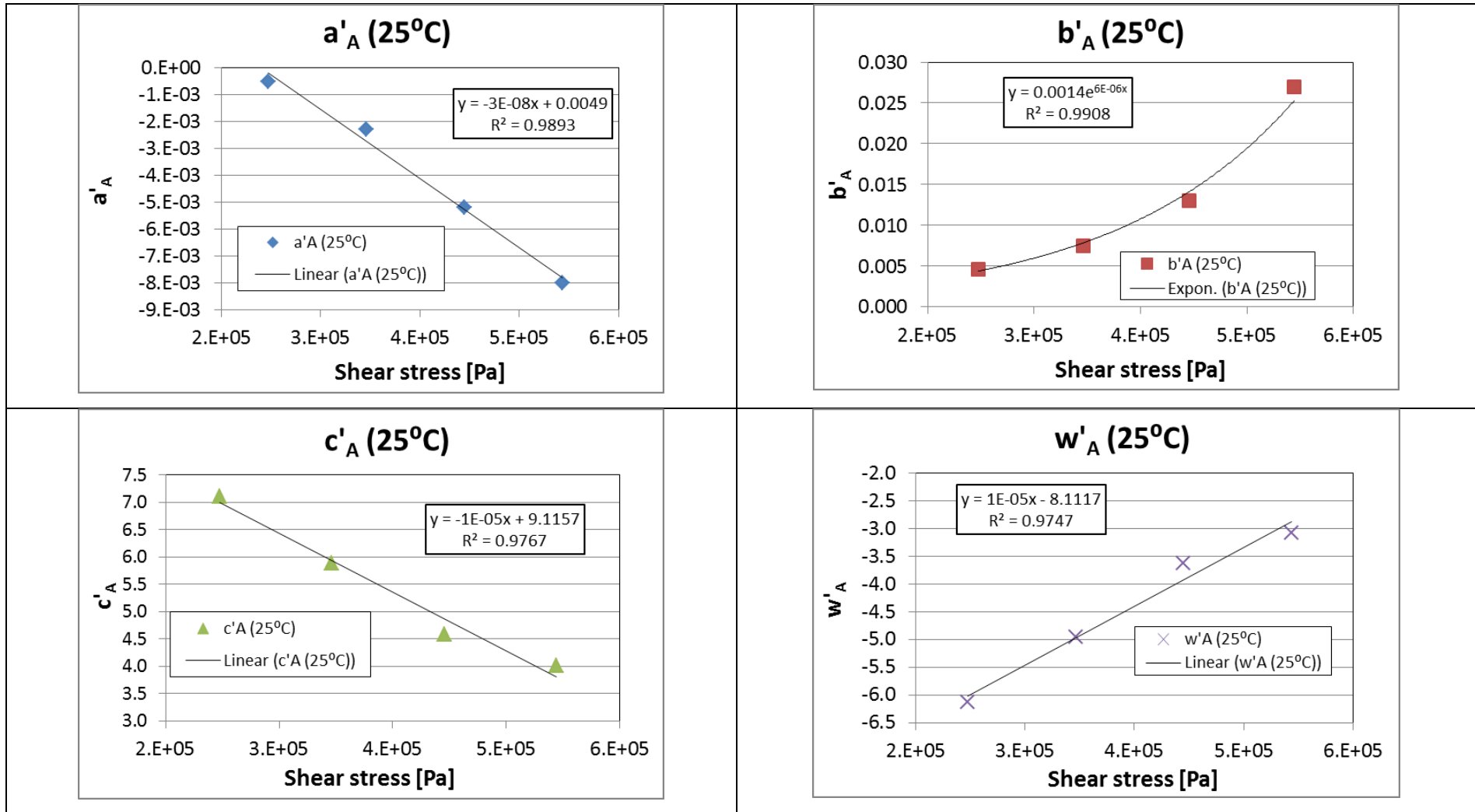


APPENDIX I

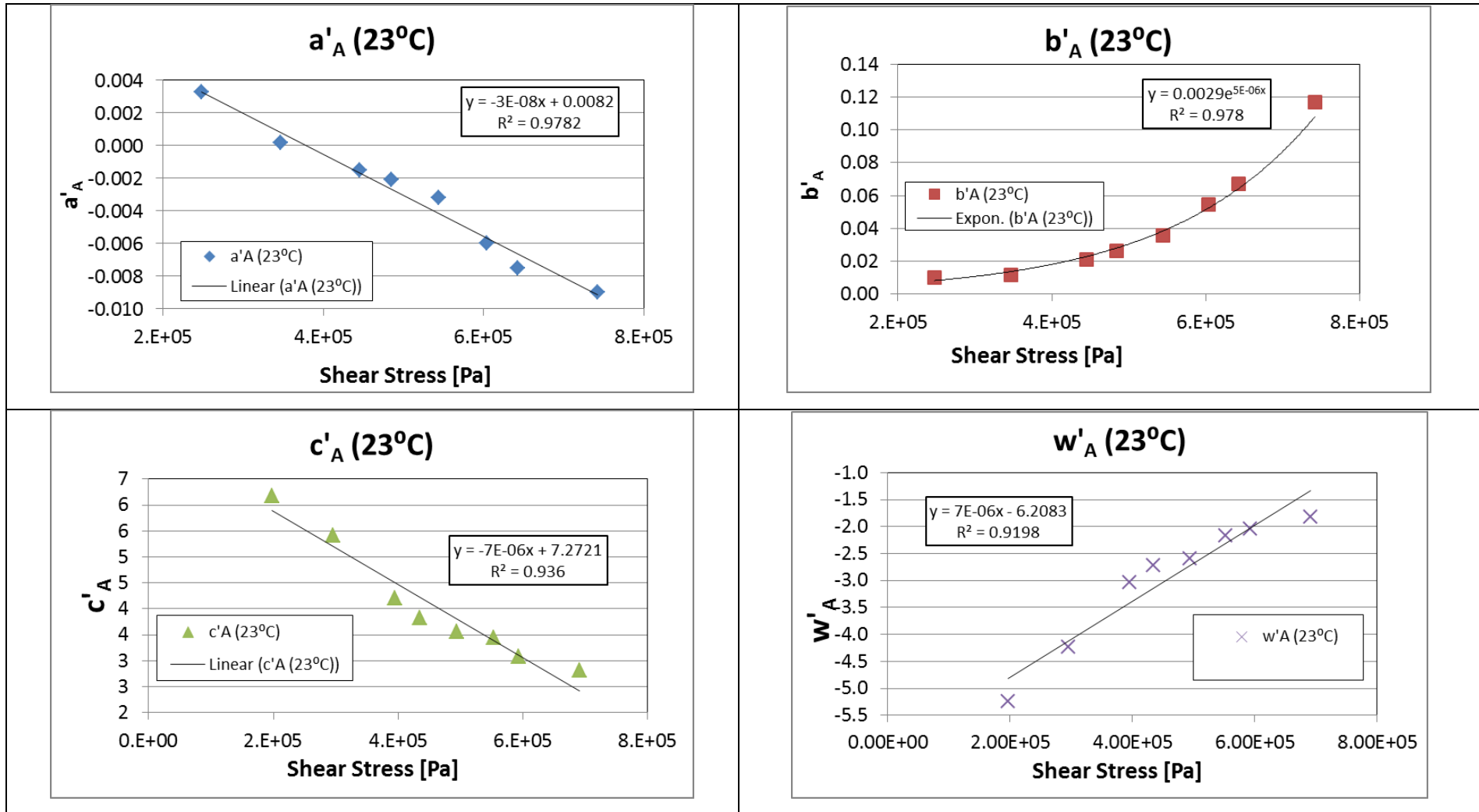


APPENDIX I

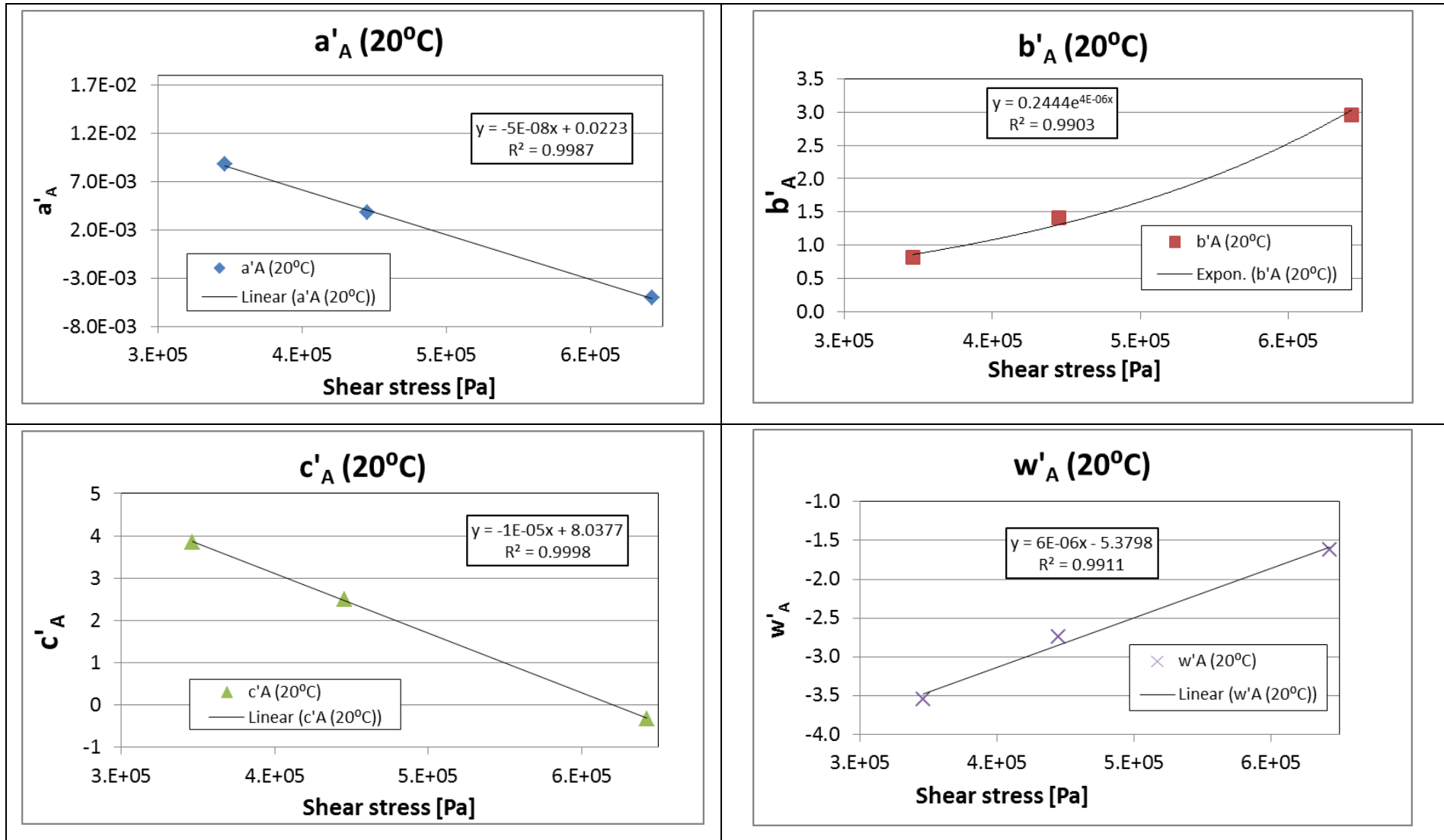
I.6 Graphic development of relationship between the initial Nelder coefficients and stress level for adhesion fatigue damage



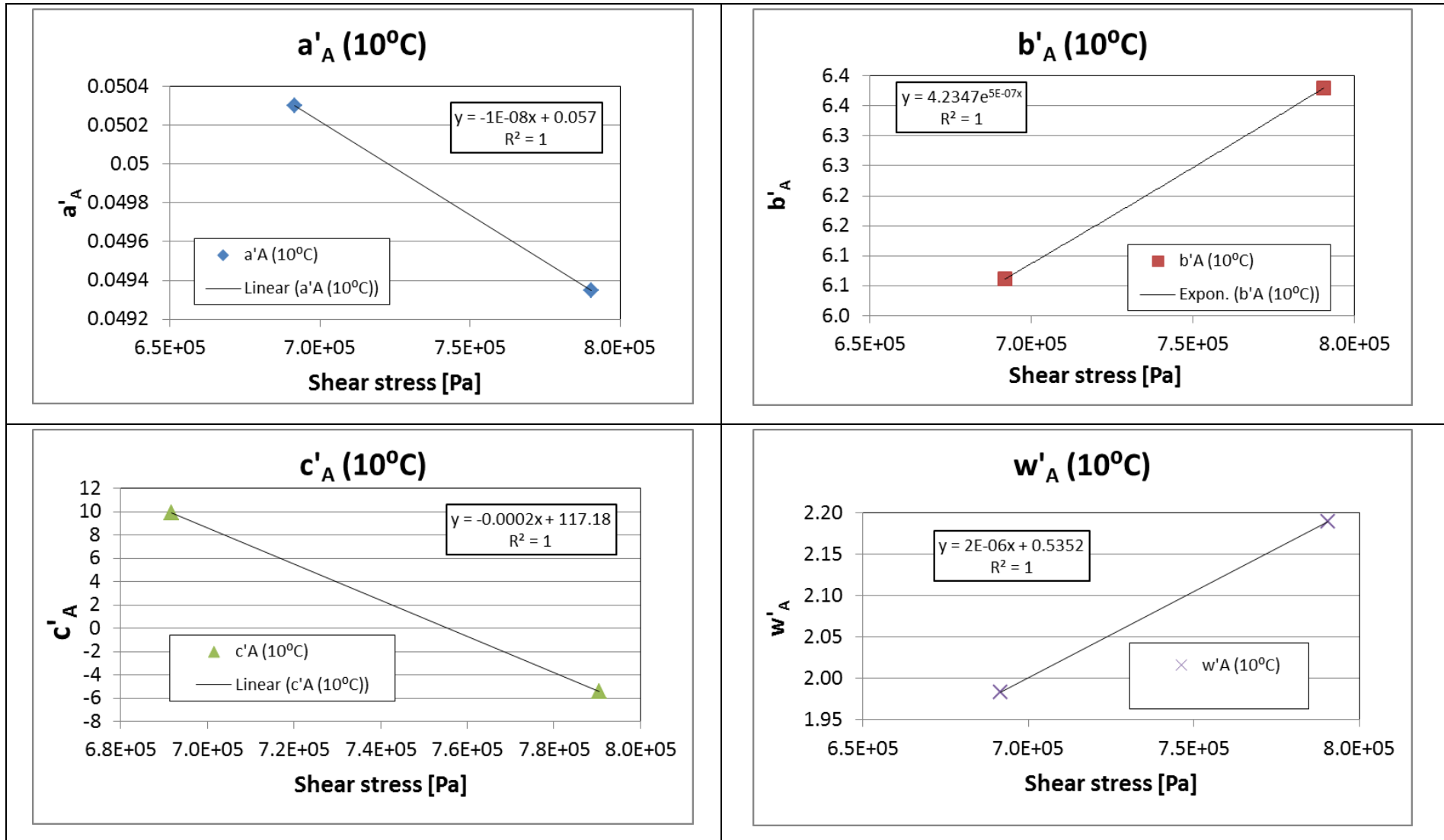
APPENDIX I



APPENDIX I



APPENDIX I

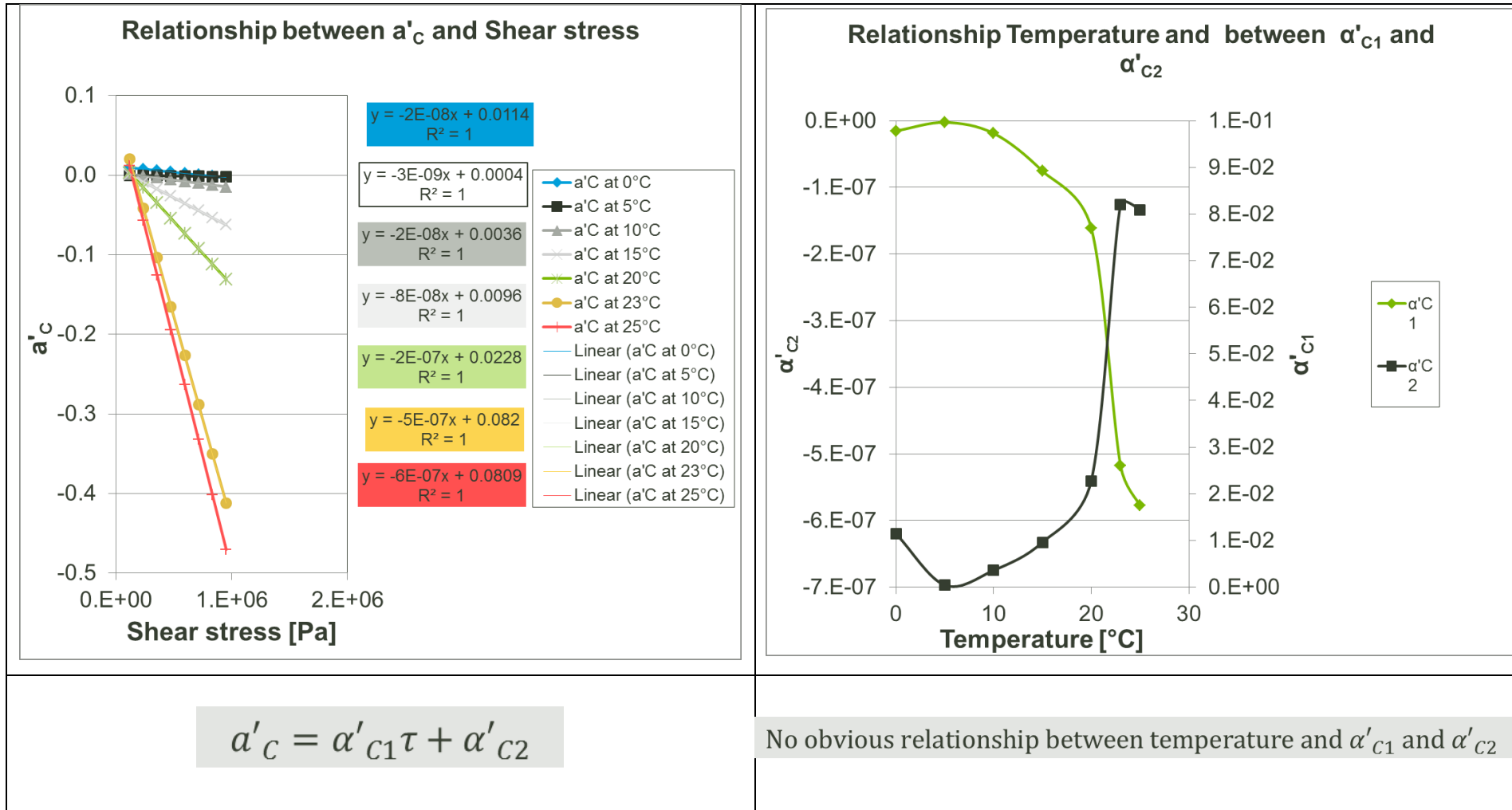


APPENDIX I

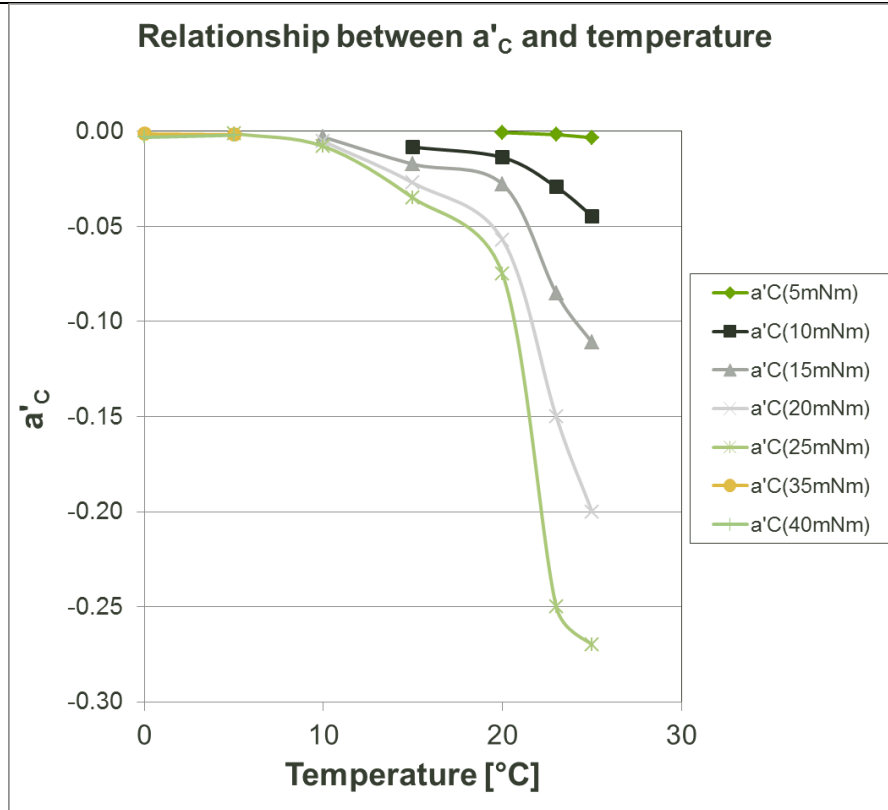
I.7 Graphic development of relationship for adjusted model coefficients and global model coefficients in the case of CFD

APPENDIX I

Coefficient "a_c"



APPENDIX I



Thus the adjusted model coefficient a_C is given by

$$a_C = \alpha_{C1}\tau + \alpha_{C2}$$

Where :

α_{C1} and α_{C2} are the model constants for cohesion, α'_{C1} and α'_{C2} are the global model coefficients, and α'_C is the initial Nelder coefficient.

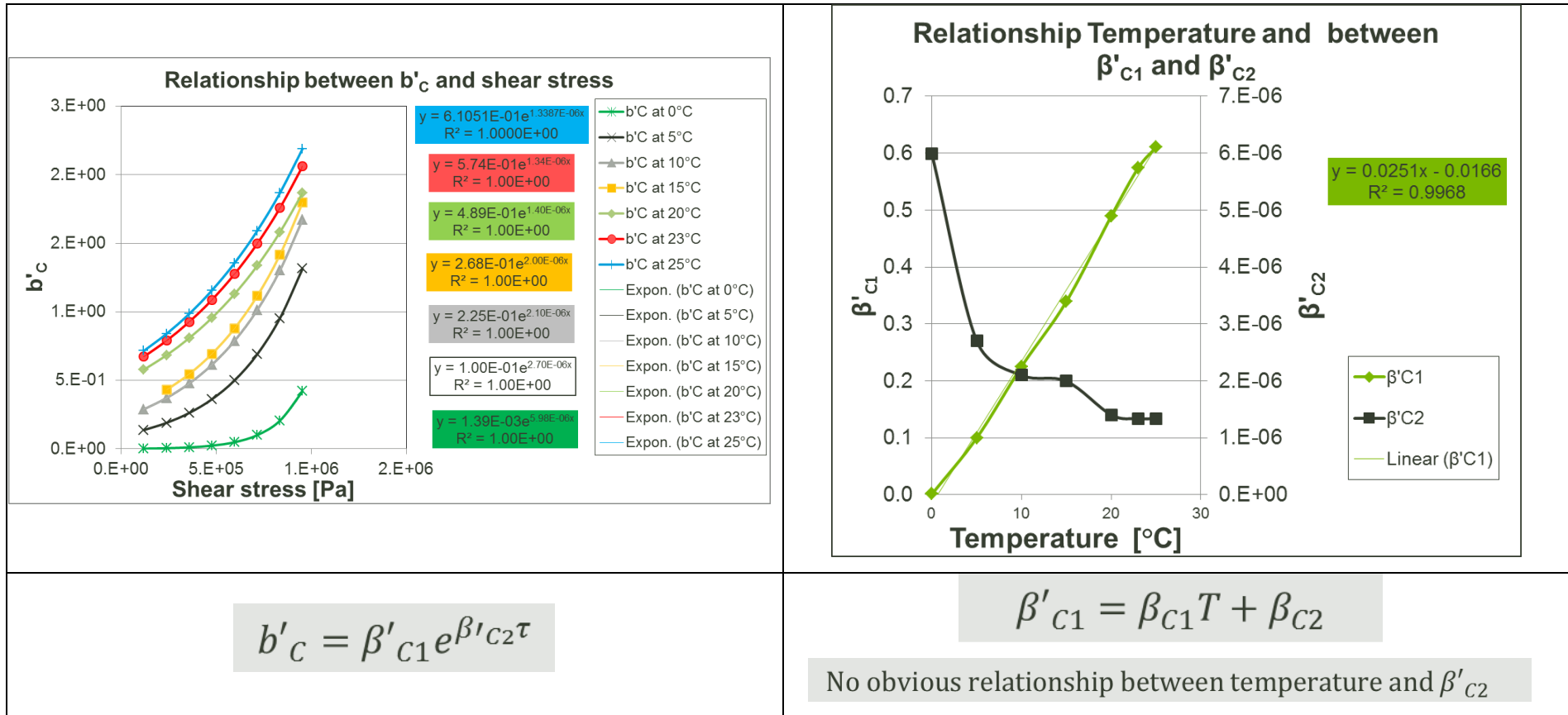
The model constants for cohesion α_{C1} and α_{C2} are respectively equal to the global model coefficients α'_{C1} and α'_{C2} , and

The adjusted coefficient a_C is equal to the initial Nelder coefficient α'_C .

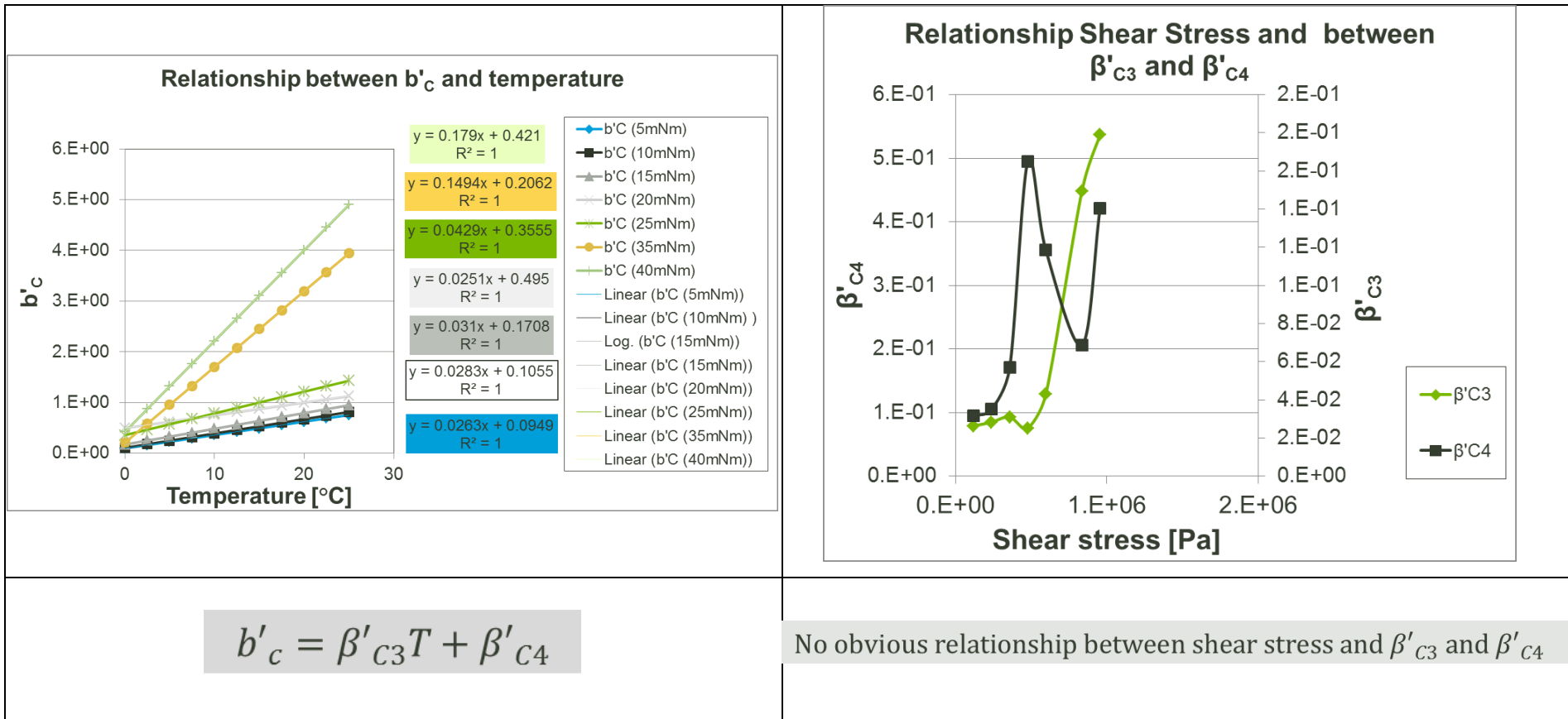
No obvious relationship between α'_C and temperature

APPENDIX I

Coefficient “b_c”



APPENDIX I



APPENDIX I

Thus the adjusted model coefficient b_c is given by

$$b_c = (\beta_{c1}T + \beta_{c2})e^{\beta_{c3}\tau}$$

Obtained from integrating :

$$\beta'_{c1} = \beta_{c1}T + \beta_{c2} \text{ in } b'_c = \beta'_{c1}e^{\beta'_{c2}\tau}$$

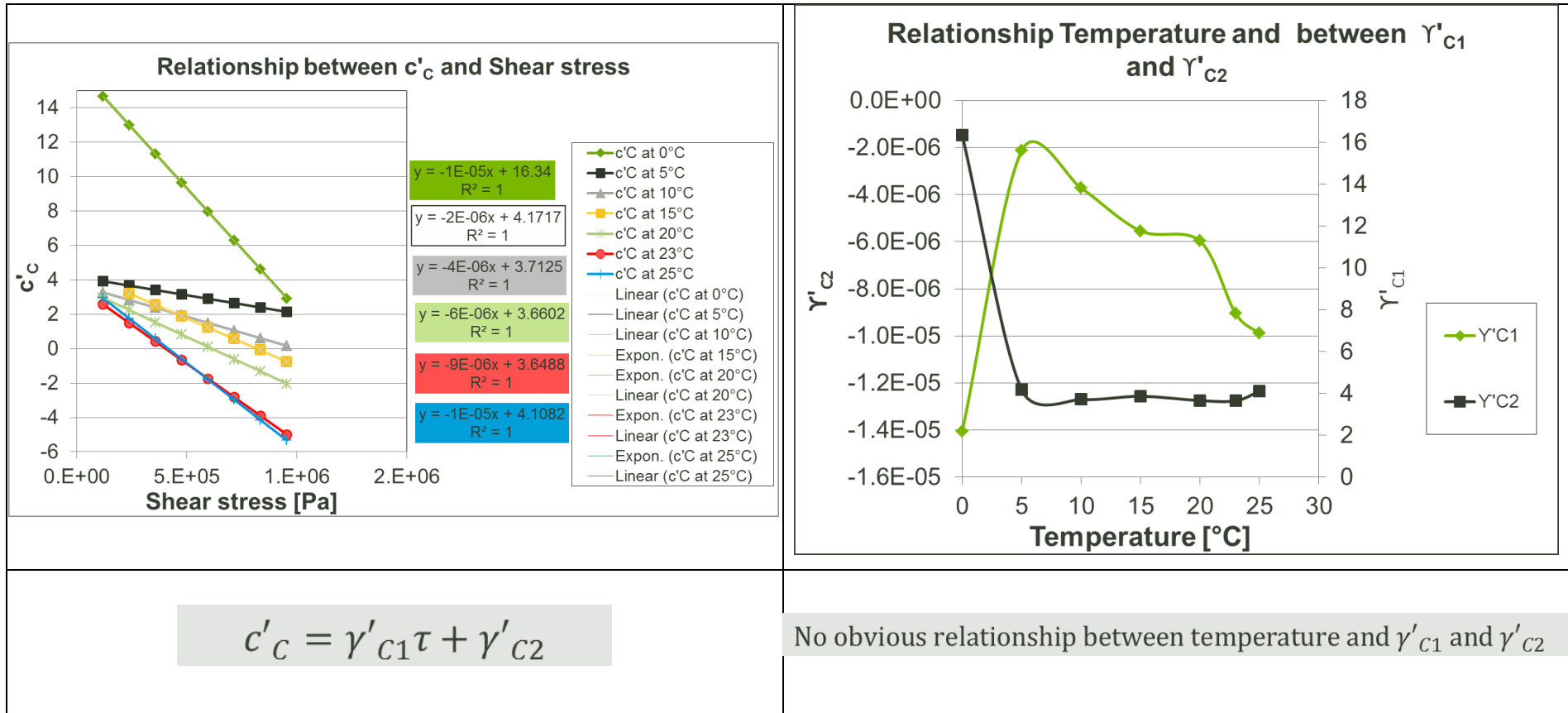
This integration was possible because β'_{c1} displayed an obvious relationship to the temperature.

Where :

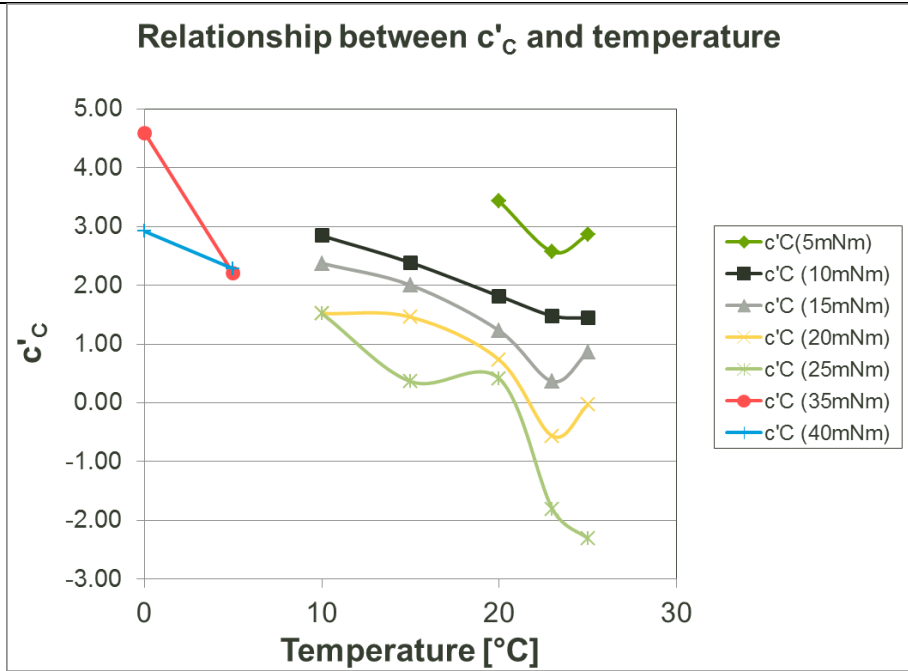
β_{c1} and β_{c2} are the model constants for cohesion, β'_{c1} and β'_{c2} are the global model coefficients, and b'_c is the initial Nelder coefficient.

APPENDIX I

Coefficient “c_c”



APPENDIX I



No obvious relationship between c'_c and temperature

Thus the adjusted model coefficient c_C is given by

$$c_C = \gamma_{C1}\tau + \gamma_{C2}$$

Where :

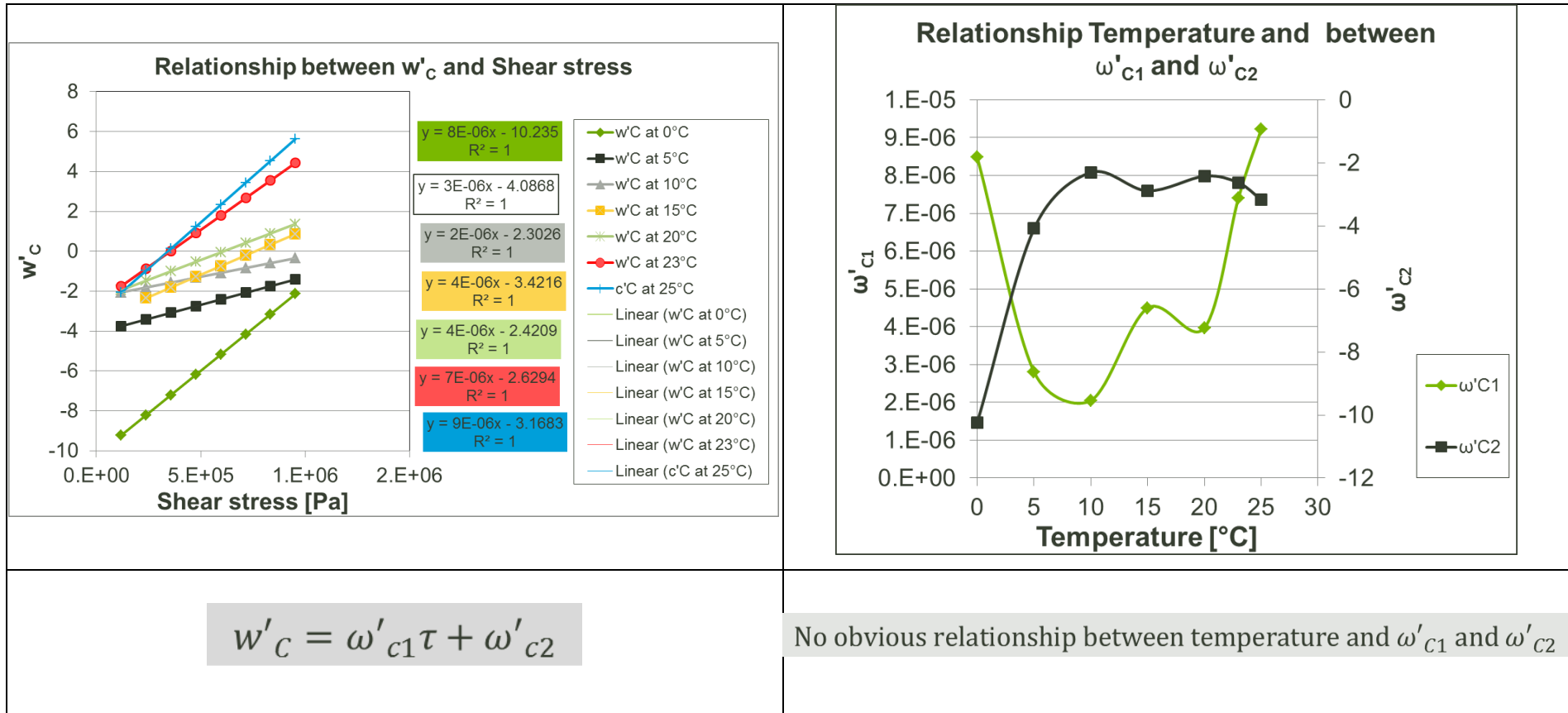
γ_{C1} and γ_{C2} are the model constants for cohesion, γ'_{C1} and γ'_{C2} are the global model coefficients, and γ'_C is the initial Nelder coefficient .

The model constants for cohesion γ_{C1} and γ_{C2} are respectively equal to the global model coefficients γ'_{C1} and γ'_{C2} ,and

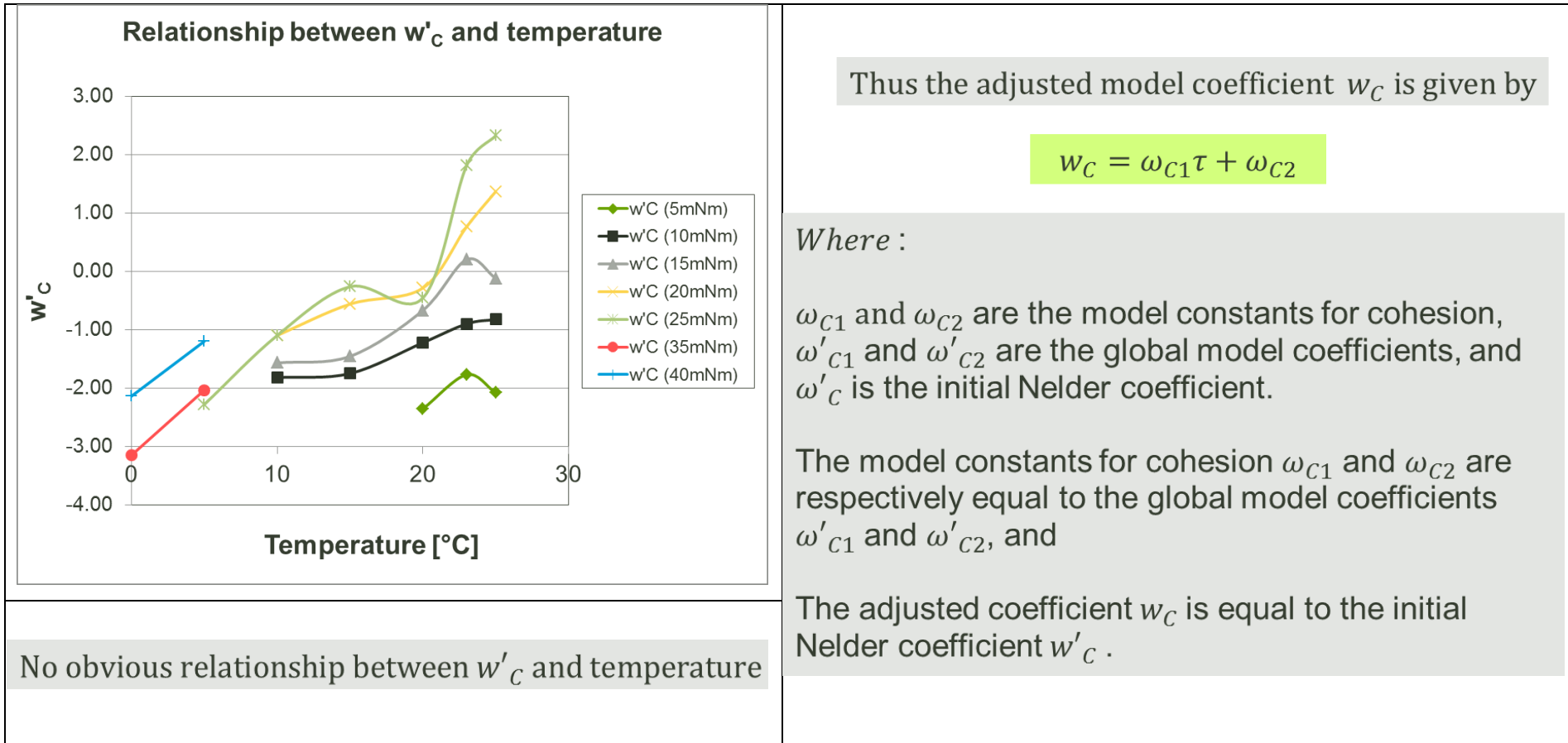
The adjusted coefficient c_C is equal to the initial Nelder coefficient c'_c .

APPENDIX I

Coefficient “w_C”



APPENDIX I

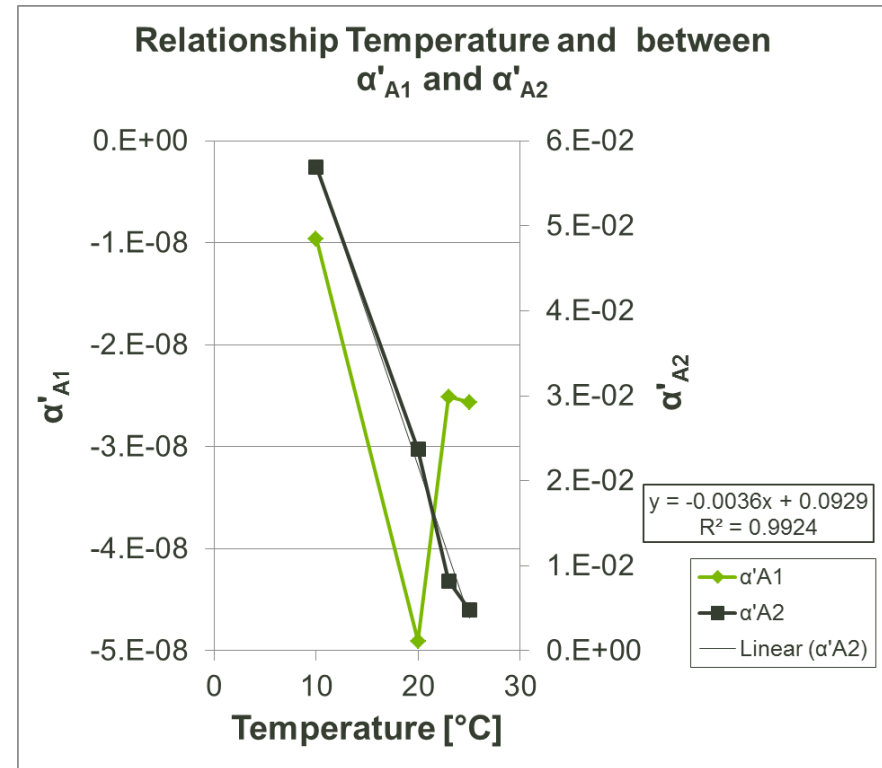
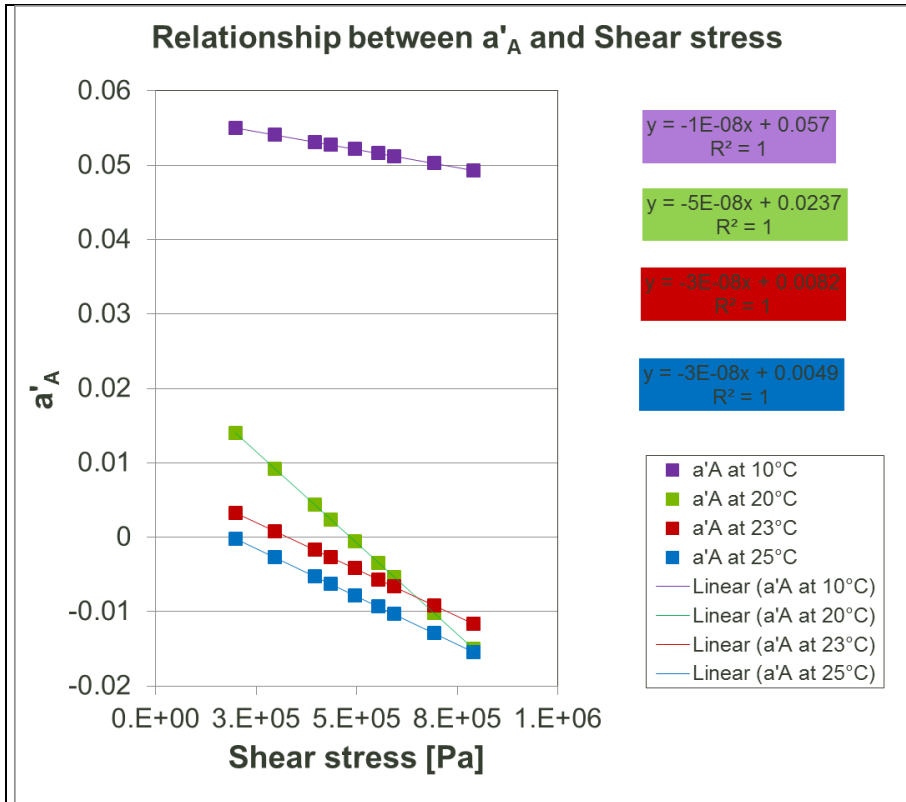


APPENDIX I

I.8 Graphic development of relationship for adjusted model coefficients and global model coefficients in the case of AFD

APPENDIX I

Coefficient “a_A”

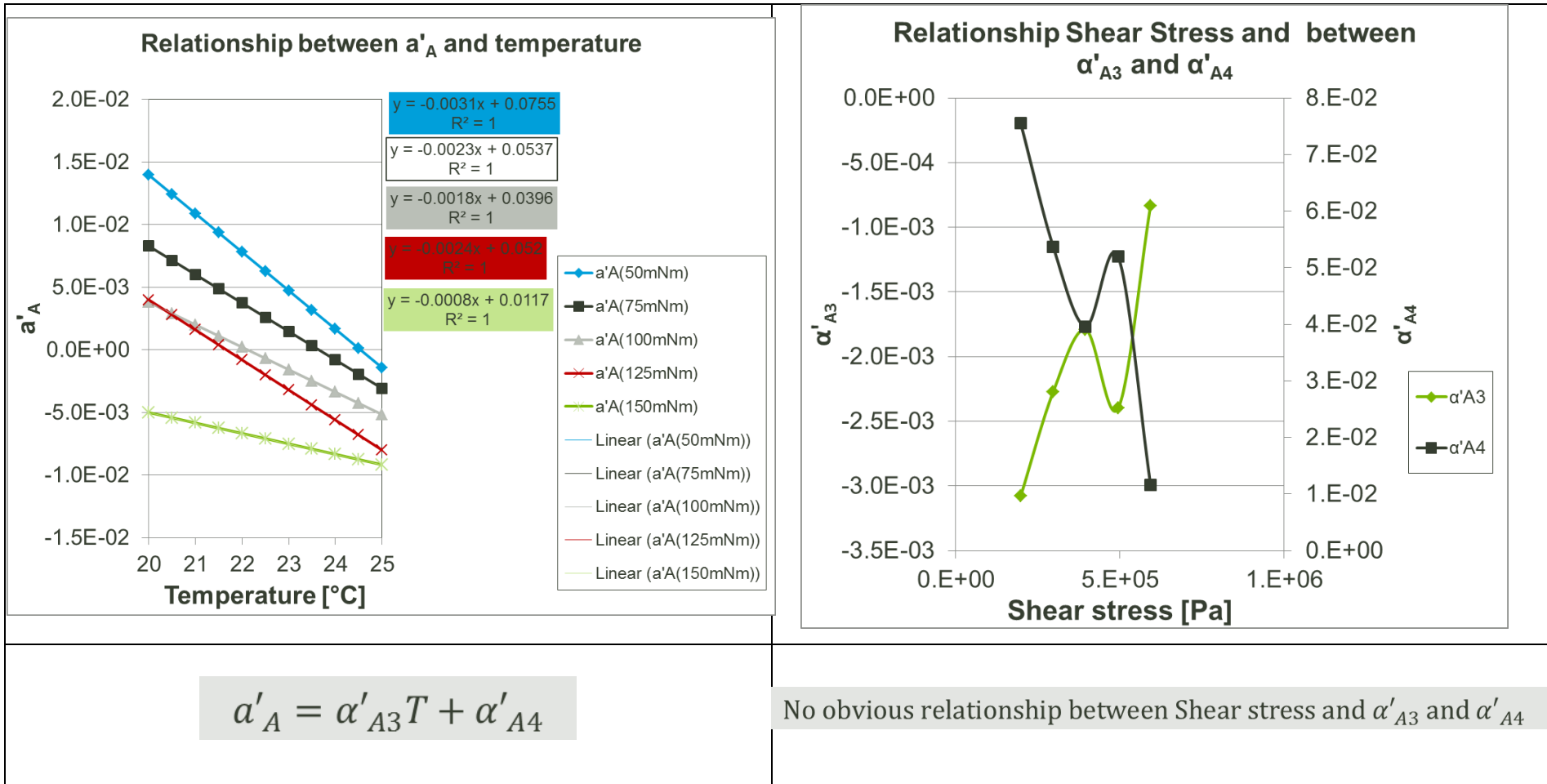


$$a'_A = \alpha'_{A1}\tau + \alpha'_{A2}$$

$$\alpha'_{A2} = \alpha_{A2}T + \alpha_{A3}$$

No obvious relationship between temperature and α'_{A1}

APPENDIX I



APPENDIX I

Thus the adjusted model coefficient a_A is given by

$$a_A = \alpha_{A1}\tau + \alpha_{A2}T + \alpha_{A3}$$

Obtained from integrating :

$$\alpha'_{A2} = \alpha_{A2}T + \alpha_{A3} \text{ in } a'_A = \alpha'_{A1}\tau + \alpha'_{A2}$$

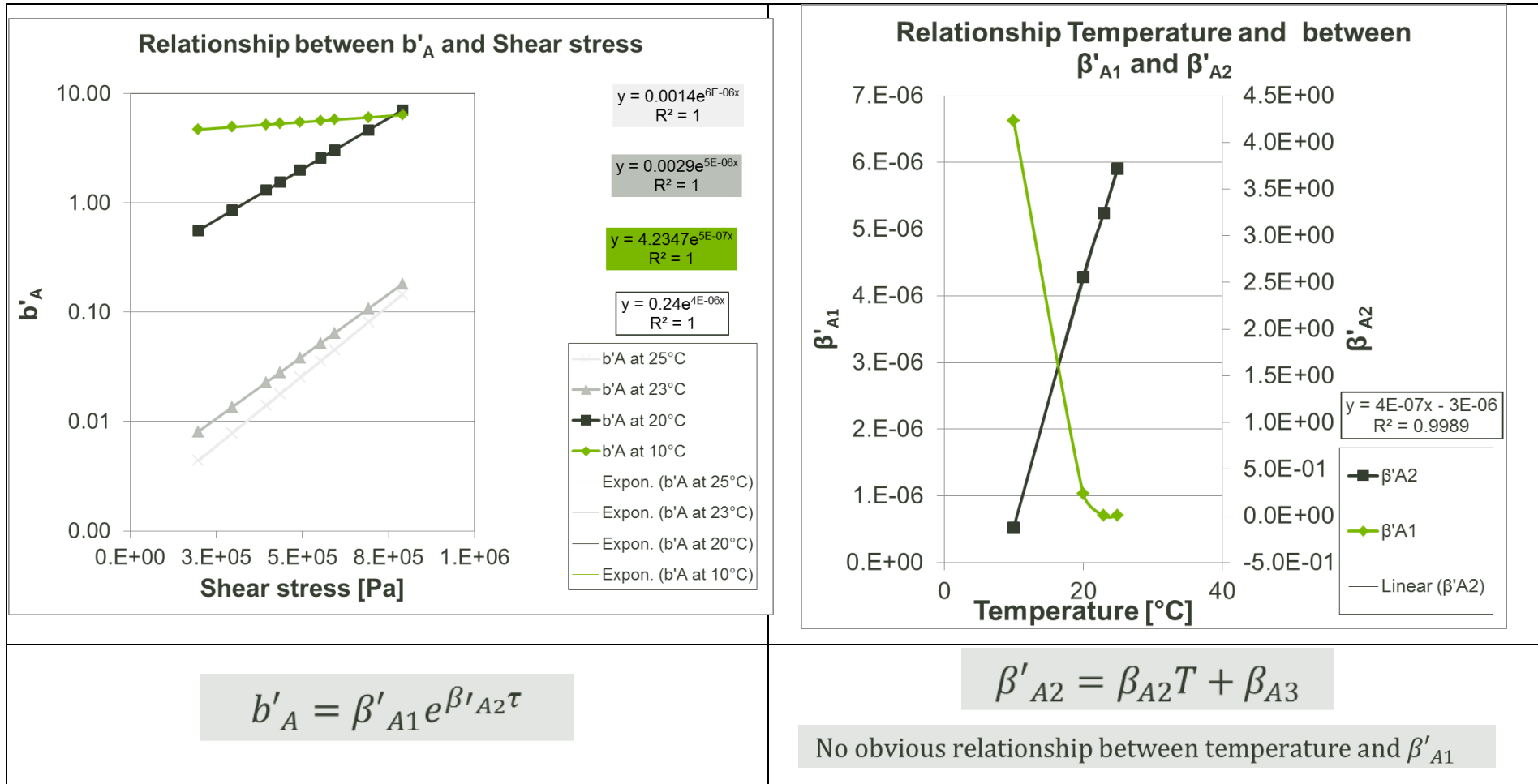
This integration was possible because α'_{A2} displayed an obvious relationship to the temperature.

Where :

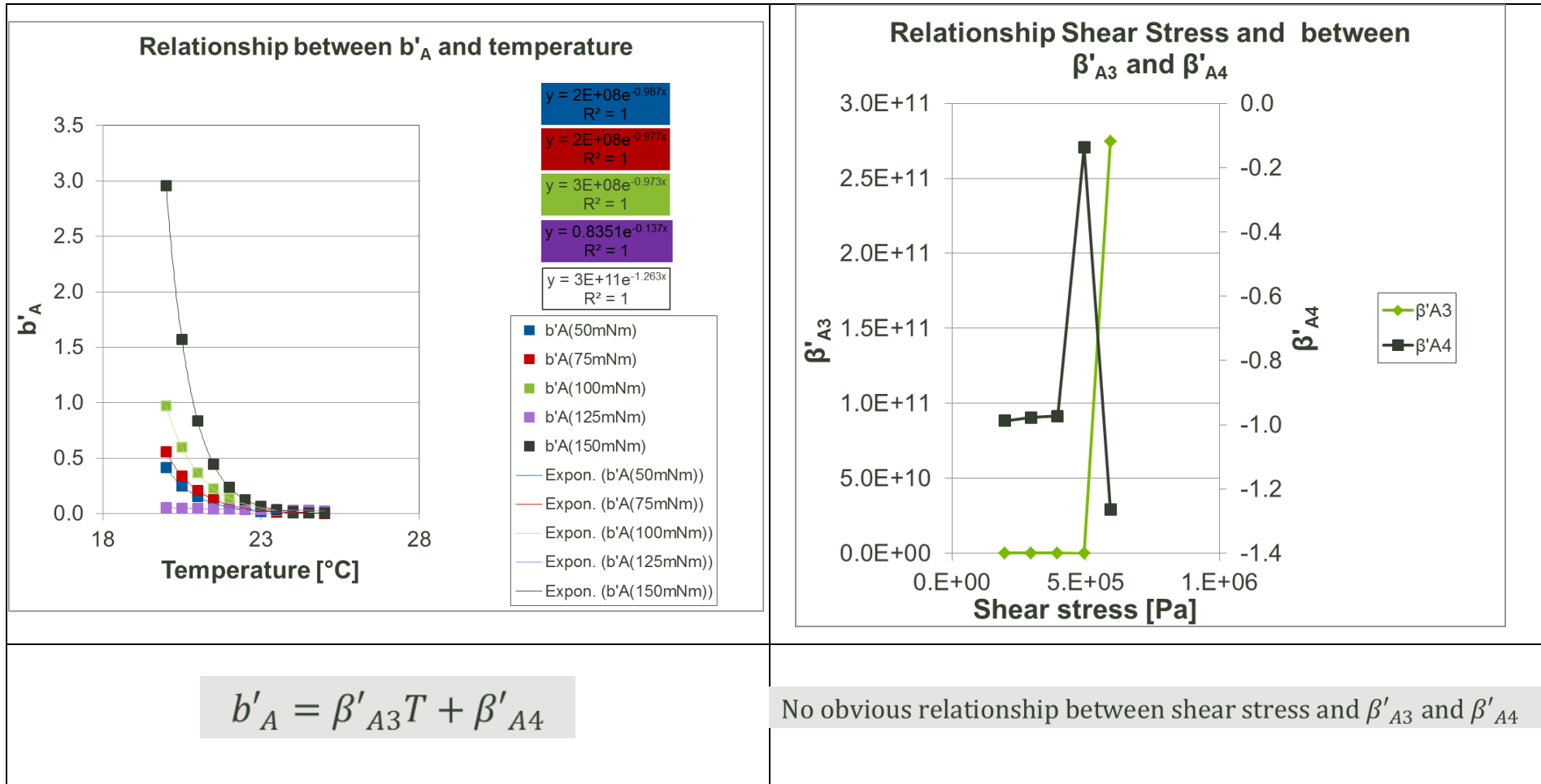
α_{A1} , α_{A2} and α_{A3} are the model constants for adhesion, α'_{A1} and α'_{A2} are the global model coefficients, and a'_A is the initial Nelder coefficient.

APPENDIX I

Coefficient “b_A”



APPENDIX I



APPENDIX I

Thus the adjusted model coefficient b_A is given b

$$b_A = \beta_{A1} e^{(\beta_{A2}T + \beta_{A3})\tau}$$

Obtained from intregating :

$$\beta'_{A2} = \beta_{A2}T + \beta_{A3} \text{ in } b'_A = \beta'_{A1} e^{\beta'_{A2}\tau}$$

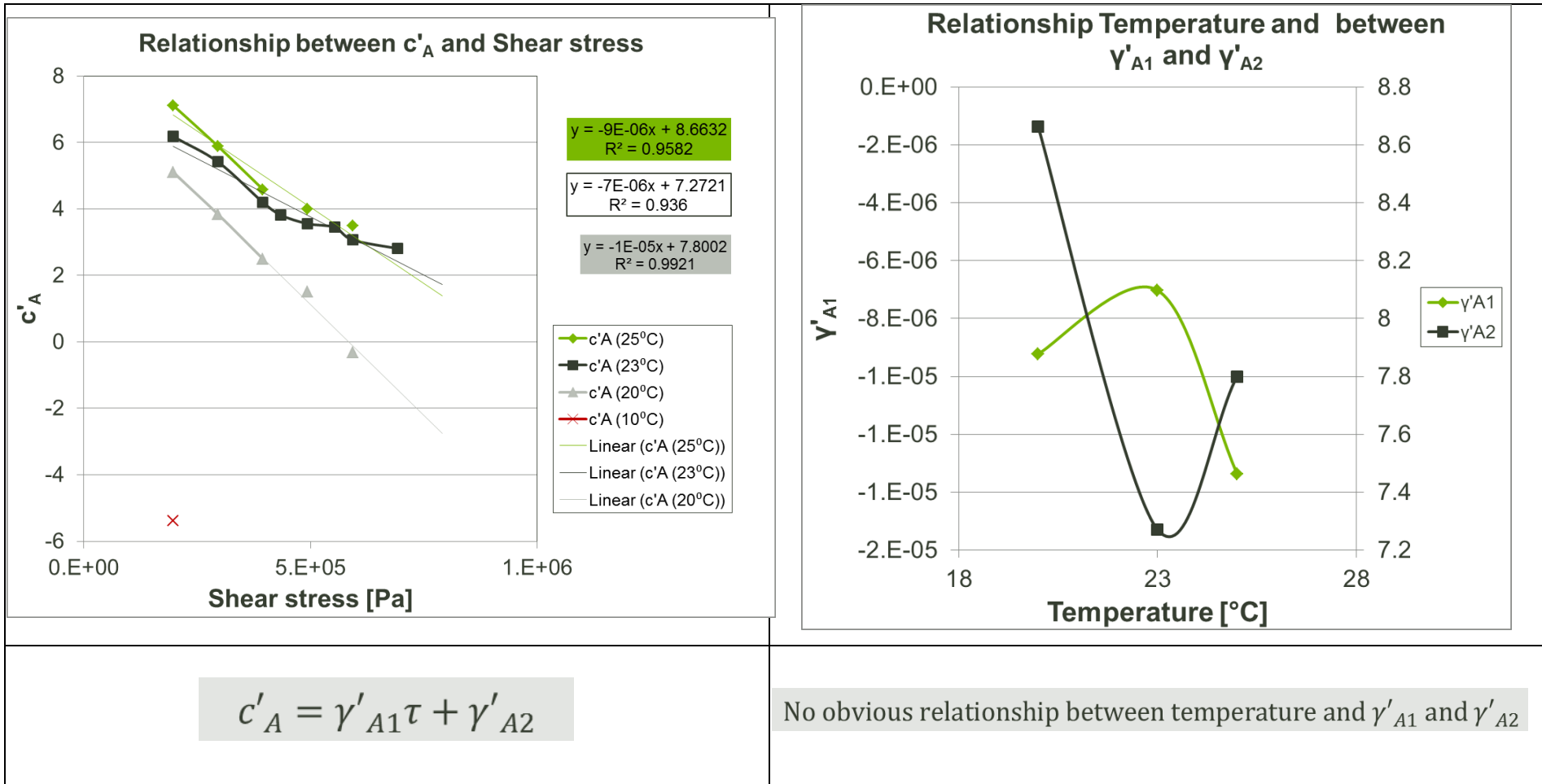
This intregation was possible because β'_{A2} displayed an obvious relationship to the temperature.

Where :

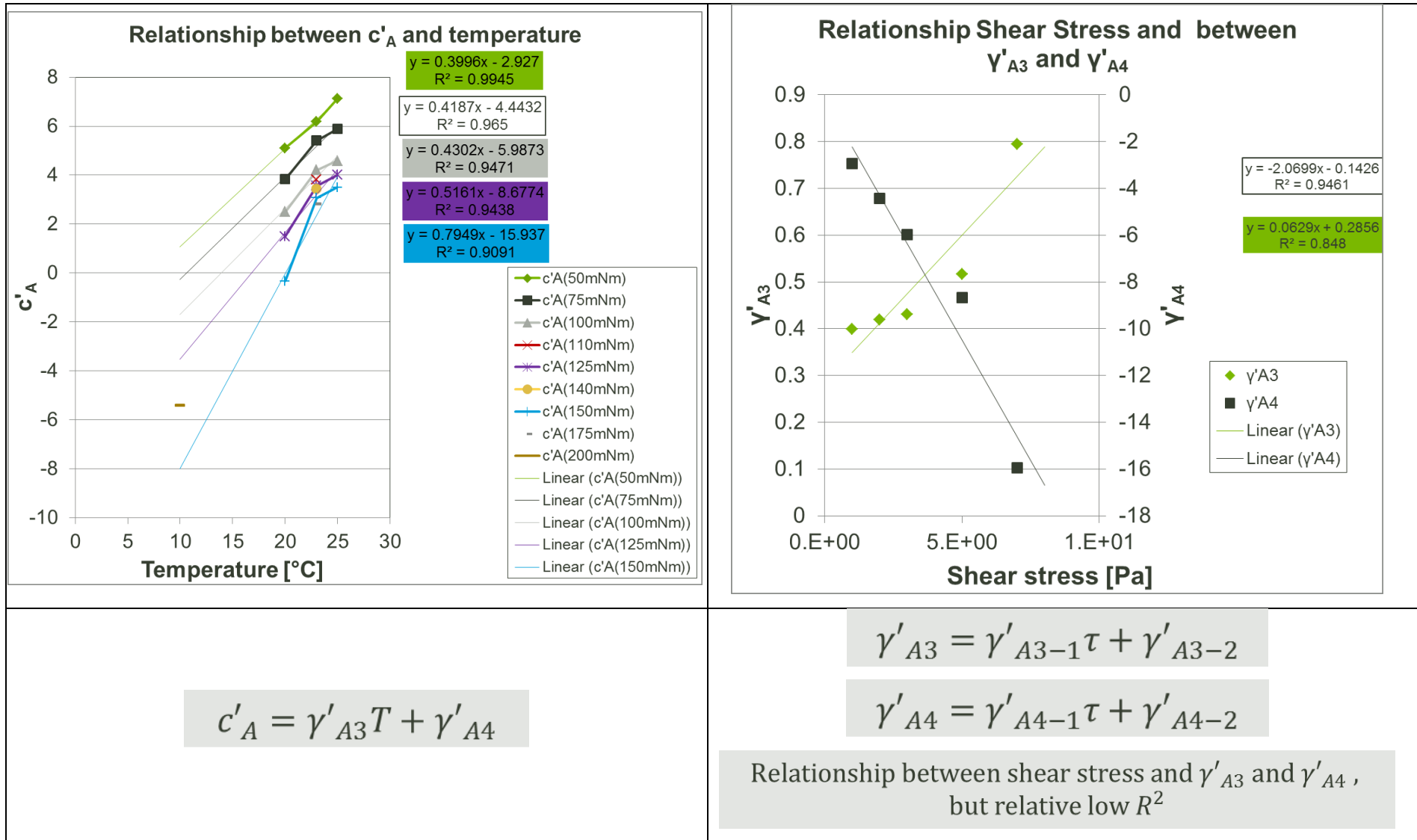
β_{A1} , β_{A2} and β_{A3} are the model constants for adhesion, β'_{A1} and β'_{A2} are the global model coefficients, and b'_A is the initial Nelder coefficient.

APPENDIX I

Coefficient “c_A”



APPENDIX I



APPENDIX I

Thus the adjusted model coefficient c_A is given by

$$c_A = \gamma_{A1}T + \gamma_{A2}$$

this relation is chosen between:

$$c'_A = \gamma'_{A3}T + \gamma'_{A4} \text{ and } c'_A = \gamma'_{A1}\tau + \gamma'_{A2}$$

Because, c_A appears to display a better relationship with the temperature than the shear stress.

Where :

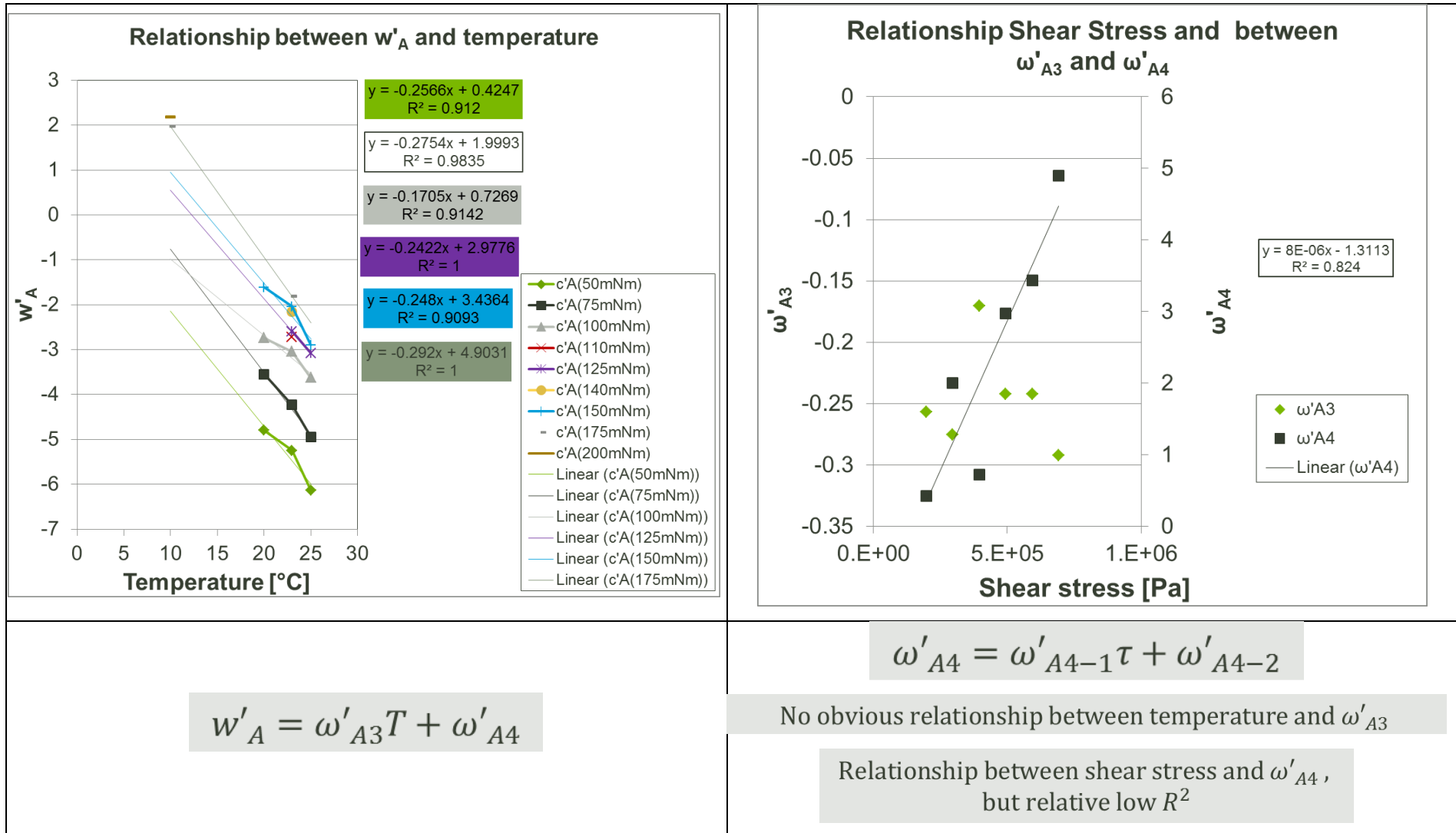
γ_{A1} and γ_{A2} are the model constants for adhesion, γ'_{A1} , γ'_{A2} , γ'_{A3} and γ'_{A4} are the global model coefficients, and γ'_A is the initial Nelder coefficient.

The model constants for adhesion γ_{A1} and γ_{A2} are respectively equal to the global model coefficients γ'_{A3} and γ'_{A4} , and

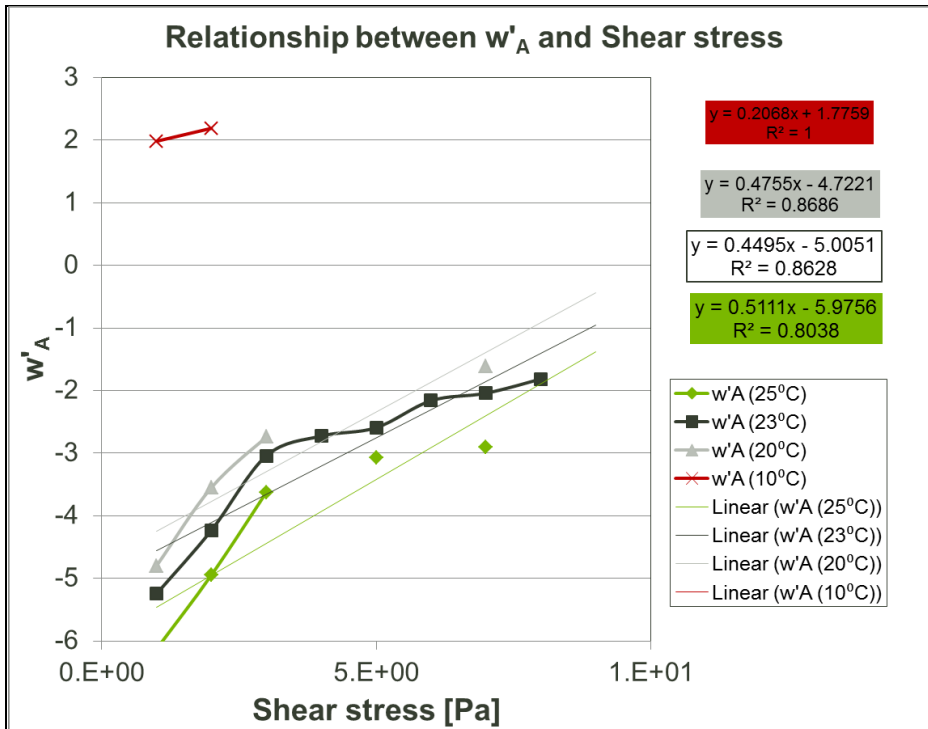
The adjusted coefficient c_A is equal to the initial Nelder coefficient c'_A .

APPENDIX I

Coefficient “wA”



APPENDIX I



Thus the adjusted model coefficient w_A is given by

$$w_A = \omega_{A1}T + \omega_{A2}$$

Where :

ω_{A1} and ω_{A2} are the model constants for adhesion, ω'_{A1} , ω'_{A2} , ω'_{A3} and ω'_{A4} are the global model coefficients, and w'_A is the initial Nelder coefficient.

The model constants for adhesion ω_{A1} and ω_{A2} are respectively equal to the global model coefficients ω'_{A3} and ω'_{A4} , and

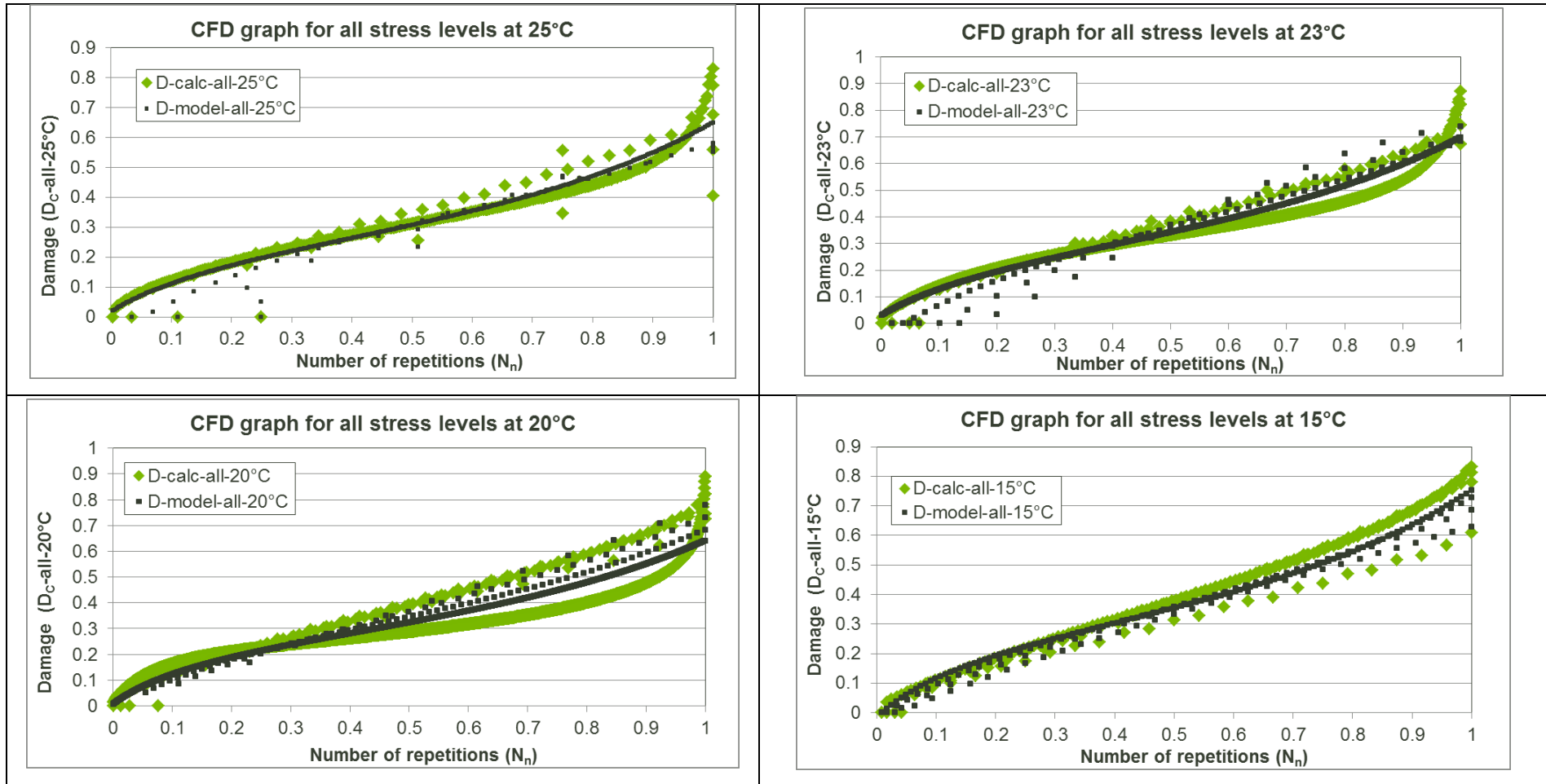
The adjusted coefficient ω_A is equal to the initial Nelder coefficient ω'_A .

$$w'_A = \omega'_{A1}\tau + \omega'_{A2}$$

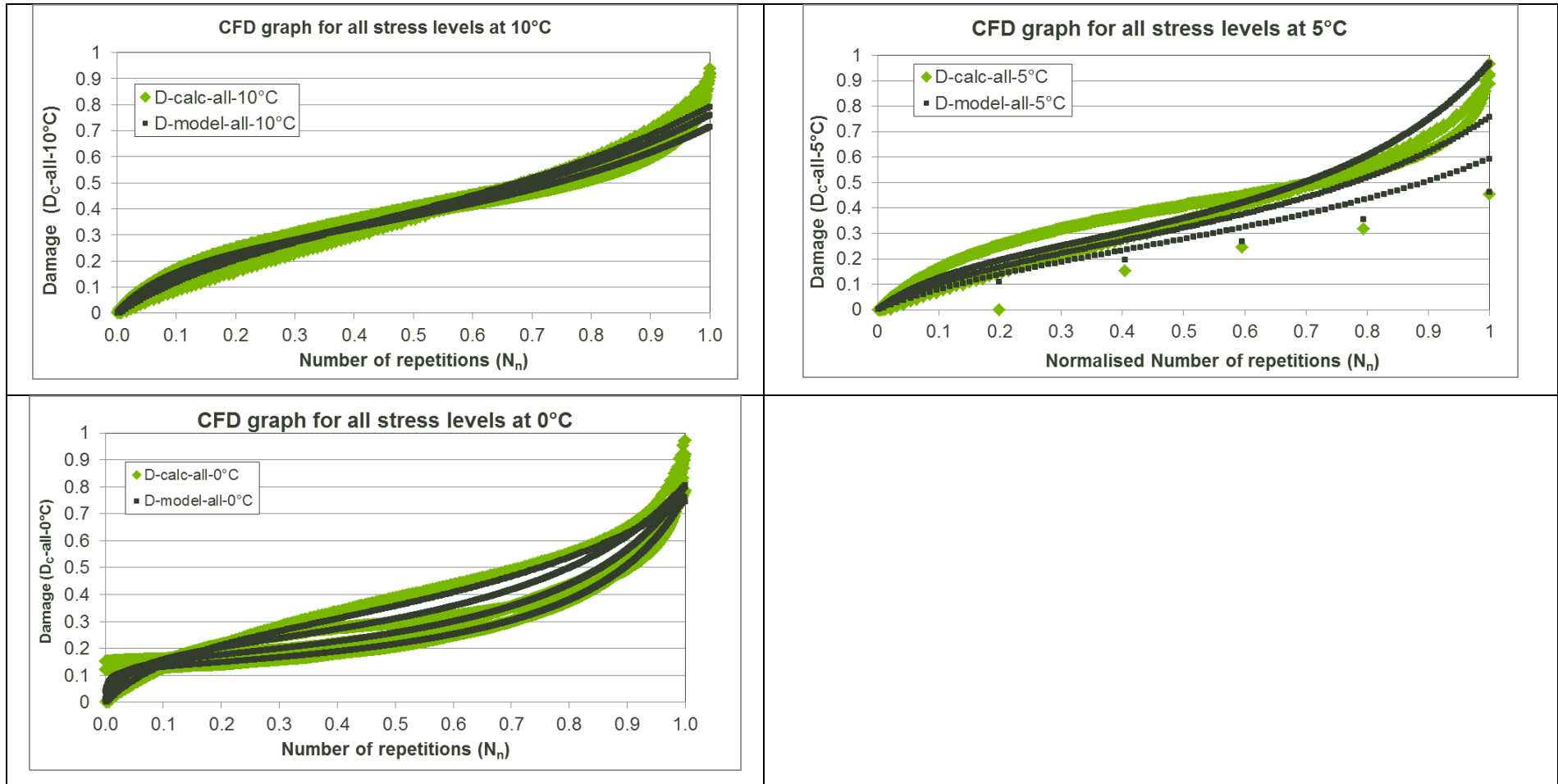
Relationship between shear stress and w'_A , but relative low R^2

APPENDIX I

1.9 Graphs of normalised cohesion fatigue damage model per temperature

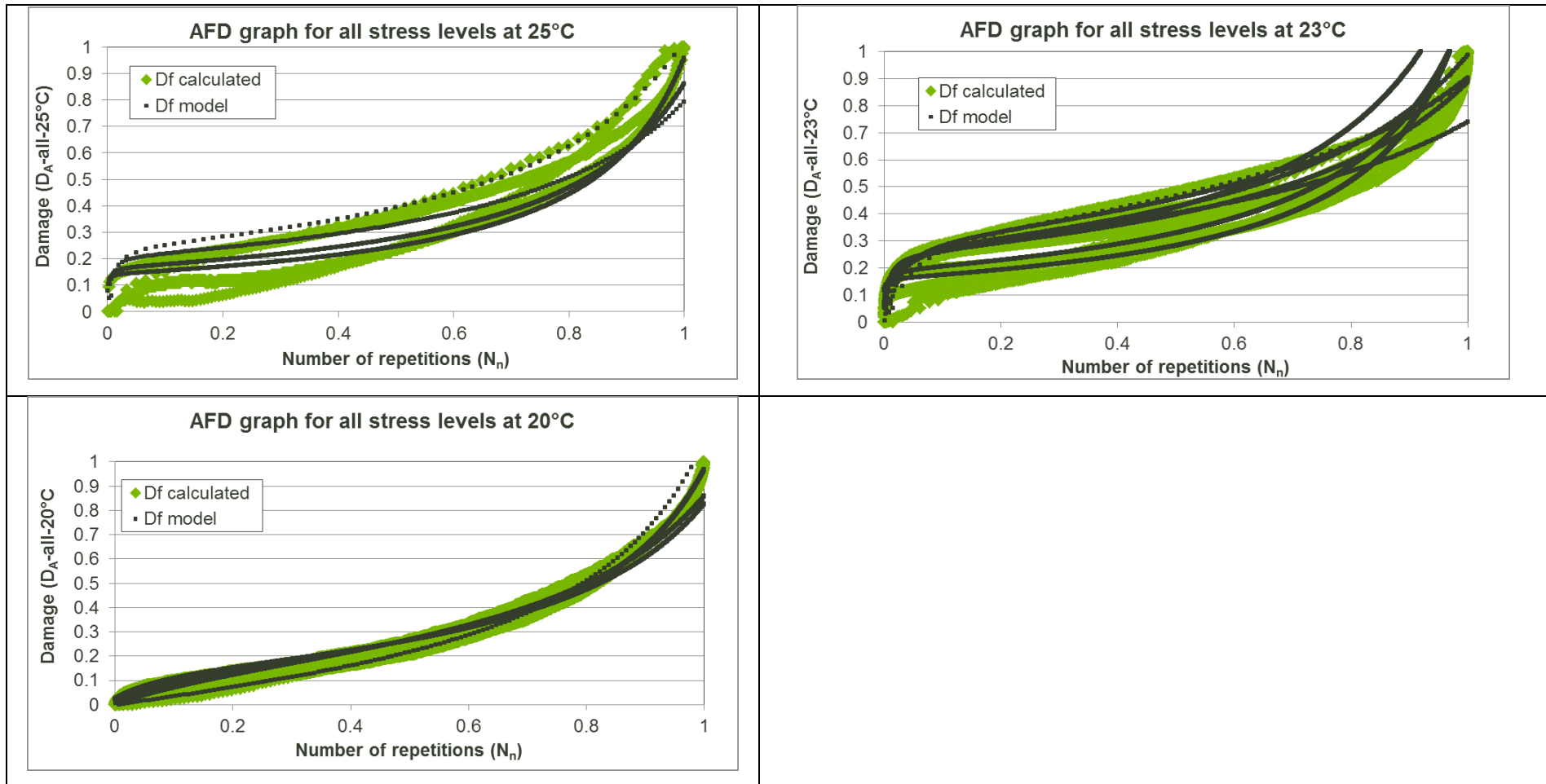


APPENDIX I



APPENDIX I

I.10 Graph of normalised adhesion fatigue damage model per temperature



APPENDIX I

I.11 Values of adjusted model coefficients in the case of cohesion fatigue damage

M [mNm]	τ [Pa]	Adjusted model coefficients for cohesion (25 ^o C)					Statistical parameter	
		α_{c1}	α_{c2}	β_{c1}	β_{c2}	β_{c3}	R ²	SEE
5	1.19.E+05	-5.77E-07	8.09E-02	2.51E-02	-1.66E-02	1.339E-06	0.90	0.03
10	2.39.E+05	-5.77E-07	8.09E-02	2.51E-02	-1.66E-02	1.339E-06		
15	3.58.E+05	-5.77E-07	8.09E-02	2.51E-02	-1.66E-02	1.339E-06		
20	4.77.E+05	-5.77E-07	8.09E-02	2.51E-02	-1.66E-02	1.339E-06		
25	5.97.E+05	-5.77E-07	8.09E-02	2.51E-02	-1.66E-02	1.339E-06		

M [mNm]	τ [Pa]	Adjusted model coefficients for cohesion (23 ^o C)					Statistical parameters	
		α_1	α_2	β_1	β_2	β_3	R ²	SEE
5	1.19E+05	-5.17E-07	8.20E-02	2.51E-02	-1.66E-02	1.3406E-06	0.95	0.04
10	2.39E+05	-5.17E-07	8.20E-02	2.51E-02	-1.66E-02	1.3406E-06		
15	3.58E+05	-5.17E-07	8.20E-02	2.51E-02	-1.66E-02	1.3406E-06		
20	4.77E+05	-5.17E-07	8.20E-02	2.51E-02	-1.66E-02	1.3406E-06		
25	5.97E+05	-5.17E-07	8.20E-02	2.51E-02	-1.66E-02	1.3406E-06		

M [mNm]	τ [Pa]	Adjusted model coefficients for cohesion (20 ^o C)					Statistical parameters	
		α_1	α_2	β_1	β_2	β_3	R ²	SEE
5	1.19E+05	-1.61E-07	2.28E-02	2.51E-02	-1.66E-02	1.34E-06	0.87	0.05
10	2.39E+05	-1.61E-07	2.28E-02	2.51E-02	-1.66E-02	1.34E-06		
15	3.58E+05	-1.61E-07	2.28E-02	2.51E-02	-1.66E-02	1.34E-06		
20	4.77E+05	-1.61E-07	2.28E-02	2.51E-02	-1.66E-02	1.34E-06		
25	5.97E+05	-1.61E-07	2.28E-02	2.51E-02	-1.66E-02	1.34E-06		

APPENDIX I

M [mNm]	τ [Pa]	Adjusted model coefficients for cohesion (15 ⁰ C)					Statistical parameters	
		α_1	α_2	β_1	β_2	β_3	R ²	SEE
5	1.19E+05	-7.55E-08	9.62E-03	2.51E-02	-1.66E-02	2.00E-06	0.96	0.04
10	2.39E+05	-7.55E-08	9.62E-03	2.51E-02	-1.66E-02	2.00E-06		
15	3.58E+05	-7.55E-08	9.62E-03	2.51E-02	-1.66E-02	2.00E-06		
20	4.77E+05	-7.55E-08	9.62E-03	2.51E-02	-1.66E-02	2.00E-06		
25	5.97E+05	-7.55E-08	9.62E-03	2.51E-02	-1.66E-02	2.00E-06		

M [mNm]	τ [Pa]	Adjusted model coefficients for cohesion (10 ⁰ C)					Statistical parameters	
		α_1	α_2	β_1	β_2	β_3	R ²	SEE
5	1.19E+05	-1.89E-08	3.59E-03	2.51E-02	-1.66E-02	2.10E-06	0.98	0.02
10	2.39E+05	-1.89E-08	3.59E-03	2.51E-02	-1.66E-02	2.10E-06		
15	3.58E+05	-1.89E-08	3.59E-03	2.51E-02	-1.66E-02	2.10E-06		
20	4.77E+05	-1.89E-08	3.59E-03	2.51E-02	-1.66E-02	2.10E-06		
25	5.97E+05	-1.89E-08	3.59E-03	2.51E-02	-1.66E-02	2.10E-06		

M [mNm]	τ [Pa]	Adjusted model coefficients for cohesion (5 ⁰ C)					Statistical parameters	
		α_1	α_2	β_1	β_2	β_3	R ²	SEE
15	3.58E+05	-2.57E-09	4.36E-04	2.51E-02	-1.66E-02	2.70E-06	0.87	0.07
20	4.77E+05	-2.57E-09	4.36E-04	2.51E-02	-1.66E-02	2.70E-06		
25	5.97E+05	-2.57E-09	4.36E-04	2.51E-02	-1.66E-02	2.70E-06		
30	7.16E+05	-2.57E-09	4.36E-04	2.51E-02	-1.66E-02	2.70E-06		
35	8.35E+05	-2.57E-09	4.36E-04	2.51E-02	-1.66E-02	2.70E-06		
40	9.54E+05	-2.57E-09	4.36E-04	2.51E-02	-1.66E-02	2.70E-06		

M [mNm]	τ [Pa]	Adjusted model coefficients for cohesion (0 ⁰ C)					Statistical parameters	
		α_1	α_2	β_1	β_2	β_3	R ²	SEE
25	5.97E+05	-1.53E-08	1.14E-02	2.51E-02	-1.66E-02	6.03E-06	0.96	0.03
30	7.16E+05	-1.53E-08	1.14E-02	2.51E-02	-1.66E-02	6.03E-06		
35	8.35E+05	-1.53E-08	1.14E-02	2.51E-02	-1.66E-02	6.03E-06		
40	9.54E+05	-1.53E-08	1.14E-02	2.51E-02	-1.66E-02	6.03E-06		

APPENDIX I

I.12 Values of adjusted model coefficients in the case of adhesion fatigue damage

M [mNm]	τ [Pa]	Adjusted model coefficients for adhesion (25°C)						Statistical parameter	
		α_1	α_2	α_3	β_1	β_2	β_3	R ²	SEE
50	1.98E+05	-2.56E-08	-3.56E-03	9.39E-02	1.36E-03	3.61E-07	-3.13E-06	0.91	0.07
75	2.96E+05	-2.56E-08	-3.56E-03	9.39E-02	1.36E-03	3.61E-07	-3.13E-06		
100	3.95E+05	-2.56E-08	-3.56E-03	9.39E-02	1.36E-03	3.61E-07	-3.13E-06		
125	4.94E+05	-2.56E-08	-3.56E-03	9.39E-02	1.36E-03	3.61E-07	-3.13E-06		

M [mNm]	τ [Pa]	Adjusted model coefficients for adhesion (23°C)						Statistical parameter	
		α_1	α_2	α_3	β_1	β_2	β_3	R ²	SEE
50	1.98E+05	-2.51E-08	-3.56E-03	9.01E-02	2.87E-03	3.61E-07	-3.06E-06	0.78	0.09
75	2.96E+05	-2.51E-08	-3.56E-03	9.01E-02	2.87E-03	3.61E-07	-3.06E-06		
100	3.95E+05	-2.51E-08	-3.56E-03	9.01E-02	2.87E-03	3.61E-07	-3.06E-06		
110	4.35E+05	-2.51E-08	-3.56E-03	9.01E-02	2.87E-03	3.61E-07	-3.06E-06		
125	4.94E+05	-2.51E-08	-3.56E-03	9.01E-02	2.87E-03	3.61E-07	-3.06E-06		
140	5.53E+05	-2.51E-08	-3.56E-03	9.01E-02	2.87E-03	3.61E-07	-3.06E-06		
150	5.93E+05	-2.51E-08	-3.56E-03	9.01E-02	2.87E-03	3.61E-07	-3.06E-06		
175	6.92E+05	-2.51E-08	-3.56E-03	9.01E-02	2.87E-03	3.61E-07	-3.06E-06		

M [mNm]	τ [Pa]	Adjusted model coefficients for adhesion (20°C)						Statistical parameter	
		α_1	α_2	α_3	β_1	β_2	β_3	R ²	SEE
50	1.98E+05	-4.90E-08	-3.56E-03	9.49E-02	2.40E-01	3.61E-07	-3.06E-06	0.98	0.03
75	2.96E+05	-4.90E-08	-3.56E-03	9.49E-02	2.40E-01	3.61E-07	-3.06E-06		
100	3.95E+05	-4.90E-08	-3.56E-03	9.49E-02	2.40E-01	3.61E-07	-3.06E-06		
150	5.93E+05	-4.90E-08	-3.56E-03	9.49E-02	2.40E-01	3.61E-07	-3.06E-06		